博士論文

Structural analysis of polymer aggregation induced by hydrophilic and hydrophobic interaction

（親水性・疎水性相互作用に起因する
高分子の凝集構造についての研究）

廣井　卓思

Abstract

In this thesis, structural analysis of polymer aggregation induced by hydrophilic and hydrophobic interaction was performed. In addition, structure control of inhomogeneity-free gels by tuning hydrophobicity was performed.

The first topic is inhomogeneities of gels from the viewpoint of dynamics. Gels are widely used in our daily life and therefore indispensable materials. For applications of gel materials, a fatal problem is that conventional gels are brittle. To solve this drawback, a gel called Tetra-PEG gel was developed. Many experimental results strongly suggest that Tetra-PEG gel is homogeneous from the viewpoint of static structure. To elucidate homogeneities from the viewpoint of dynamics, I investigated the dynamics of Tetra-PEG gels by quasi-elastic scattering techniques. By using dynamic light scattering (DLS) and neutron spin echo spectroscopy, inhomogeneity-free nature of Tetra-PEG gels was clarified.

To observe these inhomogeneities, I constructed an apparatus named DLS microscope to perform DLS with high spatial resolution. It is clarified that DLS microscope can also be applied to opaque system. This is important since conventional DLS system cannot be used for opaque dispersions because of multiple scattering or absorption occurring. This feature is proved by the size distribution measurement of polystyrene latex suspension, Chinese ink, and thermo-responsive polymer solution.

The second topic is aggregation induced by hydrophobic and hydrophilic interaction. Taking advantage of the unique feature of DLS microscope, a structural analysis of opaque system governed by hydrophobic and hydrophilic interaction was performed. As a representative hydrophobic system, concentration dependence of dispersion states of carbon nanotube (CNT) suspension was investigated. Since CNT strongly absorbs light, DLS measurement was available only for very dilute dispersion. To solve this problem, I investigated various kinds of CNT dispersions (different thickness and length) with wide concentration range by using polarized DLS microscope. As for translational Brownian motion, long CNTs showed slowing down at relatively high concentration (several wt%). As for rotational Brownian motion, the restriction of rotation was observed at relatively low concentration (0.1 wt%).

As a representative hydrophilic system, ovalbumin (OVA), a major protein in egg white, was investigated. Through the peptide treatment, *N*-terminal short peptide region is cleaved. Although the cleaved region is short, the heat-induced gels showed clear difference; cleaved OVA, called pOVA, is turbid while the intact OVA is transparent in salt-free environment. To explain this from the viewpoint of hydrophilicity, I performed structural analysis by DLS and small-angle neutron scattering (SANS). It is clarified that the amount of large aggregates is larger in pOVA solution than OVA solution, reflecting the hydrophobic nature of pOVA. This difference drastically changes the character of their heat-induced gels.

The third topic is inhomogeneity-free amphiphilic gels. From the first and second topics, inhomogeneity-free nature of Tetra-PEG gels and structure control by hydrophilic / hydrophobic interaction was elucidated. By combining these concepts, structure control of inhomogeneity-free gels by tuning hydrophobicity was performed. I prepared inhomogeneity-free amphiphilic gels through similar procedure of Tetra-PEG gels. These gels have both hydrophilic units and hydrophobic units. When the solvent is substituted by water, only the hydrophobic parts shrink and microphase-separation is induced. Microphase-separated structure was investigated by complementary use of SANS and SAXS. It is clarified that the microphase-separated structure is controlled by the size of hydrophobic units.

Contents

1 Introduction

1.1 Gels

Polymers are the molecules consisting of small unit molecules called a monomer. Usually, a monomer is in liquid or gas phase in ambient temperature. When the number of monomers within one polymer (degree of polymerization) becomes the order of several tens, the polymer becomes soft solid state due to intermolecular forces. For examples, polyethylene is one of the well-known polymers around us that is the raw materials for plastic bags. The monomer unit of polyethylene is ethylene, which is gas in ambient temperature and pressure. The origin of the softness is due to their large entropy originated from the large number of possible configuration. From this unique character, the polymer and related materials are named "soft matter" by the pioneer of this field, P. G. de Gennes [1]. From the viewpoint of physical chemistry, it is interesting that the physical properties become totally different by changing the structure even by using the same monomer unit. For examples, polyethylene is relatively stiff if there is few branch structure in the polymer, while many branch structure make the polyethylene soft like the plastic bag (Figure 1.1) [2].

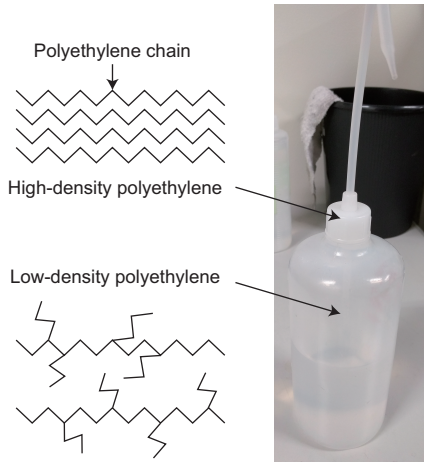

Figure 1.1: Difference between low-density polyethylene and high-density polyethylene.

Another interesting feature of polymers is crosslinking. Crosslinking can be regarded as the extension of branch structure. If two polymers are connected at a branching point, it is called that two polymers are crosslinked. By continuing crosslinking, the number of connected polymers becomes macroscopic scale. The resultant gigantic polymers are usually called polymer network. The density of crosslinking points determines the character of the polymer network. If the density of crosslinking is high, the material becomes stiff like resin. In contrast to this, if the length between each crosslinking is large enough, the material becomes soft like a rubber. This material is called elastomer. Like this, not only the chemical formula but also the structure at molecular level strongly affects the macroscopic physical properties. When the polymer network is immersed in solvent, the network sometimes absorbs solvent. This process is called swelling. The driving force of the swelling phenomena is osmotic pressure; from the viewpoint of entropy, it is better to dilute polymer network by the solvent molecules. However, polymer networks cannot be diluted infinitely even if enough amount of solvents are given. The driving force against the swelling is elasticity. As a result, polymer networks containing large amount of solvent can be stable. This system is called gels (Figure 1.2).

Gels are widely used in our daily life such as food, cosmetics, and so on (Figure 1.3). Their texture can

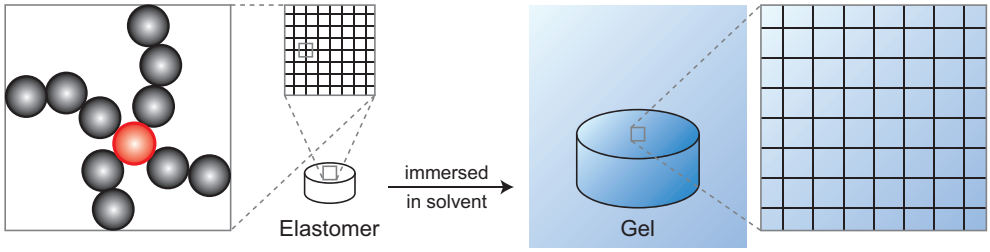

Figure 1.2: Crosslinking, elastomer, and gel.

be controlled by designing their monomers, structure, and solvent. For environmental problems, gels are promising materials. One of the recent hot topics is the application of gels to the electrolytes of batteries [3]. Electrolytes should possess both cohesive properties of solids and the diffusive properties of liquids, both of which are satisfied by using gel materials. In similar contexts, gel materials can be applied to the separator for mixed gas. By using character of their high affinity to water, hydrogels can also be used for holding soil moisture [4]. Other direction of the use of gel materials is medical application. Since the hydrogels are organic materials diluted with water, the affinity to human body is relatively high compared to other materials such as elastomer, resin, and metal. In addition, gel materials can retain other materials in their networks. By utilizing these features, the use of gel materials as a carrier of drug is one of the promising applications. As another application, an artificial joint made by gels is also promising from the viewpoint of biocompatibility. As a more familiar example, contact lenses are also hydrogels. In this case, not only the biocompatibility but also the transparency is important factor. Like this, gel materials are indispensable materials for our daily life.

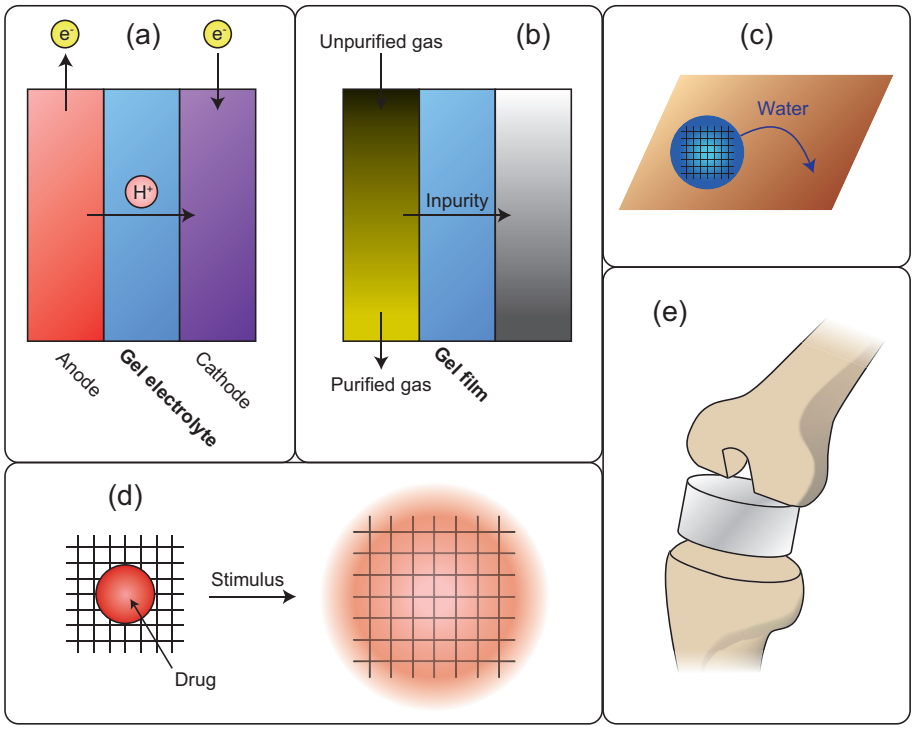

Figure 1.3: Applications of gels. (a) Gel electrolytes. (b) Separator for gas. (c) Holding soil moisture. (d) Drug delivery system. (e) Artificial articular cartilage.

1.2 Tough gels

For the application of gel materials, the fatal problem is that conventional gels are brittle. One of the origins of this weakness is that the density of crosslink is diluted by the solvent. However, conventional gels are so brittle that only the dilution effect cannot explain the origin of weakness. Currently it is well known that the origin of the weakness is inherent inhomogeneities of gel materials [5]. Conventional gels are usually prepared by using the radical reaction between polymers and crosslinkers. Since radical reaction occurs randomly, the distance between crosslinking points is uneven. This is the origin of inhomogeneities. When the stress is applied to such a inhomogeneous gel, the applied stress will be concentrated on the weak points. As a result, the gel will break with significantly smaller stress than the theoretical values.

To overcome this drawback, various kinds of tough gels have been developed such as slide-ring gel [6], nanocomposite gel [7], double-network gel [8], microsphere composite gel [9], ionically crosslinked gel [10] and so on (Figure 1.4), which are summarized in Section 5.2. Among of them, I focused on the gel called Tetra-PEG gels reported by Sakai *et al.* in 2008 [11]. Tetra-PEG gels are so strong that the breaking stress was approximately 25 MPa, which is larger that the native articular cartilage [12]. Preparation of Tetra-PEG gel is performed by mixing two tetra-arm polyethylene glycol (PEG) with different functional groups at the ends. One tetra-arm PEG has amine group while the other PEG has active ester group. These two tetra-arm PEGs can react with each other after mixing. By controlling the reaction rate by adjusting pH, the gelation proceeds. Since amine-terminated PEGs cannot react with themselves, amine-terminated PEGs and active ester-terminated PEG will be set one after the other. This preparation scheme will suppress inhomogeneities and make the Tetra-PEG gel strong.

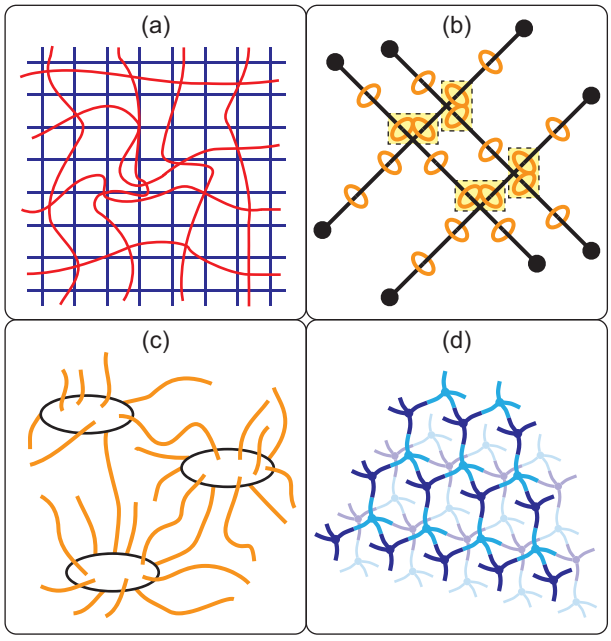

Figure 1.4: Examples of tough gels. (a) Double-network gel. (b) Slide-ring gel. (c) Nanocomposite gel. (d) Tetra-PEG gel.

1.3 Structural analysis of gels

To elucidate the origin of the strength of Tetra-PEG gels, structural analysis was performed. There are mainly two strategies for the structural analysis of soft matter; mechanical testing and scattering technique (Figure 1.5). In mechanical testing, certain stress (strain) is applied to the materials and monitor their response as a form of strain (stress). The response is quantitatively described by using some quantities such as shear modulus, bulk modulus, Young's modulus, and Poisson's ratio, summarized in Section 3.2. These macroscopic quantities can be represented by microscopic parameters such as the density of polymer chains and crosslinking, which can be controlled experimentally. From mechanical testing, it is clarified that the crosslinking reaction during the preparation of Tetra-PEG gels proceeds ideally.

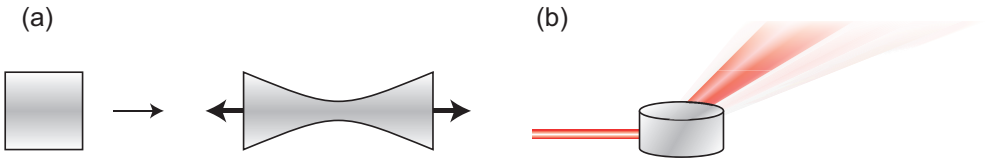

Figure 1.5: Structural analysis of soft matter. (a) Mechanical testing. (b) Scattering technique.

The other method for the investigation of soft matter is scattering. By tuning the wavelength of probe wave, the structure of materials can be recorded in reciprocal space (see Section 4). For examples, light scattering can be used for the structural analysis of colloidal suspension whose typical size is the order of μm [13]. However, for the research of gels, wavelength of visible light is usually too large for the structural analysis. To obtain structural information in the scale of polymer (typically $10 \sim 100$ nm), a short wavelength probe such as X-ray and neutrons is used [14]. By using small-angle neutron scattering (SANS) technique, structural analysis of Tetra-PEG gels was performed [15, 16]. It was shown that the scattering pattern obtained from Tetra-PEG gels are similar to that obtained from solutions. This means that inhomogeneities originated from crosslinking were suppressed significantly.

By using both mechanical testing and scattering technique, it is clarified that Tetra-PEG gels have homogeneous structure. However, all of the experiments had focused on static structure. As a matter of fact, polymer networks are fluctuating like Brownian motion of colloidal particles (Figure 1.6). Theoretical analysis for gel dynamics was performed by Tanaka *et al.* and know as Tanaka–Hocker–Benedek (THB) theory (see Section 3.2.3). This theory showed that we can obtain the mesh size of the network as a parameter called correlation length, which is extracted from the measurement of gel fluctuation. Although the correlation length gives us only qualitative information about mesh size, this parameter has been used for the characterization of gel. The reason why the correlation length gives us only qualitative picture is that inhomogeneities were not treated in the theory. This means that we may give the quantitative meaning to the correlation length for the first time by using inhomogeneity-free Tetra-PEG gels.

The two strategies for the structural analysis of soft matter can be used also for the investigation of dynamics. For the measurement of dynamics, mechanical testing is performed by applying time-dependent stress or strain. A representative example is the measurement of stress by applying oscillatory shear. By measuring the phase shift between the applied shear and measured stress, we can measure the elastic component and viscous component for viscoelastic materials. From the frequency dependence of viscoelasticity, we can obtain the information about the relaxation of polymer networks. However, dynamical mechanical testing can measure the dynamics whose characteristic time is slower than millisecond. To measure faster dynamics

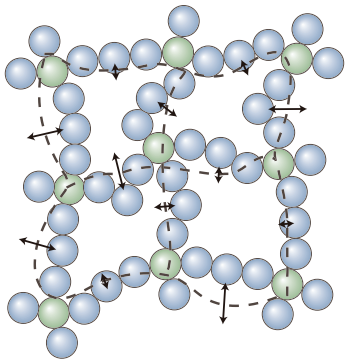

Figure 1.6: Fluctuation of a gel.

such as the fluctuation of polymer networks of gels, scattering technique is used. Therefore, I measured the dynamics of inhomogeneity-free Tetra-PEG gels by using both light (dynamic light scattering) and neutrons (neutron spin echo) as probes to clarify the quantitative meaning of the correlation length (Section 5).

1.4 Dynamic light scattering microscope

As explained in the previous subsection, Tetra-PEG gel is almost inhomogeneity-free. However, there still remain small inhomogeneities in larger scale. SANS profiles showed slight upturn in low-q region, which originates from Debye–Bueche type inhomogeneities (explained in Section 2.5.2). This upturn is clarified by the combination of SANS and light scattering [16]. Since the inhomogeneities were observed by the scattering angle dependence of visible light, we may map the inhomogeneities in real space by using the correlation length as a parameter.

Starting from this idea, I constructed the apparatus to obtain correlation length of gels with high spatial resolution; dynamic light scattering microscope (Figure 1.7, Section 6). Correlation length of gels was measured by the technique called dynamic light scattering (DLS; see Section 4.1.2). Usually, DLS is used to measure the size distribution of polymer and colloidal solutions. In addition, THB theory clarified that DLS can also measure the correlation length of gels. What we measure in DLS is the time correlation function of the intensity of scattered light. This means that we can measure correlation length from the irradiated volume. By using microscope, we can easily achieve high spatial resolution. Therefore, we can obtain the spatial map of correlation length by combining dynamic light scattering with a microscope. However, there still remains one problem. Since Tetra-PEG gel is homogeneous in the scale of irradiated volume, the intensity of scattered light is so small that we may not be able to detect enough signals to analyze. In fact, this conjecture is true; measurement of correlation length of Tetra-PEG gels by using DLS microscope is still challenging.

Instead of this, I accidentally found another application of this apparatus. DLS microscope enables us to measure the size distribution of opaque dispersion such as milk (turbid), ink (strong light absorbing) and so on (Figure 1.8). This unique point is complementary to conventional DLS system. Conventional DLS system cannot be used for opaque dispersions since multiple scattering or absorption occurring within the large irradiated volume degrade the scattered light. In contrast, DLS microscope can extract only singly scattered light by applying confocal optical system although the signal from homogeneous, transparent substance is hard to detect due to small irradiated volume. The fact that we can measure turbid system by using DLS

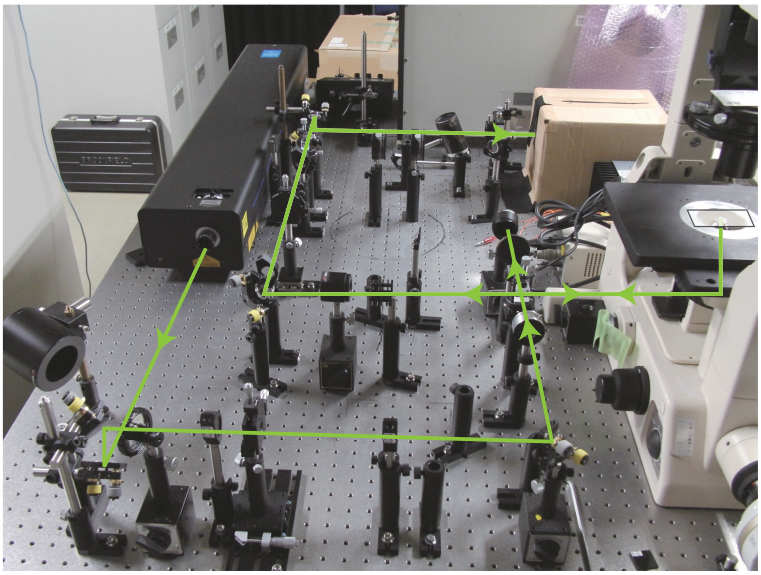

Figure 1.7: Photograph of dynamic light scattering microscope. Lines shown in the photo show the optical path.

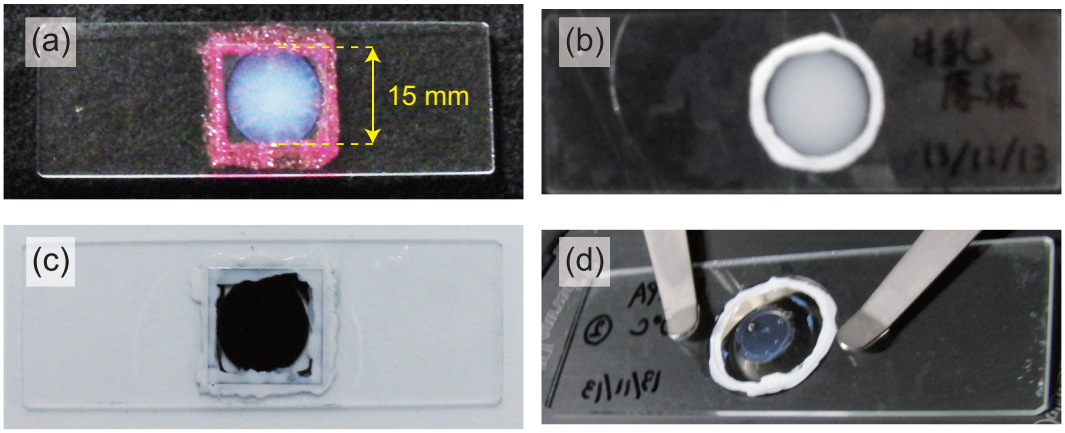

Figure 1.8: Examples of samples which are accessible by the dynamic light scattering microscope. (a) Polystyrene latex suspension. (b) Milk. (c) Chinese ink. (d) Poly(N-isopropylacrylamide) gel.

without dilution has large impact on the analysis of materials which were beyond the scope of DLS. Then I moved on the analysis of opaque systems by using scattering techniques including DLS microscope.

1.5 Hydrophilicity and hydrophobicity

For the systematic analysis of opaque systems, I focused on systems whose interaction between solutes can be manipulated systematically. Then I decided to investigate the system that is governed by hydrophilic and hydrophobic forces. The main reason for this decision is that we can manipulate hydrophilicity and hydrophobicity in gel systems at will by using Tetra-PEG gels [17, 18]. Before moving to this amphiphilic gels, I would like to introduce hydrophilicity and hydrophobicity briefly.

Interaction between molecules is interpreted by electrostatic interaction (Figure 1.9). The interaction between molecules having explicit charges (cations and anions) is called charge-charge interaction. The

interaction energy between two charged particles is proportional to r^{-1} where r is the distance between two particles. There is also an interaction between neutral molecules. If those neutral molecules have a dipole moment, the interaction is called dipole-dipole interaction. The interaction energy between two fixed dipole moments is proportional to r^{-3}. Then let us consider about the interaction between two water molecules. It is known that the interaction energy between two water molecules is approximately proportional to r^{-2} [19]. This power law is intermediate between charge-charge interaction and dipole-dipole interaction. Therefore, though the interaction between two water molecules originates from the dipole moment of water molecules, there should be qualitative difference from typical dipole-dipole interaction. This phenomenon is known as "hydrogen bonding".

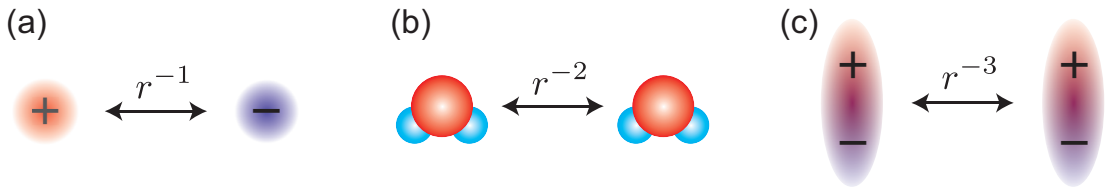

Figure 1.9: Interaction between molecules. (a) Interaction between molecules with explicit charges. (b) Interaction between water molecules. (c) Interaction between fixed molecules with dipoles.

Hydrogen bonding is formed not only between water molecules but also between a hydrogen and electronegative parts such as nitrogens, oxygens, fluorides and so on. This type of bonding strongly affects the physical properties of substances. For examples, NH_3 and HF are soluble in water while hydrocarbons are in general poorly solvable. When hydrocarbons are in water, hydrogen bondings among the solvent are disturbed by the hydrocarbons since water cannot make hydrogen bonding with the hydrocarbons. As a rule of thumb, we can classify molecules into two; the molecules that can accept hydrogen bondings are called hydrophilic while the molecules which cannot accept hydrogen bondings are called hydrophobic.

Though the interaction energy originated from hydrogen bonding is not so strong, hydrophilicity and hydrophobicity strongly affects the physical properties of polymers. This is because hydrophilicity and hydrophobicity of monomers are emphasized by polymerization. Therefore, the manipulation of hydrophilicity and hydrophobicity is one of the effective ways to design the physical properties of polymers as we want.

1.6 Carbon nanotube

To see how we can use DLS microscope for the research of hydrophilicity and hydrophobicity, I started the research of extremely hydrophobic material at first; carbon nanotube. A carbon nanotube, CNT, is a thin tube composed of carbon atoms. CNT is a very promising material because of its rigidity and electric property. To utilize these characters, CNTs are used as additive of rubbers, thin films, gels and so on. To use CNTs as additive of products, there are mainly two options; powder form or dispersion form. CNT dispersion is useful for the preparation of films via spin coat method. From the viewpoint of environmental burdens, desired solvent is water. Dissolving CNTs into water was a challenging task since CNT is extremely hydrophobic as I explained in the previous section. Recently, it is known that we can dissolve CNTs into water by using large amount of surfactants (Figure 1.10). In those dispersions, CNTs are covered by surfactants to reduce the aggregation. However, dispersion state of those solutions is not clarified yet since light scattering

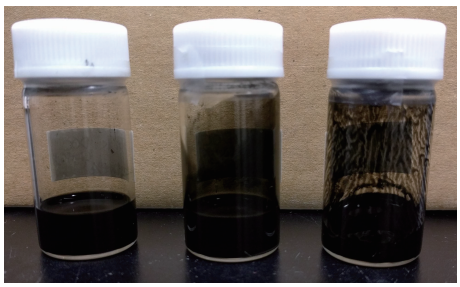

Figure 1.10: Dispersions of carbon nanotube.

technique cannot be used because of their strong light absorption. New techniques for the evaluation of dispersion states of CNT have been strongly desired.

It is clear that DLS microscope can be applied to the research of the aggregation state of CNT dispersion since strong light absorption does not affect the detection for this system. To achieve systematic research, I investigated various kinds of CNT dispersions (different thickness and length) with wide concentration range by using DLS microscope (Section 7). Through this research, aggregation induced by strong hydrophobic interaction was observed at higher concentration range. Experimental observation of this kind of aggregation was observed for the first time by using light as a probe. In addition, I found another kind of state transition serendipitously; rotational restriction. It was found that the rotational motion of carbon nanotube was restricted at relatively small concentration region (though still inaccessible by the conventional DLS system). This transition is unique for rod-like shape solutes.

1.7 Ovalbumin

Inspired by the interesting transition observed from rod-like shape solutes, I tried to investigate different rod-like shape solutes. In contrast to hydrophobic CNT, here I used hydrophilic rod-like shape solute as a sample; proteins. Proteins are composed of amino acids. Amino acids are classified into hydrophilic one and hydrophobic one by their character of side chains. Therefore, dispersion states of protein solutions are controlled by the hydrophilicity and hydrophobicity of amino acids on the surface. In solution, hydrophobic part is hidden inside the protein by folding process. Therefore, protein solution under room temperature can be regarded as a good example of hydrophilic system. The hydrophilicity of proteins can be manipulated by the change of temperature. Typical example is egg white. In spite of its name, egg white is not white but transparent under room temperature. However, like sunny-side up egg, it becomes white by heating process. During the heating process, the protein is unfolded and hydrophobic parts are exposed partially. In the case of egg white, previous research showed that the aggregates of protein becomes linear (rod-like shape) due to the balance of attractive hydrophobic interaction between exposed hydrophobic parts and repulsive Coulombic interaction between the charges on the protein [20]. Therefore, I used ovalbumin (OVA), the major protein in egg white, as a sample for the research by using DLS and SANS (Section 8).

Intact OVA is basically hydrophilic. To modify the hydrophilicity of OVA by design, I focused on peptide treatment. For the systematic understanding of OVA aggregations, experiments by using OVA with modified primary structure have been done recently by using mechanical testing [21, 22]. Through the peptide treatment, N-terminal short peptide region is cleaved and modify the hydrophilicity of OVA. Although the

cleaved region (22 amino acids) is only 6% in total, the heat-induced gels showed clear difference; cleaved OVA is turbid while the intact OVA is transparent under salt-free environment (Figure 1.11). At first glance, the result that the gel made from egg white is transparent contradicts with our common knowledge. The origin of this transparency is the concentration of salt. By controlling the concentration of OVA and salt, the structure of heat-induced gel can be manipulated. Interesting point is that the cleaved OVA is turbid even under salt-free condition. To investigate the origin of this feature, I investigated this system by using DLS and SANS technique. From the analysis, I conclude that the slight difference of dispersion state before heating significantly affects the structure of heat-induced gels. It is clarified that homogeneous OVA gels are composed of rod-like shape aggregates while the partially cleaved OVA gels contains glass-like inhomogeneities.

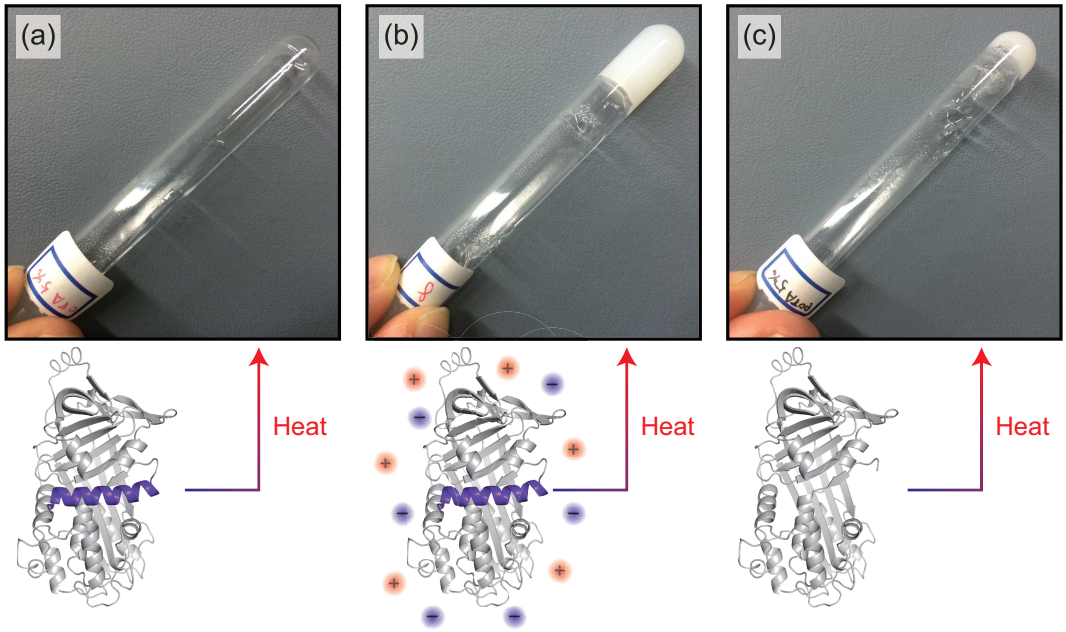

Figure 1.11: Heat-induced OVA gels. (a) Intact OVA (5 wt%). (b) Intact OVA (5 wt%) with NaCl (50 mM). (c) *N*-terminus cleaved OVA (5 wt%).

1.8 Amphiphilic co-network gels

The message from OVA experiment is that homogeneous gels can be made even the network polymer has hydrophobic component. Stimulated by this experimental result, I tried to create homogeneous amphiphilic gels by integrating the concept that I acquired. Here I briefly summarize amphiphilic network. Mixture of more than one polymer is called polymer blends. The structure of polymer blends strongly depends on the interaction parameter χ and the degree of polymerization, N (see Section 3.2.2 for details). Polymer blends show phase separation when χN is larger than the critical value [23]. In this case, phase separation extends in macroscopic scale. Other type of polymer mixture is block copolymer, which contains more than one type of monomers in one polymer. In contrast to the polymer blend, diblock or triblock copolymers tend to show phase separation in molecular dimensions due to the molecular constraint. This phenomenon is called

microphase separation and is extensively studied for a long time [24]. The interesting point of microphase-separated materials is that we can create novel physical properties by using two totally different monomers as a building block. One of the representative combinations is hydrophilic and hydrophobic monomers [25]. This combination is called amphiphilic [26]. This character is promising for many purposes. For example, amphiphilic materials can absorb both polar and nonpolar solutes. This is useful for the application of drug delivery system, which is currently limited to the delivery of hydrophilic materials [27]. Another example is soft contact lenses. Soft contact lenses demand contradictory characters; hydrophilic nature for biocompatibility and hydrophobic nature for oxygen permeability [28]. Amphiphilic materials meet these criteria. For the application, the amphiphilic materials are desired to take a network structure. However, the inhomogeneities accompanied by the introduction of cross-linking will affect their microphase-separated structure. Therefore, precise control of amphiphilic network structure is one of the main topic in this field.

Bottleneck for precise control of amphiphilic network structure is the inherent inhomogeneity. To solve this problem, I utilized Tetra-PEG module as a building block, which I investigated by using DLS and neutron spin echo (Figure 1.12, Section 9). The inhomogeneity-free amphiphilic gel is prepared by using hydrophilic Tetra-PEG and hydrophobic linear-PDMS as building blocks. SANS measurement proved the inhomogeneity-free nature of this amphiphilic gel. Then the structural analysis of the amphiphilic gels was held by varying the ratio of hydrophilic part and hydrophobic part. Complementary use of SANS and small-angle X-ray scattering (SAXS) clarified microphase-separated structure such as core-shell structure and lamellar structure. I believe that this is the first step for the precise manipulation of amphiphilic network structure.

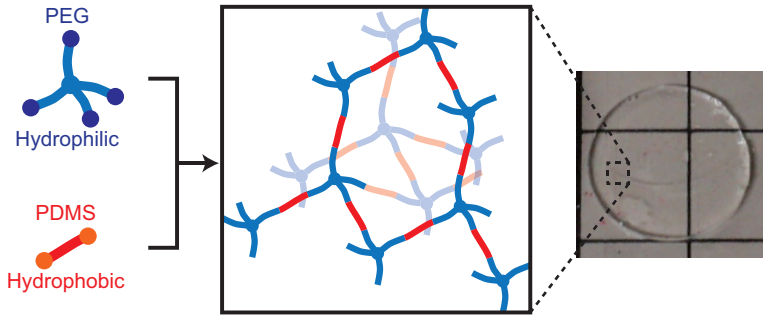

Figure 1.12: Preparation scheme of PEG–PDMS gel.

1.9 Thesis structure

In Section 2 to 4, I review the theory related to my research. I believe that this review is useful to study the field of structural analysis of soft matter. In Section 2, I introduce basic theory of scattering. Here, I review the scattering function from the viewpoint of form factors and structure factors. As for structure factors, I described from two points of view: Ornstein–Zernike equation and Landau free energy expansion. In Section 3, I introduce basic theory of physical properties of polymers. Especially, I focused on theories for three topics; fluctuation of gels, lower-critical solution temperature, and microphase separation. In Section 4, scattering techniques used in the following sections are summarized. Characteristic part is partial heterodyne method that is used for the analysis of dynamic light scattering from nonergodic system.

From Section 5, I explain my own researches. In Section 5, previous researches of Tetra-PEG gels are reviewed, followed by my research on multiscale dynamics of Tetra-PEG gels [29]. Here, I prove the homogeneity of Tetra-PEG gels from the viewpoint of dynamics. In Section 6, development and application of dynamic light scattering microscope is described [30, 31]. I successfully measured the size distribution of dense dispersions such as polystyrene latex suspension, Chinese ink, and thermo-responsive polymer solution. In addition, I measured concentrated carbon nanotube dispersion as a sample. This is the topic of Section 7; structural analysis of carbon nanotube dispersion [32]. Here, I applied polarized dynamic light scattering technique to measure rotational Brownian motion, which is unique for rod-like solutes. In Section 8, structural analysis of OVA and its derivative are described [33]. Gelation mechanism of OVA and its derivative is clarified from the viewpoint of hydrophilicity. In Section 9, I integrate the research of inhomogeneity-free gel and the research of hydrophilic and hydrophobic materials; structural analysis of amphiphilic PEG–PDMS gels [34]. In Section 10, I summarized this thesis. Graphical abstract is shown in Figure 1.13.

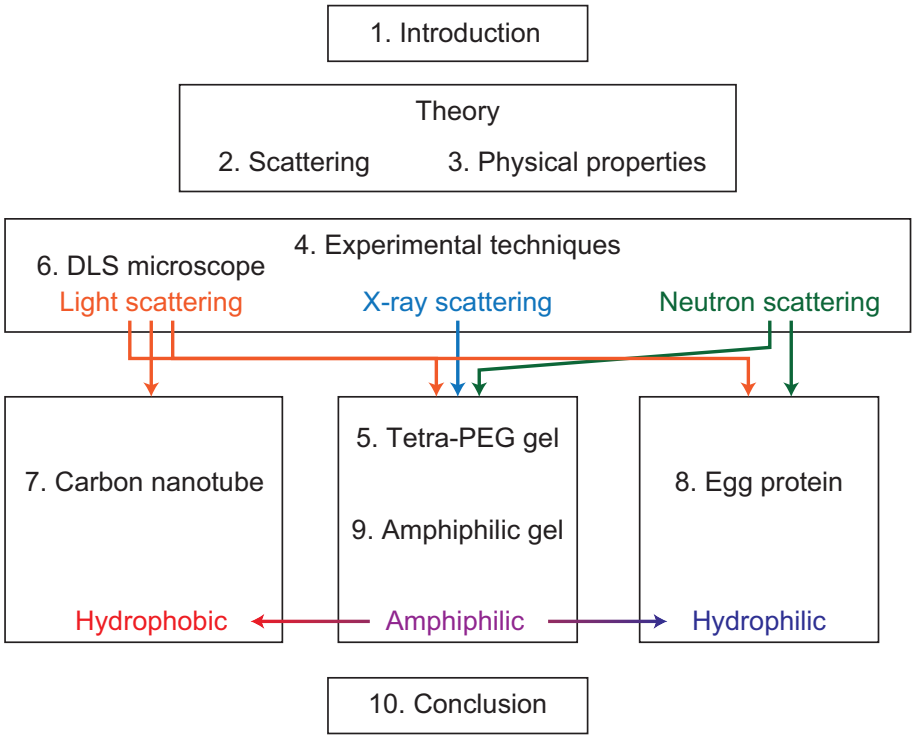

Figure 1.13: Graphical abstract of this thesis.

2 Basic Theory — Scattering

2.1 General scattering theory

This section is based on several textbook [14,35–37]. The definition is slightly different among them. Here I explicitly define several quantities used though this thesis.

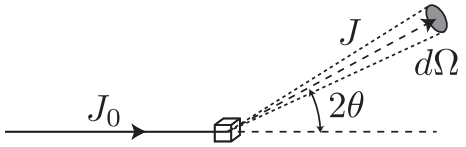

Figure 2.1: Schematics for the formulation of general scattering phenomenon.

Scattering phenomenon is described as Figure 2.1. The target is irradiated by incident wave or particles whose flux is J_0 [m^{-2}]. The flux of the scattered wave / particles are represented by J [m^{-2}]. Flux is the squared modulus of the amplitude of the wave.[1]

$$J_0 =: A_0^2 \tag{2.1.1}$$

$$J_s =: A_s^2 \tag{2.1.2}$$

Here, the scattered wave is spherical wave. Therefore, the amplitude of scattered wave, $A(R)$, will be proportional to R^{-1} where R is the distance between scattering point and observed point. In addition, $A(R)$ will also be proportional to A_0. Therefore, $A(R)$ can be represented as follows.

$$A_s(R) = A_0 \frac{b}{R} \tag{2.1.3}$$

Here, b [m] is the proportional constant called scattering length. b depends on the nature of probe (Table 2.1). Scattering phenomenon is quantitatively represented by the proportion of J_0 and J.

$$\frac{d\sigma}{d\Omega} := \frac{|A_s R|^2}{|A_0|^2} = b^2 \tag{2.1.4}$$

Here, detection area is taken as a solid angle to compensate R^{-1} dependence of scattered wave. $d\sigma/d\Omega$ has a unit of m^2 and called differential cross section. Scattered intensity, $I(q)$ [m^{-1}], is usually represented as a differential cross section per unit volume.

Let us consider the scattering from one particle consisting of z atoms whose positions are labeled by $\vec{r}_k$ (Figure 2.2(b)). In this case, we have to consider the interference between the atoms. The phase difference between the atom at the origin and at the position $\vec{r}$ is $\vec{q} \cdot \vec{r}$. Therefore, the scattering amplitude from the

Table 2.1: Scattering length

Probe	Scatterer	scattering length
Visible light	Atom	$k^2\alpha/4\pi\varepsilon\varepsilon_0$
X-ray	Electron	e^2/mc^2
Neutron	Nucleus	b_{nucleus}

[1] $A := B$ stands for "A is defined as B". $A =: B$ stands for "B is defined as A".

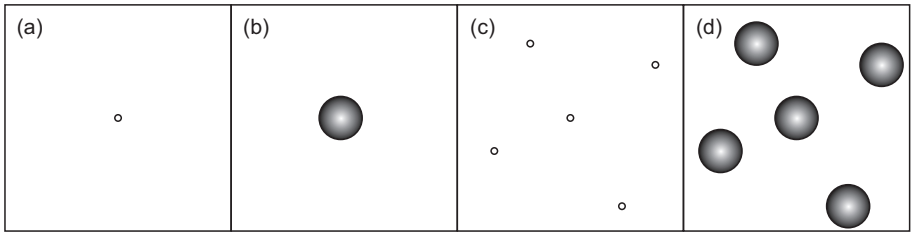

Figure 2.2: (a) Scattering from single atom. (b) Scattering from single particle. (c) Scattering from many atoms. (d) Scattering from many particles.

particle is written as follows.

$$A_s(R) = \frac{A_0}{R} \sum_{k=1}^{z} b_k e^{-i\vec{q}\cdot\vec{r}_k} \tag{2.1.5}$$

When the particle is composed of the same atoms[2], the differential cross section of the particle is written as follows.

$$\frac{d\sigma}{d\Omega} = b^2 \left| \sum_{k=1}^{z} e^{-i\vec{q}\cdot\vec{r}_k} \right|^2 =: b^2 z^2 P(\vec{q}) \tag{2.1.6}$$

$P(\vec{q})$ is called a form factor. When we treat the particle as a continuous medium, Eq.(2.1.6) is written as follows.

$$\frac{d\sigma}{d\Omega} = (\Delta\rho)^2 V_p^2 \left| \int n(\vec{r}) e^{-i\vec{q}\cdot\vec{r}} \right| =: (\Delta\rho)^2 V_p^2 P(\vec{q}) \tag{2.1.7}$$

where $\Delta\rho$, V_p, and $n(\vec{r})$ are the scattering length density, the volume of the particle, and the number density of the particle at $\vec{r}$, respectively. Note that:

$$\lim_{q\to 0} P(\vec{q}) = 1 \tag{2.1.8}$$

Next, let us consider the scattering from N atoms in irradiated volume whose positions are labeled by $\vec{R}_j$ (Figure 2.2(c)). The differential cross section of the system is written as follows.

$$\begin{aligned} \frac{d\sigma}{d\Omega} &= \left| \sum_{j=1}^{N} b_j e^{-i\vec{q}\cdot\vec{R}_j} \right|^2 \\ &= \sum_{j=1}^{N} b_j^2 + \sum_{j=1}^{N} \sum_{k\neq j}^{N} b_j b_k^* e^{-i\vec{q}\cdot\vec{R}_{jk}} \end{aligned} \tag{2.1.9}$$

where $\vec{R}_{jk} := \vec{R}_j - \vec{R}_k$. If each atom no spatial correlation (such as very dilute solution), the second term of Eq.(2.1.9) will be zero. Therefore, the scattering intensity becomes a mere summation of the scattering from each atom. If there are spatial correlation between each atom, the correlation is described as a structure

[2]We can regard monomer unit as one atom whose scattering length density is the summation of the scattering length of consisting atoms decided by their volume when the size of monomer is small compared to $1/q$.

factor, $S(\vec{q})$. When all of the atoms are the same species, $S(\vec{q})$ is defined as follows.

$$\frac{d\sigma}{d\Omega} = b^2 \left| \sum_{j=1}^{N} e^{-i\vec{q}\cdot\vec{R}_j} \right|^2 =: b^2 N S(\vec{q}) \tag{2.1.10}$$

Under this definition, note that:

$$\lim_{q\to 0} S(\vec{q}) = N \tag{2.1.11}$$

When $\vec{R}_{jk}$ has some distribution, we need to introduce a pair correlation function. The pair correlation function, $G(\vec{r})$, is defined as a Fourier transform of the structure factor.

$$\begin{aligned} G(\vec{r}) &:= \frac{1}{(2\pi)^3} \int S(\vec{q}) e^{-i\vec{q}\cdot\vec{r}} d\vec{q} \\ &= \frac{1}{N} \frac{1}{(2\pi)^3} \int \sum_{j=1}^{N} \sum_{k=1}^{N} e^{-i\vec{q}\cdot\vec{R}_{jk}} e^{-i\vec{q}\cdot\vec{r}} d\vec{q} \\ &= \frac{1}{N} \sum_{j=1}^{N} \sum_{k=1}^{N} \delta(\vec{r} + \vec{R}_j - \vec{R}_k) \\ &= \delta(\vec{r}) + \frac{1}{N} \sum_{j=1}^{N} \sum_{k\neq j}^{N} \delta(\vec{r} + \vec{R}_j - \vec{R}_k) \\ &=: \delta(\vec{r}) + g(\vec{r}) \end{aligned} \tag{2.1.12}$$

$g(\vec{r})$ is called the static pair-distribution function. $S(\vec{q})$ is the inverse Fourier transform of $G(\vec{r})$.

$$\begin{aligned} S(\vec{q}) &= \int G(\vec{r}) e^{i\vec{q}\cdot\vec{r}} d\vec{r} \\ &= \int (\delta(\vec{r}) + g(\vec{r})) e^{i\vec{q}\cdot\vec{r}} d\vec{r} = 1 + \int g(\vec{r}) e^{i\vec{q}\cdot\vec{r}} d\vec{r} \end{aligned} \tag{2.1.13}$$

Here, there is one problem which arise from the conversion from discrete $g(\vec{r})$ to continuous $g(\vec{r})$. If we substitute $g(\vec{r}) = (N-1)/V_{ir}$ where V_{ir} stands for the irradiated volume:

$$S(\vec{q}=0) = 1 + \frac{N-1}{V_{ir}} \int d\vec{r} = N \tag{2.1.14}$$

However, since constant $g(\vec{r})$ means homogeneous system (no contrast), there should be no scattering. To solve this problem, $S(\vec{q})$ is re-defined as follows.

$$S(\vec{q}) := 1 + \int (g(\vec{r}) - \varrho) e^{i\vec{q}\cdot\vec{r}} d\vec{r} \tag{2.1.15}$$

where ϱ is the average number density in the irradiated volume. Under this definition, note that:

$$\lim_{q\to 0} S(\vec{q}) = 0 \tag{2.1.16}$$

for completely homogeneous system. $S(q=0)$ is used to quantify the fluctuation of the system as shown later.

Lastly, let us consider the scattering from N particles consisting of z atoms in irradiated volume (Figure 2.2(d)). If each particle does not penetrate into other particles, the differential cross section of the system

is written as follows.

$$\begin{aligned}\frac{d\sigma}{d\Omega} &= \left|\sum_{j=1}^{N}\sum_{k_j=1}^{z} b_k e^{-i\vec{q}\cdot(\vec{R}_j+\vec{r}_{k_j})}\right|^2 \\ &= \sum_{k=1}^{z} b_k e^{-i\vec{q}\cdot\vec{r}_k}\sum_{j=1}^{N} e^{-i\vec{q}\cdot\vec{R}_j} \\ &\to N(\Delta\rho)^2 V_p^2 P(\vec{q})S(\vec{q}) \end{aligned} \tag{2.1.17}$$

Like this, scattering from dilute solution is decomposed into two factors; form factor and structure factor. In the following section, I'm going to introduce several examples of these factors, which is used in the latter part of this thesis.

2.2 Form factors

Here I summarized the form factor used in the following sections. For other form factors, please refer to The SANS Toolbox written by Boualem Hammouda [38].

2.2.1 Sphere

A sphere object of radius R with a uniform density ρ_0 is described as follows.

$$\rho(r) = \begin{cases} \rho_0 & \text{for } r \le R \\ 0 & \text{for } r > R \end{cases} \tag{2.2.1.1}$$

In this case, $\Delta\rho = \rho_0$, $V_p = \frac{4\pi}{3}R^3$, and the form factor is calculated as follows.

$$P(q) = \left[\frac{3(\sin qR - qR\cos qR)}{(qR)^3}\right]^2 \tag{2.2.1.2}$$

2.2.2 Ellipsoid

The form factor of ellipsoid is the extension of that of sphere.

$$P(q) = \int_0^1 dx \left[\frac{3\sin u - u\cos u}{u^3}\right]^2 \tag{2.2.2.1}$$

where

$$u := qR_b\sqrt{(R_a/R_b)^2x^2 + (1-x)^2} \tag{2.2.2.2}$$

2.2.3 Core-shell

Let us consider the form factor of the following core-shell structure.

$$\rho(r) = \begin{cases} \rho_c & \text{for} \quad r \leq r_c \\ \rho_s & \text{for} \quad r_c \leq r \leq R \\ \rho_0 & \text{for} \quad R < r \end{cases} \tag{2.2.3.1}$$

From Eq.(2.2.1.2):

$$P(q) = \left[(\rho_c - \rho_s) \frac{4\pi r_c^3}{3} \frac{3(\sin qr_c - qr_c \cos qr_c)}{(qr_c)^3} + (\rho_s - \rho_0) \frac{4\pi R^3}{3} \frac{3(\sin qR - qR \cos qR)}{(qR)^3} \right]^2 \tag{2.2.3.2}$$

2.2.4 Star

Star polymer is the polymer which grows more than two polymers from one crosslink point.

$$P(q) = \frac{2Z}{fu^2} \left[u - (1 - e^{-u}) + \frac{f-1}{2}(1 - e^{-u})^2 \right] \tag{2.2.4.1}$$

where f is the number of arms of the star polymer, $u := Za^2q^2/6$, Z is the degree of polymerization and a is the segment length [15].

2.2.5 Gaussian chain

Let us consider one-dimensional random walk. The length of one step is defined as b, which corresponds to the segment length. The number of steps is defined as N, which corresponds to the degree of polymerization. When $N \gg 1$, the probability that the distance between the first monomer and the last monomer is R_x is [23]:

$$P(N, R_x) = \frac{1}{\sqrt{2\pi N b^2}} \exp\left(-\frac{R_x^2}{2Nb^2} \right) \tag{2.2.5.1}$$

In 3D space, Eq.(2.2.5.1) is modified as follows.

$$P(N, \vec{R}) = \left(\frac{3}{2\pi N b^2} \right)^{3/2} \exp\left(-\frac{3R^2}{2Nb^2} \right) \tag{2.2.5.2}$$

Fourier transform of $P(N, \vec{R})$ is:

$$\begin{aligned} P(\vec{q}) &= \int d\vec{R} P(\vec{r}) e^{i\vec{q}\cdot\vec{R}} \\ &= \left(\frac{3}{2\pi N b^2} \right)^{3/2} \int d\vec{R} \exp\left(-\frac{3R^2}{2Nb^2} \right) e^{i\vec{q}\cdot\vec{R}} \\ &= \left(\frac{3}{2\pi N b^2} \right)^{3/2} \left(\frac{2\pi N b^2}{3} \right)^{3/2} \exp\left(-\frac{Nq^2b^2}{6} \right) \\ &= \exp\left(-\frac{Nq^2b^2}{6} \right) \end{aligned} \tag{2.2.5.3}$$

Here, I used the following formula.

$$\int d\vec{r} e^{-\alpha r^2} e^{i\vec{q}\cdot\vec{r}} = \left(\frac{\pi}{\alpha}\right)^{3/2} e^{-\frac{q^2}{4\alpha}} \tag{2.2.5.4}$$

Scattering from Gaussian chain is calculated by using Eq.(2.1.13). The pair correlation function, $G(\vec{r})$, is the average of $P(|i-j|, \vec{r})$.

$$G(\vec{r}) = \frac{1}{N^2} \sum_i^N \sum_j^N P(|i-j|, \vec{r}) \tag{2.2.5.5}$$

The scattering function, $P(\vec{q})$, is Fourier transform of $G(\vec{r})$:[3] [4]

$$\begin{aligned} P(\vec{q}) &= \frac{1}{N^2} \int d\vec{r} G(\vec{r}) e^{i\vec{q}\cdot\vec{r}} \\ &= \frac{1}{N^2} \sum_i^N \sum_j^N \exp\left(-\frac{q^2 b^2}{6}|i-j|\right) \end{aligned} \tag{2.2.5.6}$$

Eq.(2.2.5.6) is written as integral form.

$$\begin{aligned} P(\vec{q}) &\to \frac{1}{N^2} \int_0^N di \int_0^N dj \exp\left(-\frac{q^2 b^2}{6}|i-j|\right) \\ &= \int_0^1 ds \int_0^1 dt e^{-Q|s-t|} \\ &= \int_0^1 dt \left[\int_0^t ds e^{-Q(t-s)} + \int_t^1 ds e^{-Q(s-t)}\right] \\ &= \frac{1}{Q} \int_0^1 dt \left(2 - e^{-Qt} - e^{Qt} e^{-Q}\right) \\ &= \frac{2}{Q^2} \left(e^{-Q} + Q - 1\right) \end{aligned} \tag{2.2.5.7}$$

where

$$s := \frac{i}{N} \tag{2.2.5.8}$$

$$t := \frac{j}{N} \tag{2.2.5.9}$$

$$Q := \frac{q^2 b^2 N}{6} = \langle R_g^2 \rangle q^2 \tag{2.2.5.10}$$

Eq.(2.2.5.7) is called Debye function and used for the determination of R_g of polymers.

[3] Since this scattering function is a form factor, I used $P(\vec{q})$ instead of $S(\vec{q})$.

[4] Strictly speaking, we cannot use Eq.(2.2.5.2) when $|i-j|$ is small. Here, I neglect this point since $|i-j| \gg 1$ holds true in most terms.

2.3 Ornstein–Zernike equation

2.3.1 Canonical and grand canonical ensemble

Ornstein–Zernike equation is one of the most important equation to characterize the fluctuation in solution. Here, I derive this equation and explain the application for scattering problem [39]. First, I summarize important quantities for canonical and grand canonical ensemble. Canonical ensemble is a system whose temperature T, volume V, and the number of particles N are fixed. Let us write the Hamiltonian of identical N-particle system as follows.

$$\mathcal{H}(\vec{r}_1,\cdots,\vec{r}_N,\vec{p}_1,\cdots,\vec{p}_N) = K_N(\vec{p}_1,\cdots,\vec{p}_N) + V_N(\vec{r}_1,\cdots,\vec{r}_N) \tag{2.3.1.1}$$

where

$$K_N(\vec{p}_1,\cdots,\vec{p}_N) = \sum_{i=1}^{N} \frac{|\vec{p}_i|^2}{2m} \tag{2.3.1.2}$$

The probability that the particle coordinates and momentum are $\vec{r}_1,\cdots,\vec{r}_N$ and $\vec{p}_1,\cdots,\vec{p}_N$ is represented as follows.

$$p_N(\vec{r}_1,\cdots,\vec{r}_N,\vec{p}_1,\cdots,\vec{p}_N) = \frac{1}{h^{3N}N!}\frac{e^{-\beta\mathcal{H}}}{Q_N} \tag{2.3.1.3}$$

where a normalization constant called canonical partition function, Q_N, is

$$Q_N = \frac{1}{h^{3N}N!}\int\cdots\int e^{-\beta\mathcal{H}} d\vec{r}_1\cdots d\vec{r}_N d\vec{p}_1\cdots d\vec{p}_N \tag{2.3.1.4}$$

The factor h^{3N} is added to make the formula consistent with quantum system. The factor $N!$ means that we cannot distinguish identical N particles. Integration for momentum in Eq.(2.3.1.4) is performed separately.

$$\int\cdots\int e^{-\beta\mathcal{H}} d\vec{p}_1\cdots d\vec{p}_N = \int \exp\left[-\beta\frac{p_1^2}{2m}\right] d\vec{p}_1\cdots\int \exp\left[-\beta\frac{p_N^2}{2m}\right] d\vec{p}_N = \left(\frac{2\pi m}{\beta}\right)^{3N/2} \tag{2.3.1.5}$$

Here I used the following formula.

$$\int_{-\infty}^{\infty} e^{-\alpha x^2} dx = \sqrt{\frac{\pi}{\alpha}} \tag{2.3.1.6}$$

Substitute Eq.(2.3.1.5) to Eq.(2.3.1.4):

$$\begin{aligned} Q_N &= \frac{1}{h^{3N}N!}\left(\frac{2\pi m}{\beta}\right)^{3N/2}\int\cdots\int e^{-\beta V_N} d\vec{r}_1\cdots d\vec{r}_N \\ &= \frac{Z_N}{N!\Lambda^{3N}} \end{aligned} \tag{2.3.1.7}$$

where

$$Z_N := \int\cdots\int e^{-\beta V_N} d\vec{r}_1\cdots d\vec{r}_N \tag{2.3.1.8}$$

$$\Lambda := \left(\frac{\beta h^2}{2\pi m}\right)^{1/2} = \left(\frac{2\pi\beta\hbar^2}{m}\right)^{1/2} \tag{2.3.1.9}$$

Z_N is called configuration integral and Λ is called de Broglie thermal wavelength.

Canonical ensemble average for arbitrary quantity $A(\vec{r}_1, \cdots, \vec{r}_N, \vec{p}_1, \cdots, \vec{p}_N)$ is calculated as follows.

$$\begin{aligned}\langle A \rangle_c &:= \int \cdots \int A p_N(\vec{r}_1, \cdots, \vec{r}_N, \vec{p}_1, \cdots, \vec{p}_N) d\vec{r}_1 \cdots d\vec{r}_N d\vec{p}_1 \cdots d\vec{p}_N \\ &= \frac{\int \cdots \int A e^{-\beta \mathcal{H}} d\vec{r}_1 \cdots d\vec{r}_N d\vec{p}_1 \cdots d\vec{p}_N}{h^{3N} N! Q_N}\end{aligned} \tag{2.3.1.10}$$

If A depends only on coordinates, Eq.(2.3.1.10) becomes:

$$\begin{aligned}\langle A \rangle_c &= \frac{\int \cdots \int A e^{-\beta V_N} d\vec{r}_1 \cdots d\vec{r}_N}{h^{3N} N! Q_N} \left(\frac{2\pi m}{\beta} \right)^{3N/2} \\ &= \frac{\int \cdots \int A e^{-\beta V_N} d\vec{r}_1 \cdots d\vec{r}_N}{\left(h^2 \frac{\beta}{2\pi m} \right)^{3N/2} N! \frac{Z_N}{N! \Lambda^{3N}}} \\ &= \frac{1}{Z_N} \int \cdots \int A e^{-\beta V_N} d\vec{r}_1 \cdots d\vec{r}_N\end{aligned} \tag{2.3.1.11}$$

The probability that a particle 1 is at $\vec{r}$ is calculated as follows.

$$\begin{aligned}p_N(\vec{r}_1 = \vec{r}) &= \frac{1}{h^{3N} N! Q_N} \int \cdots \int e^{-\beta \mathcal{H}(\vec{r}, \vec{r}_2, \cdots)} d\vec{r}_2 \cdots d\vec{r}_N d\vec{p}_1 \cdots d\vec{p}_N \\ &= \frac{\int \cdots \int e^{-\beta \mathcal{H}(\vec{r}, \vec{r}_2, \cdots)} d\vec{r}_2 \cdots d\vec{r}_N d\vec{p}_1 \cdots d\vec{p}_N}{\int \cdots \int e^{-\beta \mathcal{H}(\vec{r}_1, \vec{r}_2, \cdots)} d\vec{r}_1 \cdots d\vec{r}_N d\vec{p}_1 \cdots d\vec{p}_N} \\ &= \frac{\int \cdots \int e^{-\beta V_N(\vec{r}, \vec{r}_2, \cdots)} d\vec{r}_2 \cdots d\vec{r}_N}{\int \cdots \int e^{-\beta V_N(\vec{r}_1, \vec{r}_2, \cdots)} d\vec{r}_1 \cdots d\vec{r}_N} \\ &= \frac{1}{Z_N} \int \cdots \int e^{-\beta V_N(\vec{r}, \vec{r}_2, \cdots)} d\vec{r}_2 \cdots d\vec{r}_N\end{aligned} \tag{2.3.1.12}$$

The probability for other $N-1$ particles can be calculated similarly. Particle density at $\vec{r}$, $\rho_N^{(1)}(\vec{r})$ is the summation for all of the particles.

$$\rho_N^{(1)}(\vec{r}) = \sum_{i=1}^{N} p_N(\vec{r}_i = \vec{r}) = \frac{N}{Z_N} \int \cdots \int e^{-\beta V_N(\vec{r}, \vec{r}_2, \cdots)} d\vec{r}_2 \cdots d\vec{r}_N \tag{2.3.1.13}$$

By comparing Eqs.(2.3.1.11) and (2.3.1.13), particle density is regarded as the canonical ensemble average of delta functions:

$$\begin{aligned}\langle \delta(\vec{r} - \vec{r}_1) \rangle_c &= \frac{1}{Z_N} \int \cdots \int \delta(\vec{r} - \vec{r}_1) e^{-\beta V_N(\vec{r}_1, \vec{r}_2, \cdots)} d\vec{r}_1 \cdots d\vec{r}_N \\ &= \frac{1}{Z_N} \int \cdots \int e^{-\beta V_N(\vec{r}, \vec{r}_2, \cdots)} d\vec{r}_2 \cdots d\vec{r}_N\end{aligned} \tag{2.3.1.14}$$

$$\left\langle \sum_{i=1}^{N} \delta(\vec{r} - \vec{r}_i) \right\rangle_c = \rho_N^{(1)}(\vec{r}) \tag{2.3.1.15}$$

Similar to a one-particle density, let us define two-particle density, $\rho_N^{(2)}(\vec{r}, \vec{r}')$. The probability that a particle

1 is at $\vec{r}$ and a particle 2 is at $\vec{r}'$ is calculated as follows.

$$p_N(\vec{r}_1=\vec{r},\vec{r}_2=\vec{r}') = \frac{1}{h^{3N}N!Q_N}\int\cdots\int e^{-\beta\mathcal{H}(\vec{r},\vec{r}',\vec{r}_3,\cdots)}d\vec{r}_3\cdots d\vec{r}_N d\vec{p}_1\cdots d\vec{p}_N$$
$$= \frac{1}{Z_N}\int\cdots\int e^{-\beta V_N(\vec{r},\vec{r}',\vec{r}_3,\cdots)}d\vec{r}_3\cdots d\vec{r}_N \tag{2.3.1.16}$$

$$\rho_N^{(2)}(\vec{r},\vec{r}') = \sum_{i=1}^{N}\sum_{j\neq i}^{N} p_N(\vec{r}_i=\vec{r},\vec{r}_j=\vec{r}') = \frac{N(N-1)}{Z_N}\int\cdots\int e^{-\beta V_N(\vec{r},\vec{r}',\vec{r}_3,\cdots)}d\vec{r}_3\cdots d\vec{r}_N \tag{2.3.1.17}$$
$$= \left\langle \sum_{i=1}^{N}\sum_{j\neq i}^{N}\delta(\vec{r}-\vec{r}_i)\delta(\vec{r}'-\vec{r}_j)\right\rangle_c \tag{2.3.1.18}$$

Similar to this, n-particle density, $\rho_N^{(n)}(\vec{r}_1,\cdots,\vec{r}_n)$ is defined as follows.

$$\rho_N^{(n)}(\vec{r}_1,\cdots,\vec{r}_n) := \frac{1}{Z_N}\frac{N!}{(N-n)!}\int\cdots\int e^{-\beta V_N(\vec{r}_1,\cdots,\vec{r}_N)}d\vec{r}_{N-n}\cdots d\vec{r}_N$$
$$= \left\langle \sum_{i_1=1}^{N}\cdots\sum_{i_n\neq i_1,\cdots i_{n-1}}^{N}\cdots\delta(\vec{r}_1-\vec{r}_{i_1})\cdots\delta(\vec{r}_n-\vec{r}_{i_n})\right\rangle_c \tag{2.3.1.19}$$

Energy of the system of canonical ensemble is designated by T,V,N. This energy is called Helmholtz free energy.

$$F(T,V,N) = U - TS \tag{2.3.1.20}$$
$$dF = -SdT - PdV + \mu dN \tag{2.3.1.21}$$

Helmholtz free energy is represented by the canonical partition function.

$$F = -k_BT\ln Q_N \tag{2.3.1.22}$$

When the potential V_N is decomposed into the following way,

$$V_N(\vec{r}_1,\cdots,\vec{r}_N) \to V_N(\vec{r}_1,\cdots,\vec{r}_N) + \Phi_N(\vec{r}_1,\cdots,\vec{r}_N) \tag{2.3.1.23}$$

where V_N represents the potential energy arising from interparticle interaction and Φ_N represents the potential energy arising from the interaction with external field,

$$\Phi_N(\vec{r}_1,\cdots,\vec{r}_N) = \sum_i^N \phi(\vec{r}_i) \tag{2.3.1.24}$$

In this case, configuration integral (Eq.(2.3.1.8)) is:

$$Z_N := \int\cdots\int e^{-\beta V_N}e^{-\beta(\phi(\vec{r}_1))}\cdots e^{-\beta(\phi(\vec{r}_N))}d\vec{r}_1\cdots d\vec{r}_N$$
$$= \int\cdots\int\left[\prod_{i=1}^{N}e^{-\beta(\phi(\vec{r}_i))}\right]e^{-\beta V_N}d\vec{r}_1\cdots d\vec{r}_N$$
$$=: \int\cdots\int\left[\prod_{i=1}^{N}y(\vec{r}_i)\right]e^{-\beta V_N}d\vec{r}_1\cdots d\vec{r}_N \tag{2.3.1.25}$$

where

$$y(\vec{r}_i) := e^{-\beta(\phi(\vec{r}_i))} \tag{2.3.1.26}$$

One-particle density (Eq.(2.3.1.13) or (2.3.1.15)) is: [5]

$$\begin{aligned}
\rho_N^{(1)}(\vec{r}) &= \left\langle \sum_{i=1}^{N} \delta(\vec{r}-\vec{r}_i) \right\rangle_c \\
&= \frac{1}{Z_N} \int \cdots \int \left[\prod_{i=1}^{N} y(\vec{r}_i) \right] e^{-\beta V_N(\vec{r}_1,\vec{r}_2,\cdots,\vec{r}_N)} \left(\sum_{i=1}^{N} \delta(\vec{r}-\vec{r}_i) \right) d\vec{r}_1 \cdots d\vec{r}_N \\
&= \frac{1}{Z_N} \int \cdots \int y(\vec{r}_1)y(\vec{r}_2)\cdots y(\vec{r}_N) e^{-\beta V_N(\vec{r}_1,\vec{r}_2,\cdots,\vec{r}_N)} \left(\delta(\vec{r}-\vec{r}_1)+\cdots+\delta(\vec{r}-\vec{r}_N)\right) d\vec{r}_1 \cdots d\vec{r}_N \\
&= \frac{1}{Z_N} \left[\int \cdots \int y(\vec{r})y(\vec{r}_2)\cdots y(\vec{r}_N) e^{-\beta V_N(\vec{r},\vec{r}_2,\cdots,\vec{r}_N)} d\vec{r}_2 d\vec{r}_3 \cdots d\vec{r}_N \right. \\
&\qquad + \int \cdots \int y(\vec{r}_1)y(\vec{r})\cdots y(\vec{r}_N) e^{-\beta V_N(\vec{r}_1,\vec{r},\cdots,\vec{r}_N)} d\vec{r}_1 d\vec{r}_3 \cdots d\vec{r}_N + \cdots \\
&\qquad\quad \left. + \int \cdots \int y(\vec{r}_1)y(\vec{r}_2)\cdots y(\vec{r}_{N-1}) e^{-\beta V_N(\vec{r}_1,\vec{r}_2,\cdots,\vec{r}_{N-1})} d\vec{r}_1 d\vec{r}_2 \cdots d\vec{r}_{N-1} \right] \qquad (2.3.1.27) \\
&= \frac{N y(\vec{r})}{Z_N} \int \cdots \int \left[\prod_{i=2}^{N} y(\vec{r}_i) \right] e^{-\beta V_N(\vec{r},\vec{r}_2,\cdots,\vec{r}_N)} d\vec{r}_2 \cdots d\vec{r}_N \quad \text{for } N \geq 2 \qquad (2.3.1.28)
\end{aligned}$$

Note that each term in Eq.(2.3.1.27) is the same. It is interesting to compare Eq.(2.3.1.28) with the functional derivative of configuration integral. Let us differentiate Eq.(2.3.1.25) by $y(\vec{r})$. Since $y(\vec{r})$ is a function of $\vec{r}$, Z_N is a function of the function $y(\vec{r})$. This kind of function is called functional. [6]

$$\begin{aligned}
\frac{\delta Z_N[y]}{\delta y(\vec{r})} &= \frac{\delta}{\delta y(\vec{r})} \left[\int \cdots \int \left[\prod_{i=1}^{N} y(\vec{r}_i) \right] e^{-\beta V_N(\vec{r},\vec{r}_2,\cdots,\vec{r}_N)} d\vec{r}_1 \cdots d\vec{r}_N \right] \\
&= \int \cdots \int y(\vec{r}_2)y(\vec{r}_3)\cdots y(\vec{r}_N) e^{-\beta V_N(\vec{r},\vec{r}_2,\cdots,\vec{r}_N)} d\vec{r}_2 d\vec{r}_3 \cdots d\vec{r}_N \\
&\quad + \int \cdots \int y(\vec{r}_1)y(\vec{r}_3)\cdots y(\vec{r}_N) e^{-\beta V_N(\vec{r}_1,\vec{r},\cdots,\vec{r}_N)} d\vec{r}_1 d\vec{r}_3 \cdots d\vec{r}_N + \cdots \\
&\quad\quad + \int \cdots \int y(\vec{r}_1)y(\vec{r}_2)\cdots y(\vec{r}_{N-1}) e^{-\beta V_N(\vec{r}_1,\vec{r}_2,\cdots,\vec{r}_{N-1})} d\vec{r}_1 d\vec{r}_2 \cdots d\vec{r}_{N-1} \\
&= N \int \cdots \int \left[\prod_{i=2}^{N} y(\vec{r}_i) \right] e^{-\beta V_N(\vec{r},\vec{r}_2,\cdots,\vec{r}_N)} d\vec{r}_2 \cdots d\vec{r}_N \quad \text{for } N \geq 2 \qquad (2.3.1.29)
\end{aligned}$$

Here I used the following formula.

$$\frac{\delta y(x')}{\delta y(x)} = \delta(x-x') \tag{2.3.1.30}$$

From Eqs.(2.3.1.28) and (2.3.1.29), $\rho_N^{(1)}(\vec{r})$ is expressed by $Z_N[y]$ and $y(\vec{r})$.

$$\rho_N^{(1)}(\vec{r}) = \frac{y(\vec{r})}{Z_N} \frac{\delta Z_N[y]}{\delta y(\vec{r})} \tag{2.3.1.31}$$

[5] When $N=1$, $\rho_1^{(1)}(\vec{r}) = \dfrac{y(\vec{r})}{Z_1} e^{-\beta V_1(\vec{r})}$.

[6] When $N=1$, $\dfrac{\delta Z_1[y]}{\delta y(\vec{r})} = e^{-\beta V_1(\vec{r})}$. Note that Eq.(2.3.1.31) holds when $N=1$.

By using the following equations,

$$\frac{d\ln Z_N}{dZ_N} = \frac{1}{Z_N} \tag{2.3.1.32}$$

$$\frac{d\ln y(\vec{r})}{dy(\vec{r})} = \frac{1}{y(\vec{r})} \tag{2.3.1.33}$$

$$\ln Q_N = -\beta F \tag{2.3.1.34}$$

$$\ln y(\vec{r}) = -\beta\phi(\vec{r}) \tag{2.3.1.35}$$

Eq.(2.3.1.31) is written as follows.

$$\rho_N^{(1)}(\vec{r}) = \frac{\delta\ln Z_N}{\delta\ln y(\vec{r})} = -\frac{\delta\ln Q_N}{\beta\delta\phi(\vec{r})} = \frac{\delta F}{\delta\phi(\vec{r})} \tag{2.3.1.36}$$

Next, let us summarize important feature of grand canonical ensemble. Grand canonical ensemble is a system whose temperature T, volume V, and chemical potential μ are fixed. Here, chemical potential is defined as a derivative of Helmholtz energy by N as explained in next subsection.

$$\mu := \frac{\partial F}{\partial N} \tag{2.3.1.37}$$

Difference between canonical ensemble and grand canonical ensemble is whether the total number of particles, N, is fixed or not. Grand canonical partition function, Ξ, is defined similar to Q_N (Eq.(2.3.1.4)). However, we have to sum up all of the possible N. Note that the subscript N in Q_N is no longer available for Ξ. In addition, the energy will change when the particle is added to the system even if there is no interaction between particles. This energy change is expressed by μ for one particle as shown in Eq.(2.3.1.37). When we construct partition function, this effect should be subtracted. Therefore, Ξ is expressed as follows.

$$\begin{aligned}\Xi &= \sum_{N=0}^{\infty}\frac{1}{h^{3N}N!}\int\cdots\int e^{-\beta(\mathcal{H}-N\mu)}d\vec{r}_1\cdots d\vec{r}_N d\vec{p}_1\cdots d\vec{p}_N \\ &= \sum_{N=0}^{\infty} e^{\beta N\mu}Q_N = \sum_{N=0}^{\infty} e^{\beta N\mu}\frac{Z_N}{N!\Lambda^{3N}} =: \sum_{N=0}^{\infty}\frac{z^N}{N!}Z_N\end{aligned} \tag{2.3.1.38}$$

where

$$z := \Lambda^{-3}e^{\beta\mu} \tag{2.3.1.39}$$

Grand canonical ensemble average for arbitrary quantity $A(\vec{r}_1,\cdots,\vec{r}_N,\vec{p}_1,\cdots,\vec{p}_N)$ is calculated as follows.

$$\langle A\rangle_g = \frac{1}{\Xi}\sum_{N=0}^{\infty}\frac{\int\cdots\int Ae^{-\beta(\mathcal{H}-N\mu)}d\vec{r}_1\cdots d\vec{r}_N d\vec{p}_1\cdots d\vec{p}_N}{h^{3N}N!} \tag{2.3.1.40}$$

If A depends only on coordinates, Eq.(2.3.1.40) becomes:

$$\begin{aligned}\langle A \rangle_g &= \frac{1}{\Xi}\sum_{N=0}^{\infty}\frac{\int\cdots\int Ae^{-\beta(V_N-N\mu)}d\vec{r}_1\cdots d\vec{r}_N}{h^{3N}N!}\left(\frac{2\pi m}{\beta}\right)^{3N/2} \\ &= \frac{1}{\Xi}\sum_{N=0}^{\infty}\frac{(e^{\beta\mu})^N}{\Lambda^{3N}N!}\int\cdots\int Ae^{-\beta V_N}d\vec{r}_1\cdots d\vec{r}_N \\ &= \frac{1}{\Xi}\sum_{N=0}^{\infty}\frac{z^N}{N!}\int\cdots\int Ae^{-\beta V_N}d\vec{r}_1\cdots d\vec{r}_N \\ &= \frac{1}{\Xi}\sum_{N=0}^{\infty}\frac{z^N}{N!}Z_N\langle A \rangle_c \end{aligned} \tag{2.3.1.41}$$

Energy of the system of grand canonical ensemble is designated by T, V, μ. This energy is called grand potential.

$$\Omega(T,V,\mu) = F - N\mu \tag{2.3.1.42}$$

$$d\Omega = -SdT - PdV - Nd\mu \tag{2.3.1.43}$$

Grand potential is represented by the grand canonical partition function.

$$\Omega = -k_BT\ln\Xi \tag{2.3.1.44}$$

Let us consider the case where the potential is decomposed like Eq.(2.3.1.24). In this case, grand canonical partition function is calculated by substituting Eq.(2.3.1.25) to Eq.(2.3.1.38):

$$\begin{aligned}\Xi &= \sum_{N=0}^{\infty}\frac{z^N}{N!}\int\cdots\int\left[\prod_{i=1}^{N}e^{-\beta(\phi(\vec{r}_i))}\right]e^{-\beta V_N}d\vec{r}_1\cdots d\vec{r}_N \\ &=: \sum_{N=0}^{\infty}\frac{1}{N!}\int\cdots\int\left[\prod_{i=1}^{N}z(\vec{r}_i)\right]e^{-\beta V_N}d\vec{r}_1\cdots d\vec{r}_N \end{aligned} \tag{2.3.1.45}$$

where

$$z(\vec{r}_i) := ze^{-\beta(\phi(\vec{r}_i))} = \Lambda^{-3}e^{\beta(\mu-\phi(\vec{r}_i))} =: \Lambda^{-3}e^{\beta\psi(\vec{r}_i)} \tag{2.3.1.46}$$

where

$$\psi(\vec{r}_i) := \mu - \phi(\vec{r}_i) \tag{2.3.1.47}$$

By using this grand canonical partition function, one-particle density for grand canonical ensemble, $\rho^{(1)}(\vec{r})$, is calculated as follows.

$$
\begin{aligned}
\rho^{(1)}(\vec{r}) &= \left\langle \sum_{i=1}^{N} \delta(\vec{r}-\vec{r}_i) \right\rangle_g \\
&= \frac{1}{\Xi} \sum_{N=1}^{\infty} \frac{1}{N!} \int \cdots \int \left[\prod_{i=1}^{N} z(\vec{r}_i) \right] e^{-\beta V_N(\vec{r}_1,\vec{r}_2,\cdots,\vec{r}_N)} \sum_{j=1}^{N} \delta(\vec{r}-\vec{r}_j) d\vec{r}_1 \cdots d\vec{r}_N \\
&= \frac{1}{\Xi} \sum_{N=1}^{\infty} \frac{1}{N!} \left[\int \cdots \int z(\vec{r}) z(\vec{r}_2) \cdots z(\vec{r}_N) e^{-\beta V_N(\vec{r},\vec{r}_2,\cdots,\vec{r}_N)} d\vec{r}_2 d\vec{r}_3 \cdots d\vec{r}_N \right. \\
&\qquad + \int \cdots \int z(\vec{r}_1) z(\vec{r}) \cdots z(\vec{r}_N) e^{-\beta V_N(\vec{r}_1,\vec{r},\cdots,\vec{r}_N)} d\vec{r}_1 d\vec{r}_3 \cdots d\vec{r}_N + \cdots \\
&\qquad \left. + \int \cdots \int z(\vec{r}_1) z(\vec{r}_2) \cdots z(\vec{r}_{N-1}) e^{-\beta V_N(\vec{r}_1,\vec{r}_2,\cdots,\vec{r}_{N-1})} d\vec{r}_1 d\vec{r}_2 \cdots d\vec{r}_{N-1} \right] \\
&= \frac{z(\vec{r})}{\Xi} \left[e^{-\beta V_1(\vec{r})} + \sum_{N=2}^{\infty} \frac{1}{(N-1)!} \int \cdots \int \left[\prod_{i=2}^{N} z(\vec{r}_i) \right] e^{-\beta V_N(\vec{r},\vec{r}_2,\cdots,\vec{r}_N)} d\vec{r}_2 \cdots d\vec{r}_N \right]
\end{aligned}
\tag{2.3.1.48}
$$

Let us compare Eq.(2.3.1.48) with the functional derivative of Ξ by $z(\vec{r})$.

$$
\begin{aligned}
\frac{\delta \Xi[z]}{\delta z(\vec{r})} &= \frac{\delta}{\delta z(\vec{r})} \left[\sum_{N=0}^{\infty} \frac{1}{N!} \int \cdots \int \left[\prod_{i=1}^{N} z(\vec{r}_i) \right] e^{-\beta V_N(\vec{r}_1,\vec{r}_2,\cdots,\vec{r}_N)} d\vec{r}_1 \cdots d\vec{r}_N \right] \\
&= e^{-\beta V_1(\vec{r})} + \sum_{N=2}^{\infty} \frac{1}{N!} \left[\int \cdots \int z(\vec{r}_2) z(\vec{r}_3) \cdots z(\vec{r}_N) e^{-\beta V_N(\vec{r},\vec{r}_2,\cdots,\vec{r}_N)} d\vec{r}_2 d\vec{r}_3 \cdots d\vec{r}_N \right. \\
&\quad + \int \cdots \int z(\vec{r}_1) z(\vec{r}_3) \cdots z(\vec{r}_N) e^{-\beta V_N(\vec{r}_1,\vec{r},\cdots,\vec{r}_N)} d\vec{r}_1 d\vec{r}_3 \cdots d\vec{r}_N + \cdots \\
&\quad \left. + \int \cdots \int z(\vec{r}_1) z(\vec{r}_2) \cdots z(\vec{r}_{N-1}) e^{-\beta V_N(\vec{r}_1,\vec{r}_2,\cdots,\vec{r}_{N-1})} d\vec{r}_1 d\vec{r}_2 \cdots d\vec{r}_{N-1} \right] \\
&= e^{-\beta V_1(\vec{r})} + \sum_{N=2}^{\infty} \frac{1}{(N-1)!} \int \cdots \int \left[\prod_{i=2}^{N} z(\vec{r}_i) \right] e^{-\beta V_N(\vec{r},\vec{r}_2,\cdots,\vec{r}_N)} d\vec{r}_2 \cdots d\vec{r}_N
\end{aligned}
\tag{2.3.1.49}
$$

From Eqs.(2.3.1.48) and (2.3.1.49), $\rho^{(1)}(\vec{r})$ is expressed by $\Xi[z]$ and $z(\vec{r})$.

$$
\rho^{(1)}(\vec{r}) = \frac{z(\vec{r})}{\Xi} \frac{\delta \Xi[z]}{\delta z(\vec{r})} \tag{2.3.1.50}
$$

By using the following equations,

$$
\frac{d \ln \Xi}{d \Xi} = \frac{1}{\Xi} \tag{2.3.1.51}
$$

$$
\frac{d \ln z(\vec{r})}{d z(\vec{r})} = \frac{1}{z(\vec{r})} \tag{2.3.1.52}
$$

$$
\ln \Xi = -\beta \Omega \tag{2.3.1.53}
$$

$$
\ln z(\vec{r}) = \ln \Lambda^{-3} + \beta \psi(\vec{r}) \rightarrow d \ln z(\vec{r}) = \beta d\psi(\vec{r}) = -\beta d\phi(\vec{r}) \tag{2.3.1.54}
$$

Eq.(2.3.1.50) is written as follows.

$$
\rho^{(1)}(\vec{r}) = \frac{\delta \ln \Xi}{\delta \ln z(\vec{r})} = \frac{\delta \ln \Xi}{\beta \delta \psi(\vec{r})} = -\frac{\delta \Omega}{\delta \psi(\vec{r})} = \frac{\delta \Omega}{\delta \phi(\vec{r})} \tag{2.3.1.55}
$$

2.3.2 Legendre transformation

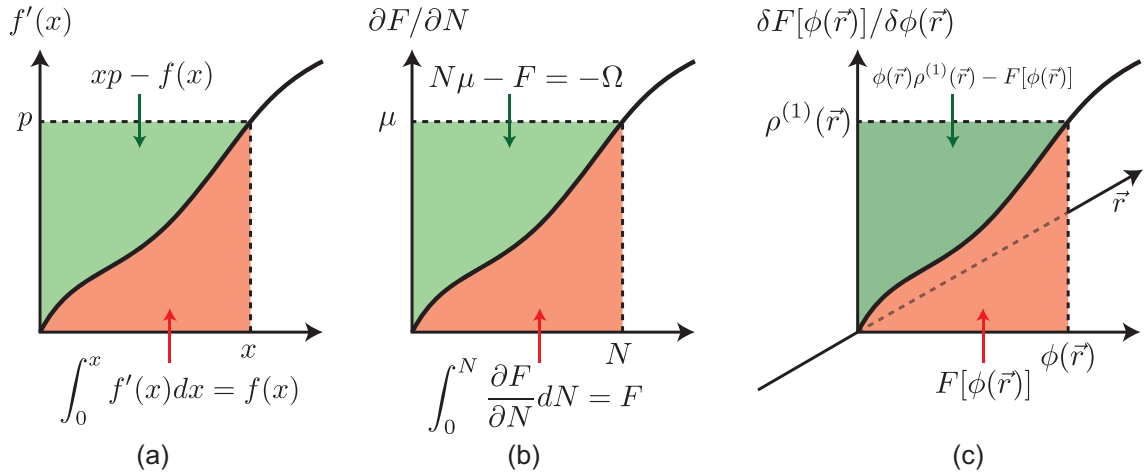

Figure 2.3: Legendre transformation of (a) $f(x)$ to $g(p)$, (b) $U(S,V,N)$ to $F(T,V,N)$, (c) $F[V(\vec{r})]$ to $F[\phi(\vec{r})]$.

Helmholtz free energy and grand potential is related to Legendre transformation (See also Section 3.3.1). Legendre transformation is used to change the variable. However, Legendre transformation is not a mere exchange of variable. Legendre transformation of a function $f(x)$ is defined as follows (Eq.(3.3.1.25)).

$$g(p) := xp - f(x) \ s.t. \ f'(x) = p \tag{2.3.2.1}$$

In Figure 2.3(a), $f(x)$ is an area of red region while $g(p)$ is an area of green region. Important point is that $f(x)$ and $g(p)$ has one-to-one correspondence when $f(x)$ is a downward-convex function ($f'(x) \geq 0 \ \forall x$). Energy, Helmholtz free energy, enthalpy, and Gibbs free energy are related to Legendre transformation as introduced later (Eqs.(3.3.1.26) $\sim$ (3.3.1.29)). Similar to these quantities, grand potential Ω is related to Helmholtz free energy F by Legendre transformation (Eq.2.3.2.1) as follows.

$$-\Omega(T,V,\mu) = N\mu - F(T,V,N) \ s.t. \ \frac{\partial F(T,V,N)}{\partial N} = \mu(T,V,N) \tag{2.3.2.2}$$

Negative sign is just a conventional one. Eq.(2.3.2.2) is graphically shown in Figure 2.3(b).

In Eq.(2.3.1.36), functional differentiation for F is done by $\phi(\vec{r})$. Similar to this, functional differentiation for Ξ is done by $\phi(\vec{r})$ in Eq.(2.3.1.55). Therefore, let us include $\phi(\vec{r})$ as a variable of F and Ξ.

$$\Omega(T,V,\mu,[\phi]) = F(T,V,N,[\phi]) - N\mu \ s.t. \ \frac{\partial F(T,V,N,[\phi])}{\partial N} = \mu(T,V,N,[\phi]) \tag{2.3.2.3}$$

By using Eq.(2.3.1.47), variables μ and $\phi(\vec{r})$ in Ω is combined to $\psi(\vec{r})$.

$$\Omega(T,V,\mu,[\phi]) \to \Omega(T,V,[\psi]) \tag{2.3.2.4}$$

Let us perform Legendre transformation of F for the variable $\psi(\vec{r})$. Legendre transformation can be extended for functionals as follows.

$$\mathcal{F}(T,V,N,[\rho^{(1)}]) = F(T,V,N,[\phi]) - \int d\vec{r}\phi(\vec{r})\rho^{(1)}(\vec{r}) \ s.t. \ \frac{\delta F(T,V,N,[\phi])}{\delta\phi(\vec{r})} = \rho^{(1)}(T,V,N,[\phi]) \tag{2.3.2.5}$$

where $\mathcal{F}$ is called intrinsic free energy. Here, I used the relation Eq.(2.3.1.36) for the differentiation of

F by $\phi(\vec{r})$. Eq.(2.3.2.5) is graphically shown in Figure 2.3(c). Since the number of particles is fixed, $\mathcal{F}(T, V, N, [\rho^{(1)}])$ is defined in canonical ensemble. $\mathcal{F}$ is extended for grand canonical ensemble by converting N as follows.

$$N \to \int d\vec{r}\rho^{(1)}(\vec{r}) \tag{2.3.2.6}$$

where $\rho^{(1)}(\vec{r})$ is one-particle density for grand canonical ensemble (Eq.(2.3.1.48)). Physical meaning of Eq.(2.3.2.6) is that the integral of one-particle density within whole space of the system stands for the number of particles in the system. Therefore, variables N and $\rho^{(1)}(\vec{r})$ in $\mathcal{F}$ is combined to $\rho^{(1)}(\vec{r})$.

$$\mathcal{F}(T, V, N, [\rho^{(1)}]) \to \mathcal{F}(T, V, [\rho^{(1)}]) \tag{2.3.2.7}$$

By using Eqs.(2.3.2.3) and (2.3.2.5), $\mathcal{F}(T, V, [\rho^{(1)}])$ is related to $\Omega(T, V, [\psi])$ as follows.

$$\begin{aligned}
\mathcal{F}(T, V, [\rho^{(1)}]) &= F(T, V, N, [\phi]) - \int d\vec{r}\phi(\vec{r})\rho^{(1)}(\vec{r}) \\
&= \Omega(T, V, [\psi]) + N\mu - \int d\vec{r}\phi(\vec{r})\rho^{(1)}(\vec{r}) \\
&= \Omega(T, V, [\psi]) + \int d\vec{r}(\mu - \phi(\vec{r}))\rho^{(1)}(\vec{r}) \\
&= \Omega(T, V, [\psi]) + \int d\vec{r}\psi(\vec{r})\rho^{(1)}(\vec{r})
\end{aligned} \tag{2.3.2.8}$$

By using Eq.(2.3.1.55), it is shown that Eq.(2.3.2.8) is also Legendre transformation.

$$\mathcal{F}(T, V, [\rho^{(1)}]) = \Omega(T, V, [\psi]) + \int d\vec{r}\psi(\vec{r})\rho^{(1)}(\vec{r}) \ s.t. \ \frac{\delta\Omega(T, V, [\psi])}{\delta\psi(\vec{r})} = -\rho^{(1)}(T, V, [\psi]) \tag{2.3.2.9}$$

2.3.3 Correlation function

From now, I use following notations for taking the average of particle density for grand canonical ensemble (see Eqs.(2.3.1.15), (2.3.1.18), (2.3.1.48)).

$$\langle\, \rho(\vec{r}) \,\rangle_g := \left\langle \sum_{i=1}^{N} \delta(\vec{r} - \vec{r}_i) \right\rangle_g = \left\langle \rho_N^{(1)}(\vec{r}) \right\rangle_g = \rho^{(1)}(\vec{r}) \tag{2.3.3.1}$$

$$\begin{aligned}
\langle\, \rho(\vec{r})\rho(\vec{r}') \,\rangle_g &:= \left\langle \sum_{i=1}^{N}\sum_{j=1}^{N} \delta(\vec{r} - \vec{r}_i)\delta(\vec{r}' - \vec{r}_j) \right\rangle_g \\
&= \left\langle \sum_{i=1}^{N}\sum_{j\neq 1}^{N} \delta(\vec{r} - \vec{r}_i)\delta(\vec{r}' - \vec{r}_j) \right\rangle_g + \left\langle \sum_{i=1}^{N} \delta(\vec{r} - \vec{r}_i)\delta(\vec{r}' - \vec{r}_i) \right\rangle_g \\
&= \left\langle \rho_N^{(2)}(\vec{r}, \vec{r}') \right\rangle_g + \left\langle \rho_N^{(1)}(\vec{r})\delta(\vec{r} - \vec{r}') \right\rangle_g \\
&= \rho^{(2)}(\vec{r}, \vec{r}') + \rho^{(1)}(\vec{r})\delta(\vec{r} - \vec{r}')
\end{aligned} \tag{2.3.3.2}$$

$\rho^{(1)}(\vec{r})$ is one-particle density for grand canonical ensemble as shown in Eq.(2.3.1.48). $\rho^{(2)}(\vec{r},\vec{r}')$ is two-particle density for grand canonical ensemble:

$$\begin{aligned}
\rho^{(2)}(\vec{r}) &:= \left\langle \sum_{i=1}^{N}\sum_{j\neq 1}^{N} \delta(\vec{r}-\vec{r}_i)\delta(\vec{r}'-\vec{r}_j) \right\rangle_g \\
&= \frac{1}{\Xi}\sum_{N=1}^{\infty}\frac{1}{N!}\int\cdots\int\left[\prod_{i=1}^{N} z(\vec{r}_i)\right] e^{-\beta V_N(\vec{r}_1,\vec{r}_2,\cdots,\vec{r}_N)} \left(\sum_{j=1}^{N}\delta(\vec{r}-\vec{r}_j)\right)\left(\sum_{k\neq j}^{N}\delta(\vec{r}-\vec{r}_k)\right) d\vec{r}_1\cdots d\vec{r}_N \\
&= \frac{1}{\Xi}\sum_{N=1}^{\infty}\frac{1}{N!}\left[\int\cdots\int z(\vec{r})z(\vec{r}')z(\vec{r}_3)\cdots z(\vec{r}_N) e^{-\beta V_N(\vec{r},\vec{r}',\vec{r}_3,\cdots,\vec{r}_N)} d\vec{r}_3\cdots d\vec{r}_N + \cdots\right] \\
&= \frac{z(\vec{r})z(\vec{r}')}{\Xi}\left[e^{-\beta V_2(\vec{r},\vec{r}')} + \sum_{N=3}^{\infty}\frac{1}{(N-2)!}\int\cdots\int\left[\prod_{i=3}^{N} z(\vec{r}_i)\right] e^{-\beta V_N(\vec{r},\vec{r}',\vec{r}_3,\cdots,\vec{r}_N)} d\vec{r}_3\cdots d\vec{r}_N\right]
\end{aligned} \tag{2.3.3.3}$$

Let us compare Eq.(2.3.3.3) with the functional derivative of Ξ by $z(\vec{r})$ and $z(\vec{r}')$.

$$\begin{aligned}
\frac{\delta^2\Xi[z]}{\delta z(\vec{r})\delta z(\vec{r}')} &= \frac{\delta^2}{\delta z(\vec{r})\delta z(\vec{r}')}\left[\sum_{N=0}^{\infty}\frac{1}{N!}\int\cdots\int\left[\prod_{i=1}^{N} z(\vec{r}_i)\right] e^{-\beta V_N(\vec{r}_1,\vec{r}_2,\cdots,\vec{r}_N)} d\vec{r}_1\cdots d\vec{r}_N\right] \\
&= e^{-\beta V_2(\vec{r},\vec{r}')} + \sum_{N=3}^{\infty}\frac{1}{(N-2)!}\int\cdots\int\left[\prod_{i=3}^{N} z(\vec{r}_i)\right] e^{-\beta V_N(\vec{r},\vec{r}',\vec{r}_3,\cdots,\vec{r}_N)} d\vec{r}_3\cdots d\vec{r}_N
\end{aligned} \tag{2.3.3.4}$$

From Eqs.(2.3.3.3) and (2.3.3.4), $\rho^{(2)}(\vec{r},\vec{r}')$ is expressed by $\Xi[z]$ and $z(\vec{r})$. [7]

$$\rho^{(2)}(\vec{r},\vec{r}') = \frac{z(\vec{r})z(\vec{r}')}{\Xi}\frac{\delta^2\Xi[z]}{\delta z(\vec{r})\delta z(\vec{r}')} \tag{2.3.3.5}$$

Substitute Eq.(2.3.1.50) to Eq.(2.3.3.5):

$$\rho^{(2)}(\vec{r},\vec{r}') = \frac{z(\vec{r})z(\vec{r}')}{\Xi}\frac{\delta}{\delta z(\vec{r}')}\left[\frac{\Xi[z]}{z(\vec{r})}\rho^{(1)}(\vec{r})\right] \tag{2.3.3.6}$$

Differentiation in Eq.(2.3.3.6) is calculated as follows.

$$\frac{\delta\Xi[z]}{\delta z(\vec{r}')} = \frac{\Xi}{z(\vec{r}')}\rho^{(1)}(\vec{r}') \tag{2.3.3.7}$$

$$\frac{\delta z(\vec{r})^{-1}}{\delta z(\vec{r}')} = \frac{\delta z(\vec{r})}{\delta z(\vec{r}')}\frac{\delta z(\vec{r})^{-1}}{\delta z(\vec{r})} = -\frac{1}{z(\vec{r})^2}\delta(\vec{r}-\vec{r}') \tag{2.3.3.8}$$

$$\frac{\delta\rho^{(1)}(\vec{r})}{\delta z(\vec{r}')} = \frac{\delta\ln z(\vec{r}')}{\delta z(\vec{r}')}\frac{\delta\rho^{(1)}(\vec{r})}{\delta\ln z(\vec{r}')} = \frac{1}{z(\vec{r}')}\frac{\delta\rho^{(1)}(\vec{r})}{\delta\ln z(\vec{r}')} \tag{2.3.3.9}$$

Substitute Eqs.(2.3.3.7) $\sim$ (2.3.3.9) to Eq.(2.3.3.6):

$$\begin{aligned}
\rho^{(2)}(\vec{r},\vec{r}') &= \frac{z(\vec{r})z(\vec{r}')}{\Xi}\left[\frac{\Xi}{z(\vec{r})z(\vec{r}')}\rho^{(1)}(\vec{r})\rho^{(1)}(\vec{r}') - \frac{\Xi}{z(\vec{r})^2}\rho^{(1)}(\vec{r})\delta(\vec{r}-\vec{r}') + \frac{\Xi}{z(\vec{r})z(\vec{r}')}\frac{\delta\rho^{(1)}(\vec{r})}{\delta\ln z(\vec{r}')}\right] \\
&= \rho^{(1)}(\vec{r})\rho^{(1)}(\vec{r}') - \rho^{(1)}(\vec{r})\delta(\vec{r}-\vec{r}') + \frac{\delta\rho^{(1)}(\vec{r})}{\delta\ln z(\vec{r}')}
\end{aligned} \tag{2.3.3.10}$$

[7] In general, $\rho^{(n)}(\vec{r}_1,\cdots,\vec{r}_n) = \dfrac{z(\vec{r}_1)\cdots z(\vec{r}_n)}{\Xi}\dfrac{\delta^n\Xi[z]}{\delta z(\vec{r}_1)\cdots\delta z(\vec{r}_n)}$.

Let us define density correlation function as follows.

$$H^{(n)}(\vec{r}_1,\cdots,\vec{r}_n) := \left\langle \left[\rho(\vec{r}_1)-\rho^{(1)}(\vec{r}_1)\right]\cdots\left[\rho(\vec{r}_n)-\rho^{(1)}(\vec{r}_n)\right]\right\rangle_g \tag{2.3.3.11}$$

Following this definition and Eqs.(2.3.3.1), (2.3.3.2), $H^{(1)}(\vec{r})$ and $H^{(2)}(\vec{r},\vec{r}')$ are calculated as follows.

$$H^{(1)}(\vec{r}) = \left\langle \rho(\vec{r})-\rho^{(1)}(\vec{r})\right\rangle_g = \langle\,\rho(\vec{r})\,\rangle_g - \rho^{(1)}(\vec{r}) = 0 \tag{2.3.3.12}$$

$$\begin{aligned} H^{(2)}(\vec{r},\vec{r}') &= \left\langle \left[\rho(\vec{r})-\rho^{(1)}(\vec{r})\right]\left[\rho(\vec{r}')-\rho^{(1)}(\vec{r}')\right]\right\rangle_g \\ &= \langle\,\rho(\vec{r})\rho(\vec{r}')\,\rangle_g - \langle\,\rho(\vec{r})\,\rangle_g\rho^{(1)}(\vec{r}') - \rho^{(1)}(\vec{r})\langle\,\rho(\vec{r}')\,\rangle_g + \rho^{(1)}(\vec{r})\rho^{(1)}(\vec{r}') \\ &= \rho^{(2)}(\vec{r},\vec{r}') + \rho^{(1)}(\vec{r})\delta(\vec{r}-\vec{r}') - \rho^{(1)}(\vec{r})\rho^{(1)}(\vec{r}') \end{aligned} \tag{2.3.3.13}$$

Let us define n-particle distribution function, $g^{(n)}(\vec{r}_1,\cdots,\vec{r}_n)$, and pair correlation function, $h^{(2)}(\vec{r},\vec{r}')$, as follows.

$$g^{(n)}(\vec{r}_1,\cdots,\vec{r}_n) := \frac{\rho^{(n)}(\vec{r}_1,\cdots,\vec{r}_n)}{\prod_{i=1}^n \rho^{(1)}(\vec{r}_i)} \tag{2.3.3.14}$$

$$h^{(2)}(\vec{r},\vec{r}') := g^{(2)}(\vec{r},\vec{r}') - 1 \tag{2.3.3.15}$$

Substitute Eqs.(2.3.3.14) and (2.3.3.15) to Eq.(2.3.3.13):

$$\begin{aligned} H^{(2)}(\vec{r},\vec{r}') &= \rho^{(1)}(\vec{r})\rho^{(1)}(\vec{r}')(g^{(2)}(\vec{r},\vec{r}')-1) + \rho^{(1)}(\vec{r})\delta(\vec{r}-\vec{r}') \\ &= \rho^{(1)}(\vec{r})\rho^{(1)}(\vec{r}')h^{(2)}(\vec{r},\vec{r}') + \rho^{(1)}(\vec{r})\delta(\vec{r}-\vec{r}') \end{aligned} \tag{2.3.3.16}$$

Another form is obtained by substitute Eqs.(2.3.3.10) and (2.3.1.54) to Eq.(2.3.3.13):

$$H^{(2)}(\vec{r},\vec{r}') = \frac{\delta\rho^{(1)}(\vec{r})}{\delta\ln z(\vec{r}')} = \frac{1}{\beta}\frac{\delta\rho^{(1)}(\vec{r})}{\delta\psi(\vec{r}')} \tag{2.3.3.17}$$

To extract the effect of particle interactions on the density profile, let us decompose the intrinsic free energy, $\mathcal{F}[\rho^{(1)}]$, into two parts[8]; ideal part, $\mathcal{F}^{id}[\rho^{(1)}]$, which is calculated by setting the potential V and ϕ to be 0, and excess part, $\mathcal{F}^{ex}[\rho^{(1)}]$.

$$\mathcal{F}[\rho^{(1)}] =: \mathcal{F}^{id}[\rho^{(1)}] + \mathcal{F}^{ex}[\rho^{(1)}] \tag{2.3.3.18}$$

When $\phi = 0$, $\mathcal{F}$ is equal to Helmholtz energy, F (see Eq.(2.3.2.5)). Therefore, $\mathcal{F}^{id}[\rho^{(1)}]$ is calculated from Helmholtz energy by setting $V_N = 0$. When $V_N = 0$, Z_N is (see Eq.(2.3.1.8):

$$Z_N^{id} = \int\cdots\int d\vec{r}_1\cdots d\vec{r}_N = V^N \tag{2.3.3.19}$$

Substitute Eq.(2.3.3.19) to Eq.(2.3.1.7):

$$Q_N^{id} = \frac{Z_N^{id}}{N!\Lambda^{3N}} = \frac{V^N}{N!\Lambda^{3N}} \tag{2.3.3.20}$$

[8]From now, I omit the other variables, T and V, for simplicity.

Substitute Eq.(2.3.3.20) to Eq.(2.3.1.22):

$$\begin{aligned}\mathcal{F}^{id}[\rho^{(1)}] = F^{id} &= -k_BT \ln Q_N^{id} \\ &= -k_BT \left(N \ln[\Lambda^{-3}V] - \ln N!\right) \\ &\simeq k_BT \left(N \ln[\Lambda^3 V^{-1}] + N \ln N - N\right) \\ &= k_BTN \left(\ln[\Lambda^3 N/V] - 1\right) \end{aligned} \tag{2.3.3.21}$$

where Stirling's formula, $\ln N! \simeq N \ln N - N$ is used. When there is no interaction between particles, one-particle density, $\rho_N^{(1)}$, should be N/V. Therefore,

$$\begin{aligned}\mathcal{F}^{id}[\rho^{(1)}] &\simeq k_BTN \left(\ln[\Lambda^3 \rho_N^{(1)}] - 1\right) \\ &\to k_BT \int d\vec{r} \rho^{(1)}(\vec{r}) \left(\ln[\Lambda^3 \rho^{(1)}(\vec{r})] - 1\right) \end{aligned} \tag{2.3.3.22}$$

Here, the number of particles are substituted by the integral of one-particle density (Eq.(2.3.2.6)). Functional derivative of $\mathcal{F}^{id}[\rho^{(1)}]$ is calculated as follows.

$$\begin{aligned}\delta\mathcal{F}^{id}[\rho^{(1)}] &= k_BT \int d\vec{r} \left[\delta\rho^{(1)}(\vec{r}) \left(\ln[\Lambda^3 \rho^{(1)}(\vec{r})] - 1\right) + \rho^{(1)}(\vec{r}) \delta \left(\ln[\Lambda^3 \rho^{(1)}(\vec{r})] - 1\right)\right] \\ &= k_BT \int d\vec{r} \left[\delta\rho^{(1)}(\vec{r}) \left(\ln[\Lambda^3 \rho^{(1)}(\vec{r})] - 1\right) + \rho^{(1)}(\vec{r}) \delta \left(\ln \rho^{(1)}(\vec{r})\right)\right] \\ &= k_BT \int d\vec{r} \left[\delta\rho^{(1)}(\vec{r}) \left(\ln[\Lambda^3 \rho^{(1)}(\vec{r})] - 1\right) + \rho^{(1)}(\vec{r}) \frac{\delta\rho^{(1)}(\vec{r})}{\rho^{(1)}(\vec{r})}\right] \\ &= k_BT \int d\vec{r} \delta\rho^{(1)}(\vec{r}) \ln[\Lambda^3 \rho^{(1)}(\vec{r})] \end{aligned} \tag{2.3.3.23}$$

$$\frac{\delta\mathcal{F}^{id}[\rho^{(1)}]}{\delta\rho^{(1)}(\vec{r})} = k_BT \int d\vec{r}' \delta(\vec{r} - \vec{r}') \ln[\Lambda^3 \rho^{(1)}(\vec{r}')] = \frac{1}{\beta} \ln[\Lambda^3 \rho^{(1)}(\vec{r})] \tag{2.3.3.24}$$

As for excess part, let us define new function called direct correlation function as follows.

$$\frac{\delta\mathcal{F}^{ex}[\rho^{(1)}]}{\delta\rho^{(1)}(\vec{r})} =: -\frac{1}{\beta} c^{(1)}(\vec{r}) \tag{2.3.3.25}$$

Higher order direct correlation functions are defined as follows.

$$\frac{\delta^n\mathcal{F}^{ex}[\rho^{(1)}]}{\delta\rho^{(1)}(\vec{r}_1) \cdots \delta\rho^{(1)}(\vec{r}_n)} =: -\frac{1}{\beta} c^{(n)}(\vec{r}_1, \cdots, \vec{r}_n)] \tag{2.3.3.26}$$

By using Eqs.(2.3.3.24) and (2.3.3.25), functional derivative of $\mathcal{F}[\rho^{(1)}]$ is:

$$\beta \frac{\delta\mathcal{F}[\rho^{(1)}]}{\delta\rho^{(1)}(\vec{r})} = \ln[\Lambda^3 \rho^{(1)}(\vec{r})] - c^{(1)}(\vec{r}) \tag{2.3.3.27}$$

Functional derivative of $\mathcal{F}[\rho^{(1)}]$ is also calculated by using Eq.(2.3.2.8).

$$\begin{aligned}&\delta\mathcal{F}(T, V, [\rho^{(1)}]) = \delta\Omega(T, V, [\psi]) + \int d\vec{r} \psi(\vec{r}) \delta\rho^{(1)}(\vec{r}) \\ &\to \frac{\delta\mathcal{F}[\rho^{(1)}]}{\delta\rho^{(1)}(\vec{r})} = \psi(\vec{r}) \end{aligned} \tag{2.3.3.28}$$

From Eqs.(2.3.3.26) and (2.3.3.28):

$$\beta\psi(\vec{r}) = \ln[\Lambda^3\rho^{(1)}(\vec{r})] - c^{(1)}(\vec{r}) \tag{2.3.3.29}$$

Finally, I'm going to derive Ornstein–Zernike equation. Starting point is the following identity.

$$\int H^{(2)}(\vec{r}_1,\vec{r}_3)(H^{(2)})^{-1}(\vec{r}_3,\vec{r}_2)d\vec{r}_3 = \delta(\vec{r}_1-\vec{r}_2) \tag{2.3.3.30}$$

$(H^{(2)})^{-1}(\vec{r},\vec{r}')$ is an inversion function of $H^{(2)}(\vec{r},\vec{r}')$, which is calculated by using Eq.(2.3.3.17).

$$(H^{(2)})^{-1}(\vec{r},\vec{r}') = \beta\frac{\delta\psi(\vec{r})}{\delta\rho^{(1)}(\vec{r}')} \tag{2.3.3.31}$$

By using Eqs.(2.3.3.29) and (2.3.3.26),

$$\begin{aligned}(H^{(2)})^{-1}(\vec{r},\vec{r}') &= \frac{\delta}{\delta\rho^{(1)}(\vec{r}')}\left[\ln\Lambda^3 + \ln\rho^{(1)}(\vec{r}) - c^{(1)}(\vec{r})\right] \\ &= \frac{1}{\rho^{(1)}(\vec{r})}\delta(\vec{r}-\vec{r}') - c^{(2)}(\vec{r},\vec{r}')\end{aligned} \tag{2.3.3.32}$$

Substitute Eqs.(2.3.3.16) and (2.3.3.32) to Eq.(2.3.3.30):

$$\begin{aligned}&\int\left[\rho^{(1)}(\vec{r}_1)\rho^{(1)}(\vec{r}_3)h^{(2)}(\vec{r}_1,\vec{r}_3) + \rho^{(1)}(\vec{r}_1)\delta(\vec{r}_1-\vec{r}_3)\right]\left[\frac{1}{\rho^{(1)}(\vec{r}_3)}\delta(\vec{r}_3-\vec{r}_2) - c^{(2)}(\vec{r}_3,\vec{r}_2)\right]d\vec{r}_3 = \delta(\vec{r}_1-\vec{r}_2) \\ &\to \int\Big[\rho^{(1)}(\vec{r}_1)h^{(2)}(\vec{r}_1,\vec{r}_3)\delta(\vec{r}_3-\vec{r}_2) - \rho^{(1)}(\vec{r}_1)\rho^{(1)}(\vec{r}_3)h^{(2)}(\vec{r}_1,\vec{r}_3)c^{(2)}(\vec{r}_3,\vec{r}_2) \\ &\qquad + \frac{\rho^{(1)}(\vec{r}_1)}{\rho^{(1)}(\vec{r}_3)}\delta(\vec{r}_1-\vec{r}_3)\delta(\vec{r}_3-\vec{r}_2) - \rho^{(1)}(\vec{r}_1)c^{(2)}(\vec{r}_3,\vec{r}_2)\delta(\vec{r}_1-\vec{r}_3)\Big]d\vec{r}_3 = \delta(\vec{r}_1-\vec{r}_2) \\ &\to \rho^{(1)}(\vec{r}_1)h^{(2)}(\vec{r}_1,\vec{r}_2) - \int\rho^{(1)}(\vec{r}_1)\rho^{(1)}(\vec{r}_3)h^{(2)}(\vec{r}_1,\vec{r}_3)c^{(2)}(\vec{r}_3,\vec{r}_2)d\vec{r}_3 + \delta(\vec{r}_1-\vec{r}_2) - \rho^{(1)}(\vec{r}_1)c^{(2)}(\vec{r}_1,\vec{r}_2) = \delta(\vec{r}_1-\vec{r}_2) \\ &\to h^{(2)}(\vec{r}_1,\vec{r}_2) = c^{(2)}(\vec{r}_1,\vec{r}_2) + \int\rho^{(1)}(\vec{r}_3)h^{(2)}(\vec{r}_1,\vec{r}_3)c^{(2)}(\vec{r}_3,\vec{r}_2)d\vec{r}_3\end{aligned} \tag{2.3.3.33}$$

Eq.(2.3.3.33) is called Ornstein–Zernike equation. When $h^{(2)}(\vec{r},\vec{r}')$ and $c^{(2)}(\vec{r},\vec{r}')$ depends only on the distance between $\vec{r}$ and $\vec{r}'$ and $\rho^{(1)}(\vec{r})$ is regarded as an uniform, Eq.(2.3.3.33) becomes more simple.

$$\begin{aligned}h^{(2)}(|\vec{r}_1-\vec{r}_2|) &= c^{(2)}(|\vec{r}_1-\vec{r}_2|) + \rho\int h^{(2)}(|\vec{r}_1-\vec{r}_3|)c^{(2)}(|\vec{r}_3-\vec{r}_2|)d\vec{r}_3 \\ &= c^{(2)}(|\vec{r}_1-\vec{r}_2|) + \rho\int h^{(2)}(|\vec{r}_1-\vec{r}_3|)c^{(2)}(|\vec{r}_2-\vec{r}_3|)d\vec{r}_3 \\ &= c^{(2)}(|\vec{r}_1-\vec{r}_2|) + \rho\int h^{(2)}(|-\vec{r}_3|)c^{(2)}(|\vec{r}_2-\vec{r}_1-\vec{r}_3|)d\vec{r}_3\end{aligned} \tag{2.3.3.34}$$

By defining $\vec{r} := \vec{r}_2 - \vec{r}_1$, $r := |\vec{r}|$:

$$h^{(2)}(r) = c^{(2)}(r) + \rho\int h^{(2)}(r')c^{(2)}(|\vec{r}-\vec{r}'|)d\vec{r}' \tag{2.3.3.35}$$

2.3.4 Application to scattering function

Let us see the relationship between the direct correlation function, $c^{(2)}(r)$, and structure factor, $S(q)$ (Eq.(2.1.15)) [39]. From here, we consider the isotropic case. By comparing the definition of static pair-distribution function, $g(r)$ (Eq.(2.1.12)) and two-particle distribution function, $g^{(2)}(r)$ (Eq.(2.3.3.14), $r := |\vec{r} - \vec{r}'|$), these two quantities are connected as follows.

$$g^{(2)}(r) = \frac{g(r)}{\rho} \tag{2.3.4.1}$$

where ρ in Eq.(2.3.4.1) is expressed as ϱ in Eq.(2.1.15). Substitute Eq.(2.3.4.1) to Eq.(2.1.15):

$$S(q) := 1 + \rho \int (g^{(2)}(r) - 1) e^{i\vec{q}\cdot\vec{r}} d\vec{r} = 1 + \rho \int h^{(2)}(r) e^{i\vec{q}\cdot\vec{r}} d\vec{r} = 1 + \rho h^{(2)}(q) \tag{2.3.4.2}$$

$h^{(2)}(q)$ is a Fourier transform of $h^{(2)}(r)$. Fourier transform of Eq.(2.3.3.35) is a form of convolution and calculated as follows.

$$\begin{aligned} h^{(2)}(q) &= \int h^{(2)}(r) e^{i\vec{q}\cdot\vec{r}} d\vec{r} \\ &= \int c^{(2)}(r) e^{i\vec{q}\cdot\vec{r}} d\vec{r} + \rho \int d\vec{r} \int d\vec{r}' h^{(2)}(r') c^{(2)}(|\vec{r} - \vec{r}'|) e^{i\vec{q}\cdot\vec{r}} \\ &= c^{(2)}(q) + \rho \int d(\vec{r} - \vec{r}') \int d\vec{r}' h^{(2)}(r') c^{(2)}(|\vec{r} - \vec{r}'|) e^{i\vec{q}\cdot(\vec{r}-\vec{r}')} e^{i\vec{q}\cdot\vec{r}'} \\ &= c^{(2)}(q) + \rho h^{(2)}(q) c^{(2)}(q) \end{aligned} \tag{2.3.4.3}$$

Therefore, $h^{(2)}(q)$ and $S(q)$ is expressed as a function of $c^{(2)}(q)$.

$$h^{(2)}(q) = \frac{c^{(2)}(q)}{1 - \rho c^{(2)}(q)} \tag{2.3.4.4}$$

$$S(q) = 1 + \frac{\rho c^{(2)}(q)}{1 - \rho c^{(2)}(q)} = \frac{1}{1 - \rho c^{(2)}(q)} \tag{2.3.4.5}$$

2.4 Structure factors

2.4.1 Closure relation

Let us use Eq.(2.3.4.5) to calculate scattering functions. To achieve this goal, we have to know the relationship between $c^{(2)}(r)$ and $h^{(2)}(r)$, otherwise we cannot solve Ornstein–Zernike equation, Eq.(2.3.3.35). This relationship is called closure relation. Let us assume that the potential $V_N(\vec{r}_1, \cdots, \vec{r}_N)$ in Eq.(2.3.1.1) is expressed by the summation of potential energy between each particle pair.

$$V_N(\vec{r}_1, \cdots, \vec{r}_N) = \sum_{i=1}^{N} \sum_{j>i}^{N} v(\vec{r}_i, \vec{r}_j) \tag{2.4.1.1}$$

Then, let us consider the case where one particle is added to the origin of the system, $\vec{r}_0$. As a result, the number of particle is modified to $N+1$ and the potential energy is modified to:

$$V_{N+1}(\vec{r}_0, \vec{r}_1, \cdots, \vec{r}_N) = \sum_{i=0}^{N+1} \sum_{j>i}^{N+1} v(\vec{r}_i, \vec{r}_j) \tag{2.4.1.2}$$

$V_{N+1}(\vec{r}_0, \vec{r}_1, \cdots, \vec{r}_N)$ can be decomposed into two terms; interactions with the new particle at $\vec{r}_0$ and else.

$$V_{N+1}(\vec{r}_0, \vec{r}_1, \cdots, \vec{r}_N) = \sum_{i=1}^{N} \sum_{j>i}^{N} v(\vec{r}_i, \vec{r}_j) + \sum_{i=1}^{N} v(\vec{r}_0, \vec{r}_i) =: V_N(\vec{r}_1, \cdots, \vec{r}_N) + \sum_{i=1}^{N} \phi(\vec{r}_i) \tag{2.4.1.3}$$

This is similar to Eq.(2.3.1.23). Then, let us assume that the reference system is $N+1$-particle system whose potential energy is $V_N(\vec{r}_1, \cdots, \vec{r}_N)$ and the term $\sum_{i=1}^{N} \phi(\vec{r}_i)$ is assumed to be an external field. From now, I attach the subscript 0 for the quantities of reference system. For examples, one-particle density in canonical ensemble is written by let $y(\vec{r})$ be 0 in Eq.(2.3.1.28).

$$\begin{aligned}
\rho_{N,0}^{(1)}(\vec{r}) &= \frac{1}{Z_{N,0}} \int \cdots \int e^{-\beta V_N(\vec{r}_1, \cdots, \vec{r}_N)} \left(\sum_{i=1}^{N} \delta(\vec{r} - \vec{r}_i) \right) d\vec{r}_1 \cdots d\vec{r}_N \\
&= \frac{N}{Z_{N,0}} \int \cdots \int e^{-\beta V_N(\vec{r}, \vec{r}_2, \cdots, \vec{r}_N)} d\vec{r}_2 \cdots d\vec{r}_N
\end{aligned} \tag{2.4.1.4}$$

where

$$Z_{N,0} := \int \cdots \int e^{-\beta V_N(\vec{r}_1, \vec{r}_2, \cdots, \vec{r}_N)} d\vec{r}_1 \cdots d\vec{r}_N \tag{2.4.1.5}$$

In grand canonical ensemble,

$$\rho_0^{(1)}(\vec{r}) = \frac{1}{\Xi_0} \sum_{N=1}^{\infty} \frac{z^N}{N!} Z_{N,0} \rho_{N,0}^{(1)}(\vec{r}) \tag{2.4.1.6}$$

where

$$\Xi_0 := \sum_{N=0}^{\infty} \frac{z^N}{N!} Z_{N,0} \tag{2.4.1.7}$$

Two-particle density is:

$$\rho_{N,0}^{(2)}(\vec{r}, \vec{r}') = \frac{N(N-1)}{Z_{N,0}} \int \cdots \int e^{-\beta V_N(\vec{r}, \vec{r}', \vec{r}_3, \cdots, \vec{r}_N)} d\vec{r}_3 \cdots d\vec{r}_N \tag{2.4.1.8}$$

$$\begin{aligned}
\rho_0^{(2)}(\vec{r}, \vec{r}') &= \frac{1}{\Xi_0} \sum_{N=2}^{\infty} \frac{z^N}{N!} Z_{N,0} \rho_{N,0}^{(2)}(\vec{r}, \vec{r}') \\
&= \frac{1}{\Xi_0} \sum_{N=2}^{\infty} \frac{z^N}{(N-2)!} \int \cdots \int e^{-\beta V_N(\vec{r}, \vec{r}', \vec{r}_3, \cdots, \vec{r}_N)} d\vec{r}_3 \cdots d\vec{r}_N
\end{aligned} \tag{2.4.1.9}$$

Let us see the relationship between reference system and actual system. Grand canonical partition function for actual system is decomposed to:

$$\begin{aligned}\Xi &= \sum_{N=0}^{\infty} \frac{z^N}{N!} \int \cdots \int e^{-\beta V_{N+1}(\vec{r}_0, \vec{r}_1, \cdots, \vec{r}_N)} d\vec{r}_1 \cdots d\vec{r}_N \\ &= \frac{\Xi_0}{z} \sum_{N=0}^{\infty} \frac{1}{\Xi_0} \frac{z^{N+1}}{N!} \int \cdots \int e^{-\beta V_{N+1}(\vec{r}_0, \vec{r}_1, \cdots, \vec{r}_N)} d\vec{r}_1 \cdots d\vec{r}_N \\ &= \frac{\Xi_0}{z} \sum_{N=1}^{\infty} \frac{1}{\Xi_0} \frac{z^N}{(N-1)!} \int \cdots \int e^{-\beta V_N(\vec{r}_0, \vec{r}_1, \cdots, \vec{r}_{N-1})} d\vec{r}_1 \cdots d\vec{r}_{N-1}\end{aligned} \tag{2.4.1.10}$$

Here,

$$\begin{aligned}&\int \cdots \int e^{-\beta V_N(\vec{r}_0, \vec{r}_1, \cdots, \vec{r}_{N-1})} d\vec{r}_1 \cdots d\vec{r}_{N-1} \\ &= \int \cdots \int e^{-\beta V_N(\vec{r}_0, \vec{r}_2, \cdots, \vec{r}_N)} d\vec{r}_2 \cdots d\vec{r}_N = \frac{Z_{N,0} \rho_{N,0}^{(1)}(\vec{r}_0)}{N}\end{aligned} \tag{2.4.1.11}$$

Substitute Eq.(2.4.1.11) to (2.4.1.10):

$$\Xi = \frac{\Xi_0}{z} \sum_{N=1}^{\infty} \frac{1}{\Xi_0} \frac{z^N}{N!} Z_{N,0} \rho_{N,0}^{(1)}(\vec{r}_0) = \frac{\Xi_0}{z} \rho_0^{(1)} \tag{2.4.1.12}$$

Here, I use the fact that $\rho_0^{(1)}(\vec{r})$ does not depend on $\vec{r}$ since the potential is homogeneous.

Next, let us decompose $\rho^{(1)}(\vec{r}_1)$ (Eq.(2.3.1.48)). By using Eq.(2.4.1.12):

$$\begin{aligned}\rho^{(1)}(\vec{r}_1) &= \frac{1}{\Xi} \sum_{N=1}^{\infty} \frac{z^N}{(N-1)!} \int \cdots \int e^{-\beta V_{N+1}(\vec{r}_0, \vec{r}_1, \vec{r}_2, \cdots, \vec{r}_N)} d\vec{r}_2 \cdots d\vec{r}_N \\ &= \frac{1}{\rho_0^{(1)} \Xi_0} \sum_{N=1}^{\infty} \frac{z^{N+1}}{(N-1)!} \int \cdots \int e^{-\beta V_{N+1}(\vec{r}_0, \vec{r}_1, \vec{r}_2, \cdots, \vec{r}_N)} d\vec{r}_2 \cdots d\vec{r}_N \\ &= \frac{1}{\rho_0^{(1)} \Xi_0} \sum_{N=2}^{\infty} \frac{z^N}{(N-2)!} \int \cdots \int e^{-\beta V_N(\vec{r}_0, \vec{r}_1, \vec{r}_2, \cdots, \vec{r}_{N-1})} d\vec{r}_2 \cdots d\vec{r}_{N-1} \\ &= \frac{1}{\rho_0^{(1)} \Xi_0} \sum_{N=2}^{\infty} \frac{z^N}{(N-2)!} \int \cdots \int e^{-\beta V_N(\vec{r}_0, \vec{r}_1, \vec{r}_3, \cdots, \vec{r}_N)} d\vec{r}_3 \cdots d\vec{r}_N\end{aligned} \tag{2.4.1.13}$$

Substitute Eq.(2.4.1.9) to (2.4.1.13):

$$\rho^{(1)}(\vec{r}_1) = \frac{\rho_0^{(2)}(\vec{r}_0, \vec{r}_1)}{\rho_0^{(1)}} \tag{2.4.1.14}$$

For reference system, Eq.(2.3.3.14) becomes:

$$g_0^{(2)}(\vec{r}_0, \vec{r}_1) = \frac{\rho_0^{(2)}(\vec{r}_0, \vec{r}_1)}{\rho_0^{(1)}(\vec{r}_0) \rho_0^{(1)}(\vec{r}_1)} = \frac{\rho_0^{(2)}(\vec{r}_0, \vec{r}_1)}{\left(\rho_0^{(1)}\right)^2} \tag{2.4.1.15}$$

Substitute Eq.(2.4.1.15) to (2.4.1.14):

$$\rho^{(1)}(\vec{r}_1) = g_0^{(2)}(\vec{r}_0, \vec{r}_1) \rho_0^{(1)} \tag{2.4.1.16}$$

Eq.(2.4.1.16) means that one-particle density for actual system is expressed by the particle densities of reference system. This technique is called random phase approximation (See also Section 3.3.3). Here, let us approximate that $g_0^{(2)}(\vec{r}_0, \vec{r}_1)$ is two-particle distribution function of the actual system.

$$g_0^{(2)}(\vec{r}_0, \vec{r}_1) \to g^{(2)}(|\vec{r}_0 - \vec{r}_1|) = g^{(2)}(r_1) \tag{2.4.1.17}$$

Note that $\vec{r}_0$ is the origin.

By using this approximation, let us see the relationship between $g^{(2)}(r)$ and $c^{(2)}(r)$. First, let us expand $c^{(1)}(\vec{r})$ around the reference system by $\rho^{(1)}(\vec{r})$.

$$c^{(1)}(\vec{r}) \simeq c_0^{(1)} + \int \Delta\rho^{(1)}(\vec{r}') \left.\frac{\delta c^{(1)}(\vec{r})}{\delta\rho^{(1)}(\vec{r}')}\right|_{\phi=0} d\vec{r}' \tag{2.4.1.18}$$

$c_0^{(1)}$ is a direct correlation function of the reference system. From Eq.(2.3.3.29):

$$\begin{aligned} &\beta\mu_0 = \ln[\Lambda^3\rho_0^{(1)}(\vec{r})] - c_0^{(1)}(\vec{r}) \\ &\to c_0^{(1)} = \ln[\Lambda^3\rho_0^{(1)}] - \beta\mu_0 \end{aligned} \tag{2.4.1.19}$$

Note that $\psi(\vec{r})$ of the reference state is μ since $\phi(\vec{r}) = 0$. From Eqs.(2.3.3.25) and (2.3.3.26):

$$\frac{\delta c^{(1)}(\vec{r})}{\delta\rho^{(1)}(\vec{r}')} = c^{(2)}(\vec{r}, \vec{r}') \tag{2.4.1.20}$$

Substitute Eqs.(2.4.1.19) and (2.4.1.20) to Eq.(2.4.1.18):

$$c^{(1)}(\vec{r}) \to \ln[\Lambda^3\rho_0^{(1)}] - \beta\mu_0 + \int \Delta\rho^{(1)}(\vec{r}')c_0^{(2)}(\vec{r}, \vec{r}')d\vec{r}' \tag{2.4.1.21}$$

From Eq.(2.3.3.29), $c^{(1)}(\vec{r})$ is expressed as follows.

$$c^{(1)}(\vec{r}) = \ln[\Lambda^3\rho^{(1)}(\vec{r})] - \beta\mu + \beta\phi(\vec{r}) \tag{2.4.1.22}$$

Here, we assume that the chemical potential of actual system is the same as the reference system.

$$\mu \to \mu_0 \tag{2.4.1.23}$$

$\phi(\vec{r})$ is a pairwise potential (Eq.(2.4.1.1)), $v(r)$, where $r = |\vec{r}|$ is distance between two particles. Therefore,

$$c^{(1)}(\vec{r}) \to \ln[\Lambda^3\rho^{(1)}(\vec{r})] - \beta\mu_0 + \beta v(r) \tag{2.4.1.24}$$

By comparing Eqs.(2.4.1.21) and (2.4.1.24):

$$\begin{aligned} &\ln[\Lambda^3\rho_0^{(1)}] - \beta\mu_0 + \int \Delta\rho^{(1)}(\vec{r}')c_0^{(2)}(\vec{r}, \vec{r}')d\vec{r}' = \ln[\Lambda^3\rho^{(1)}(\vec{r})] - \beta\mu_0 + \beta v(r) \\ &\to \rho^{(1)}(\vec{r}) = \rho_0^{(1)} \exp\left[-\beta v(r) + \int \Delta\rho^{(1)}(\vec{r}')c_0^{(2)}(\vec{r}, \vec{r}')d\vec{r}'\right] \end{aligned} \tag{2.4.1.25}$$

$\Delta\rho^{(1)}(\vec{r})$ is calculated by using Eq.(2.4.1.16):

$$\Delta\rho^{(1)}(\vec{r}) = \rho^{(1)}(\vec{r}) - \rho_0^{(1)} = \rho_0^{(1)}(g^{(2)}(r) - 1) = \rho_0^{(1)}h^{(2)}(r) \tag{2.4.1.26}$$

Here, we assume that $c^{(2)}(\vec{r},\vec{r}')$ of actual system is the same as the reference system.

$$c_0^{(2)}(\vec{r},\vec{r}') \to c^{(2)}(\vec{r},\vec{r}') = c^{(2)}(|\vec{r}-\vec{r}'|) \tag{2.4.1.27}$$

By using Ornstein–Zernike equation (Eq.(2.3.3.35)), the integral in Eq.(2.4.1.25) becomes:

$$\int \Delta\rho^{(1)}(\vec{r}')c^{(2)}(|\vec{r}-\vec{r}'|)d\vec{r}' = \rho_0^{(1)}\int h^{(2)}(r')c^{(2)}(|\vec{r}-\vec{r}'|)d\vec{r}' = h^{(2)}(r) - c^{(2)}(r) \tag{2.4.1.28}$$

Substitute Eqs.(2.4.1.16) and (2.4.1.28) to Eq.(2.4.1.25):

$$g^{(2)}(r) = \exp\left[-\beta v(r) + h^{(2)}(r) - c^{(2)}(r)\right] \tag{2.4.1.29}$$

Eq.(2.4.1.29) is called hypernetted chain (HNC) approximation.

Another closure relation is obtained by starting from $e^{c^{(1)}(\vec{r})}$.

$$\exp\left[c^{(1)}(\vec{r})\right] \simeq \exp\left[c_0^{(1)}(\vec{r})\right] + \int \Delta\rho^{(1)}(\vec{r}')\left.\frac{\delta\exp[c^{(1)}(\vec{r})]}{\delta\rho^{(1)}(\vec{r}')}\right|_{\phi=0} d\vec{r}' \tag{2.4.1.30}$$

Functional derivative in Eq.(2.4.1.30) is calculated as follows.

$$\left.\frac{\delta\exp[c^{(1)}(\vec{r})]}{\delta\rho^{(1)}(\vec{r}')}\right|_{\phi=0} = \left.\frac{\delta c^{(1)}(\vec{r})}{\delta\rho^{(1)}(\vec{r}')}\right|_{\phi=0}\left.\frac{\delta\exp[c^{(1)}(\vec{r})]}{\delta c^{(1)}(\vec{r})}\right|_{\phi=0} = c_0^{(2)}(\vec{r},\vec{r}')\exp[c_0^{(1)}(\vec{r})] \to c^{(2)}(|\vec{r}-\vec{r}'|)\exp[c_0^{(1)}(\vec{r})] \tag{2.4.1.31}$$

By taking exponential of Eqs.(2.4.1.19) and (2.4.1.24):

$$\exp\left[c^{(1)}(\vec{r})\right] = \Lambda^3\rho^{(1)}(\vec{r})e^{-\beta\mu_0}e^{\beta v(r)} \tag{2.4.1.32}$$

$$\exp\left[c_0^{(1)}(\vec{r})\right] = \Lambda^3\rho_0^{(1)}e^{-\beta\mu_0} \tag{2.4.1.33}$$

Substitute Eqs.(2.3.3.35), (2.4.1.16), (2.4.1.26), (2.4.1.31) $\sim$ (2.4.1.33) to Eq.(2.4.1.30):

$$\begin{aligned}
&\exp\left[c^{(1)}(\vec{r})\right] = \exp\left[c_0^{(1)}(\vec{r})\right]\left(1 + \int \rho_0^{(1)}h^{(2)}(r')c_0^{(2)}(|\vec{r}-\vec{r}'|)d\vec{r}'\right)\\
&\to \Lambda^3\rho^{(1)}(\vec{r})e^{-\beta\mu_0}e^{\beta v(r)} = \Lambda^3\rho_0^{(1)}e^{-\beta\mu_0}\left(1 + h^{(2)}(r) - c^{(2)}(r)\right)\\
&\to \rho^{(1)}e^{\beta v(r)} = \rho_0^{(1)}e^{-\beta v(r)}\left(1 + h^{(2)}(r) - c^{(2)}(r)\right)
\end{aligned}$$

$$g^{(2)}(r) = e^{-\beta v(r)}\left[1 + h^{(2)}(r) - c^{(2)}(r)\right] \tag{2.4.1.34}$$

Eq.(2.4.1.34) is called Percus–Yevick (PY) approximation [40]. By using Eq.(2.3.3.15), $c^{(2)}(r)$ is expressed as follows.

$$\begin{aligned}
&g^{(2)}(r) = e^{-\beta v(r)}\left[g^{(2)}(r) - c^{(2)}(r)\right]\\
&\to c^{(2)}(r) = g^{(2)}(r)\left[1 - e^{\beta v(r)}\right]
\end{aligned} \tag{2.4.1.35}$$

2.4.2 Percus–Yevick equation for a hard sphere

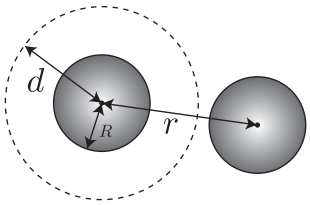

Figure 2.4: Configuration for hard sphere model.

Let us calculate the scattering function from a hard sphere. The potential is defined as follows.

$$v(r) = \begin{cases} \infty & \text{for } r < d = 2R \\ 0 & \text{for } r \geq d = 2R \end{cases} \tag{2.4.2.1}$$

Here, d represents the diameter of a hard sphere and R is the radius (Figure 2.4). The center of mass between two particles cannot be less than d since hard sphere cannot penetrate into other particles. This means that two-particle distribution function is 0 for $r < d$.

$$g^{(2)}(r) = 0 \quad \text{for } r < d \tag{2.4.2.2}$$

Under Percus–Yevick approximation, $h^{(2)}(r)$ and $c^{(2)}(r)$ is expressed as follows (Eqs.(2.3.3.15) and (2.4.1.35)).

$$h^{(2)}(r) = \begin{cases} -1 & \text{for } r < d \\ g^{(2)}(r) - 1 & \text{for } r \geq d \end{cases} \tag{2.4.2.3}$$

$$c^{(2)}(r) = \begin{cases} g^{(2)}(r)\left[1 - e^{\beta v(r)}\right] & \text{for } r < d \\ 0 & \text{for } r \geq d \end{cases} \tag{2.4.2.4}$$

The task is the calculation of $c^{(2)}(r)$ for $r < d$. Note that $g^{(2)}(r) = 0$ while $e^{\beta v(r)} = \infty$ for $r < d$. Analytical solution was given by Wertheim and Thiele in 1963 by using inverse Laplace transformation [41–43]. Here, I introduce more simple derivation presented by Kelbg [44]. Calculation is performed by direct differentiation of Ornstein–Zernike equation, Eq.(2.3.3.35). I'm going to use the following modified equation.

$$\begin{aligned} h^{(2)}(r) &= c^{(2)}(r) + \rho \int h^{(2)}(r')c^{(2)}(|\vec{r} - \vec{r}'|)d\vec{r}' \\ &= c^{(2)}(r) + \rho \int h^{(2)}(|\vec{r}' - \vec{r}|)c^{(2)}(|\vec{r} - \vec{r}' - \vec{r}|)d\vec{r}' \\ &= c^{(2)}(r) + \rho \int c^{(2)}(r')h^{(2)}(|\vec{r} - \vec{r}'|)d\vec{r}' \end{aligned} \tag{2.4.2.5}$$

By setting

$$\vec{r} := (r, 0, 0) \tag{2.4.2.6}$$

$$\vec{r}' := (s, \theta, \varphi) \tag{2.4.2.7}$$

$$|\vec{r} - \vec{r}'| =: t \tag{2.4.2.8}$$

Eq.(2.4.2.5) becomes:

$$\begin{aligned} h^{(2)}(r) &= c^{(2)}(r) + \rho \int_{s=0}^{\infty} \int_{\theta=0}^{\pi} \int_{\varphi=0}^{2\pi} c^{(2)}(s) h^{(2)}(t) s^2 ds \sin\theta d\theta d\varphi \\ &= c^{(2)}(r) + 2\pi\rho \int_{s=0}^{\infty} \int_{\theta=0}^{\pi} c^{(2)}(s) h^{(2)}(t) s^2 ds \sin\theta d\theta \end{aligned} \tag{2.4.2.9}$$

Let us convert the variable from θ to t by using the following relation.

$$\begin{aligned} & t^2 = r^2 + s^2 - 2rs\cos\theta \\ & \rightarrow \frac{dt^2}{d\theta}\left(= 2t\frac{dt}{d\theta}\right) = 2rs\sin\theta \\ & \rightarrow \sin\theta d\theta = \frac{tdt}{rs} \end{aligned} \tag{2.4.2.10}$$

Note that r and s do not depend on θ. By substituting Eq.(2.4.2.10) to (2.4.2.9):

$$h^{(2)}(r) = c^{(2)}(r) + 2\pi\rho \int_{s=0}^{\infty} \int_{t=|r-s|}^{r+s} c^{(2)}(s) h^{(2)}(t) \frac{ts}{r} ds dt \tag{2.4.2.11}$$

Note that $t = |r - s|$ when $\theta = 0$ while $t = r + s$ when $\theta = \pi$. Here, let us define two quantities.

$$H(r) := rh^{(2)}(r) = \begin{cases} -r & \text{for } r < d \\ r\left[g^{(2)}(r) - 1\right] & \text{for } r \geq d \end{cases} \tag{2.4.2.12}$$

$$C(r) := rc^{(2)}(r) = \begin{cases} rg^{(2)}(r)\left[1 - e^{\beta v(r)}\right] & \text{for } r < d \\ 0 & \text{for } r \geq d \end{cases} \tag{2.4.2.13}$$

By using Eqs.(2.4.2.12) and (2.4.2.13), Eq.(2.4.2.11) becomes:

$$\begin{aligned} H(r) &= C(r) + 2\pi\rho \int_0^{\infty} dsC(s) \int_{|r-s|}^{r+s} dtH(t) \\ &= C(r) + 2\pi\rho \int_0^{r} dsC(s) \int_{r-s}^{r+s} dtH(t) + 2\pi\rho \int_r^{\infty} dsC(s) \int_{s-r}^{r+s} dtH(t) \\ &=: C(r) + 2\pi\rho \int_0^{r} dsC(s)K(r,s) + 2\pi\rho \int_r^{\infty} dsC(s)K(s,r) \end{aligned} \tag{2.4.2.14}$$

where

$$K(r,s) := \int_{r-s}^{r+s} dtH(t) \tag{2.4.2.15}$$

$$K(s,r) := \int_{s-r}^{r+s} dtH(t) \tag{2.4.2.16}$$

$$K(r,r) := \int_0^{2r} dtH(t) \tag{2.4.2.17}$$

To obtain derivative of Eq.(2.4.2.14), I use the following formulae:

$$\begin{aligned}\int_{x+dx}^{a} g(y)f(x+dx,y)dy &= \int_{x+dx}^{a} g(y)\left[f(x,y)+\frac{\partial f(x,y)}{\partial x}dx\right]dy \\ &= \int_{x}^{a} g(y)f(x,y)dy - \int_{x}^{x+dx} g(y)f(x,y)dy \\ &\quad + \left(\int_{x}^{a} g(y)\frac{\partial f(x,y)}{\partial x}dy\right)dx - \left(\int_{x}^{x+dx} g(y)\frac{\partial f(x,y)}{\partial x}dy\right)dx \end{aligned} \tag{2.4.2.18}$$

By using Eq.(2.4.2.18):

$$\begin{aligned}&\frac{\partial}{\partial x}\int_{x}^{a} g(y)f(x,y)dy \\ &= \left[\int_{x+dx}^{a} g(y)f(x+dx,y)dy - \int_{x}^{a} g(y)f(x,y)dy\right]/(dx) \\ &\simeq \left[-\int_{x}^{x+dx} g(y)f(x,y)dy + \left(\int_{x}^{a} g(y)\frac{\partial f(x,y)}{\partial x}dy\right)dx\right]/(dx) \\ &\to \int_{x}^{a} g(y)\frac{\partial f(x,y)}{\partial x}dy - g(x)f(x,x)\end{aligned} \tag{2.4.2.19}$$

$$\begin{aligned}&\int_{a}^{z(x+dx)} g(y)f(z(x+dx),y)dy \\ &= \int_{a}^{z(x)+(\partial z/\partial x)dx} g(y)\left[f(z(x),y)+\frac{\partial f(z,y)}{\partial z}\frac{\partial z}{\partial x}dx\right]dy \\ &= \int_{a}^{z(x)} g(y)f(z(x),y)dy + \int_{z(x)}^{z(x)+(\partial z/\partial x)dx} g(y)f(z(x),y)dy \\ &\quad + \left(\int_{a}^{z(x)} g(y)\frac{\partial f(z,y)}{\partial z}\frac{\partial z}{\partial x}dy\right)dx + \left(\int_{z(x)}^{z(x)+(\partial z/\partial x)dx} g(y)\frac{\partial f(z,y)}{\partial z}\frac{\partial z}{\partial x}dy\right)dx\end{aligned} \tag{2.4.2.20}$$

By using Eq.(2.4.2.20):

$$\begin{aligned}&\frac{\partial}{\partial x}\int_{a}^{z(x)} g(y)f(z(x),y)dy \\ &= \left[\int_{a}^{z(x+dx)} g(y)f(z(x+dx),y)dy - \int_{a}^{z(x)} g(y)f(z(x),y)dy\right]/(dx) \\ &\simeq \left[\int_{z(x)}^{z(x)+(\partial z/\partial x)dx} g(y)f(z(x),y)dy + \left(\int_{a}^{z(x)} g(y)\frac{\partial f(z,y)}{\partial z}\frac{\partial z}{\partial x}dy\right)dx\right]/(dx) \\ &\to \int_{a}^{z(x)} g(y)\frac{\partial f(z,y)}{\partial z}\frac{\partial z}{\partial x}dy + g(z)f(z,z)\frac{\partial z}{\partial x}\end{aligned} \tag{2.4.2.21}$$

Differentiation of the second term of Eq.(2.4.2.14) is calculated by using Eq.(2.4.2.21).

$$\begin{aligned}\frac{\partial}{\partial r}\int_{0}^{r} C(s)K(r,s)ds &= \int_{0}^{r} C(s)\frac{\partial K(r,s)}{\partial r}\frac{\partial r}{\partial r}ds + C(r)K(r,r)\frac{\partial r}{\partial r} \\ &= \int_{0}^{r} C(s)\frac{\partial}{\partial r}\left[\int_{r-s}^{r+s} dtH(t)\right]ds + C(r)K(r,r) \\ &= \int_{0}^{r} dsC(s)\left[H(r+s)-H(r-s)\right] + C(r)\int_{0}^{2r} dtH(t)\end{aligned} \tag{2.4.2.22}$$

Differentiation of the third term of Eq.(2.4.2.14) is calculated by using Eq.(2.4.2.19).

$$\begin{aligned}\frac{\partial}{\partial r}\int_r^\infty C(s)K(s,r)ds &= \int_r^\infty C(s)\frac{\partial K(s,r)}{\partial r}ds - C(r)K(r,r)\\ &= \int_r^\infty C(s)\frac{\partial}{\partial r}\left[\int_{s-r}^{r+s} dtH(t)\right]ds - C(r)K(r,r)\\ &= \int_r^\infty dsC(s)\left[H(r+s)-H(s-r)\right] - C(r)\int_0^{2r} dtH(t)\end{aligned} \tag{2.4.2.23}$$

Substitute Eqs.(2.4.2.22) and (2.4.2.23) to the differentiation of Eqs.(2.4.2.14):

$$\begin{aligned}\frac{dH(r)}{dr} =: \frac{dC(r)}{dr} &+ 2\pi\rho\left[\int_0^r dsC(s)\left[H(r+s)-H(r-s)\right] + C(r)\int_0^{2r} dtH(t)\right.\\ &\left.+\int_r^\infty dsC(s)\left[H(r+s)-H(s-r)\right] - C(r)\int_0^{2r} dtH(t)\right]\\ = \frac{dC(r)}{dr} &+ 2\pi\rho\left[\int_0^\infty dsC(s)H(r+s) - \int_0^r dsC(s)H(r-s) + \int_r^\infty dsC(s)H(s-r)\right]\end{aligned} \tag{2.4.2.24}$$

By using the following relation,

$$\begin{aligned}&g^{(2)}(r) = g^{(2)}(-r)\\ &\rightarrow h^{(2)}(r) = h^{(2)}(-r)\\ &\rightarrow H(r) = -H(-r)\end{aligned} \tag{2.4.2.25}$$

Eq.(2.4.2.24) becomes as follows.

$$\begin{aligned}\frac{dH(r)}{dr} &= \frac{dC(r)}{dr} + 2\pi\rho\left[\int_0^\infty dsC(s)H(r+s) - \int_0^r dsC(s)H(r-s) - \int_r^\infty dsC(s)H(r-s)\right]\\ &= \frac{dC(r)}{dr} + 2\pi\rho\int_0^\infty dsC(s)\left[H(r+s)-H(r-s)\right]\end{aligned} \tag{2.4.2.26}$$

Substitute Eqs.(2.4.2.12) and (2.4.2.13) to Eq.(2.4.2.26):

$$\frac{dH(r)}{dr} = \frac{dC(r)}{dr} + 2\pi\rho\int_0^d dsC(s)\left[-(r+s)+(r-s)\right] = \frac{dC(r)}{dr} - 4\pi\rho\int_0^d dssC(s) \tag{2.4.2.27}$$

When $r = 0$:

$$\begin{aligned}-1 &= \left.\frac{dC(r)}{dr}\right|_{r=0} - 4\pi\rho\int_0^d dssC(s)\\ \rightarrow \left.\frac{dC(r)}{dr}\right|_{r=0} &= -1 + 4\pi\rho\int_0^d dssC(s)\end{aligned} \tag{2.4.2.28}$$

Next, let us calculate second derivative of $C(r)$ at $r = 0$. First term in Eq.(2.4.2.26) is expressed as follows:

$$\int_0^\infty dsC(s)H(r+s) = \int_0^\infty dsC(s)H(r+s) - \int_0^\infty dsH(s)H(r+s) + \int_0^\infty dsH(s)H(r+s) \tag{2.4.2.29}$$

By defining $s' := d + s$:

$$\begin{aligned}\int_0^\infty dsH(s)H(r+s) &= \int_r^\infty ds'H(s'-r)H(s') \\ &= -\int_r^\infty ds'H(r-s')H(s') \\ &= -\int_0^\infty ds'H(r-s')H(s') + \int_0^r ds'H(r-s')H(s') \end{aligned} \tag{2.4.2.30}$$

Substitute Eq.(2.4.2.30) to Eq.(2.4.2.29):

$$\begin{aligned}&\int_0^\infty dsC(s)H(r+s) \\ &= \int_0^\infty ds\left[C(s)H(r+s) - H(s)H(r+s) - H(r-s)H(s)\right] + \int_0^r dsH(r-s)H(s) \\ &= \int_0^\infty ds\left[C(s)H(r+s) - H(s)H(r+s) + C(s)H(r-s) - H(s)H(r-s)\right] \\ &\quad - \int_0^\infty dsC(s)H(r-s) + \int_0^r dsH(s)H(r-s) \\ &= \int_0^\infty ds\left[C(s) - H(s)\right]\left[H(r+s) + H(r-s)\right] - \int_0^\infty dsC(s)H(r-s) + \int_0^r dsH(s)H(r-s) \end{aligned} \tag{2.4.2.31}$$

From now, let us focus the case where $r < d$. In this case, by using Eqs.(2.4.2.12) and (2.4.2.13), 2nd and 3rd terms in Eq.(2.4.2.31) is:

$$\begin{aligned}\int_0^\infty dsC(s)H(r-s) &= \int_0^d dsC(s)H(r-s) = \int_0^d dsC(s)(s-r) \\ &= \int_0^d dssC(s) - r\int_0^d dsC(s) \quad (r<d) \end{aligned} \tag{2.4.2.32}$$

$$\begin{aligned}\int_0^r dsH(s)H(r-s) &= \int_0^r ds(-s)(s-r) \\ &= \left[-\frac{s^3}{3} + \frac{s^2 r}{2}\right]_{s=0}^r = \frac{r^3}{6} \quad (r<d) \end{aligned} \tag{2.4.2.33}$$

Substitute Eqs.(2.4.2.31), (2.4.2.32), (2.4.2.33) to Eq.(2.4.2.26):

$$\begin{aligned}\frac{dH(r)}{dr} &= \frac{dC(r)}{dr} + 2\pi\rho\left[\int_0^\infty ds\left[C(s) - H(s)\right]\left[H(r+s) + H(r-s)\right]\right. \\ &\qquad \left. -2\int_0^\infty dsC(s)H(r-s) + \int_0^r dsH(s)H(r-s)\right] \\ &= \frac{dC(r)}{dr} + 2\pi\rho\int_0^\infty ds\left[C(s) - H(s)\right]\left[H(r+s) + H(r-s)\right] \\ &\qquad + 4\pi\rho r\int_0^d dsC(s) - 4\pi\rho\int_0^d dssC(s) + \frac{\pi\rho r^3}{3} \quad (r<d) \end{aligned} \tag{2.4.2.34}$$

Next, let us calculate the r-derivative of the first integral in Eq.(2.4.2.34). Here, I use the following conversion.

$$\frac{d([C(s) - H(s)][H(r+s) + H(r-s)])}{dr} = [C(s) - H(s)]\frac{d[H(r+s) - H(r-s)]}{ds} \tag{2.4.2.35}$$

Therefore, the integral after differentiation is:

$$\begin{aligned}
&\int_0^\infty ds \frac{d([C(s)-H(s)][H(r+s)+H(r-s)])}{dr} \\
&= \int_0^\infty ds[C(s)-H(s)]\frac{d[H(r+s)-H(r-s)]}{ds} \\
&= [[C(s)-H(s)][H(r+s)-H(r-s)]]_{s=0}^{\infty} - \int_0^\infty ds \frac{d[C(s)-H(s)]}{ds}[H(r+s)-H(r-s)] \qquad (2.4.2.36)
\end{aligned}$$

From Eqs.(2.4.2.12) and (2.4.2.13), $C(s=0) = H(s=0) = 0$. In addition, $H(s \to \infty) = H(s \to -\infty) = 0$ since $g^{(2)}(r=\infty) = 1$. Therefore, the first integral of Eq.(2.4.2.36) vanishes. To calculate the second integral of Eq.(2.4.2.36), let us use Eq.(2.4.2.26):

$$\frac{d[C(s)-H(s)]}{ds} = -2\pi\rho \int_0^\infty dt C(t)[H(s+t)-H(s-t)] = -2\pi\rho \int_0^d dt C(t)[H(s+t)-H(s-t)] \qquad (2.4.2.37)$$

Substitute Eq.(2.4.2.37) to Eq.(2.4.2.36):

$$\begin{aligned}
&\int_0^\infty ds \frac{d([C(s)-H(s)][H(r+s)+H(r-s)])}{dr} \\
&= 2\pi\rho \int_0^d dt C(t) \int_0^\infty ds[H(r+s)-H(r-s)][H(s+t)-H(s-t)] \qquad (2.4.2.38)
\end{aligned}$$

Integral for s in Eq.(2.4.2.38) is evaluated as follows.

$$\int_0^\infty ds H(r+s)H(s+t) \to \int_r^\infty du H(u)H(t+u-r) \quad (u := r+s) \qquad (2.4.2.39)$$

$$-\int_0^\infty ds H(r+s)H(s-t) \to -\int_r^\infty du H(u)H(u-r-t) \quad (u := r+s) \qquad (2.4.2.40)$$

$$\begin{aligned}
-\int_0^\infty ds H(r-s)H(s+t) &\to -\int_t^\infty du H(r-u+t)H(u) \quad (u := s+t) \\
&= \int_t^\infty du H(u)H(u-r-t) \qquad (2.4.2.41)
\end{aligned}$$

$$\begin{aligned}
\int_0^\infty ds H(r-s)H(s-t) &\to \int_{-t}^\infty du H(r-u+t)H(u) \quad (u := s-t) \\
&= -\int_{-t}^\infty du H(u)H(t+u-r) \qquad (2.4.2.42)
\end{aligned}$$

From Eqs.(2.4.2.39) and (2.4.2.42):

$$\begin{aligned}
&\int_0^\infty ds H(r+s)H(s+t) + \int_0^\infty ds H(r-s)H(s-t) \\
&= -\int_{-t}^r du H(u)H(t+u-r) \\
&= -\int_{-t}^r du(-u)(-u+r-t) \\
&= -\left[\frac{u^3}{3} - \frac{u^2}{2}(r-t)\right]_{u=-t}^{r} = -\frac{r^3+t^3}{3} + \frac{r^2-t^2}{2}(r-t) \qquad (2.4.2.43)
\end{aligned}$$

From Eqs.(2.4.2.40) and (2.4.2.41):

$$\begin{aligned}
&-\int_0^\infty dsH(r+s)H(s-t)-\int_0^\infty dsH(r-s)H(s+t)\\
&=\int_t^r duH(u)H(u-r-t)\\
&=\int_t^r du(-u)(-u+r+t)\\
&=\left[\frac{u^3}{3}-\frac{u^2}{2}(r+t)\right]_{u=t}^{r}=\frac{r^3-t^3}{3}-\frac{r^2-t^2}{2}(r+t)
\end{aligned} \tag{2.4.2.44}$$

Substitute Eqs.(2.4.2.43) and (2.4.2.44) to Eq.(2.4.2.38):

$$\begin{aligned}
&\int_0^\infty ds\frac{d([C(s)-H(s)][H(r+s)+H(r-s)])}{dr}\\
&=2\pi\rho\int_0^d dtC(t)\left(-\frac{r^3+t^3}{3}+\frac{r^2-t^2}{2}(r-t)+\frac{r^3-t^3}{3}-\frac{r^2-t^2}{2}(r+t)\right)\\
&=2\pi\rho\int_0^d dtC(t)\left(\frac{t^3}{3}-tr^2\right)
\end{aligned} \tag{2.4.2.45}$$

By using Eq.(2.4.2.45), differentiation of Eq.(2.4.2.34) is performed as follows.

$$\begin{aligned}
\frac{d^2H(r)}{dr^2}&=\frac{d^2C(r)}{dr^2}+2\pi\rho\int_0^\infty ds\frac{d([C(s)-H(s)][H(r+s)+H(r-s)])}{dr}+4\pi\rho\int_0^d dsC(s)+\pi\rho r^2\\
&=\frac{d^2C(r)}{dr^2}+\frac{4\pi^2\rho^2}{3}\int_0^d dss^3C(s)-4\pi^2\rho^2r^2\int_0^d dssC(s)+4\pi\rho\int_0^d dsC(s)+\pi\rho r^2\quad(r<d)
\end{aligned} \tag{2.4.2.46}$$

When $r=0$:

$$\begin{aligned}
0&=\left.\frac{d^2C(r)}{dr^2}\right|_{r=0}+\frac{4\pi^2\rho^2}{3}\int_0^d dss^3C(s)+4\pi\rho\int_0^d dsC(s)\\
&\rightarrow\left.\frac{d^2C(r)}{dr^2}\right|_{r=0}=-4\pi\rho\int_0^d ds\left[\frac{\pi\rho s^3}{3}+1\right]C(s)
\end{aligned} \tag{2.4.2.47}$$

Higher order derivatives can be calculated by using Eq.(2.4.2.46) as follows.

$$\frac{d^3H(r)}{dr^3}=\frac{d^3C(r)}{dr^3}-8\pi^2\rho^2r\int_0^d dssC(s)+2\pi\rho r\quad(r<d) \tag{2.4.2.48}$$

$$\frac{d^4H(r)}{dr^4}=\frac{d^4C(r)}{dr^4}-8\pi^2\rho^2\int_0^d dssC(s)+2\pi\rho\quad(r<d) \tag{2.4.2.49}$$

All higher derivatives vanish. When $r=0$:

$$\left.\frac{d^3C(r)}{dr^3}\right|_{r=0}=0 \tag{2.4.2.50}$$

$$\left.\frac{d^4C(r)}{dr^4}\right|_{r=0}=2\pi\rho\left[-1+4\pi\rho\int_0^d dssC(s)\right] \tag{2.4.2.51}$$

From Eqs.(2.4.2.28), (2.4.2.47), (2.4.2.50), and (2.4.2.51), $C(r)$ is expanded as follows:

$$\begin{aligned} C(r) &= C(0) + \left.\frac{dC(r)}{dr}\right|_{r=0} r + \frac{1}{2}\left.\frac{d^2C(r)}{dr^2}\right|_{r=0} r^2 + \frac{1}{6}\left.\frac{d^3C(r)}{dr^3}\right|_{r=0} r^3 + \frac{1}{24}\left.\frac{d^4C(r)}{dr^4}\right|_{r=0} r^4 \\ &= r\left[-1 + 4\pi\rho\int_0^d dssC(s)\right] + \frac{1}{2}r^2\left[-4\pi\rho\int_0^d ds\left[\frac{\pi\rho s^3}{3}+1\right]C(s)\right] + \frac{1}{24}r^4 2\pi\rho\left[-1+4\pi\rho\int_0^d dssC(s)\right] \\ &=: a_1 r + a_2 r^2 + a_4 r^4 \quad (r<d) \end{aligned} \tag{2.4.2.52}$$

Integrals in Eq.(2.4.2.52) are formally calculated as follows:

$$\int_0^d dssC(s) = \int_0^d ds(a_1 s^2 + a_2 s^3 + a_4 s^5) = \frac{a_1}{3}d^3 + \frac{a_2}{4}d^4 + \frac{a_4}{6}d^6 \tag{2.4.2.53}$$

$$\begin{aligned} \int_0^d ds\left[1+\frac{\pi\rho s^3}{3}\right]C(s) &= \int_0^d ds(a_1 s + a_2 s^2 + a_4 s^4) + \frac{\pi\rho}{3}\int_0^d ds(a_1 s^4 + a_2 s^5 + a_4 s^7) \\ &= \left[\frac{a_1}{2}d^2 + \frac{a_2}{3}d^3 + \frac{a_4}{5}d^5\right] + \frac{\pi\rho}{3}\left[\frac{a_1}{5}d^5 + \frac{a_2}{6}d^6 + \frac{a_4}{8}d^8\right] \end{aligned} \tag{2.4.2.54}$$

Substitute Eqs.(2.4.2.53) and (2.4.2.54) to Eq.(2.4.2.52):

$$\begin{aligned} a_1 r + a_2 r^2 + a_4 r^4 = &- r + 4\pi\rho r\left[\frac{a_1}{3}d^3 + \frac{a_2}{4}d^4 + \frac{a_4}{6}d^6\right] \\ &- 2\pi\rho r^2\left[\frac{a_1}{2}d^2 + \frac{a_2}{3}d^3 + \frac{a_4}{5}d^5 + \frac{\pi\rho}{3}\left(\frac{a_1}{5}d^5 + \frac{a_2}{6}d^6 + \frac{a_4}{8}d^8\right)\right] \\ &+ \frac{\pi\rho}{12}r^4\left[-1 + 4\pi\rho\left(\frac{a_1}{3}d^3 + \frac{a_2}{4}d^4 + \frac{a_4}{6}d^6\right)\right] \end{aligned} \tag{2.4.2.55}$$

Let us use following quantities:

$$\alpha := a_1 \tag{2.4.2.56}$$

$$\beta := da_2 \tag{2.4.2.57}$$

$$\gamma := d^3 a_4 \tag{2.4.2.58}$$

$$\phi := \frac{\pi d^3\rho}{6} = \frac{4\pi R^3\rho}{3} \tag{2.4.2.59}$$

where $R := d/2$ stands for the radius of each hard sphere. ϕ represents the volume fraction. By equating the same order terms of r,

$$\alpha = -1 + 4\pi\rho\left[\frac{\alpha}{3} + \frac{\beta}{4} + \frac{\gamma}{6}\right]d^3 = -1 + \phi[8\alpha + 6\beta + 4\gamma] \tag{2.4.2.60}$$

$$\begin{aligned} \beta &= -2\pi\rho r^2\left[\frac{\alpha}{2} + \frac{\beta}{3} + \frac{\gamma}{5}\right]d^3 - \frac{2\pi^2\rho^2}{3}\left[\frac{\alpha}{5} + \frac{\beta}{6} + \frac{\gamma}{8}\right]d^6 \\ &= -\phi\left[6\alpha + 4\beta + \frac{12}{5}\gamma\right] - \phi^2\left[\frac{24}{5}\alpha + 4\beta + 3\gamma\right] \end{aligned} \tag{2.4.2.61}$$

$$\gamma = -\frac{\pi\rho}{12}d^3 + \frac{\pi^2\rho^2}{3}\left[\frac{\alpha}{3} + \frac{\beta}{4} + \frac{\gamma}{6}\right]d^3 = -\frac{\phi}{2} + \phi^2[4\alpha + 3\beta + 2\gamma] \tag{2.4.2.62}$$

From Eqs.(2.4.2.60) and (2.4.2.62):

$$\gamma = \frac{\phi}{2}\alpha \tag{2.4.2.63}$$

Substitute Eq.(2.4.2.63) to Eq.(2.4.2.60):

$$\begin{aligned} \alpha &= -1 + \phi[8\alpha + 6\beta + 2\phi\alpha] \\ &\rightarrow \beta = \frac{1 - (2\phi^2 + 8\phi - 1)\alpha}{6\phi} \end{aligned} \tag{2.4.2.64}$$

Substitute Eqs.(2.4.2.63) and (2.4.2.64) to Eq.(2.4.2.61):

$$\begin{aligned} \beta &= \left(-6\phi - \frac{6}{5}\phi^2 - \frac{24}{5}\phi^2 - \frac{3}{2}\phi^3\right)\alpha + (-4\phi - 4\phi^2)\beta \\ &\rightarrow \left(\frac{3}{2}\phi^3 + 6\phi^2 + 6\phi\right)\alpha = (-4\phi^2 - 4\phi - 1)\frac{1 - (2\phi^2 + 8\phi - 1)\alpha}{6\phi} \end{aligned}$$

As a result, α is obtained as follows.

$$\alpha = -\frac{(1 + 2\phi)^2}{(1 - \phi)^4} \tag{2.4.2.65}$$

Substitute Eq.(2.4.2.65) to Eqs.(2.4.2.64) and (2.4.2.63):

$$\beta = 6\phi\frac{(1 + \frac{\phi}{2})^2}{(1 - \phi)^4} \tag{2.4.2.66}$$

$$\gamma = -\frac{\phi(1 + 2\phi)^2}{2(1 - \phi)^4} \tag{2.4.2.67}$$

By using the analytical solution, we can calculate the analytical formula of the structure factor of hard spheres. Substitute Eqs.(2.4.2.13) and (2.4.2.56) $\sim$ (2.4.2.58) to Eq.(2.4.2.52):

$$c^{(2)}(r) = \begin{cases} \alpha + \beta\dfrac{r}{2R} + \gamma\left(\dfrac{r}{2R}\right)^3 & \text{for } \ r < d \\ 0 & \text{for } \ r \geq d \end{cases} \tag{2.4.2.68}$$

Let us calculate the Fourier transform of $c^{(2)}(r)$:

$$\begin{aligned} c^{(2)}(q) &= \int_{r=0}^{\infty}\int_{\theta=0}^{\pi}\int_{\varphi=0}^{2\pi} c^{(2)}(r)e^{i\vec{q}\cdot\vec{r}}r^2\sin\theta dr d\theta d\varphi \\ &= 2\pi\int_{r=0}^{\infty}\int_{u=-1}^{1} c^{(2)}(r)e^{iqru}r^2 dr du \quad (u := \cos\theta) \\ &= 2\pi\int_{r=0}^{\infty} c^{(2)}(r)\left[\frac{e^{iqru}}{iqr}\right]_{u=-1}^{1} r^2 dr \\ &= 4\pi\int_{0}^{2R} c^{(2)}(r)\frac{\sin qr}{qr}r^2 dr \\ &= 4\pi\int_{0}^{2R}\left(\alpha + \beta\frac{r}{2R} + \gamma\left(\frac{r}{2R}\right)^3\right)\frac{\sin qr}{qr}r^2 dr \end{aligned} \tag{2.4.2.69}$$

Each integral in Eq.(2.4.2.69) is calculated as follows:

$$\begin{aligned}\int_0^{2R} r\sin qr dr &= \left[-\frac{r\cos qr}{q}\right]_0^{2R} + \int_0^{2R}\frac{\cos qr}{q}dr \\ &= -\frac{2R\cos 2qR}{q} + \frac{1}{q}\left[-\frac{\sin qr}{q}\right]_0^{2R} \\ &= -\frac{2R\cos 2qR}{q} + \frac{\sin 2qR}{q^2} \\ &= -\frac{1}{q^2}A\cos A + \frac{1}{q^2}\sin A \end{aligned} \tag{2.4.2.70}$$

$$\begin{aligned}\int_0^{2R} r^2\sin qr dr &= \left[-\frac{r^2\cos qr}{q}\right]_0^{2R} + \int_0^{2R}\frac{2r\cos qr}{q}dr \\ &= -\frac{4R^2\cos 2qR}{q} + \frac{2}{q}\left\{\left[\frac{r\sin qr}{q}\right]_0^{2R} - \int_0^{2R}\frac{\sin qr}{q}dr\right\} \\ &= -\frac{4R^2\cos 2qR}{q} + \frac{2}{q}\frac{2R\sin 2qR}{q} - \frac{2}{q^2}\left[-\frac{\cos qr}{q}\right]_0^{2R} \\ &= -\frac{4R^2\cos 2qR}{q} + \frac{4R\sin 2qR}{q^2} + \frac{2\cos 2qR}{q^3} - \frac{2}{q^3} \\ &= -\frac{1}{q^3}A^2\cos A + \frac{2}{q^3}A\sin A + \frac{2}{q^3}\cos A - \frac{2}{q^3} \end{aligned} \tag{2.4.2.71}$$

$$\begin{aligned}&\int_0^{2R} r^4\sin qr dr \\ &= \left[-\frac{r^4\cos qr}{q}\right]_0^{2R} + \int_0^{2R}\frac{4r^3\cos qr}{q}dr \\ &= -\frac{16R^4\cos 2qR}{q} + \frac{4}{q}\left\{\left[\frac{r^3\sin qr}{q}\right]_0^{2R} - \int_0^{2R}\frac{3r^2\sin qr}{q}dr\right\} \\ &= -\frac{16R^4\cos 2qR}{q} + \frac{4}{q}\frac{8R^3\sin 2qR}{q} - \frac{12}{q^2}\int_0^{2R} r^2\sin qr dr \\ &= -\frac{16R^4\cos 2qR}{q} + \frac{32R^3\sin 2qR}{q^2} + \frac{48R^2\cos 2qR}{q^3} - \frac{48R\sin 2qR}{q^4} - \frac{24\cos 2qR}{q^5} + \frac{24}{q^5} \\ &= -\frac{1}{q^5}A^4\cos A + \frac{4}{q^5}A^3\sin A + \frac{12}{q^5}A^2\cos A - \frac{24}{q^5}A\sin A - \frac{24}{q^5}\cos A + \frac{24}{q^5} \end{aligned} \tag{2.4.2.72}$$

where

$$A := 2qR \tag{2.4.2.73}$$

Substitute Eqs.(2.4.2.70)∼(2.4.2.72) into Eq.(2.4.2.69):

$$\begin{aligned}c^{(2)}(q) = 4\pi\Bigg[&\frac{\alpha}{q^3}(-A\cos A + \sin A) + \frac{\beta}{2qR}\frac{1}{q^3}(-A^2\cos A + 2A\sin A + 2\cos A - 2) \\ &+\frac{\gamma}{8q^3R^3}\frac{1}{q^3}(-A^4\cos A + 4A^3\sin A + 12A^2\cos A - 24A\sin A - 24\cos A + 24)\Bigg]\end{aligned} \tag{2.4.2.74}$$

Substitute Eq.(2.4.2.74) into Eq.(2.3.4.5):

$$S(q) = \frac{1}{1 - \frac{4\pi R^3 \rho}{3} \frac{3}{4\pi R^3} c^{(2)}(q)} = \frac{1}{1 + \phi f_{\mathrm{PY}}(\phi, A)} \tag{2.4.2.75}$$

where

$$\begin{aligned} f_{\mathrm{PY}}(\phi, A) := -24 \Bigg[& \frac{\alpha}{A^3}(-A\cos A + \sin A) + \frac{\beta}{A^4}(-A^2\cos A + 2A\sin A + 2\cos A - 2) \\ & + \frac{\gamma}{A^6}(-A^4\cos A + 4A^3\sin A + 12A^2\cos A - 24A\sin A - 24\cos A + 24) \Bigg] \end{aligned} \tag{2.4.2.76}$$

Notice that α, β and γ is the functions of ϕ.

2.4.3 Modified Percus–Yevick equation

In the case of Percus–Yevick equation, we can determine the value of ϕ from the constituents of the sample. However, the radius of rigid spheres, R, may not correspond to the range of the inter-particle potential. In modified Percus–Yevick equation, we assume the following inter-particle potential instead of Eq.(2.4.2.1): [45]

$$v(r) = \begin{cases} \infty & \text{for } \ r \le 2D \\ 0 & \text{for } \ r > 2D \end{cases} \tag{2.4.3.1}$$

where $D > R$ determine the size of an effective repulsive potential wall. By using this potential, we modify the original Percus–Yevick equation as follows:

Structure factor, $S(q)$, is represented as follows under isotropic environment:

$$S(q) = \frac{1}{1 + \phi f_{PY}(\phi', A')} \tag{2.4.3.2}$$

where

$$A' := 2qD \tag{2.4.3.3}$$

$$\phi' := \phi \left(\frac{D}{R} \right)^3 \tag{2.4.3.4}$$

2.4.4 Square-Well structure factor

In the case of Percus–Yevick approximation, inter-particle potential is defined as Eq.(2.4.2.1). From now, we treat another type of inter-particle potential. First example is square-well potential described as follows:

$$v(r) = \begin{cases} \infty & \text{for } \ r \le 2R \\ -\epsilon & \text{for } \ 2R \le r \le 2\lambda R \\ 0 & \text{for } \ r > 2\lambda R \end{cases} \tag{2.4.4.1}$$

Structure factor originated from this square-well potential was derived analytically by Sharma and Sharma [46]. The result is quite similar to that of Percus–Yevick equation:

$$S(q) = \frac{1}{1 + \phi f_{\mathrm{SW}}(\phi, A, \epsilon, \lambda, T)} \tag{2.4.4.2}$$

where

$$f_{\mathrm{SW}}(\phi, A, \epsilon, \lambda) := 24\left[\frac{\alpha_{\mathrm{SW}}}{A^3}(-A\cos A + \sin A) + \frac{\beta_{\mathrm{SW}}}{A^4}(-A^2\cos A + 2A\sin A + 2\cos A - 2)\right.$$
$$+ \frac{\gamma_{\mathrm{SW}}}{A^6}(-A^4\cos A + 4A^3\sin A + 12A^2\cos A - 24A\sin A - 24\cos A + 24)$$
$$\left. -\frac{\epsilon}{k_B T}\frac{1}{A^3}(\sin\lambda A - \lambda A\cos\lambda A + A\cos A - \sin A)\right] \tag{2.4.4.3}$$

where

$$\alpha_{\mathrm{SW}} := \frac{(1+2\phi)^2 + \phi^3(\phi-4)}{(1-\phi)^4} \tag{2.4.4.4}$$

$$\beta_{\mathrm{SW}} := -\frac{\phi(18 + 20\phi - 12\phi^2 + \phi^4)}{3(1-\phi)^4} \tag{2.4.4.5}$$

$$\gamma_{\mathrm{SW}} := \frac{\phi((1+2\phi)^2 + \phi^3(\phi-4))}{2(1-\phi)^4} \tag{2.4.4.6}$$

2.4.5 Hayter-Penfold equation

Second example is repulsive potential described as follows:

$$v(r) = \begin{cases} \infty & \text{for } r \le 2R \\ 4\pi\varepsilon_0\varepsilon R^2\psi_0^2\dfrac{\exp(-\kappa(r-2R))}{r} & \text{for } r > 2R \end{cases} \tag{2.4.5.1}$$

where ε is the dielectric constant of the solvent medium, ε_0 is the permittivity of free space, ψ_0 is the surface potential and κ is the Debye–Hückel inverse screening length. The surface potential, ψ_0, is related to the electronic charge, z_m, on the macroion:

$$\psi_0 = \frac{z_m}{4\pi\varepsilon_0\varepsilon R(1+\kappa R)} \tag{2.4.5.2}$$

The Debye–Hückel inverse screening length, κ, is related to the ion strength. Ion strength is determined by both macroions themselves and the concentration of salt, c_{salt}:[9]

$$\kappa = \sqrt{\frac{e^2}{\varepsilon k_B T}\left(z_m\frac{\phi}{4\pi R^3/3} + 2N_A c_{\mathrm{salt}}\right)} \tag{2.4.5.3}$$

Analytical form of structure factor is derived by Hayter and Penfold [47]:

$$S(q) = \frac{1}{1 - \phi f_{\mathrm{HP}}(\phi, A, z_m, c_{\mathrm{salt}}, \varepsilon, T)} \tag{2.4.5.4}$$

[9]Here, the unit of c_{salt} is mol/m^3.

where

$$
\begin{aligned}
f_{\mathrm{HP}}(\phi, A, z_m, c_{\mathrm{salt}}, \varepsilon, T) := 24 \Bigg[& \frac{A_{\mathrm{HP}}}{A^3}(-A\cos A + \sin A) \\
& + \frac{B_{\mathrm{HP}}}{A^4}(-A^2\cos A + 2A\sin A + 2\cos A - 2) \\
& + \frac{G_{\mathrm{HP}}}{A^6}(-A^4\cos A + 4A^3\sin A + 12A^2\cos A - 24A\sin A - 24\cos A + 24) \\
& + \frac{C_{\mathrm{HP}}}{A(A^2+k^2)}(k\cosh k\sin A - A\sinh k\cos A) \\
& + \frac{F_{\mathrm{HP}}}{A(A^2+k^2)}(k\sinh k\sin A - A(\cosh k\cos A - 1)) \\
& + \frac{F_{\mathrm{HP}}}{A^2}(\cos A - 1) \\
& - \frac{\gamma\exp(-k)}{A(A^2+k^2)}(k\sin A + A\cos A) \Bigg]
\end{aligned} \tag{2.4.5.5}
$$

where

$$k := 2\kappa R \tag{2.4.5.6}$$

$$\gamma := \frac{4\pi\varepsilon_0\varepsilon R^2\psi_0^2}{k_B T}\exp(-k) \tag{2.4.5.7}$$

$$A_{\mathrm{HP}} := a_1 + a_2 C_{\mathrm{HP}} + a_3 F_{\mathrm{HP}} \tag{2.4.5.8}$$

$$B_{\mathrm{HP}} := b_1 + b_2 C_{\mathrm{HP}} + b_3 F_{\mathrm{HP}} \tag{2.4.5.9}$$

$$C_{\mathrm{HP}} := -\frac{\omega_{16}F_{\mathrm{HP}}^2 + \omega_{15}F_{\mathrm{HP}} + \omega_{14}}{\omega_{13}F_{\mathrm{HP}} + \omega_{12}} \tag{2.4.5.10}$$

$$G_{\mathrm{HP}} := \frac{\phi}{2}A_{\mathrm{HP}} \tag{2.4.5.11}$$

F_{HP} is one of roots of following equation:

$$\omega_4 F^4 + \omega_3 F^3 + \omega_2 F^2 + \omega_1 F + \omega_0 = 0 \tag{2.4.5.12}$$

There are four candidates as F_{HP}. To determine appropriate solution, corresponding radial distribution functions are calculated for each solution:

$$g(x) = 1 + \frac{R}{6\pi\phi r}\int_0^\infty (S(A) - 1)A\sin\frac{Ar}{2R}dA \tag{2.4.5.13}$$

Appropriate solution satisfy physically reasonable condition, $g(x) = 0$, inside the particle. Definition of parameters in Eqs.(2.4.5.8)∼(2.4.5.12) are shown in Appendix 11.2.

2.4.6 Single contact theory

Let us start from the first line of Eq.(2.1.17):

$$\frac{d\sigma}{d\Omega} = \left| \sum_{j=1}^{N}\sum_{k_j=1}^{z} b_k e^{-i\vec{q}\cdot(\vec{R}_j + \vec{r}_{k_j})} \right|^2 \tag{2.4.6.1}$$

Here, we are going to discuss dilute polymer solution. In this case, b is regarded as the summation of the scattering length of consisting atoms normalized by their volume.

$$\frac{d\sigma}{d\Omega} \to (\Delta\rho v_u)^2 \left| \sum_{j=1}^{N} \sum_{k_j=1}^{z} e^{-i\vec{q}\cdot(\vec{R}_j+\vec{r}_{k_j})} \right|^2 \tag{2.4.6.2}$$

When there is no interaction between polymers, Eq.(2.4.6.2) is decomposed into the form Eq.(2.1.17).

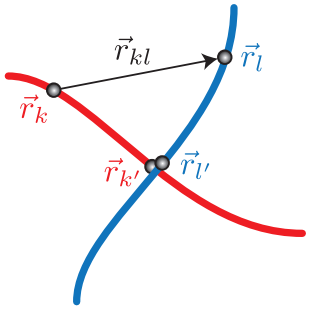

Figure 2.5: Schematics for polymers with single contact.

Here, let us consider what happen if there is single contact between polymers.

$$\frac{d\sigma}{d\Omega} = (\Delta\rho v_u)^2 \left[N \left| \sum_{k=1}^{z} e^{-i\vec{q}\cdot\vec{r}_k} \right|^2 + N(N-1) \sum_{k=1}^{z} \sum_{l=1}^{z} \langle\, e^{-i\vec{q}\cdot\vec{r}_{kl}} \,\rangle \right] \tag{2.4.6.3}$$

As for second term, time (or, for ergodic media, spatial) average is taken since the measured quantities should be time-averaged one. The first term of Eq.(2.4.6.3) describes the form factor of each polymer. The second term of Eq.(2.4.6.3) is decomposed into three terms as follows (Figure 2.5).

$$\langle\, e^{-i\vec{q}\cdot\vec{r}_{kl}} \,\rangle = \langle\, e^{-i\vec{q}\cdot\vec{r}_{kk'}} \,\rangle \langle\, e^{-i\vec{q}\cdot\vec{r}_{k'l'}} \,\rangle \langle\, e^{-i\vec{q}\cdot\vec{r}_{l'l}} \,\rangle \tag{2.4.6.4}$$

The first term and third term in Eq.(2.4.6.4) stand for form factors while the second term stands for excluded volume, v_{ex}/V_{ir} [36]. Therefore,

$$\frac{d\sigma}{d\Omega} \to (\Delta\rho v_u)^2 \left[N z^2 P(\vec{q}) + N^2 \left[-\frac{v_{ex}}{V_{ir}} (z^2 P(\vec{q}))^2 \right] \right] \tag{2.4.6.5}$$

Here, $N(N-1) \simeq N^2$ is used. Let us use the volume fraction of polymers, ϕ, defined as follows:

$$\phi := \frac{z v_u N}{V_{ir}} \tag{2.4.6.6}$$

Substitute Eq.(2.4.6.6) into Eq.(2.4.6.5):

$$\begin{aligned} \frac{d\sigma}{d\Omega} &\to (\Delta\rho v_u)^2 \left[\frac{\phi V_{ir}}{z v_u} z^2 P(\vec{q}) - \frac{\phi^2 V_{ir}^2}{z^2 v_u^2} \frac{v_{ex}}{V_{ir}} z^4 P(\vec{q})^2 \right] \\ &= (\Delta\rho)^2 V_{ir} v_u \left[z\phi P(\vec{q}) - \frac{v_{ex}}{v_u} (z\phi P(\vec{q}))^2 \right] \end{aligned} \tag{2.4.6.7}$$

Let us see the relationship between χ parameter and excluded volume v_{ex}. When the polymer fraction of

solution, ϕ, is small, Helmholtz free energy of mixing per lattice is expanded as follows.

$$\begin{aligned}\Delta\bar{F}_{mix} &= k_BT\left[\frac{\phi}{N}\ln\phi + (1-\phi)\ln(1-\phi) + \chi\phi(1-\phi)\right] \\ &\simeq k_BT\left[\frac{\phi}{N}\ln\phi + (1-\phi)\left(-\phi - \frac{\phi^2}{2}\right) + \chi\phi(1-\phi)\right] \\ &= k_BT\left[\frac{\phi}{N}\ln\phi + (\chi-1)\phi + \left(\frac{1}{2}-\chi\right)\phi^2 + \frac{1}{2}\phi^3\right] \end{aligned} \tag{2.4.6.8}$$

Next, let us derive $\Delta\bar{F}_{mix}$ by taking excluded volume into consideration. Here, we regard one polymer as the object whose volume is v_{ex}. Then we use lattice model whose lattice size is v_u. In this case, the number of lattices available to the first polymer, Ω_1, is V/v_u [10]. Like this, the number of lattice available to the ith polymer, Ω_i, is:

$$\Omega_i = \frac{V-(i-1)v_{ex}}{v_u} \tag{2.4.6.9}$$

By using Eq.(2.4.6.9), entropy of mixing is calculated as follows.

$$\begin{aligned}\Delta S_{mix} &= k_B\ln[\Omega_1\Omega_2\cdots\Omega_{N_p}] \\ &= k_B\ln\left[\frac{V}{v_u}\frac{V-v_{ex}}{v_u}\cdots\frac{V-(N_p-1)v_{ex}}{v_u}\right] \\ &= k_B\ln\left[\left(\frac{V}{v_u}\right)^{N_p}1\cdot\left(1-\frac{v_{ex}}{V}\right)\cdots\left(1-\frac{(N_p-1)v_{ex}}{V}\right)\right] \\ &= k_BN_p\ln\frac{V}{v_u} + k_B\sum_{i=0}^{N_p-1}\ln\left(1-i\frac{v_{ex}}{V}\right) \\ &\simeq k_BN_p\ln\frac{V}{v_u} + k_B\sum_{i=0}^{N_p-1}-i\frac{v_{ex}}{V} \\ &\simeq k_BN_p\ln\frac{V}{v_u} - k_B\frac{v_{ex}}{V}\frac{N_p^2}{2} \end{aligned} \tag{2.4.6.10}$$

Since $V = v_uN_t$ and $\phi = N_p/N_t$, entropy of mixing per lattice is expressed as follows.

$$\begin{aligned}\Delta\bar{S}_{mix} &\simeq k_B\frac{N_p}{N_t}\ln N_t - k_B\frac{1}{N_t}\frac{v_{ex}}{v_uN_t}\frac{N_p^2}{2} \\ &= k_B\phi\ln N_t - k_B\frac{v_{ex}}{v_u}\frac{\phi^2}{2} \end{aligned} \tag{2.4.6.11}$$

When we consider the volume of polymer as v_{ex}, interaction energy between polymer and solvent is automatically included. Therefore, $\Delta\bar{F}_{mix}$ is expressed as follows.

$$\Delta\bar{F}_{mix} = -T\Delta\bar{S}_{mix} = -k_BT\phi\ln N + k_BT\frac{v_{ex}}{v_u}\frac{\phi^2}{2} \tag{2.4.6.12}$$

Comparing ϕ^2 term in Eqs.(2.4.6.8) and (2.4.6.12), following result is obtained.

$$\frac{v_{ex}}{v_u} = 1-2\chi \tag{2.4.6.13}$$

[10] Here we ignore disorientation entropy. Ω_1 is the number of vacant lattice sites.

In addition, let us use the following relationships.

$$1 - x \simeq \frac{1}{1+x} \quad \text{for} \quad x \ll 1 \tag{2.4.6.14}$$

Then $I(\vec{q})$ is represented as follows.

$$I(\vec{q}) = \frac{d\sigma}{d\Omega}\frac{1}{V_{ir}} = (\Delta\rho)^2 v_u \frac{z\phi P(\vec{q})}{1 + (1-2\chi)zP(\vec{q})} \tag{2.4.6.15}$$

2.5 Phenomenological models

2.5.1 Landau free energy expansion

Here, I derive some structure factors from the effect of fluctuation of the volume fraction of polymers on free energy [48, 49]. Let us expand the free energy of the system as follows.

$$F = \int d\vec{r}\left[a_0 + a_1\varphi(\vec{r}) + a_2\varphi(\vec{r})^2 + a_3\varphi(\vec{r})^3 + \cdots + c_1(\nabla\varphi(\vec{r}))^2 + c_2(\Delta\varphi(\vec{r}))^2 + \cdots\right] \tag{2.5.1.1}$$

This expansion is just mathematical manipulation. Here, let us see the following special case.

$$F := \int d\vec{r}\left[a_2|\delta\varphi(\vec{r})|^2 + c_1|\nabla\delta\varphi(\vec{r})|^2 + c_2|\Delta\delta\varphi(\vec{r})|^2\right] \tag{2.5.1.2}$$

$\delta\varphi(\vec{r})$ stands for the deviation of φ from average value at $\vec{r}$. Here I assume that the system is isotropic: $\varphi(\vec{r}) = \varphi(r)$. Fourier transformation of $\delta\varphi(\vec{r})^2$, $(\nabla\delta\varphi(\vec{r}))^2$, and $(\Delta\delta\varphi(\vec{r}))^2$ are calculated as follows.

$$\delta\varphi(\vec{r}) = \frac{1}{(2\pi)^{3/2}}\int d\vec{q}\delta\varphi(\vec{q})e^{-i\vec{q}\cdot\vec{r}} \tag{2.5.1.3}$$

$$\nabla\delta\varphi(\vec{r}) = \frac{1}{(2\pi)^{3/2}}\int d\vec{q}(-i\vec{q})\delta\varphi(\vec{q})e^{-i\vec{q}\cdot\vec{r}} \tag{2.5.1.4}$$

$$\Delta\delta\varphi(\vec{r}) = \frac{1}{(2\pi)^{3/2}}\int d\vec{q}(-q^2)\delta\varphi(\vec{q})e^{-i\vec{q}\cdot\vec{r}} \tag{2.5.1.5}$$

$$\begin{aligned}
\int d\vec{r}|\delta\varphi(\vec{r})|^2 &= \frac{1}{(2\pi)^3}\int d\vec{r}\int d\vec{q}\int d\vec{q}'\left[\delta\varphi^*(\vec{q})e^{i\vec{q}\cdot\vec{r}}\right]\left[\delta\varphi(\vec{q}')e^{-i\vec{q}'\cdot\vec{r}}\right] \\
&= \frac{1}{(2\pi)^3}\int d\vec{q}\int d\vec{q}'\delta\varphi^*(\vec{q})\delta\varphi(\vec{q}')\int d\vec{r}e^{i(\vec{q}-\vec{q}')\cdot\vec{r}} \\
&= \frac{1}{(2\pi)^{3/2}}\int d\vec{q}\int d\vec{q}'\delta\varphi^*(\vec{q})\delta\varphi(\vec{q}')\delta(\vec{q}-\vec{q}') \\
&= \frac{1}{(2\pi)^{3/2}}\int d\vec{q}|\delta\varphi(\vec{q})|^2
\end{aligned} \tag{2.5.1.6}$$

$$\begin{aligned}
\int d\vec{r}|\nabla\delta\varphi(\vec{r})|^2 &= \frac{1}{(2\pi)^3}\int d\vec{r}\int d\vec{q}\int d\vec{q}'\left[i\vec{q}\delta\varphi^*(\vec{q})e^{i\vec{q}\cdot\vec{r}}\right]\left[-i\vec{q}'\delta\varphi(\vec{q}')e^{-i\vec{q}'\cdot\vec{r}}\right] \\
&= \frac{1}{(2\pi)^3}\int d\vec{q}\int d\vec{q}'\delta\varphi^*(\vec{q})\delta\varphi(\vec{q}')\vec{q}\cdot\vec{q}'\int d\vec{r}e^{i(\vec{q}-\vec{q}')\cdot\vec{r}} \\
&= \frac{1}{(2\pi)^{3/2}}\int d\vec{q}\int d\vec{q}'\delta\varphi^*(\vec{q})\delta\varphi(\vec{q}')\vec{q}\cdot\vec{q}'\delta(\vec{q}-\vec{q}') \\
&= \frac{1}{(2\pi)^{3/2}}\int d\vec{q}q^2|\delta\varphi(\vec{q})|^2
\end{aligned} \tag{2.5.1.7}$$

$$\begin{aligned}\int d\vec{r}|\Delta\delta\varphi(\vec{r})|^2 &= \frac{1}{(2\pi)^3}\int d\vec{r}\int d\vec{q}\int d\vec{q}'\left[(-q^2)\delta\varphi^*(\vec{q})e^{i\vec{q}\cdot\vec{r}}\right]\left[(-q'^2)\delta\varphi(\vec{q}')e^{-i\vec{q}'\cdot\vec{r}}\right]\\ &= \frac{1}{(2\pi)^3}\int d\vec{q}\int d\vec{q}'\delta\varphi^*(\vec{q})\delta\varphi(\vec{q}')q^2q'^2\int d\vec{r}e^{i(\vec{q}-\vec{q}')\cdot\vec{r}}\\ &= \frac{1}{(2\pi)^{3/2}}\int d\vec{q}\int d\vec{q}'\delta\varphi^*(\vec{q})\delta\varphi(\vec{q}')q^2q'^2\delta(\vec{q}-\vec{q}')\\ &= \frac{1}{(2\pi)^{3/2}}\int d\vec{q}q^4|\delta\varphi(\vec{q})|^2 \end{aligned} \tag{2.5.1.8}$$

Substitute Eqs.(2.5.1.6) $\sim$ (2.5.1.8) into Eq.(2.5.1.2):

$$F = \int d\vec{r}\left[a_2|\delta\varphi(\vec{r})|^2 + c_1|\nabla\delta\varphi(\vec{r})|^2 + c_2|\Delta\delta\varphi(\vec{r})|^2\right] = \frac{1}{(2\pi)^{3/2}}\int d\vec{q}[a_2 + c_1q^2 + c_2q^4]|\delta\varphi(\vec{q})|^2 \tag{2.5.1.9}$$

To calculate $|\delta\varphi(\vec{q})|$, I define $\delta\varphi(\vec{q}) =: x$ for a certain q. Then the thermal average of x^2 is calculated as follows.

$$\langle\, x^2\,\rangle = \frac{\displaystyle\int dx'x'^2\exp[-\beta\mathcal{H}_q(x')]}{\displaystyle\int dx'\exp[-\beta\mathcal{H}_q(x')]} \tag{2.5.1.10}$$

where

$$\mathcal{H}_q(x) := \frac{1}{(2\pi)^{3/2}}(a_2 + c_1q^2 + c_2q^4)x^2 =: \frac{\alpha}{\beta}x^2 \tag{2.5.1.11}$$

Here, $\mathcal{H}_q(x)$ stands for the energy contribution of q component to the whole energy F. To calculate further, I use the following formulae.

$$\int dx\exp[-\alpha x^2] = \sqrt{\frac{\pi}{\alpha}} \tag{2.5.1.12}$$

$$\int dxx^2\exp[-\alpha x^2] = \frac{1}{2\alpha}\sqrt{\frac{\pi}{\alpha}} \tag{2.5.1.13}$$

Substitute Eqs.(2.5.1.11) $\sim$ (2.5.1.13) to Eq.(2.5.1.10):

$$\begin{aligned}\langle\, x^2\,\rangle &= \frac{\displaystyle\int dx'x'^2\exp[-\alpha x^2]}{\displaystyle\int dx'\exp[-\alpha x^2]} = \frac{1}{2\alpha}\\ \rightarrow \langle\, |\delta\varphi(\vec{q})|^2\,\rangle &= \frac{1}{2\beta}\frac{(2\pi)^{3/2}}{a_2 + c_1q^2 + c_2q^4}\end{aligned} \tag{2.5.1.14}$$

Let us relate $\langle\, |\delta\varphi(\vec{q})|^2\,\rangle$ to scattering function, $S(\vec{q})$. Amplitude of neutron scattering from one nucleus, j, is represented as follows:

$$A_j(\vec{q},t) = A_0b_je^{i(\omega t - \vec{q}\cdot\vec{R}_j)} \tag{2.5.1.15}$$

For continuous media, we extend this equation as follows:

$$A(\vec{q},t) = A_0\int_V \Delta\rho\delta\varphi(\vec{r})e^{i(\omega t-\vec{q}\cdot\vec{r})}d\vec{r} \tag{2.5.1.16}$$

where $\Delta\rho$ is the difference of the scattering length density between solvents and polymers, $\delta\varphi(\vec{r})$ is a deviation

of the volume fraction of polymers at $\vec{r}$. Here, we concentrate on small angle region so as not to consider the small scale inhomogeneity such as one polymer coil and one mesh unit. Then scattering intensity is represented as follows:

$$\begin{aligned} I(\vec{q}) &= \frac{A(\vec{q},t)^2}{A_0^2 V} \\ &= \frac{\Delta\rho^2}{V}\int d\vec{r}\int d\vec{r}'\,\delta\varphi(\vec{r})\delta\varphi(\vec{r}')e^{i\vec{q}\cdot(\vec{r}-\vec{r}')} \\ &=: \Delta\rho^2\langle\delta\varphi^2\rangle\int d\vec{r}\gamma(\vec{r})e^{i\vec{q}\cdot\vec{r}} \end{aligned} \tag{2.5.1.17}$$

where $\gamma(\vec{r})$ a correlation function. Here, we use the following relation:

$$\langle\varphi(\vec{r})\delta\varphi(\vec{r}')\rangle = \gamma(\vec{r}-\vec{r}')\langle\delta\varphi^2\rangle =: \gamma(\vec{R})\langle\delta\varphi^2\rangle \tag{2.5.1.18}$$

Fourier transform of $\delta\varphi(\vec{r})\delta\varphi(\vec{r}')$ is $\langle\,|\delta\varphi(\vec{q})|^2\,\rangle$.

$$\begin{aligned} \int d\vec{r}\int d\vec{r}'\,\delta\varphi(\vec{r})\delta\varphi(\vec{r}')e^{i\vec{q}\cdot(\vec{r}-\vec{r}')} &= \int d\vec{r}\int d\vec{R}\delta\varphi(\vec{R}+\vec{r})\delta\varphi(\vec{R})e^{i\vec{q}\cdot\vec{r}} \\ &= \int d\vec{r}\int d\vec{R}\frac{1}{(2\pi)^3}\int d\vec{q}_1\delta\varphi(\vec{q}_1)e^{-i\vec{q}_1\cdot(\vec{R}+\vec{r})}\int d\vec{q}_2\delta\varphi(\vec{q}_2)e^{-i\vec{q}_2\cdot\vec{R}}e^{i\vec{q}\cdot\vec{r}} \\ &= \frac{1}{(2\pi)^3}\int d\vec{q}_1\int d\vec{q}_2\delta\varphi(\vec{q}_1)\delta\varphi(\vec{q}_2)\int d\vec{r}e^{i(\vec{q}-\vec{q}_1)\cdot\vec{r}}\int d\vec{R}e^{i(-\vec{q}_1-\vec{q}_2)\cdot\vec{R}} \\ &= \int d\vec{q}_1\int d\vec{q}_2\delta\varphi(\vec{q}_1)\delta\varphi(\vec{q}_2)\delta(\vec{q}-\vec{q}_1)\delta(-\vec{q}_1-\vec{q}_2) \\ &= \delta\varphi(\vec{q})\delta\varphi(-\vec{q}) \to \langle\,|\delta\varphi(\vec{q})|^2\,\rangle \end{aligned} \tag{2.5.1.19}$$

From Eqs.(2.5.1.14), (2.5.1.17), and (2.5.1.19), $I(\vec{q})$ from the system Eq.(2.5.1.2) is represented as follows.

$$I(\vec{q}) \propto \frac{1}{a_2 + c_1 q^2 + c_2 q^4} \tag{2.5.1.20}$$

Eq.(2.5.1.20) is called Teubner–Strey model and used to explain a peak observed in the scattering profile of microemulsions [49]. In the case of microemulsions, there is a tendency to create interfaces spontaneously (negative microscopic surface tension). To include this concept, $c_1 < 0$ is required. To make the system stable, additional term $c_2|\Delta\delta\varphi(\vec{r})|^2$ is required. To judge whether the system is stable or not, we use Eq.(2.5.1.9). If $a_2 + c_1q^2 + c_2q^4$ becomes negative, such q component is favorable compared to the reference state where $\delta\varphi(\vec{r}) = 0$ in all $\vec{r}$. Therefore, the fluctuation whose wavevector is q will grow and assumption Eq.(2.5.1.2) will no longer be acceptable. To prevent this, the following stability condition should be fulfilled.

$$c_1^2 - 4a_2c_2 < 0 \tag{2.5.1.21}$$

When $c_1 > 0$, the following energy expansion is also valid.

$$F := \int d\vec{r}\left[a_2|\delta\varphi(\vec{r})|^2 + c_1|\nabla\delta\varphi(\vec{r})|^2\right] \tag{2.5.1.22}$$

By setting $c_2 = 0$ in the previous derivation, the scattering function $I(\vec{q})$ from the system Eq.(2.5.1.22) is

represented as follows.

$$I(\vec{q}) \propto \frac{1}{a_2 + c_1 q^2} \tag{2.5.1.23}$$

Eq.(2.5.1.22) is called Ornstein–Zernike function and used to explain the scattering profile of semidilute solution and the vicinity of critical points [50]. I will show the different derivation of Eqs.(2.5.1.20) and (2.5.1.23) to see the physical meaning of parameters a_2, c_1, and c_2.

2.5.2 Debye-Bueche function

In Debye–Bueche function, we set $\gamma(\vec{r})$ (Eq.(2.5.1.18)) as follows:

$$\gamma(r) := e^{-r/\Xi} \tag{2.5.2.1}$$

where Ξ is a kind of correlation length. Since this function is isotropic (see Eq.(**??**)):

$$\begin{aligned} I(\vec{q}) &= \Delta\rho^2 \langle \delta\varphi^2 \rangle 4\pi \int_0^\infty r^2 \gamma(r) \frac{\sin qr}{qr} dr \\ &= \Delta\rho^2 \langle \delta\varphi^2 \rangle 4\pi \frac{1}{q} \int_0^\infty r e^{-r/\Xi} \sin qr dr \end{aligned} \tag{2.5.2.2}$$

Integral part of Eq.(2.5.2.2) is calculated as follows[11]:

$$\begin{aligned} \int_0^\infty r e^{-r/\Xi} \sin qr dr &= \Im \left(\int_0^\infty r e^{-r/\Xi} e^{iqr} dr \right) \\ &= \Im \left(\int_0^\infty r e^{(iq - \frac{1}{\Xi})r} dr \right) \\ &= \Im \left(\left[\frac{r}{iq - \frac{1}{\Xi}} e^{(iq - \frac{1}{\Xi})r} \right]_0^\infty - \frac{1}{iq - \frac{1}{\Xi}} \int_0^\infty e^{(iq - \frac{1}{\Xi})r} dr \right) \\ &= \Im \left(-\frac{1}{(iq - \frac{1}{\Xi})^2} \left[e^{(iq - \frac{1}{\Xi})r} \right]_0^\infty \right) \\ &= \Im \left(\frac{1}{(iq - \frac{1}{\Xi})^2} \frac{(iq + \frac{1}{\Xi})^2}{(iq + \frac{1}{\Xi})^2} \right) \\ &= \Im \left(\frac{-q^2 + 2i\frac{q}{\Xi} + \frac{1}{\Xi^2}}{(-q^2 - \frac{1}{\Xi^2})^2} \right) \\ &= 2\frac{q}{\Xi} \frac{1}{(-q^2 - \frac{1}{\Xi^2})^2} \\ &= 2q \frac{\Xi^3}{(1 + q^2\Xi^2)^2} \end{aligned} \tag{2.5.2.3}$$

Substitute Eq.(2.5.2.3) into Eq.(2.5.2.2):

$$I(\vec{q}) = \Delta\rho^2 \langle \delta\varphi^2 \rangle \frac{8\pi\Xi^3}{(1 + q^2\Xi^2)^2} \tag{2.5.2.4}$$

[11] $\Im$ represents the extraction of an imaginary part.

2.5.3 Ornstein–Zernike function

Let us consider the SANS profile from semi-dilute solution. Scattering from semi-dilute solution is originated from the fluctuation of concentration. This fluctuation is quantitatively represented by a parameter K_{os}, called osmotic modulus as mentioned later. In the case of Ornstein–Zernike function, we set $\gamma(\vec{r})$ as follows:

$$\gamma(r) := \frac{\xi}{r} e^{-r/\xi} \tag{2.5.3.1}$$

where ξ is a kind of correlation length. Since this function is isotropic:

$$\begin{aligned} I(\vec{q}) &= \Delta\rho^2 \langle \delta\varphi^2 \rangle 4\pi \int_0^\infty r^2 \gamma(r) \frac{\sin qr}{qr} dr \\ &= \Delta\rho^2 \langle \delta\varphi^2 \rangle \frac{4\pi\xi}{q} \int_0^\infty e^{-r/\xi} \sin qr dr \end{aligned} \tag{2.5.3.2}$$

Integral part of Eq.(2.5.3.2) is calculated as follows:

$$\begin{aligned} \int_0^\infty e^{-r/\xi} \sin qr dr &= \Im \left(\int_0^\infty e^{-r/\xi} e^{iqr} dr \right) \\ &= \Im \left(\int_0^\infty e^{(iq - \frac{1}{\xi})r} dr \right) \\ &= \Im \left(\left[\frac{1}{iq - \frac{1}{\xi}} e^{(iq - \frac{1}{\xi})r} \right]_0^\infty \right) \\ &= \Im \left(-\frac{1}{iq - \frac{1}{\xi}} \right) \\ &= \Im \left(-\frac{iq + \frac{1}{\xi}}{(iq - \frac{1}{\xi})(iq + \frac{1}{\xi})} \right) \\ &= \Im \left(\frac{iq + \frac{1}{\xi}}{q^2 + \frac{1}{\xi^2}} \right) \\ &= \frac{q}{q^2 + \frac{1}{\xi^2}} \end{aligned} \tag{2.5.3.3}$$

Substitute Eq.(2.5.3.3) into Eq.(2.5.3.2):

$$I(\vec{q}) = \Delta\rho^2 \langle \delta\varphi^2 \rangle \frac{4\pi\xi^3}{1 + q^2\xi^2} \tag{2.5.3.4}$$

Intensity at $q = 0$

Let us consider the scattering intensity at $q = 0$. This means that we do not have to care the interference effect. Our start point is Eq.(2.1.15):

$$\begin{aligned} S(\vec{q}) &= 1 + \int (g(\vec{r}) - \varrho_2) e^{i\vec{q}\cdot\vec{r}} d\vec{r} \\ \rightarrow S(0) &= 1 + \int (g(\vec{r}) - \varrho_2) d\vec{r} \end{aligned} \tag{2.5.3.5}$$

where ϱ_2 is the number density of monomer units. Notice that we use the density of monomer units instead of polymers. This assumption is based on the fact that the physical properties at semi-dilute region is depends

only on polymer fraction and does not depend on the degree of polymerization.

Let us define N_2 as the number of monomer units in the irradiated volume V_0:

$$N_2 := \varrho_2 V_0 \tag{2.5.3.6}$$

Then the average value of N_2^2 is represented as follows:

$$\begin{aligned}
\langle N_2^2 \rangle &= \varrho_2 \int_{V_0} \int_{V_0} G(\vec{r}_2 - \vec{r}_1, t=0) d\vec{r}_1 d\vec{r}_2 \\
&= \langle N_2 \rangle \int_{V_0} (\delta(\vec{r}_2 - \vec{r}_1) + g(\vec{r}_2 - \vec{r}_1)) d\vec{r}_2 \\
&= \langle N_2 \rangle \left(1 + \int_{V_0} g(\vec{r}) d\vec{r} \right)
\end{aligned} \tag{2.5.3.7}$$

where

$$\langle N_2 \rangle = \int_{V_0} \varrho_2 d\vec{r} \tag{2.5.3.8}$$

is the average value of N_2.

Substitute Eq.(2.5.3.7) into Eq.(2.5.3.5):

$$\begin{aligned}
S(0) &= \frac{\langle N_2 \rangle \left(\int g(\vec{r}) d\vec{r} \right)}{\langle N_2 \rangle} + \int \varrho_2 d\vec{r} \\
&= \frac{\langle N_2^2 \rangle}{\langle N_2 \rangle} - \langle N_2 \rangle \\
&= \frac{\langle N_2^2 \rangle - \langle N_2 \rangle^2}{\langle N_2 \rangle} \\
&= \frac{\langle N_2^2 - 2N_2 \langle N_2 \rangle + \langle N_2 \rangle^2 \rangle}{\langle N_2 \rangle} \\
&= \frac{\langle (N_2 - \langle N_2 \rangle)^2 \rangle}{\langle N_2 \rangle} = \frac{\langle (\Delta N_2)^2 \rangle}{\langle N_2 \rangle}
\end{aligned} \tag{2.5.3.9}$$

where

$$\Delta N_2 := N_2 - \langle N_2 \rangle \tag{2.5.3.10}$$

Under equilibrium condition, ΔN_2 is represented as follows:

$$\langle (\Delta N_2)^2 \rangle = \frac{\int (\Delta N_2)^2 P(\Delta N_2) d(\Delta N_2)}{\int P(\Delta N_2) d(\Delta N_2)} \tag{2.5.3.11}$$

where

$$P(\Delta N_2) := C \exp \left[\frac{\Delta G(\Delta N_2)}{k_B T} \right] \tag{2.5.3.12}$$

$P(\Delta N_2)$ represents the Boltzmann distribution. Notice that the denominator of Eq.(2.5.3.12) is $k_B T$ (instead of RT) since we consider the change of Gibbs energy caused by the change of number (instead of number of moles).

From now, we relate Eq.(2.5.3.11) to the chemical potential of the solution, and then osmotic pressure. ΔG is represented by using chemical potential, μ, and the number of moles of solvents in the irradiated volume, n_1:

$$\Delta G = \int dG = \int_{n_1}^{n_1'} (\mu' - \mu) dx = \int_{n_1}^{n_1'} \frac{\partial \mu}{\partial n_1}(x - n_1) dx = \frac{1}{2}\frac{\partial \mu}{\partial n_1}(\Delta n_1)^2 \tag{2.5.3.13}$$

where

$$\Delta n_1 := n_1' - n_1 \tag{2.5.3.14}$$

Since $n_1 = N_1/N_A$,

$$\Delta G = \frac{1}{2}\frac{\partial \mu}{\partial N_1}\frac{dN_1}{n_1}\left(\frac{1}{N_A} N_A \Delta n_1\right)^2 = \frac{1}{2N_A}\frac{\partial \mu}{\partial N_1}(\Delta N_1)^2 \tag{2.5.3.15}$$

Then, we relate ΔN_1 (the change of number of solvents) to ΔN_2 (the change of number of monomers) via the change of number concentration, Δc. The number concentration, c [m^{-3}], is represented as follows:

$$c = \frac{N_2}{V_0} \simeq \frac{N_2}{N_1 \overline{V}_1 / N_A} \tag{2.5.3.16}$$

Differentiate both sides of Eq.(2.5.3.16) by N_1:

$$\frac{\partial c}{\partial N_1} \simeq -\frac{N_2}{N_1^2 \overline{V}_1 / N_A} \simeq -\frac{c}{N_1} \simeq -\frac{c\overline{V}_1}{V_0 N_A} \tag{2.5.3.17}$$

By using Eqs.(2.5.3.16) and (2.5.3.17):

$$\Delta c = \frac{\Delta N_2}{V_0} = \frac{c\overline{V}_1}{V_0 N_A}\Delta N_1 \tag{2.5.3.18}$$

Then, we can relate ΔN_1 and ΔN_2 as follows:

$$\Delta N_1 = -\frac{N_A}{c\overline{V}_1}\Delta N_2 \tag{2.5.3.19}$$

Substitute Eq.(2.5.3.19) into Eq.(2.5.3.15):

$$\begin{aligned}
\Delta G &= \frac{1}{2N_A}\frac{\partial \mu}{\partial N_2}\frac{N_2}{N_1}\left(\frac{N_A}{c\overline{V}_1}\right)^2 (\Delta N_2)^2 \\
&= -\frac{1}{2N_A}\frac{\partial \mu}{\partial N_2}\frac{c\overline{V}_1}{N_A}\left(\frac{N_A}{c\overline{V}_1}\right)^2 (\Delta N_2)^2 \\
&= -\frac{1}{2}\frac{\partial \mu}{\partial N_2}\frac{1}{c\overline{V}_1}(\Delta N_2)^2
\end{aligned} \tag{2.5.3.20}$$

Substitute Eq.(2.5.3.20) into Eq.(2.5.3.12) and then into Eq.(2.5.3.11) [12]:

$$\begin{aligned}\langle\,(\Delta N_2)^2\,\rangle &= \frac{\displaystyle\int (\Delta N_2)^2 \exp\left[-\frac{1}{2k_BTc\overline{V}_1}\frac{\partial\mu}{\partial N_2}(\Delta N_2)^2\right] d(\Delta N_2)}{\displaystyle\int \exp\left[-\frac{1}{2k_BTc\overline{V}_1}\frac{\partial\mu}{\partial N_2}(\Delta N_2)^2\right] d(\Delta N_2)} \\ &= -k_BTc\overline{V}_1\left(\frac{\partial\mu}{\partial N_2}\right)^{-1} \end{aligned} \tag{2.5.3.21}$$

From now, we relate μ to the osmotic pressure, Π. Let us define μ° as the chemical potential of solvent and μ as that of solution. Definition of osmotic pressure, Π, is as follows: we contact the solvent and solution via semipermeable membrane. Then, this system shows difference of pressure between the solvent and solution at equilibrium. Mathematically, this condition is represented as follows since the chemical potential of two liquid should be the same at equilibrium:

$$\mu^\circ(P_0) = \mu(P_0+\Pi) =: \mu(P_0) + \Delta\mu \tag{2.5.3.22}$$

where P_0 implies ordinary pressure. Additional chemical potential, $\Delta\mu$, is represented by the following integral form:

$$\Delta\mu = \int_{P_0}^{P_0+\Pi} \frac{\partial\mu}{\partial P} dP \tag{2.5.3.23}$$

Here, we use the definition of chemical potential:

$$\mu = \frac{\partial G}{\partial n_1} \tag{2.5.3.24}$$

Then $\partial\mu/\partial P$ is represented as follows:

$$\frac{\partial\mu}{\partial P} = \frac{\partial}{\partial P}\left(\frac{\partial G}{\partial n_1}\right) = \frac{\partial}{\partial n_1}\left(\frac{\partial G}{\partial P}\right) = \frac{\partial V}{\partial n_1} = \overline{V}_1 \tag{2.5.3.25}$$

since

$$\begin{aligned} dG &= V\,dP - S\,dT \\ \rightarrow \frac{\partial G}{\partial P} &= V \end{aligned} \tag{2.5.3.26}$$

where V is the volume of solution and $\overline{V}_1$ is partial molar volume of the solvent.

Let us assume that $\overline{V}_1$ remains constant under the pressure $P = P_0 \sim P_0 + \Pi$. Then, substitute Eq.(2.5.3.25) into Eq.(2.5.3.23):

$$\Delta\mu = \int_{P_0}^{P_0+\Pi} \overline{V}_1 dP = \Pi\overline{V}_1 dP \tag{2.5.3.27}$$

Then, we can see the relationship between μ and Π:

$$\Pi = \frac{\mu^\circ - \mu}{\overline{V}_1} \tag{2.5.3.28}$$

[12] $\displaystyle\int_{-\infty}^{\infty} \exp\left(-ax^2\right) dx = \sqrt{\pi}a^{-1/2}$, $\displaystyle\int_{-\infty}^{\infty} x^2 \exp\left(-ax^2\right) dx = \sqrt{\pi}a^{-3/2}/2$.

Let us differentiate both sides of Eq.(2.5.3.28) by c (use Eq.(2.5.3.16)):

$$\frac{\partial \Pi}{\partial c} = -\frac{1}{\overline{V}_1}\frac{\partial \mu}{\partial c} = -\frac{1}{\overline{V}_1}\frac{\partial \mu}{\partial N_2}\frac{dN_2}{dc} = -\frac{V_0}{\overline{V}_1}\frac{\partial \mu}{\partial N_2} \tag{2.5.3.29}$$

Substitute Eqs.(2.5.3.16), (2.5.3.21) and (2.5.3.29) into Eq.(2.5.3.9):

$$S(0) = \frac{-k_B T c \overline{V}_1 \left(-\dfrac{\overline{V}_1}{V_0}\dfrac{\partial \Pi}{\partial c}\right)^{-1}}{cV_0} = k_B T \left(\frac{\partial \Pi}{\partial c}\right)^{-1} \tag{2.5.3.30}$$

Next, we define the quantity called osmotic modulus. This quantity is similar to bulk modulus defined for elastic bodies. Bulk modulus, K, for an elastic body whose volume is V is defined as follows:

$$K := -V\frac{\partial P}{\partial V} \simeq \frac{\Delta P}{-\Delta V/V} \tag{2.5.3.31}$$

This quantity implies how large the pressure is required for changing the volume. To say briefly, this shows the stiffness of the matter.

Osmotic modulus is defined for solutions. Bulk modulus, K_{os}, for a solution whose monomer fraction is ϕ is defined as follows:

$$K_{os} := \phi\frac{\partial \Pi}{\partial \phi} \simeq \frac{\Delta \Pi}{\Delta\phi/\phi} \tag{2.5.3.32}$$

Notice that the sign is different between K and K_{os} since the behavior against $\Delta P > 0$ is opposite; the volume is decreased ($\Delta V < 0$) while the monomer fraction is increased ($\Delta\phi > 0$).

Now let us represent $S(0)$ by using K_{os}. Before that, we represent ϕ by using c. Here, we use the lattice model whose mesh size is a. Then, c (the number concentration of monomer units) is represented as follows:

$$c = \frac{\phi}{a^3} \tag{2.5.3.33}$$

Substitute Eqs.(2.5.3.32) and (2.5.3.33) into Eq.(2.5.3.30):

$$S(0) = k_B T \left(\frac{\partial \Pi}{\partial \phi}\frac{d\phi}{dc}\right)^{-1} = k_B T \left(\frac{1}{\phi}\frac{\partial \Pi}{\partial \phi}a^3\right)^{-1} = \frac{k_B T \phi}{a^3 K_{os}} \tag{2.5.3.34}$$

Then we convert Eq.(2.5.3.34) into the absolute intensity of SANS experiment [13]:

$$I(q) = \frac{1}{V_0}\left.\frac{d\sigma}{d\Omega}\right|_{coh} = \frac{1}{V_0}(\langle\, \Delta b \,\rangle)^2 N_2 S(q) \tag{2.5.3.35}$$

Here, the number of solutes in the irradiated volume, N_2, is represented by using ϕ and a:

$$N_2 = \frac{V_0}{a^3}\phi \tag{2.5.3.36}$$

Notice that V_0/a^3 implies the total number of lattice in the irradiated volume. In the context of the lattice model, the difference of scattering length density, $\Delta\rho$, is represented as follows:

$$\Delta\rho = \frac{\langle\, \Delta b \,\rangle}{a^3} \tag{2.5.3.37}$$

[13] We ignore the incoherent component.

Substitute Eqs.(2.5.3.34), (2.5.3.36) and (2.5.3.37) into Eq.(2.5.3.35):

$$I(0) = \frac{1}{V_0}(\langle b \rangle)^2 \frac{V_0}{a^3}\phi \frac{k_B T \phi}{a^3 K_{os}} = \frac{(\Delta\rho)^2 k_B T \phi^2}{K_{os}} \tag{2.5.3.38}$$

2.5.4 Teubner–Strey function

In the case of Teubner–Strey function, we set $\gamma(\vec{r})$ as follows:

$$\gamma(r) := \frac{d}{2\pi r} e^{-r/\xi} \sin \frac{2\pi r}{d} \tag{2.5.4.1}$$

Here two length parameters, d and ξ, is introduced.

Since this function is isotropic:

$$\begin{aligned} I(\vec{q}) &= \Delta\rho^2 \langle \delta\varphi^2 \rangle 4\pi \int_0^\infty r^2 \gamma(r) \frac{\sin qr}{qr} dr \\ &= \Delta\rho^2 \langle \delta\varphi^2 \rangle \frac{2d}{q} \int_0^\infty e^{-r/\xi} \sin qr \sin \frac{2\pi r}{d} dr \\ &= \Delta\rho^2 \langle \delta\varphi^2 \rangle \frac{d}{q} \int_0^\infty e^{-r/\xi} \left[-\cos\left(q + \frac{2\pi}{d}\right) r + \cos\left(q - \frac{2\pi}{d}\right) r \right] dr \end{aligned} \tag{2.5.4.2}$$

Here, I use the following relationship.

$$\begin{aligned} \int_0^\infty e^{-r/\xi} \cos \alpha r dr &= \Re \left(\int_0^\infty e^{(i\alpha - \frac{1}{\xi})r} dr \right) \\ &= \Re \left(\frac{i\alpha + \frac{1}{\xi}}{\alpha^2 + \frac{1}{\xi^2}} \right) \\ &= \frac{\xi}{1 + \alpha^2 \xi^2} \end{aligned} \tag{2.5.4.3}$$

Substitute Eq.(2.5.4.3) to Eq.Eq.(2.5.4.2):

$$\begin{aligned} &\frac{d}{q} \int_0^\infty e^{-r/\xi} \left[-\cos\left(q + \frac{2\pi}{d}\right) r + \cos\left(q - \frac{2\pi}{d}\right) r \right] dr \\ &= \frac{d}{q} \left[-\frac{\xi}{1 + (q + \frac{2\pi}{d})^2 \xi^2} + \frac{\xi}{1 + (q - \frac{2\pi}{d})^2 \xi^2} \right] \\ &= \frac{8\pi\xi^3}{(1 + \frac{4\pi^2}{d^2}\xi^2)^2 + (2\xi^2 - \frac{8\pi^2}{d^2}\xi^4) q^2 + \xi^4 q^4} \end{aligned} \tag{2.5.4.4}$$

Substitute Eq.(2.5.4.4) into Eq.(2.5.4.2):

$$I(\vec{q}) = \Delta\rho^2 \langle \delta\varphi^2 \rangle \frac{8\pi\xi^3}{(1 + \frac{4\pi^2}{d^2}\xi^2)^2 + (2\xi^2 - \frac{8\pi^2}{d^2}\xi^4) q^2 + \xi^4 q^4} \tag{2.5.4.5}$$

3 Basic Theory — Physical Properties

3.1 Dynamics of polymers

As mentioned later (Eq.(4.2.4.30)), what we obtain from a neutron spin echo experiment is normalized intermediate functions, $I(\vec{q},t)$ and $I_s(\vec{q},t)$ (Eqs.(4.2.1.40) and (4.2.1.41)):

$$I(\vec{q},t) := \frac{1}{N}\sum_{j,j'}\langle e^{-i\vec{q}\cdot\vec{R}_{j'}(0)}e^{i\vec{q}\cdot\vec{R}_j(t)}\rangle \tag{3.1.1}$$

$$I_s(\vec{q},t) := \frac{1}{N}\sum_{j}\langle e^{-i\vec{q}\cdot\vec{R}_{j}(0)}e^{i\vec{q}\cdot\vec{R}_j(t)}\rangle \tag{3.1.2}$$

Eq.(3.1.1) is a coherent part and Eq.(3.1.2) is an incoherent part. In the Gaussian approximation, the distribution of particle positions is described by a Gaussian distribution, as follows [51]:

$$I(\vec{q},t) = \frac{1}{N}\sum_{j,j'}\exp\left[-\frac{q^2}{6}\langle(\vec{R}_j(t)-\vec{R}_{j'}(0))^2\rangle\right] \tag{3.1.3}$$

$$I_s(\vec{q},t) = \frac{1}{N}\sum_{j}\exp\left[-\frac{q^2}{6}\langle(\vec{R}_j(t)-\vec{R}_{j}(0))^2\rangle\right] \tag{3.1.4}$$

The form of $I(\vec{q},t)$ is more complicated compared to $I_s(\vec{q},t)$ since we have to consider correlations between all of the monomers. So we first derive the representation of $I_s(\vec{q},t)$ briefly. Then we move on to the representation of $I(\vec{q},t)$.

3.1.1 Incoherent component

From now, we derive $\langle(\vec{R}_j(t)-\vec{R}_j(0))^2\rangle$ for various motions [23]. This corresponds to the dynamics of self correlation. In this subsection, we omit the subscript j.

Brownian motion

If the monomers feel only the stochastic force, the motion becomes Brownian motion. In this case, the displacement of monomers is described by using their diffusion constant, D:

$$\langle(\vec{R}(t)-\vec{R}(0))^2\rangle = 6Dt \tag{3.1.1.1}$$

This means that the relaxation rate is proportional to t:

$$I_s(\vec{q},t) \propto \exp\left[-q^2Dt\right] \tag{3.1.1.2}$$

Rouse mode

Then let us think about the effect of connectivity on polymer dynamics. Here, we use the concept of relaxation time. Relaxation time is time required for a certain chain section to move a distance of order of its own size. For all unentangled polymers which is composed of N monomers, there are N different relaxation modes. These modes are labeled by mode index $p = 1, 2, 3, \ldots, N$. Each mode has corresponding

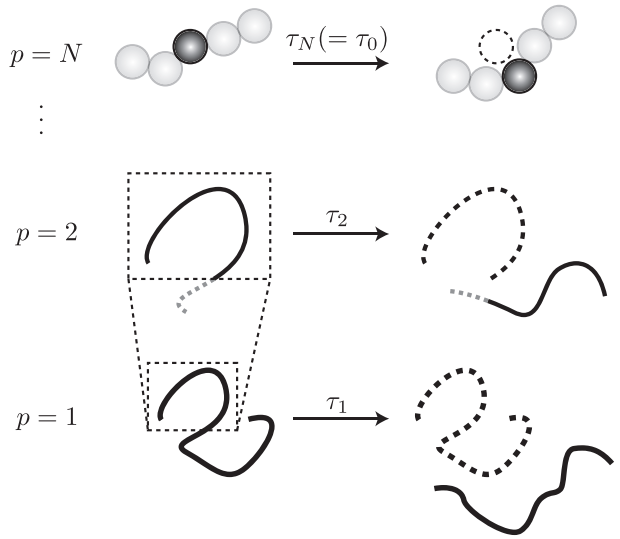

Figure 3.1: The concept of relaxation time. Relaxation time τ_p is time required for a chain section whose length is N/p to move a distance of order of its own size. In the case where $p = 1$, τ_1 implies the relaxation time of a whole polymer. In the case where $p = N$, τ_N implies the relaxation time of one monomer. This relaxation time is referred to as τ_0.

relaxation time represented by τ_p. τ_p is the relaxation time of a chain section whose length is N/p. $\tau_N =: \tau_0$ is the relaxation time of monomer and τ_1 is that of whole polymer (Fig.3.1).

Let us think about the unentangled melt. In this case, each section can be regarded as an ideal Gaussian chain. From the definition of relaxation time, $\langle(\vec{R}(\tau_p^R) - \vec{R}(0))^2\rangle$ is the order of the square of their own size, $b(N/p)^{1/2}$ (ideal chain):

$$\langle(\vec{R}(\tau_p^R) - \vec{R}(0))^2\rangle \simeq \left(b\left(\frac{N}{p}\right)^{1/2}\right)^2 = b^2\frac{N}{p} \tag{3.1.1.3}$$

where b is the length of one monomer. Superscript R implies Rouse mode, as mentioned later.

From now, we connect τ_p^R and N/p. For a polymer composed of N monomers, the longest relaxation time, τ_1^R, can be represented formally as follows by using Eq.(3.1.1.1):

$$\tau_1^R \simeq \frac{\langle(\vec{R}(t) - \vec{R}(0))^2\rangle}{6D_R} \simeq \frac{(bN^{1/2})^2}{D_R} \tag{3.1.1.4}$$

where D_R is a diffusion constant of the polymer. A difference from simple Brownian motion is the N-dependence of the diffusion constant. This diffusion constant is calculated by using a friction coefficient of the polymer, ζ_R (the Einstein relation):

$$D_R = \frac{k_B T}{\zeta_R} \tag{3.1.1.5}$$

Here, we assume that the friction coefficient of the polymer is the sum of that of monomers, ζ_0: [14]

$$\zeta_R := N\zeta_0 \tag{3.1.1.6}$$

[14] In the case of Brownian motion, $\zeta \propto \eta_s R$. Although there is no concept of relaxation in the case of Brownian motion, the representation of ζ is the same as Zimm mode, as mentioned later.

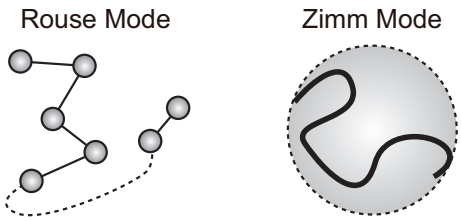

Figure 3.2: Model of Rouse mode and Zimm mode. Left: Model of Rouse mode. A polymer is assumed to be composed of the beads connected by springs. The number of beads is the same as that of monomers. Right: Model of Zimm mode. Since each monomer interacts each other via hydrodynamic interactions, a section of N/p monomers is treated as one sphere.

This means we assume that ζ_0 is additive quantity. The physical meaning of this is that each monomer feels force independently. In this respect, the bead-spring model is used for this situation (Fig.3.2, left).

Substitute Eq.(3.1.1.5) and (3.1.1.6) into Eq.(3.1.1.4):

$$\tau_1^R \simeq \frac{\zeta_0 b^2}{k_B T} N^2 =: \tau_0 N^2 \tag{3.1.1.7}$$

By using this relation, we can calculate the relaxation time of mode p:

$$\tau_p^R \simeq \tau_0 \left(\frac{N}{p}\right)^2 \tag{3.1.1.8}$$

Substitute Eq.(3.1.1.8) into Eq.(3.1.1.3):

$$\langle (\vec{R}(\tau_p^R) - \vec{R}(0))^2 \rangle \simeq b^2 \left(\frac{\tau_p^R}{\tau_0}\right)^{1/2} \tag{3.1.1.9}$$

This can be generalized as follows:

$$\langle (\vec{R}(t) - \vec{R}(0))^2 \rangle \simeq b^2 \left(\frac{t}{\tau_0}\right)^{1/2} \quad \text{for} \quad \tau_0 < t < \tau_1^R \tag{3.1.1.10}$$

This means that the segment correlation function is proportional to $t^{1/2}$. Notice that the Brownian motion follows linear t-dependence (Eq.(3.1.1.1)). This can be qualitatively understood that the monomer shows Brownian motion on the Brownian motion of the polymer. This motion is a kind of subdiffusive motion and referred to as Rouse mode. After complete relaxation ($\tau_1^R < t$), polymer begins to show the Brownian (diffusive) motion.

Zimm mode

In the case of Rouse mode (polymer melt), there is no long-range force from the surrounding solvent, called hydrodynamic interaction. The motion under the existence of hydrodynamic interaction is called Zimm mode. In this motion, N-dependence of the friction coefficient, ζ_Z, is different from that of Rouse

mode ($\zeta_R \propto N$, Eq.(3.1.1.6)). Here, we use the relationship called Stokes law:

$$\zeta_Z \simeq \eta_s R = \eta_s b N^\nu \tag{3.1.1.11}$$

where η_s is the viscosity of solvent, R is the radius of polymer in the solution called hydrodynamic radius, ν is the swelling exponent. Notice that ζ_0 does not affect ζ. This is because each section is regarded as one sphere due to hydrodynamic interactions (Fig.3.2, right). Then, the longest relaxation time, τ_1^Z, can be derived similar to Eq.(3.1.1.4)[15]:

$$\tau_1^Z \simeq \frac{(bN^\nu)^2}{D_Z} \simeq \frac{(bN^\nu)^2}{k_B T/(\eta_s b N^\nu)} = \frac{\eta_s b^3}{k_B T} N^{3\nu} =: \tau_0 N^{3\nu} \tag{3.1.1.12}$$

and

$$\tau_p^Z \simeq \tau_0 \left(\frac{N}{p}\right)^{3\nu} \tag{3.1.1.13}$$

From definition of relaxation time (similar to Eq.(3.1.1.3)),

$$\langle (\vec{R}(\tau_p^Z) - \vec{R}(0))^2 \rangle \simeq \left(b \left(\frac{N}{p}\right)^\nu \right)^2 = b^2 \left(\frac{N}{p}\right)^{2\nu} \tag{3.1.1.14}$$

Substitute Eq.(3.1.1.13) into Eq.(3.1.1.14):

$$\langle (\vec{R}(\tau_p^Z) - \vec{R}(0))^2 \rangle \simeq b^2 \left(\frac{\tau_p^Z}{\tau_0}\right)^{2/3} \tag{3.1.1.15}$$

This can be generalized as follows:

$$\langle (\vec{R}(t) - \vec{R}(0))^2 \rangle \simeq b^2 \left(\frac{t}{\tau_0}\right)^{2/3} \quad \text{for} \quad \tau_0 < t < \tau_1^Z \tag{3.1.1.16}$$

This means that the segment correlation function is proportional to $t^{2/3}$.

3.1.2 Coherent component

From now, we see $\langle (\vec{R}_j(t) - \vec{R}_{j'}(0))^2 \rangle$ for various motions. We skip the derivation since it is quite complicated. Instead of this, we see the important results during the derivation [23, 52].

Rouse mode

In the case of polymer melt without entanglement, the dynamics of jth monomer in a polymer is described by a following equation:

$$\zeta_0 \frac{\partial \vec{R}_j}{\partial t} = \nabla_j V(\vec{R}_j) + \vec{f}_j(t) \tag{3.1.2.1}$$

where $\vec{R}_j$ is the position of jth monomer, $V(\vec{R}_j)$ is the free energy of the polymer chain and $\vec{f}_j(t)$ is the

[15] Although this derivation is qualitative, τ_0 should be the same as that of Rouse mode (Eq.(3.1.1.7)) in principle.

stochastic force from the heat bath on jth monomer. The force $\nabla_j V(\vec{R}_j)$ is considered to be a contribution of entropic springs. In this case, we can write Eq.(3.1.2.1) in more concrete form:

$$\zeta_0 \frac{\partial \vec{R}_j}{\partial t} = \frac{3k_BT}{b^2} \frac{\partial^2 \vec{R}_j}{\partial j^2} + \vec{f}_j(t) \tag{3.1.2.2}$$

where k_BT/b^2 is a spring constant. Here, we regard j as a continuous variable.

By solving this equation, we can calculate the time-dependent thermally averaged mean square displacement:

$$\langle (\vec{R}_j(t) - \vec{R}_{j'}(0))^2 \rangle = 6D_R t + |j - j'|b^2 + \frac{4Nb^2}{\pi^2} \sum_{p=1}^{N} \frac{1}{p^2} \cos\frac{p\pi j}{N} \cos\frac{p\pi j'}{N} \left(1 - \exp\left(-\frac{p^2 t}{\tau_1^R}\right)\right) \tag{3.1.2.3}$$

Briefly speaking, the first term implies the diffusive motion of center of gravity ($\langle\langle (\vec{R}_j(t) - \vec{R}_j(0))^2 \rangle\rangle$). The second term implies the average distance between jth and j'th monomers ($\langle\langle (\vec{R}_j(t) - \vec{R}_{j'}(t))^2 \rangle\rangle$). The third term is the summation of a characteristic term of Rouse mode: effect of connectivity. p is the index of the relaxation modes.

When $j = j'$ (incoherent term) and $t < \tau_1^R$, this can be calculated as the following brief form:

$$\langle (\vec{R}_j(t) - \vec{R}_j(0))^2 \rangle = 2b^2 \left(\frac{3k_BTt}{\pi\zeta_0 b^2}\right)^{1/2} \propto b^2 \left(\frac{t}{\tau_0}\right)^{1/2} \tag{3.1.2.4}$$

Here, we used Eq.(3.1.1.7). This result is the same as that of Eq.(3.1.1.10).

Substitute Eq.(3.1.2.4) into Eq.(3.1.4):

$$\begin{aligned} I_s(\vec{q}, t) &= \exp\left[-\frac{q^2}{6} 2b^2 \left(\frac{3k_BTt}{\pi\zeta_0 b^2}\right)^{1/2}\right] \\ &= \exp\left[-\frac{2}{\pi^{1/2}} \left(\frac{1}{12} k_BT \frac{b^2}{\zeta_0} q^4 t\right)^{1/2}\right] \end{aligned} \tag{3.1.2.5}$$

Let us define the characteristic rate of the Rouse dynamics, $\Omega_R(q)$:

$$\Omega_R(q) := \frac{1}{12} k_BT \frac{b^2}{\zeta_0} q^4 \tag{3.1.2.6}$$

Substitute Eq.(3.1.2.6) into Eq.(3.1.2.5):

$$\boxed{I_s(\vec{q}, t) = \exp\left[-\frac{2}{\pi^{1/2}} \left(\Omega_R(q) t\right)^{1/2}\right]} \tag{3.1.2.7}$$

To see the coherent term ($j \neq j'$), let us substitute Eq.(3.1.2.3) into Eq.(3.1.3):

$$\begin{aligned} &I(\vec{q}, t) \\ &= \frac{1}{N} \sum_{j,j'} \exp\left[-q^2 D_R t - \frac{1}{6}|j - j'|q^2 b^2 - \frac{2Nb^2q^2}{3\pi^2} \sum_{p} \frac{1}{p^2} \cos\frac{p\pi j}{N} \cos\frac{p\pi j'}{N} \left(1 - \exp\left(-\frac{p^2 t}{\tau_1^R}\right)\right)\right] \end{aligned} \tag{3.1.2.8}$$

First, let us see the case where q is small. When $q(bN^{1/2}) \ll 1$, we cannot see the internal motion of polymers. In this case, what we see is the diffusive motion of the center of gravity of the polymer. This

statement is verified mathematically:

$$I(\vec{q},t) \simeq \frac{1}{N}\sum_{j,j'} \exp\left[-q^2 D_R t\right] = N\exp\left[-q^2 D_R t\right] \quad \text{for} \quad q(bN^{1/2}) \ll 1 \tag{3.1.2.9}$$

Then let use see the opposite case: $q(bN^{1/2}) \gg 1$. In this case, we concentrate on short time behavior ($t < \tau_1^R$) since the signal completely decays when t is large. Eq.(3.1.2.3) is converted into the following form:

$$\begin{aligned}
&\langle(\vec{R}_j(t) - \vec{R}_{j'}(0))^2\rangle \\
&= 6D_R t + |j-j'|b^2 + \frac{2Nb^2}{\pi^2}\sum_{p=1}^{N}\frac{1}{p^2}\left[\cos\frac{p\pi(j+j')}{N} + \cos\frac{p\pi(j-j')}{N}\right]\left(1-\exp\left(-\frac{p^2 t}{\tau_1^R}\right)\right)
\end{aligned} \tag{3.1.2.10}$$

Here, we can ignore the first term since t is small. In addition to this, we can also ignore the first cosine term in the third term since the summation of the third term is dominated by large p values[16] and this cosine term oscillates rapidly.

Then we substitute Eq.(3.1.2.10) into Eq.(3.1.3). From now, we consider j, j' and p as continuous variables. This means that we represent Eq.(3.1.3) in an integral form:

$$\begin{aligned}
&I(\vec{q},t) \\
&\simeq \frac{1}{N}\sum_{j,j'}\exp\left[-\frac{1}{6}q^2|j-j'|b^2 - \frac{q^2Nb^2}{3\pi^2}\sum_p \frac{1}{p^2}\cos\frac{p\pi(j-j')}{N}\left(1-\exp\left[-\frac{tp^2}{\tau_1^R}\right]\right)\right] \\
&\to \frac{1}{N}\int_0^\infty dj\int_0^\infty dj' \\
&\qquad \exp\left[-\frac{1}{6}q^2|j-j'|b^2 - \frac{q^2Nb^2}{3\pi^2}\int_0^\infty dp\frac{1}{p^2}\cos\frac{p\pi(j-j')}{N}\left(1-\exp\left[-\frac{tp^2}{\tau_1^R}\right]\right)\right] \\
&= 2\int_{-\infty}^\infty d(j-j')\exp\left[-\frac{1}{6}q^2|j-j'|b^2 - \frac{q^2Nb^2}{3\pi^2}\int_0^\infty dp\frac{1}{p^2}\cos\frac{p\pi(j-j')}{N}\left(1-\exp\left[-\frac{tp^2}{\tau_1^R}\right]\right)\right]
\end{aligned} \tag{3.1.2.11}$$

Here, we define the following variables:

$$u := \frac{|j-j'|q^2b^2}{6} \tag{3.1.2.12}$$

$$W := \frac{3k_BT}{\zeta_0 b^2} \tag{3.1.2.13}$$

$$x := \frac{\pi(Wt)^{1/2}}{N}p = \left(\frac{3\pi^2 k_B T t}{\zeta_0 N^2 b^2}\right)^{1/2} p \tag{3.1.2.14}$$

In addition to this, we use the exact value of τ_1^R:[17]

$$\tau_1^R = \frac{\zeta_0 b^2}{3\pi^2 k_B T}N^2 = \frac{N^2}{\pi^2 W} \tag{3.1.2.15}$$

[16] Large p corresponds to the relaxation of a section composed of N/p monomers. This means that large p corresponds to short relaxation terms. In other words, we do not have to consider the relaxation of long sections since those does not relax in the discussed time region.

[17] Notice that Eq.(3.1.1.7) holds true.

Then,

$$
\begin{aligned}
I(\vec{q},t) &= 2\int_{-\infty}^{\infty}\frac{6}{q^2b^2}\frac{q^2b^2}{6}d(j-j')\exp\left[-\frac{|j-j'|q^2b^2}{6}-\frac{q^2b^2}{6}(Wt)^{1/2}\frac{2}{\pi}\right.\\
&\qquad\left.\int_0^{\infty}dp\frac{\pi}{N}(Wt)^{1/2}\frac{\cos\left[\frac{\pi p}{N}(Wt)^{1/2}\frac{|j-j'|q^2b^2}{6}\frac{6}{q^2b^2}(Wt)^{-1/2}\right]}{\frac{\pi^2p^2}{N^2}Wt}\left(1-\exp\left[-\frac{\pi^2p^2}{N^2}Wt\right]\right)\right]\\
&= \frac{12}{q^2b^2}\int_0^{\infty}du\exp\left[-u-(\Omega_Rt)^{1/2}\frac{2}{\pi}\int_0^{\infty}dx\frac{\cos(xu(\Omega_Rt)^{-1/2})}{x^2}\left(1-\exp(-x^2)\right)\right]\\
&= \frac{12}{q^2b^2}\int_0^{\infty}du\exp\left[-u-(\Omega_Rt)^{1/2}h(u(\Omega_Rt)^{-1/2})\right] \qquad (3.1.2.16)
\end{aligned}
$$

where

$$
(\Omega_Rt)^{1/2} := \left(\frac{1}{12}k_BT\frac{b^2}{\zeta_0}q^4t\right)^{1/2} = \frac{q^2b^2}{6}(Wt)^{1/2} \qquad (3.1.2.17)
$$

$$
h(y) := \frac{2}{\pi}\int_0^{\infty}dx\frac{\cos(xy)}{x^2}\left(1-\exp(-x^2)\right) \qquad (3.1.2.18)
$$

Although the form of equation is complicated, it is important to notice that this function depends only one variable, Ω_R, similar to the incoherent term (Eq.(3.1.2.7))[18].

It is known that the long time behavior ($\Omega_Rt > 1$) becomes a simple exponential form:

$$
\frac{I(\vec{q},t)}{I(\vec{q},0)} = \exp\left[-2^{1/2}(\Omega_Rt)^{1/2}\right] \quad \text{for} \quad \Omega_Rt > 1 \qquad (3.1.2.19)
$$

Zimm mode

In the case of polymer solutions, we have to add the effect of hydrodynamic interactions into Eq.(3.1.2.2). This can be represented by the dragging force, $\zeta_0\vec{v}(\vec{R}_j)$ where $\vec{v}(\vec{R}_j)$ is the velocity of jth monomer:

$$
\nabla_jV(\vec{R}_j) = \frac{3k_BT}{b^2}\frac{\partial^2\vec{R}_j}{\partial j^2} + \zeta_0\vec{v}(\vec{R}_j) \qquad (3.1.2.20)
$$

The velocity of jth monomer, $\vec{v}(\vec{R}_j)$, is determined from the force made by all of the other monomers. The force on j'th monomer and the resulting flow field at jth monomer is connected by a 3×3 tensor called Oseen tensor, $\mathbf{T}^{jj'}$:

$$
\mathbf{T}^{jj'} := \frac{1}{8\pi\eta_s|\vec{R}_j-\vec{R}_{j'}|}\left(\mathbf{E}-\frac{(\vec{R}_j-\vec{R}_{j'})(\vec{R}_j-\vec{R}_{j'})}{(\vec{R}_j-\vec{R}_{j'})^2}\right) \qquad (3.1.2.21)
$$

where $\mathbf{E}$ is an unit matrix and $(\vec{R}_j-\vec{R}_{j'})(\vec{R}_j-\vec{R}_{j'})$ is dyadic. Then,

$$
\vec{v}(\vec{R}_j) = \sum_{j\neq j'}\mathbf{T}^{jj'}\vec{F}(\vec{R}_{j'}) \qquad (3.1.2.22)
$$

[18]Notice that the prefactor $12/(q^2b^2)$ is not a fitting parameter since what we obtain is a normalized function.

where $\vec{F}(\vec{R}_{j'})$ is the force on j'th monomer:

$$\vec{F}(\vec{R}_{j'}) = \frac{3k_BT}{b^2}\frac{\partial^2\vec{R}_{j'}}{\partial j'^2} + \vec{f}_{j'}(t) \tag{3.1.2.23}$$

Notice that we do not take $\zeta_0\vec{v}(\vec{R}_{j'})$ term into consideration for Eq.(3.1.2.23). The term $j = j'$ should be omitted since the force on jth monomer does not make the flow field at the position of oneself. Substitute Eq.(3.1.2.20), (3.1.2.22) and (3.1.2.23) into Eq.(3.1.2.1):

$$\begin{aligned}\zeta_0\frac{\partial\vec{R}_j}{\partial t} &= \zeta_0\vec{v}(\vec{R}_j) + \frac{3k_BT}{b^2}\frac{\partial^2\vec{R}_j}{\partial j^2} + \vec{f}_j(t) \\ &= \zeta_0\sum_{j\neq j'}\mathbf{T}^{jj'}\left(\frac{3k_BT}{b^2}\frac{\partial^2\vec{R}_{j'}}{\partial j'^2} + \vec{f}_{j'}(t)\right) + \frac{3k_BT}{b^2}\frac{\partial^2\vec{R}_j}{\partial j^2} + \vec{f}_j(t)\end{aligned} \tag{3.1.2.24}$$

Here, we define that[19]

$$\mathbf{T}^{jj} := \frac{1}{\zeta_0}\mathbf{E} \tag{3.1.2.25}$$

then we can write the equation briefly:

$$\frac{\partial\vec{R}_j}{\partial t} = \sum_{j'}\mathbf{T}^{jj'}\left(\frac{3k_BT}{b^2}\frac{\partial^2\vec{R}_{j'}}{\partial j'^2} + \vec{f}_{j'}(t)\right) \tag{3.1.2.26}$$

Notice that j' runs from 1 to N, including j. Although this equation cannot solve analytically, we can linearize this equation by using a number of approximations. The result is:

$$\frac{\partial\vec{R}_j}{\partial t} = W\frac{\partial^2\vec{R}_j}{\partial j^2} + \frac{1}{\zeta_0}\vec{f}_j(t) + WB\sum_{j\neq j'}\left(\frac{1}{|j-j'|^{1/2}} + \vec{f}_{j'}(t)\right) \tag{3.1.2.27}$$

where W is the same as Eq.(3.1.2.13) and B is a parameter called draining parameter:

$$B := \frac{1}{6^{1/2}\pi^{3/2}}\frac{\zeta_0}{\eta_s b} \tag{3.1.2.28}$$

This parameter implies the strength of hydrodynamic interaction. $B = 0.4$ in the case of Zimm mode and hydrodynamic interaction is dominant. $B = 0$ implies the Rouse limit and Eq.(3.1.2.28) reproduces Eq.(3.1.2.2).

When $j = j'$ (incoherent term) and $t < \tau_1^Z$, this can be calculated as the following brief form:

$$\langle(\vec{R}_j(t) - \vec{R}_j(0))^2\rangle = \frac{16}{9}\frac{1}{\pi^{3/2}}\left(\frac{(3\pi)^{1/2}k_BT}{\eta_s}t\right)^{2/3} \propto b^2\left(\frac{k_BT}{\eta_s b^3}t\right)^{2/3} \propto b^2\left(\frac{t}{\tau_0}\right)^{2/3} \tag{3.1.2.29}$$

Here, we used Eq.(3.1.1.12). This result is the same as that of Eq.(3.1.1.16).

[19] We can define $\mathbf{T}^{jj}$ arbitrarily since this term is not used for the calculation of flow field.

Substitute Eq.(3.1.2.29) into Eq.(3.1.4):

$$\begin{aligned} I_s(\vec{q},t) &= \exp\left[-\frac{8}{27}\frac{q^2}{\pi^{3/2}}\left(\frac{(3\pi)^{1/2}k_BT}{\eta_s}t\right)^{2/3}\right] \\ &= \exp\left[-\frac{8\cdot 2^{2/3}}{9\pi^{1/2}}\frac{q^2}{2^{2/3}3\pi}\left(\frac{(3\pi)^{1/2}k_BT}{\eta_s}t\right)^{2/3}\right] \\ &= \exp\left[-\frac{2^{11/3}}{9\pi^{1/2}}\left(\frac{q^3}{2(3\pi)^{3/2}}\frac{(3\pi)^{1/2}k_BT}{\eta_s}t\right)^{2/3}\right] \\ &= \exp\left[-\frac{2^{11/3}}{9\pi^{1/2}}\left(\frac{1}{6\pi}\frac{k_BT}{\eta_s}q^3t\right)^{2/3}\right] \end{aligned} \tag{3.1.2.30}$$

Let us define the characteristic rate of the Zimm dynamics, $\Omega_Z(q)$:

$$\Omega_Z(q) := \frac{1}{6\pi}\frac{k_BT}{\eta_s}q^3 \tag{3.1.2.31}$$

Substitute Eq.(3.1.2.31) into Eq.(3.1.2.30):

$$I_s(\vec{q},t) = \exp\left[-\frac{2^{11/3}}{9\pi^{1/2}}\left(\Omega_Z(q)t\right)^{2/3}\right] \tag{3.1.2.32}$$

It is known that the coherent term also depends only on $(\Omega_Z t)^{2/3}$:

$$I_s(\vec{q},t) = \frac{12}{q^2b^2}\int_0^\infty du\exp\left[-u-(\Omega_Z t)^{2/3}g(u(\Omega_Z t)^{-2/3})\right] \tag{3.1.2.33}$$

where

$$g(y) := \frac{2}{\pi}\int_0^\infty dx\frac{\cos(xy)}{x^2}\left(1-\exp(-2^{-1/2}x^{3/2})\right) \tag{3.1.2.34}$$

It is known that the long time behavior ($\Omega_Z t > 1$) becomes a simple exponential form, similar to Rouse mode (Eq.(3.1.2.19)):

$$\frac{I(\vec{q},t)}{I(\vec{q},0)} = \exp\left[-\frac{2^{2/3}}{\pi}\Gamma\left(\frac{1}{3}\right)(\Omega_Z t)^{2/3}\right] \quad \text{for} \quad \Omega_R t > 1 \tag{3.1.2.35}$$

where $\Gamma(x)$ is the Gamma function.

3.2 Physical properties of polymers

3.2.1 Viscoelasticity

To characterize the materials, what we focus on at the first time is the phase of the materials. Here, I stick on only solid and liquid phases. In the case of solids, their physical properties can be characterized by checking how stiff they are. To specify the stiffness quantitatively, there are some representative parameters to characterize the solids. These characters are called elasticity. In the case of liquids, their physical properties can be characterized by checking how flow they will. To specify the flow quantitatively, we usually use the parameter called viscosity. In contrast to the materials such as metals and low-molecular liquid, polymers have both elasticity and viscosity for most of the case. These character is called viscoelasticity. In this subsection, I introduce the basic theory of viscoelasticity necessary to understand previous and my current research.

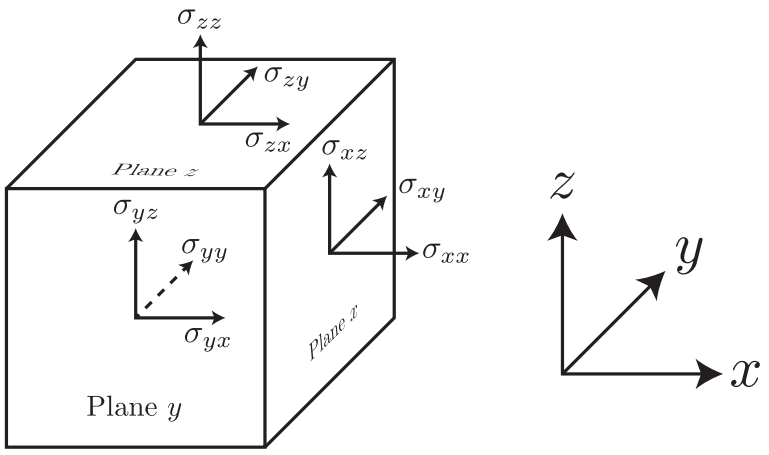

Figure 3.3: Definition of stress.

Figure 3.3 shows the definition of stress applied on a certain unit volume. Stress is defined as the force applied to the area.

$$\sigma_{ij} := \frac{F_j}{A_i} \tag{3.2.1.1}$$

where F_j is the force parallel to j axis and A_i is the area perpendicular to i axis. $\sigma_{zz} > 0$ corresponds to the stretching of the materials and $\sigma_{zz} < 0$ corresponds to the compression. σ_{ij} $(i \neq j)$ is the force parallel to j axis and applied to the plane i. These type of force is called shear. By applying certain stress, the body will be deformed. If the unit length L_i becomes $L_i + dL_i$ $(i = x, y, z)$, strain γ_i is defined as follows.

$$\gamma_i := \frac{dL_i}{L_i} \tag{3.2.1.2}$$

For a perfect elastic solid, shear stress σ_{ij} $(i \neq j)$ is proportional to the strain γ_j. This proportional constant is called shear modulus, G.[20]

$$G := \frac{\sigma_{ij}}{\gamma_j} \tag{3.2.1.3}$$

[20] For isotropic materials, G does not depend on i and j.

In contrast to this, for a simple liquid, shear stress is proportional to the time variation of the strain, $\dot{\gamma}$. This proportional constant is called viscosity, η.[21]

$$\eta := \frac{\sigma_{ij}}{\dot{\gamma}_j} \tag{3.2.1.4}$$

In the case of polymer systems, there are both an elastic term and a viscous term.

$$\sigma_{ij} = G\gamma_j^e = \eta\dot{\gamma}_j^v \tag{3.2.1.5}$$

where the total strain, γ is decided into two terms.

$$\gamma_j =: \gamma_j^e + \gamma_j^v \tag{3.2.1.6}$$

Here I'm going to show that G and η is not independent but strongly related to each other. Let us consider a step strain γ_j is applied to the viscoelastic body at $t = 0$. At that time, the stress σ_{ij} will be produced on plane i. As time goes on, the stress will be relaxed since the body has viscous component. This means that the stress becomes time-dependent for the step strain. By using Eq.(3.2.1.3), we can define time-dependent shear modulus.

$$G(t) := \frac{\sigma_{ij}(t)}{\gamma_j} \tag{3.2.1.7}$$

By using this time-dependent shear modulus, the stress at $t = t$ can be represented by the summation of small stress originated from small step strain applied at $t = t_i$.

$$\begin{aligned}\sigma_{ij}(t) &= \sum_k G(t - t_k)\delta(\gamma_j)_k = \sum_k G(t - t_k)(\dot{\gamma}_j)_k\delta t_k \\ &\to \int_{-\infty}^{t} G(t - t')\dot{\gamma}_j(t')dt'\end{aligned} \tag{3.2.1.8}$$

When $\dot{\gamma}_j$ is a constant (steady shear):

$$\sigma_{ij}(t) = \dot{\gamma}_j \int_{-\infty}^{t} G(t - t')dt' = \dot{\gamma}_j \int_0^{\infty} G(s)ds \tag{3.2.1.9}$$

where $s := t - t'$. In most of the case, the applied stress will also become constant under steady shear. In that case, we can use Eq.(3.2.1.4). As a result, the relationship between G and η is derived as follows.

$$\eta = \int_0^{\infty} G(t)dt \tag{3.2.1.10}$$

Next, let us connect the macroscopic quantity G to the microscopic quantities by using rubber as an example. First, let us see entropy for a single chain. Probability that end-to-end distance is R is calculated as follows.

$$P(R) = \exp\left[-\frac{3R^2}{2Nb^2}\right] \tag{3.2.1.11}$$

where N and b is the number of polymerization and length of one segment, respectively. Entropy of the

[21] For isotropic materials, η does not depend on i and j.

chain is calculated by regarding $P(R)$ as the number of state in Boltzmann's equation.

$$s(R) = k_B \ln P(R) = -\frac{3k_B R^2}{2Nb^2} \tag{3.2.1.12}$$

Here, let us consider the deformation called affine deformation. Under this assumption, deformation ratio for macroscopic scale is the same as that for each polymer. Let us define the deformation ratio as $(\lambda_x, \lambda_y, \lambda_z)$. In addition, we assume that $\lambda_x\lambda_y\lambda_z = 1$. This means that the total volume does not change by deformation. In this case, entropy change for each polymer is calculated as follows.

$$\Delta s = s(R) - s_(R_0) = -\frac{k_B}{2Nb^2}(\lambda_x^2 + \lambda_y^2 + \lambda_z^2 - 3)r_0^2 \tag{3.2.1.13}$$

Here, we assume isotropic distribution before deformation: $x_0^2 = y_0^2 = z_0^2 = r_0^2/3$. Therefore, entropy change per unit volume is represented as follows.

$$\begin{aligned}\Delta S &= -\frac{1}{2}Nk_B(\lambda_x^2 + \lambda_y^2 + \lambda_z^2 - 3) \\ &= -\frac{1}{2}\nu R(\lambda_x^2 + \lambda_y^2 + \lambda_z^2 - 3)\end{aligned} \tag{3.2.1.14}$$

where N is the number of polymers in a unit volume and $\nu := N/N_A$. When there is no internal energy (enthalpy) change, change of Gibbs free energy by deformation is represented as follows.

$$\Delta G = -T\Delta S = \frac{1}{2}\nu RT(\lambda_x^2 + \lambda_y^2 + \lambda_z^2 - 3) \tag{3.2.1.15}$$

For simple shear, the relationship between λ and γ is calculated as follows:

$$\lambda_x := \lambda, \lambda_y = 1, \lambda_z = \frac{1}{\lambda} \Rightarrow \gamma = \lambda - \frac{1}{\lambda} \tag{3.2.1.16}$$

By substituting Eq.(3.2.1.16) into Eq.(3.2.1.15):

$$\Delta G = \frac{1}{2}\nu RT\gamma^2 \tag{3.2.1.17}$$

The work done on the body per unit area is calculated by a differentiation of ΔG by γ. This work is nothing but stress.

$$\sigma = \frac{d(\Delta G)}{d\gamma} = \nu RT\gamma \tag{3.2.1.18}$$

By comparing Eq.(3.2.1.3) and (3.2.1.18), shear modulus G is represented as follows.

$$G = \nu RT \tag{3.2.1.19}$$

G is also called elastic modulus.

Eq.(3.2.1.19) shows that shear modulus is proportional to the number of chains in a unit volume. This notion is extended to the polymer melt and solution. As shown in Section 3.1, polymer segment start relaxing after setting them to the state far from equilibrium. After the relaxation, shear modulus is proportional to the number of (relaxed) chains in a unit volume. The number density of chains is equal to ϕ/Nb^3 where Nb^3

is the volume of each polymer, therefore:

$$G(\tau) \simeq k_B T \frac{\phi}{Nb^3} \tag{3.2.1.20}$$

Here, $\sigma(t)$ is time-dependent stress. τ is the relaxation time and defined by using Eq.(3.2.1.5).

$$\tau := \frac{\eta}{G} \tag{3.2.1.21}$$

Qualitatively speaking, viscoelastic body is regarded as a solid at $t < \tau$ (before relaxation) while is regraded as a liquid at $t > \tau$ (after relaxation). By substituting Eqs.(3.2.1.21) and (3.2.1.6) into Eq.(3.2.1.5):

$$\tau \frac{d\gamma_j^v}{dt} = \gamma_j^e = \gamma_j - \gamma_j^v \rightarrow \gamma_j^e = \gamma_j \exp[-t/\tau] \tag{3.2.1.22}$$

$$\sigma_{ij}(t) = G\gamma_j \exp[-t/\tau] \tag{3.2.1.23}$$

From Eq.(3.2.1.23), we define time-dependent shear modulus as follows.

$$G(t) = G \exp[-t/\tau] \tag{3.2.1.24}$$

First, let us use the following rough estimation to obtain viscosity.

$$\eta = \int_0^\infty G(t)dt = \int_0^\infty G \exp[-t/\tau]dt \simeq G(\tau)\tau \tag{3.2.1.25}$$

This result is obtained by substituting $G(\tau)$ into G in Eq.(3.2.1.23). There are several forms to represent viscosity for polymer solution. From experimental point of view, the definition of viscosity is Eq.(3.2.1.4). By using this definition, let us write the viscosity of solvent and polymer solution (whose concentration is c) as η_0 and η_p, respectively. Then the following definition is used.

$$\text{Relative viscosity, } \eta_r \ : \ \frac{\eta_p}{\eta_0} \tag{3.2.1.26}$$

$$\text{Specific viscosity, } \eta_s \ : \ \frac{\eta_p - \eta_0}{\eta_0} \tag{3.2.1.27}$$

$$\text{Reduced viscosity, } \eta_s/c \ : \ \frac{\eta_p - \eta_0}{c\eta_0} \tag{3.2.1.28}$$

$$\text{Intrinsic viscosity, } [\eta] \ : \ \lim_{c\to 0} \frac{\eta_s}{c} \tag{3.2.1.29}$$

The viscosity of polymer solution shown in Eq.(3.2.1.25) consider the contribution only from polymers. Therefore, η in Eq.(3.2.1.25) can be written as $\eta_p - \eta_0$. By using this fact, we can calculate intrinsic viscosity as follows.

$$[\eta] \simeq \lim_{c\to 0} \frac{G(\tau)\tau}{c\eta_0} = \frac{k_B T N_A}{\eta_0 M_0 N}\tau \tag{3.2.1.30}$$

Here, I used the fact that the mass concentration, c, is written by using polymer fraction, ϕ and molar mass of a monomer, M_0, as follows.

$$c = \frac{\phi}{b^3}\frac{M_0}{N_A} \tag{3.2.1.31}$$

From the viewpoint of each polymer, relaxation time corresponds to the longest relaxation time of Zimm

mode, Eq.(3.1.1.12).

$$\tau = \frac{\eta_0 (bN^\nu)^3}{k_B T} = \frac{\eta_0 R^3}{k_B T} \tag{3.2.1.32}$$

By substituting Eq.(3.2.1.32) into Eq.(3.2.1.30):

$$[\eta] \simeq \frac{R^3 N_A}{M_0 N} \tag{3.2.1.33}$$

To compensate the error originated from rough approximation (Eq.(3.2.1.25)), let us introduce numerical factor Φ.

$$[\eta] = \Phi \frac{R^3}{M} \tag{3.2.1.34}$$

where $M := M_0 N$ is the molar mass of the polymer. $\Phi = 2.5 \times 10^{23}$ mol^{-1} is a universal constant for all polymer-solvent systems [23]. Eq.(3.2.1.34) is known as Fox–Flory equation.

Let us see the concentration dependence of viscosity. Our starting point is Eq.(3.2.1.10). To calculate this, we have to know $G(t)$. At the longest relaxation time of polymer in solution (Zimm mode), $t = \tau_1^Z$, $G(\tau_1^Z)$ is expressed as Eq.(3.2.1.20). When $t < \tau_1^Z$, not all modes are relaxed within one polymer chain. Before realization, each unrelaxed mode will contribute $k_B T$ to the shear modulus. In other words, p unrelaxed modes can be regarded as p chains which contribute the elasticity of the system. Since the number of unrelaxed modes at $t = \tau_p^Z$ is p, we can write the shear modulus when $t < \tau_1^Z$ as follows.

$$G(\tau_p^Z) \simeq k_B T \frac{\phi}{Nb^3} p \tag{3.2.1.35}$$

By using Eq.(3.1.1.13), we can obtain $G(t)$ as follows:

$$\begin{aligned} G(\tau_p^Z) &\simeq k_B T \frac{\phi}{Nb^3} N \left(\frac{\tau_p^Z}{\tau_0} \right)^{-1/3\nu} \\ \rightarrow G(t) &\simeq \frac{k_B T}{b^3} \phi \left(\frac{t}{\tau_0} \right)^{-1/3\nu} \quad \text{for } \tau_0 < t < \tau_1^Z \end{aligned} \tag{3.2.1.36}$$

At $t > \tau_1^Z$, the system is regarded as liquid and shear modulus will decrease exponentially as Eq.(3.2.1.24). By combining these expressions, the time dependence of $G(t)$ is approximated as follows.

$$G(t) \simeq \frac{k_B T}{b^3} \phi \left(\frac{t}{\tau_0} \right)^{-1/3\nu} \exp(-t/\tau_1^Z) \tag{3.2.1.37}$$

By substituting Eq.(3.2.1.37) into Eq.(3.2.1.10) (with $\eta \rightarrow \eta_p - \eta_0$), viscosity can be calculated as follows.

$$\eta_p - \eta_0 = \int_0^\infty G(t) dt = \eta_0 \phi N^{3\nu - 1} \tag{3.2.1.38}$$

For polymer melt, we can use similar discussion for Rouse mode (Eq.(3.1.1.8)).

$$\begin{aligned} G(\tau_p^R) &\simeq k_B T \frac{\phi}{Nb^3} N \left(\frac{\tau_p^R}{\tau_0} \right)^{-1/2} \\ \rightarrow G(t) &\simeq \frac{k_B T}{b^3} \phi \left(\frac{t}{\tau_0} \right)^{-1/2} \exp(-t/\tau_1^R) \end{aligned} \tag{3.2.1.39}$$

$$\eta = \int_0^\infty G(t)dt = \eta_0 \phi N \tag{3.2.1.40}$$

For semidilute, unentangled solution, relaxation mode is changed from Zimm mode to Rouse mode at the size of correlation length, ξ. As a result, their viscosity becomes:

$$\eta_p - \eta_0 = \int_0^\infty G(t)dt = \eta_0 \phi^{1/(3\nu-1)} N \tag{3.2.1.41}$$

3.2.2 Osmotic modulus

As shown in Section 2.5.3, scattering intensity is related to the fluctuation of irradiated molecules. To specify this fluctuation quantitatively, we introduced the parameter called osmotic modulus, K_{os} (Eq.(2.5.3.32)). Let us see the explicit form of K_{os}. In addition, I'm going to expand this notion from polymer solutions to polymer gels. Here I'm going to use lattice model. By using the lattice model, mixing entropy and enthalpy per lattice is calculated as follows (See Eq.(3.2.4.14)).

$$\Delta \bar{S}_{mix} = -k_B \left(\frac{\phi}{N} \ln \phi + (1-\phi) \ln(1-\phi) \right) \tag{3.2.2.1}$$

$$\Delta \bar{H}_{mix} = k_B T \chi \phi (1-\phi) \tag{3.2.2.2}$$

where ϕ and N is the volume fraction of polymers and the degree of polymerization, respectively. χ is the parameter called Flory interaction parameter. Let us assume that there are n_s mole of solvent molecules and n_p mole of polymers in a unit volume. In this case, the number of lattice in a unit volume, N_{tot} becomes:

$$N_{tot} = N_A(n_s + n_p N) \tag{3.2.2.3}$$

Therefore, the mixing entropy and enthalpy per unit volume is:

$$\Delta S_{mix} = N_{tot} \Delta \bar{S} = -k_B N_{tot} \left(\frac{N_A n_p N}{N_{tot}} \frac{1}{N} \ln \phi + \frac{N_A n_s}{N_{tot}} \ln(1-\phi) \right) = -R(n_p \ln \phi + n_s \ln(1-\phi)) \tag{3.2.2.4}$$

$$\Delta H_{mix} = N_{tot} \Delta \bar{H} = k_B T \chi N_{tot} \phi \frac{N_A n_s}{N_{tot}} = RT \chi \phi n_s \tag{3.2.2.5}$$

From Eqs.(3.2.2.4) and (3.2.2.5), the Gibbs free energy of mixing per unit volume is written as follows.

$$\Delta G = \Delta H_{mix} - T \Delta S_{mix} = RT(n_p \ln \phi + n_s \ln(1-\phi) + \chi \phi n_s) \tag{3.2.2.6}$$

The Gibbs free energy of mixing is the difference of Gibbs free energy between solution and (solvent + solute).

$$\Delta G = \Delta G_{\text{solution}} - \Delta G_{\text{solvent}} - \Delta G_{\text{solute}} \tag{3.2.2.7}$$

Differentiation of Gibbs free energy by the mole of solvent, n_s, is the chemical potential as shown in Eq.(2.5.3.24).

$$\left. \frac{\partial \Delta G}{\partial n_s} \right|_{T,P,n_p} = \left. \frac{\partial \Delta G_{\text{solution}}}{\partial n_s} \right|_{T,P,n_p} - \left. \frac{\partial \Delta G_{\text{solvent}}}{\partial n_s} \right|_{T,P,n_p} = \mu - \mu^\circ \tag{3.2.2.8}$$

By substituting Eq.(3.2.2.8) into Eq.(2.5.3.28):

$$\Pi = -\frac{1}{\overline{V}_s}\left.\frac{\partial \Delta G}{\partial n_s}\right|_{T,P,n_p} \tag{3.2.2.9}$$

Differentiation of Eq.(3.2.2.6) can be done as follows.

$$\frac{\partial(n_p \ln\phi)}{\partial n_s} = n_p \frac{\partial\phi}{\partial n_s}\frac{d(\ln\phi)}{d\phi} = n_p \frac{\partial}{\partial n_s}\left[\frac{n_p N}{n_p N + n_s}\right]\frac{1}{\phi} = -\frac{\phi}{N} \tag{3.2.2.10}$$

$$\frac{\partial(n_s \ln(1-\phi))}{\partial n_s} = \ln(1-\phi) + n_s \frac{\partial\phi}{\partial n_s}\frac{d\ln(1-\phi)}{d\phi} = \ln(1-\phi) + \phi \tag{3.2.2.11}$$

$$\frac{\partial(\chi\phi n_s)}{\partial n_s} = \chi \frac{\partial}{\partial n_s}\left[\frac{n_p n_s N}{n_p N + n_s}\right] = \phi^2 \tag{3.2.2.12}$$

Substitute Eqs.(3.2.2.6), (3.2.2.10) $\sim$ (3.2.2.12) into Eq.(3.2.2.9):

$$\Pi = -\frac{RT}{\overline{V}_s}\left[\ln(1-\phi) + \left(1 - \frac{1}{N}\right)\phi + \chi\phi^2\right] \tag{3.2.2.13}$$

Substitute Eq.(3.2.2.13) into Eq.(2.5.3.32):

$$K_{os} = \phi\frac{\partial\Pi}{\partial\phi} = \frac{RT\phi}{\overline{V}_s}\left[\left(\frac{1}{1-\phi} + 2\chi\right)\phi + \frac{1}{N}\right] \tag{3.2.2.14}$$

To take the effect of the difference of partial volume of solvent and solute into consideration, the degree of polymerization, N, is changed to the reduced degree of polymerization.

$$N \to \frac{\overline{V}_m}{\overline{V}_s}N \tag{3.2.2.15}$$

where $\overline{V}_m$ stands for the partial volume of one monomer in the polymer. By using this expression, Eq.(3.2.2.14) is written as follows.

$$K_{os} = \frac{RT\phi}{\overline{V}_m N}\left[1 + \left(\frac{1}{1-\phi} + 2\chi\right)\phi\frac{\overline{V}_m}{\overline{V}_s}N\right] \tag{3.2.2.16}$$

In the case of solution, the origin of entropy change is mixing only. In contrast to this, we have to consider the entropy originated from crosslinking in the case of gels. Here, the entropy change is measured by comparing uncrossklinked, undeformed network and crosslinked, deformed network. This means that we cannot use Eq.(3.2.1.14) since the volume of the system will changed significantly due to swelling. By using more precise discussion, it is proved that there are two effects which cause entropy change. First term is an elastic term.

$$\Delta S_{el} = -\frac{1}{2}\nu R(\lambda_x^2 + \lambda_y^2 + \lambda_z^2 - 3 - 2\ln\lambda_x\lambda_y\lambda_z) \tag{3.2.2.17}$$

Note that the term $\ln\lambda_x\lambda_y\lambda_z$ becomes 0 when there is no volume change. In this case, Eq.(3.2.2.17) becomes

Eq.(3.2.1.14). Second term is a network term.

$$\Delta S_{net} = -\frac{2\nu R}{f} \ln \lambda_x \lambda_y \lambda_z \tag{3.2.2.18}$$

where f is a functionality of the crosslink point. The origin of this term is the entropy loss by a restriction of crosslinking points. As a result, additional entropy change originated from crosslinking becomes as follows when $f = 4$.

$$\begin{aligned} \Delta S_{el} + \Delta S_{net} &= -\frac{1}{2}\nu R(\lambda_x^2 + \lambda_y^2 + \lambda_z^2 - 3 - \ln \lambda_x \lambda_y \lambda_z) \\ &= -\frac{1}{2}\nu R \left[3 \left(\frac{\phi}{\phi_0} \right)^{-2/3} - 3 + \ln \left(\frac{\phi}{\phi_0} \right) \right] \end{aligned} \tag{3.2.2.19}$$

where we assume the following relationship (isotropic swelling).

$$\lambda_x = \lambda_y = \lambda_z = \left(\frac{\phi}{\phi_0} \right)^{-1/3} \tag{3.2.2.20}$$

Here, ϕ_0 and ϕ stand for the polymer volume fraction of as-prepared state and swollen state, respectively. From Eq.(3.2.2.19), we can calculate the osmotic pressure of gel systems.

$$\Pi = -\frac{1}{\overline{V}_s} \left. \frac{\partial \Delta G}{\partial n_s} \right|_{T,P,n_p} = -\frac{1}{\overline{V}_s} \frac{\partial}{\partial n_s} (\Delta H_{mix} - T(\Delta S_{mix} + \Delta S_{el} + \Delta S_{net})) \tag{3.2.2.21}$$

Differentiation of Eq.(3.2.2.21) can be done as follows.

$$\begin{aligned} \frac{\partial(\Delta S_{el} + \Delta S_{net})}{\partial n_s} &= \frac{\partial(\phi/\phi_0)}{\partial n_s} \frac{d(\Delta S_{el} + \Delta S_{net})}{d(\phi/\phi_0)} \\ &= -\frac{1}{2}\nu R \left(-\frac{\phi}{\phi_0} \frac{1}{n_p N + n_s} \right) \left[-2 \left(\frac{\phi}{\phi_0} \right)^{-5/3} + \left(\frac{\phi}{\phi_0} \right)^{-1} \right] \\ &= -\frac{1}{2}\nu R V_s \left[2 \left(\frac{\phi}{\phi_0} \right)^{-2/3} - 1 \right] \end{aligned} \tag{3.2.2.22}$$

where we assume that the partial molar volume of solvent ($\overline{V}_s$) and monomer ($\overline{V}_m$) are the same.

$$\frac{1}{n_p N + n_s} = \overline{V}_s = \overline{V}_m \tag{3.2.2.23}$$

Eq.(3.2.2.22) is defined for a unit volume of as-prepared state. Therefore, it should be multiplied by ϕ/ϕ_0 to redefine it for a unit volume of swollen state. By using Eqs.(3.2.2.13) and (3.2.2.22) to Eq.(3.2.2.21), osmotic pressure for gel system becomes as follows.

$$\Pi = -\frac{RT}{\overline{V}_s} \left[\ln(1-\phi) + \phi + \chi\phi^2 \right] + \nu RT \left[\frac{1}{2} \frac{\phi}{\phi_0} - \left(\frac{\phi}{\phi_0} \right)^{1/3} \right] \tag{3.2.2.24}$$

Here, $1/N$ term is neglected since N is large. Then osmotic modulus for gel system becomes:

$$K = \phi \frac{\partial \Pi}{\partial \phi} = \frac{RT\phi^2}{\overline{V}_s} \left(\frac{1}{1-\phi} + 2\chi \right) + \nu RT \left[\frac{1}{2} \frac{\phi}{\phi_0} - \frac{1}{3} \left(\frac{\phi}{\phi_0} \right)^{1/3} \right] \tag{3.2.2.25}$$

Here, both osmotic pressure and crosslinking contribute to K. Therefore, K is called bulk modulus.

3.2.3 Tanaka–Hocker–Benedek theory

The theory of dynamics of gel network was proposed by Tanaka *et al.* to obtain microscopic information of gels by light scattering [53]. Here I'm going to review their theory for the application of my research. Starting point of this theory is the following equation of motion for a displacement vector of gel networks.

$$\rho\frac{\partial^2\vec{u}}{\partial t^2} = \vec{\nabla}\cdot\sigma - f\frac{\partial\vec{u}}{\partial t} \tag{3.2.3.1}$$

where $\vec{u}(\vec{r},t)$ is a displacement vector of a unit cube whose average position is $\vec{r}$, ρ is the density of the network, f is the friction constant, and σ is the stress tensor. The stress tensor is related to the shear modulus and bulk modulus which I explained in Section 3.2.1 and 3.2.2 as follows.

$$\sigma_{ij} = K(\vec{\nabla}\cdot\vec{u})\delta_{ij} + 2G\left[\frac{1}{2}\left(\frac{\partial u_j}{\partial x_i}+\frac{\partial u_i}{\partial x_j}\right) - \frac{1}{3}(\vec{\nabla}\cdot\vec{u})\delta_{ij}\right] \tag{3.2.3.2}$$

Substituting Eq.(3.2.3.2) into Eq.(3.2.3.2) gives:

$$\rho\frac{\partial^2 u_i}{\partial t^2} = \sum_j \frac{\partial}{\partial r_j}\left[\left(K-\frac{2}{3}G\right)(\vec{\nabla}\cdot\vec{u})\delta_{ji} + G\left(\frac{\partial u_i}{\partial x_j}+\frac{\partial u_j}{\partial x_i}\right)\right] - f\frac{\partial u_i}{\partial t} \tag{3.2.3.3}$$

since

$$\vec{\nabla}\cdot\sigma = \begin{bmatrix}\frac{\partial}{\partial x} & \frac{\partial}{\partial y} & \frac{\partial}{\partial z}\end{bmatrix}\begin{bmatrix}\sigma_{xx} & \sigma_{xy} & \sigma_{xz}\\ \sigma_{yx} & \sigma_{yy} & \sigma_{yz}\\ \sigma_{zx} & \sigma_{zy} & \sigma_{zz}\end{bmatrix} = \begin{bmatrix}\sum_i \frac{\partial}{\partial r_i}\sigma_{ix} & \sum_i \frac{\partial}{\partial r_i}\sigma_{iy} & \sum_i \frac{\partial}{\partial r_i}\sigma_{iz}\end{bmatrix} \tag{3.2.3.4}$$

Here,

$$\sum_i \frac{\partial}{\partial r_i}\left[(\vec{\nabla}\cdot\vec{u})\delta_{ik}\right] = \frac{\partial}{\partial r_i}(\vec{\nabla}\cdot\vec{u}) = \nabla_i(\vec{\nabla}\cdot\vec{u}) \tag{3.2.3.5}$$

$$\begin{aligned}&\sum_j \frac{\partial}{\partial r_j}\left(\frac{\partial u_i}{\partial x_j}+\frac{\partial u_j}{\partial x_i}\right)\\ &= \frac{\partial^2 u_i}{\partial x^2}+\frac{\partial^2 u_i}{\partial y^2}+\frac{\partial^2 u_i}{\partial z^2}+\frac{\partial^2 u_x}{\partial x\partial r_i}+\frac{\partial^2 u_y}{\partial y\partial r_i}+\frac{\partial^2 u_z}{\partial z\partial r_i}\\ &= \Delta u_i + \nabla_i(\vec{\nabla}\cdot\vec{u})\end{aligned} \tag{3.2.3.6}$$

Substitute Eqs.(3.2.3.5) and (3.2.3.6) into Eq.(3.2.3.3):

$$\begin{aligned}\rho\frac{\partial^2 u_i}{\partial t^2} &= G\Delta u_i + \left(K+\frac{1}{3}G\right)\nabla_i(\vec{\nabla}\cdot\vec{u}) - f\frac{\partial u_i}{\partial t}\\ \rightarrow \rho\frac{\partial^2\vec{u}}{\partial t^2} &= G\Delta\vec{u} + \left(K+\frac{1}{3}G\right)\vec{\nabla}(\vec{\nabla}\cdot\vec{u}) - f\frac{\partial\vec{u}}{\partial t}\end{aligned} \tag{3.2.3.7}$$

Eq.(3.2.3.7) is easily solved by using Fourier transformation.

$$u_i(\vec{r},t) = \frac{1}{(2\pi)^2}\iint u_i(\vec{q},\omega)\exp[i(\vec{q}\cdot\vec{r}+\omega t)]d\vec{q}d\omega \tag{3.2.3.8}$$

$$\frac{\partial}{\partial t}u_i(\vec{r},t) = \frac{1}{(2\pi)^2}\iint i\omega u_i(\vec{q},\omega)\exp[i(\vec{q}\cdot\vec{r}+\omega t)]d\vec{q}d\omega \tag{3.2.3.9}$$

$$\frac{\partial^2}{\partial t^2}u_i(\vec{r},t) = \frac{1}{(2\pi)^2}\iint -\omega^2 u_i(\vec{q},\omega)\exp[i(\vec{q}\cdot\vec{r}+\omega t)]d\vec{q}d\omega \tag{3.2.3.10}$$

$$\left(\frac{\partial^2}{\partial x^2}+\frac{\partial^2}{\partial y^2}+\frac{\partial^2}{\partial z^2}\right)u_i(\vec{r},t) = \frac{1}{(2\pi)^2}\iint -q^2 u_i(\vec{q},\omega)\exp[i(\vec{q}\cdot\vec{r}+\omega t)]d\vec{q}d\omega \tag{3.2.3.11}$$

Here, we can set $\vec{q} := (0,0,q)$ without loss of generality since the fluctuation of gel is isotropic. Under this assumption:

$$\begin{aligned}\frac{\partial}{\partial r_i}\left(\frac{\partial u_x}{\partial x}+\frac{\partial u_y}{\partial y}+\frac{\partial u_z}{\partial z}\right)u_i(\vec{r},t) &= \frac{1}{(2\pi)^2}\frac{\partial}{\partial r_i}\iint iqu_z(\vec{q},\omega)\exp[i(\vec{q}\cdot\vec{r}+\omega t)]d\vec{q}d\omega \\ &= \begin{cases} 0 & i=x,y \\ \dfrac{1}{(2\pi)^2}\iint -q^2 u_z(\vec{q},\omega)\exp[i(\vec{q}\cdot\vec{r}+\omega t)]d\vec{q}d\omega & i=z \end{cases}\end{aligned} \tag{3.2.3.12}$$

By using Eqs.(3.2.3.8) $\sim$ (3.2.3.12), Eq.(3.2.3.7) is written as follows.

$$\begin{cases} \dfrac{1}{(2\pi)^2}\iint \left[\rho\omega^2 - if\omega - Gq^2\right]u_i(\vec{q},\omega)\exp[i(\vec{q}\cdot\vec{r}+\omega t)]d\vec{q}d\omega = 0 & i=x,y \\ \dfrac{1}{(2\pi)^2}\iint \left[\rho\omega^2 - if\omega - \left(K+\dfrac{4}{3}G\right)q^2\right]u_z(\vec{q},\omega)\exp[i(\vec{q}\cdot\vec{r}+\omega t)]d\vec{q}d\omega = 0 & i=z \end{cases} \tag{3.2.3.13}$$

Eq.(3.2.3.13) is rewritten as follows:

$$\begin{cases} \left[\rho\omega^2 - if\omega - \rho c_t^2 q^2\right]u_i(\vec{q},\omega) = 0 & i=x,y \\ \left[\rho\omega^2 - if\omega - \rho c_l^2 q^2\right]u_z(\vec{q},\omega) = 0 & i=z \end{cases} \tag{3.2.3.14}$$

where

$$c_t := \sqrt{\frac{G}{\rho}} \tag{3.2.3.15}$$

$$c_l := \sqrt{\frac{K+\frac{4}{3}G}{\rho}} \tag{3.2.3.16}$$

Eqs.(3.2.3.15) and (3.2.3.16) correspond to the transverse and longitudinal sound velocities, respectively. From now, we use c to express both c_t and c_l. By using this notation, two equations in Eqs.(3.2.3.14) can be treated simultaneously. When $u_i(\vec{q},\omega)$ has non-trivial solution, Eqs.(3.2.3.14) becomes:

$$\rho\omega^2 - if\omega - \rho c^2 q^2 = 0 \tag{3.2.3.17}$$

The solution of Eq.(3.2.3.17) is:

$$i\omega = -\frac{1}{\tau_0}(1 \pm \sqrt{1-\omega_0^2\tau_0^2}) \tag{3.2.3.18}$$

where

$$\omega_0 := cq \tag{3.2.3.19}$$

$$\tau_0 := \frac{2\rho}{f} \tag{3.2.3.20}$$

When $\omega_0\tau_0 \gg 1$, Eq.(3.2.3.18) is solved as follows:

$$\omega = \pm\omega_0 + \frac{i}{\tau_0} \tag{3.2.3.21}$$

From Eq.(3.2.3.21), the meaning of ω_0 and τ_0 are clarified. ω_0 stands for the angular frequency of the propagating wave (sound wave). τ_0 stands for the relaxation time of the non-propagating wave. Note that $e^{i\omega t} = e^{\pm i\omega_0 t}e^{-t/\tau_0}$. When $\omega_0\tau_0 \ll 1$, which is the case for gels, Eq.(3.2.3.18) is solved as follows:

$$\omega = \begin{cases} if/\rho = 2i/\tau_0 \\ i\rho c^2 q^2/f = i\tau_0\omega_0^2/2 \end{cases} \tag{3.2.3.22}$$

Each solution is purely imaginary. This means that there are only non-propagating waves. The first solution in Eq.(3.2.3.22) can be obtained by assuming that the elastic term is negligibly small. In other words, $c \to 0$ in Eq.(3.2.3.17).

$$\rho\omega^2 - if\omega = 0 \Rightarrow \omega = i\frac{f}{\rho} \tag{3.2.3.23}$$

Usually, this frequency is too large (fast) to be observed by using dynamic light scattering (the order of nanoseconds^{-1}). In contrast to this, the second solution in Eq.(3.2.3.22) can be obtained by assuming that the acceleration term is negligibly small. In other words, $\rho\omega^2 \to 0$ in Eq.(3.2.3.17).

$$-if\omega - \rho c^2 q^2 = 0 \Rightarrow \omega = i\frac{\rho c^2 q^2}{f} \tag{3.2.3.24}$$

This frequency is suitable for the measurement by using dynamic light scattering (the order of milliseconds^{-1}). In real space, this approximation makes Eq.(3.2.3.7) diffusion equation. By assuming that $\vec{q} = (0, 0, q)$, Eq.(3.2.3.7) without acceleration term (light hand side) can be written as follows.

$$\begin{aligned} & G\Delta u_i + \left(K + \frac{1}{3}G\right)\nabla_i(\vec{\nabla}\cdot\vec{u}) - f\frac{\partial u_i}{\partial t} \\ & = G\left(\frac{\partial^2 u_i}{\partial x^2} + \frac{\partial^2 u_i}{\partial y^2} + \frac{\partial^2 u_i}{\partial z^2}\right) + \left(K + \frac{1}{3}G\right)\frac{\partial}{\partial r_i}\left(+\frac{\partial u_x}{\partial x} + \frac{\partial u_y}{\partial y} + \frac{\partial u_z}{\partial z}\right) - f\frac{\partial u_i}{\partial t} \\ & = \begin{cases} G\dfrac{\partial^2 u_i}{\partial z^2} - f\dfrac{\partial u_i}{\partial t} = 0 & i = x, y \\ \left(K + \dfrac{4}{3}G\right)\dfrac{\partial^2 u_i}{\partial z^2} - f\dfrac{\partial u_i}{\partial t} = 0 & i = z \end{cases} \end{aligned} \tag{3.2.3.25}$$

Eq.(3.2.3.25) is summarized as follows.

$$\frac{\partial\vec{u}}{\partial t} = \frac{M}{f}\frac{\partial^2\vec{u}}{\partial z^2} \tag{3.2.3.26}$$

where

$$M = \begin{cases} G & \text{for transverse modes} \\ K + \dfrac{4}{3}G & \text{for a longitudinal mode} \end{cases} \tag{3.2.3.27}$$

Eq.(3.2.3.26) has the same form as the diffusion equation.

$$\frac{\partial \phi(\vec{r}, t)}{\partial t} = D\Delta\phi(\vec{r}, t) \tag{3.2.3.28}$$

Therefore, M/f represents the diffusion constants for the fluctuation of network strands in the gel. When we apply Einstein–Stokes relationship, characteristic length, ξ, is called correlation length. ξ is sometimes interpreted as the mesh size of the network. Eq.(3.2.3.26) has the same form as the diffusion equation.

$$\frac{M}{f} =: \frac{k_B T}{6\pi\eta\xi} \tag{3.2.3.29}$$

3.2.4 Polymers with lower critical solution temperature

Solubility of solid substance usually increases as the temperature increases. This is mainly due to the entropy term. When solid substance dissolve is dissolved in liquid, solute can move freely in solution. This means that dissolution is preferable from the viewpoint of entropy [22]. Contribution of entropic change, ΔS, to the free energy is $-T\Delta S$ where T is absolute temperature. Therefore, the tendency of dissolution is strengthen when temperature increases. In the case of polymer solution, situation becomes more complicated. First I'm going to explain the phase separation by using lattice model [54]. Let us consider how to set N_s solvents and N_p polymers to N_t lattice whose coordination number is z (Figure 3.4). Here, the degree of polymerization of the polymers is assume to be N. In this case, $N_t = N_s + NN_p$.

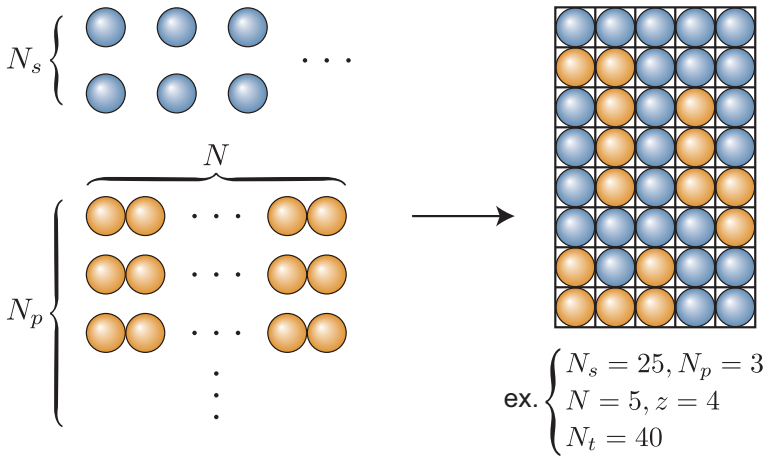

Figure 3.4: Lattice model.

To calculate entropy of mixing, let us consider the number of ways of putting the first polymer to the lattice, ν_1. The number of ways to put the first monomer is the number of lattice sites, N_t. Next monomer can be set to either z sites next to the first monomer. Third monomer can be set to either $z - 1$ sites next

[22] The same discussion holds true for dissolution of liquid. In the case of gas substance, dissolution restrict the motion of gas molecule. Therefore, dissolution of gas is not preferable from the viewpoint of entropy. This is the main reason why solubility of gas substance usually decreases as the temperature increases

to the second monomer. Like this, other monomers can be set to either $z-1$ sites next to the previous monomer if other previous monomers do not interfere. As a result, ν_1 is represented as follows.

$$\nu_1 = N_t z(z-1)^{N-2} \tag{3.2.4.1}$$

Next, let us consider the number of ways of putting the second polymer to the lattice, ν_1. The number of ways to put the first monomer is the number of unoccupied lattice sites, $N_t - N$. Next monomer can be set to either z sites next to the first monomer if they are unoccupied. Here we assume that the probability that the site next to the monomers of the second polymer is approximated to be $(N_t - N)/N_t$, the occupancy of all the lattice sites. By using this assumption, ν_2 is represented as follows.

$$\begin{aligned}\nu_2 &= (N_t - N)\left(z\frac{N_t - N}{N_t}\right)\left((z-1)\frac{N_t - N}{N_t}\right)\left((z-1)\frac{N_t - N}{N_t}\right)\cdots \\ &= (N_t - N)z(z-1)^{N-2}\left(\frac{N_t - N}{N_t}\right)^{N-1}\end{aligned} \tag{3.2.4.2}$$

By using the similar discussion, the number of ways of putting the $i+1$th polymer to the lattice, ν_i is represented as follows.

$$\nu_{i+1} = (N_t - iN)z(z-1)^{N-2}\left(\frac{N_t - iN}{N_t}\right)^{N-1} \tag{3.2.4.3}$$

Eq.(3.2.4.3) is mathematically approximated as follows.

$$\begin{aligned}\nu_{i+1} &\simeq (N_t - iN)(z-1)^{N-1}\left(\frac{N_t - iN}{N_t}\right)^{N-1} \\ &= (N_t - iN)^N\left(\frac{z-1}{N_t}\right)^{N-1} \\ &\simeq (N_t - iN)(N_t - iN - 1)\cdots(N_t - (i+1)N + 1)\left(\frac{z-1}{N_t}\right)^{N-1} \\ &= \frac{(N_t - iN)!}{(N_t - (i+1)N)!}\left(\frac{z-1}{N_t}\right)^{N-1}\end{aligned} \tag{3.2.4.4}$$

Total number of ways of putting all N_p polymers to the lattice, Ω_{sp} is therefore calculated as follows.

$$\begin{aligned}\Omega_{sp} &= \frac{1}{N_p!}\Pi_{i=1}^{N_p}\nu_i \\ &\simeq \frac{1}{N_p!}\frac{N_t!}{(N_t - N)!}\frac{(N_t - N)!}{(N_t - 2N)!}\cdots\frac{(N_t - (N_p - 1)N)!}{(N_t - N_pN)!}\left(\frac{z-1}{N_t}\right)^{N_p(N-1)} \\ &= \frac{N_t!}{(N_t - N_pN)!N_p!}\left(\frac{z-1}{N_t}\right)^{N_p(N-1)} \\ &= \frac{N_t!}{N_s!N_p!}\left(\frac{z-1}{N_t}\right)^{N_p(N-1)}\end{aligned} \tag{3.2.4.5}$$

Here, $1/N_p!$ is added since we cannot distinguish each polymer. By using Stirling's approximation,

$$\ln X! \simeq X\ln X - X \quad \text{when} \quad X \gg 1 \tag{3.2.4.6}$$

logarithm of Eq.(3.2.4.5) is:

$$\begin{aligned}\ln \Omega_{sp} &\simeq (N_t \ln N_t - N_t) - (N_s \ln N_s - N_s) - (N_p \ln N_p - N_p) + N_p(N-1)(\ln(z-1) - \ln N_t) \\ &= (N_s \ln N_t + N_p \ln N_t + (N-1)N_p \ln N_t - (N_s + NN_p)) \\ &\quad - (N_s \ln N_s - N_s) - (N_p \ln N_p - N_p) + N_p(N-1)\ln(z-1) - N_p(N-1)\ln N_t \\ &= -N_s \ln \frac{N_s}{N_t} - N_p \ln \frac{N_p}{N_t} + N_p(N-1)(\ln(z-1) - 1) \end{aligned} \tag{3.2.4.7}$$

Entropy of mixing, ΔS_{mix} is calculated by subtracting the entropy of pure solvents, S_s, and pure polymers, S_p, from the entropy of solution, S_{sp}. Entropies of pure solvent, pure polymers, and mixture are obtained as follows.

$$S_{sp} = k_B \ln \Omega_{sp} \tag{3.2.4.8}$$

$$S_s = k_B \ln \Omega_{sp}(N_p = 0) = k_B N_s \ln \frac{N_s}{N_s} = 0 \tag{3.2.4.9}$$

$$\begin{aligned} S_p &= k_B \ln \Omega_{sp}(N_s = 0) = k_B \left(-N_p \ln \frac{N_p}{NN_p} + N_p(N-1)(\ln(z-1) - 1) \right) \\ &= k_B N_p \ln \frac{N(z-1)^{N-1}}{e^{N-1}} \end{aligned} \tag{3.2.4.10}$$

Since we cannot distinguish each solute, the entropy of pure solvents is zero. In contrast to this, the entropy of pure polymers is nonzero since each polymer has internal degree of freedom. Eq.(3.2.4.10) is called the entropy of disorientation. By using Eqs.(3.2.4.8) $\sim$ (3.2.4.10), entropy of mixing is calculated as follows.

$$\Delta S_{mix} = S_{sp} - S_s - S_p = -N_s \ln \frac{N_s}{N_t} - N_p \ln \frac{N_p}{N_t} - N_p \ln N = -N_s \ln \phi_s - N_p \ln \phi_p \tag{3.2.4.11}$$

where ϕ_s and ϕ_p stand for the fraction of solvents and polymers, respectively.

$$\phi_s := \frac{N_s}{N_t} \tag{3.2.4.12}$$

$$\phi_p := \frac{NN_p}{N_t} \tag{3.2.4.13}$$

Note that $\phi_s + \phi_p = 1$. The mixing entropy pre lattice is (Eq.(3.2.2.1)):

$$\Delta \bar{S}_{mix} = \frac{\Delta S_{mix}}{N_t} = -k_B \left(\phi_s \ln \phi_s - \frac{\phi_p}{N} \ln \phi_p \right) \tag{3.2.4.14}$$

Next, let us consider the enthalpy term. In the case of lattice model, pressure and volume is regarded as a constant. Therefore, mixing enthalpy is equal to the change of energy.

$$\Delta H_{mix} = \Delta(U_{mix} - PV) = \Delta U_{mix} \tag{3.2.4.15}$$

Pairwise interaction energies between two solvents, two monomers, and a solvent and a monomer are defined as u_{ss}, u_{pp}, u_{sp}, respectively. By calculating the number of contacts, internal energies of pure solvent, U_s and pure polymers, U_p, are obtained as follows.

$$U_s = N_t \phi_s z u_{ss}/2 \tag{3.2.4.16}$$

$$U_p = N_t \phi_p z u_{pp}/2 \tag{3.2.4.17}$$

Here, $N_t\phi_s z/2$ and $N_t\phi_p z/2$ are the number of contacts in pure solvent and pure polymers, respectively. To calculate the internal energies of solution, U_{sp}, we assume that the number of contacts between two solvents is $N_t\phi_s^2$, the number of contacts between two polymers is $N_t\phi_p^2$, and the number of contacts between a solvent and a monomer is $2N_t\phi_s\phi_p$, respectively. In actual, the number of contacts between two polymers will be larger than $N_t\phi_p^2$ because of the connectivity. However, the effect of the connectivity is neglected in this assumption. Therefore, mixing enthalpy is calculated as follows.

$$U_{sp} = N_t(u_{ss}\phi_s^2 + u_{pp}\phi_p^2 + 2u_{sp}\phi_s\phi_p)z/2 \tag{3.2.4.18}$$

$$\begin{aligned}\Delta H_{mix} &= U_{sp} - U_s - U_p \\ &= N_t(u_{ss}\phi_s^2 + u_{pp}\phi_p^2 + 2u_{sp}\phi_s\phi_p - \phi_s u_{ss} - \phi_p u_{pp})z/2 \\ &= N_t(u_{ss}\phi_s(\phi_s - 1) + u_{pp}\phi_p(\phi_p - 1) + 2u_{sp}\phi_s\phi_p)z/2 \\ &= N_t\phi_s\phi_p(2u_{sp} - u_{ss} - u_{pp})z/2 \qquad (3.2.4.19) \\ &=: k_B T N_t \chi \phi_s \phi_p \qquad (3.2.4.20)\end{aligned}$$

where

$$\chi := \frac{z}{2}\frac{2u_{sp} - u_{ss} - u_{pp}}{k_B T} \tag{3.2.4.21}$$

The mixing entropy per lattice is (Eq.(3.2.2.2)):

$$\Delta\bar{H}_{mix} = \frac{\Delta H_{mix}}{N_t} = k_B T \chi \phi_s \phi_p \tag{3.2.4.22}$$

By using Eqs.(3.2.4.14) and (3.2.4.22), Gibbs energy for mixing per lattice is calculated as follows.

$$\Delta\bar{G}_{mix} = \Delta\bar{H}_{mix} - T\Delta\bar{S}_{mix} = k_B T\left[\frac{\phi}{N}\ln\phi + (1-\phi)\ln(1-\phi) + \chi\phi(1-\phi)\right] \tag{3.2.4.23}$$

where $\phi := \phi_p$ stands for polymer fraction. When $N = 1$, Eq.(3.2.4.23) becomes the Gibbs energy for mixing of two solvent. In this case, phase separation occurs as a function of temperature. Figure 3.5 shows ϕ-dependence of $\Delta\bar{G}_{mix}$. When the temperature is fixed, phase separation occurs when χT is large. In extreme case, phase separation never occurs when $\chi = 0$. Physical meaning is that phase separation is induced by the interaction energy between solvents and solutes. When χT is fixed, phase separation occurs when T is small since the entropy term becomes small relative to the enthalpy term. This type of phase separation is called upper critical solution temperature (UCST) type phase transition. When $N > 1$, ϕ-dependence of $\Delta\bar{G}_{mix}$ becomes asymmetric. Although phase separation can be explained similar to the case of $N = 1$, only UCST type phase separation is described.

In contrast to this, there is an opposite phenomenon called lower critical solution temperature (LCST) type phase transition. Typical example of LCST is poly(N-isopropylacrylamide) (PNIPA) [55] whose solution becomes turbid at temperature higher than 32 °C. The gel prepared by PNIPA shows volume phase separation at 34 °C and can be used for application such as drug delivery system [56]. Here I'm going to describe the theory to explain LCST by using lattice model developed by Matsuyama and Tanaka [57].

In this model, we consider association of a polymer and solvents (Figure 3.6). These clusters are in equilibrium. Polymer fraction before mixing is ϕ. After mixing, several solvents are attached to each polymer. These equilibrium is expressed as equilibrium constants, K_i where i is the number of associated

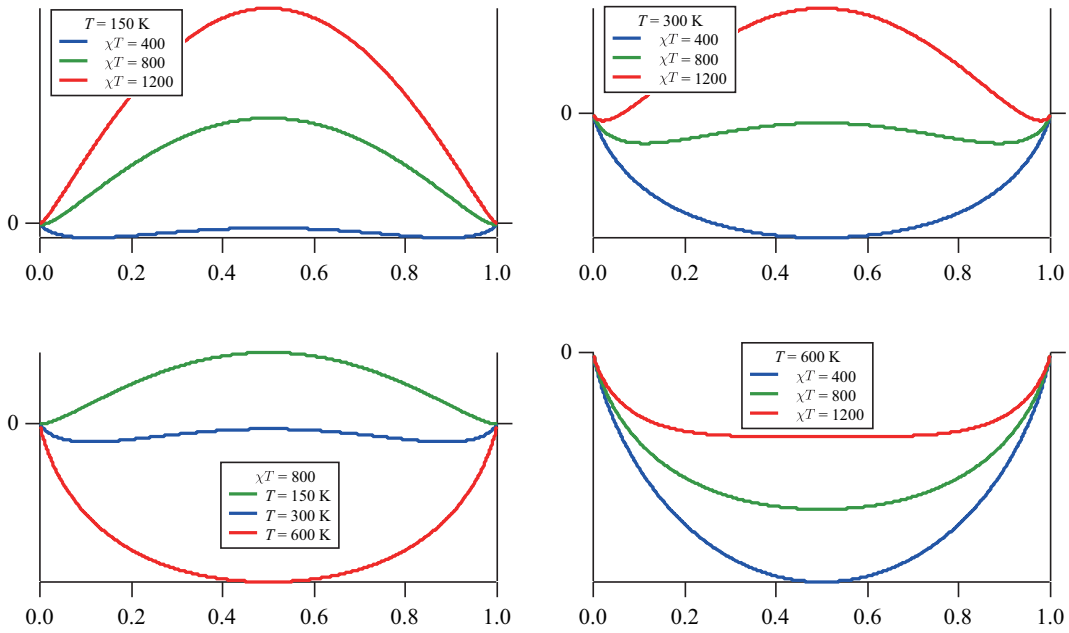

Figure 3.5: ϕ-dependence of $\Delta\bar{G}_{mix}$ of liquid mixture with different χ and T.

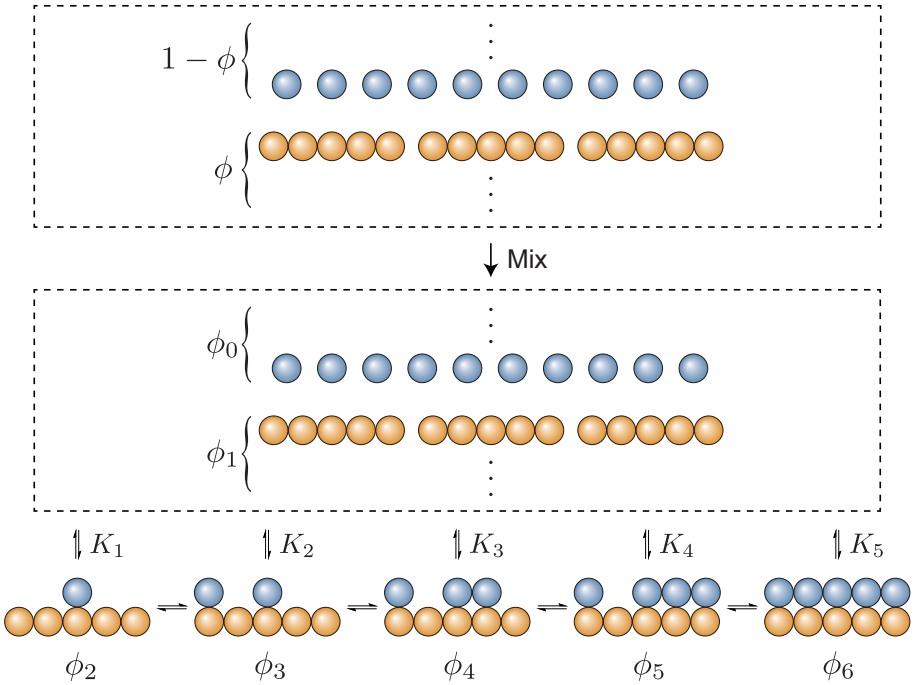

Figure 3.6: Extended lattice model for LCST. As an example, $N = 5$ and $f = N$ is assumed in this figure.

solvents. Degree of polymerization is set to be N and the maximum association number is set to be f. Volume fraction of pure solvent after mixing is expressed as ϕ_0. Volume fractions of clusters with i solvents (i cluster, $0 \leq i \leq f$) are expressed as ϕ_{i+1}. Here, 0 cluster stands for the unbonded polymer. To apply this system to lattice model, we set the number of solvents as N_0 and the number of i clusters as N_{i+1}. From

these definitions, we can obtain the following relationship.

$$N_t = N_0 + \sum_{i=0}^{f}(N+i)N_{i+1} \tag{3.2.4.24}$$

$$\phi = \sum_{i=0}^{f}\frac{N}{N+i}\phi_{i+1} = \sum_{i=0}^{f}\frac{NN_{i+1}}{N_t} \tag{3.2.4.25}$$

The free energy of this system, G, is the summation of two terms. The first term is the free energy of isolated system, G_{ref}.

$$G_{ref} := N_0\mu_0^\circ + \sum_{i=0}^{f}N_{i+1}\mu_{i+1}^\circ \tag{3.2.4.26}$$

where μ_0° is the chemical potential of an isolated solvent and μ_i° is that of an isolated i cluster. The second term is the free energy of mixing, G_{mix}. This term is expressed by extending the expression Eq.(3.2.4.23).

$$\begin{aligned} G_{mix} &:= N_t k_B T\left[\phi_0\ln\phi_0 + \sum_{i=0}^{f}\frac{\phi_{i+1}}{N+i}\ln\phi_{i+1} + \chi\phi(1-\phi)\right] \\ &= k_B T\left[N_0\ln\phi_0 + \sum_{i=0}^{f}N_{i+1}\ln\phi_{i+1} + \chi N_t\phi(1-\phi)\right] \end{aligned} \tag{3.2.4.27}$$

Here, I used the following relationship.

$$\frac{\phi_{i+1}}{N+i} = \frac{(N+i)N_{i+1}}{N_t}\frac{1}{N+i} = \frac{N_{i+1}}{N_t} \tag{3.2.4.28}$$

For the calculation of enthalpy, the interaction energy of polymer and associated solvents is neglected. In other words, u_{sp} used for χ stands for the pairwise interaction energy between a free solvent and a monomer.

Next issue is the determination of ϕ_0 and ϕ_{i+1} for $0 \le i \le f$. To determine the volume fractions, we use the equilibrium condition of i cluster. When the free solvents and polymers are in equilibrium with i clusters, the following relationship should hold.

$$\phi_{i+1} = K_i\phi_1\phi_0^i \tag{3.2.4.29}$$

$$\mu_{i+1} = \mu_1 + i\mu_0 \tag{3.2.4.30}$$

Here, μ_0 and μ_{i+1} $(0 \le i \le f)$ stands for the chemical potential of free solvent and that of i cluster in the mixture and represented as follows.

$$\mu_0 = \frac{\partial G}{\partial N_0} = \frac{\partial G_{ref}}{\partial N_0} + \frac{\partial G_{mix}}{\partial N_0} \tag{3.2.4.31}$$

$$\mu_{i+1} = \frac{\partial G}{\partial N_{i+1}} \tag{3.2.4.32}$$

To calculate Eq.(3.2.4.31) explicitly, following relationships are used.

$$\frac{\partial N_t}{\partial N_0} = 1 \tag{3.2.4.33}$$

$$\frac{\partial}{\partial N_0}\ln\phi_0 = \frac{\partial\phi_0}{\partial N_0}\frac{1}{\phi_0} = \frac{\partial}{\partial N_0}\left(\frac{N_0}{N_t}\right)\frac{N_t}{N_0}$$
$$= \left[\frac{1}{N_t} + N_0\frac{\partial N_t}{\partial N_0}\frac{dN_t^{-1}}{dN_t}\right]\frac{N_t}{N_0} = \frac{1}{N_0} - \frac{1}{N_t} \tag{3.2.4.34}$$

$$\frac{\partial}{\partial N_0}\ln\phi_{i+1} = \frac{\partial\phi_{i+1}}{\partial N_0}\frac{1}{\phi_{i+1}} = \frac{\partial}{\partial N_0}\left(\frac{(N+i)N_{i+1}}{N_t}\right)\frac{N_t}{(N+i)N_{i+1}}$$
$$= \frac{\partial N_t}{\partial N_0}\frac{dN_t^{-1}}{dN_t}N_t = -\frac{1}{N_t} \tag{3.2.4.35}$$

$$\frac{\partial\phi}{\partial N_0} = \frac{\partial}{\partial N_0}\sum_{i=0}^{f}\frac{NN_{i+1}}{N_t} = \sum_{i=0}^{f}NN_{i+1}\frac{\partial N_t}{\partial N_0}\frac{dN_t^{-1}}{dN_t} = -\frac{\phi}{N_t} \tag{3.2.4.36}$$

$$\frac{\partial}{\partial N_0}[\phi(1-\phi)] = \frac{\partial\phi}{\partial N_0}(1-2\phi) = -\frac{\phi(1-2\phi)}{N_t} \tag{3.2.4.37}$$

By using Eqs.(3.2.4.33) $\sim$ (3.2.4.37), Eq.(3.2.4.31) is calculated as follows.

$$\beta\mu_0 = \beta\mu_0^\circ + \frac{\partial}{\partial N_0}\left[N_0\ln\phi_0 + \sum_{i=0}^{f}N_{i+1}\ln\phi_{i+1} + \chi N_t\phi(1-\phi)\right]$$
$$= \beta\mu_0^\circ + \left[\ln\phi_0 + N_0\left(\frac{1}{N_0} - \frac{1}{N_t}\right) - \sum_{i=0}^{f}\frac{N_{i+1}}{N_t} + \chi[\phi(1-\phi) - \phi(1-2\phi)]\right]$$
$$= \beta\mu_0^\circ + \ln\phi_0 + 1 - \left[\phi_0 + \frac{\phi}{N}\right] + \chi\phi^2 \tag{3.2.4.38}$$

where $\beta := (k_BT)^{-1}$. To calculate Eq.(3.2.4.32) explicitly, following relationships are used.

$$\frac{\partial N_t}{\partial N_{i+1}} = N + i \tag{3.2.4.39}$$

$$\frac{\partial}{\partial N_{i+1}}\ln\phi_0 = \frac{\partial\phi_0}{\partial N_{i+1}}\frac{1}{\phi_0} = \frac{\partial}{\partial N_{i+1}}\left(\frac{N_0}{N_t}\right)\frac{N_t}{N_0}$$
$$= \frac{\partial N_t}{\partial N_{i+1}}\frac{dN_t^{-1}}{dN_t}N_t = -\frac{N+i}{N_t} \tag{3.2.4.40}$$

$$\frac{\partial}{\partial N_{i+1}}\ln\phi_{k+1} = \frac{\partial\phi_{k+1}}{\partial N_{i+1}}\frac{1}{\phi_{k+1}} = \frac{\partial}{\partial N_{i+1}}\left(\frac{(N+k)N_{k+1}}{N_t}\right)\frac{N_t}{(N+k)N_{k+1}}$$
$$= \frac{\partial N_t}{\partial N_0}\frac{dN_t^{-1}}{dN_t}N_t = -\frac{N+i}{N_t} \tag{3.2.4.41}$$

$$\frac{\partial}{\partial N_{i+1}}\ln\phi_{i+1} = \frac{\partial\phi_{i+1}}{\partial N_{i+1}}\frac{1}{\phi_{i+1}} = \frac{\partial}{\partial N_{i+1}}\left(\frac{(N+i)N_{i+1}}{N_t}\right)\frac{N_t}{(N+i)N_{i+1}}$$
$$= \left[\frac{1}{N_t} + N_{i+1}\frac{\partial N_t}{\partial N_{i+1}}\frac{dN_t^{-1}}{dN_t}\right]\frac{N_t}{N_{i+1}} = \frac{1}{N_{i+1}} - \frac{N+i}{N_t} \tag{3.2.4.42}$$

$$\frac{\partial\phi}{\partial N_{i+1}} = \frac{\partial}{\partial N_{i+1}}\sum_{k=0}^{f}\frac{NN_{k+1}}{N_t} = \frac{N}{N_t} + \sum_{k=0}^{f} NN_{k+1}\frac{\partial N_t}{\partial N_{i+1}}\frac{dN_t^{-1}}{dN_t}$$
$$= \frac{N}{N_t} - \sum_{k=0}^{f} NN_{k+1}\frac{N+i}{N_t^2} = \frac{N}{N_t} - \frac{N+i}{N_t}\phi \tag{3.2.4.43}$$

$$\frac{\partial}{\partial N_{i+1}}[\phi(1-\phi)] = \frac{\partial\phi}{\partial N_{i+1}}(1-2\phi) = \left[\frac{N}{N_t} - \frac{N+i}{N_t}\phi\right](1-2\phi) \tag{3.2.4.44}$$

By using Eqs.(3.2.4.39) $\sim$ (3.2.4.44), Eq.(3.2.4.32) is calculated as follows.

$$\beta\mu_{i+1} = \beta\mu_{i+1}^{\circ} + \frac{\partial}{\partial N_{i+1}}\left[N_0\ln\phi_0 + \sum_{k=0}^{f} N_{k+1}\ln\phi_{k+1} + \chi N_t\phi(1-\phi)\right]$$
$$= \beta\mu_{i+1}^{\circ} + \left[-N_0\frac{N+i}{N_t} + \ln\phi_{i+1} + 1 - \sum_{k=0}^{f} N_{k+1}\frac{N+i}{N_t} + (N+i)\chi\phi(1-\phi) + \chi(N-(N+i)\phi)(1-2\phi)\right]$$
$$= \beta\mu_{i+1}^{\circ} + \ln\phi_{i+1} + 1 - (N+i)\left[\phi_0 + \frac{\phi}{N}\right] + N\chi\left[(1-\phi)^2 + \frac{i}{N}\phi^2\right] \tag{3.2.4.45}$$

Substitute Eqs.(3.2.4.38) and (3.2.4.45) into Eq.(3.2.4.30):

$$\beta\mu_{i+1}^{\circ} + \ln\phi_{i+1} + 1 - (N+i)\left[\phi_0 + \frac{\phi}{N}\right] + \chi[N(1-\phi)^2 + i\phi^2]$$
$$= \beta\mu_1^{\circ} + \ln\phi_1 + 1 - N\left[\phi_0 + \frac{\phi}{N}\right] + \chi[N(1-\phi)^2]$$
$$+ i\beta\mu_0^{\circ} + \ln\phi_0^i + i - i\left[\phi_0 + \frac{\phi}{N}\right] + \chi[i\phi^2]$$

$$\rightarrow \beta\mu_{i+1}^{\circ} + \ln\phi_{i+1} = \beta\mu_1^{\circ} + \ln\phi_1 + i\beta\mu_0^{\circ} + \ln\phi_0^i + i \tag{3.2.4.46}$$

From Eq.(3.2.4.46), K_i is calculated as follows.

$$\ln\frac{\phi_{i+1}}{\phi_1\phi_0^i} = i - \beta(\mu_{i+1}^{\circ} - \mu_1^{\circ} - i\mu_0^{\circ}) =: i - \Delta_i$$
$$\rightarrow \phi_{i+1} = \exp[i-\Delta_i]\phi_1\phi_0^i =: K_i\phi_1\phi_0^i \tag{3.2.4.47}$$

Remaining task is the determination of Δ_i, the difference of chemical potentials before and after the association in isolated environment. Let us this term into entropy part and enthalpy part (Figure 3.7).

$$\Delta_i := \beta(\mu_{i+1}^{\circ} - \mu_1^{\circ} - i\mu_0^{\circ})$$
$$=: \beta(\Delta H - T\Delta S) \tag{3.2.4.48}$$

Enthalpy part is simply represented by the summation of association energy between a monomer and a solvent, $\Delta\varepsilon(>0)$.

$$\Delta H = -i\Delta\varepsilon \tag{3.2.4.49}$$

Note that i cluster has i association sites.

Entropy part is further decomposed into two contributions. First one is combinatorial entropy. This term

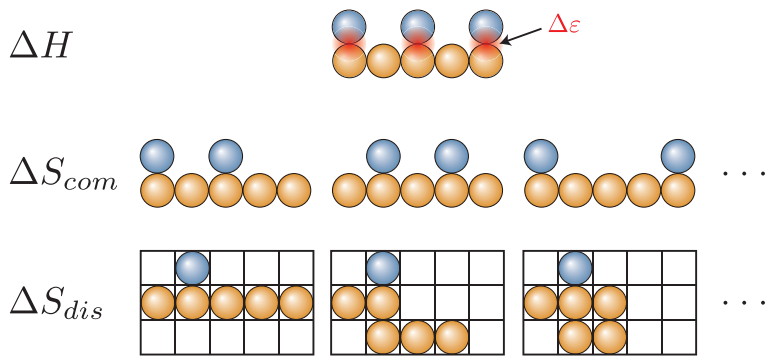

Figure 3.7: Decomposition of Δ_i into entropy part and enthalpy part.

originates from the number of ways to choose i sites from f sites, which is calculated as follows.

$$\Delta S_{com} = k_B \ln \frac{f!}{i!(f-i)!} \tag{3.2.4.50}$$

Second one is disorientation entropy. This term originates from the number of ways to put i cluster into $N+i$ lattice cells, which has already calculated in Eq.(3.2.4.10). I define this entropy as $S(N,i)$. The disorientation entropy of one unbonded polymer whose degree of polymerization is N is:

$$S(N,0) = k_B \ln \frac{N(z-1)^{N-1}}{\sigma e^{N-1}} \tag{3.2.4.51}$$

Here, σ, the symmetry number, is added. When we can distinguish the direction of the polymer, $\sigma = 1$. When we cannot distinguish the direction of the polymer, $\sigma = 2$ since the way of filling from the first to the last monomer is the same of that from the last to the first monomer. Eq.(3.2.4.51) can be extended to the case of i clusters as follows.

$$S(N,i) = k_B \ln \left[\frac{(N+i)(z-1)^{N+i-1}}{\sigma e^{N+i-1}} w^i \right] \tag{3.2.4.52}$$

where $\ln w$ stands for the decrease of entropy due to one bond formation. Then disorientation entropy is calculated as follows.

$$\begin{aligned}
\Delta S_{dis}/k_B &= (S(n,i) - S(n,0) - iS(1,0))/k_B \\
&= \ln(N+i) + (N+i-1)\ln(z-1) + \ln w^i - \ln\sigma - (N+i-1) \\
&\quad - \ln N - (N-1)\ln(z-1) + \ln\sigma + (N-1) + m\ln\sigma \\
&= \ln\frac{N+i}{N} + i\ln(z-1) + \ln w^i + i\ln\sigma - i \\
&= \ln\left[\frac{N+i}{N}\left(\frac{(z-1)w\sigma}{e}\right)^i\right] =: \ln\left[\frac{N+i}{N}\lambda_0^i\right]
\end{aligned} \tag{3.2.4.53}$$

By substituting Eqs.(3.2.4.49), (3.2.4.50), and (3.2.4.53) into Eq.(3.2.4.48), Δ_i is represented as follows.

$$\Delta_i = -i\beta\Delta\varepsilon - \ln\frac{N+i}{N}\frac{f!}{i!(f-i)!} - \ln\lambda_0^i \tag{3.2.4.54}$$

Substitute Eq.(3.2.4.54) into Eq.(3.2.4.47), K_i is calculated as follows.

$$K_i = \frac{N+i}{N}\frac{f!}{i!(f-i)!}\lambda(T)^i \tag{3.2.4.55}$$

where

$$\lambda(T) := \lambda_0 e^{1+\beta\Delta\varepsilon} \tag{3.2.4.56}$$

Eq.(3.2.4.55) shows that K_i does not depend on ϕ and changes as a function of T. We can calculate ϕ_i for given ϕ under the condition of Eq.(3.2.4.25). From this information, we can calculate the free energy from Eqs.(3.2.4.26) and (3.2.4.27). Matsuyama and Tanaka showed that there are certain parameter sets which reproduce LCST type phase separation, which reproduce the phase diagram of polyethylene glycol [57]. Later, phase separation of PNIPA was also reproduced by taking the effect of cooperative association [58]. Here, the interaction between bonded solutes are included. Once one solute is bonded to the polymer, other free solutes can be easily bonded to the site next to the bonded solute. This kind of cooperative association was observed experimentally by dielectric relaxation techniques [59].

3.3 Microphase separation

3.3.1 Helmholtz free energy as a functional of $\phi(\vec{r})$

First, let us describe Helmholtz free energy of the system with M polymers. Here, we assume that all of the polymers are homopolymers with $N+1$ segments. To specify this system, what we have to designate is the coordinates of all of the segments. The space spanned by these coordinates are called Γ.

$$\Gamma := \left\{(\vec{r}_0^{(1)},\cdots,\vec{r}_N^{(1)}),(\vec{r}_0^{(2)},\cdots,\vec{r}_N^{(2)}),\cdots(\vec{r}_0^{(M)},\cdots,\vec{r}_N^{(M)})\right\} =: \Gamma_1\Gamma_2\cdots\Gamma_M \tag{3.3.1.1}$$

where $\vec{r}_j^{(i)}$ is the coordinate of jth segments of ith polymer. Subspace spanned by ith polymer is represented as Γ_i. The energy of the system Γ without any interaction is defined as $\hat{\mathcal{H}}_0(\Gamma)$.[23]

$$\hat{\mathcal{H}}_0(\Gamma_i) := \frac{3k_BT}{2b^2}\sum_{j=0}^{N-1}\left|\vec{r}_{j+1}^{(i)} - \vec{r}_j^{(i)}\right|^2 \tag{3.3.1.2}$$

$$\hat{\mathcal{H}}_0(\Gamma) := \sum_{i=1}^{M}\hat{\mathcal{H}}_0(\Gamma_i) \tag{3.3.1.3}$$

Here, I apply bond-beads model. In this model, energy of the system is expressed as the summation of the potential energy of spring whose spring constant is $3k_BT/b^2$. [24]

The energy of the system Γ originated from interactions between polymers are represented as $\hat{\mathcal{W}}(\Gamma)$. Therefore, total Hamiltonian of the system is:

$$\hat{\mathcal{H}}(\Gamma) = \hat{\mathcal{H}}_0(\Gamma) + \hat{\mathcal{W}}(\Gamma) \tag{3.3.1.4}$$

[23] The symbol $\hat{A}$ means that the quantity A is related to the microscopic state defined by certain configuration Γ.

[24] The minimum value of $\hat{\mathcal{H}}_0(\Gamma_i)$ is 0 when $\vec{r}_0^{(i)} = \vec{r}_1^{(i)} = \cdots = \vec{r}_N^{(i)}$. However, Γ_i becomes a point when $\hat{\mathcal{H}}_0(\Gamma_i) = 0$. Therefore, the most probable energy is determined as the balance of energy of each configuration Γ and the size of Γ. The size of Γ stands for the effect of entropy.

When the energy of certain Γ is large, the probability that the system takes the configuration Γ, $P(\Gamma)$, decreases. This probability is represented as follows.

$$P(\Gamma) = \exp\left[-\beta\hat{\mathcal{H}}(\Gamma)\right]/Z \tag{3.3.1.5}$$

where Z is normalization constant called state sum:

$$Z = \frac{1}{M!}\int d\Gamma \exp[-\beta\hat{\mathcal{H}}(\Gamma)] \tag{3.3.1.6}$$

Here $1/M!$ means that we cannot distinguish M polymers. $\int d\Gamma$ stands for the integration through all of possible Γ. By using $P(\Gamma)$, concentration distribution of segments at $\vec{r}$ is calculated as follows.[25]

$$\phi(\vec{r}) = \langle\, \hat{\phi}(\vec{r};\Gamma)\,\rangle = \frac{1}{M!Z}\int d\Gamma \hat{\phi}(\vec{r};\Gamma)\exp\left[-\beta\hat{\mathcal{H}}(\Gamma)\right] \tag{3.3.1.7}$$

Next, we assume that $\hat{\mathcal{W}}(\Gamma)$ is characterized only by the information $\hat{\phi}(\vec{r};\Gamma)$. Here, $\hat{\mathcal{W}}$ becomes a function of $\hat{\phi}(\vec{r};\Gamma)$. Function of some functions are called functional and represented like $\hat{\mathcal{W}}[\hat{\phi}(\vec{r};\Gamma)]$. Our task is to find Helmholtz free energy as a functional of $\phi(\vec{r})$. Helmholtz free energy is related to the state sum as follows.

$$F[\phi(\vec{r})] = -\frac{1}{\beta}\ln Z \tag{3.3.1.8}$$

Helmholtz free energy of the system will be the minimum of Eq.(3.3.1.8). To obtain concrete expression of Eq.(3.3.1.8), I express Eq.(3.3.1.6) by using Eq.(11.5.2) and (11.5.4) as follows.

$$\begin{aligned}
Z &= \frac{1}{M!}\int d\Gamma \exp\left[-\beta\left(\hat{\mathcal{H}}_0(\Gamma) + \hat{\mathcal{W}}[\hat{\phi}(\vec{r};\Gamma)]\right)\right] \\
&= \frac{1}{M!}\int d\Gamma \exp\left[-\beta\hat{\mathcal{H}}_0(\Gamma)\right]\int D\{\varphi(\vec{r})\}\delta\left[\varphi(\vec{r}) - \hat{\phi}(\vec{r};\Gamma)\right]\exp\left[-\beta\mathcal{W}[\varphi(\vec{r})]\right] \\
&= \frac{1}{M!}\int d\Gamma \exp\left[-\beta\hat{\mathcal{H}}_0(\Gamma)\right]\int D\{\varphi(\vec{r})\}\int D\{w(\vec{r})\}\exp\left[i\int d\vec{r}\left(\varphi(\vec{r}) - \hat{\phi}(\vec{r};\Gamma)\right)w(\vec{r})\right]\exp\left[-\beta\mathcal{W}[\varphi(\vec{r})]\right]
\end{aligned} \tag{3.3.1.9}$$

Then let us define $\mathcal{V}(\vec{r})$ as follows.

$$\mathcal{V}(\vec{r}) := \frac{iw(\vec{r})}{\beta} \tag{3.3.1.10}$$

Then $\phi(\vec{r})$ is expressed as follows.

$$\begin{aligned}
Z = \frac{1}{M!}\int D\{\varphi(\vec{r})\}\int D\{w(\vec{r})\}\exp\left[-\beta\mathcal{W}[\varphi(\vec{r})] + i\int d\vec{r}\varphi(\vec{r})w(\vec{r})\right] \\
\int d\Gamma \exp\left[-\beta\hat{\mathcal{H}}_0(\Gamma) - i\int d\vec{r}\hat{\phi}(\vec{r};\Gamma)w(\vec{r})\right] \\
= \frac{1}{M!}\frac{\beta}{i}\int D\{\varphi(\vec{r})\}\int D\{\mathcal{V}(\vec{r})\}\exp\left[-\beta\left(\mathcal{W}[\varphi(\vec{r})] - \int d\vec{r}\varphi(\vec{r})\mathcal{V}(\vec{r})\right)\right] \\
\int d\Gamma \exp\left[-\beta\left(\hat{\mathcal{H}}_0(\Gamma) + \int d\vec{r}\hat{\phi}(\vec{r};\Gamma)\mathcal{V}(\vec{r})\right)\right]
\end{aligned} \tag{3.3.1.11}$$

The final term of Eq.(3.3.1.11) is regarded as the state sum of ideal polymers under external field $\mathcal{V}(\vec{r})$,

[25] After the integration over Γ, $\phi(\vec{r})$ is no longer related to certain microscopic state. Therefore, there is no $\hat{}$ on $\phi(\vec{r})$.

$\mathcal{Z}[\mathcal{V}(\vec{r})]$. When $\hat{\mathcal{H}}_0(\Gamma)$ is Eq.(3.3.1.3), $\mathcal{Z}[\mathcal{V}(\vec{r})]$ is calculated as follows.

$$\begin{aligned}\mathcal{Z}[\mathcal{V}(\vec{r})] &:= \int d\Gamma \exp\left[-\beta\left(\hat{\mathcal{H}}_0(\Gamma) + \int d\vec{r}\hat{\phi}(\vec{r};\Gamma)\mathcal{V}(\vec{r})\right)\right] \\ &= \int d\Gamma \exp\left[-\beta\left(\hat{\mathcal{H}}_0(\Gamma) + \sum_{i=1}^{M}\sum_{j=0}^{N}\mathcal{V}(\vec{r}_j^{(i)})\right)\right] \\ &= \left[\int d\Gamma_1 \exp\left[-\beta\left(\hat{\mathcal{H}}_0(\Gamma_1) + \sum_{j=0}^{N}\mathcal{V}(\vec{r}_j^{(1)})\right)\right]\right]^M =: \mathcal{Z}_1^M \end{aligned} \tag{3.3.1.12}$$

By using $\mathcal{Z}$, Eq.(3.3.1.11) is summarized as follows.

$$Z = \frac{1}{M!}\frac{\beta}{i}\int D\{\varphi(\vec{r})\}\int D\{\mathcal{V}(\vec{r})\}\exp\left[-\beta\left(-\frac{1}{\beta}\ln\mathcal{Z}[\mathcal{V}(\vec{r})] + \mathcal{W}[\varphi(\vec{r})] - \int d\vec{r}\varphi(\vec{r})\mathcal{V}(\vec{r})\right)\right] \tag{3.3.1.13}$$

Compared to Eq.(3.3.1.6), Eq.(3.3.1.13) is integrated by functions $\varphi(\vec{r})$ and $V(\vec{r})$ instead of Γ. By substituting Eq.(3.3.1.13) into Eq.(3.3.1.8), we can obtain $F[\phi(\vec{r})]$. Calculation is performed by using saddle point method (Eq.(11.5.10)).

$$-\frac{1}{\beta}\ln Z \simeq -\frac{1}{\beta}\ln\frac{\beta}{M!i} + \left[-\frac{1}{\beta}\ln\mathcal{Z}[V(\vec{r})] + \mathcal{W}[\phi(\vec{r})] - \int d\vec{r}\phi(\vec{r})V(\vec{r})\right] \tag{3.3.1.14}$$

such that

$$\frac{\delta}{\delta\mathcal{V}(\vec{r})}\left[-\frac{1}{\beta}\ln\mathcal{Z}[\mathcal{V}(\vec{r})] + \mathcal{W}[\varphi(\vec{r})] - \int d\vec{r}\varphi(\vec{r})\mathcal{V}(\vec{r})\right]\Big|_{\mathcal{V}(\vec{r})=V(\vec{r})} = 0 \tag{3.3.1.15}$$

$$\frac{\delta}{\delta\varphi(\vec{r})}\left[-\frac{1}{\beta}\ln\mathcal{Z}[\mathcal{V}(\vec{r})] + \mathcal{W}[\varphi(\vec{r})] - \int d\vec{r}\varphi(\vec{r})\mathcal{V}(\vec{r})\right]\Big|_{\varphi(\vec{r})=\phi(\vec{r})} = 0 \tag{3.3.1.16}$$

Eqs.(3.3.1.15) and (3.3.1.16) is calculated as follows.

$$-\frac{1}{\beta\mathcal{Z}[\mathcal{V}(\vec{r})]}\frac{\delta\mathcal{Z}[V(\vec{r})]}{\delta\mathcal{V}(\vec{r})}\Big|_{\mathcal{V}(\vec{r})=V(\vec{r})} - \phi(\vec{r}) = 0 \tag{3.3.1.17}$$

$$\frac{\delta\mathcal{W}[\varphi(\vec{r})]}{\delta\varphi(\vec{r})}\Big|_{\varphi(\vec{r})=\phi(\vec{r})} - V(\vec{r}) = 0 \tag{3.3.1.18}$$

By neglecting the 1st term of Eq.(3.3.1.14) and substituting Eqs.(3.3.1.17) and (3.3.1.18), the final result is obtained.

$$\boxed{F[\phi(\vec{r})] = -\frac{1}{\beta}\ln\mathcal{Z}[V(\vec{r})] + \mathcal{W}[\phi(\vec{r})] - \int d\vec{r}\phi(\vec{r})V(\vec{r})} \tag{3.3.1.19}$$

such that

$$\phi(\vec{r}) = -\frac{1}{\beta\mathcal{Z}[\mathcal{V}(\vec{r})]}\frac{\delta\mathcal{Z}[V(\vec{r})]}{\delta\mathcal{V}(\vec{r})}\Big|_{\mathcal{V}(\vec{r})=V(\vec{r})} \tag{3.3.1.20}$$

$$V(\vec{r}) = \frac{\delta\mathcal{W}[\varphi(\vec{r})]}{\delta\varphi(\vec{r})}\Big|_{\varphi(\vec{r})=\phi(\vec{r})} \tag{3.3.1.21}$$

When there are n polymer species, Eq.(3.3.1.19) is extended as follows.

$$F[\{\phi_K(\vec{r})\}] = -\frac{1}{\beta}\ln \mathcal{Z}[\{V_K(\vec{r})\}] + \mathcal{W}[\{\phi_K(\vec{r})\}] - \sum_K \int d\vec{r}\phi_K(\vec{r})V_K(\vec{r}) \tag{3.3.1.22}$$

where $\{\phi_K(\vec{r})\}$ and $\{V_K(\vec{r})\}$ stands for the list of concentration distributions and external field for the polymer species K. Until now, we take the reference state as the bond-beads model. Instead of this, we can take the state where $\{\phi_K(\vec{r})\} = \{\bar{\phi}_K\}$ as a reference state. This new reference state is completely homogeneous state where the concentration distributions do not depend on $\vec{r}$. Since the interaction between polymers is already included in this reference state, we can set $\hat{\mathcal{W}}(\Gamma) = 0$. Therefore, Eq.(3.3.1.19) becomes as follows.

$$F[\{\delta\phi_K(\vec{r})\}] = -\frac{1}{\beta}\ln \mathcal{Z}[\{V_K(\vec{r})\}] - \sum_K \int d\vec{r}\delta\phi_K(\vec{r})V_K(\vec{r}) \tag{3.3.1.23}$$

Here, the concentration distribution is expressed as a deviation from the reference state.

$$\delta\phi_K(\vec{r}) := \phi_K(\vec{r}) - \bar{\phi}_K \tag{3.3.1.24}$$

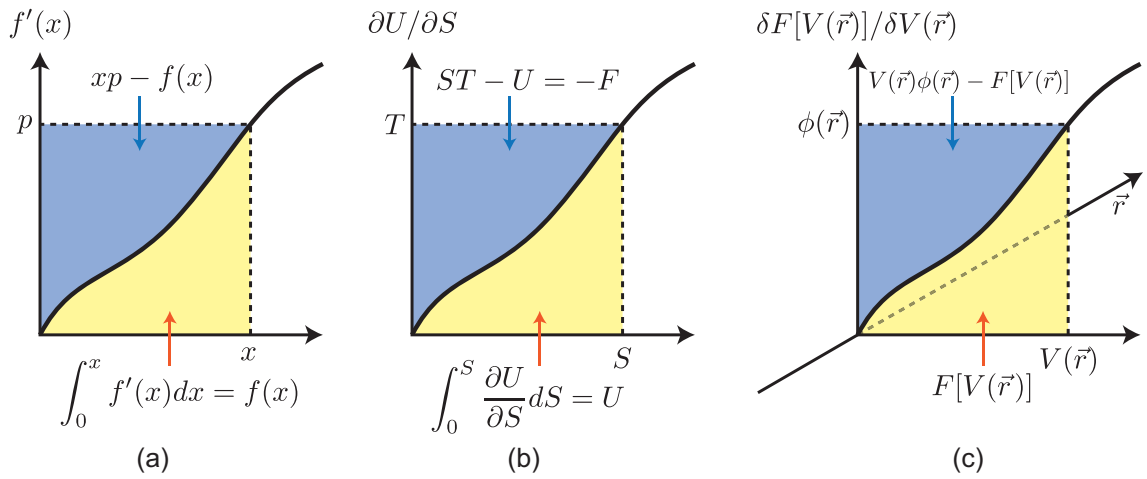

Figure 3.8: Legendre transformation of (a) $f(x)$ to $g(p)$, (b) $U(S,V,N)$ to $F(T,V,N)$, (c) $F[V(\vec{r})]$ to $F[\phi(\vec{r})]$

Eq.(3.3.1.24) is regarded as Legendre transformation. Legendre transformation is used to change variable of a function. The simplest transformation is represented as follows.

$$g(p) := xp - f(x) \ s.t. \ f'(x) = p \tag{3.3.1.25}$$

As a whole, the variable of f is transformed from x to p. Graphical image of Eq.(3.3.1.25) is shown in Figure 3.8(a). The yellow area stands for $f(x)$ while the blue area stands for $g(p)$. If $f'(x)$ is a monotonically increasing function, $f(x)$ and $g(p)$ has one-to-one correspondence. In other words, $f(x)$ and $g(p)$ has the same information while their variables are different. One of the most well known applications of Legendre

transformation is construction of thermodynamic functions.

$$F(T,V,N) := U(S,V,N) - ST \quad s.t. \quad \frac{\partial U(S,V,N)}{\partial S} = T(S,V,N) \tag{3.3.1.26}$$

$$H(S,P,N) := U(S,V,N) + VP \quad s.t. \quad \frac{\partial U(S,V,N)}{\partial V} = -P(S,V,N) \tag{3.3.1.27}$$

$$G(T,P,N) := F(T,V,N) + VP \quad s.t. \quad \frac{\partial F(T,V,N)}{\partial V} = -P(T,V,N) \tag{3.3.1.28}$$

$$= H(S,P,N) - ST \quad s.t. \quad \frac{\partial H(S,P,N)}{\partial S} = T(S,P,N) \tag{3.3.1.29}$$

where U, F, H, and G are energy, Helmholtz free energy, enthalpy, and Gibbs free energy, respectively. Graphical image of Eq.(3.3.1.26) is shown in Figure 3.8(b). Difference of sign in Eq.(3.3.1.25) and Eqs.(3.3.1.26) $\sim$ (3.3.1.29) is just conventional one. By extending this concept to a functional, we can change the variable of the Helmholtz free energy of the system from $V(\vec{r})$ to $\phi(\vec{r})$ as shown in Eq.(3.3.1.23).

$$F[\phi(\vec{r})] = F[V(\vec{r})] - \int d\vec{r} V(\vec{r})\phi(\vec{r}) \quad s.t. \quad \frac{\delta F[V(\vec{r})]}{\delta V(\vec{r})} = \phi(\vec{r}) \tag{3.3.1.30}$$

Here, $F[V(\vec{r})]$ is the Helmholtz energy of ideal polymer system under external field $V(\vec{r})$ and calculated by using Eqs.(3.3.1.8) and (3.3.1.11).

$$F[V(\vec{r})] = -\frac{1}{\beta} \ln \mathcal{Z}[V(\vec{r})] \tag{3.3.1.31}$$

$$\frac{\delta F[V(\vec{r})]}{\delta V(\vec{r})} = -\frac{1}{\beta \mathcal{Z}[V(\vec{r})]} \frac{\delta \mathcal{Z}[V(\vec{r})]}{\delta V(\vec{r})} \tag{3.3.1.32}$$

Substituting Eq.(3.3.1.31) to Eq.(3.3.1.30), Eq.(3.3.1.23) for one polymer species is obtained. Eq.(3.3.1.32) shows the condition Eq.(3.3.1.20).

Legendre transformation is applicable only if $V(\vec{r})$ and $\phi(\vec{r})$ has one-to-one correspondence. Mathematically, this means that $\phi(\vec{r})$ is monotonically increasing function with respect to $V(\vec{r})$. Since $\phi(\vec{r})$ is defined as a derivative of $F[V(\vec{r})]$, $F[V(\vec{r})]$ should be a concave function. This assumption is reasonable when the deviation from homogeneous state is small.

3.3.2 Ginzburg–Landau model

Next task is to expand Eq.(3.3.1.23) by $\{\delta\phi_K(\vec{r})\}$. To make the formulation simple, we use excess energy instead of Eq.(3.3.1.23) as follows.

$$F[\{\delta\phi_K(\vec{r})\}] - F[\{0\}] = -\frac{1}{\beta}\ln\frac{\mathcal{Z}[\{V_K(\vec{r})\}]}{\mathcal{Z}[\{0\}]} - \sum_K \int d\vec{r}\delta\phi_K(\vec{r})V_K(\vec{r}) \tag{3.3.2.1}$$

Let us expand the first term of Eq.(3.3.2.1) by $\{V_K(\vec{r})\}$. By extending Eq.(3.3.1.12) to n polymer species:

$$\begin{aligned}\frac{\mathcal{Z}[\{V_K(\vec{r})\}]}{\mathcal{Z}[\{0\}]} &= \frac{\prod_K \frac{1}{M_K!}\int d\Gamma \exp\left[-\beta\left(\hat{\mathcal{H}}_S(\Gamma) + \int d\vec{r}\delta\hat{\phi}_K(\vec{r};\Gamma)V_K(\vec{r})\right)\right]}{\prod_K \frac{1}{M_K!}\int d\Gamma \exp\left[-\beta\hat{\mathcal{H}}_S(\Gamma)\right]} \\ &= \frac{\int d\Gamma \exp\left[-\beta\left(\hat{\mathcal{H}}_S(\Gamma) + \sum_K\int d\vec{r}\delta\hat{\phi}_K(\vec{r};\Gamma)V_K(\vec{r})\right)\right]}{\int d\Gamma \exp\left[-\beta\hat{\mathcal{H}}_S(\Gamma)\right]}\end{aligned} \tag{3.3.2.2}$$

where $\hat{\mathcal{H}}_S(\Gamma)$ is Hamiltonian for homogeneous system. Eq.(3.3.2.2) is regarded as the statistical average for reference state whose energy is expressed as $\hat{\mathcal{H}}_0(\Gamma)$.

$$\frac{\mathcal{Z}[\{V_K(\vec{r})\}]}{\mathcal{Z}[\{0\}]} =: \left\langle \exp\left[-\beta\sum_K\int d\vec{r}\delta\hat{\phi}_K(\vec{r};\Gamma)V_K(\vec{r})\right]\right\rangle \tag{3.3.2.3}$$

By regarding Eq.(11.5.13) as a moment-generating function (see Eq.(3.3.2.3) for details), let us calculate the moment. To achieve this, let us expand Eq.(3.3.2.3) as a polynomial of $\{V_K(\vec{r})\}$.

$$\begin{aligned}\frac{\mathcal{Z}[\{V_K(\vec{r})\}]}{\mathcal{Z}[\{0\}]} &= 1 - \beta\left\langle\sum_{K_1}\int d\vec{r}_1\delta\hat{\phi}_{K_1}(\vec{r}_1;\Gamma)V_{K_1}(\vec{r}_1)\right\rangle \\ &\quad + \frac{(-\beta)^2}{2}\left\langle\sum_{K_1}\sum_{K_2}\int d\vec{r}_1\int d\vec{r}_2\delta\hat{\phi}_{K_1}(\vec{r}_1;\Gamma)\delta\hat{\phi}_{K_2}(\vec{r}_2;\Gamma)V_{K_1}(\vec{r}_1)V_{K_2}(\vec{r}_2)\right\rangle + \cdots \\ &= 1 - \beta\sum_{K_1}\int d\vec{r}_1 V_{K_1}(\vec{r}_1)\left\langle\delta\hat{\phi}_{K_1}(\vec{r}_1;\Gamma)\right\rangle \\ &\quad + \frac{(-\beta)^2}{2}\sum_{K_1}\sum_{K_2}\int d\vec{r}_1\int d\vec{r}_2 V_{K_1}(\vec{r}_1)V_{K_2}(\vec{r}_2)\left\langle\delta\hat{\phi}_{K_1}(\vec{r}_1;\Gamma)\delta\hat{\phi}_{K_2}(\vec{r}_2;\Gamma)\right\rangle + \cdots \\ &= \sum_n^\infty \frac{1}{n!}\sum_{K_1,\cdots,K_n}\int d\vec{r}_1\cdots\int d\vec{r}_n V_{K_1}(\vec{r}_1)\cdots V_{K_n}(\vec{r}_n)(-\beta)^n\left\langle\delta\hat{\phi}_{K_1}(\vec{r}_1;\Gamma)\cdots\delta\hat{\phi}_{K_n}(\vec{r}_n;\Gamma)\right\rangle\end{aligned} \tag{3.3.2.4}$$

Comparing Eq.(3.3.2.4) and (11.5.31), nth moment is represented as follows.

$$M_n^{K_1,\cdots,K_n}(\vec{r}_1,\cdots,\vec{r}_n) = \left\langle\delta\hat{\phi}_{K_1}(\vec{r}_1;\Gamma)\cdots\delta\hat{\phi}_{K_n}(\vec{r}_n;\Gamma)\right\rangle \tag{3.3.2.5}$$

By using this notation, Eq.(3.3.2.3) and its logarithm is expanded as follows.

$$\frac{\mathcal{Z}[\{V_K(\vec{r})\}]}{\mathcal{Z}[\{0\}]} = \sum_n^\infty \frac{1}{n!} \sum_{K_1,\cdots,K_n} \int d\vec{r}_1 \cdots \int d\vec{r}_n (-\beta)^n M_n^{K_1,\cdots,K_n}(\vec{r}_1,\cdots,\vec{r}_n) V_{K_1}(\vec{r}_1)\cdots V_{K_n}(\vec{r}_n) \quad (3.3.2.6)$$

$$\ln \frac{\mathcal{Z}[\{V_K(\vec{r})\}]}{\mathcal{Z}[\{0\}]} = \sum_n^\infty \frac{1}{n!} \sum_{K_1,\cdots,K_n} \int d\vec{r}_1 \cdots \int d\vec{r}_n (-\beta)^n C_n^{K_1,\cdots,K_n}(\vec{r}_1,\cdots,\vec{r}_n) V_{K_1}(\vec{r}_1)\cdots V_{K_n}(\vec{r}_n) \quad (3.3.2.7)$$

Eq.(3.3.2.7) is cumulant expansion and the cumulants $C_n^{K_1,\cdots,K_n}(\vec{r}_1,\cdots,\vec{r}_n)$ is related to the moments Eq.(3.3.2.5) through Eqs.(11.5.36), (11.5.37), (11.5.38), and so on.

Next task is the expansion by $\{\delta\phi_K(\vec{r})\}$ instead of $\{V_K(\vec{r})\}$. $\delta\phi_K(\vec{r})$ is calculated by using the condition Eq.(3.3.1.15) for the system Eq.(3.3.2.1).

$$\frac{\delta}{\delta V_K(\vec{r})}\left[-\frac{1}{\beta}\ln\frac{\mathcal{Z}[\{V_K(\vec{r})\}]}{\mathcal{Z}[\{0\}]} - \sum_K \int d\vec{r}\,\delta\phi_K(\vec{r})V_K(\vec{r})\right]\Bigg|_{\{V_K(\vec{r})\}=\{0\}} = 0 \quad (3.3.2.8)$$

As a result, following expansion is obtained for $\delta\phi_K(\vec{r})$.

$$\begin{aligned}
\delta\phi_K(\vec{r}) &= -\frac{1}{\beta}\frac{\delta}{\delta V_K(\vec{r})}\ln\frac{\mathcal{Z}[\{V_K(\vec{r})\}]}{\mathcal{Z}[\{0\}]} \\
&= -\frac{1}{\beta}\frac{\delta}{\delta V_K(\vec{r})}\left[\sum_n^\infty \frac{(-\beta)^n}{n!}\sum_{K_1,\cdots,K_n}\int d\vec{r}_1\cdots\int d\vec{r}_n C_n^{K_1,\cdots,K_n}(\vec{r}_1,\cdots,\vec{r}_n)V_{K_1}(\vec{r}_1)\cdots V_{K_n}(\vec{r}_n)\right] \\
&= \sum_n^\infty \frac{(-\beta)^{n-1}}{(n-1)!}\sum_{K_2,\cdots,K_n}\int d\vec{r}_2\cdots\int d\vec{r}_n C_n^{K,K_2,\cdots,K_n}(\vec{r},\vec{r}_2,\cdots,\vec{r}_n)V_{K_2}(\vec{r}_2)\cdots V_{K_n}(\vec{r}_n) \\
&= C_1^K(\vec{r}) + (-\beta)\sum_{K_2}\int d\vec{r}_2 C_2^{K,K_2}(\vec{r},\vec{r}_2)V_{K_2}(\vec{r}_2) \\
&\quad + \frac{(-\beta)^2}{2}\sum_{K_2}\sum_{K_3}\int d\vec{r}_2\int d\vec{r}_3 C_3^{K,K_2,K_3}(\vec{r},\vec{r}_2,\vec{r}_3)V_{K_2}(\vec{r}_2)V_{K_3}(\vec{r}_3) \\
&\quad + \frac{(-\beta)^3}{6}\sum_{K_2}\sum_{K_3}\sum_{K_4}\int d\vec{r}_2\int d\vec{r}_3\int d\vec{r}_4 C_4^{K,K_2,K_3,K_4}(\vec{r},\vec{r}_2,\vec{r}_3,\vec{r}_4)V_{K_2}(\vec{r}_2)V_{K_3}(\vec{r}_3)V_{K_4}(\vec{r}_4) + \cdots
\end{aligned} \quad (3.3.2.9)$$

Here, 1st cumulant is zero from definition.

$$C_1^K(\vec{r}) = \left\langle \delta\hat{\phi}_K(\vec{r}_1;\Gamma)\right\rangle = 0 \quad (3.3.2.10)$$

From Eq.(3.3.2.9), we can solve the power of $V_K(\vec{r})$ as a function of $\delta\phi_K(\vec{r})$. First order term is:

$$\delta\phi_{K_1}(\vec{r}_1) \simeq -\beta\sum_{K_2}\int d\vec{r}_2 C_2^{K_1,K_2}(\vec{r}_1,\vec{r}_2)V_{K_2}(\vec{r}_2) \quad (3.3.2.11)$$

This is solved inversely as follows.

$$
\begin{aligned}
&-\frac{1}{\beta}\sum_{K_3}\int d\vec{r}_3\left(C_2^{K_1,K_3}(\vec{r}_1,\vec{r}_3)\right)^{-1}\delta\phi_{K_3}(\vec{r}_3)\\
&=\sum_{K_2}\sum_{K_3}\int d\vec{r}_2\int d\vec{r}_3\left(C_2^{K_1,K_3}(\vec{r}_1,\vec{r}_3)\right)^{-1}C_2^{K_3,K_2}(\vec{r}_3,\vec{r}_2)V_{K_2}(\vec{r}_2)\\
&=\sum_{K_2}\int d\vec{r}_2\delta_{K_1,K_2}\delta(\vec{r}_1-\vec{r}_2)V_{K_2}(\vec{r}_2)=V_{K_1}(\vec{r}_1)
\end{aligned}
\tag{3.3.2.12}
$$

where $\left(C_2^{K,K'}(\vec{r},\vec{r}')\right)^{-1}$ is inverse function of $C_2^{K,K'}(\vec{r},\vec{r}')$: [26]

$$
\sum_{K''}\int d\vec{r}''\left(C_2^{K,K''}(\vec{r},\vec{r}'')\right)^{-1}\left(C_2^{K'',K'}(\vec{r}'',\vec{r}')\right)=\delta_{K,K'}\delta(\vec{r}-\vec{r}')
\tag{3.3.2.13}
$$

By using Eq.(3.3.2.11), 2nd order term is calculated as follows.

$$
(-\beta)^{-2}\delta\phi_{K_1}(\vec{r}_1)\delta\phi_{K_1'}(\vec{r}_1')\simeq\sum_{K_2}\sum_{K_2'}\int d\vec{r}_2\int d\vec{r}_2'C_2^{K_1,K_2}(\vec{r}_1,\vec{r}_2)C_2^{K_1',K_2'}(\vec{r}_1',\vec{r}_2')V_{K_2}(\vec{r}_2)V_{K_2'}(\vec{r}_2')
\tag{3.3.2.14}
$$

$$
\begin{aligned}
&(-\beta)^{-2}\sum_{K_3}\sum_{K_3'}\int d\vec{r}_3\int d\vec{r}_3'\left(C_2^{K_1,K_3}(\vec{r}_1,\vec{r}_3)\right)^{-1}\left(C_2^{K_1',K_3'}(\vec{r}_1',\vec{r}_3')\right)^{-1}\delta\phi_{K_3}(\vec{r}_3)\delta\phi_{K_3'}(\vec{r}_3')\\
&=\sum_{K_2}\sum_{K_2'}\sum_{K_3}\sum_{K_3'}\int d\vec{r}_2\int d\vec{r}_2'\int d\vec{r}_3\int d\vec{r}_3'\\
&\qquad\left(C_2^{K_1,K_3}(\vec{r}_1,\vec{r}_3)\right)^{-1}\left(C_2^{K_1',K_3'}(\vec{r}_1',\vec{r}_3')\right)^{-1}C_2^{K_3,K_2}(\vec{r}_3,\vec{r}_2)C_2^{K_3',K_2'}(\vec{r}_3',\vec{r}_2')V_{K_2}(\vec{r}_2)V_{K_2'}(\vec{r}_2')\\
&=\sum_{K_2}\sum_{K_2'}\int d\vec{r}_2\int d\vec{r}_2'\delta_{K_1,K_2}\delta_{K_1',K_2'}\delta(\vec{r}_1-\vec{r}_2)\delta(\vec{r}_1'-\vec{r}_2')V_{K_2}(\vec{r}_2)V_{K_2'}(\vec{r}_2')\\
&=V_{K_1}(\vec{r}_1)V_{K_1'}(\vec{r}_1')
\end{aligned}
\tag{3.3.2.15}
$$

Similarly, higher order terms are calculated as follows.

$$
\begin{aligned}
&V_{K_1}(\vec{r}_1)V_{K_1'}(\vec{r}_1')V_{K_1''}(\vec{r}_1'')\\
&=(-\beta)^{-3}\sum_{K_3}\sum_{K_3'}\sum_{K_3''}\int d\vec{r}_3\int d\vec{r}_3'\int d\vec{r}_3''\\
&\qquad\left(C_2^{K_1,K_3}(\vec{r}_1,\vec{r}_3)\right)^{-1}\left(C_2^{K_1',K_3'}(\vec{r}_1',\vec{r}_3')\right)^{-1}\left(C_2^{K_1'',K_3''}(\vec{r}_1'',\vec{r}_3'')\right)^{-1}\delta\phi_{K_3}(\vec{r}_3)\delta\phi_{K_3'}(\vec{r}_3')\delta\phi_{K_3''}(\vec{r}_3'')
\end{aligned}
\tag{3.3.2.16}
$$

[26] Qualitatively speaking, Eq.(3.3.2.11) is written by using matrix representation as follows.

$$
\begin{bmatrix}\delta\phi_1\\ \vdots\\ \delta\phi_p\end{bmatrix}=-\frac{1}{\beta}\begin{bmatrix}C_2^{11}&\cdots&C_2^{p1}\\ \vdots&\ddots&\vdots\\ C_2^{p1}&\cdots&C_2^{pp}\end{bmatrix}\begin{bmatrix}V_1\\ \vdots\\ V_p\end{bmatrix}
$$

Then $\{V_K\}$ is calculated by using $\{\delta\phi_K\}$ and inverse matrix of $C_2^{K,K'}$ (Eq.(3.3.2.12)).

$$
\begin{bmatrix}V_1\\ \vdots\\ V_p\end{bmatrix}=-\beta\begin{bmatrix}C_2^{11}&\cdots&C_2^{p1}\\ \vdots&\ddots&\vdots\\ C_2^{p1}&\cdots&C_2^{pp}\end{bmatrix}^{-1}\begin{bmatrix}\delta\phi_1\\ \vdots\\ \delta\phi_p\end{bmatrix}
$$

$$
\begin{aligned}
&V_{K_1}(\vec{r}_1)V_{K_1'}(\vec{r}_1')V_{K_1''}(\vec{r}_1'')V_{K_1'''}(\vec{r}_1''') \\
&= (-\beta)^{-4}\sum_{K_3}\sum_{K_3'}\sum_{K_3''}\sum_{K_3'''}\int d\vec{r}_3\int d\vec{r}_3'\int d\vec{r}_3''\int d\vec{r}_3''' \\
&\quad \left(C_2^{K_1,K_3}(\vec{r}_1,\vec{r}_3)\right)^{-1}\left(C_2^{K_1',K_3'}(\vec{r}_1',\vec{r}_3')\right)^{-1}\left(C_2^{K_1'',K_3''}(\vec{r}_1'',\vec{r}_3'')\right)^{-1}\left(C_2^{K_1''',K_3'''}(\vec{r}_1''',\vec{r}_3''')\right)^{-1} \\
&\quad \delta\phi_{K_3}(\vec{r}_3)\delta\phi_{K_3'}(\vec{r}_3')\delta\phi_{K_3''}(\vec{r}_3'')\delta\phi_{K_3'''}(\vec{r}_3''') \qquad (3.3.2.17)
\end{aligned}
$$

Next, let us calculate the higher term of Eq.(3.3.2.11). To make the expression simple, I rewrite Eq.(3.3.2.9) to simple form as follows.

$$\phi = -\beta C_2 V + \frac{\beta^2}{2}C_3V^2 - \frac{\beta^3}{6}C_4V^3 + \cdots \qquad (3.3.2.18)$$

$$\phi^2 = \beta^2C_2^2V^2 - \beta^3C_2C_3V^3 + \beta^4\left(\frac{1}{3}C_2C_4 + \frac{1}{4}C_3^2\right)V^4 + \cdots \qquad (3.3.2.19)$$

$$\phi^3 = -\beta^3C_2^3V^3 + \frac{3}{2}\beta^4C_2^2C_3V^4 + \cdots \qquad (3.3.2.20)$$

$$\phi^4 = \beta^4C_2^4V^4 + \cdots \qquad (3.3.2.21)$$

By using this notation, Eqs.(3.3.2.12), (3.3.2.15) $\sim$ (3.3.2.17) is rewritten as follows.

$$(-\beta)^nV^n = (C_2^{-1})^n\phi^n \qquad (3.3.2.22)$$

Expansion of V up to ϕ^2 is achieved as follows.

$$
\begin{aligned}
&\beta^2V^2 = (C_2^{-1})^2\phi^2 \\
&\to \phi = -\beta C_2V + \frac{1}{2}C_3(C_2^{-1})^2\phi^2 \\
&\to \beta V = -C_2^{-1}\phi + \frac{1}{2}C_3(C_2^{-1})^3\phi^2 \qquad (3.3.2.23)
\end{aligned}
$$

Higher order terms are calculated as follows.

$$
\begin{aligned}
&\beta^3V^3 = -(C_2^{-1})^3\phi^3 \\
&\to \phi^2 = \beta^2C_2^2V^2 + C_3(C_2^{-1})^2\phi^3 \\
&\to \beta^2V^2 = (C_2^{-1})^2\phi^2 - C_3(C_2^{-1})^4\phi^3 \\
&\to \phi = -\beta C_2V + \frac{1}{2}C_3(C_2^{-1})^2\phi^2 - \frac{1}{2}C_3^2(C_2^{-1})^4\phi^3 + \frac{1}{6}C_4(C_2^{-1})^3\phi^3 \\
&\to \beta V = -C_2^{-1}\phi + \frac{1}{2}C_3(C_2^{-1})^3\phi^2 + \left[-\frac{1}{2}C_3^2(C_2^{-1})^5 + \frac{1}{6}C_4(C_2^{-1})^4\right]\phi^3 \qquad (3.3.2.24)
\end{aligned}
$$

$$
\begin{aligned}
&\beta^4V^4 = (C_2^{-1})^4\phi^4 \\
&\to \beta^3V^3 = -(C_2^{-1})^3\phi^3 + \frac{3}{2}C_3(C_2^{-1})^5\phi^4 \\
&\to \beta^2V^2 = (C_2^{-1})^2\phi^2 - C_3(C_2^{-1})^4\phi^3 + \left[\frac{5}{4}C_3^2(C_2^{-1})^6 - \frac{1}{3}C_4(C_2^{-1})^5\right]\phi^4 \qquad (3.3.2.25)
\end{aligned}
$$

Then let us expand Eq.(3.3.2.1) by $\{\delta\phi_K\}$. By substituting Eqs.(3.3.2.7) and (3.3.2.9) to Eq.(3.3.2.1):

$$
\begin{aligned}
&F[\{\delta\phi_K(\vec{r})\}] - F[\{0\}] \\
&= -\frac{1}{\beta}\left[\sum_n^\infty \frac{(-\beta)^n}{n!} \sum_{K_1,\cdots,K_n} \int d\vec{r}_1 \cdots \int d\vec{r}_n C_n^{K_1,\cdots,K_n}(\vec{r}_1,\cdots,\vec{r}_n) V_{K_1}(\vec{r}_1)\cdots V_{K_n}(\vec{r}_n)\right] \\
&+ \frac{1}{\beta}\sum_{K_1}\int d\vec{r}_1 \left[\sum_n^\infty \frac{(-\beta)^n}{(n-1)!} \sum_{K_2,\cdots,K_n} \int d\vec{r}_2 \cdots \int d\vec{r}_n C_n^{K_1,K_2,\cdots,K_n}(\vec{r}_1,\vec{r}_2,\cdots,\vec{r}_n) V_{K_2}(\vec{r}_2)\cdots V_{K_n}(\vec{r}_n)\right] V_{K_1}(\vec{r}_1) \\
&= \frac{1}{\beta}\left[\sum_n^\infty \frac{n-1}{n!}(-\beta)^n \sum_{K_1,\cdots,K_n} \int d\vec{r}_1 \cdots \int d\vec{r}_n C_n^{K_1,\cdots,K_n}(\vec{r}_1,\cdots,\vec{r}_n) V_{K_1}(\vec{r}_1)\cdots V_{K_n}(\vec{r}_n)\right] \qquad (3.3.2.26)
\end{aligned}
$$

Eq.(3.3.2.26) is rewritten as follows by using the previous notation.

$$\beta\Delta F = \frac{1}{2}C_2(-\beta V)^2 + \frac{1}{3}C_3(-\beta V)^3 + \frac{1}{8}C_4(-\beta V)^4 + \cdots \qquad (3.3.2.27)$$

By substituting Eq.(3.3.2.25) to Eq.(3.3.2.27), $\beta\Delta F$ is expanded by ϕ. ϕ^2 term is:

$$\frac{1}{2}C_2(C_2^{-1})^2\phi^2 = \frac{1}{2}C_2^{-1}\phi^2 \qquad (3.3.2.28)$$

ϕ^3 term is created from V^2 term and V^3 term:

$$\frac{1}{2}C_2\left[-C_3(C_2^{-1})^4\right]\phi^3 + \frac{1}{3}C_3(C_2^{-1})^3\phi^3 = -\frac{1}{6}C_3(C_2^{-1})^3\phi^3 \qquad (3.3.2.29)$$

ϕ^4 term is created from V^2 term, V^3 term, and V^4 term:

$$
\begin{aligned}
&\frac{1}{2}C_2\left[\frac{5}{4}C_3^2(C_2^{-1})^6 - \frac{1}{3}C_4(C_2^{-1})^5\right]\phi^4 + \frac{1}{3}C_3\left[-\frac{3}{2}C_3(C_2^{-1})^5\right]\phi^4 + \frac{1}{8}C_4(C_2^{-1})^4\phi^4 \\
&= \left[-\frac{1}{24}C_4(C_2^{-1})^4 + \frac{1}{8}C_3^2(C_2^{-1})^5\right]\phi^4 \qquad (3.3.2.30)
\end{aligned}
$$

As a result, Eq.(3.3.2.27) is expanded as follows.

$$\Delta F = \frac{1}{2\beta}C_2^{-1}\phi^2 - \frac{1}{6\beta}C_3(C_2^{-1})^3\phi^3 + \frac{1}{24\beta}\left[-C_4(C_2^{-1})^4 + 3C_3^2(C_2^{-1})^5\right]\phi^4 + \cdots \qquad (3.3.2.31)$$

Complete description of Eq.(3.3.2.33) is as follows.

$$
\begin{aligned}
&F[\{\delta\phi_K(\vec{r})\}] - F[\{0\}] \\
&= \frac{1}{2\beta}\sum_{K_1,K_2}\int d\vec{r}_1 \int d\vec{r}_2 \left(C_2^{K_1,K_2}(\vec{r}_1,\vec{r}_2)\right)^{-1} \delta\phi_{K_1}(\vec{r}_1)\delta\phi_{K_2}(\vec{r}_2) \\
&- \frac{1}{6\beta}\sum_{K_1,\cdots,K_6}\int d\vec{r}_1 \cdots \int d\vec{r}_6 C_3^{K_1,K_2,K_3}(\vec{r}_1,\vec{r}_2,\vec{r}_3) \\
&\qquad \left(C_2^{K_1,K_4}(\vec{r}_1,\vec{r}_4)\right)^{-1}\left(C_2^{K_2,K_5}(\vec{r}_2,\vec{r}_5)\right)^{-1}\left(C_2^{K_3,K_6}(\vec{r}_3,\vec{r}_6)\right)^{-1}\delta\phi_{K_4}(\vec{r}_4)\delta\phi_{K_5}(\vec{r}_5)\delta\phi_{K_6}(\vec{r}_6) + \cdots \\
&\qquad\qquad\qquad\qquad\qquad\qquad\qquad\qquad\qquad\qquad\qquad\qquad\qquad\qquad (3.3.2.32)
\end{aligned}
$$

Eqs.(3.3.2.9) and (3.3.2.32) are the description in real space. By Fourier transformation, these equations are rewritten in q-space. Let us perform Fourier transformation of the following equation, which is similar to Eq.(3.3.2.9).

$$\begin{aligned} f(\vec{r}_1) &= (-\beta)\int d\vec{r}_2 g_2(\vec{r}_1,\vec{r}_2)h_a(\vec{r}_2) \\ &+ \frac{(-\beta)^2}{2}\int d\vec{r}_2\int d\vec{r}_3 g_3(\vec{r}_1,\vec{r}_2,\vec{r}_3)h_a(\vec{r}_2)h_b(\vec{r}_3) \\ &+ \frac{(-\beta)^3}{6}\int d\vec{r}_2\int d\vec{r}_3\int d\vec{r}_4 g_4(\vec{r}_1,\vec{r}_2,\vec{r}_3,\vec{r}_4)h_a(\vec{r}_2)h_b(\vec{r}_3)h_c(\vec{r}_4)+\cdots \end{aligned} \tag{3.3.2.33}$$

Here, we assume the translational invariance for $g_2(\vec{r}_1,\vec{r}_2)$:

$$g_2(\vec{r}_1,\vec{r}_2) = g_2(\vec{r}_1-\vec{r},\vec{r}_2-\vec{r}) \tag{3.3.2.34}$$

Substitute $\vec{r}=\vec{r}_2$ to Eq.(3.3.2.34), the number of variables of g_2 is reduced.

$$g_2(\vec{r}_1,\vec{r}_2) \to g_2(\vec{r}_1-\vec{r}_2) \tag{3.3.2.35}$$

Fourier transform of f is:

$$f(\vec{q}_1) = \int d\vec{r}_1 f(\vec{r}_1)e^{i\vec{q}_1\cdot\vec{r}_1} \quad\Longleftrightarrow\quad f(\vec{r}_1) = \frac{1}{(2\pi)^3}\int d\vec{q}_1 f(\vec{q}_1)e^{-i\vec{q}_1\cdot\vec{r}_1} \tag{3.3.2.36}$$

Therefore, 1st term of the right hand side of Eq.(3.3.2.33) is calculated as follows.

$$\begin{aligned} &\int d\vec{r}_1\left[\int d\vec{r}_2 g_2(\vec{r}_1-\vec{r}_2)h_a(\vec{r}_2)\right]e^{i\vec{q}_1\cdot\vec{r}_1} \\ &= \frac{1}{(2\pi)^6}\int d\vec{r}_1\int d\vec{r}_2\int d\vec{q}_2\int d\vec{q}_3 g_2(\vec{q}_2)e^{-i\vec{q}_2\cdot(\vec{r}_1-\vec{r}_2)}h_a(\vec{q}_3)e^{-i\vec{q}_3\cdot\vec{r}_2}e^{i\vec{q}_1\cdot\vec{r}_1} \\ &= \frac{1}{(2\pi)^6}\int d\vec{r}_1\int d\vec{r}_2\int d\vec{q}_2\int d\vec{q}_3 g_2(\vec{q}_2)h_a(\vec{q}_3)e^{i(\vec{q}_1-\vec{q}_2)\cdot\vec{r}_1}e^{i(\vec{q}_2-\vec{q}_3)\cdot\vec{r}_2} \\ &= \frac{1}{(2\pi)^6}\int d\vec{q}_2\int d\vec{q}_3 g_2(\vec{q}_2)h_a(\vec{q}_3)\delta(\vec{q}_1-\vec{q}_2)\delta(\vec{q}_2-\vec{q}_3) \\ &= g_2(\vec{q}_1)h_a(\vec{q}_1) \end{aligned} \tag{3.3.2.37}$$

Here, I used the following form of delta function.

$$\delta(\vec{q}_1) = \int d\vec{r}_1 e^{i\vec{q}_1\cdot\vec{r}_1} \quad\Longleftrightarrow\quad \delta(\vec{r}_1) = \frac{1}{(2\pi)^3}\int d\vec{q}_1 e^{-i\vec{q}_1\cdot\vec{r}_1} \tag{3.3.2.38}$$

$$f(\vec{q}) = \frac{1}{(2\pi)^3}\int d\vec{q}_1 f(\vec{q}_1)\delta(\vec{q}-\vec{q}_1) \quad\Longleftrightarrow\quad f(\vec{r}) = \int d\vec{r}_1 f(\vec{r}_1)\delta(\vec{r}-\vec{r}_1) \tag{3.3.2.39}$$

2nd term of the right hand side of Eq.(3.3.2.33) is calculated as follows.

$$\begin{aligned} &\int d\vec{r}_1\left[\int d\vec{r}_2\int d\vec{r}_3 g_3(\vec{r}_1,\vec{r}_2,\vec{r}_3)h_a(\vec{r}_2)h_b(\vec{r}_3)\right]e^{i\vec{q}_1\cdot\vec{r}_1} \\ &= \frac{1}{(2\pi)^{15}}\int d\vec{r}_1\cdots\int d\vec{r}_3\int d\vec{q}_2\cdots\int d\vec{q}_6 g_3(\vec{q}_2,\vec{q}_3,\vec{q}_4)h_a(\vec{q}_5)h_b(\vec{q}_6)e^{i(\vec{q}_1-\vec{q}_2)\cdot\vec{r}_1}e^{i(-\vec{q}_3-\vec{q}_5)\cdot\vec{r}_2}e^{i(-\vec{q}_4-\vec{q}_6)\cdot\vec{r}_3} \\ &= \frac{1}{(2\pi)^{15}}\int d\vec{q}_2\cdots\int d\vec{q}_6 g_3(\vec{q}_2,\vec{q}_3,\vec{q}_4)h_a(\vec{q}_5)h_b(\vec{q}_6)\delta(\vec{q}_1-\vec{q}_2)\delta(-\vec{q}_3-\vec{q}_5)\delta(-\vec{q}_4-\vec{q}_6) \\ &= \frac{1}{(2\pi)^6}\int d\vec{q}_3\int d\vec{q}_4 g_3(\vec{q}_1,\vec{q}_3,\vec{q}_4)h_a(-\vec{q}_3)h_b(-\vec{q}_4) \end{aligned} \tag{3.3.2.40}$$

3rd term of the right hand side of Eq.(3.3.2.33) is calculated as follows.

$$\begin{aligned}
&\int d\vec{r}_1 \left[\int d\vec{r}_2 \int d\vec{r}_3 \int d\vec{r}_4 g_4(\vec{r}_1, \vec{r}_2, \vec{r}_3, \vec{r}_4) h_a(\vec{r}_2) h_b(\vec{r}_3) h_c(\vec{r}_4) \right] e^{i\vec{q}_1 \cdot \vec{r}_1} \\
&= \frac{1}{(2\pi)^9} \int d\vec{q}_2 \int d\vec{q}_3 \int d\vec{q}_4 g_4(\vec{q}_1, \vec{q}_2, \vec{q}_3, \vec{q}_4) h_a(-\vec{q}_2) h_b(-\vec{q}_3) h_c(-\vec{q}_4)
\end{aligned} \tag{3.3.2.41}$$

Substitute Eqs.(3.3.2.36), (3.3.2.37), (3.3.2.40), (3.3.2.41) to Eq.(3.3.2.33) (original form is Eq.(3.3.2.9)):

$$\begin{aligned}
\delta\phi_K(\vec{q}_1) = (-\beta) &\sum_{K_2} C_2^{K,K_2}(\vec{q}_1) V_{K_2}(\vec{q}_1) \\
&+ \frac{(-\beta)^2}{2} \frac{1}{(2\pi)^6} \sum_{K_2} \sum_{K_3} \int d\vec{q}_2 \int d\vec{q}_3 C_3^{K,K_2,K_3}(\vec{q}_1, \vec{q}_2, \vec{q}_3) V_{K_2}(\vec{q}_2) V_{K_3}(\vec{q}_3) \\
&+ \frac{(-\beta)^3}{6} \frac{1}{(2\pi)^9} \sum_{K_2} \sum_{K_3} \sum_{K_4} \int d\vec{q}_2 \int d\vec{q}_3 \int d\vec{q}_4 C_4^{K,K_2,K_3,K_4}(\vec{q}_1, \vec{q}_2, \vec{q}_3, \vec{q}_4) V_{K_2}(\vec{q}_2) V_{K_3}(\vec{q}_3) V_{K_4}(\vec{q}_4) + \cdots
\end{aligned} \tag{3.3.2.42}$$

Here I used the inversion symmetry of the system.

$$V_K(\vec{q}) = V_K(-\vec{q}) \tag{3.3.2.43}$$

Next, let us perform Fourier transformation of the following equation, which is similar to Eq.(3.3.2.32).

$$\begin{aligned}
\Delta F = &\frac{1}{2\beta} \int d\vec{r}_1 \int d\vec{r}_2 g_2(\vec{r}_1 - \vec{r}_2) h_a(\vec{r}_1) h_b(\vec{r}_2) \\
&- \frac{1}{6\beta} \int d\vec{r}_1 \cdots \int d\vec{r}_6 g_3(\vec{r}_1, \vec{r}_2, \vec{r}_3) g_{2a}(\vec{r}_1 - \vec{r}_4) g_{2b}(\vec{r}_2 - \vec{r}_5) g_{2c}(\vec{r}_3 - \vec{r}_6) h_a(\vec{r}_4) h_b(\vec{r}_5) h_c(\vec{r}_6) + \cdots
\end{aligned} \tag{3.3.2.44}$$

1st term of the right hand side of Eq.(3.3.2.44) is calculated as follows.

$$\begin{aligned}
&\int d\vec{r}_1 \int d\vec{r}_2 g_2(\vec{r}_1 - \vec{r}_2) h_a(\vec{r}_1) h_b(\vec{r}_2) \\
&= \frac{1}{(2\pi)^9} \int d\vec{r}_1 \int d\vec{r}_2 \int d\vec{q}_1 \int d\vec{q}_2 \int d\vec{q}_3 g_2(\vec{q}_1) e^{-i\vec{q}_1 \cdot (\vec{r}_1 - \vec{r}_2)} h_a(\vec{q}_2) e^{-i\vec{q}_2 \cdot \vec{r}_1} h_b(\vec{q}_3) e^{-i\vec{q}_3 \cdot \vec{r}_2} \\
&= \frac{1}{(2\pi)^9} \int d\vec{r}_1 \int d\vec{r}_2 \int d\vec{q}_1 \int d\vec{q}_2 \int d\vec{q}_3 g_2(\vec{q}_1) h_a(\vec{q}_2) h_b(\vec{q}_3) e^{i(-\vec{q}_1 - \vec{q}_2) \cdot \vec{r}_1} e^{i(\vec{q}_1 - \vec{q}_3) \cdot \vec{r}_2} \\
&= \frac{1}{(2\pi)^9} \int d\vec{q}_1 \int d\vec{q}_2 \int d\vec{q}_3 g_2(\vec{q}_1) h_a(\vec{q}_2) h_b(\vec{q}_3) \delta(-\vec{q}_1 - \vec{q}_2) \delta(\vec{q}_1 - \vec{q}_3) \\
&= \frac{1}{(2\pi)^3} \int d\vec{q}_1 g_2(\vec{q}_1) h_a(-\vec{q}_1) h_b(\vec{q}_1)
\end{aligned} \tag{3.3.2.45}$$

2nd term of the right hand side of Eq.(3.3.2.44) is calculated as follows.

$$\begin{aligned}
&\int d\vec{r}_1 \cdots \int d\vec{r}_6 g_3(\vec{r}_1,\vec{r}_2,\vec{r}_3) g_{2a}(\vec{r}_1-\vec{r}_4) g_{2b}(\vec{r}_2-\vec{r}_5) g_{2c}(\vec{r}_3-\vec{r}_6) h_a(\vec{r}_4) h_b(\vec{r}_5) h_c(\vec{r}_6) \\
&= \frac{1}{(2\pi)^{27}} \int d\vec{r}_1 \cdots \int d\vec{r}_6 \int d\vec{q}_1 \cdots \int d\vec{q}_9 g_3(\vec{q}_1,\vec{q}_2,\vec{q}_3) g_{2a}(\vec{q}_4) g_{2b}(\vec{q}_5) g_{2c}(\vec{q}_6) h_a(\vec{q}_7) h_b(\vec{q}_8) h_c(\vec{q}_9) \\
&\qquad\qquad e^{i(-\vec{q}_1-\vec{q}_4)\cdot\vec{r}_1} e^{i(-\vec{q}_2-\vec{q}_5)\cdot\vec{r}_2} e^{i(-\vec{q}_3-\vec{q}_6)\cdot\vec{r}_3} e^{i(\vec{q}_4-\vec{q}_7)\cdot\vec{r}_4} e^{i(\vec{q}_5-\vec{q}_8)\cdot\vec{r}_5} e^{i(\vec{q}_6-\vec{q}_9)\cdot\vec{r}_6} \\
&= \frac{1}{(2\pi)^9} \int d\vec{q}_1 \int d\vec{q}_2 \int d\vec{q}_3 g_3(\vec{q}_1,\vec{q}_2,\vec{q}_3) g_{2a}(-\vec{q}_1) g_{2b}(-\vec{q}_2) g_{2c}(-\vec{q}_3) h_a(-\vec{q}_1) h_b(-\vec{q}_2) h_c(-\vec{q}_3) \qquad (3.3.2.46)
\end{aligned}$$

Substitute Eqs.(3.3.2.45) and (3.3.2.46) to Eq.(3.3.2.44) (original form is Eq.(3.3.2.32)):

$$\begin{aligned}
&F[\{\delta\phi_K(\vec{q})\}] - F[\{0\}] \\
&= \frac{1}{2\beta} \frac{1}{(2\pi)^3} \sum_{K_1,K_2} \int d\vec{q}_1 \left(C_2^{K_1,K_2}(\vec{q}_1) \right)^{-1} \delta\phi_{K_1}(\vec{q}_1) \delta\phi_{K_2}(-\vec{q}_1) \\
&- \frac{1}{6\beta} \frac{1}{(2\pi)^9} \sum_{K_1,\cdots,K_6} \int d\vec{q}_1 \int d\vec{q}_2 \int d\vec{q}_3 C_3^{K_1,K_2,K_3}(\vec{q}_1,\vec{q}_2,\vec{q}_3) \\
&\qquad \left(C_2^{K_1,K_4}(\vec{q}_1) \right)^{-1} \left(C_2^{K_2,K_5}(\vec{q}_2) \right)^{-1} \left(C_2^{K_3,K_6}(\vec{q}_3) \right)^{-1} \delta\phi_{K_4}(\vec{q}_1) \delta\phi_{K_5}(\vec{q}_2) \delta\phi_{K_6}(\vec{q}_3) + \cdots \\
&\qquad\qquad (3.3.2.47)
\end{aligned}$$

Let us restrict our discussion to the case of two-component system where[27]

$$\delta\phi_1(\vec{r}) + \delta\phi_2(\vec{r}) = 0 \quad \forall\vec{r} \qquad (3.3.2.48)$$

holds true, which is the case of $\hat{\mathcal{H}}_S(\Gamma)$. In this special case, cumulants for each order is represented by only one value. For examples, 2nd order cumulants is:

$$\begin{aligned}
C_2^{1,1}(\vec{r}_1,\vec{r}_2) &= \left\langle \delta\hat{\phi}_1(\vec{r}_1;\Gamma) \delta\hat{\phi}_1(\vec{r}_1;\Gamma) \right\rangle =: C_2(\vec{r}_1,\vec{r}_2) \qquad (3.3.2.49) \\
C_2^{1,2}(\vec{r}_1,\vec{r}_2) &= \left\langle \delta\hat{\phi}_1(\vec{r}_1;\Gamma) \delta\hat{\phi}_2(\vec{r}_2;\Gamma) \right\rangle \\
&= -\left\langle \delta\hat{\phi}_1(\vec{r}_1;\Gamma) \delta\hat{\phi}_1(\vec{r}_2;\Gamma) \right\rangle = -C_2(\vec{r}_1,\vec{r}_2) \qquad (3.3.2.50) \\
C_2^{2,1}(\vec{r}_1,\vec{r}_2) &= \left\langle \delta\hat{\phi}_2(\vec{r}_1;\Gamma) \delta\hat{\phi}_1(\vec{r}_2;\Gamma) \right\rangle \\
&= -\left\langle \delta\hat{\phi}_1(\vec{r}_1;\Gamma) \delta\hat{\phi}_1(\vec{r}_2;\Gamma) \right\rangle = -C_2(\vec{r}_1,\vec{r}_2) \qquad (3.3.2.51) \\
C_2^{2,2}(\vec{r}_1,\vec{r}_2) &= \left\langle \delta\hat{\phi}_2(\vec{r}_1;\Gamma) \delta\hat{\phi}_2(\vec{r}_2;\Gamma) \right\rangle \\
&= (-1)^2 \left\langle \delta\hat{\phi}_1(\vec{r}_1;\Gamma) \delta\hat{\phi}_1(\vec{r}_2;\Gamma) \right\rangle = C_2(\vec{r}_1,\vec{r}_2) \qquad (3.3.2.52)
\end{aligned}$$

Similar to this, 3rd order and 4th order cumulant is expressed as follows (Explicit expression is shown in

[27] $\forall$ stands for "for all".

Eqs.(3.3.3.1) $\sim$ (3.3.3.3)).

$$\begin{aligned}
&C_3(\vec{r}_1,\vec{r}_2,\vec{r}_3) =: C_3^{1,1,1}(\vec{r}_1,\vec{r}_2,\vec{r}_3)\\
&= -C_3^{1,1,2}(\vec{r}_1,\vec{r}_2,\vec{r}_3) = -C_3^{1,2,1}(\vec{r}_1,\vec{r}_2,\vec{r}_3) = -C_3^{2,1,1}(\vec{r}_1,\vec{r}_2,\vec{r}_3)\\
&= C_3^{1,2,2}(\vec{r}_1,\vec{r}_2,\vec{r}_3) = C_3^{2,1,2}(\vec{r}_1,\vec{r}_2,\vec{r}_3) = C_3^{2,2,1}(\vec{r}_1,\vec{r}_2,\vec{r}_3)\\
&= -C_3^{2,2,2}(\vec{r}_1,\vec{r}_2,\vec{r}_3)
\end{aligned} \tag{3.3.2.53}$$

$$\begin{aligned}
&C_4(\vec{r}_1,\vec{r}_2,\vec{r}_3,\vec{r}_4) =: C_4^{1,1,1,1}(\vec{r}_1,\vec{r}_2,\vec{r}_3,\vec{r}_4)\\
&= -C_4^{1,1,1,2}(\vec{r}_1,\vec{r}_2,\vec{r}_3,\vec{r}_4) = -C_4^{1,1,2,1}(\vec{r}_1,\vec{r}_2,\vec{r}_3,\vec{r}_4) = -C_4^{1,2,1,1}(\vec{r}_1,\vec{r}_2,\vec{r}_3,\vec{r}_4) = -C_4^{2,1,1,1}(\vec{r}_1,\vec{r}_2,\vec{r}_3,\vec{r}_4)\\
&= C_4^{1,1,2,2}(\vec{r}_1,\vec{r}_2,\vec{r}_3,\vec{r}_4) = C_4^{1,2,1,2}(\vec{r}_1,\vec{r}_2,\vec{r}_3,\vec{r}_4) = C_4^{2,1,1,2}(\vec{r}_1,\vec{r}_2,\vec{r}_3,\vec{r}_4)\\
&= C_4^{1,2,2,1}(\vec{r}_1,\vec{r}_2,\vec{r}_3,\vec{r}_4) = C_4^{2,1,2,1}(\vec{r}_1,\vec{r}_2,\vec{r}_3,\vec{r}_4) = C_4^{2,2,1,1}(\vec{r}_1,\vec{r}_2,\vec{r}_3,\vec{r}_4)\\
&= -C_4^{1,2,2,2}(\vec{r}_1,\vec{r}_2,\vec{r}_3,\vec{r}_4) = -C_4^{2,1,2,2}(\vec{r}_1,\vec{r}_2,\vec{r}_3,\vec{r}_4) = -C_4^{2,2,1,2}(\vec{r}_1,\vec{r}_2,\vec{r}_3,\vec{r}_4) = -C_4^{2,2,2,1}(\vec{r}_1,\vec{r}_2,\vec{r}_3,\vec{r}_4)\\
&= C_4^{2,2,2,2}(\vec{r}_1,\vec{r}_2,\vec{r}_3,\vec{r}_4)
\end{aligned} \tag{3.3.2.54}$$

Here, the problem is that we cannot define inverse matrix of Eq.(3.3.2.13) since matrix $C_2^{K,K'}(\vec{r},\vec{r}')$ is singular.

$$C_2^{K,K'}(\vec{r},\vec{r}') = C_2(\vec{r}_1,\vec{r}_2)\begin{bmatrix} 1 & -1 \\ -1 & 1 \end{bmatrix} \tag{3.3.2.55}$$

To avoid this difficulty, let us rewrite the equations above without using matrix representation. By using Eqs.(3.3.2.49) $\sim$ (3.3.2.52), 2nd order cumulant term in Eq.(3.3.2.9) is written as follows when $K = 1$.

$$\sum_{K_2}\int d\vec{r}_2 C_2^{1,K_2}(\vec{r},\vec{r}_2)V_{K_2}(\vec{r}_2) = \int d\vec{r}_2 C_2(\vec{r},\vec{r}_2)\left[V_1(\vec{r}_2) - V_2(\vec{r}_2)\right] = \int d\vec{r}_2 C_2(\vec{r},\vec{r}_2)U(\vec{r}_2) \tag{3.3.2.56}$$

where

$$U(\vec{r}) := V_1(\vec{r}) - V_2(\vec{r}) \tag{3.3.2.57}$$

For 3rd order term:

$$\begin{aligned}
&\sum_{K_2}\sum_{K_3}\int d\vec{r}_2\int d\vec{r}_3 C_3^{1,K_2,K_3}(\vec{r},\vec{r}_2,\vec{r}_3)V_{K_2}(\vec{r}_2)V_{K_3}(\vec{r}_3)\\
&= \int d\vec{r}_2\int d\vec{r}_3 C_3(\vec{r},\vec{r}_2,\vec{r}_3)\left[V_1(\vec{r}_2)V_1(\vec{r}_3) - V_1(\vec{r}_2)V_2(\vec{r}_3) - V_2(\vec{r}_2)V_1(\vec{r}_3) + V_2(\vec{r}_2)V_2(\vec{r}_3)\right]\\
&= \int d\vec{r}_2\int d\vec{r}_3 C_3(\vec{r},\vec{r}_2,\vec{r}_3)U(\vec{r}_2)U(\vec{r}_3)
\end{aligned} \tag{3.3.2.58}$$

For 4th order term:

$$\begin{aligned}
&\sum_{K_2}\sum_{K_3}\sum_{K_4}\int d\vec{r}_2\int d\vec{r}_3\int d\vec{r}_4 C_4^{1,K_2,K_3,K_4}(\vec{r},\vec{r}_2,\vec{r}_3,\vec{r}_4)V_{K_2}(\vec{r}_2)V_{K_3}(\vec{r}_3)V_{K_4}(\vec{r}_4)\\
&= \int d\vec{r}_2\int d\vec{r}_3\int d\vec{r}_4 C_4(\vec{r},\vec{r}_2,\vec{r}_3,\vec{r}_4)U(\vec{r}_2)U(\vec{r}_3)U(\vec{r}_4)
\end{aligned} \tag{3.3.2.59}$$

As a result, expansion of concentration fluctuation is:

$$\begin{aligned}\delta\psi(\vec{r}_1) = (-\beta)\int d\vec{r}_2 C_2(\vec{r}_1,\vec{r}_2)U(\vec{r}_2) \\ + \frac{(-\beta)^2}{2}\int d\vec{r}_2\int d\vec{r}_3 C_3(\vec{r},\vec{r}_2,\vec{r}_3)U(\vec{r}_2)U(\vec{r}_3) \\ + \frac{(-\beta)^3}{6}\int d\vec{r}_2\int d\vec{r}_3\int d\vec{r}_4 C_4(\vec{r},\vec{r}_2,\vec{r}_3,\vec{r}_4)U(\vec{r}_2)U(\vec{r}_3)U(\vec{r}_4)+\cdots\end{aligned} \tag{3.3.2.60}$$

where order parameter $\delta\psi(\vec{r})$ is defined as follows.

$$\delta\psi(\vec{r}) := \delta\phi_1(\vec{r}) = -\delta\phi_2(\vec{r}) \tag{3.3.2.61}$$

By using the same calculation schemes, Eqs.(3.3.2.32), (3.3.2.42), and (3.3.2.47) is expressed as follows.

$$\begin{aligned}&F[\delta\psi(\vec{r})] - F[0] \\ &= \frac{1}{2\beta}\int d\vec{r}_1\int d\vec{r}_2 C_2^{-1}(\vec{r}_1,\vec{r}_2)\delta\psi(\vec{r}_1)\delta\psi(\vec{r}_2) \\ &- \frac{1}{6\beta}\int d\vec{r}_1\cdots\int d\vec{r}_6 C_3(\vec{r}_1,\vec{r}_2,\vec{r}_3)C_2^{-1}(\vec{r}_1,\vec{r}_4)C_2^{-1}(\vec{r}_2,\vec{r}_5)C_2^{-1}(\vec{r}_3,\vec{r}_6)\delta\psi(\vec{r}_4)\delta\psi(\vec{r}_5)\delta\psi(\vec{r}_6)+\cdots\end{aligned} \tag{3.3.2.62}$$

$$\begin{aligned}\delta\psi(\vec{q}_1) = (-\beta)C_2(\vec{q}_1)U(\vec{q}_1) \\ + \frac{(-\beta)^2}{2}\frac{1}{(2\pi)^6}\int d\vec{q}_2\int d\vec{q}_3 C_3(\vec{q}_1,\vec{q}_2,\vec{q}_3)U(\vec{q}_2)U(\vec{q}_3) \\ + \frac{(-\beta)^3}{6}\frac{1}{(2\pi)^9}\int d\vec{q}_2\int d\vec{q}_3\int d\vec{q}_4 C_4(\vec{q}_1,\vec{q}_2,\vec{q}_3,\vec{q}_4)U(\vec{q}_2)U(\vec{q}_3)U(\vec{q}_4)+\cdots\end{aligned} \tag{3.3.2.63}$$

$$\begin{aligned}&F[\delta\psi(\vec{q})] - F[0] \\ &= \frac{1}{2\beta}\frac{1}{(2\pi)^3}\int d\vec{q}_1 C_2^{-1}(\vec{q}_1)\delta\psi(\vec{q}_1)\delta\psi(-\vec{q}_1) \\ &- \frac{1}{6\beta}\frac{1}{(2\pi)^9}\int d\vec{q}_1\int d\vec{q}_2\int d\vec{q}_3 C_3(\vec{q}_1,\vec{q}_2,\vec{q}_3)C_2^{-1}(\vec{q}_1)C_2^{-1}(\vec{q}_2)C_2^{-1}(\vec{q}_3)\delta\psi(\vec{q}_1)\delta\psi(\vec{q}_2)\delta\psi(\vec{q}_3)+\cdots\end{aligned} \tag{3.3.2.64}$$

where $C_2^{-1}(\vec{r}_1,\vec{r}_2)$ is defined as follows (Eqs.(3.3.2.13)).

$$\int d\vec{r}_3 C_2^{-1}(\vec{r}_1,\vec{r}_3)C_2(\vec{r}_3,\vec{r}_2) = \delta(\vec{r}_1-\vec{r}_2) \tag{3.3.2.65}$$

By using Eq.(3.3.2.35), Fourier transform of left hand side of Eq.(3.3.2.65) is calculated as follows.

$$\begin{aligned}
&\frac{1}{(2\pi)^6}\int d\vec{r}_3\int d\vec{q}_1\int d\vec{q}_2 C_2^{-1}(\vec{q}_1)C_2(\vec{q}_2)e^{-i\vec{q}_1\cdot(\vec{r}_1-\vec{r}_3)}e^{-i\vec{q}_2\cdot(\vec{r}_3-\vec{r}_2)}\\
&=\frac{1}{(2\pi)^6}\int d\vec{q}_1\int d\vec{q}_2\int d\vec{r}_3 C_2^{-1}(\vec{q}_1)C_2(\vec{q}_2)e^{i(\vec{q}_1-\vec{q}_2)\cdot\vec{r}_3}e^{-i\vec{q}_1\cdot\vec{r}_1}e^{i\vec{q}_2\cdot\vec{r}_2}\\
&=\frac{1}{(2\pi)^6}\int d\vec{q}_1\int d\vec{q}_2 C_2^{-1}(\vec{q}_1)C_2(\vec{q}_2)\delta(\vec{q}_1-\vec{q}_2)e^{-i\vec{q}_1\cdot\vec{r}_1}e^{i\vec{q}_2\cdot\vec{r}_2}\\
&=\frac{1}{(2\pi)^3}\int d\vec{q}_1 C_2^{-1}(\vec{q}_1)C_2(\vec{q}_1)e^{-i\vec{q}_1\cdot(\vec{r}_1-\vec{r}_2)}
\end{aligned}\tag{3.3.2.66}$$

By using Eq.(3.3.2.38), Fourier transform of right hand side of Eq.(3.3.2.65) is calculated as follows.

$$\delta(\vec{r}_1-\vec{r}_2)=\frac{1}{(2\pi)^3}\int d\vec{q}_1 e^{-i\vec{q}_1\cdot(\vec{r}_1-\vec{r}_2)}\tag{3.3.2.67}$$

By comparing Eqs.(3.3.2.66) and (3.3.2.67),

$$C_2^{-1}(\vec{q})C_2(\vec{q})=1\quad\forall\vec{q}\tag{3.3.2.68}$$

3.3.3 Random-phase approximation

To calculate Eq.(3.3.2.47), we have to know the coefficients for each term. These terms are expressed by the combination of cumulants as follows (See Eqs.(3.3.2.5), (11.5.36), (11.5.37), (11.5.38), and so on.).

$$C_2^{K_1,K_2}(\vec{r}_1,\vec{r}_2)=M_2^{K_1,K_2}(\vec{r}_1,\vec{r}_2)=\left\langle\delta\hat{\phi}_{K_1}(\vec{r}_1;\Gamma)\delta\hat{\phi}_{K_2}(\vec{r}_2;\Gamma)\right\rangle\tag{3.3.3.1}$$

$$C_3^{K_1,K_2,K_3}(\vec{r}_1,\vec{r}_2,\vec{r}_3)=M_3^{K_1,K_2,K_3}(\vec{r}_1,\vec{r}_2,\vec{r}_3)=\left\langle\delta\hat{\phi}_{K_1}(\vec{r}_1;\Gamma)\delta\hat{\phi}_{K_2}(\vec{r}_2;\Gamma)\delta\hat{\phi}_{K_3}(\vec{r}_3;\Gamma)\right\rangle\tag{3.3.3.2}$$

$$\begin{aligned}
&C_4^{K_1,K_2,K_3,K_4}(\vec{r}_1,\vec{r}_2,\vec{r}_3,\vec{r}_4)\\
&=M_4^{K_1,K_2,K_3,K_4}(\vec{r}_1,\vec{r}_2,\vec{r}_3,\vec{r}_4)\\
&\quad-M_2^{K_1,K_2}(\vec{r}_1,\vec{r}_2)M_2^{K_3,K_4}(\vec{r}_3,\vec{r}_4)-M_2^{K_1,K_3}(\vec{r}_1,\vec{r}_3)M_2^{K_2,K_4}(\vec{r}_2,\vec{r}_4)-M_2^{K_1,K_4}(\vec{r}_1,\vec{r}_4)M_2^{K_2,K_3}(\vec{r}_2,\vec{r}_3)\\
&=\left\langle\delta\hat{\phi}_{K_1}(\vec{r}_1;\Gamma)\delta\hat{\phi}_{K_2}(\vec{r}_2;\Gamma)\delta\hat{\phi}_{K_3}(\vec{r}_3;\Gamma)\delta\hat{\phi}_{K_4}(\vec{r}_4;\Gamma)\right\rangle-\left\langle\delta\hat{\phi}_{K_1}(\vec{r}_1;\Gamma)\delta\hat{\phi}_{K_2}(\vec{r}_2;\Gamma)\right\rangle\left\langle\delta\hat{\phi}_{K_3}(\vec{r}_3;\Gamma)\delta\hat{\phi}_{K_4}(\vec{r}_4;\Gamma)\right\rangle\\
&\quad-\left\langle\delta\hat{\phi}_{K_1}(\vec{r}_1;\Gamma)\delta\hat{\phi}_{K_3}(\vec{r}_3;\Gamma)\right\rangle\left\langle\delta\hat{\phi}_{K_2}(\vec{r}_2;\Gamma)\delta\hat{\phi}_{K_4}(\vec{r}_4;\Gamma)\right\rangle-\left\langle\delta\hat{\phi}_{K_1}(\vec{r}_1;\Gamma)\delta\hat{\phi}_{K_4}(\vec{r}_4;\Gamma)\right\rangle\left\langle\delta\hat{\phi}_{K_2}(\vec{r}_2;\Gamma)\delta\hat{\phi}_{K_3}(\vec{r}_3;\Gamma)\right\rangle
\end{aligned}\tag{3.3.3.3}$$

where

$$\left\langle\delta\hat{\phi}_{K_1}(\vec{r}_1;\Gamma)\cdots\delta\hat{\phi}_{K_n}(\vec{r}_n;\Gamma)\right\rangle=\frac{\displaystyle\int d\Gamma\exp\left[-\beta\hat{\mathcal{H}}_S(\Gamma)\right]\sum_{K_1,\cdots,K_n}\int d\vec{r}_1\cdots\int d\vec{r}_n\delta\hat{\phi}_{K_1}(\vec{r}_1;\Gamma)\cdots\delta\hat{\phi}_{K_n}(\vec{r}_n;\Gamma)}{\displaystyle\int d\Gamma\exp\left[-\beta\hat{\mathcal{H}}_S(\Gamma)\right]}\tag{3.3.3.4}$$

In q-space, Eqs.(3.3.3.1) $\sim$ (3.3.3.3) is expressed as follows.

$$C_2^{K_1,K_2}(\vec{q}_1)=\left\langle\delta\hat{\phi}_{K_1}(\vec{q}_1)\delta\hat{\phi}_{K_2}(-\vec{q}_1)\right\rangle\tag{3.3.3.5}$$

$$C_3^{K_1,K_2,K_3}(\vec{q}_1,\vec{q}_2,\vec{q}_3) = \left\langle \delta\hat{\phi}_{K_1}(\vec{q}_1)\delta\hat{\phi}_{K_2}(\vec{q}_2)\delta\hat{\phi}_{K_2}(\vec{q}_3)\right\rangle \tag{3.3.3.6}$$

$$\begin{aligned}
&C_4^{K_1,K_2,K_3,K_4}(\vec{q}_1,\vec{q}_2,\vec{q}_3,\vec{q}_4)\\
&= \left\langle \delta\hat{\phi}_{K_1}(\vec{q}_1)\delta\hat{\phi}_{K_2}(\vec{q}_2)\delta\hat{\phi}_{K_3}(\vec{q}_3)\delta\hat{\phi}_{K_4}(\vec{q}_4)\right\rangle - \left\langle \delta\hat{\phi}_{K_1}(\vec{q}_1)\delta\hat{\phi}_{K_2}(\vec{q}_2)\right\rangle \left\langle \delta\hat{\phi}_{K_3}(\vec{q}_3)\delta\hat{\phi}_{K_4}(\vec{q}_4)\right\rangle\\
&\quad - \left\langle \delta\hat{\phi}_{K_1}(\vec{q}_1)\delta\hat{\phi}_{K_3}(\vec{q}_3)\right\rangle \left\langle \delta\hat{\phi}_{K_2}(\vec{q}_2)\delta\hat{\phi}_{K_4}(\vec{q}_4)\right\rangle - \left\langle \delta\hat{\phi}_{K_1}(\vec{q}_1)\delta\hat{\phi}_{K_4}(\vec{q}_4)\right\rangle \left\langle \delta\hat{\phi}_{K_2}(\vec{q}_2)\delta\hat{\phi}_{K_3}(\vec{q}_3)\right\rangle
\end{aligned} \tag{3.3.3.7}$$

where the translational invariance Eq.(3.3.2.35) is used. [28] Calculation of Eq.(3.3.3.4) is usually difficult since $\hat{\mathcal{H}}_S(\Gamma)$ contains the information about interaction between polymers (see the statements above Eq.(3.3.1.23)). Instead of Eq.(3.3.3.4), we can calculate the following correlation function:

$$\left\langle \delta\hat{\phi}_{K_1}(\vec{r}_1;\Gamma)\cdots\delta\hat{\phi}_{K_n}(\vec{r}_n;\Gamma)\right\rangle_0 = \frac{\displaystyle\int d\Gamma \exp\left[-\beta\hat{\mathcal{H}}_0(\Gamma)\right]\sum_{K_1,\cdots,K_n}\int d\vec{r}_1\cdots\int d\vec{r}_n\delta\hat{\phi}_{K_1}(\vec{r}_1;\Gamma)\cdots\delta\hat{\phi}_{K_n}(\vec{r}_n;\Gamma)}{\displaystyle\int d\Gamma\exp\left[-\beta\hat{\mathcal{H}}_0(\Gamma)\right]} \tag{3.3.3.8}$$

where $\hat{\mathcal{H}}_0(\Gamma)$ is the Hamiltonian without any interaction (Eq.(3.3.1.3)). Let us define cumulants for $\hat{\mathcal{H}}_0(\Gamma)$ system as follows.

$$G_2^{K_1,K_2}(\vec{q}_1) = \left\langle \delta\hat{\phi}_{K_1}(\vec{q}_1)\delta\hat{\phi}_{K_2}(-\vec{q}_1)\right\rangle_0 \tag{3.3.3.9}$$

$$G_3^{K_1,K_2,K_3}(\vec{q}_1,\vec{q}_2,\vec{q}_3) = \left\langle \delta\hat{\phi}_{K_1}(\vec{q}_1)\delta\hat{\phi}_{K_2}(\vec{q}_2)\delta\hat{\phi}_{K_2}(\vec{q}_3)\right\rangle_0 \tag{3.3.3.10}$$

$$\begin{aligned}
&G_4^{K_1,K_2,K_3,K_4}(\vec{q}_1,\vec{q}_2,\vec{q}_3,\vec{q}_4)\\
&= \left\langle \delta\hat{\phi}_{K_1}(\vec{q}_1)\delta\hat{\phi}_{K_2}(\vec{q}_2)\delta\hat{\phi}_{K_3}(\vec{q}_3)\delta\hat{\phi}_{K_4}(\vec{q}_4)\right\rangle_0 - \left\langle \delta\hat{\phi}_{K_1}(\vec{q}_1)\delta\hat{\phi}_{K_2}(\vec{q}_2)\right\rangle_0 \left\langle \delta\hat{\phi}_{K_3}(\vec{q}_3)\delta\hat{\phi}_{K_4}(\vec{q}_4)\right\rangle_0\\
&\quad - \left\langle \delta\hat{\phi}_{K_1}(\vec{q}_1)\delta\hat{\phi}_{K_3}(\vec{q}_3)\right\rangle_0 \left\langle \delta\hat{\phi}_{K_2}(\vec{q}_2)\delta\hat{\phi}_{K_4}(\vec{q}_4)\right\rangle_0 - \left\langle \delta\hat{\phi}_{K_1}(\vec{q}_1)\delta\hat{\phi}_{K_4}(\vec{q}_4)\right\rangle_0 \left\langle \delta\hat{\phi}_{K_2}(\vec{q}_2)\delta\hat{\phi}_{K_3}(\vec{q}_3)\right\rangle_0
\end{aligned} \tag{3.3.3.11}$$

We can calculate Eq.(3.3.3.9) $\sim$ (3.3.3.11) since we do not have to consider complex interactions between polymers.

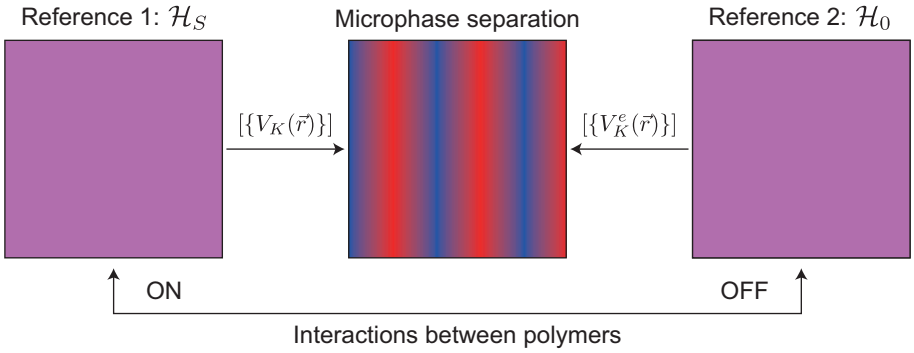

Figure 3.9: Qualitative explanation of random-phase approximation.

[28] In Eq.(3.3.3.7), translational invariance is not assumed. However, all of the variables of 2nd order cumulants in Eq.(3.3.3.7) is reduced to single value for the calculation of Eq.(3.3.2.47).

To express cumulants Eq.(3.3.3.5) $\sim$ (3.3.3.7) by using Eq.(3.3.3.9) $\sim$ (3.3.3.11), the technique called random-phase approximation is useful [50]. Under this approximation, Eq.(3.3.2.42) is expressed as follows (Figure 3.9).

$$\begin{aligned}\delta\phi_K(\vec{q}_1) = &\sum_{K_2} G_2^{K,K_2}(\vec{q}_1)V_{K_2}^e(\vec{q}_1) \\ &+ \frac{1}{2\beta}\frac{1}{(2\pi)^6}\sum_{K_2}\sum_{K_3}\int d\vec{q}_2\int d\vec{q}_3 G_3^{K,K_2,K_3}(\vec{q}_1,\vec{q}_2,\vec{q}_3)V_{K_2}^e(\vec{q}_2)V_{K_3}^e(\vec{q}_3) \\ &- \frac{1}{6\beta}\frac{1}{(2\pi)^9}\sum_{K_2}\sum_{K_3}\sum_{K_4}\int d\vec{q}_2\int d\vec{q}_3\int d\vec{q}_4 G_4^{K,K_2,K_3,K_4}(\vec{q}_1,\vec{q}_2,\vec{q}_3,\vec{q}_4)V_{K_2}^e(\vec{q}_2)V_{K_3}^e(\vec{q}_3)V_{K_4}^e(\vec{q}_4)+\cdots\end{aligned} \tag{3.3.3.12}$$

Here, reference state is changed from $\hat{\mathcal{H}}_S(\Gamma)$ to $\hat{\mathcal{H}}_0(\Gamma)$. To compensate the difference, artificial external field is changed from $[\{V_K(\vec{r})\}]$ to $[\{V_K^e(\vec{r})\}]$.

From now, we restrict our discussion to two-component system. Interactions between polymers are represented by using pairwise interaction energies (see Eq.(3.2.4.15) and discussions below.).[29]

$$\begin{aligned}&\left[zu_{11}(\bar{\phi}_1+\delta\phi_1(\vec{r}))+zu_{12}\phi_2(\bar{\phi}_2+\delta\phi_2(\vec{r}))\right]-\left[zu_{11}\bar{\phi}_1-zu_{12}\bar{\phi}_2\right] \\ &\qquad = zu_{11}\delta\phi_1(\vec{r})+zu_{12}\delta\phi_2(\vec{r}) \quad \text{for component 1}\end{aligned} \tag{3.3.3.13}$$

$$\begin{aligned}&\left[zu_{12}(\bar{\phi}_1+\delta\phi_1(\vec{r}))+zu_{22}\phi_2(\bar{\phi}_2+\delta\phi_2(\vec{r}))\right]-\left[zu_{12}\bar{\phi}_1-zu_{22}\bar{\phi}_2\right] \\ &\qquad = zu_{12}\delta\phi_1(\vec{r})+zu_{22}\delta\phi_2(\vec{r}) \quad \text{for component 2}\end{aligned} \tag{3.3.3.14}$$

By introducing polymer interactions, the condition of incompressibility is no longer fulfilled. To modify this condition, additional potential V is required. Note that this potential does not depend on the polymer species. One of the examples of this kind of potential is external pressure. As a result, V_K^e is expressed as follows in q-space.

$$V_1^e(\vec{q}) = V_1(\vec{q})+zu_{11}\delta\phi_1(\vec{q})+zu_{12}\delta\phi_2(\vec{q})+V(\vec{q}) \tag{3.3.3.15}$$

$$V_2^e(\vec{q}) = V_2(\vec{q})+zu_{12}\delta\phi_1(\vec{q})+zu_{22}\delta\phi_2(\vec{q})+V(\vec{q}) \tag{3.3.3.16}$$

In addition, incompressibility is imposed as follows.

$$\delta\phi_1(\vec{q})+\delta\phi_2(\vec{q})=0 \tag{3.3.3.17}$$

Note that Eq.(3.3.2.48) is no longer valid for $\hat{\mathcal{H}}_0(\Gamma)$. [30]

[29] Here, z is the number of sites next to a certain site. Though we can formulate without using lattice model, I formally defined as Eqs.(3.3.3.13) and (3.3.3.14) to make the discussion clear.

[30] Fourier transformation of Eq.(3.3.3.17) is

$$\int d\vec{r}\,[\delta\phi_1(\vec{r})+\delta\phi_2(\vec{r})]\,e^{i\vec{q}\cdot\vec{r}}=0$$

Therefore, incompressibility holds true in total. However, incompressibility is not fulfilled at each point. Note that Fourier transformation of Eq.(3.3.2.48) is

$$\frac{1}{(2\pi)^3}\int d\vec{q}\,[\delta\phi_1(\vec{q})+\delta\phi_2(\vec{q})]\,e^{-i\vec{q}\cdot\vec{r}}=0$$

Let us compare Eqs.(3.3.2.63) and (3.3.3.12):

$$\begin{aligned}
\delta\psi(\vec{q}_1) &= (-\beta)C_2(\vec{q}_1)U(\vec{q}_1) \\
&\quad + \frac{(-\beta)^2}{2}\frac{1}{(2\pi)^6}\int d\vec{q}_2 \int d\vec{q}_3 C_3(\vec{q}_1,\vec{q}_2,\vec{q}_3)U(\vec{q}_2)U(\vec{q}_3) \\
&\quad + \frac{(-\beta)^3}{6}\frac{1}{(2\pi)^9}\int d\vec{q}_2 \int d\vec{q}_3 \int d\vec{q}_4 C_4(\vec{q}_1,\vec{q}_2,\vec{q}_3,\vec{q}_4)U(\vec{q}_2)U(\vec{q}_3)U(\vec{q}_4) + \cdots \\
&= (-\beta)\sum_{K_2} G_2^{1,K_2}(\vec{q}_1)V_{K_2}^e(\vec{q}_1) \\
&\quad + \frac{(-\beta)^2}{2}\frac{1}{(2\pi)^6}\sum_{K_2}\sum_{K_3}\int d\vec{q}_2 \int d\vec{q}_3 G_3^{1,K_2,K_3}(\vec{q}_1,\vec{q}_2,\vec{q}_3)V_{K_2}^e(\vec{q}_2)V_{K_3}^e(\vec{q}_3) \\
&\quad + \frac{(-\beta)^3}{6}\frac{1}{(2\pi)^9}\sum_{K_2}\sum_{K_3}\sum_{K_4}\int d\vec{q}_2 \int d\vec{q}_3 \int d\vec{q}_4 G_4^{1,K_2,K_3,K_4}(\vec{q}_1,\vec{q}_2,\vec{q}_3,\vec{q}_4)V_{K_2}^e(\vec{q}_2)V_{K_3}^e(\vec{q}_3)V_{K_4}^e(\vec{q}_4) + \cdots \\
&= -(-\beta)\sum_{K_2} G_2^{2,K_2}(\vec{q}_1)V_{K_2}^e(\vec{q}_1) \\
&\quad - \frac{(-\beta)^2}{2}\frac{1}{(2\pi)^6}\sum_{K_2}\sum_{K_3}\int d\vec{q}_2 \int d\vec{q}_3 G_3^{2,K_2,K_3}(\vec{q}_1,\vec{q}_2,\vec{q}_3)V_{K_2}^e(\vec{q}_2)V_{K_3}^e(\vec{q}_3) \\
&\quad - \frac{(-\beta)^3}{6}\frac{1}{(2\pi)^9}\sum_{K_2}\sum_{K_3}\sum_{K_4}\int d\vec{q}_2 \int d\vec{q}_3 \int d\vec{q}_4 G_4^{2,K_2,K_3,K_4}(\vec{q}_1,\vec{q}_2,\vec{q}_3,\vec{q}_4)V_{K_2}^e(\vec{q}_2)V_{K_3}^e(\vec{q}_3)V_{K_4}^e(\vec{q}_4) + \cdots
\end{aligned} \tag{3.3.3.18}$$

Note that $K_2, K_3, K_4, \ldots$ run only 1 or 2. To solve Eq.(3.3.3.18), let us expand $\delta\psi(\vec{q})$ in powers of the external potentials.[31]

$$\delta\psi(\vec{q}) =: \delta\psi^{(1)}(\vec{q}) + \delta\psi^{(2)}(\vec{q}) + \delta\psi^{(3)}(\vec{q}) + \cdots \tag{3.3.3.19}$$

$$V_K^e(\vec{q}) =: V_K^{e(1)}(\vec{q}) + V_K^{e(2)}(\vec{q}) + V_K^{e(3)}(\vec{q}) + \cdots \tag{3.3.3.20}$$

where

$$V_1^{e(1)}(\vec{q}) = V_1(\vec{q}) + zu_{11}\delta\psi^{(1)}(\vec{q}) - zu_{12}\delta\psi^{(1)}(\vec{q}) + V^{(1)}(\vec{q}) \tag{3.3.3.21}$$

$$V_2^{e(1)}(\vec{q}) = V_2(\vec{q}) + zu_{12}\delta\psi^{(1)}(\vec{q}) - zu_{22}\delta\psi^{(1)}(\vec{q}) + V^{(1)}(\vec{q}) \tag{3.3.3.22}$$

$$V_1^{e(2)}(\vec{q}) = zu_{11}\delta\psi^{(2)}(\vec{q}) - zu_{12}\delta\psi^{(2)}(\vec{q}) + V^{(2)}(\vec{q}) \tag{3.3.3.23}$$

$$V_2^{e(2)}(\vec{q}) = zu_{12}\delta\psi^{(2)}(\vec{q}) - zu_{22}\delta\psi^{(2)}(\vec{q}) + V^{(2)}(\vec{q}) \tag{3.3.3.24}$$

$$V_1^{e(3)}(\vec{q}) = zu_{11}\delta\psi^{(3)}(\vec{q}) - zu_{12}\delta\psi^{(3)}(\vec{q}) + V^{(3)}(\vec{q}) \tag{3.3.3.25}$$

$$V_2^{e(3)}(\vec{q}) = zu_{12}\delta\psi^{(3)}(\vec{q}) - zu_{22}\delta\psi^{(3)}(\vec{q}) + V^{(3)}(\vec{q}) \tag{3.3.3.26}$$

where I used the following conditions (extension of Eq.(3.3.3.17)).

$$\delta\psi^{(n)}(\vec{q}) = \delta\phi_1^{(n)}(\vec{q}) = -\delta\phi_2^{(n)}(\vec{q}) \quad \forall n \tag{3.3.3.27}$$

[31] Here, "solve" means to express C_n by using G_n since we can calculate G_n for specific systems.

As for $\delta\psi^{(1)}(\vec{q})$, Eq.(3.3.3.18) shows that:

$$\begin{aligned}-\frac{1}{\beta}\delta\psi^{(1)}(\vec{q}) &= C_2(\vec{q})\left[V_1(\vec{q}) - V_2(\vec{q})\right] \\ &= G_2^{1,1}(\vec{q})V_1^{e(1)}(\vec{q}) + G_2^{1,2}(\vec{q})V_2^{e(1)}(\vec{q}) \\ &= -G_2^{2,1}(\vec{q})V_1^{e(1)}(\vec{q}) - G_2^{2,2}(\vec{q})V_2^{e(1)}(\vec{q}) \end{aligned} \tag{3.3.3.28}$$

Let us define correlation functions G_2 as follows.[32]

$$S_{11}(\vec{q}) := G_2^{1,1}(\vec{q}) \tag{3.3.3.29}$$

$$S_{22}(\vec{q}) := G_2^{2,2}(\vec{q}) \tag{3.3.3.30}$$

$$S_c(\vec{q}) := G_2^{1,2}(\vec{q}) = G_2^{2,1}(\vec{q}) \tag{3.3.3.31}$$

By omitting $(\vec{q})$ for simplicity, we can solve Eq.(3.3.3.28) as follows.

$$\begin{aligned}&(S_{11} + S_c)V_1^{e(1)} = -(S_c + S_{22})V_2^{e(1)} \\ &\rightarrow \frac{V_2^{e(1)}}{V_1^{e(1)}} = -\frac{S_{11} + S_c}{S_c + S_{22}}\end{aligned} \tag{3.3.3.32}$$

$$\begin{aligned}V_1^{e(1)} - V_2^{e(1)} &= V_1 - V_2 + z(u_{11} + u_{22} - 2u_{12})\delta\psi^{(1)} = V_1 - V_2 - \frac{2\chi}{\beta}\delta\psi^{(1)} \\ &= V_1 - V_2 + 2\chi C_2(V_1 - V_2) = (1 + 2\chi C_2)\left(V_1 - V_2\right) \\ &= (1 + 2\chi C_2)\,\frac{S_{11}V_1^{e(1)} + S_c V_2^{e(1)}}{C_2}\end{aligned} \tag{3.3.3.33}$$

From Eqs.(3.3.3.32) and (3.3.3.33):

$$\begin{aligned}1 - \frac{V_2^{e(1)}}{V_1^{e(1)}} &= 1 + \frac{S_{11} + S_c}{S_c + S_{22}} \\ &= (1 + 2\chi C_2)\,\frac{S_{11} + S_c\frac{V_2^{e(1)}}{V_1^{e(1)}}}{C_2} = (1 + 2\chi C_2)\left[\frac{S_{11}}{C_2} - \frac{S_c}{C_2}\frac{S_{11} + S_c}{S_c + S_{22}}\right]\end{aligned} \tag{3.3.3.34}$$

Here, we define the following two quantities:

$$A(\vec{q}) := S_{11}(\vec{q}) + 2S_c(\vec{q}) + S_{22}(\vec{q}) \tag{3.3.3.35}$$

$$W(\vec{q}) := S_{11}(\vec{q})S_{22}(\vec{q}) - S_c^2(\vec{q}) \tag{3.3.3.36}$$

By using Eqs.(3.3.3.35) and (3.3.3.36), Eq.(3.3.3.34) becomes:

$$\begin{aligned}&\frac{S_c + S_{22} + S_{11} + S_c}{S_c + S_{22}} = \frac{1}{C_2(S_c + S_{22})}\left(1 + 2\chi C_2\right)\left(S_{11}(S_c + S_{22}) - S_c(S_{11} + S_c)\right) \\ &\rightarrow A = \frac{1}{C_2}\left(1 + 2\chi C_2\right)W\end{aligned} \tag{3.3.3.37}$$

[32] $S_{11} \neq S_{12}$ and $S_{11} \neq -S_c$ since Eq.(3.3.2.48) is no longer valid.

Finally, C_2 is expressed by $G_2^{K,K'}$ as follows.

$$C_2(\vec{q}) = \frac{W(\vec{q})}{A(\vec{q}) - 2\chi W(\vec{q})} \tag{3.3.3.38}$$

As for $\delta\psi^{(2)}(\vec{q})$, Eq.(3.3.3.18) shows that:

$$\begin{aligned}
\delta\psi^{(2)}(\vec{q}) &= \frac{(-\beta)^2}{2}\frac{1}{(2\pi)^6}\int d\vec{q}_2 \int d\vec{q}_3 C_3(\vec{q}_1,\vec{q}_2,\vec{q}_3)U(\vec{q}_2)U(\vec{q}_3) \\
&= (-\beta)\left(G_2^{1,1}(\vec{q})V_1^{e(2)}(\vec{q}) + G_2^{1,2}(\vec{q})V_2^{e(2)}(\vec{q})\right) \\
&\quad + \frac{(-\beta)^2}{2}\frac{1}{(2\pi)^6}\sum_{K_2}\sum_{K_3}\int d\vec{q}_2 \int d\vec{q}_3 G_3^{1,K_2,K_3}(\vec{q}_1,\vec{q}_2,\vec{q}_3)V_{K_2}^{e(1)}(\vec{q}_2)V_{K_3}^{e(1)}(\vec{q}_3) \\
&= -(-\beta)\left(G_2^{2,1}(\vec{q})V_1^{e(2)}(\vec{q}) + G_2^{2,2}(\vec{q})V_2^{e(2)}(\vec{q})\right) \\
&\quad - \frac{(-\beta)^2}{2}\frac{1}{(2\pi)^6}\sum_{K_2}\sum_{K_3}\int d\vec{q}_2 \int d\vec{q}_3 G_3^{2,K_2,K_3}(\vec{q}_1,\vec{q}_2,\vec{q}_3)V_{K_2}^{e(1)}(\vec{q}_2)V_{K_3}^{e(1)}(\vec{q}_3)
\end{aligned} \tag{3.3.3.39}$$

From Eq.(3.3.3.39), C_3 is expressed as follows.

$$\begin{aligned}
&C_3(\vec{q}_1,\vec{q}_2,\vec{q}_3) = C_2(\vec{q}_1)C_2(\vec{q}_2)C_2(\vec{q}_3)\sum_{K_1,K_2,K_3} G_3^{K_1,K_2,K_3}(\vec{q}_1,\vec{q}_2,\vec{q}_3) \\
&\left[\left(G_2^{K_1,1}(\vec{q}_1)\right)^{-1} - \left(G_2^{K_1,2}(\vec{q}_1)\right)^{-1}\right]\left[\left(G_2^{K_2,1}(\vec{q}_2)\right)^{-1} - \left(G_2^{K_2,2}(\vec{q}_2)\right)^{-1}\right]\left[\left(G_2^{K_3,1}(\vec{q}_3)\right)^{-1} - \left(G_2^{K_3,2}(\vec{q}_3)\right)^{-1}\right]
\end{aligned} \tag{3.3.3.40}$$

By substituting Eqs.(3.3.3.38) and (3.3.3.40) to Eq.(3.3.2.64):

$$\begin{aligned}
&F[\delta\psi(\vec{q})] - F[0] \\
&= \frac{1}{2\beta}\frac{1}{(2\pi)^3}\int d\vec{q}_1 \left[\frac{S(\vec{q}_1)}{W(\vec{q}_1)} - 2\chi\right]\delta\psi(\vec{q}_1)\delta\psi(-\vec{q}_1) \\
&- \frac{1}{6\beta}\frac{1}{(2\pi)^9}\int d\vec{q}_1 \int d\vec{q}_2 \int d\vec{q}_3 \sum_{K_1,K_2,K_3} G_3^{K_1,K_2,K_3}(\vec{q}_1,\vec{q}_2,\vec{q}_3) \\
&\quad \left[\left(G_2^{K_1,1}(\vec{q}_1)\right)^{-1} - \left(G_2^{K_1,2}(\vec{q}_1)\right)^{-1}\right]\left[\left(G_2^{K_2,1}(\vec{q}_2)\right)^{-1} - \left(G_2^{K_2,2}(\vec{q}_2)\right)^{-1}\right]\left[\left(G_2^{K_3,1}(\vec{q}_3)\right)^{-1} - \left(G_2^{K_3,2}(\vec{q}_3)\right)^{-1}\right] \\
&\quad \delta\psi(\vec{q}_1)\delta\psi(\vec{q}_2)\delta\psi(\vec{q}_3) + \cdots
\end{aligned} \tag{3.3.3.41}$$

Until now, I assume the translational invariance only for 2nd order cumulant (Eq.(3.3.2.35)). At this point, let us assume the translational invariance for higher order terms.

$$g_3(\vec{r}_1,\vec{r}_2,\vec{r}_3) \to g_3(\vec{r}_1 - \vec{r}_3, \vec{r}_2 - \vec{r}_3) \tag{3.3.3.42}$$

$$g_4(\vec{r}_1,\vec{r}_2,\vec{r}_3,\vec{r}_4) \to g_4(\vec{r}_1 - \vec{r}_4, \vec{r}_2 - \vec{r}_4, \vec{r}_3 - \vec{r}_4) \tag{3.3.3.43}$$

Under this assumption, Eq.(3.3.2.40) becomes:

$$
\begin{aligned}
&\int d\vec{r}_1 \int d\vec{r}_2 \int d\vec{r}_3 g_3(\vec{r}_1-\vec{r}_3,\vec{r}_2-\vec{r}_3)h_a(\vec{r}_2)h_b(\vec{r}_3)e^{i\vec{q}_1\cdot\vec{r}_1} \\
&= \frac{1}{(2\pi)^{12}} \int d\vec{r}_1 \cdots \int d\vec{r}_3 \int d\vec{q}_2 \cdots \int d\vec{q}_5 g_3(\vec{q}_2,\vec{q}_3)h_a(\vec{q}_4)h_b(\vec{q}_5)e^{i\vec{q}_1\cdot\vec{r}_1}e^{-i\vec{q}_2\cdot(\vec{r}_1-\vec{r}_3)}e^{-i\vec{q}_3\cdot(\vec{r}_2-\vec{r}_3)}e^{-i\vec{q}_4\cdot\vec{r}_2}e^{-i\vec{q}_5\cdot\vec{r}_3} \\
&= \frac{1}{(2\pi)^{12}} \int d\vec{r}_1 \cdots \int d\vec{r}_3 \int d\vec{q}_2 \cdots \int d\vec{q}_5 g_3(\vec{q}_2,\vec{q}_3)h_a(\vec{q}_4)h_b(\vec{q}_5)e^{i(\vec{q}_1-\vec{q}_2)\cdot\vec{r}_1}e^{i(-\vec{q}_3-\vec{q}_4)\cdot\vec{r}_2}e^{i(\vec{q}_2+\vec{q}_3-\vec{q}_5)\cdot\vec{r}_3} \\
&= \frac{1}{(2\pi)^{12}} \int d\vec{q}_2 \cdots \int d\vec{q}_5 g_3(\vec{q}_2,\vec{q}_3)h_a(\vec{q}_4)h_b(\vec{q}_5)\delta(\vec{q}_1-\vec{q}_2)\delta(-\vec{q}_3-\vec{q}_4)\delta(\vec{q}_2+\vec{q}_3-\vec{q}_5) \\
&= \frac{1}{(2\pi)^3} \int d\vec{q}_3 g_3(\vec{q}_1,\vec{q}_3)h_a(-\vec{q}_3)h_b(\vec{q}_1+\vec{q}_3) \\
&\to \frac{1}{(2\pi)^6} \int d\vec{q}_2 \int d\vec{q}_3 \delta(\vec{q}_1+\vec{q}_2+\vec{q}_3)g_3(\vec{q}_1,\vec{q}_3,\vec{q}_2)h_a(-\vec{q}_3)h_b(-\vec{q}_2)
\end{aligned}
\tag{3.3.3.44}
$$

Similar to this, Eq.(3.3.2.46) becomes:

$$
\begin{aligned}
&\int d\vec{r}_1 \cdots \int d\vec{r}_6 g_3(\vec{r}_1-\vec{r}_3,\vec{r}_2-\vec{r}_3)g_{2a}(\vec{r}_1-\vec{r}_4)g_{2b}(\vec{r}_2-\vec{r}_5)g_{2c}(\vec{r}_3-\vec{r}_6)h_a(\vec{r}_4)h_b(\vec{r}_5)h_c(\vec{r}_6) \\
&= \frac{1}{(2\pi)^{24}} \int d\vec{r}_1 \cdots \int d\vec{r}_6 \int d\vec{q}_1 \cdots \int d\vec{q}_8 g_3(\vec{q}_1,\vec{q}_2)g_{2a}(\vec{q}_3)g_{2b}(\vec{q}_4)g_{2c}(\vec{q}_5)h_a(\vec{q}_6)h_b(\vec{q}_7)h_c(\vec{q}_8) \\
&\qquad e^{-i\vec{q}_1\cdot(\vec{r}_1-\vec{r}_3)}e^{-i\vec{q}_2\cdot(\vec{r}_2-\vec{r}_3)}e^{-i\vec{q}_3\cdot(\vec{r}_1-\vec{r}_4)}e^{-i\vec{q}_4\cdot(\vec{r}_2-\vec{r}_5)}e^{-i\vec{q}_5\cdot(\vec{r}_3-\vec{r}_6)}e^{-i\vec{q}_6\cdot\vec{r}_4}e^{-i\vec{q}_7\cdot\vec{r}_5}e^{-i\vec{q}_8\cdot\vec{r}_6} \\
&= \frac{1}{(2\pi)^{24}} \int d\vec{r}_1 \cdots \int d\vec{r}_6 \int d\vec{q}_1 \cdots \int d\vec{q}_8 g_3(\vec{q}_1,\vec{q}_2)g_{2a}(\vec{q}_3)g_{2b}(\vec{q}_4)g_{2c}(\vec{q}_5)h_a(\vec{q}_6)h_b(\vec{q}_7)h_c(\vec{q}_8) \\
&\qquad e^{i(-\vec{q}_1-\vec{q}_3)\cdot\vec{r}_1}e^{i(-\vec{q}_2-\vec{q}_4)\cdot\vec{r}_2}e^{i(\vec{q}_1+\vec{q}_2-\vec{q}_5)\cdot\vec{r}_3}e^{i(\vec{q}_3-\vec{q}_6)\cdot\vec{r}_4}e^{i(\vec{q}_4-\vec{q}_7)\cdot\vec{r}_5}e^{i(\vec{q}_5-\vec{q}_8)\cdot\vec{r}_6} \\
&= \frac{1}{(2\pi)^6} \int d\vec{q}_1 \int d\vec{q}_2 g_3(\vec{q}_1,\vec{q}_2)g_{2a}(-\vec{q}_1)g_{2b}(-\vec{q}_2)g_{2c}(\vec{q}_1+\vec{q}_2)h_a(-\vec{q}_1)h_b(-\vec{q}_2)h_c(\vec{q}_1+\vec{q}_2) \\
&\to \frac{1}{(2\pi)^9} \int d\vec{q}_1 \int d\vec{q}_2 \int d\vec{q}_3 \delta(\vec{q}_1+\vec{q}_2+\vec{q}_3)g_3(\vec{q}_1,\vec{q}_2,\vec{q}_3)g_{2a}(-\vec{q}_1)g_{2b}(-\vec{q}_2)g_{2c}(-\vec{q}_3)h_a(-\vec{q}_1)h_b(-\vec{q}_2)h_c(-\vec{q}_3)
\end{aligned}
\tag{3.3.3.45}
$$

4th order term is also calculated in similar way. These calculation show that the translational invariance impose the condition $\sum_i \vec{q}_i = 0$ in q-space. Eq.(3.3.3.41) becomes:

$$
\begin{aligned}
&F[\delta\psi(\vec{q})] - F[0] \\
&= \frac{1}{2\beta}\frac{1}{(2\pi)^3} \int d\vec{q}_1 \left[\frac{A(\vec{q}_1)}{W(\vec{q}_1)} - 2\chi\right] \delta\psi(\vec{q}_1)\delta\psi(-\vec{q}_1) \\
&- \frac{1}{6\beta}\frac{1}{(2\pi)^9} \int d\vec{q}_1 \int d\vec{q}_2 \int d\vec{q}_3 \delta(\vec{q}_1+\vec{q}_2+\vec{q}_3) \sum_{K_1,K_2,K_3} G_3^{K_1,K_2,K_3}(\vec{q}_1,\vec{q}_2,\vec{q}_3) \\
&\quad \left[\left(G_2^{K_1,1}(\vec{q}_1)\right)^{-1} - \left(G_2^{K_1,2}(\vec{q}_1)\right)^{-1}\right] \left[\left(G_2^{K_2,1}(\vec{q}_2)\right)^{-1} - \left(G_2^{K_2,2}(\vec{q}_2)\right)^{-1}\right] \left[\left(G_2^{K_3,1}(\vec{q}_3)\right)^{-1} - \left(G_2^{K_3,2}(\vec{q}_3)\right)^{-1}\right] \\
&\quad \delta\psi(\vec{q}_1)\delta\psi(\vec{q}_2)\delta\psi(\vec{q}_3) + \cdots
\end{aligned}
\tag{3.3.3.46}
$$

3.3.4 Correlation functions for block copolymer melt

To calculate Eq.(3.3.3.41), we have to know the correlation functions for ideal chains (polymer melt), Eqs.(3.3.3.9) $\sim$ (3.3.3.11). These quantity is calculated by using the procedure similar to the derivation of Debye function, Eq.(2.2.5.7).

Correlation function between Ith segment and Jth segment in real space, $G_{IJ}(\vec{r}_1, \vec{r}_2)$, is:[33]

$$\begin{aligned} G_{IJ}(\vec{r}_1, \vec{r}_2) &:= \left\langle \delta\hat{\phi}_I(\vec{r}_1;\Gamma)\delta\hat{\phi}_J(\vec{r}_2;\Gamma) \right\rangle_0 \\ &= \left\langle \left(\hat{\phi}_I(\vec{r}_1;\Gamma) - \bar{\phi}_I\right)\left(\hat{\phi}_J(\vec{r}_2;\Gamma) - \bar{\phi}_J\right) \right\rangle_0 \\ &= \left\langle \hat{\phi}_I(\vec{r}_1;\Gamma)\hat{\phi}_J(\vec{r}_2;\Gamma) \right\rangle_0 - \left\langle \hat{\phi}_I(\vec{r}_1;\Gamma) \right\rangle_0 \bar{\phi}_J - \left\langle \hat{\phi}_J(\vec{r}_2;\Gamma) \right\rangle_0 \bar{\phi}_I + \bar{\phi}_I\bar{\phi}_J \\ &= \left\langle \hat{\phi}_I(\vec{r}_1;\Gamma)\hat{\phi}_J(\vec{r}_2;\Gamma) \right\rangle_0 - \frac{1}{N^2} \end{aligned} \tag{3.3.4.1}$$

Here, I used the following relationships.

$$\left\langle \hat{\phi}_I(\vec{r}_1;\Gamma) \right\rangle_0 = \left\langle \hat{\phi}_J(\vec{r}_2;\Gamma) \right\rangle_0 = \frac{1}{N} \tag{3.3.4.2}$$

$$\bar{\phi}_I = \bar{\phi}_J = \frac{1}{N} \tag{3.3.4.3}$$

Note that ϕ represents the monomer fraction. Here, we consider polymer melt and therefore total polymer fraction is 1. $\left\langle \hat{\phi}_I(\vec{r}_1;\Gamma)\hat{\phi}_J(\vec{r}_2;\Gamma) \right\rangle_0$ is divided into two contributions; correlation between the same chain and between different chains. First contribution is approximated by the probability Eq.(2.2.5.2) multiplied by $1/N$, which express the probability that the monomer at $\vec{r}_1$ is Ith segment. Second contribution is $(1/N)^2$ since we assume that there are no interaction between different polymers.

$$\left\langle \hat{\phi}_I(\vec{r}_1;\Gamma)\hat{\phi}_J(\vec{r}_2;\Gamma) \right\rangle_0 \simeq \frac{1}{N} P(|I-J|, \vec{r}_1 - \vec{r}_2) + \frac{1}{N^2} \tag{3.3.4.4}$$

Substitute Eq.(3.3.4.4) to Eq.(3.3.4.1):

$$G_{IJ}(\vec{r}_1, \vec{r}_2) = \frac{1}{N} P(|I-J|, \vec{r}_1 - \vec{r}_2) \tag{3.3.4.5}$$

3rd order correlation function, $G_{IJK}(\vec{r}_1, \vec{r}_2, \vec{r}_3)$ is:

$$\begin{aligned} G_{IJK}(\vec{r}_1, \vec{r}_2, \vec{r}_3) &:= \left\langle \delta\hat{\phi}_I(\vec{r}_1;\Gamma)\delta\hat{\phi}_J(\vec{r}_2;\Gamma)\delta\hat{\phi}_K(\vec{r}_3;\Gamma) \right\rangle_0 \\ &= \left\langle \hat{\phi}_I(\vec{r}_1;\Gamma)\hat{\phi}_J(\vec{r}_2;\Gamma)\hat{\phi}_K(\vec{r}_3;\Gamma) \right\rangle_0 \\ &- \frac{1}{N}\left\langle \hat{\phi}_I(\vec{r}_1;\Gamma)\hat{\phi}_J(\vec{r}_2;\Gamma) \right\rangle_0 - \frac{1}{N}\left\langle \hat{\phi}_I(\vec{r}_1;\Gamma)\hat{\phi}_K(\vec{r}_3;\Gamma) \right\rangle_0 - \frac{1}{N}\left\langle \hat{\phi}_J(\vec{r}_2;\Gamma)\hat{\phi}_K(\vec{r}_3;\Gamma) \right\rangle_0 \\ &+ \frac{1}{N^2}\left\langle \hat{\phi}_I(\vec{r}_1;\Gamma) \right\rangle_0 + \frac{1}{N^2}\left\langle \hat{\phi}_J(\vec{r}_2;\Gamma) \right\rangle_0 + \frac{1}{N^2}\left\langle \hat{\phi}_K(\vec{r}_3;\Gamma) \right\rangle_0 \\ &- \frac{1}{N^3} \end{aligned} \tag{3.3.4.6}$$

[33] At this stage, there is no assumption for monomer types of Ith segment and Jth segment.

Here,

$$\begin{aligned}
&\left\langle \hat{\phi}_I(\vec{r}_1;\Gamma)\hat{\phi}_J(\vec{r}_2;\Gamma)\hat{\phi}_K(\vec{r}_3;\Gamma)\right\rangle_0 \\
&\simeq \frac{1}{N}P_{IJK}(|I-J|,\vec{r}_1-\vec{r}_2;|J-K|,\vec{r}_2-\vec{r}_3) \\
&+\frac{1}{N^2}P(|I-J|,\vec{r}_1-\vec{r}_2)+\frac{1}{N^2}P(|J-K|,\vec{r}_2-\vec{r}_3)+\frac{1}{N^2}P(|K-I|,\vec{r}_3-\vec{r}_1)+\frac{1}{N^3}
\end{aligned} \tag{3.3.4.7}$$

1st term of the right hand side of Eq.(3.3.4.7) is the probability that Ith segment at $\vec{r}_1$, Jth segment at $\vec{r}_2$, and Kth segment at $\vec{r}_3$ are on the same chain, 2nd term is the probability that Ith segment at $\vec{r}_1$ and Jth segment at $\vec{r}_2$ are on the same chain while Kth segment at $\vec{r}_3$ is on different chain, and so on. Substitute Eqs.(3.3.4.2), (3.3.4.4), and (3.3.4.7) to Eq.(3.3.4.6),

$$G_{IJK}(\vec{r}_1,\vec{r}_2,\vec{r}_3)=\frac{1}{N}P_{IJK}(|I-J|,\vec{r}_1-\vec{r}_2;|J-K|,\vec{r}_2-\vec{r}_3) \tag{3.3.4.8}$$

Here, $P_{IJK}(|I-J|,\vec{r}_1-\vec{r}_2;|J-K|,\vec{r}_2-\vec{r}_3)$ is the product of 2nd order correlation function.

$$\begin{aligned}
P_{IJK}(|I-J|,\vec{r}_1-\vec{r}_2;|J-K|,\vec{r}_2-\vec{r}_3) &= P_{IJ}(|I-J|,\vec{r}_1-\vec{r}_2)P_{JK}(|J-K|,\vec{r}_2-\vec{r}_3) \\
&\text{for } I<J<K \text{ or } \ K<J<I
\end{aligned} \tag{3.3.4.9}$$

When $I<J<K$ or $K<J<I$ do not hold, labeling order should be exchanged.

By using similar procedure, 4th order correlation function, $G_{IJKL}(\vec{r}_1,\vec{r}_2,\vec{r}_3,\vec{r}_4)$ is:

$$G_{IJKL}(\vec{r}_1,\vec{r}_2,\vec{r}_3,\vec{r}_4)=\frac{1}{N}P_{IJKL}(|I-J|,\vec{r}_1-\vec{r}_2;|J-K|,\vec{r}_2-\vec{r}_3;|K-L|,\vec{r}_3-\vec{r}_4) \tag{3.3.4.10}$$

where

$$\begin{aligned}
&P_{IJKL}(|I-J|,\vec{r}_1-\vec{r}_2;|J-K|,\vec{r}_2-\vec{r}_3;|K-L|,\vec{r}_3-\vec{r}_4) \\
&= P_{IJ}(|I-J|,\vec{r}_1-\vec{r}_2)P_{JK}(|J-K|,\vec{r}_2-\vec{r}_3)P_{KL}(|K-L|,\vec{r}_3-\vec{r}_4) \\
&\text{for } I<J<K<L \text{ or } \ L<K<J<I
\end{aligned} \tag{3.3.4.11}$$

By using correlation functions Eqs.(3.3.4.5), (3.3.4.8), and (3.3.4.10), correlation functions Eqs.(3.3.3.9) $\sim$ (3.3.3.11) are calculated. First, let us see $G_2^{11}(\vec{q})$ for the case of block copolymer where the fraction of species 1 is defined as f by referring to Eqs.(2.2.5.6) and (2.2.5.7). Since I and J run from 1 to fN:

$$\begin{aligned}
S_{11}(\vec{q},f)=G_2^{11}(\vec{q},f) &= \int d\vec{r}\left[\sum_{I=1}^{fN}\sum_{J=1}^{fN}G_{IJ}(\vec{r})\right]e^{i\vec{q}\cdot\vec{r}} \\
&= \frac{1}{N}\sum_{I=1}^{fN}\sum_{J=1}^{fN}\exp\left(-\frac{q^2b^2}{6}|I-J|\right) \\
&\to \frac{1}{N}\int_0^{fN}dI\int_0^{fN}dJ\exp\left(-\frac{q^2b^2}{6}|I-J|\right) \\
&= f^2N\int_0^1 ds\int_0^1 dt\exp\left(-Q|s-t|\right) \\
&= f^2N\frac{2}{Q^2}\left(e^{-Q}+Q-1\right) \\
&=: N\frac{2}{x^2}\left[e^{-fx}+fx-1\right] =: Ng_1(x,f)
\end{aligned} \tag{3.3.4.12}$$

where

$$s := \frac{I}{fN} \tag{3.3.4.13}$$

$$t := \frac{J}{fN} \tag{3.3.4.14}$$

$$Q := \frac{q^2b^2}{6} fN = f\langle R_g^2 \rangle q^2 \tag{3.3.4.15}$$

$$x := \frac{q^2b^2}{6} N = \langle R_g^2 \rangle q^2 = \frac{Q}{f} \tag{3.3.4.16}$$

Similar to this,

$$\begin{aligned} S_{22}(\vec{q}, f) = G_2^{22}(\vec{q}, f) &= \int d\vec{r} \left[\sum_{I=fN+1}^{N} \sum_{J=fN+1}^{N} G_{IJ}(\vec{r}) \right] e^{i\vec{q}\cdot\vec{r}} \\ &\to \frac{1}{N} \int_{fN}^{1} dI \int_{fN}^{1} dJ \exp\left(-\frac{q^2b^2}{6} |I - J| \right) \\ &= \frac{1}{N} \int_{0}^{(1-f)N} dI \int_{0}^{(1-f)N} dJ \exp\left(-\frac{q^2b^2}{6} |I - J| \right) \\ &= N g_1(x, 1-f) \end{aligned} \tag{3.3.4.17}$$

By using Eqs.(3.3.4.12) and (3.3.4.17):

$$\begin{aligned} S_c(\vec{q}, f) = G_2^{12}(\vec{q}, f) &= \int d\vec{r} \left[\sum_{I=1}^{fN} \sum_{J=fN+1}^{N} G_{IJ}(\vec{r}) \right] e^{i\vec{q}\cdot\vec{r}} \\ &\to \frac{1}{N} \int_{0}^{fN} dI \int_{fN}^{1} dJ \exp\left(-\frac{q^2b^2}{6} |I - J| \right) \\ &= \frac{1}{2N} \left[\int_{0}^{N} dI \int_{0}^{N} dJ \exp\left(-\frac{q^2b^2}{6} |I - J| \right) \right. \\ &\qquad \left. - \int_{0}^{fN} dI \int_{0}^{fN} dJ \exp\left(-\frac{q^2b^2}{6} |I - J| \right) - \int_{fN}^{N} dI \int_{fN}^{N} dJ \exp\left(-\frac{q^2b^2}{6} |I - J| \right) \right] \\ &= \frac{N}{2} \left[g_1(x, 1) - g_1(x, f) - g_1(x, 1-f) \right] \end{aligned} \tag{3.3.4.18}$$

Next, let us calculate $G_3^{111}(\vec{q}_1, \vec{q}_2, \vec{q}_3)$. In this case, we have to take care the order of I, J, K of $G_{IJK}(\vec{r}_1, \vec{r}_2, \vec{r}_3)$. There are six patterns of the order of I, J, K as follows.

$$I < J < K : G_{IJK}(\vec{r}_1, \vec{r}_2, \vec{r}_3) = \frac{1}{N} P(J - I, \vec{r}_1 - \vec{r}_2) P(K - J, \vec{r}_2 - \vec{r}_3) \tag{3.3.4.19}$$

$$I < K < J : G_{IJK}(\vec{r}_1, \vec{r}_2, \vec{r}_3) = \frac{1}{N} P(K - I, \vec{r}_1 - \vec{r}_3) P(J - K, \vec{r}_3 - \vec{r}_2) \tag{3.3.4.20}$$

$$J < I < K : G_{IJK}(\vec{r}_1, \vec{r}_2, \vec{r}_3) = \frac{1}{N} P(I - J, \vec{r}_2 - \vec{r}_1) P(K - I, \vec{r}_1 - \vec{r}_3) \tag{3.3.4.21}$$

$$J < K < I : G_{IJK}(\vec{r}_1, \vec{r}_2, \vec{r}_3) = \frac{1}{N} P(K - J, \vec{r}_2 - \vec{r}_3) P(I - K, \vec{r}_3 - \vec{r}_1) \tag{3.3.4.22}$$

$$K < I < J : G_{IJK}(\vec{r}_1, \vec{r}_2, \vec{r}_3) = \frac{1}{N} P(I - K, \vec{r}_3 - \vec{r}_1) P(J - I, \vec{r}_1 - \vec{r}_2) \tag{3.3.4.23}$$

$$K < J < I : G_{IJK}(\vec{r}_1, \vec{r}_2, \vec{r}_3) = \frac{1}{N} P(J - K, \vec{r}_3 - \vec{r}_2) P(I - J, \vec{r}_2 - \vec{r}_1) \tag{3.3.4.24}$$

By using Eqs.(3.3.4.19) $\sim$ (3.3.4.24), $G_3^{111}(\vec{q}_1,\vec{q}_2,\vec{q}_3)$ is represented as follows.

$$NG_3^{111}(\vec{q}_1,\vec{q}_2,\vec{q}_3) \to \int_0^{fN} dk \int_0^k dj \int_0^j di P_{ij}(\vec{q}_1)P_{jk}(\vec{q}_3) \tag{3.3.4.25}$$

$$+ \int_0^{fN} dj \int_0^j dk \int_0^k di P_{ik}(\vec{q}_1)P_{kj}(\vec{q}_2) \tag{3.3.4.26}$$

$$+ \int_0^{fN} dk \int_0^k di \int_0^i dj P_{ji}(\vec{q}_2)P_{ik}(\vec{q}_3) \tag{3.3.4.27}$$

$$+ \int_0^{fN} di \int_0^i dk \int_0^k dj P_{jk}(\vec{q}_2)P_{ki}(\vec{q}_1) \tag{3.3.4.28}$$

$$+ \int_0^{fN} dj \int_0^j di \int_0^i dk P_{ki}(\vec{q}_3)P_{ij}(\vec{q}_2) \tag{3.3.4.29}$$

$$+ \int_0^{fN} di \int_0^i dj \int_0^j dk P_{kj}(\vec{q}_3)P_{ji}(\vec{q}_1) \tag{3.3.4.30}$$

where $P_{ij}(\vec{q})$ corresponds to one term in Eq.(2.2.5.6).

$$P_{ij}(\vec{q}) := \exp\left(-\frac{q^2b^2}{6}|i-j|\right) \tag{3.3.4.31}$$

Note that $P_{ij}(\vec{q})$ depends only on the magnitude of $\vec{q}$. In the following calculation, what we need is the case where $|\vec{q}_1|^2 = |\vec{q}_2|^2 = q^2$ and $|\vec{q}_3|^2 = hq^2$. Under this assumption, Eqs.(3.3.4.25), (3.3.4.27), (3.3.4.29), and (3.3.4.30) become the same and Eqs.(3.3.4.26) and (3.3.4.28) become the same. As a result:

$$NG_3^{111}(\vec{q}_1,\vec{q}_2,\vec{q}_3) \to \int_0^{fN} di \int_0^i dj \int_0^j dk \left(4P_{ij}(q)P_{jk}(h^{1/2}q) + 2P_{ij}(q)P_{jk}(q)\right) \tag{3.3.4.32}$$

When $h \neq 0, 1$, 1st term of Eq.(3.3.4.32) is calculated as follows. [34]

$$\begin{aligned}
&\int_0^{fN} di \int_0^i dj \int_0^j dk P_{ij}(q)P_{jk}(h^{1/2}q) \\
&= \int_0^{fN} di \int_0^i dj \int_0^j dk \exp\left[-\frac{q^2b^2}{6}(i-j) - \frac{hq^2b^2}{6}(j-k)\right] \\
&= N^3 \int_0^f ds \int_0^s dt \int_0^t du \exp\left[-x(s-t) - hx(t-u)\right] \\
&= N^3 \frac{1}{hx} \int_0^f ds \int_0^s dt e^{-xs}\left[e^{xt} - e^{(1-h)xt}\right] \\
&= N^3 \frac{1}{hx^2} \int_0^f ds \left[1 - \frac{h}{h-1}e^{-xs} + \frac{1}{h-1}e^{-hxs}\right] \\
&= N^3 \frac{1}{hx^3}\left[fx - 1 - \frac{1}{h} + \frac{h}{h-1}e^{-fx} - \frac{1}{h(h-1)}e^{-hfx}\right] =: N^3 g_2(f,h) \quad (h \neq 0,1)
\end{aligned} \tag{3.3.4.33}$$

where $s := i/N, t := j/N, u := k/N$ and x is Eq.(3.3.4.16). Like this, 2nd term of Eq.(3.3.4.32) is:

$$\int_0^{fN} di \int_0^i dj \int_0^j dk P_{ij}(q)P_{jk}(q) = N^3 \frac{1}{x^3}\left[fxe^{-fx} + fx - 2 + 2e^{-fx}\right] =: N^3 g_2(f,1) \tag{3.3.4.34}$$

Substitute Eqs.(3.3.4.33) and (3.3.4.34) to Eq.(3.3.4.32):

$$G_3^{111}(\vec{q}_1,\vec{q}_2,\vec{q}_3) \to G_3^{111}(q,f,h) = 2N^2(2g_2(f,h) + g_2(f,1)) \tag{3.3.4.35}$$

[34] In original paper, $h \neq 0, 1, 3, 4$ was assumed. However, Eq.(3.3.4.33) is valid for the case where $h \neq 3, 4$.

When $h = 0$:

$$g_2(f,0) := \frac{1}{x^3}\left[\frac{f^2x^2}{2} - fx + 1 - e^{-fx}\right] \tag{3.3.4.36}$$

Other 3rd order cumulants (moments) are calculated in similar way. In the case of $G_3^{112}(\vec{q}_1,\vec{q}_2,\vec{q}_3)$, the order of I and J should be considered.

$$I < J : G_{IJK}(\vec{r}_1,\vec{r}_2,\vec{r}_3) = \frac{1}{N}P(J-I,\vec{r}_1-\vec{r}_2)P(K-J,\vec{r}_2-\vec{r}_3) \tag{3.3.4.37}$$

$$J < I : G_{IJK}(\vec{r}_1,\vec{r}_2,\vec{r}_3) = \frac{1}{N}P(I-J,\vec{r}_2-\vec{r}_1)P(K-I,\vec{r}_1-\vec{r}_3) \tag{3.3.4.38}$$

$$\begin{aligned} G_3^{112}(\vec{q}_1,\vec{q}_2,\vec{q}_3) &\to G_3^{112}(q,f,h) \\ &= \frac{1}{N}\int_0^{fN} dj \int_0^{j} di \int_{fN}^{N} dk P_{ij}(q_1)P_{jk}(q_3) + \frac{1}{N}\int_0^{fN} di \int_0^{i} dj \int_{fN}^{N} dk P_{ji}(q_2)P_{ik}(q_3) \\ &= \frac{2}{N}\int_0^{fN} di \int_0^{i} dj \int_{fN}^{N} dk P_{ij}(q)P_{jk}(h^{1/2}q) \\ &= 2N^2 g_3(f,h) \end{aligned} \tag{3.3.4.39}$$

where

$$g_3(f,h) := \frac{1}{hx^3}\left[1-e^{-h(1-f)x}\right]\left[\frac{1}{h} - \frac{1}{h-1}e^{-fx} + \frac{1}{h(h-1)}e^{-hfx}\right] \quad \text{for } h \neq 0,1 \tag{3.3.4.40}$$

$$g_3(f,0) := \frac{1-f}{x^2}\left[fx + e^{-fx} - 1\right] \tag{3.3.4.41}$$

$$g_3(f,1) := \frac{1}{x^3}\left[1-e^{-(1-f)x}\right]\left[1 - fxe^{-fx} - e^{-fx}\right] \tag{3.3.4.42}$$

In the case of $G_3^{121}(\vec{q}_1,\vec{q}_2,\vec{q}_3)$, the order of I and K should be considered.

$$I < K : G_{IJK}(\vec{r}_1,\vec{r}_2,\vec{r}_3) = \frac{1}{N}P(K-I,\vec{r}_1-\vec{r}_3)P(J-K,\vec{r}_3-\vec{r}_2) \tag{3.3.4.43}$$

$$K < I : G_{IJK}(\vec{r}_1,\vec{r}_2,\vec{r}_3) = \frac{1}{N}P(I-K,\vec{r}_3-\vec{r}_1)P(J-I,\vec{r}_1-\vec{r}_2) \tag{3.3.4.44}$$

$$\begin{aligned} G_3^{121}(\vec{q}_1,\vec{q}_2,\vec{q}_3) &\to G_3^{121}(q,f,h) \\ &\to \frac{1}{N}\int_0^{fN} dk \int_0^{k} di \int_{fN}^{N} dj P_{ik}(q_1)P_{kj}(q_2) + \frac{1}{N}\int_0^{fN} di \int_0^{i} dk \int_{fN}^{N} dj P_{ki}(q_3)P_{ij}(q_2) \\ &= \frac{1}{N}\int_0^{fN} di \int_0^{i} dj \int_{fN}^{N} dk \left(P_{ij}(q)P_{jk}(q) + P_{ij}(q)P_{jk}(h^{1/2}q)\right) \\ &= N^2\left[g_4(f,h) + g_3(f,1)\right] \end{aligned} \tag{3.3.4.45}$$

where[35]

$$g_4(f,h) := \frac{1}{hx^3}\left[1-e^{-(1-f)x}\right]\left[1+\frac{1}{h-1}e^{-hfx}-\frac{h}{(h-1)}e^{-fx}\right] \quad \text{for } h \neq 0,1 \tag{3.3.4.46}$$

$$g_4(f,0) := \frac{1}{x^3}\left[1-e^{-(1-f)x}\right]\left[fx-1+e^{-fx}\right] \tag{3.3.4.47}$$

$$g_4(f,1) := g_3(f,1) \tag{3.3.4.48}$$

By using Eqs.(3.3.4.35), (3.3.4.39), and (3.3.4.45),

$$G_3^{211}(q,f,h) = G_3^{121}(q,f,h) = N^2\left[g_4(f,h)+g_3(f,1)\right] \tag{3.3.4.49}$$

$$G_3^{221}(q,f,h) = G_3^{112}(q,1-f,h) = 2N^2 g_3(1-f,h) \tag{3.3.4.50}$$

$$G_3^{212}(q,f,h) = G_3^{121}(q,1-f,h) = N^2\left[g_4(1-f,h)+g_3(1-f,1)\right] \tag{3.3.4.51}$$

$$G_3^{122}(q,f,h) = G_3^{211}(q,1-f,h) = N^2\left[g_4(1-f,h)+g_3(1-f,1)\right] \tag{3.3.4.52}$$

$$G_3^{222}(q,f,h) = G_3^{111}(q,1-f,h) = 2N^2(2g_2(1-f,h)+g_2(1-f,1)) \tag{3.3.4.53}$$

By using the similar calculation scheme, 4th order moments are obtained as follows.

$$G_4^{1111}(q,f,h_1,h_2) = 8N^3\left[f_1(f,h_1)+f_1(f,4-h_1-h_2)+f_1(f,h_2)\right] \tag{3.3.4.54}$$

$$\begin{aligned} G_4^{1112}(q,f,h_1,h_2) &= G_4^{1121}(q,f,h_1,h_2) = G_4^{1211}(q,f,h_1,h_2) = G_4^{2111}(q,f,h_1,h_2) \\ &= 2N^3\left[f_2(f,h_1)+f_2(f,4-h_1-h_2)+f_2(f,h_2)\right] \end{aligned} \tag{3.3.4.55}$$

$$\begin{aligned} G_4^{1122}(q,f,h_1,h_2) &= G_4^{2211}(q,f,h_1,h_2) \\ &= 4N^3 f_3(f,h_1)f_3(1-f,h_1) \end{aligned} \tag{3.3.4.56}$$

$$\begin{aligned} G_4^{1221}(q,f,h_1,h_2) &= G_4^{2112}(q,f,h_1,h_2) \\ &= 4N^3 f_3(f,4-h_1-h_2)f_3(1-f,4-h_1-h_2) \end{aligned} \tag{3.3.4.57}$$

$$\begin{aligned} G_4^{1212}(q,f,h_1,h_2) &= G_4^{2121}(q,f,h_1,h_2) \\ &= 4N^3 f_3(f,h_2)f_3(1-f,h_2) \end{aligned} \tag{3.3.4.58}$$

$$\begin{aligned} G_4^{2221}(q,f,h_1,h_2) &= G_4^{2212}(q,f,h_1,h_2) = G_4^{2122}(q,f,h_1,h_2) = G_4^{1222}(q,f,h_1,h_2) \\ &= 2N^3\left[f_2(1-f,h_1)+f_2(1-f,4-h_1-h_2)+f_2(1-f,h_2)\right] \end{aligned} \tag{3.3.4.59}$$

$$G_4^{2222}(q,f,h_1,h_2) = 8N^3\left[f_1(1-f,h_1)+f_1(1-f,4-h_1-h_2)+f_1(1-f,h_2)\right] \tag{3.3.4.60}$$

[35] In original paper, there is a typo for $g_4(f,h)$ (Eq.(3.3.4.46)).

where

$$f_1(f,h) := \frac{1}{x^4}\left[\frac{fx}{h} + \frac{fx}{h-1}e^{-fx} + \frac{2h-3}{(h-1)^2}e^{-fx} + \frac{1}{h^2(h-1)^2}e^{-fhx} - \frac{2h+1}{h^2}\right] \quad \text{for } h \neq 0,1 \tag{3.3.4.61}$$

$$f_1(f,0) := \frac{1}{x^4}\left[\frac{f^2x^2}{2} - fxe^{-fx} - 3e^{-fx} - 2fx + 3\right] \tag{3.3.4.62}$$

$$f_1(f,1) := \frac{1}{x^4}\left[\frac{f^2x^2}{2}e^{-fx} + fx + 2fxe^{-fx} + 3e^{-fx} - 3\right] \tag{3.3.4.63}$$

$$f_2(f,h) := \frac{1}{x^4}\left[1 - e^{(f-1)x}\right]\left[\frac{1}{h} - \frac{h-2}{(h-1)^2}e^{-fx} - \frac{1}{h(h-1)^2}e^{-fhx} - \frac{fx}{h-1}e^{-fx}\right] \quad \text{for } h \neq 0,1 \tag{3.3.4.64}$$

$$f_2(f,0) := \frac{1}{x^4}\left[1 - e^{(f-1)x}\right]\left[2e^{-fx} + fxe^{-fx} - 2 + fx\right] \tag{3.3.4.65}$$

$$f_2(f,1) := \frac{1}{x^4}\left[1 - e^{(f-1)x}\right]\left[1 - e^{-fx} - \frac{f^2x^2}{2}e^{-fx} - fxe^{-fx}\right] \tag{3.3.4.66}$$

$$f_3(f,h) := \frac{1}{h(h-1)x^2}\left[h - 1 - he^{-fx} + e^{-hfx}\right] \quad \text{for } h \neq 0,1 \tag{3.3.4.67}$$

$$f_3(f,0) := \frac{1}{2}g_1(f,x) \tag{3.3.4.68}$$

$$f_3(f,1) := \frac{1}{x^2}\left[1 - e^{-fx} - fxe^{-fx}\right] \tag{3.3.4.69}$$

3.3.5 Energy expansion for specific morphology

$C_2(\vec{r}_1,\vec{r}_2)$ (Eq.(3.3.2.49)) is proportional to the pair correlation function, Eq.(2.1.12). Therefore, its Fourier transform, $C_2(\vec{q})$ (Eq.(3.3.3.38)), is proportional to the scattering function, Eq.(2.1.13). Substitute Eqs.(3.3.4.12), (3.3.4.17), and (3.3.4.18) to Eqs.(3.3.3.35) and (3.3.3.36) and then to Eq.(3.3.3.38):

$$\begin{aligned} C_2(q) &= \frac{1}{\frac{A(\vec{q})}{W(\vec{q})} - 2\chi} \\ &= \frac{N}{\frac{g_1(1,x)}{g_1(f,x)g_1(1-f,x) - (g_1(1,x) - g_1(f,x) - g_1(1-f,x))^2/4} - 2\chi N} \end{aligned} \tag{3.3.5.1}$$

Note that C_2 depends only on their magnitude.

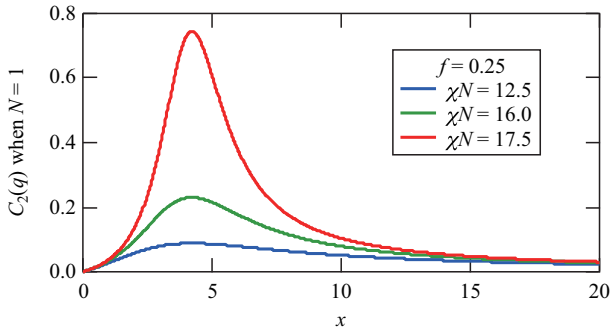

Figure 3.10: χN dependence of $C_2(\vec{q})$ for $f = 0.25$.

Figure 3.10 shows $C_2(q)$ for $f = 0.25$. It is clearly shown that $C_2(q)$ diverge at certain value of χN. This point corresponds to the spinodal point and χN of this point, $(\chi N)_s$, is calculated as follows.

$$\frac{A(q^*)}{W(q^*)}N = 2(\chi N)_s \tag{3.3.5.2}$$

q^* is the value of $\vec{q}$ at the spinodal point. By using q^*, x^* is defined as follows (see Eq.(3.3.4.16)).

$$x^* := \frac{(q^*)^2 b^2}{6} N \tag{3.3.5.3}$$

As seen in Figure 3.10, q^* and x^* depends only on f and do not depend on χN. Figure 3.11 shows the calculation results of $(\chi N)_s$ and x^* as a function of f.

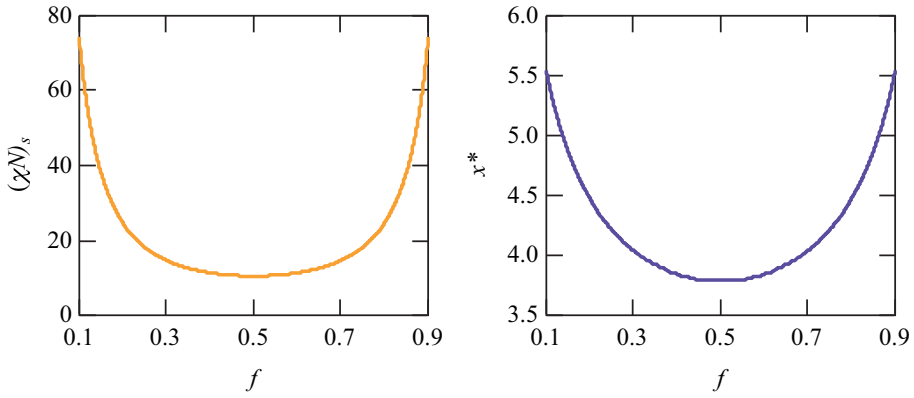

Figure 3.11: $(\chi N)_s$ and x^* as a function of f.

Free energy expansion Eq.(3.3.3.46) shows that 2nd order term of $\psi(q)$ becomes small around $\chi N = (\chi N)_s$. In contrast to this, 3rd and higher order term does not depend on χN as shown in the previous subsection. By taking this into consideration, let us define Fourier transform of $\delta\psi(\vec{r})$ as follows (original one is Eq.(3.3.2.36)).

$$\begin{aligned} \delta\psi(\vec{r}) &= \frac{1}{(2\pi)^3} \int d\vec{q}_1 \delta\psi(\vec{q}) e^{-i\vec{q}\cdot\vec{r}} \\ \rightarrow \delta\psi(\vec{r}) &= \frac{1}{\sqrt{n}} \psi_n \sum_{k=1}^{n} \left(e^{i(\vec{Q}_k\cdot\vec{r}+\varphi_k)} + e^{-i(\vec{Q}_k\cdot\vec{r}+\varphi_k)} \right) \end{aligned} \tag{3.3.5.4}$$

where n is the number of possible $\vec{q}^*$, which is determined by the morphology of microphase separated structure. $\vec{Q}_k$ stands for one of $\vec{q}^*$. Fourier transform of Eq.(3.3.5.4) is:

$$\begin{aligned} \delta\psi(\vec{q}) &= \int d\vec{r} \delta\psi(\vec{r}) e^{i\vec{q}\cdot\vec{r}} \\ &= \frac{1}{\sqrt{n}} \psi_n \sum_{k=1}^{n} \int d\vec{r} \left(e^{i(\vec{q}+\vec{Q}_k)\cdot\vec{r}} e^{i\varphi_k} + e^{i(\vec{q}-\vec{Q}_k)\cdot\vec{r}} e^{-i\varphi_k} \right) \\ &= \frac{1}{\sqrt{n}} \psi_n \sum_{k=1}^{n} \left(\delta(\vec{q}+\vec{Q}_k) e^{i\varphi_k} + \delta(\vec{q}-\vec{Q}_k) e^{-i\varphi_k} \right) \end{aligned} \tag{3.3.5.5}$$

The meaning of Eqs.(3.3.5.4) and (3.3.5.5) is that we consider only specific $\vec{q}$ for the energy expansion. By using Eq.(3.3.5.5), let us see free energy expansion again (Eq.(3.3.3.46)).

$$
\begin{aligned}
&\beta N\left(F[\delta\psi(\vec{q})]-F[0]\right)\\
&=\frac{1}{2}\frac{1}{(2\pi)^3}\int d\vec{q}_1\left[\frac{A(\vec{q}_1)}{W(\vec{q}_1)}N-2\chi N\right]\delta\psi(\vec{q}_1)\delta\psi(-\vec{q}_1)\\
&+\frac{N}{6}\frac{1}{(2\pi)^9}\int d\vec{q}_1\int d\vec{q}_2\int d\vec{q}_3\delta(\vec{q}_1+\vec{q}_2+\vec{q}_3)\Gamma_3(\vec{q}_1,\vec{q}_2,\vec{q}_3)\delta\psi(\vec{q}_1)\delta\psi(\vec{q}_2)\delta\psi(\vec{q}_3)\\
&+\frac{N}{24}\frac{1}{(2\pi)^{12}}\int d\vec{q}_1\int d\vec{q}_2\int d\vec{q}_3\int d\vec{q}_4\delta(\vec{q}_1+\vec{q}_2+\vec{q}_3+\vec{q}_4)\Gamma_4(\vec{q}_1,\vec{q}_2,\vec{q}_3,\vec{q}_4)\delta\psi(\vec{q}_1)\delta\psi(\vec{q}_2)\delta\psi(\vec{q}_3)\delta\psi(\vec{q}_4)+\cdots
\end{aligned}
\tag{3.3.5.6}
$$

2nd order term of Eq.(3.3.5.6) is expanded as follows.

$$
\begin{aligned}
&\frac{1}{2}\frac{1}{(2\pi)^3}\int d\vec{q}\left[\frac{A(\vec{q})}{W(\vec{q})}N-2\chi N\right]\delta\psi(\vec{q})\delta\psi(-\vec{q})\\
&=\frac{1}{2}\frac{1}{(2\pi)^3}\left(\frac{1}{\sqrt{n}}\psi_n\right)^2\int d\vec{q}\left[\frac{A(\vec{q})}{W(\vec{q})}N-2\chi N\right]\\
&\qquad\sum_{k=1}^{n}\sum_{l=1}^{n}\left(\delta(\vec{q}+\vec{Q}_k)e^{i\varphi_k}+\delta(\vec{q}-\vec{Q}_k)e^{-i\varphi_k}\right)\left(\delta(-\vec{q}+\vec{Q}_l)e^{i\varphi_l}+\delta(-\vec{q}-\vec{Q}_l)e^{-i\varphi_l}\right)\\
&=\frac{1}{2}\frac{1}{(2\pi)^3}\frac{1}{n}\psi_n^2\int d\vec{q}\left[\frac{A(\vec{q})}{W(\vec{q})}N-2\chi N\right]\\
&\qquad\sum_{k=1}^{n}\left(\delta(\vec{q}+\vec{Q}_k)e^{i\varphi_k}+\delta(\vec{q}-\vec{Q}_k)e^{-i\varphi_k}\right)\left(\delta(-\vec{q}+\vec{Q}_k)e^{i\varphi_k}+\delta(-\vec{q}-\vec{Q}_k)e^{-i\varphi_k}\right)\\
&=\frac{1}{2}\frac{1}{(2\pi)^3}\frac{1}{n}\psi_n^2\int d\vec{q}\left[\frac{A(\vec{q})}{W(\vec{q})}N-2\chi N\right]\sum_{k=1}^{n}\left(\delta(\vec{q}+\vec{Q}_k)e^{i\varphi_k}e^{-i\varphi_k}+\delta(\vec{q}-\vec{Q}_k)e^{-i\varphi_k}e^{i\varphi_k}\right)\\
&=\frac{1}{n}\psi_n^2\sum_{k=1}^{n}\left[\frac{A(\vec{Q}_k)}{W(\vec{Q}_k)}N-2\chi N\right]\\
&=2N(\chi_s-\chi)\psi_n^2
\end{aligned}
\tag{3.3.5.7}
$$

To calculate 3rd and higher order terms, we have to specify the morphology of microphase separated structure. Here we consider three morphology; lamellar, hexagonal, and bcc phase (Figure 3.12). In q-space, these morphologies are characterized by one, three, and six vectors, $\{\vec{Q}_k\}$. 3rd order term of Eq.(3.3.5.6) is expanded as follows. [36]

$$
\begin{aligned}
&\frac{N}{6}\frac{1}{(2\pi)^9}\int d\vec{q}_1\int d\vec{q}_2\int d\vec{q}_3\delta(\vec{q}_1+\vec{q}_2+\vec{q}_3)\Gamma_3(\vec{q}_1,\vec{q}_2,\vec{q}_3)\delta\psi(\vec{q}_1)\delta\psi(\vec{q}_2)\delta\psi(\vec{q}_3)\\
&=\frac{N}{6}\left(\frac{1}{\sqrt{n}}\psi_n\right)^3\sum_{k=1}^{n}\sum_{l=1}^{n}\sum_{m=1}^{n}\delta(\pm\vec{Q}_k\pm\vec{Q}_l\pm\vec{Q}_m)\Gamma_3(\pm\vec{Q}_k,\pm\vec{Q}_l,\pm\vec{Q}_m)\exp\left[i(\mp\varphi_k\mp\varphi_l\mp\varphi_m)\right]
\end{aligned}
\tag{3.3.5.8}
$$

Here, the delta function in the first line is defined for continuous variable as shown in Eqs.(3.3.2.38) and (3.3.2.39). In contrast to this, the delta function in the second line is defined for discrete variable. In this case, definition becomes:

$$
\delta(\vec{Q})=\begin{cases}0 & \text{for } \vec{Q}\neq 0\\ 1 & \text{for } \vec{Q}=0\end{cases}
\tag{3.3.5.9}
$$

[36] Here, $\pm\vec{Q}_k\pm\vec{Q}_l\pm\vec{Q}_m$ indicates all of the possible 8 combination of the signs.

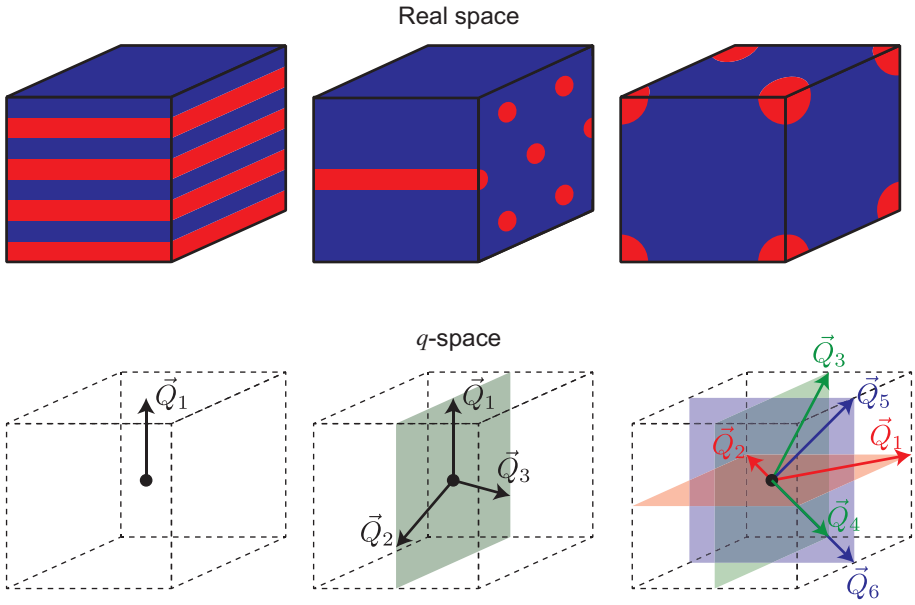

Figure 3.12: Morphology of (left) lamellar, (center) hexagonal, (right) bcc phase in real and q-space.

Let us consider the combination which makes the delta function in Eq.(3.3.5.8) to be 1.

$$\pm\vec{Q}_k \pm \vec{Q}_l \pm \vec{Q}_m = 0 \tag{3.3.5.10}$$

In the case of lamellar ($n = 1$), there is no combination which satisfy Eq.(3.3.5.10). This means that 3rd order term of Eq.(3.3.5.6) vanishes for lamellar phase.

In the case of hexagonal phase ($n = 3$), there are 12 combinations which satisfy Eq.(3.3.5.10).

$$\begin{aligned}
&\vec{Q}_1 + \vec{Q}_2 + \vec{Q}_3 = \vec{Q}_2 + \vec{Q}_3 + \vec{Q}_1 = \vec{Q}_3 + \vec{Q}_1 + \vec{Q}_2 \\
&= \vec{Q}_3 + \vec{Q}_2 + \vec{Q}_1 = \vec{Q}_2 + \vec{Q}_1 + \vec{Q}_3 = \vec{Q}_1 + \vec{Q}_3 + \vec{Q}_2 = 0 \qquad (3.3.5.11) \\
&-\vec{Q}_1 - \vec{Q}_2 - \vec{Q}_3 = -\vec{Q}_2 - \vec{Q}_3 - \vec{Q}_1 = -\vec{Q}_3 - \vec{Q}_1 - \vec{Q}_2 \\
&= -\vec{Q}_3 - \vec{Q}_2 - \vec{Q}_1 = -\vec{Q}_2 - \vec{Q}_1 - \vec{Q}_3 = -\vec{Q}_1 - \vec{Q}_3 - \vec{Q}_2 = 0 \qquad (3.3.5.12)
\end{aligned}$$

$\Gamma_3(\pm\vec{Q}_k, \pm\vec{Q}_l, \pm\vec{Q}_m)$ for Eqs.(3.3.5.11) and (3.3.5.12) are the same. We write this quantity simply as Γ_3. From the combination of Eq.(3.3.5.11), the final exponential term in Eq.(3.3.5.8) becomes $e^{-i(\varphi_1+\varphi_2+\varphi_3)}$ while it becomes $e^{i(\varphi_1+\varphi_2+\varphi_3)}$ for the combination of Eq.(3.3.5.12). As a result, Eq.(3.3.5.8) is calculated as follows.

$$\begin{aligned}
&\frac{N}{6}\left(\frac{1}{\sqrt{n}}\psi_n\right)^3 \sum_{k=1}^{n}\sum_{l=1}^{n}\sum_{m=1}^{n} \delta(\pm\vec{Q}_k \pm \vec{Q}_l \pm \vec{Q}_m)\Gamma_3(\pm\vec{Q}_k, \pm\vec{Q}_l, \pm\vec{Q}_m)\exp\left[i(\mp\varphi_k \mp \varphi_l \mp \varphi_m)\right] \quad \text{for } n = 3 \\
&= \frac{N}{6}\frac{1}{3\sqrt{3}}\psi_3^3 6\Gamma_3\left(e^{i(\varphi_1+\varphi_2+\varphi_3)} + e^{-i(\varphi_1+\varphi_2+\varphi_3)}\right) \\
&= \frac{2N}{3\sqrt{3}}\Gamma_3\cos(\varphi_1+\varphi_2+\varphi_3)\psi_3^3 \qquad (3.3.5.13)
\end{aligned}$$

Phase factor $\varphi_1 + \varphi_2 + \varphi_3$ is determined to make Eq.(3.3.5.13) minimum. As shown later, Γ_3 is negative for $f < 0.5$ and positive for $f > 0.5$. Therefore, $\cos(\varphi_1 + \varphi_2 + \varphi_3)$ should be 1 for $f < 0.5$ and -1 for $f > 0.5$.

In the case of bcc phase ($n = 6$), there are 4 sets which satisfy Eq.(3.3.5.10) (Figure 3.13). For each set,

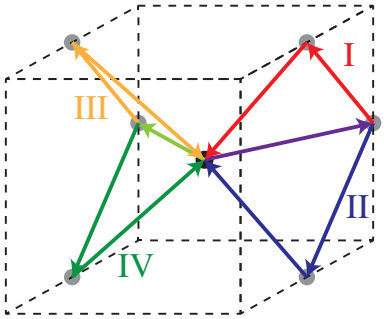

Figure 3.13: 4 sets which satisfy Eq.(3.3.5.10) for bcc phase ($n = 6$). I: Eq.(3.3.5.14) / II: Eq.(3.3.5.15) / III: Eq.(3.3.5.16) / IV: Eq.(3.3.5.17).

cosine terms are created as follows.

$$(\pm\vec{Q}_1, \mp\vec{Q}_3, \mp\vec{Q}_6) \to 2\cos(\varphi_1 - \varphi_3 - \varphi_6) =: 2\cos\alpha \tag{3.3.5.14}$$

$$(\pm\vec{Q}_1, \mp\vec{Q}_4, \mp\vec{Q}_5) \to 2\cos(\varphi_1 - \varphi_4 - \varphi_5) =: 2\cos\beta \tag{3.3.5.15}$$

$$(\pm\vec{Q}_2, \mp\vec{Q}_4, \pm\vec{Q}_6) \to 2\cos(\varphi_2 - \varphi_4 + \varphi_6) =: 2\cos\gamma \tag{3.3.5.16}$$

$$(\pm\vec{Q}_2, \mp\vec{Q}_3, \pm\vec{Q}_5) \to 2\cos(\varphi_2 - \varphi_3 + \varphi_5) = 2\cos(\alpha - \beta + \gamma) \tag{3.3.5.17}$$

There are 12 combinations for each set and each set creates $12\cos(\cdots)$ term. [37] As a result, Eq.(3.3.5.8) is calculated as follows.

$$\begin{aligned}&\frac{N}{6}\left(\frac{1}{\sqrt{n}}\psi_n\right)^3 \sum_{k=1}^{n}\sum_{l=1}^{n}\sum_{m=1}^{n} \delta(\pm\vec{Q}_k \pm \vec{Q}_l \pm \vec{Q}_m)\Gamma_3(\pm\vec{Q}_k, \pm\vec{Q}_l, \pm\vec{Q}_m)\exp\left[i(\mp\varphi_k \mp \varphi_l \mp \varphi_m)\right] \quad \text{for } n = 6 \\ &= \frac{N}{6}\frac{1}{6\sqrt{6}}\psi_6^3\Gamma_3 12\left(\cos\alpha + \cos\beta + \cos\gamma + \cos(\alpha - \beta + \gamma)\right)\end{aligned} \tag{3.3.5.18}$$

Phase factor α, β and γ is determined to make Eq.(3.3.5.18) minimum. Therefore, $\alpha = \beta = \gamma = 0$ for $f < 0.5$ and $\alpha = \beta = \gamma = \pi$ for $f > 0.5$.

Let us move on to the 4th order term of Eq.(3.3.5.6).

$$\begin{aligned}&\frac{N}{24}\frac{1}{(2\pi)^{12}}\int d\vec{q}_1 \int d\vec{q}_2 \int d\vec{q}_3 \int d\vec{q}_4 \delta(\vec{q}_1 + \vec{q}_2 + \vec{q}_3 + \vec{q}_4)\Gamma_4(\vec{q}_1, \vec{q}_2, \vec{q}_3, \vec{q}_4)\delta\psi(\vec{q}_1)\delta\psi(\vec{q}_2)\delta\psi(\vec{q}_3)\delta\psi(\vec{q}_4) \\ &= \frac{N}{24}\left(\frac{1}{\sqrt{n}}\psi_n\right)^4 \sum_{j=1}^{n}\sum_{k=1}^{n}\sum_{l=1}^{n}\sum_{m=1}^{n} \delta(\pm\vec{Q}_j \pm \vec{Q}_k \pm \vec{Q}_l \pm \vec{Q}_m) \\ &\qquad \Gamma_4(\pm\vec{Q}_j, \pm\vec{Q}_k, \pm\vec{Q}_l, \pm\vec{Q}_m)\exp\left[i(\mp\varphi_j \mp \varphi_k \mp \varphi_l \mp \varphi_m)\right]\end{aligned} \tag{3.3.5.19}$$

From now, we use the representation $\Gamma_4(h_1, h_2)$ instead of $\Gamma_4(\vec{Q}_a, \vec{Q}_b, \vec{Q}_c, \vec{Q}_d)$. h_1 and h_2 are defined as

[37] For example, from a set of Eq.(3.3.5.14),

$$\vec{Q}_1 - \vec{Q}_3 - \vec{Q}_6 = -\vec{Q}_3 - \vec{Q}_6 + \vec{Q}_1 = -\vec{Q}_6 + \vec{Q}_1 - \vec{Q}_3 = -\vec{Q}_6 - \vec{Q}_3 + \vec{Q}_1 = -\vec{Q}_3 + \vec{Q}_1 - \vec{Q}_6 = \vec{Q}_1 - \vec{Q}_6 - \vec{Q}_3 = 0$$
$$-\vec{Q}_1 + \vec{Q}_3 + \vec{Q}_6 = \vec{Q}_3 + \vec{Q}_6 - \vec{Q}_1 = \vec{Q}_6 - \vec{Q}_1 + \vec{Q}_3 = \vec{Q}_6 + \vec{Q}_3 - \vec{Q}_1 = \vec{Q}_3 - \vec{Q}_1 + \vec{Q}_6 = -\vec{Q}_1 + \vec{Q}_6 + \vec{Q}_3 = 0$$

First line creates $e^{-i(\varphi_1 - \varphi_3 - \varphi_6)}$ term while second line creates $e^{i(\varphi_1 - \varphi_3 - \varphi_6)}$ term. As a result, the contribution of this set to Eq.(3.3.5.8) is $12\cos\alpha$.

follows.

$$|\vec{Q}_a + \vec{Q}_b|^2 = h_1(q^*)^2 \tag{3.3.5.20}$$

$$|\vec{Q}_a + \vec{Q}_d|^2 = h_2(q^*)^2 \tag{3.3.5.21}$$

Under this assumption, $|\vec{Q}_a + \vec{Q}_c|^2$ is calculated as follows.

$$\begin{aligned}|\vec{Q}_a + \vec{Q}_c|^2 &= |\vec{Q}_a|^2 + 2\vec{Q}_a \cdot (-\vec{Q}_a - \vec{Q}_b - \vec{Q}_d) + |\vec{Q}_c|^2 \\ &= |\vec{Q}_a|^2 - 2|\vec{Q}_a|^2 - 2\vec{Q}_a \cdot \vec{Q}_b - 2\vec{Q}_a \cdot \vec{Q}_d + |\vec{Q}_c|^2 \\ &= -2\vec{Q}_a \cdot \vec{Q}_b - 2\vec{Q}_a \cdot \vec{Q}_d \\ &= -|\vec{Q}_a + \vec{Q}_b|^2 - |\vec{Q}_a + \vec{Q}_b|^2 + 4(q^*)^2 = (4 - h_1 - h_2)(q^*)^2\end{aligned} \tag{3.3.5.22}$$

Note that $\vec{Q}_c = -\vec{Q}_a - \vec{Q}_b - \vec{Q}_d$ and $|\vec{Q}_a|^2 = |\vec{Q}_c|^2 = (q^*)^2$.

Similar to the case of 3rd order term (Eq.(3.3.5.10)), let us consider the combination which makes the delta function in Eq.(3.3.5.19) to be 1.

$$\pm\vec{Q}_j \pm \vec{Q}_k \pm \vec{Q}_l \pm \vec{Q}_m = 0 \tag{3.3.5.23}$$

In the case of lamellar phase ($n = 1$), there are 6 combinations which satisfy Eq.(3.3.5.23).

$$\begin{aligned}&\vec{Q}_1 + \vec{Q}_1 - \vec{Q}_1 - \vec{Q}_1 = \vec{Q}_1 - \vec{Q}_1 + \vec{Q}_1 - \vec{Q}_1 = -\vec{Q}_1 + \vec{Q}_1 + \vec{Q}_1 - \vec{Q}_1 \\ &= \vec{Q}_1 - \vec{Q}_1 - \vec{Q}_1 + \vec{Q}_1 = -\vec{Q}_1 + \vec{Q}_1 - \vec{Q}_1 + \vec{Q}_1 = -\vec{Q}_1 - \vec{Q}_1 + \vec{Q}_1 + \vec{Q}_1 = 0\end{aligned} \tag{3.3.5.24}$$

Phase factor $\mp\varphi_j \mp \varphi_k \mp \varphi_l \mp \varphi_m = 0$ for all of the terms of Eq.(3.3.5.24). Γ_4 term for these terms are the same and represented as $\Gamma_4(0,0)$; for $\Gamma_4(\vec{Q}_1, -\vec{Q}_1, \vec{Q}_1, -\vec{Q}_1)$, $h_1 = h_2 = 0$ (Eqs.(3.3.5.20) and (3.3.5.21)). [38] Then Eq.(3.3.5.19) becomes:

$$\begin{aligned}&\frac{N}{24}\left(\frac{1}{\sqrt{n}}\psi_n\right)^4 \sum_{j=1}^{n}\sum_{k=1}^{n}\sum_{l=1}^{n}\sum_{m=1}^{n} \delta(\pm\vec{Q}_j \pm \vec{Q}_k \pm \vec{Q}_l \pm \vec{Q}_m) \\ &\qquad \Gamma_4(\pm\vec{Q}_j, \pm\vec{Q}_k, \pm\vec{Q}_l, \pm\vec{Q}_m) \exp\left[i(\mp\varphi_j \mp \varphi_k \mp \varphi_l \mp \varphi_m)\right] \quad \text{for } n = 1 \\ &= \frac{N}{24}\psi_1^4 6\Gamma_4(0,0)\end{aligned} \tag{3.3.5.25}$$

In the case of hexagonal phase ($n = 3$), there are 2 sets which satisfy Eq.(3.3.5.23). For each set, cosine terms are created as follows.

$$(\pm\vec{Q}_i, \pm\vec{Q}_i, \mp\vec{Q}_i, \mp\vec{Q}_i) \to 2\cos(\varphi_i + \varphi_i - \varphi_i - \varphi_i) = 2 \quad [i = 1,2,3] \tag{3.3.5.26}$$

$$(\pm\vec{Q}_i, \pm\vec{Q}_j, \mp\vec{Q}_i, \mp\vec{Q}_j) \to 2\cos(\varphi_i + \varphi_j - \varphi_i - \varphi_j) = 2 \quad [i = 1,2,3 \ / \ j(\neq i) = 1,2,3] \tag{3.3.5.27}$$

Eq.(3.3.5.26) has 6 terms for each i as shown in Eq.(3.3.5.24). Eq.(3.3.5.27) has $4! = 24$ terms for each (i,j). Combination of (i,j) is 3; $(1,2), (2,3), (3,1)$. As for Γ_4 part, a set of Eq.(3.3.5.26) is $\Gamma_4(0,0)$, which is the same as the case of lamellar. A set of Eq.(3.3.5.27) is $\Gamma_4(0,1)$; for $\Gamma_4(\vec{Q}_1, -\vec{Q}_1, -\vec{Q}_2, \vec{Q}_2)$, $|\vec{Q}_1 - \vec{Q}_1|^2 = 0(q^*)^2$ and $|\vec{Q}_1 + \vec{Q}_2|^2 = |-\vec{Q}_3|^2 = (q^*)^2$. As a result, a set of Eq.(3.3.5.26) results $18\Gamma_4(0,0)$ and a set of Eq.(3.3.5.27)

[38] Note that $\Gamma_4(\vec{Q}_j, \vec{Q}_k, \vec{Q}_l, \vec{Q}_m)$ does not change by the exchange of variables.

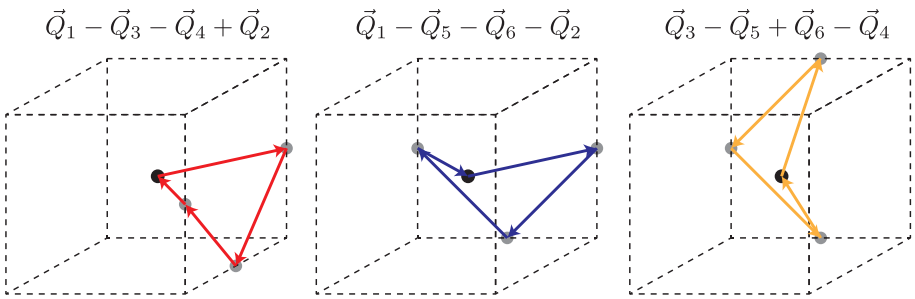

Figure 3.14: 4 sets which satisfy Eq.(3.3.5.10) for bcc phase ($n = 6$). I: Eq.(3.3.5.14) / II: Eq.(3.3.5.15) / III: Eq.(3.3.5.16) / IV: Eq.(3.3.5.17).

results $72\Gamma_4(0,1)$. Then Eq.(3.3.5.19) becomes:

$$\begin{aligned}
&\frac{N}{24}\left(\frac{1}{\sqrt{n}}\psi_n\right)^4 \sum_{j=1}^{n}\sum_{k=1}^{n}\sum_{l=1}^{n}\sum_{m=1}^{n} \delta(\pm\vec{Q}_j \pm \vec{Q}_k \pm \vec{Q}_l \pm \vec{Q}_m) \\
&\qquad\qquad \Gamma_4(\pm\vec{Q}_j, \pm\vec{Q}_k, \pm\vec{Q}_l, \pm\vec{Q}_m) \exp\left[i(\mp\varphi_j \mp \varphi_k \mp \varphi_l \mp \varphi_m)\right] \quad \text{for } n = 3 \\
&= \frac{N}{24}\frac{1}{9}\psi_1^4 \left(18\Gamma_4(0,0) + 72\Gamma_4(0,1)\right) \qquad (3.3.5.28)
\end{aligned}$$

In the case of bcc phase ($n = 3$), there are 4 sets which satisfy Eq.(3.3.5.23). 3 sets and corresponding cosine terms are as follows.

$$(\pm\vec{Q}_i, \pm\vec{Q}_i, \mp\vec{Q}_i, \mp\vec{Q}_i) \to 2\cos(\varphi_i + \varphi_i - \varphi_i - \varphi_i) = 2 \quad [i = 1 \sim 6] \qquad (3.3.5.29)$$

$$\begin{aligned}
&(\pm\vec{Q}_i, \pm\vec{Q}_j, \mp\vec{Q}_i, \mp\vec{Q}_j) \to 2\cos(\varphi_i + \varphi_j - \varphi_i - \varphi_j) = 2 \\
&\qquad [(i,j) = (1,3), (1,4), (1,5), (1,6), (2,3), (2,2), (2,5), (2,6), (3,5), (3,6), (4,5), (4,6)] \qquad (3.3.5.30)
\end{aligned}$$

$$(\pm\vec{Q}_i, \pm\vec{Q}_j, \mp\vec{Q}_i, \mp\vec{Q}_j) \to 2\cos(\varphi_i + \varphi_j - \varphi_i - \varphi_j) = 2 \quad [(i,j) = (1,2), (3,4), (5,6)] \qquad (3.3.5.31)$$

The last set is shown in Figure 3.14.

$$(\pm\vec{Q}_1, \pm\vec{Q}_2, \mp\vec{Q}_3, \mp\vec{Q}_4) \to 2\cos(\varphi_1 + \varphi_2 - \varphi_3 - \varphi_4) = 2\cos(\alpha + \gamma) \qquad (3.3.5.32)$$

$$(\pm\vec{Q}_1, \mp\vec{Q}_2, \mp\vec{Q}_5, \mp\vec{Q}_6) \to 2\cos(\varphi_1 - \varphi_2 - \varphi_5 - \varphi_6) = 2\cos(\beta - \gamma) \qquad (3.3.5.33)$$

$$(\pm\vec{Q}_3, \mp\vec{Q}_4, \mp\vec{Q}_5, \pm\vec{Q}_6) \to 2\cos(\varphi_3 - \varphi_4 - \varphi_5 + \varphi_6) = 2\cos(\beta - \alpha) \qquad (3.3.5.34)$$

Eq.(3.3.5.29) has 6 terms for each i. Eq.(3.3.5.30) has 24 terms for each (i,j). Combination of (i,j) is 12 as mentioned. Eq.(3.3.5.31) has 24 terms for each (i,j). Combination of (i,j) is 3 as mentioned. Eqs.(3.3.5.32) $\sim$ (3.3.5.34) has 48 terms. As for Γ_4 part, a set of Eq.(3.3.5.29) is $\Gamma_4(0,0)$. A set of Eq.(3.3.5.30) is $\Gamma_4(0,1)$; for $\Gamma_4(\vec{Q}_1, -\vec{Q}_1, \vec{Q}_3, -\vec{Q}_3)$, $|\vec{Q}_1 - \vec{Q}_1|^2 = 0(q^*)^2$ and $|\vec{Q}_1 - \vec{Q}_3|^2 = |\vec{Q}_6|^2 = (q^*)^2$. A set of Eq.(3.3.5.31) is $\Gamma_4(0,2)$; for $\Gamma_4(\vec{Q}_1, -\vec{Q}_1, \vec{Q}_2, -\vec{Q}_2)$, $|\vec{Q}_1 - \vec{Q}_1|^2 = 0(q^*)^2$ and $|\vec{Q}_1 - \vec{Q}_2|^2 = 2(q^*)^2$ (see Figure 3.12). Eqs.(3.3.5.32) $\sim$ (3.3.5.34) is $\Gamma_4(1,2)$; for $\Gamma_4(\vec{Q}_1, -\vec{Q}_3, -\vec{Q}_4, \vec{Q}_2)$, $|\vec{Q}_1 - \vec{Q}_3|^2 = |\vec{Q}_6|^2 = (q^*)^2$ and $|\vec{Q}_1 + \vec{Q}_2|^2 = 2(q^*)^2$. As a result, a set of Eq.(3.3.5.29) results $36\Gamma_4(0,0)$, a set of Eq.(3.3.5.30) results $288\Gamma_4(0,1)$, a set of Eq.(3.3.5.31) results $72\Gamma_4(0,2)$, and Eqs.(3.3.5.32) $\sim$ (3.3.5.34) result $48\Gamma_4(1,2)\cos(\cdots)$ for each. Then Eq.(3.3.5.19)

becomes:

$$\frac{N}{24}\left(\frac{1}{\sqrt{n}}\psi_n\right)^4 \sum_{j=1}^{n}\sum_{k=1}^{n}\sum_{l=1}^{n}\sum_{m=1}^{n}\delta(\pm\vec{Q}_j \pm \vec{Q}_k \pm \vec{Q}_l \pm \vec{Q}_m)$$
$$\Gamma_4(\pm\vec{Q}_j, \pm\vec{Q}_k, \pm\vec{Q}_l, \pm\vec{Q}_m)\exp\left[i(\mp\varphi_j \mp \varphi_k \mp \varphi_l \mp \varphi_m)\right] \quad \text{for } n=6$$
$$= \frac{N}{24}\frac{1}{36}\psi_1^4\left(36\Gamma_4(0,0) + 288\Gamma_4(0,1) + 72\Gamma_4(0,2)\right.$$
$$\left. +48\Gamma_4(1,2)\cos(\alpha+\gamma) + 48\Gamma_4(1,2)\cos(\beta-\gamma) + 48\Gamma_4(1,2)\cos(\beta-\alpha)\right) \tag{3.3.5.35}$$

Eq.(3.3.5.35) is minimized under the condition where $\alpha=\beta=\gamma=0$ or $\alpha=\beta=\gamma=\pi$, which is the same as the case for 3rd order term (Eq.(3.3.5.18)).

By substituting Eqs.(3.3.5.7), (3.3.5.13), (3.3.5.18), (3.3.5.25), (3.3.5.28), and (3.3.5.35) into Eq.(3.3.5.6), energy expansion is summarized as follows.

$$\beta N\left(F[\delta\psi(\vec{q})] - F[0]\right) \simeq 2N(\chi_s - \chi)\psi_n^2 + \alpha_n\psi_n^3 + \beta_n\psi_n^4 \tag{3.3.5.36}$$

where

$$\alpha_1 = 0 \tag{3.3.5.37}$$
$$\alpha_3 = \begin{cases} +\frac{2}{3\sqrt{3}}N\Gamma_3 & \text{for } f \le 0.5 \\ -\frac{2}{3\sqrt{3}}N\Gamma_3 & \text{for } f \ge 0.5 \end{cases} \tag{3.3.5.38}$$
$$\alpha_6 = \begin{cases} +\frac{4}{3\sqrt{6}}N\Gamma_3 & \text{for } f \le 0.5 \\ -\frac{4}{3\sqrt{6}}N\Gamma_3 & \text{for } f \ge 0.5 \end{cases} \tag{3.3.5.39}$$

$$\beta_1 = \frac{1}{4}N\Gamma_4(0,0) \tag{3.3.5.40}$$
$$\beta_3 = \frac{1}{12}N\left(\Gamma_4(0,0) + 4\Gamma_4(0,1)\right) \tag{3.3.5.41}$$
$$\beta_6 = \frac{1}{24}N\left(\Gamma_4(0,0) + 8\Gamma_4(0,1) + 2\Gamma_4(0,2) + 4\Gamma_4(1,2)\right) \tag{3.3.5.42}$$

3.3.6 Phase diagram for microphase separation

Phase diagram for microphase separation is constructed by comparing the energy Eq.(3.3.5.36) for lamellar ($n=1$), hexagonal ($n=3$), and bcc ($n=6$) phase. To calculate, we need the value of Γ_3 and $\Gamma_4(h_1,h_2)$. These value depends only on f. Explicit form of Γ_3 is (see Eq.(3.3.3.46)):

$$\Gamma_3 = -\sum_i\sum_j\sum_k G_3^{ijk}(q^*,1)\left[S_{i1}^{-1}(q^*) - S_{i2}^{-1}(q^*)\right]\left[S_{j1}^{-1}(q^*) - S_{j2}^{-1}(q^*)\right]\left[S_{k1}^{-1}(q^*) - S_{k2}^{-1}(q^*)\right] \tag{3.3.6.1}$$

where S_{ij}^{-1} is the matrix element of the inverse matrix of S_{ij}.

$$\begin{bmatrix} S_{11}^{-1} & S_{12}^{-1} \\ S_{21}^{-1} & S_{22}^{-1} \end{bmatrix} = \begin{bmatrix} S_{11} & S_{12} \\ S_{21} & S_{22} \end{bmatrix}^{-1} = \frac{1}{S_{11}S_{22} - S_{12}S_{21}}\begin{bmatrix} S_{22} & -S_{12} \\ -S_{21} & S_{11} \end{bmatrix} \tag{3.3.6.2}$$

Explicit form of $G_3^{ijk}(q,h)$ and $S_{ij}(q)$ are shown in Section 3.3.4. Explicit form of $\Gamma_4(h_1,h_2)$ is:

$$\Gamma_4(h_1,h_2) = -\sum_i \sum_j \sum_k \sum_l \gamma_{ijkl}(q^*,h_1,h_2) \\ \left[S_{i1}^{-1}(q^*) - S_{i2}^{-1}(q^*)\right]\left[S_{j1}^{-1}(q^*) - S_{j2}^{-1}(q^*)\right]\left[S_{k1}^{-1}(q^*) - S_{k2}^{-1}(q^*)\right]\left[S_{l1}^{-1}(q^*) - S_{l2}^{-1}(q^*)\right] \quad (3.3.6.3)$$

where

$$\gamma_{ijkl}(q^*,h_1,h_2) = \sum_m \sum_n \Big[G_3^{ijm}(q^*,h_1)S_{mn}^{-1}(h_1x^*)G_3^{kln}(q^*,h_1) \\ + G_3^{ikm}(q^*,4-h_1-h_2)S_{mn}^{-1}((4-h_1-h_2)x^*)G_3^{jln}(q^*,4-h_1-h_2) \\ + G_3^{ilm}(q^*,h_2)S_{mn}^{-1}(h_2x^*)G_3^{jkn}(q^*,h_2)\Big] - G_4^{ijkl}(q^*,h_1,h_2) \quad (3.3.6.4)$$

Explicit form of $G_4^{ijkl}(q,h_1,h_2)$ are shown in Section 3.3.4. Γ_3 Γ_3 and $\Gamma_4(h_1,h_2)$ are shown in Figure 3.15 as functions of f.

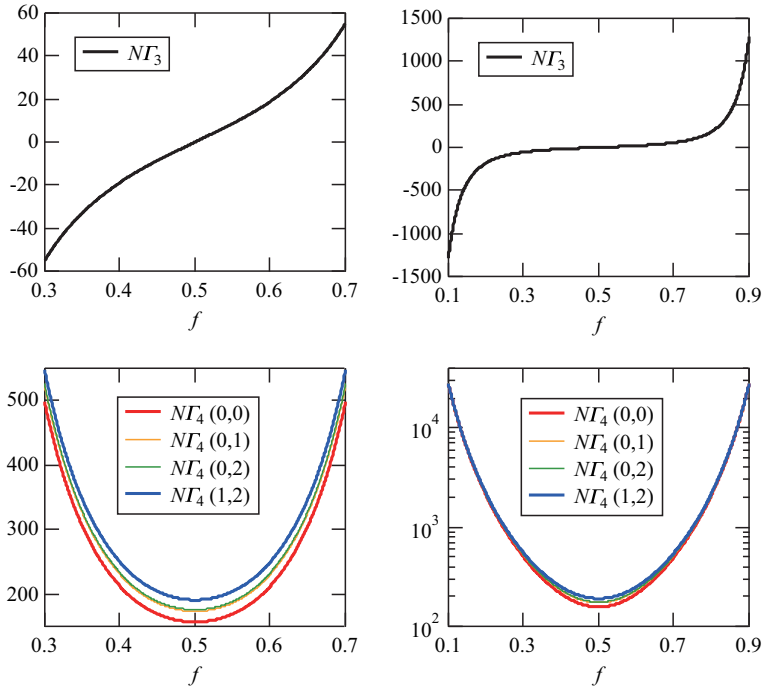

Figure 3.15: $N\Gamma_3$ and $N\Gamma_4(h_1,h_2)$ as functions of f. $\Gamma_4(0,1)$ and $\Gamma_4(0,2)$ are overlap.

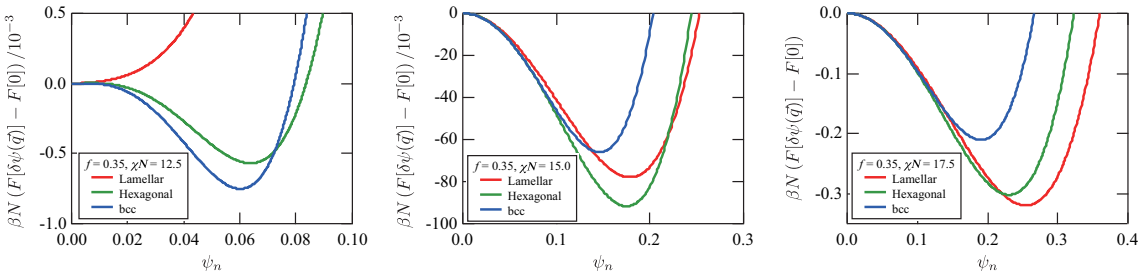

Figure 3.16: $\beta N\,(F[\delta\psi(\vec{q})]-F[0])$ of lamellar, hexagonal, and bcc phases at $f=0.35$ as functions of ψ_n. $\chi N=12.5, 15.0, 17.5$ are shown.

Once f is given, we can calculate $(\chi N)_s$, q^*, α_n, and β_n. Therefore, Eq.(3.3.5.36) is calculated as a function of f and χN for each n ($n=1,3,6$). As an example, the case of $f=0.35$ and $\chi N=12.5, 15.0, 17.5$ are shown in Figure 3.16. When $\chi N=12.5$, bcc phase is energetically favorable ($\psi_n\simeq 0.060$). When $\chi N=15.0$, hexagonal phase is energetically favorable ($\psi_n\simeq 0.175$). When $\chi N=17.5$, lamellar phase is energetically favorable ($\psi_n\simeq 0.255$). To analyze which phase is energetically favorable, let us calculate ψ_n at the minimum value of $\beta N\,(F[\delta\psi(\vec{q})]-F[0])$. This value, $\overline{\psi}$, satisfy the following equations.

$$\left.\frac{\partial F[\delta\psi(\vec{q})]}{\partial\psi_n}\right|_{\psi_n=\overline{\psi}_n}=0 \tag{3.3.6.5}$$

$$\left.\frac{\partial^2 F[\delta\psi(\vec{q})]}{\partial\psi_n^2}\right|_{\psi_n=\overline{\psi}_n}>0 \tag{3.3.6.6}$$

$$F[\delta\psi(\vec{q})](\psi_n=\overline{\psi}_n,\chi=\chi_t)=0 \tag{3.3.6.7}$$

Eq.(3.3.6.5) is the condition of extreme value. Eq.(3.3.6.6) is the condition of local minimum. Eq.(3.3.6.7) means that the energy at transition point ($\chi=\chi_t$) should be the same as that of disordered phase. For $n=3,6$ ($\alpha_n\neq 0$), from Eq.(3.3.6.5),

$$\begin{aligned}&\left.\frac{\partial F[\delta\psi(\vec{q})]}{\partial\psi_n}\right|_{\psi_n=\overline{\psi}_n}=4N(\chi_s-\chi)\overline{\psi}_n+3\alpha_n\overline{\psi}_n^2+4\beta_n\overline{\psi}_n^3=0\\ &\to\overline{\psi}_n=0,\ \frac{-3\alpha_n\pm\sqrt{9\alpha_n^2-64N\beta_n(\chi_s-\chi)}}{8\beta_n}=:0,\ \frac{-3\alpha_n(1\pm\gamma_n)}{8\beta_n}\end{aligned} \tag{3.3.6.8}$$

where

$$\gamma_n:=\left(1-\frac{64N\beta_n(\chi_s-\chi)}{9\alpha_n^2}\right)^{1/2} \tag{3.3.6.9}$$

For example, $\overline{\psi}_6$ for $f=0.35$, $\chi N=12.5$ is $-0.06, 0, 0.06$ as shown in Figure 3.16. The solution of Eq.(3.3.6.8) which satisfy Eq.(3.3.6.6) is the value of larger ψ_n and therefore: [39]

$$\overline{\psi}_n=-\frac{3\alpha_n(1+\gamma_n)}{8\beta_n} \tag{3.3.6.10}$$

[39] The smaller ψ_n corresponds to local maximum value when $\chi\leq\chi_s$. (See Figure 3.19.) When $\chi>\chi_s$, Eq.(3.3.6.10) is the sole solution.

From the conditions Eqs.(3.3.6.5) and (3.3.6.7),

$$2N(\chi_s - \chi_t) + \alpha_n \overline{\psi}_n + \beta_n \overline{\psi}_n^2 = 0 \tag{3.3.6.11}$$

$$4N(\chi_s - \chi_t) + 3\alpha_n \overline{\psi}_n + 4\beta_n \overline{\psi}_n^2 = 0 \tag{3.3.6.12}$$

From Eqs.(3.3.6.11) and (3.3.6.12):

$$\begin{aligned} &2\alpha_n \overline{\psi}_n + 2\beta_n \overline{\psi}_n^2 = 3\alpha_n \overline{\psi}_n + 4\beta_n \overline{\psi}_n^2 \\ &\rightarrow \overline{\psi}_n = -\frac{\alpha_n}{2\beta_n} \quad \text{for } \chi = \chi_t \end{aligned} \tag{3.3.6.13}$$

By comparing Eqs.(3.3.6.10) and (3.3.6.13):

$$\begin{aligned} &\overline{\psi}_n = -\frac{3\alpha_n(1+\gamma_n)}{8\beta_n} = -\frac{\alpha_n}{2\beta_n} \\ &\rightarrow \gamma_n = \frac{1}{3} \quad \text{for } \chi = \chi_t \end{aligned} \tag{3.3.6.14}$$

χ_t is calculated from Eqs.(3.3.6.9) and (3.3.6.14):

$$\begin{aligned} &\gamma_n^2 = 1 - \frac{64N\beta_n(\chi_s - \chi_t)}{9\alpha_n^2} = \frac{1}{9} \\ &\rightarrow N\chi_t = N\chi_s - \frac{\alpha_n^2}{8\beta_n} \end{aligned} \tag{3.3.6.15}$$

Let us substitute Eq.(3.3.6.10) to Eq.(3.3.5.36). From Eq.(3.3.6.9):

$$\begin{aligned} &\gamma_n^2 = 1 - \frac{64N\beta_n(\chi_s - \chi)}{9\alpha_n^2} \\ &\rightarrow N(\chi_s - \chi) = \frac{9\alpha_n^2}{64\beta_n}(1 - \gamma_n^2) \end{aligned} \tag{3.3.6.16}$$

Substitute Eqs.(3.3.6.10) and (3.3.6.16) to Eq.(3.3.5.36):

$$\begin{aligned} &\beta N \left(F[\delta\psi(\vec{q})] - F[0]\right) \\ &\simeq \frac{9\alpha_n^2}{32\beta_n}(1-\gamma_n^2)\left(-\frac{3\alpha_n(1+\gamma_n)}{8\beta_n}\right)^2 + \alpha_n\left(-\frac{3\alpha_n(1+\gamma_n)}{8\beta_n}\right)^3 + \beta_n\left(-\frac{3\alpha_n(1+\gamma_n)}{8\beta_n}\right)^4 \\ &= \frac{27\alpha_n^4}{4096\beta_n^3}(1+\gamma_n)^3(1-3\gamma_n) \quad \text{for } n = 3, 6 \end{aligned} \tag{3.3.6.17}$$

For $n = 1$ ($\alpha_1 = 0$),

$$\begin{aligned} &\left.\frac{\partial F[\delta\psi(\vec{q})]}{\partial \psi_n}\right|_{\psi_n = \overline{\psi}_n} = 4N(\chi_s - \chi)\overline{\psi}_n + 4\beta_n \overline{\psi}_n^3 = 0 \\ &\rightarrow \overline{\psi}_n^2 = 0, -\frac{N(\chi_s - \chi)}{\beta_n} \quad \text{for } \chi_s < \chi \end{aligned} \tag{3.3.6.18}$$

From Eq.(3.3.6.6), $\overline{\psi}_n = 0$ is rejected. Substitute Eq.(3.3.6.18) to Eq.(3.3.5.36):

$$\begin{aligned}
&\beta N\left(F[\delta\psi(\vec{q})]-F[0]\right)\\
&\simeq 2N(\chi_s-\chi)\left(-\frac{N(\chi_s-\chi)}{\beta_n}\right)+\beta_n(\chi_s-\chi)\left(-\frac{N(\chi_s-\chi)}{\beta_n}\right)^2\\
&=-\frac{N^2(\chi_s-\chi)^2}{\beta_n}\quad \text{for } n=1
\end{aligned} \tag{3.3.6.19}$$

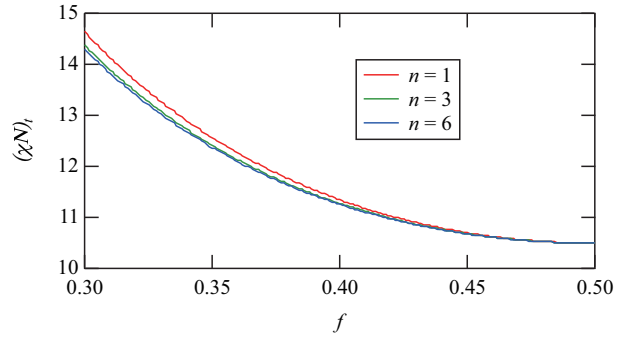

Figure 3.17: Comparison of $(\chi N)_t$ for $n = 1, 3, 6$.

Construction of phase diagram is performed by comparing Eqs.(3.3.6.17) and (3.3.6.19) for $n = 1, 3, 6$ under the condition where $\chi > \chi_t$ for each n. χ_t for $n = 3, 6$ are calculated by Eq.(3.3.6.15). χ_t for $n = 1$ is equal to χ_s as mentioned in Eq.(3.3.6.18). χ_t for all of n are shown in Figure 3.17. This shows that $\chi_t(n = 6) < \chi_t(n = 3) < \chi_t(n = 1)$ for all f. Therefore, the phase which appear first is bcc phase ($n = 6$) when $\chi = \chi_t(n = 6)$. In the range where $\chi_t(n = 6) < \chi < \chi_t(n = 3)$, microphase separation shows bcc phase in all χ region. In the range where $\chi_t(n = 3) < \chi < \chi_t(n = 1)$, the morphology of microphase separation is determined by the comparison of Eq.(3.3.6.17) for $n = 3$ and $n = 6$. [40] In the range where $\chi_t(n = 1) < \chi$, the morphology of microphase separation is determined by the comparison of Eqs.(3.3.6.17) and (3.3.6.19) for $n = 1, 3, 6$. Through this procedure, phase diagram is created as shown in Figure 3.18. This analysis clearly shows that the morphology of microphase separation is determined by χN and f. The size of polymer, N, is not directly related to the morphology. Note that microphase separation can occur even when $\chi \leq \chi_s$ if $\chi_t \leq \chi$. In this χ range, there is small energy barrier from $\psi_n = 0$ to $\overline{\psi}_n$ (Figure 3.19). Therefore, this is not spinodal point. In other words, disordered state is meta stable. However, this energy barrier is small compared to thermal energy. The domain size of microphase-separated structure is calculated from the value of x^* as shown in Figure 3.11.

[40] Calculation result shows that bcc phase is favorable in all χ region in this range.

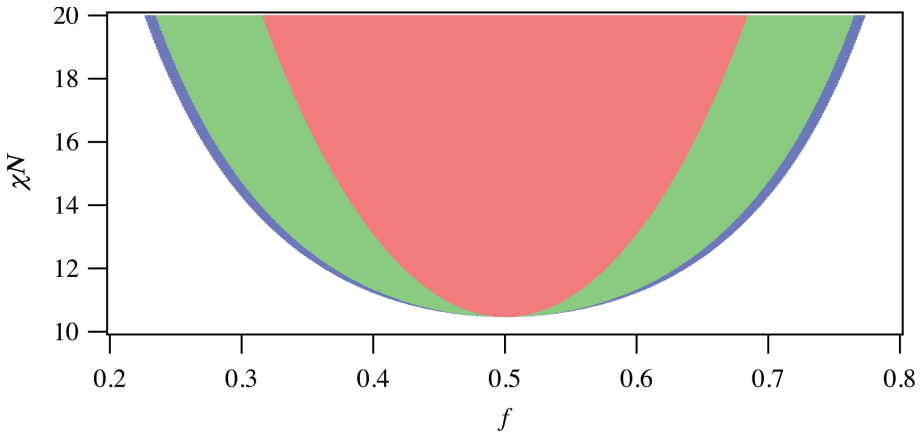

Figure 3.18: Phase diagram for microphase separation. Red region: lamellar, Green region: hexagonal, Blue region: bcc, Blank region: disordered state.

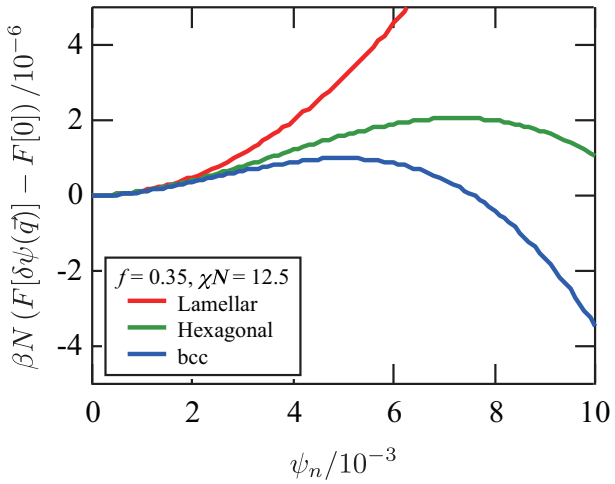

Figure 3.19: Expansion of Figure 3.16 for $\chi N = 12.5$.

4 Scattering Methods

4.1 Light scattering

4.1.1 Basic theory of light scattering

In this subsection, we are going to derive a scattered electric field from one dipole moment induced by monochromatic light wave such as laser [60, 61].

We start from Maxwell's equations:

$$\nabla \cdot \vec{D} = \rho \tag{4.1.1.1}$$

$$\nabla \cdot \vec{B} = 0 \tag{4.1.1.2}$$

$$\nabla \times \vec{E} = -\frac{\partial \vec{B}}{\partial t} \tag{4.1.1.3}$$

$$\nabla \times \vec{H} = \vec{J} + \frac{\partial \vec{D}}{\partial t} \tag{4.1.1.4}$$

where

$$\vec{D} = \varepsilon\varepsilon_0 \vec{E} \tag{4.1.1.5}$$

$$\vec{H} = \frac{1}{\mu\mu_0} \vec{B} \tag{4.1.1.6}$$

Here, $\vec{E}$ and $\vec{B}$ are the electric and magnetic fields in free space, $\vec{D}$ and $\vec{H}$ are the corresponding modified fields in material media, ρ is charge density, $\vec{J}$ is current density, ε_0 and μ_0 are the permittivity and permeability of free space, ε and μ are the dielectric constant and magnetic permeability of the media.

In the case where medium is homogeneous, there is no free charges and zero conductivity:

$$\nabla \cdot \vec{D} = 0 \tag{4.1.1.7}$$

$$\nabla \cdot \vec{B} = 0 \tag{4.1.1.8}$$

$$\nabla \times \vec{E} = -\frac{\partial \vec{B}}{\partial t} \tag{4.1.1.9}$$

$$\nabla \times \vec{H} = \frac{\partial \vec{D}}{\partial t} \tag{4.1.1.10}$$

Taking the curl from the left hand side of Eq.(4.1.1.9) and substituting Eq.(4.1.1.10) gives[41]:

$$\nabla \times \nabla \times \vec{E} = -\mu\mu_0 \nabla \times \frac{\partial \vec{H}}{\partial t} = -\mu\mu_0 \frac{\partial^2 \vec{D}}{\partial t^2} \tag{4.1.1.11}$$

These relations hold true for both an incident field and a scattered field. Here, we assume that a local dielectric constant is written as the following tensor form:

$$\varepsilon\varepsilon_0 \to \varepsilon\varepsilon_0 \boldsymbol{I} + \delta\boldsymbol{\epsilon} \tag{4.1.1.12}$$

where $\boldsymbol{I}$ implies an unit matrix.

This is a general representation of permittivity for non-spherical molecules. From here, we use a subscript i for an incident field, s for a scattered field. A total field is represented without any subscript.

[41] $\nabla \times \nabla \times \vec{\pi} := \nabla \times (\nabla \times \vec{\pi})$.

A total electric displacement, $\vec{D}$, is written as follows:

$$\begin{aligned}\vec{D} &= \vec{D}_i + \vec{D}_s = (\varepsilon\varepsilon_0 \boldsymbol{I} + \delta\boldsymbol{\epsilon})(\vec{E}_i + \vec{E}_s) \\ &= \varepsilon\varepsilon_0\vec{E}_i + \delta\boldsymbol{\epsilon}\cdot\vec{E}_i + \varepsilon\varepsilon_0\vec{E}_s + \delta\boldsymbol{\epsilon}\cdot\vec{E}_s \end{aligned} \tag{4.1.1.13}$$

Since $\vec{D}_i = \varepsilon\varepsilon_0\vec{E}_i$:

$$\vec{D}_s \simeq \delta\boldsymbol{\epsilon}\cdot\vec{E}_i + \varepsilon\varepsilon_0\vec{E}_s \tag{4.1.1.14}$$

Here, we neglect the term $\delta\boldsymbol{\epsilon}\cdot\vec{E}_s$ which is second perturbation.

Then, substitute Eq.(4.1.1.14) into Eq.(4.1.1.11):

$$\begin{aligned}&\nabla\times\nabla\times\vec{E}_s = -\mu\mu_0\frac{\partial^2\vec{D}_s}{\partial t^2} \\ &\rightarrow \frac{1}{\varepsilon\varepsilon_0}\nabla\times\nabla\times(\vec{D}_s - \delta\boldsymbol{\epsilon}\cdot\vec{E}_i) = -\mu\mu_0\frac{\partial^2\vec{D}_s}{\partial t^2}\end{aligned} \tag{4.1.1.15}$$

Here, we use the following vector identity:

$$\nabla\times\nabla\times\vec{D}_s = -\nabla^2\vec{D}_s + \nabla(\nabla\cdot\vec{D}_s) \tag{4.1.1.16}$$

By substituting Eqs.(4.1.1.7) and (4.1.1.16) into Eq.(4.1.1.15):

$$\begin{aligned}&-\frac{1}{\varepsilon\varepsilon_0}\nabla^2\vec{D}_s + \mu\mu_0\frac{\partial^2\vec{D}_s}{\partial t^2} = \frac{1}{\varepsilon\varepsilon_0}\nabla\times\nabla\times(\delta\boldsymbol{\epsilon}\cdot\vec{E}_i) \\ &\rightarrow \nabla^2\vec{D}_s - \frac{1}{v^2}\frac{\partial^2\vec{D}_s}{\partial t^2} = \nabla\times\nabla\times(\delta\boldsymbol{\epsilon}\cdot\vec{E}_i)\end{aligned} \tag{4.1.1.17}$$

where the velocity of light, v, is [42]:

$$v := (\varepsilon\varepsilon_0\mu\mu_0)^{-1/2} \tag{4.1.1.18}$$

Here, we define the following vector $\vec{\pi}$ called Hertz vector:

$$\vec{D}_s =: \nabla\times\nabla\times\vec{\pi} \tag{4.1.1.19}$$

By using $\vec{\pi}$, Eq.(4.1.1.17) is rewritten as follows:

$$\nabla^2\vec{\pi} - \frac{1}{v^2}\frac{\partial^2\vec{\pi}}{\partial t^2} = \delta\boldsymbol{\epsilon}\cdot\vec{E}_i \tag{4.1.1.20}$$

The formal solution of Eq.(4.1.1.20) is well-known as follows:

$$\vec{\pi}(\vec{R},t) = \frac{1}{4\pi}\int_V d\vec{r}\frac{\delta\boldsymbol{\epsilon}(\vec{r},t')}{|\vec{R}-\vec{r}|}\cdot\vec{E}_i(\vec{r},t') \tag{4.1.1.21}$$

where $\vec{R}$ and $\vec{r}$ are the position of a detector and an atom, respectively, defined in Fig.4.1 [43]. t' is the

[42] When $\delta\boldsymbol{\epsilon} = 0$ (isotropic environment),

$$\nabla^2\vec{D}_s - \frac{1}{v^2}\frac{\partial^2\vec{D}_s}{\partial t^2} = 0$$

This is a wave equation whose velocity is v.

[43] In this definition, $\nabla = \partial/\partial\vec{R}$.

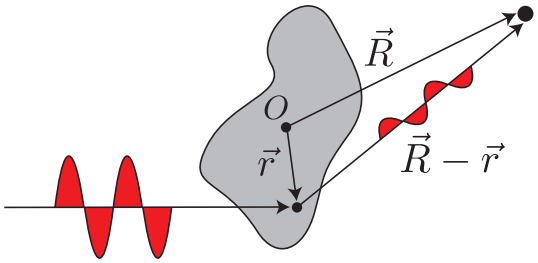

Figure 4.1: Coordination definitions. $\vec{R}$ and $\vec{r}$ are the position of a detector and an atom, respectively.

retarded time:

$$t' := t - \frac{|\vec{R}-\vec{r}|}{v} \tag{4.1.1.22}$$

We define the incident electric field as follows:

$$\vec{E}_i(\vec{r},t) := \vec{e}_i E_0 \exp[i(\vec{k}_i\cdot\vec{r}-\omega_i t)] \tag{4.1.1.23}$$

Then, the scattered electric field is calculated as follows:

$$\begin{aligned}\vec{E}_s(\vec{R},t) &= \frac{1}{\varepsilon\varepsilon_0}\vec{D}_s \\ &= \frac{1}{\varepsilon\varepsilon_0}\nabla\times\nabla\times\left[\frac{1}{4\pi}\int_V d\vec{r}\frac{\delta\boldsymbol{\epsilon}(\vec{r},t')}{|\vec{R}-\vec{r}|}\cdot\vec{e}_i E_0\exp\left[i(\vec{k}_i\cdot\vec{r}-\omega_i t')\right]\right] \\ &= \nabla\times\nabla\times\left[\frac{E_0}{4\pi\varepsilon\varepsilon_0}\int_V d\vec{r}\frac{1}{|\vec{R}-\vec{r}|}(\delta\boldsymbol{\epsilon}(\vec{r},t')\cdot\vec{e}_i)\exp\left[i(\vec{k}_i\cdot\vec{r}-\omega_i t')\right]\right]\end{aligned} \tag{4.1.1.24}$$

Let us decompose the dielectric tensor $\delta\boldsymbol{\epsilon}(\vec{r},t')$ into Fourier components:

$$\delta\boldsymbol{\epsilon}(\vec{r},t') =: \sum_p \delta\boldsymbol{\epsilon}_p(\vec{r})\exp[i\Omega_p t'] \tag{4.1.1.25}$$

Ω_p represent frequency components in the system such as translational, rotational and vibrational motions of the system. This formulation comes from the assumption that the fluctuation of the dielectric constant is produced by translational, rotational or vibrational motions of the molecules in the media. This works well in most of the case since $\omega_i(\sim 10^{15}\ \mathrm{s}^{-1}) \gg \Omega_p(< 10^{10}\ \mathrm{s}^{-1}$ for translational, $\sim 10^{12}\ \mathrm{s}^{-1}$ for rotational, $\sim 10^{13}\ \mathrm{s}^{-1}$ for vibrational motions) [44].

In addition to this, we use the assumption that $|\vec{R}| \gg |\vec{r}|$. Under this assumption, the retarded time is:

$$\begin{aligned}t' &= t - \frac{1}{v}(R^2 - 2\vec{R}\cdot\vec{r}+r^2)^{1/2} \\ &\simeq t - \frac{R}{v}\left(1-\frac{2\vec{R}\cdot\vec{r}}{R^2}\right)^{1/2} \\ &\simeq t - \frac{1}{v}\left(R - \frac{\vec{R}\cdot\vec{r}}{R}\right) \\ &= t - \frac{1}{v}(R - \vec{r}\cdot\vec{n}_s)\end{aligned} \tag{4.1.1.26}$$

[44] From the viewpoint of the wavenumber $(1/\lambda)$, $\omega_i(\sim 20000\ \mathrm{cm}^{-1}) \gg \Omega_p(< 1\ \mathrm{cm}^{-1}$ for translational, $\sim 100\ \mathrm{cm}^{-1}$ for rotational, $\sim 1000\ \mathrm{cm}^{-1}$ for vibrational motions)

where $\vec{n}_s$ is an unit vector of a wavevector of the scattered field.

Substitute Eqs.(4.1.1.25) and (4.1.1.26) into Eq.(4.1.1.24):

$$\begin{aligned}\vec{E}_s(\vec{R},t) &\simeq \frac{E_0}{4\pi\varepsilon\varepsilon_0 R}\nabla\times\nabla\times\int_V d\vec{r}\sum_p \delta\boldsymbol{\epsilon}_p(\vec{r})\cdot\vec{e}_i\exp[i\Omega_p t']\exp[i(\vec{k}_i\cdot\vec{r}-\omega_i t')] \\ &= \frac{E_0}{4\pi\varepsilon\varepsilon_0 R}\nabla\times\nabla\times \\ &\quad \int_V d\vec{r}\sum_p \delta\boldsymbol{\epsilon}_p(\vec{r})\cdot\vec{e}_i\exp[i\vec{k}_i\cdot\vec{r}]\exp[-i\omega_i t]\exp[i\Omega_p t]\exp\left[i(\omega_i-\Omega_p)\frac{1}{v}(R-\vec{r}\cdot\vec{n}_s)\right] \end{aligned} \tag{4.1.1.27}$$

Here, we regard $1/|\vec{R}-\vec{r}|\simeq 1/R$. Now let us define $\vec{k}_p$ as follows:

$$\frac{\omega_i-\Omega_p}{v}\vec{n}_s =: \frac{\omega_s}{v}\vec{n}_s =: \vec{k}_p \tag{4.1.1.28}$$

By using Eq.(4.1.1.28) [45]:

$$\begin{aligned}&\vec{E}_s(\vec{R},t) \\ &= \frac{E_0}{4\pi\varepsilon\varepsilon_0 R}\nabla\times\nabla\times\int_V d\vec{r}\sum_p \delta\boldsymbol{\epsilon}_p(\vec{r})\cdot\vec{e}_i\exp[i(\vec{k}_i-\vec{k}_p)\cdot\vec{r}]\exp[-i\omega_i t]\exp[i\Omega_p t]\exp[ik_p R] \\ &= -\frac{E_0}{4\pi\varepsilon\varepsilon_0 R}\sum_p \exp[i(\vec{k}_p\cdot\vec{R}-\omega_i t)]\vec{k}_p\times\left(\vec{k}_p\times\int_V d\vec{r}\exp[i(\vec{k}_i-\vec{k}_p)\cdot\vec{r}]\exp[i\Omega_p t]\delta\boldsymbol{\epsilon}_p(\vec{r})\cdot\vec{e}_i\right)\end{aligned} \tag{4.1.1.29}$$

Here we use the fact that $\nabla\times\nabla\times e^{i\vec{k}_p\cdot\vec{R}} = -\vec{k}_p\times\vec{k}_p\times e^{i\vec{k}_p\cdot\vec{R}}$. Notice that $k_p R = \vec{k}_p\cdot\vec{R}$ since $\vec{k}_p \parallel \vec{R}$.

Since $\omega_i \gg \Omega_p$,

$$\vec{k}_p \simeq \frac{\omega_i}{v}\vec{n}_s = \vec{k}_s \tag{4.1.1.30}$$

Then,

$$\begin{aligned}&\vec{E}_s(\vec{R},t) \\ &\simeq -\frac{E_0}{4\pi\varepsilon\varepsilon_0 R}\exp[i(\vec{k}_s\cdot\vec{R}-\omega_i t)]\vec{k}_s\times\left(\vec{k}_s\times\int_V d\vec{r}\exp[i(\vec{k}_i-\vec{k}_s)\cdot\vec{r}]\sum_p\exp[i\Omega_p t]\delta\boldsymbol{\epsilon}_p(\vec{r})\cdot\vec{e}_i\right)\end{aligned} \tag{4.1.1.31}$$

We define $\vec{q}$ and $\delta\boldsymbol{\epsilon}(\vec{r},t')$ as follows:

$$\vec{q} := \vec{k}_i - \vec{k}_s \tag{4.1.1.32}$$

$$\delta\boldsymbol{\epsilon}(\vec{r},t) := \sum_p \delta\boldsymbol{\epsilon}_p(\vec{r})\exp[i\Omega_p t] \tag{4.1.1.33}$$

Substitute Eqs.(4.1.1.32) and (4.1.1.33) into Eq.(4.1.1.31):

$$\boxed{\vec{E}_s(\vec{R},t) \simeq -\frac{E_0}{4\pi\varepsilon\varepsilon_0 R}\exp[i(\vec{k}_s\cdot\vec{R}-\omega_i t)]\int_V d\vec{r}\exp[i\vec{q}\cdot\vec{r}]\vec{k}_s\times(\vec{k}_s\times[\delta\boldsymbol{\epsilon}(\vec{r},t)\cdot\vec{e}_i])} \tag{4.1.1.34}$$

Eq.(4.1.1.34) is the start point of the derivation of dynamic light scattering discussed in the later subsection. Let us see one simple example; scattering from one spherical molecule at $\vec{r}=\vec{r}_j$ (Fig.4.2). In this case,

[45] From now, we represent $|\vec{A}| := A$ for arbitrary vector quantity.

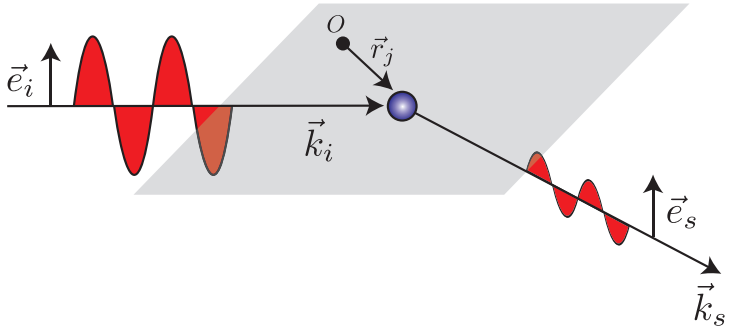

Figure 4.2: Coordination definitions. $\vec{r}_j$ is a position of a spherical molecule. $\vec{e}_i$ and $\vec{e}_s$ are the polarization of incident and scattered light. $\vec{k}_i$ and $\vec{k}_s$ are the wavevector of incident and scattered light.

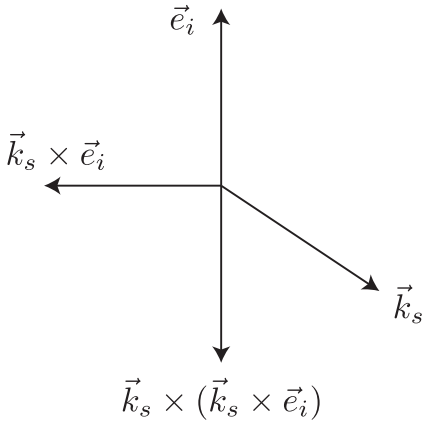

Figure 4.3: Calculation of cross products (Eq.(4.1.1.37)).

$\delta\boldsymbol{\epsilon}(\vec{r},t)$ is replaced by the polarizability of the molecule:

$$\delta\boldsymbol{\epsilon}(\vec{r},t) \to \alpha\delta(\vec{r}-\vec{r}_j) \tag{4.1.1.35}$$

Notice that α is a scalar since the molecule is assumed to be spherical.

Substitute Eq.(4.1.1.35) into Eq.(4.1.1.34):

$$\vec{E}_s(\vec{R},t) = -\frac{\alpha E_0}{4\pi\varepsilon\varepsilon_0 R}\exp[i(\vec{k}_s\cdot\vec{R}-\omega_i t)]\int_V d\vec{r}\exp[i\vec{q}\cdot\vec{r}]\delta(\vec{r}-\vec{r}_j)(\vec{k}_s\times(\vec{k}_s\times\vec{e}_i)) \tag{4.1.1.36}$$

First, we assume that $\vec{e}_i \perp \vec{k}_s$ as shown in Fig.4.2. In this case (see Fig.4.3),

$$\vec{k}_s\times(\vec{k}_s\times\vec{e}_i) = -k_s^2\vec{e}_i \tag{4.1.1.37}$$

so

$$\begin{aligned}
\vec{E}_s(\vec{R},t) &= \frac{\alpha E_0 k_s^2}{4\pi\varepsilon\varepsilon_0 R}\exp[i(\vec{k}_s\cdot\vec{R}-\omega_i t)]\int_V d\vec{r}\exp[i\vec{q}\cdot\vec{r}]\delta(\vec{r}-\vec{r}_j)\vec{e}_i \\
&= \frac{\alpha E_0 k_s^2}{4\pi\varepsilon\varepsilon_0 R}\exp[i(\vec{k}_s\cdot\vec{R}-\omega_i t)]\exp[i\vec{q}\cdot\vec{r}_j]\vec{e}_i \\
&= \frac{k_s^2}{4\pi\varepsilon\varepsilon_0 R}\exp[i\vec{k}_s\cdot(\vec{R}-\vec{r}_j)]\alpha\vec{e}_i E_0\exp[i(\vec{k}_i\cdot\vec{r}_j-\omega_i t)] \\
&= \frac{k_s^2}{4\pi\varepsilon\varepsilon_0 R}\exp[i\vec{k}_s\cdot(\vec{R}-\vec{r}_j)]\alpha\vec{E}_i(\vec{r}_j,t)
\end{aligned} \tag{4.1.1.38}$$

Eq.(4.1.1.38) clearly shows that the incident light at $\vec{r}_j$ ($\vec{E}_i(\vec{r}_j,t) \propto \exp[i\vec{k}_i\cdot\vec{r}_j]$) is the source of the scattered light ($\propto \exp[i\vec{k}_s\cdot(\vec{R}-\vec{r}_j)]$).

Here, we define the induced electric dipole moment $\vec{\mu}$ as follows:

$$\vec{\mu}(\vec{r},t) := \alpha\vec{E}_i(\vec{r},t) \tag{4.1.1.39}$$

By using the fact that $k_i \simeq k_s$ (elastic scattering), Eq.(4.1.1.38) is then transformed into:

$$\begin{aligned}\vec{E}_s(\vec{R},t) &= \frac{1}{4\pi\varepsilon\varepsilon_0 R}\frac{\omega_i^2}{v^2}\vec{\mu}(\vec{r},t)\exp[i\vec{k}_s\cdot(\vec{R}-\vec{r_j})] \\ &= -\frac{1}{4\pi\varepsilon\varepsilon_0 R}\frac{1}{v^2}\ddot{\vec{\mu}}(\vec{r},t)\exp[i\vec{k}_s\cdot(\vec{R}-\vec{r_j})] \\ &= -\frac{\mu\mu_0}{4\pi R}\ddot{\vec{\mu}}(\vec{r},t)\exp[i\vec{k}_s\cdot(\vec{R}-\vec{r_j})] \end{aligned} \tag{4.1.1.40}$$

Then consider the case where $\vec{e}_i$ is not perpendicular to $\vec{k}_s$ as shown in Fig.4.4. In this case (see Fig.4.5),

$$\begin{aligned}\vec{k}_s\times(\vec{k}_s\times\vec{e}_i) &= \vec{k}_s\times(\vec{k}_s\times(\vec{e}_i-\vec{n}_s(\vec{e}_i\cdot\vec{n}_s))) \\ &= -k_s^2(\vec{e}_i-\vec{n}_s(\vec{e}_i\cdot\vec{n}_s)) \\ &= -k_s^2\vec{e}_s\cos\psi \end{aligned} \tag{4.1.1.41}$$

so

$$\boxed{\vec{E}_s(\vec{R},t) = -\frac{\mu\mu_0|\ddot{\vec{\mu}}(\vec{r}_j,t)|}{4\pi R}\exp[i\vec{k}_s\cdot(\vec{R}-\vec{r_j})]\vec{e}_s\cos\psi = -\frac{\mu\mu_0}{4\pi R}\exp[i\vec{k}_s\cdot(\vec{R}-\vec{r_j})](\ddot{\vec{\mu}}-\vec{n}_s(\ddot{\vec{\mu}}\cdot\vec{n}_s))} \tag{4.1.1.42}$$

Eq.(4.1.1.42) is visualized in Fig.4.6 as the amplitude of the electric field.

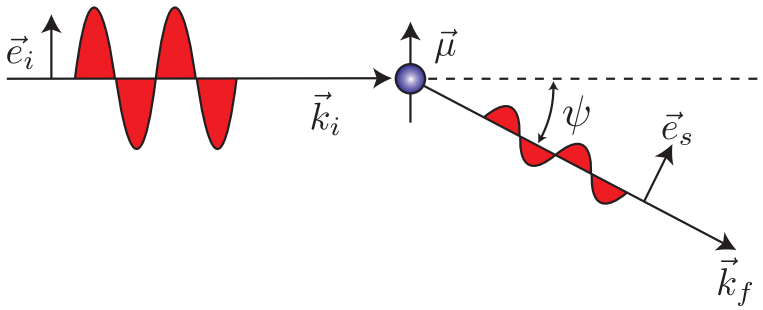

Figure 4.4: Coordination definitions. μ is an induced electric dipole moment. ψ is an angle between the plain containing incident light whose perpendicular line is parallel to $\vec{e}_i$ and that of scattered light. $\vec{e}_i$ and $\vec{e}_s$ are the polarization of incident and scattered light. $\vec{k}_i$ and $\vec{k}_s$ are the wavevector of incident and scattered light.

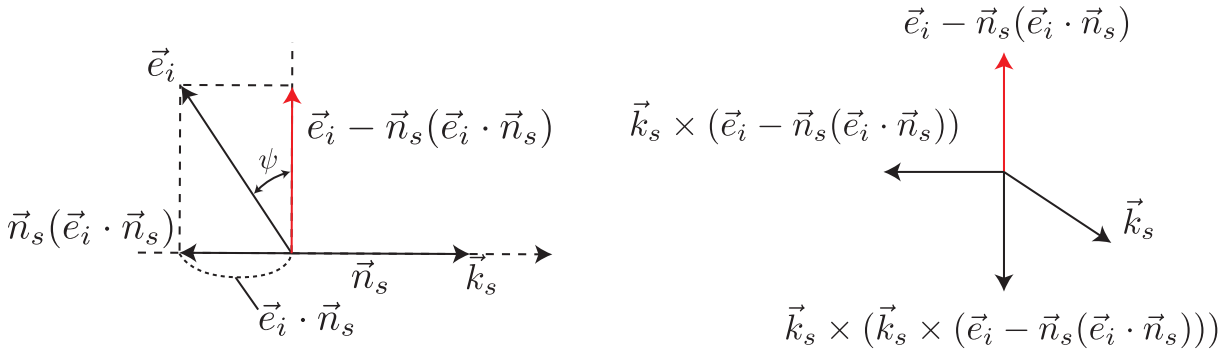

Figure 4.5: Calculation of cross products (Eq.(4.1.1.41)).

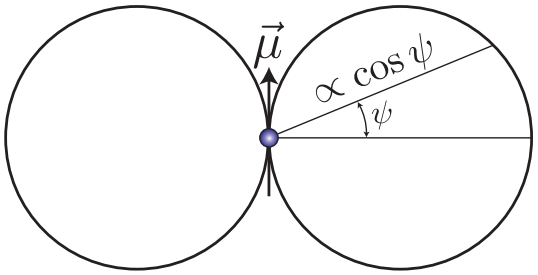

Figure 4.6: Visualization of the scattered electric field (Eq.(4.1.1.42)).

4.1.2 Dynamic light scattering

Dynamic light scattering is a method to characterize the size distribution of the solute such as macromolecules, colloid and so on. In principle, dynamic light scattering is quasi-elastic light scattering originated from Doppler effect. In practice, the observable is a time correlation function of electric current at the detector originated from the scattered electric field. The electric current, i, is proportional to a square of electric field, $\vec{E}$, at the detector:

$$i_s = A|\vec{E}| \tag{4.1.2.1}$$

where A is a real proportional constant. Then, what we observe in dynamic light scattering is:

$$\langle\, i_s(0) i_s(\tau)\,\rangle_T = A^2 \langle\, |\vec{E}_s(0)|^2 |\vec{E}_s(\tau)|^2\,\rangle_T \tag{4.1.2.2}$$

where $\langle\cdots\rangle_T$ denotes time average.

In this subsection, we derive how to determine the size of the solution from the time correlation function, Eq.(4.1.2.2) [61, 62].

Our starting point is Eq.(4.1.1.34):

$$\vec{E}_s(\vec{R},t) \simeq -\frac{E_0}{4\pi\varepsilon\varepsilon_0 R}\exp[i(\vec{k}_s\cdot\vec{R}-\omega_i t)]\int_V d\vec{r}\exp[i\vec{q}\cdot\vec{r}]\vec{k}_s\times(\vec{k}_s\times[\delta\boldsymbol{\epsilon}(\vec{r},t)\cdot\vec{e}_i])$$

$\delta\boldsymbol{\epsilon}(\vec{r},t)$ is replaced by the polarizability of molecules in the irradiated volume:

$$\delta\boldsymbol{\epsilon}(\vec{r},t) \to \sum_j \boldsymbol{\alpha}_j(t)\delta(\vec{r}-\vec{r}_j(t)) \tag{4.1.2.3}$$

where $\boldsymbol{\alpha}_j(t)$ is the polarizability tensor of a molecule j whose position is $\vec{r}_j(t)$. j runs all of the molecules in the irradiated volume. We assume that the polarizability tensor is scalar; $\boldsymbol{\alpha}_j(t) \to \alpha_j(t)$. In other words, we assume that the molecule is spherical.

We ignore the fact that the molecule j gets out of the irradiated volume during the time t. This is good approximation since the time scale to get out of the irradiated volume is much larger than the time scale we are interested in[46].

[46] For example, consider the case of the polystyrene beads whose radius is 20 nm. The diffusion constant of this sphere in water at room temperature is calculated by using Stokes–Einstein equation:

$$D = \frac{k_B T}{6\pi\eta R_h} = \frac{1.38\times10^{-23}\ [\mathrm{J/K}]\cdot 298\ [\mathrm{K}]}{6\pi\cdot 0.895\times10^{-3}[\mathrm{Pa{\cdot}s}]\cdot 20\times10^{-9}\ [\mathrm{m}]} \simeq 1\times10^{-11}[\mathrm{m^2/s}]$$

Typical dimensional order of the irradiated volume is about 100 μm. Time to across the Brownian particle at a distance $L =$

Substitute Eq.(4.1.2.3) into Eq.(4.1.1.34):

$$\begin{aligned}
&\vec{E}_s(\vec{R},t) \\
&\simeq -\frac{E_0}{4\pi\varepsilon\varepsilon_0 R}\exp[i(\vec{k}_s\cdot\vec{R}-\omega_i t)]\int_V d\vec{r}\exp[i\vec{q}\cdot\vec{r}]\vec{k}_s\times\left(\vec{k}_s\times\left[\sum_j \alpha_j(t)\delta(\vec{r}-\vec{r}_j(t))\cdot\vec{e}_i\right]\right) \\
&= \frac{E_0 k_s^2}{4\pi\varepsilon\varepsilon_0 R}\exp[i(\vec{k}_s\cdot\vec{R}-\omega_i t)]\int_V d\vec{r}\exp[i\vec{q}\cdot\vec{r}]\sum_j \alpha_j(t)\delta(\vec{r}-\vec{r}_j(t))\cdot\vec{e}_i \\
&= \frac{E_0 k_s^2\vec{e}_i}{4\pi\varepsilon\varepsilon_0 R}\exp[i(\vec{k}_s\cdot\vec{R}-\omega_i t)]\sum_j \alpha_j(t)\exp[i\vec{q}\cdot\vec{r}_j(t)] \qquad (4.1.2.4)
\end{aligned}$$

Here, we assume that $\vec{k}_s \perp \vec{e}_i$. In the case where α_j is constant for all of the molecules, α:

$$\begin{aligned}
\vec{E}_s(\vec{R},t) &= \frac{\alpha E_0 k_s^2\vec{e}_i}{4\pi\varepsilon\varepsilon_0 R}e^{i(\vec{k}_s\cdot\vec{R}-\omega_i t)}\sum_j e^{i\vec{q}\cdot\vec{r}_j(t)} \\
&= \vec{B}e^{i(\vec{k}_s\cdot\vec{R}-\omega_i t)}\psi(\vec{q},t) \qquad (4.1.2.5)
\end{aligned}$$

where

$$\vec{B} := \frac{\alpha E_0 k_s^2}{4\pi\varepsilon\varepsilon_0 R}\vec{e}_i \qquad (4.1.2.6)$$

$$\psi(\vec{q},t) := \sum_j e^{i\vec{q}\cdot\vec{r}_j(t)} \qquad (4.1.2.7)$$

Substitute Eq.(4.1.2.5) into Eq.(4.1.2.2)

$$\begin{aligned}
\langle\, i_s(0)i_s(\tau)\,\rangle_T &= A^2\langle\, E_s^*(0)E_s(0)E_s^*(\tau)E_s(\tau)\,\rangle_T \\
&= A^2B^4\langle\,\psi^*(\vec{q},0)\psi(\vec{q},0)\psi^*(\vec{q},\tau)\psi(\vec{q},\tau)\,\rangle_T \qquad (4.1.2.8)
\end{aligned}$$

where $E_s := |\vec{E}_s|$.

Since each molecule is moving around:

$$\langle\, e^{i\vec{q}\cdot\vec{r}_j(t)}\,\rangle_E = 0 \qquad (4.1.2.9)$$

where $\langle\cdots\rangle_E$ denotes ensemble average. Therefore, by using central limit theorem, $E_s(\vec{R},t)$ is a complex Gaussian distribution since $E_s(\vec{R},t)$ is the sum of $e^{i\vec{q}\cdot\vec{r}_j(t)}$. It is known that the 4th order moment of a complex Gaussian distribution is decomposed to the product of 2nd order moment (See Appendix 11.3):

100 μm, τ, is calculated as follows:

$$\tau \sim \frac{L^2}{D} \sim \frac{(100\times10^{-6}\ [\mathrm{m}])^2}{1\times10^{-11}[\mathrm{m}^2/\mathrm{s}]} \sim 1\times10^3\ [\mathrm{s}]$$

which is sufficiently large compared to the correlation time we are interested in (several millisecond).

$$
\begin{aligned}
&\langle\, \psi^*(\vec{q},0)\psi(\vec{q},0)\psi^*(\vec{q},\tau)\psi(\vec{q},\tau)\,\rangle_T \\
&= \langle\, \psi^*(\vec{q},0)\psi(\vec{q},0)\,\rangle_T \langle\, \psi^*(\vec{q},\tau)\psi(\vec{q},\tau)\,\rangle_T \\
&\quad + \langle\, \psi^*(\vec{q},0)\psi^*(\vec{q},\tau)\,\rangle_T \langle\, \psi(\vec{q},0)\psi(\vec{q},\tau)\,\rangle_T + \langle\, \psi^*(\vec{q},0)\psi(\vec{q},\tau)\,\rangle_T \langle\, \psi(\vec{q},0)\psi^*(\vec{q},\tau)\,\rangle_T \\
&= \langle\, \psi^*(\vec{q},0)\psi(\vec{q},0)\,\rangle_T \langle\, \psi^*(\vec{q},\tau)\psi(\vec{q},\tau)\,\rangle_T + \langle\, \psi^*(\vec{q},0)\psi(\vec{q},\tau)\,\rangle_T \langle\, \psi(\vec{q},0)\psi^*(\vec{q},\tau)\,\rangle_T \\
&= \langle\, |\psi(\vec{q},0)|^2\,\rangle_T^2 + |\langle\, \psi^*(\vec{q},0)\psi(\vec{q},\tau)\,\rangle_T|^2
\end{aligned}
\tag{4.1.2.10}
$$

Notice that $\langle\, \psi\psi\,\rangle_T = \langle\, \psi^*\psi^*\,\rangle_T = 0$.

Eq.(4.1.2.10) shows that what we can obtain from $\langle\, i_s(0)i_s(\tau)\,\rangle_T$ is represented by $\langle\, \psi^*(\vec{q},0)\psi(\vec{q},\tau)\,\rangle_T$. Let us expand this quantity:

$$
\begin{aligned}
\langle\, \psi^*(\vec{q},0)\psi(\vec{q},\tau)\,\rangle_T &= \left\langle \sum_j \sum_k e^{i\vec{q}\cdot(\vec{r}_k(\tau)-\vec{r}_j(0))} \right\rangle_T \\
&= \left\langle \sum_j e^{i\vec{q}\cdot(\vec{r}_j(\tau)-\vec{r}_j(0))} \right\rangle_T + \left\langle \sum_j e^{-i\vec{q}\cdot\vec{r}_j(0)} \sum_{k\neq j} e^{i\vec{q}\cdot\vec{r}_k(\tau)} \right\rangle_T
\end{aligned}
\tag{4.1.2.11}
$$

Since each particle is statistically independent, the second term of Eq.(4.1.2.11) can be separated as follows:

$$
\begin{aligned}
\left\langle \sum_j e^{-i\vec{q}\cdot\vec{r}_j(0)} \sum_{k\neq j} e^{i\vec{q}\cdot\vec{r}_k(\tau)} \right\rangle_T &= \left\langle \sum_j e^{-i\vec{q}\cdot\vec{r}_j(0)} \right\rangle_T \left\langle \sum_{k\neq j} e^{i\vec{q}\cdot\vec{r}_k(\tau)} \right\rangle_T \\
&= \left\langle \sum_j e^{-i\vec{q}\cdot\vec{r}_j(0)} \right\rangle_E \left\langle \sum_{k\neq j} e^{i\vec{q}\cdot\vec{r}_k(\tau)} \right\rangle_E = 0
\end{aligned}
\tag{4.1.2.12}
$$

From the first line to the second line, we use the fact that the medium is ergodic when the irradiated volume is sufficiently large. Notice that these terms are zero (Eq.(4.1.2.9)). So,

$$
\langle\, \psi^*(\vec{q},0)\psi(\vec{q},\tau)\,\rangle_T = \left\langle \sum_j e^{i\vec{q}\cdot(\vec{r}_j(\tau)-\vec{r}_j(0))} \right\rangle_T = N \left\langle e^{i\vec{q}\cdot(\vec{r}_j(\tau)-\vec{r}_j(0))} \right\rangle_T =: N F_s(\vec{q},\tau)
\tag{4.1.2.13}
$$

where N is the number of molecules in the irradiated volume and

$$
\boxed{F_s(\vec{q},t) := \left\langle e^{i\vec{q}\cdot(\vec{r}_j(t)-\vec{r}_j(0))} \right\rangle_T}
\tag{4.1.2.14}
$$

$F_s(\vec{q},t)$ is one of the most important quantity called self-intermediate scattering function. To clarify the physical meaning of this function, let us convert to a real space domain by Fourier transformation:

$$
\begin{aligned}
\frac{1}{(2\pi)^3}\int_{-\infty}^{\infty} d\vec{q} e^{-i\vec{q}\cdot\vec{x}} F_s(\vec{q},t) &= \frac{1}{(2\pi)^3}\int_{-\infty}^{\infty} d\vec{q} \langle \exp[i\vec{q}\cdot((\vec{r}_j(t)-\vec{r}_j(0))-\vec{x})]\rangle_T \\
&= \langle\, \delta((\vec{r}_j(t)-\vec{r}_j(0))-\vec{x})\,\rangle_T \\
&= \langle\, \delta(\vec{x}-(\vec{r}_j(t)-\vec{r}_j(0)))\,\rangle_T =: G_s(\vec{x},t)
\end{aligned}
\tag{4.1.2.15}
$$

Here, we use the following formula:

$$\delta(\vec{x}) = \frac{1}{(2\pi)^3}\int_{-\infty}^{\infty} d\vec{q}e^{i\vec{q}\cdot\vec{x}} \tag{4.1.2.16}$$

$$\delta(\vec{x}) = \delta(-\vec{x}) \tag{4.1.2.17}$$

$G_s(\vec{x},t)$ is called van–Hove self space-time correlation function. Physical meaning of $G_s(\vec{x},t)$ is clear; $G_s(\vec{x},t)d\vec{x}$ is the probability that particle j will suffer a displacement $\vec{x}$ in time t (Fig.4.7).

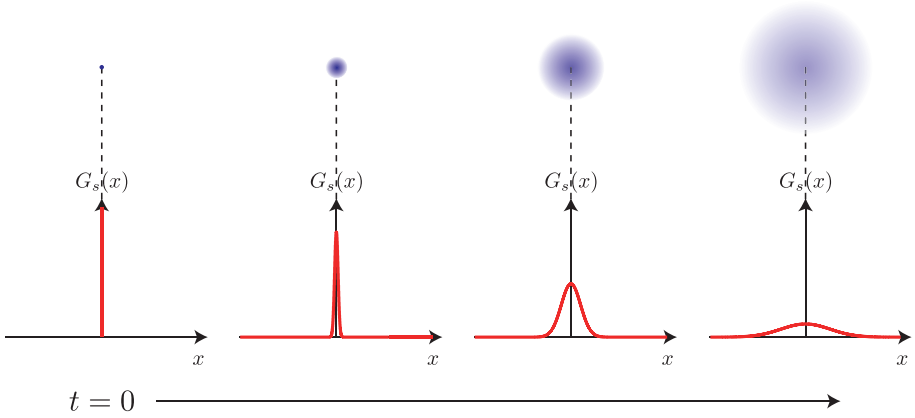

Figure 4.7: Visualization of time variation of $G_s(\vec{x},\tau)$ in the case of Brownian motion in 1D space (Eq.(4.1.2.15)). The position of the Brownian particle is strictly defined at $x = 0$ at $t = 0$. This is mathematically described as a delta function. As the time proceeds, the distribution of probability that the particle exists at x becomes broaden.

Let us calculate $F_s(\vec{q},t)$ of Brownian particles by using $G_s(\vec{x},t)$. The probability density, $P(\vec{x})$, of a Brownian particle follows the diffusion equation:

$$\frac{\partial}{\partial t}P(\vec{x}) = D\nabla^2 P(\vec{x}) \tag{4.1.2.18}$$

where D is a diffusion constant of the particle. Since $G_s(\vec{x},t)$ implies the probability density, $G_s(\vec{x},t)$ also follows the diffusion equation:

$$\frac{\partial}{\partial t}G_s(\vec{x},t) = D\nabla^2 G_s(\vec{x},\tau) \tag{4.1.2.19}$$

Substitute Eq.(4.1.2.15) into Eq.(4.1.2.19):

$$\begin{aligned}
&\frac{\partial}{\partial t}\left[\frac{1}{(2\pi)^3}\int_{-\infty}^{\infty} d\vec{q}e^{-i\vec{q}\cdot\vec{x}}F_s(\vec{q},t)\right] = D\nabla^2\left[\frac{1}{(2\pi)^3}\int_{-\infty}^{\infty} d\vec{q}e^{-i\vec{q}\cdot\vec{x}}F_s(\vec{q},t)\right] \\
&\rightarrow \frac{1}{(2\pi)^3}\int_{-\infty}^{\infty} d\vec{q}e^{-i\vec{q}\cdot\vec{x}}\frac{\partial F_s(\vec{q},t)}{\partial t} = \frac{1}{(2\pi)^3}\int_{-\infty}^{\infty} d\vec{q}e^{-i\vec{q}\cdot\vec{x}}(-q^2 DF_s(\vec{q},t)) \\
&\rightarrow \frac{\partial F_s(\vec{q},t)}{\partial t} = -q^2 DF_s(\vec{q},t)
\end{aligned} \tag{4.1.2.20}$$

Eq.(4.1.2.20) is easily solved:

$$F_s(\vec{q},t) = e^{-q^2 Dt} \tag{4.1.2.21}$$

Constant of integration is determined from the fact that $F_s(\vec{q},0)=1$ (see Eq.(4.1.2.14)).

Now go back to Eq.(4.1.2.8). Substitute Eq.(4.1.2.13) into Eq.(4.1.2.10) and then into Eq.(4.1.2.8):

$$\langle\, i_s(0)i_s(\tau)\,\rangle_T = A^2B^4(|NF_s(\vec{q},0)|^2+|NF_s(\vec{q},\tau)|^2) =: |G^{(1)}(0)|^2+|G^{(1)}(\tau)|^2 =: G^{(2)}(\tau) \tag{4.1.2.22}$$

where

$$G^{(1)}(\tau) := AB^2NF_s(\vec{q},\tau) \tag{4.1.2.23}$$

What we usually observe is its normalized form:

$$g^{(1)}(\tau) := \frac{G^{(1)}(\tau)}{G^{(1)}(0)} \tag{4.1.2.24}$$

$$g^{(2)}(\tau) := \frac{G^{(2)}(\tau)}{|G^{(1)}(0)|^2} \tag{4.1.2.25}$$

Substitute Eqs.(4.1.2.24) and (4.1.2.25) into Eq.(4.1.2.22):

$$\boxed{g^{(2)}(\tau) = 1+|g^{(1)}(\tau)|^2} \tag{4.1.2.26}$$

This is what we observe in dynamic light scattering experiment. Eq.(4.1.2.26) is called Siegert relation.

In the case where the scatterers are Brownian particles, substitute Eq.(4.1.2.21) into Eq.(4.1.2.23), (4.1.2.24) and (4.1.2.26):

$$G^{(1)}(\tau) = AB^2Ne^{-q^2D\tau} \tag{4.1.2.27}$$

$$g^{(1)}(\tau) = e^{-q^2D\tau} \tag{4.1.2.28}$$

$$\boxed{g^{(2)}(\tau) = 1+e^{-2q^2D\tau}} \tag{4.1.2.29}$$

Most of the cases, DLS data is analyzed by Eq.(4.1.2.29).

In the case of polydisperse Brownian particles, Eq.(4.1.2.13) becomes:

$$\langle\, \psi^*(\vec{q},0)\psi(\vec{q},\tau)\,\rangle_T = N_1F_{s1}(\vec{q},\tau)+N_2F_{s2}(\vec{q},\tau)+\cdots \tag{4.1.2.30}$$

where $F_{si}(\vec{q},\tau) := e^{-q^2D_i\tau}$ (Eq.(4.1.2.21)). In general, Eq.(4.1.2.30) becomes an integral form:

$$\langle\, \psi^*(\vec{q},0)\psi(\vec{q},\tau)\,\rangle_T = \int_0^\infty N(\Gamma)e^{-\Gamma\tau}d\Gamma \tag{4.1.2.31}$$

where $N(\Gamma)$ is the number of particles whose relaxation rate is $\Gamma := q^2D$. Then,

$$g^{(1)}(\tau) = \int_0^\infty G(\Gamma)e^{-\Gamma\tau}d\Gamma \tag{4.1.2.32}$$

where $G(\Gamma)$ is the normalized distribution function. Substitute Eq.(4.1.2.32) into Eq.(4.1.2.26):

$$g^{(2)}(\tau) = 1+\left|\int_0^\infty G(\Gamma)e^{-\Gamma\tau}d\Gamma\right|^2 \tag{4.1.2.33}$$

It is impossible to solve this equation analytically (inverse Laplace transformation). Instead of this, $G(\Gamma)$ is calculated by the numerical calculation such as a constrained regularization program, CONTIN. Figure 4.8 shows typical experiment results for polystyrene latex suspension. Measurements was performed by DLS/SLS-5000 compact goniometer (ALV, Langen), coupled with an ALV photon correlator. The incident light of the conventional DLS system is a 22 mW He–Ne laser whose wavelength is 632.8 nm. Scattered angle was set to be 90° and the measurement time was 30 seconds. Figure 4.8(a) shows the time correlation functions of scattered light intensity. All of data are fitted by a single exponential function, Eq.(4.1.2.29), which are also shown in the figure as dashed lines. By applying CONTIN, Figure 4.8(a) are converted to the distribution functions of relaxation rate. Relaxation rate, Γ, is converted to hydrodynamic radius, R_h, by using Einstein–Stokes relationship:

$$\Gamma = q^2 D = q^2 \frac{k_B T}{6\pi\eta R_h} \tag{4.1.2.34}$$

where η is viscosity of solvent. [47] As a result, we can obtain the distribution functions of hydrodynamic radius as shown in Figure 4.8(b).

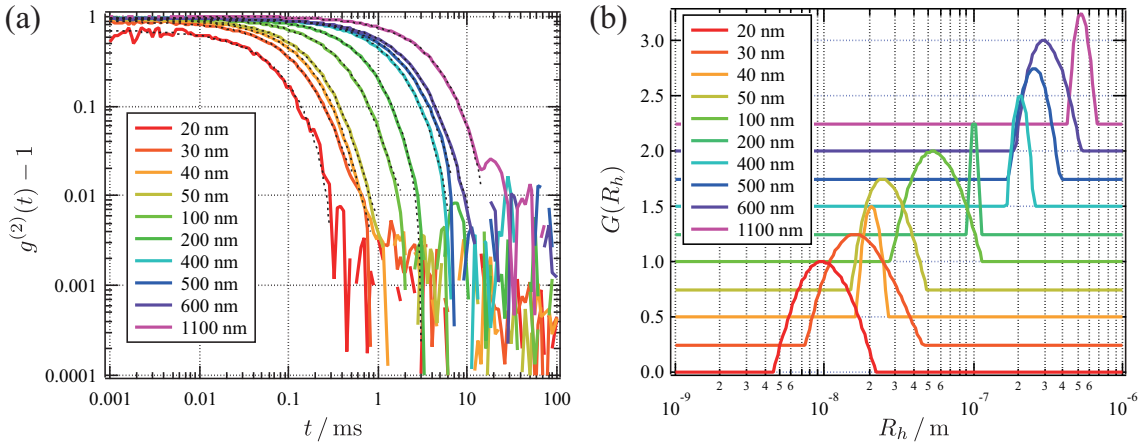

Figure 4.8: Typical measurement results for DLS. The samples are polystyrene latex suspensions whose concentration is 0.001 wt%. Diameter for each sample is shown in the figures. (a) Time correlation functions of scattered light intensity. Dashed lines are the fitting result by using Eq.(4.1.2.29). (b) Size distribution functions calculated from the time correlation functions.

[47] 0.890 cP = 8.90 × 10^{-4} Pa·s for water at 25 °C.

Qualitative description

As I mentioned, dynamic light scattering is regarded as a Doppler effect originated from Brownian motion of solutes. Here, I describe DLS from this point of view. When the light is irradiated to a polymer solution, secondary radiation from the solutes has the same frequency of the incident light. The frequency of light that solutes feel will slightly deviate from the original wavelength when the solutes are moving toward or against the direction of incident light. Similarly, the frequency of light that a detector detects also show slight deviation when the solutes are moving toward or against the detector. Since the velocity distribution of polymers are related to their Brownian motion, we may be able to detect the distribution of the frequency of scattered light (Doppler shift) to determine the diffusion constant. However, it is almost impossible to detect this broadening. To detect the distribution of the frequency of scattered light, we use a spectrometer (Figure 4.9(a)). However, this broadening is so small that we cannot detect. As a typical example, let us consider the Doppler shift of He–Ne laser ($\lambda = 632.8$ nm) from particles in water whose diameter is 100 nm. In the case of Brownian motion, full-width-half-maximum (FWHM) is evaluated as $2Dq^2$ (Eq.(4.1.2.21)). In this case, the diffusion constant $D \sim 5 \times 10^{-12}$ m^2 s^{-1}, the magnitude of scattering vector $q \simeq 2 \times 10^7$ m^{-1}, and therefore $2Dq^2 \sim 10^3$ Hz. This corresponds to 10^{-8} nm while typical resolution of spectrometers is 0.1 nm. Therefore, it is very difficult to detect this broadening. [48]

To overcome this difficulty, let us consider the measurement of scattered light intensity. Scattered light intensity, I_s, is proportional to the squared modulus of electric field E_s. Here, E_s is the summation of the secondary radiation from all of the particles in the irradiated volume. Therefore, I_s is expressed as follows.

$$I_s(\omega) = |E_s|^2 = E_s^* E_s = \left(\sum_i E_{s0}^* e^{i\omega_i t} \right) \left(\sum_j E_{s0} e^{-i\omega_j t} \right) \tag{4.1.2.35}$$

where i and j are the label of particles in the irradiated volume, ω_i and ω_j are the angular frequency of secondary radiation from particle i and j. By decomposing ω_i and ω_j into the angular frequency of incident light, ω_0, and the deviation from ω_0:

$$I_s(\omega) = \left(\sum_i E_{s0}^* e^{i(\omega_0 + \Delta\omega_i)t} \right) \left(\sum_j E_{s0} e^{-i(\omega_0 + \Delta\omega_j)t} \right) = |E_{s_0}|^2 \left(\sum_i \sum_j e^{i(\Delta\omega_i - \Delta\omega_j)t} \right) \tag{4.1.2.36}$$

The peak of $I_s(\omega)$ will be at $\omega = 0$. Therefore, the Doppler shift can be detected as a broadening around $\omega = 0$ (Figure 4.9(b)). Note that the peak of $E_s(\omega)$ is at ω_0, which is significantly larger than the Doppler shift. Doppler shift of one particle i depends on time since the Doppler shift is priginated from Brownian motion. Therefore, $\Delta\omega_i - \Delta\omega_j$ in Eq.(4.1.2.36) is also time dependent. However, this variation is spatially averaged when there are many particles inside the irradiated volume. [49] As a result, $I_s(\omega)$ is time independent. The frequency distribution of such a signal is called power spectrum.

Frequency distribution expressed in Eq.(4.1.2.36) is detected by using spectrum analyzer. Detection scheme to detect the scattered light intensity directly is called homodyne detection. However, it is sometimes hard to detect the motion of particles by homedyne detection when the motion is not Brownian motion. As an example, let us consider the particle moving with the same velocity. When the colloidal particles with

[48] In addition, typical line width of monochromatic laser is $\sim 10^5$ Hz $> 2Dq^2$.

[49] When the number of particles inside the irradiated volume is very small, we observe the number fluctuation. This is a basic idea for fluorescence correlation spectroscopy.

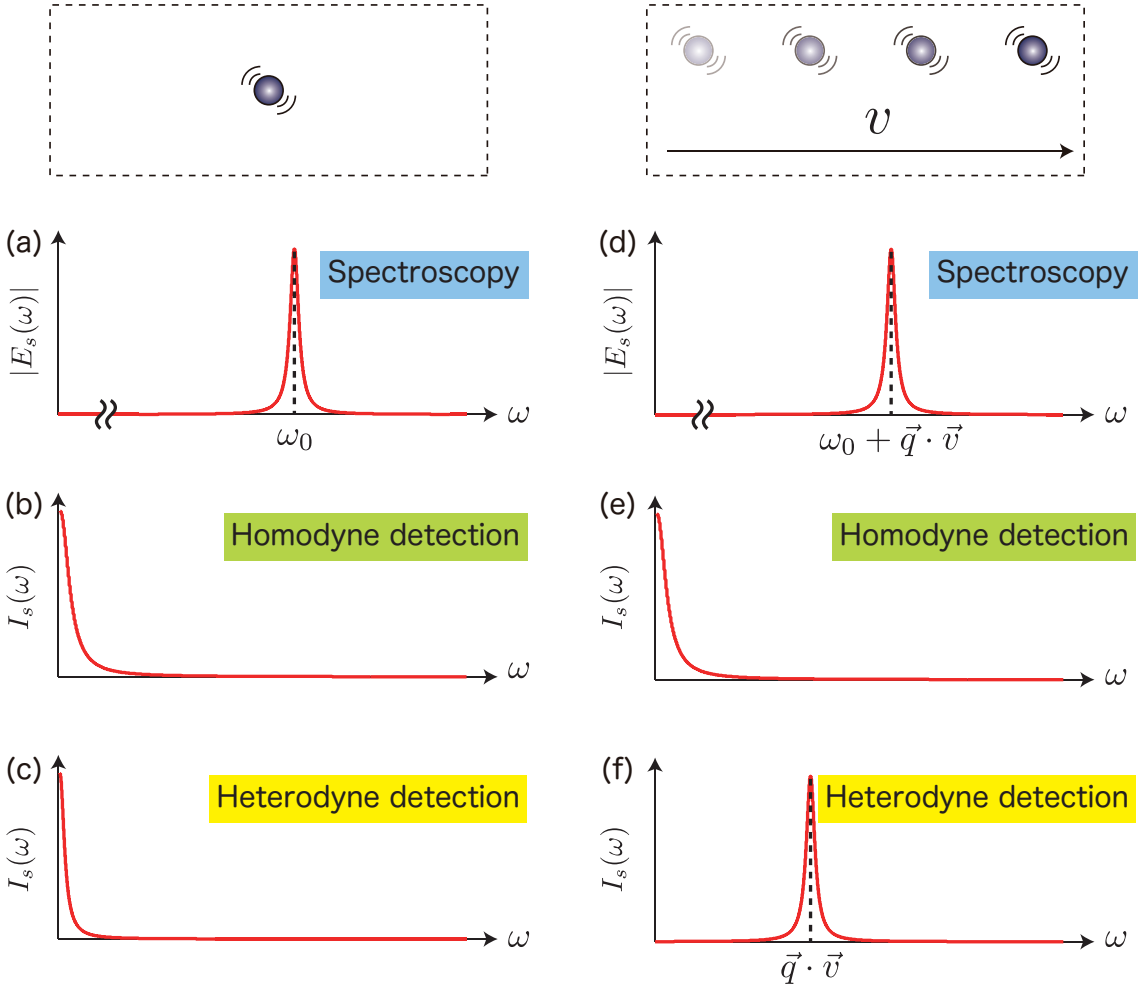

Figure 4.9: Summary of dynamic light scattering in frequency region.

charges are set in static electric field, equation of motion is expressed as follows.

$$m\frac{d^2\vec{r}}{dt^2} = Ze\vec{E} - 6\pi\eta R_h v \tag{4.1.2.37}$$

where m is the mass of the particle, Ze is the charges on the particle, η is the velocity of solvent, R_h is the hydrodynamic radius, and v is the velocity. When the force from electric field and viscosity are balanced, the velocity becomes constant. Then let us consider the expression of I_s. When $v = 0$ and the particle motion is only Brownian motion, the summation of the electric field of scattered light from all of the particles in the irradiated volume is:

$$E_s = A\sum_i e^{i(\vec{q}\cdot\vec{r}_i - \omega_0 t)} \tag{4.1.2.38}$$

Here, $\vec{q}\cdot\vec{r}_i$ stands for the difference of phase from the scattered light from $\vec{r} = 0$. Note that $\vec{r}_i$ depends on time. Scattered light intensity is expressed as follows.

$$I_s = E_s^* E_s = A^2 \sum_i \sum_j e^{i\vec{q}\cdot(\vec{r}_i - \vec{r}_j)} \tag{4.1.2.39}$$

When all of the particle has the same velocity $\vec{v}$:

$$E_s = A\sum_i e^{i(\vec{q}\cdot(\vec{r}_i+\vec{v}t)-\omega_0 t)} \tag{4.1.2.40}$$

Scattered light intensity is:

$$I_s = A^2\sum_i\sum_j e^{i\vec{q}\cdot(\vec{r}_i-\vec{r}_j)} \tag{4.1.2.41}$$

Eqs.(4.1.2.39) and (4.1.2.39) are the same. Therefore, homodyne detection cannot detect the uniform motion of the particles (Figure 4.9(d))

To overcome this difficulty, let us consider that additional laser called local oscillator is irradiated simultaneously to the detector. By setting the amplitude of scattered light as A_s and that of local oscillator as A_{LO}, the electric field and the scattered light intensity on the detector become:

$$E = A_s\sum_i e^{i(\vec{q}\cdot(\vec{r}_i+\vec{v}t)-\omega_0 t)} + A_{\mathrm{LO}}e^{-i\omega_0 t} \tag{4.1.2.42}$$

$$I = A_{\mathrm{LO}}^2 + A_{\mathrm{LO}}^* A_s\sum_i e^{i(\vec{q}\cdot(\vec{r}_i+\vec{v}t)-\omega_0 t)} + A_s^* A_{\mathrm{LO}}\sum_i e^{-i(\vec{q}\cdot(\vec{r}_i+\vec{v}t)-\omega_0 t)} + A_s^2\sum_i\sum_j e^{i\vec{q}\cdot(\vec{r}_i-\vec{r}_j)} \tag{4.1.2.43}$$

The second term and third terms in Eq.(4.1.2.43) contain the information about $\vec{v}$. Usually, we neglect the fourth term in Eq.(4.1.2.43) by setting $A_{\mathrm{LO}} \gg A_s$. This detection scheme is called heterodyne detection. When we explicitly consider the existence of the fourth term, the scheme is called partial heterodyne scheme, which is introduced in Section 4.1.3. Explicit formula of spectra is expressed as a form of Lorentzian [62]:

$$E_s \sim \frac{Dq^2}{(\omega-(\omega_0+\vec{q}\cdot\vec{v}))^2+(Dq^2)^2} \tag{4.1.2.44}$$

$$I_{\mathrm{homodyne}} \sim \frac{2Dq^2}{\omega^2+(2Dq^2)^2} \tag{4.1.2.45}$$

$$I_{\mathrm{heterodyne}} \sim \frac{Dq^2}{(\omega-\vec{q}\cdot\vec{v})^2+(Dq^2)^2} \tag{4.1.2.46}$$

In the case of heterodyne detection, the center of frequency distribution is shifted to $\vec{q}\cdot\vec{v}$. As a result, not only the information of Brownian motion, D, but also the velocity of the particle, v, is obtained (Figure 4.9(f)). Heterodyne detection is widely used for electrophoretic light scattering.

Up to here, I stick on the measurement in frequency domain. The same information can be obtained in time domain. In the case of the measurement in time domain, observed quantity is the time correlation function of the scattered light intensity defined as follows:

$$\langle I_s(0)I_s(\tau)\rangle_T := \lim_{T\to\infty}\frac{1}{2T}\int_{-T}^{T} I_s(t)I_s(t+\tau)dt \tag{4.1.2.47}$$

The fact that we can obtain the same information in frequency domain and time domain is a consequence of the Wiener–Khintchin theorem. This theorem shows that the power spectrum and the time correlation function are connected via Fourier transformation (Figure 4.10).

$$\langle I_s(0)I_s(\tau)\rangle_T = \frac{1}{2\pi}\int_{-\infty}^{\infty} I_s(\omega)e^{i\omega\tau}d\omega \tag{4.1.2.48}$$

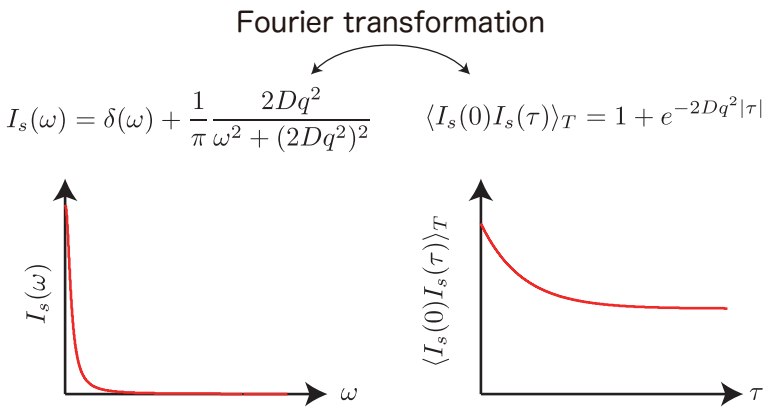

Figure 4.10: Wiener–Khintchin theorem

By using Eq.(4.1.2.48), let us calculate the time correlation function of scattered light intensity from the particles with Brownian motion. Let us use the power spectrum Eq.(4.1.2.45) as a starting point.

$$I_s(\omega) = \delta(\omega) + \frac{1}{\pi}\frac{2Dq^2}{\omega^2 + (2Dq^2)^2} \tag{4.1.2.49}$$

Here, delta function $\delta(\omega)$ is included to express DC component which has no relationship with the fluctuation of scattered light intensity [63]. By using Eq.(4.1.2.48), expression in time domain is obtained. [50]

$$\begin{aligned}\langle I_s(0)I_s(\tau)\rangle_T &= \frac{1}{2\pi}\int_{-\infty}^{\infty}\left(\delta(\omega) + \frac{1}{\pi}\frac{2Dq^2}{\omega^2 + (2Dq^2)^2}\right)e^{i\omega\tau}d\omega \\ &= 1 + e^{-2Dq^2|t|}\end{aligned} \tag{4.1.2.50}$$

In the case of time domain observation, measured time correlation function is fitted by exponential function, and diffusion constant D is estimated by using Eq.(4.1.2.50). In the case of heterodyne detection, power spectrum is governed by strong local oscillator.

$$I_s(\omega) \simeq \delta(\omega) \tag{4.1.2.51}$$

Corresponding time correlation function is:

$$\langle I_s(0)I_s(\tau)\rangle_T \simeq \frac{1}{2\pi}\int_{-\infty}^{\infty}\delta(\omega)e^{i\omega\tau}d\omega = 1 \tag{4.1.2.52}$$

Therefore, heterodyne detection is not useful in time domain. Next section, I explain the third detection scheme, partial heterodyne detection.

[50] Mathematically, time t is expressed as a form of absolute value. However, we measure only the region on $t > 0$. Therefore, the symbol of absolute value is usually omitted.

4.1.3 Partial heterodyne method

The total scattered electric field[51], $E(\vec{q},t)$, is represented by a summation of the scattered electric field from particles within a scattered volume, V:

$$E(\vec{q},t) = \sum_{j\in V}^{N} b_j \exp[i\vec{q}\cdot\vec{r}_j(t)] \tag{4.1.3.1}$$

where $\vec{q}$ is a wavevector, b_j is the amplitude of the electric field from the particle j,[52] $\vec{r_j}$ is the position of the particle j. In the case of non-ergodic media, $\vec{r}_j$ is decomposed to the two components; their fixed position, $\vec{R}_j$, and the displacements, $\vec{\Delta}_j(t)$:

$$\vec{r}_j(t) = \vec{R}_j + \vec{\Delta}_j(t) \tag{4.1.3.2}$$

$$\vec{R}_j = \langle\, \vec{r}_j(t)\,\rangle_T \tag{4.1.3.3}$$

$$\langle\, \vec{\Delta}_j(t)\,\rangle_T = 0 \tag{4.1.3.4}$$

Here, $\langle\cdots\rangle_T$ denotes time average.

Substitute Eq.(4.1.3.2) into Eq.(4.1.3.1):

$$\begin{aligned} E(\vec{q},t) &= \sum_{j\in V}^{N} b_j \exp[i\vec{q}\cdot\vec{R}_j]\exp[i\vec{q}\cdot\vec{\Delta}_j(t)] \\ &= \sum_{j\in V}^{N} b_j \exp[i\vec{q}\cdot\vec{R}_j](\exp[i\vec{q}\cdot\vec{\Delta}_j(t)] - w_j) + \sum_{j\in V}^{N} b_j \exp[i\vec{q}\cdot\vec{R}_j]w_j \\ &=: E_F(\vec{q},t) + E_C(\vec{q}) \end{aligned} \tag{4.1.3.5}$$

where

$$w_j := \langle\, \exp[i\vec{q}\cdot\vec{\Delta}_j(t)]\,\rangle_T \tag{4.1.3.6}$$

denotes the time average of the phase of the electric field from the particle j.

The first term of Eq.(4.1.3.5) is time- and position-dependent. Since the time-dependent part, $\exp[i\vec{q}\cdot\vec{\Delta}_j(t)] - w_j$, denotes the displacement from their average position, this term is zero-mean quantity. [53] We call this term as $E_F(\vec{q},t)$, a fluctuating component. The second term of Eq.(4.1.3.5) is position-dependent and time-independent. We call this term as $E_C(\vec{q},t)$, a constant component.

What we want to know is $g^{(2)}(\tau)-1$ of the scattered electric field from non-ergodic media like a gel. From now, we represent $g^{(2)}(\tau)-1$ in two different forms. $g^{(2)}(\tau)-1$ is written as follows:

$$\begin{aligned} g^{(2)}(\tau) - 1 &:= \frac{\langle\, I(\vec{q},0)I(\vec{q},\tau)\,\rangle_T}{\langle\, I(\vec{q})\,\rangle_T^2} - 1 \\ &= \frac{\langle\, I(\vec{q},0)I(\vec{q},\tau)\,\rangle_T - \langle\, I(\vec{q})\,\rangle_T^2}{\langle\, I(\vec{q})\,\rangle_T^2} \end{aligned} \tag{4.1.3.7}$$

[51] We ignore the vector nature of the electric field and treat it as scalar wave. In other words, we do not consider the polarization.

[52] In reality, b_j is $\vec{q}$-dependent. We omit $(\vec{q})$ for simplicity.

[53] If we assume that each particle shows restricted Brownian motion, this term is Gaussian.

where

$$I(\vec{q},\tau) := E^*(\vec{q},\tau)E(\vec{q},\tau) = |E(\vec{q},\tau)|^2 \tag{4.1.3.8}$$

is the intensity of scattered light at $t = \tau$.

By using Eqs.(4.1.3.5) and (4.1.3.8), a first term of the numerator of Eq.(4.1.3.7) is written as follows [54][55]:

$$\begin{aligned}
&\langle\, I(\vec{q},0)I(\vec{q},\tau)\,\rangle_T \\
&= \langle\, |E_F(0)+E_C|^2|E_F(\tau)+E_C|^2\,\rangle \\
&= \langle\, (E_F^2(0)+E_F^*(0)E_C+E_F(0)E_C^*+E_C^2)(E_F^2(\tau)+E_F^*(\tau)E_C+E_F(\tau)E_C^*+E_C^2)\,\rangle \\
&= \langle\, E_F^2(0)E_F^2(\tau)\,\rangle + I_C\langle\, E_F^2(0)\,\rangle + I_C\langle\, E_F^*(0)E_F(\tau)\,\rangle \\
&\quad + I_C\langle\, E_F(0)E_F^*(\tau)\,\rangle + I_C\langle\, E_F^2(\tau)\,\rangle + I_C^2 \\
&= \langle\, I_F(\vec{q},0)I_F(\vec{q},\tau)\,\rangle_T + 2I_C(\vec{q})\langle\, E_F(\vec{q},0)E_F^*(\vec{q},\tau)\,\rangle_T + 2\langle\, I_F(\vec{q})\,\rangle_T I_C(\vec{q}) + I_C^2(\vec{q})
\end{aligned} \tag{4.1.3.9}$$

The first term of Eq.(4.1.3.9) is rewritten to be:

$$\begin{aligned}
\langle\, I_F(\vec{q},0)I_F(\vec{q},\tau)\,\rangle_T &= \langle\, E_F^*(0)E_F(0)E_F^*(\tau)E_F(\tau)\,\rangle \\
&= \langle\, E_F^*(0)E_F(0)\,\rangle\langle\, E_F^*(\tau)E_F(\tau)\,\rangle \\
&\quad + \langle\, E_F^*(0)E_F^*(\tau)\,\rangle\langle\, E_F(0)E_F(\tau)\,\rangle + \langle\, E_F^*(0)E_F(\tau)\,\rangle\langle\, E_F(0)E_F^*(\tau)\,\rangle \\
&= \langle\, I_F(\vec{q})\,\rangle_T^2 + \langle\, E_F^*(\vec{q},0)E_F(\vec{q},\tau)\,\rangle_T^2
\end{aligned} \tag{4.1.3.10}$$

By definition (Eqs.(4.1.3.5)),

$$\begin{aligned}
&\langle\, E_F^*(\vec{q},0)E_F(\vec{q},\tau)\,\rangle_T \\
&= \sum_{j=1}^{N}\sum_{k=1}^{N} b_j^* b_k \exp[i\vec{q}\cdot(\vec{R}_k-\vec{R}_j)]\langle\,(\exp[-i\vec{q}\cdot\vec{\Delta}_j(0)]-w_j^*)(\exp[i\vec{q}\cdot\vec{\Delta}_k(\tau)]-w_k)\,\rangle_T \\
&= \sum_{j=1}^{N}\sum_{k=1}^{N} b_j^* b_k \exp[i\vec{q}\cdot(\vec{R}_k-\vec{R}_j)](\langle\,\exp[-i\vec{q}\cdot\vec{\Delta}_j(0)]\exp[i\vec{q}\cdot\vec{\Delta}_k(\tau)]\,\rangle_T \\
&\quad - w_k\langle\,\exp[-i\vec{q}\cdot\vec{\Delta}_j(0)]\,\rangle_T - w_j^*\langle\,\exp[i\vec{q}\cdot\vec{\Delta}_k(\tau)]\,\rangle_T + w_j^* w_k) \\
&= \sum_{j=1}^{N}\sum_{k=1}^{N} b_j^* b_k \exp[i\vec{q}\cdot(\vec{R}_k-\vec{R}_j)](\langle\,\exp[i\vec{q}\cdot(\vec{\Delta}_k(\tau)-\vec{\Delta}_j(0)]\,\rangle_T - w_k w_j^* - w_j^* w_k + w_j^* w_k) \\
&= \sum_{j=1}^{N}\sum_{k=1}^{N} b_j^* b_k \exp[i\vec{q}\cdot(\vec{R}_k-\vec{R}_j)](\langle\,\exp[i\vec{q}\cdot(\vec{\Delta}_k(\tau)-\vec{\Delta}_j(0)]\,\rangle_T - w_j^* w_k)
\end{aligned} \tag{4.1.3.11}$$

To proceed, let us define an intermediate scattering function, $F(\vec{q},\tau)$, as:

$$F(\vec{q},\tau) := \frac{1}{N\overline{b^2}}\sum_{j=1}^{N}\sum_{k=1}^{N}\langle\, b_j^* b_k \exp[i\vec{q}\cdot(\vec{r}_k(\tau)-\vec{r}_j(0))]\,\rangle_E \tag{4.1.3.12}$$

Notice that the average is taken as ensemble, not time.

[54] From here, we stop writing the explicit representation of the variable $(\vec{q})$ during calculations for simplicity.

[55] We regard $E^*E =: I$ although the prefactor is required. This does not matter since what we obtain is normalized quantity.

This function implies Fourier transformation of the probability distribution function, $G(\vec{R},\tau)$:

$$G(\vec{R},\tau) := \frac{1}{N\overline{b^2}}\sum_{j=1}^{N}\sum_{k=1}^{N}\langle\, b_j^* b_k \delta(\vec{R}-[\vec{r}_k(\tau)-\vec{r}_j(0)])\,\rangle_E \tag{4.1.3.13}$$

$$F(\vec{R},\tau) = \int d^3\vec{R} e^{i\vec{q}\cdot\vec{R}} G(\vec{R},\tau) \tag{4.1.3.14}$$

In the case where $\tau = 0$, $F(\vec{q},0)$ simply implies the ensemble average of scattered intensity. This is easily proved by substituting Eq.(4.1.3.1) into Eq.(4.1.3.8):

$$\begin{aligned}\langle\, I(\vec{q})\,\rangle_E &= \sum_{j=1}^{N}\sum_{k=1}^{N}\langle\, b_j^* b_k \exp[-i\vec{q}\cdot\vec{r_j}(0)]\exp[i\vec{q}\cdot\vec{r_k}(0)]\,\rangle_E \\ &= \sum_{j=1}^{N}\sum_{k=1}^{N}\langle\, b_j^* b_k \exp[i\vec{q}\cdot(\vec{r_k}-\vec{r_j})]\,\rangle_E = N\overline{b^2}F(\vec{q},0)\end{aligned} \tag{4.1.3.15}$$

Although $F(\vec{q},\tau)$ is ensemble average, we can connect this quantity to time average quantity. By substituting Eq.(4.1.3.2) into Eq.(4.1.3.12):

$$\begin{aligned}N\overline{b^2}F(\vec{q},\tau) &= \sum_{j=1}^{N}\sum_{k=1}^{N}\langle\, b_j^* b_k \exp[i\vec{q}\cdot(\vec{R}_k-\vec{R}_j)]\exp[i\vec{q}\cdot(\vec{\Delta}_k(\tau)-\vec{\Delta}_j(0)]\,\rangle_E \\ &= \sum_{j=1}^{N}\sum_{k=1}^{N}\langle\, b_j^* b_k \exp[i\vec{q}\cdot(\vec{R}_k-\vec{R}_j)]\langle\exp[i\vec{q}\cdot(\vec{\Delta}_k(\tau)-\vec{\Delta}_j(0)]\,\rangle_T\,\rangle_E\end{aligned} \tag{4.1.3.16}$$

From the first line to the second line, we assumed that $\vec{\Delta}_j$ and $\vec{\Delta}_k$ are time-independent. If the scattering volume is sufficiently large, $\langle\cdots\rangle_E$ is redundant:

$$N\overline{b^2}F(\vec{q},\tau) = \sum_{j=1}^{N}\sum_{k=1}^{N} b_j^* b_k \exp[i\vec{q}\cdot(\vec{R}_k-\vec{R}_j)]\langle\exp[i\vec{q}\cdot(\vec{\Delta}_k(\tau)-\vec{\Delta}_j(0)]\,\rangle_T \tag{4.1.3.17}$$

Then,

$$\begin{aligned}N\overline{b^2}F(\vec{q},\infty) &= \sum_{j=1}^{N}\sum_{k=1}^{N} b_j^* b_k \exp[i\vec{q}(\vec{R}_k-\vec{R}_j)]\langle\exp[-i\vec{q}\cdot\vec{\Delta}_j(0)]\,\rangle_T\langle\exp[i\vec{q}\cdot\vec{\Delta}_k(\infty)]\,\rangle_T \\ &= \sum_{j=1}^{N}\sum_{k=1}^{N} b_j^* b_k \exp[i\vec{q}(\vec{R}_k-\vec{R}_j)] w_j^* w_k\end{aligned} \tag{4.1.3.18}$$

Substitute Eqs.(4.1.3.15), (4.1.3.17) and (4.1.3.18) into Eq.(4.1.3.11):

$$\begin{aligned}\langle\, E_F^*(\vec{q},0)E_F(\vec{q},\tau)\,\rangle_T &= N\overline{b^2}(F(\vec{q},\tau)-F(\vec{q},\infty)) \\ &= \frac{\langle\, I(\vec{q})\,\rangle_E}{F(\vec{q},0)}(F(\vec{q},\tau)-F(\vec{q},\infty)) = \langle\, I(\vec{q})\,\rangle_E(f(\vec{q},\tau)-f(\vec{q},\infty))\end{aligned} \tag{4.1.3.19}$$

where $f(\vec{q},\tau)$ is a normalized intermediate scattering function:

$$f(\vec{q},\tau) := \frac{F(\vec{q},\tau)}{F(\vec{q},0)} \tag{4.1.3.20}$$

Substituting $\tau = 0$ into Eq.(4.1.3.19) shows the intensity from the fluctuating component:

$$\begin{aligned}\langle I_F(\vec{q})\rangle_T &= \langle E_F^*(\vec{q},0)E_F(\vec{q},0)\rangle_T \\ &= \langle I(\vec{q})\rangle_E(1-f(\vec{q},\infty))\end{aligned} \tag{4.1.3.21}$$

since by definition

$$f(\vec{q},0) = 1 \tag{4.1.3.22}$$

Substituting Eq.(4.1.3.19) and (4.1.3.21) into Eq.(4.1.3.10):

$$\langle I_F(\vec{q},0)I_F(\vec{q},\tau)\rangle_T = \langle I(\vec{q})\rangle_E^2[(1-f(\vec{q},\infty))^2 + (f(\vec{q},\tau)-f(\vec{q},\infty))^2] \tag{4.1.3.23}$$

Let us get back on the track. Our aim is to calculate Eq.(4.1.3.7). Substituting Eqs.(4.1.3.19) and (4.1.3.23) into the numerator of Eq.(4.1.3.7):

$$\begin{aligned}&\langle I(\vec{q},0)I(\vec{q},\tau)\rangle_T - \langle I(\vec{q})\rangle_T^2 \\ &= \langle I_F(\vec{q},0)I_F(\vec{q},\tau)\rangle_T + 2I_C(\vec{q})\langle E_F(\vec{q},0)E_F^*(\vec{q},\tau)\rangle_T + 2\langle I_F(\vec{q})\rangle_T I_C(\vec{q}) + I_C^2(\vec{q}) - \langle I(\vec{q})\rangle_T^2 \\ &= \langle I(\vec{q})\rangle_E^2[(1-f(\vec{q},\infty))^2 + (f(\vec{q},\tau)-f(\vec{q},\infty))^2] \\ &\quad + 2I_C(\vec{q})\langle I(\vec{q})\rangle_E(f(\vec{q},\tau)-f(\vec{q},\infty)) + 2\langle I_F(\vec{q})\rangle_T I_C(\vec{q}) + I_C^2(\vec{q}) - \langle I(\vec{q})\rangle_T^2 \\ &= \langle I(\vec{q})\rangle_E^2(f(\vec{q},\tau)-f(\vec{q},\infty))^2 + 2I_C(\vec{q})\langle I(\vec{q})\rangle_E(f(\vec{q},\tau)-f(\vec{q},\infty))\end{aligned} \tag{4.1.3.24}$$

By using Eq.(4.1.3.21), $I_C(\vec{q})$ is:

$$\begin{aligned}I_C(\vec{q}) &= \langle I(\vec{q})\rangle_T - \langle I_F(\vec{q})\rangle_T \\ &= \langle I(\vec{q})\rangle_T - \langle I(\vec{q})\rangle_E(1-f(\vec{q},\infty))\end{aligned} \tag{4.1.3.25}$$

Then,

$$\begin{aligned}&g^{(2)}(\tau) - 1 \\ &= \left(\frac{\langle I(\vec{q})\rangle_E}{\langle I(\vec{q})\rangle_T}\right)^2 (f(\vec{q},\tau)-f(\vec{q},\infty))^2 + 2\frac{\langle I(\vec{q})\rangle_E}{\langle I(\vec{q})\rangle_T}\frac{I_C(\vec{q})}{\langle I(\vec{q})\rangle_T}(f(\vec{q},\tau)-f(\vec{q},\infty)) \\ &= Y^2(f(\vec{q},\tau)-f(\vec{q},\infty))^2 + 2Y\frac{\langle I(\vec{q})\rangle_T - \langle I(\vec{q})\rangle_E(1-f(\vec{q},\infty))}{\langle I(\vec{q})\rangle_T}(f(\vec{q},\tau)-f(\vec{q},\infty)) \\ &= Y^2(f(\vec{q},\tau)-f(\vec{q},\infty))^2 + 2Y(f(\vec{q},\tau)-f(\vec{q},\infty)) - 2Y^2(1-f(\vec{q},\infty))(f(\vec{q},\tau)-f(\vec{q},\infty)) \\ &= Y^2(f(\vec{q},\tau)^2 - f(\vec{q},\infty)^2) + 2Y(1-Y)(f(\vec{q},\tau)-f(\vec{q},\infty))\end{aligned} \tag{4.1.3.26}$$

where

$$Y := \frac{\langle I(\vec{q})\rangle_E}{\langle I(\vec{q})\rangle_T} \tag{4.1.3.27}$$

Before going any further, we assume the following relationship:

$$f(\vec{q},\tau) \simeq 1 - D_N q^2\tau \quad \text{when } \tau \ll D_N q^2 \tag{4.1.3.28}$$

This is merely the short time expansion of $f(\vec{q},\tau)$. q^2-dependence comes from the assumption of Brownian

motion for a short time. However, the coefficient D_N has no physical meaning since $f(\vec{q},\tau)$ contains the effect of $E_C(\vec{q})$ which is totally coherent. This mixing is the origin of the name, "Partially Heterodyne Method."

What we want to know is the diffusion coefficient originated only from the fluctuating component:

$$f_f(\vec{q},\tau) := \frac{\langle E_F^*(\vec{q},0)E_F(\vec{q},\tau)\rangle_T}{\langle I_F(\vec{q})\rangle_T} \simeq 1 - Dq^2\tau \quad \text{when } \tau \ll Dq^2 \tag{4.1.3.29}$$

although this quantity cannot be measured directly because of the contamination of $E_C(\vec{q})$.

Let us move on to the calculation of $g^{(2)}(\tau)-1$ again. Substitute Eq.(4.1.3.28) into Eq.(4.1.3.26):

$$\begin{aligned} g^{(2)}(\tau)-1 &= Y^2((1-D_Nq^2\tau)^2 - f(\vec{q},\infty)^2) + 2Y(1-Y)((1-D_Nq^2\tau) - f(\vec{q},\infty)) \\ &=: \sigma_I^2 - 2D_NYq^2\tau + O(\tau^2) \\ &= \sigma_I^2\left(1 - 2\frac{D_NY}{\sigma_I^2}q^2\tau\right) + O(\tau^2) \\ &=: \sigma_I^2(1-2D_Aq^2\tau) + O(\tau^2) \end{aligned} \tag{4.1.3.30}$$

where

$$\sigma_I^2 := g^{(2)}(0) - 1 \tag{4.1.3.31}$$

$$D_A := \frac{D_NY}{\sigma_I^2} \tag{4.1.3.32}$$

σ_I^2 is calculated straightforwardly:

$$\sigma_I^2 := Y(1-f(\vec{q},\infty))(2-Y(1-f(\vec{q},\infty))) \tag{4.1.3.33}$$

Eq.(4.1.3.30) is one of the most important results. This equation shows that the time correlation function $g^{(2)}(\tau)-1$ from non-ergodic media like a gel decays linearly[56] when $\tau \ll 1$. In other words, what we can obtain from experiment is D_A. As mentioned above, what we want to know is D, the diffusion coefficient of fluctuating component (Eq.(4.1.3.29)). So let us find the relationship between D and D_A. At first, let us represent Eq.(4.1.3.7) in a different way. Substituting Eqs.(4.1.3.9), (4.1.3.10) and (4.1.3.25) into Eq.(4.1.3.7):

$$\begin{aligned} & g^{(2)}(\tau)-1 \\ &:= \frac{\langle I(\vec{q},0)I(\vec{q},\tau)\rangle_T}{\langle I(\vec{q})\rangle_T^2} - 1 \\ &= \frac{\langle I_F(\vec{q},0)I_F(\vec{q},\tau)\rangle_T + 2I_C(\vec{q})\langle E_F(\vec{q},0)E_F^*(\vec{q},\tau)\rangle_T + 2\langle I_F(\vec{q})\rangle_TI_C(\vec{q}) + I_C^2(\vec{q})}{\langle I(\vec{q})\rangle_T^2} - 1 \\ &= \frac{\langle I_F(\vec{q},0)I_F(\vec{q},\tau)\rangle_T + 2I_C(\vec{q})\langle E_F(\vec{q},0)E_F^*(\vec{q},\tau)\rangle_T + 2\langle I_F(\vec{q})\rangle_TI_C(\vec{q}) + I_C^2(\vec{q})}{\langle I(\vec{q})\rangle_T^2} \\ &\quad - \frac{(\langle I_F(\vec{q})\rangle_T + I_C(\vec{q}))^2}{\langle I(\vec{q})\rangle_T^2} \\ &= \frac{\langle I_F(\vec{q})\rangle_T^2 + \langle E_F^*(\vec{q},0)E_F(\vec{q},\tau)\rangle_T^2 + 2I_C(\vec{q})\langle E_F(\vec{q},0)E_F^*(\vec{q},\tau)\rangle_T - \langle I_F(\vec{q})\rangle_T^2}{\langle I(\vec{q})\rangle_T^2} \\ &= \frac{\langle E_F^*(\vec{q},0)E_F(\vec{q},\tau)\rangle_T^2 + 2I_C(\vec{q})\langle E_F(\vec{q},0)E_F^*(\vec{q},\tau)\rangle_T}{\langle I(\vec{q})\rangle_T^2} \end{aligned} \tag{4.1.3.34}$$

[56] If we treat Eq.(4.1.3.28) as exponential function, Eq.(4.1.3.30) may also shows exponential decay.

By substituting $\tau = 0$ and using Eqs.(4.1.3.21) and (4.1.3.31):

$$\sigma_I^2 = \frac{\langle I_F(\vec{q})\rangle_T^2 + 2I_C\langle I_F(\vec{q})\rangle_T}{\langle I(\vec{q})\rangle_T^2} \tag{4.1.3.35}$$

From Eqs.(4.1.3.25), (4.1.3.29), (4.1.3.34) and (4.1.3.35):

$$\begin{aligned}
&g^{(2)}(\tau) - \sigma_I^2 \\
&= \frac{\langle I_F(\vec{q})\rangle_T^2 f_f(\vec{q},\tau)^2 + 2I_C(\vec{q})\langle I_F(\vec{q})\rangle_T f_f(\vec{q},\tau)}{\langle I(\vec{q})\rangle_T^2} + 1 - \frac{\langle I_F(\vec{q})\rangle_T^2 + 2I_C(\vec{q})\langle I_F(\vec{q})\rangle_T}{\langle I(\vec{q})\rangle_T^2} \\
&= \frac{\langle I_F(\vec{q})\rangle_T^2 f_f(\vec{q},\tau)^2 + 2(\langle I(\vec{q})\rangle_T - \langle I_F(\vec{q})\rangle_T)\langle I_F(\vec{q})\rangle_T f_f(\vec{q},\tau) + \langle I(\vec{q})\rangle_T^2}{\langle I(\vec{q})\rangle_T^2} \\
&\quad + \frac{\langle I(\vec{q})\rangle_T^2 - 2\langle I(\vec{q})\rangle_T\langle I_F(\vec{q})\rangle_T - 2\langle I_F(\vec{q})\rangle_T^2}{\langle I(\vec{q})\rangle_T^2} \\
&= \left[(f_f(\vec{q},\tau) - 1)\frac{\langle I_F(\vec{q})\rangle_T}{\langle I(\vec{q})\rangle_T} + 1\right]^2
\end{aligned} \tag{4.1.3.36}$$

So,

$$(f_f(\vec{q},\tau) - 1)X + 1 = \sqrt{g^{(2)}(\tau) - \sigma_I^2} \tag{4.1.3.37}$$

where

$$X := \frac{\langle I_F(\vec{q})\rangle_T}{\langle I(\vec{q})\rangle_T} \tag{4.1.3.38}$$

Substitute $\tau \to \infty$ into Eq.(4.1.3.37):

$$-X + 1 = \sqrt{1 - \sigma_I^2} \quad \to \quad \sigma_I^2 = X(2 - X) \tag{4.1.3.39}$$

since

$$f_f(\vec{q},\infty) = 0 \tag{4.1.3.40}$$

$$g^{(2)}(\infty) = 1 \tag{4.1.3.41}$$

This can also be represented as follows:

$$1 - \sqrt{1 - \sigma_I^2} = X \tag{4.1.3.42}$$

Substituting Eqs.(4.1.3.29) and (4.1.3.39) into Eq.(4.1.3.34):

$$\begin{aligned}
g^{(2)}(\tau) - 1 &= \frac{\langle I_F(\vec{q})\rangle_T^2 f_f(\vec{q},\tau)^2 + 2(\langle I(\vec{q})\rangle_T - \langle I_F(\vec{q})\rangle_T)\langle I_F(\vec{q})\rangle_T f_f(\vec{q},\tau)}{\langle I(\vec{q})\rangle_T^2} \\
&= X^2 f_f(\vec{q},\tau)^2 + 2X(1-X) f_f(\vec{q},\tau) \\
&= X^2(1 - Dq^2\tau)^2 + 2X(1-X)(1 - Dq^2\tau) \\
&= (2X - X^2) - 2DXq^2\tau + O(\tau^2) \\
&= \sigma_I^2\left(1 - 2\frac{DX}{\sigma_I^2}q^2\tau\right) + O(\tau^2)
\end{aligned} \tag{4.1.3.43}$$

By comparing Eqs.(4.1.3.30) and (4.1.3.43), we can obtain the relationship between D and D_A:

$$D_A = \frac{X}{\sigma_I^2} D \tag{4.1.3.44}$$

By using Eq.(4.1.3.39):

$$D_A = \frac{D}{2 - X} = \frac{1 - \sqrt{1 - \sigma_I^2}}{\sigma_I^2} D \tag{4.1.3.45}$$

The coefficient of Eq.(4.1.3.45) is shown in Figure 4.11.

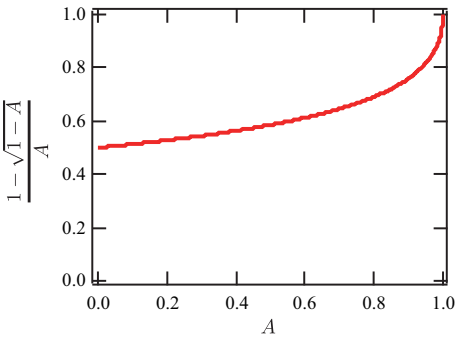

Figure 4.11: Coefficient of Eq.(4.1.3.45).

It is instructive to consider the extreme cases of Eq.(4.1.3.45). When the scattered media is ergodic, $X = 1$ since $\langle I_F(\vec{q}) \rangle_T = \langle I(\vec{q}) \rangle_T$ (Eq.(4.1.3.38)). Then, $D_A = D$. This is obvious since the detection is totally homodyne. Opposite extreme case is $X \to 0$, the media which is frozen. In this case, $D_A = D/2$. This is consistent with the representation of heterodyne detection since the local oscillator, $E_C(\vec{q})$ is sufficiently larger than $E_F(\vec{q}, t)$.

At the end, let us write Eq.(4.1.3.45) in another form to make an analysis easy [64]. Substituting Eq.(4.1.3.38) into Eq.(4.1.3.45):

$$D_A = \frac{D}{2 - (\langle I_F(\vec{q}) \rangle_T / \langle I(\vec{q}) \rangle_T)} \to \frac{\langle I(\vec{q}) \rangle_T}{D_A} = \frac{2}{D} \langle I(\vec{q}) \rangle_T - \frac{\langle I_F(\vec{q}) \rangle_T}{D} \tag{4.1.3.46}$$

4.1.4 Polarized dynamic light scattering

Eq.(4.1.1.42) shows that the polarization of scattered light is the same as the incident light if the scatterers are isotropic. If the scatterers are anisotropic, scattered light may contain polarized light whose polarization is orthogonal to the polarization of incident light. This light is called depolarized light. Polarized dynamic light scattering is a technique to measure the relaxation time of both polarized and depolarized light. Polarized light is measured by using two polarizers with the same direction (VV configuration) while depolarized light is measured with the polarizers which are orthogonal with each other (VH configuration). Experimental set up is shown in Figure 4.12. This technique is useful for the measurements of anisotropic substances such as rod-like solutes. It is reported that the relaxation rates obtained with VV and VH configurations for rod-like solutes are calculated as follows: [65]

$$\Gamma_{VV} = D_t q^2 \tag{4.1.4.1}$$

$$\Gamma_{VH} = D_t q^2 + 6D_r \tag{4.1.4.2}$$

where q is the magnitude of scattering vector, D_t is the translational diffusion coefficient and D_r is the rotational diffusion coefficient. Two diffusion constants, D_t and D_r, are related to the form of solutes as follows:

$$D_t = \frac{k_B T}{6\pi\eta_s a}\left[\ln\frac{2a}{b} + \ln 2 - 1\right] \tag{4.1.4.3}$$

$$D_r = \frac{3k_B T}{8\pi\eta_s a^3}\left[\frac{(\frac{a}{b})^2(\ln(\frac{a}{b}))^2}{(\frac{a}{b})^2(\ln(\frac{a}{b}) + \ln 2 - 1) + 0.651(\ln(\frac{a}{b}))^2}\right] \tag{4.1.4.4}$$

where k_B, T, η_s, a, b are Boltzmann constant, the absolute temperature, the viscosity of solvent, the half-length of solutes and radius of solutes, respectively. Here, D_t and D_r are functions of a and b. By using Eq.(4.1.4.4), we can estimate a and b and therefore aspect ratio by dynamic light scattering though the obtained value is rough estimation.

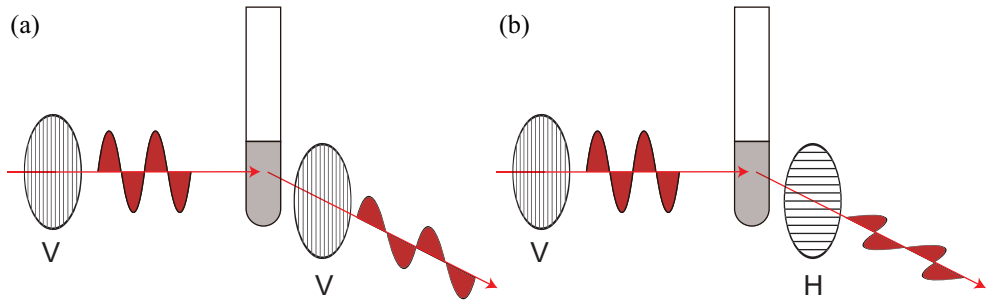

Figure 4.12: Polarized DLS by using conventional DLS system. (a) VV (polarized) and (b) VH (depolarized) configuration.

4.2 Neutron scattering

4.2.1 Basic theory of neutron scattering

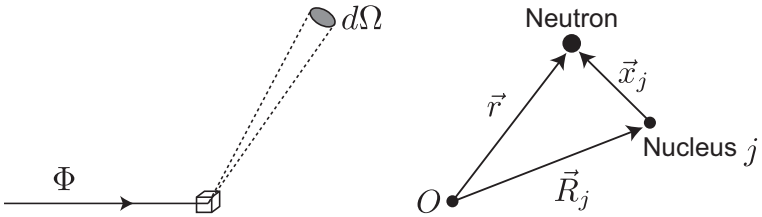

Figure 4.13: Coordination definitions for neutron scattering.

Let us define varying kinds of cross sections [14, 35]. Total scattering cross section is defined as follows:

$$\sigma_{tot} := \frac{\text{Total number of scattered neutrons in all directions per second}}{\Phi} \tag{4.2.1.1}$$

where Φ is the flux of the incident neutrons. This quantity is determined only by the species of atoms in the scattering volume and is not affected by the position of atoms.

The quantity of scattered neutrons is different as the scattering angle. Then, we define new cross section called differential scattering cross section as follows (See Fig.4.13, left.):

$$\frac{d\sigma}{d\Omega} := \frac{\text{The number of scattered neutrons into } d\Omega \text{ per second}}{\Phi d\Omega} \tag{4.2.1.2}$$

This quantity does not depend on the distance from the scattering system to the observed point since we use solid angle.

For the precise formulation of neutron scattering, we have to care the energy exchange between neutrons and the scattering system. To treat such a situation, we define another cross section called partial differential scattering cross section as follows:

$$\frac{d^2\sigma}{d\Omega dE'} := \frac{\text{The number of scattered neutrons into } d\Omega \text{ with final energy between } E' \text{ and } E'+dE' \text{ per second}}{\Phi d\Omega dE'} \tag{4.2.1.3}$$

These three cross sections are related in the form of integration:

$$\frac{d\sigma}{d\Omega} = \int_0^\infty \frac{d^2\sigma}{d\Omega dE'} dE' \tag{4.2.1.4}$$

$$\sigma_{tot} = \int \frac{d\sigma}{d\Omega} d\Omega \tag{4.2.1.5}$$

These cross sections have all of the information about neutron scattering. Our task is to relate these cross sections to the structural information. From now, we are going to derive the most general form of the partial differential scattering cross section [35]. Let us define $\vec{k}$ and λ as the wavevector and wavelength of the incident neutrons, respectively. Here, the wavevector is defined to have magnitude

$$k := \frac{2\pi}{\lambda} \tag{4.2.1.6}$$

and its direction being that of velocity, $\vec{v}$. Incident neutrons, the scattering system and the whole system

are represented by wavefunctions as $\psi_{\vec{k}}$, χ_λ and $\psi_{\vec{k}}\chi_\lambda$, respectively [57]. We assume that $\psi_{\vec{k}}$ is a plane wave and represented as follows:

$$\psi_{\vec{k}} := \frac{1}{\sqrt{Y}} e^{i\vec{k}\cdot\vec{r}} \tag{4.2.1.7}$$

Here we assume that there is one neutron in the box of volume Y. In this manner, we represent the flux of the incident neutrons, Φ, as follows[58]:

$$\Phi = \frac{v}{Y} = \frac{mv}{mY} = \frac{\hbar k}{Ym} \tag{4.2.1.8}$$

where m is the mass of a neutron.

Differential scattering cross section that the scattering system changes from λ to λ' is written as follows:

$$\left.\frac{d\sigma}{d\Omega}\right|_{\lambda\to\lambda'} = \frac{1}{\Phi}\frac{1}{d\Omega}\sum_{\vec{k}' \text{ in } d\Omega} W_{\vec{k},\lambda\to\vec{k}',\lambda'} \tag{4.2.1.9}$$

where $W_{\vec{k},\lambda\to\vec{k}',\lambda'}$ is the number of transitions per second from the state $\vec{k},\lambda$ to $\vec{k}',\lambda'$ (See Fig.4.14). By using Fermi's golden rule, $W_{\vec{k},\lambda\to\vec{k}',\lambda'}$ is represented as follows:

$$\sum_{\vec{k}' \text{ in } d\Omega} W_{\vec{k},\lambda\to\vec{k}',\lambda'} = \frac{2\pi}{\hbar}\rho_{\vec{k}'}\left|\int\int \chi^*_{\lambda'}\psi^*_{\vec{k}'} V \psi_{\vec{k}}\chi_\lambda d\vec{R}d\vec{r}\right|^2 \tag{4.2.1.10}$$

where $\vec{R}$ is the position of nucleus, $\vec{r}$ is the position of neutrons (See Fig.4.13, right.) and $\rho_{\vec{k}'}$ is the density of states,

$$\rho_{\vec{k}'} = \frac{Y}{(2\pi)^3}k'\frac{m}{\hbar^2}d\Omega \tag{4.2.1.11}$$

Substitute Eq.(4.2.1.7) into the integral part of Eq.(4.2.1.10):

$$\int\int \chi^*_{\lambda'}\psi^*_{\vec{k}'} V \psi_{\vec{k}}\chi_\lambda d\vec{R}d\vec{r} = \frac{1}{Y}\int\int \chi^*_{\lambda'} e^{-i\vec{k}'\cdot\vec{r}} V e^{i\vec{k}\cdot\vec{r}}\chi_\lambda d\vec{R}d\vec{r} =: \frac{1}{Y}\langle\vec{k}',\lambda'|V|\vec{k},\lambda\rangle \tag{4.2.1.12}$$

Substitute Eq.(4.2.1.8), (4.2.1.10), (4.2.1.11) and (4.2.1.12) into Eq.(4.2.1.9):

$$\left.\frac{d\sigma}{d\Omega}\right|_{\lambda\to\lambda'} = \frac{Ym}{\hbar k}\frac{1}{d\Omega}\frac{2\pi}{\hbar}\frac{Y}{(2\pi)^3}k'\frac{m}{\hbar^2}d\Omega\frac{1}{Y^2}|\langle\vec{k}',\lambda'|V|\vec{k},\lambda\rangle|^2 = \frac{k'}{k}\left(\frac{m}{2\pi\hbar^2}\right)^2|\langle\vec{k}',\lambda'|V|\vec{k},\lambda\rangle|^2 \tag{4.2.1.13}$$

The term k'/k in Eq.(4.2.1.13) implies that the scattering cross section increase as the density of states

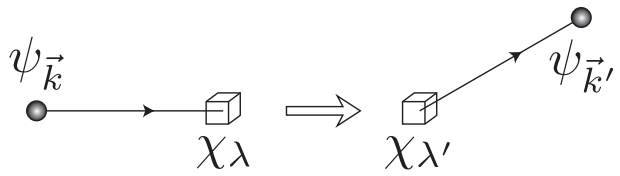

Figure 4.14: Definitions of wavefunctions. $\psi_{\vec{k}}, \psi_{\vec{k}'}, \chi_\lambda, \chi_{\lambda'}$ are wave functions of the neutron before scattering, of the neutron after scattering, of the scattering system before scattering and of the scattering system after scattering, respectively.

[57] From now, we denote these functions as $\vec{k}$, λ and $(\vec{k},\lambda)$, respectively.
[58] Flux $[\mathrm{m}^{-2}\cdot\mathrm{s}^{-1}]$ = density (Y^{-1}) $[\mathrm{m}^{-3}]$ × velocity (v) $[\mathrm{m}\cdot\mathrm{s}^{-1}]$.

increase (k') and decrease as the incident neutron becomes fast (k^{-1}).

In light of energy conservation law, we can express the partial differential scattering cross section as follows:

$$\left.\frac{d^2\sigma}{d\Omega dE'}\right|_{\lambda\to\lambda'} = \frac{k'}{k}\left(\frac{m}{2\pi\hbar^2}\right)^2 |\langle\vec{k}',\lambda'|V|\vec{k},\lambda\rangle|^2\delta(E_\lambda - E_{\lambda'} + E - E') \tag{4.2.1.14}$$

where $E_\lambda, E_{\lambda'}, E$ and E' indicates the energy of $\chi_\lambda, \chi_{\lambda'}, \psi_{\vec{k}}$ and $\psi_{\vec{k}'}$, respectively. Then we explicitly calculate the matrix elements in Eq.(4.2.1.14):

$$\begin{aligned}
\langle\vec{k}',\lambda'|V|\vec{k},\lambda\rangle &= \int\int \chi^*_{\lambda'} e^{-i\vec{k}'\cdot\vec{r}} V e^{-i\vec{k}\cdot\vec{r}} \chi_\lambda d\vec{R}d\vec{r} \\
&= \sum_j \int\int \chi^*_{\lambda'} e^{-i\vec{k}'\cdot\vec{r}} V_j(\vec{r}-\vec{R}_j) e^{-i\vec{k}\cdot\vec{r}} \chi_\lambda d\vec{R}_j d\vec{r} \\
&= \sum_j \int\int \chi^*_{\lambda'} e^{-i\vec{k}'\cdot(\vec{x}_j+\vec{R}_j)} V_j(\vec{x}_j) e^{-i\vec{k}\cdot(\vec{x}_j+\vec{R}_j)} \chi_\lambda d\vec{R}_j d\vec{x}_j \\
&= \sum_j \int V_j(\vec{x}_j) e^{i(\vec{k}-\vec{k}')\cdot\vec{x}_j} d\vec{x}_j \int \chi^*_{\lambda'} e^{i(\vec{k}-\vec{k}')\cdot\vec{R}_j} \chi_\lambda d\vec{R}_j \\
&= \sum_j V_j(\vec{q}) \langle\lambda'|e^{i\vec{q}\cdot\vec{R}_j}|\lambda\rangle
\end{aligned} \tag{4.2.1.15}$$

where $\vec{x}_j := \vec{r} - \vec{R}_j$ (Fig.4.13, right) and $\vec{q} := \vec{k} - \vec{k}'$. Here, $V_j(\vec{q})$ is the Fourier transform of the potential $V_j(\vec{x}_j)$:

$$V_j(\vec{q}) := \int V_j(\vec{x}_j) e^{i\vec{q}\cdot\vec{x}_j} d\vec{x}_j \tag{4.2.1.16}$$

$V_j(\vec{x}_j)$ is the potential at $\vec{r}$ caused by the nucleus j. In the case of neutron scattering, $V_j(\vec{x}_j)$ is assumed to be the following Fermi pseudopotential:

$$V_j(\vec{x}_j) = \frac{2\pi\hbar^2}{m} b_j \delta(\vec{x}_j) \tag{4.2.1.17}$$

where b_j is the scattering length of the atom at $\vec{R}_j$. This value is determined by their nuclear species and spin states. We treat the effect of neutron polarization on the scattering length in the next subsection. Substitute Eq.(4.2.1.17) into Eq.(4.2.1.16):

$$V_j(\vec{q}) = \frac{2\pi\hbar^2}{m} b_j \tag{4.2.1.18}$$

Substitute Eq.(4.2.1.15) and (4.2.1.18) into Eq.(4.2.1.14):

$$\left.\frac{d^2\sigma}{d\Omega dE'}\right|_{\lambda\to\lambda'} = \frac{k'}{k}\left|\sum_j b_j \langle\lambda'|e^{i\vec{q}\cdot\vec{R}_j}|\lambda\rangle\right|^2 \delta(E_\lambda - E_{\lambda'} + E - E') \tag{4.2.1.19}$$

This is the general form of the partial differential scattering cross section.

From now, we derive the thermal average of Eq.(4.2.1.19) by calculating the matrix elements. A delta function can be represented as the following integral form:

$$\delta(\omega) = \frac{1}{2\pi}\int_{-\infty}^{\infty} e^{i\omega t} dt = \frac{1}{2\pi}\int_{-\infty}^{\infty} e^{-i\omega t} dt \tag{4.2.1.20}$$

By using Eq.(4.2.1.20), the delta function in Eq.(4.2.1.19) is transformed into the following integral form:

$$\begin{aligned}\delta(E_\lambda - E_{\lambda'} + E - E') &=: \delta(\hbar(\omega_\lambda - \omega_{\lambda'} + \omega_i - \omega_f)) \\ &= \frac{1}{2\pi\hbar}\int_{-\infty}^{\infty} \exp[-i(\omega_\lambda - \omega_{\lambda'} + \omega_i - \omega_f)t]dt \\ &= \frac{1}{2\pi\hbar}\int_{-\infty}^{\infty} \exp\left[i\frac{E_{\lambda'} - E_\lambda}{\hbar}t\right] e^{-i\omega t}dt \end{aligned} \tag{4.2.1.21}$$

where

$$\omega := \omega_i - \omega_f \tag{4.2.1.22}$$

Substitute Eq.(4.2.1.21) into Eq.(4.2.1.19):

$$\begin{aligned}&\left.\frac{d^2\sigma}{d\Omega dE'}\right|_{\lambda\to\lambda'} \\ &= \frac{k'}{k}\sum_{j,j'} b_j b_{j'} \langle\lambda|e^{-i\vec{q}\cdot\vec{R}_{j'}}|\lambda'\rangle\langle\lambda'|e^{i\vec{q}\cdot\vec{R}_j}|\lambda\rangle \frac{1}{2\pi\hbar}\int_{-\infty}^{\infty} \exp\left[i\frac{E_{\lambda'} - E_\lambda}{\hbar}t\right] e^{-i\omega t}dt \\ &= \frac{k'}{k}\frac{1}{2\pi\hbar}\sum_{j,j'} b_j b_{j'} \int_{-\infty}^{\infty} \langle\lambda|e^{-i\vec{q}\cdot\vec{R}_{j'}}|\lambda'\rangle \left\langle\lambda'\left|\exp\left[i\frac{E_{\lambda'}}{\hbar}t\right] e^{i\vec{q}\cdot\vec{R}_j} \exp\left[-i\frac{E_\lambda}{\hbar}t\right]\right|\lambda\right\rangle e^{-i\omega t}dt \end{aligned} \tag{4.2.1.23}$$

We want to use the following closure relation:

$$\sum_{\lambda'}\langle\lambda|\hat{A}|\lambda'\rangle\langle\lambda'|\hat{B}|\lambda\rangle = \langle\lambda|\hat{A}\hat{B}|\lambda\rangle \tag{4.2.1.24}$$

To use this relation, the operator $\hat{A}$ and $\hat{B}$ should not depend on λ'. However, there is the term $E_{\lambda'}$ (the eigenvalue of the scattering system $\chi_{\lambda'}$) in Eq.(4.2.1.23). This problem is solved by using the following expression:

$$\exp\left[-i\frac{E_\lambda}{\hbar}t\right]\left|\lambda\right\rangle = \exp\left[-i\frac{\hat{\mathcal{H}}}{\hbar}t\right]\left|\lambda\right\rangle \tag{4.2.1.25}$$

$$\left\langle\lambda'\left|\exp\left[i\frac{E_{\lambda'}}{\hbar}t\right]\right. = \left\langle\lambda'\right|\exp\left[i\frac{\hat{\mathcal{H}}}{\hbar}t\right] \tag{4.2.1.26}$$

where $\hat{\mathcal{H}}$ is the Hamiltonian of the scattering system. Substitute Eq.(4.2.1.25) and (4.2.1.26) into Eq.(4.2.1.23):

$$\begin{aligned}\left.\frac{d^2\sigma}{d\Omega dE'}\right|_{\lambda\to\lambda'} &= \frac{k'}{k}\frac{1}{2\pi\hbar}\sum_{j,j'} b_j b_{j'} \int_{-\infty}^{\infty} \langle\lambda|e^{-i\vec{q}\cdot\vec{R}_{j'}}|\lambda'\rangle \left\langle\lambda'\left|\exp\left[i\frac{\hat{\mathcal{H}}}{\hbar}t\right] e^{i\vec{q}\cdot\vec{R}_j} \exp\left[-i\frac{\hat{\mathcal{H}}}{\hbar}t\right]\right|\lambda\right\rangle e^{-i\omega t}dt \\ &= \frac{k'}{k}\frac{1}{2\pi\hbar}\sum_{j,j'} b_j b_{j'} \int_{-\infty}^{\infty} \langle\lambda|e^{-i\vec{q}\cdot\vec{R}_{j'}(0)}|\lambda'\rangle\langle\lambda'|e^{i\vec{q}\cdot\vec{R}_j(t)}|\lambda\rangle e^{-i\omega t}dt \end{aligned} \tag{4.2.1.27}$$

Here we used the Heisenberg representation:

$$\exp\left[i\frac{\mathcal{H}}{\hbar}t\right] e^{i\vec{q}\cdot\vec{R}_j} \exp\left[-i\frac{\mathcal{H}}{\hbar}t\right] = e^{i\vec{q}\cdot\vec{R}_j(t)} \tag{4.2.1.28}$$

Notice that Schrödinger representation shows the same expression of Heisenberg representation at $t = 0$. Then we average the all initial states, $|\lambda\rangle$, and final states, $|\lambda'\rangle$. Let us assume that the initial states are in thermal equilibrium state. In this case, the probability that the initial state is $|\lambda\rangle$, p_λ, is represented as

follows (the Boltzmann distribution):

$$p_\lambda = \frac{e^{-E_\lambda \beta}}{\sum_\lambda e^{-E_\lambda \beta}} =: \frac{e^{-E_\lambda \beta}}{Z} \tag{4.2.1.29}$$

where $\beta := 1/k_B T$. By using Eq.(4.2.1.24) and (4.2.1.29), thermal average of Eq.(4.2.1.27) is [59]:

$$\begin{aligned}
\frac{d^2\sigma}{d\Omega dE'} &= \sum_{\lambda,\lambda'} p_\lambda \left.\frac{d^2\sigma}{d\Omega dE'}\right|_{\lambda\to\lambda'} \\
&= \frac{k'}{k}\frac{1}{2\pi\hbar}\sum_{j,j'} b_j b_{j'} \int_{-\infty}^{\infty} \sum_\lambda p_\lambda \langle\lambda| e^{-i\vec{q}\cdot\vec{R}_{j'}(0)} e^{i\vec{q}\cdot\vec{R}_j(t)} |\lambda\rangle e^{-i\omega t} dt \\
&= \frac{k'}{k}\frac{1}{2\pi\hbar}\sum_{j,j'} b_j b_{j'} \int_{-\infty}^{\infty} \langle e^{-i\vec{q}\cdot\vec{R}_{j'}(0)} e^{i\vec{q}\cdot\vec{R}_j(t)} \rangle e^{-i\omega t} dt
\end{aligned} \tag{4.2.1.30}$$

where $\langle\cdots\rangle$ denotes thermal average. Note that $e^{-i\vec{q}\cdot\vec{R}_{j'}(0)} e^{i\vec{q}\cdot\vec{R}_j(t)}$ is not necessarily the same as $e^{i\vec{q}\cdot(\vec{R}_j(t)-\vec{R}_{j'}(0))}$ since $\vec{R}_{j'}(0)$ and $\vec{R}_j(t)$ do not commute in general [60].

Then we separate Eq.(4.2.1.30) into two terms. Let us define the ensemble average of scattering length as follows:

$$\bar{b} := \sum_i f_i b_i \tag{4.2.1.31}$$

$$\overline{b^2} := \sum_i f_i b_i^2 \tag{4.2.1.32}$$

where f_i is the fraction of an atom which has the scattering length b_i. By using Eq.(4.2.1.31) and (4.2.1.32):

$$\begin{aligned}
&\sum_{j,j'} b_j b_{j'} \int_{-\infty}^{\infty} \langle e^{-i\vec{q}\cdot\vec{R}_{j'}(0)} e^{i\vec{q}\cdot\vec{R}_j(t)} \rangle e^{-i\omega t} dt \\
&= \sum_{j\neq j'} b_j b_{j'} \int_{-\infty}^{\infty} \langle e^{-i\vec{q}\cdot\vec{R}_{j'}(0)} e^{i\vec{q}\cdot\vec{R}_j(t)} \rangle e^{-i\omega t} dt + \sum_j b_j^2 \int_{-\infty}^{\infty} \langle e^{-i\vec{q}\cdot\vec{R}_j(0)} e^{i\vec{q}\cdot\vec{R}_j(t)} \rangle e^{-i\omega t} dt \\
&\to (\bar{b})^2 \sum_{j\neq j'} \int_{-\infty}^{\infty} \langle e^{-i\vec{q}\cdot\vec{R}_{j'}(0)} e^{i\vec{q}\cdot\vec{R}_j(t)} \rangle e^{-i\omega t} dt + \overline{b^2} \sum_j \int_{-\infty}^{\infty} \langle e^{-i\vec{q}\cdot\vec{R}_j(0)} e^{i\vec{q}\cdot\vec{R}_j(t)} \rangle e^{-i\omega t} dt \\
&\quad + (\bar{b})^2 \sum_j \int_{-\infty}^{\infty} \langle e^{-i\vec{q}\cdot\vec{R}_j(0)} e^{i\vec{q}\cdot\vec{R}_j(t)} \rangle e^{-i\omega t} dt - (\bar{b})^2 \sum_j \int_{-\infty}^{\infty} \langle e^{-i\vec{q}\cdot\vec{R}_j(0)} e^{i\vec{q}\cdot\vec{R}_j(t)} \rangle e^{-i\omega t} dt \\
&= (\bar{b})^2 \sum_{j,j'} \int_{-\infty}^{\infty} \langle e^{-i\vec{q}\cdot\vec{R}_{j'}(0)} e^{i\vec{q}\cdot\vec{R}_j(t)} \rangle e^{-i\omega t} dt + (\overline{b^2} - (\bar{b})^2) \sum_j \int_{-\infty}^{\infty} \langle e^{-i\vec{q}\cdot\vec{R}_j(0)} e^{i\vec{q}\cdot\vec{R}_j(t)} \rangle e^{-i\omega t} dt
\end{aligned} \tag{4.2.1.33}$$

[59] $p_{\lambda'}$ is already included as a form of $W_{\vec{k},\lambda\to\vec{k}',\lambda'}$.

[60] This can be proved as follows:

$$\begin{aligned}
e^{-i\vec{q}\cdot\vec{R}_{j'}(0)} e^{i\vec{q}\cdot\vec{R}_j(t)} &= \left(1 - i\vec{q}\cdot\vec{R}_{j'}(0) + \frac{1}{2}(-i\vec{q}\cdot\vec{R}_{j'}(0))^2 + \cdots\right)\left(1 + i\vec{q}\cdot\vec{R}_j(t) + \frac{1}{2}(i\vec{q}\cdot\vec{R}_j(t))^2 + \cdots\right) \\
&= 1 + i\vec{q}\cdot(\vec{R}_j(t) - \vec{R}_{j'}(0)) + \frac{1}{2}(2\vec{q}\cdot\vec{R}_{j'}(0)\vec{q}\cdot\vec{R}_j(t) - (\vec{q}\cdot\vec{R}_{j'}(0))^2 - (\vec{q}\cdot\vec{R}_j(t))^2) + \cdots \\
e^{i\vec{q}\cdot(\vec{R}_j(t)-\vec{R}_{j'}(0))} &= 1 + i\vec{q}\cdot(\vec{R}_j(t) - \vec{R}_{j'}(0)) + \frac{1}{2}(i\vec{q}\cdot(\vec{R}_j(t) - \vec{R}_{j'}(0)))^2 + \cdots \\
&= 1 + i\vec{q}\cdot(\vec{R}_j(t) - \vec{R}_{j'}(0)) + \frac{1}{2}(\vec{q}\cdot\vec{R}_j(t)\vec{q}\cdot\vec{R}_{j'}(0) + \vec{q}\cdot\vec{R}_{j'}(0)\vec{q}\cdot\vec{R}_j(t) - (\vec{q}\cdot\vec{R}_{j'}(0))^2 - (\vec{q}\cdot\vec{R}_j(t))^2) + \cdots
\end{aligned}$$

In general, $[\vec{R}_{j'}(0), \vec{R}_j(t)] = \vec{R}_{j'}(0)\cdot\vec{R}_j(t) - \vec{R}_j(t)\cdot\vec{R}_{j'}(0) \neq 0$. This means that

$$2\vec{q}\cdot\vec{R}_{j'}(0)\vec{q}\cdot\vec{R}_j(t) \neq \vec{q}\cdot\vec{R}_j(t)\vec{q}\cdot\vec{R}_{j'}(0) + \vec{q}\cdot\vec{R}_{j'}(0)\vec{q}\cdot\vec{R}_j(t)$$

so $e^{-i\vec{q}\cdot\vec{R}_{j'}(0)} e^{i\vec{q}\cdot\vec{R}_j(t)} \neq e^{-i\vec{q}\cdot(\vec{R}_j(t)-\vec{R}_{j'}(0))}$ in general.

Here, we used the relationship that $\sum_{j,j'} b_j b_{j'} = (\bar{b})^2$ since b_j and $b_{j'}$ are independent. Substitute Eq.(4.2.1.33) into Eq.(4.2.1.30):

$$\frac{d^2\sigma}{d\Omega dE'} = \frac{k'}{k}\frac{1}{2\pi\hbar}(\bar{b})^2 \sum_{j,j'} \int_{-\infty}^{\infty} \langle e^{-i\vec{q}\cdot\vec{R}_{j'}(0)} e^{i\vec{q}\cdot\vec{R}_j(t)} \rangle e^{-i\omega t} dt + \frac{k'}{k}\frac{1}{2\pi\hbar}(\overline{b^2} - (\bar{b})^2) \sum_{j} \int_{-\infty}^{\infty} \langle e^{-i\vec{q}\cdot\vec{R}_j(0)} e^{i\vec{q}\cdot\vec{R}_j(t)} \rangle e^{-i\omega t} dt \tag{4.2.1.34}$$

We define the following cross section [61]:

$$\sigma_{coh} := 4\pi(\bar{b})^2 \tag{4.2.1.35}$$

$$\sigma_{inc} := 4\pi(\overline{b^2} - (\bar{b})^2) \tag{4.2.1.36}$$

Substitute Eq.(4.2.1.35) and (4.2.1.36) into Eq.(4.2.1.34):

$$\frac{d^2\sigma}{d\Omega dE'} = \frac{k'}{k}\frac{1}{2\pi\hbar}\frac{\sigma_{coh}}{4\pi} \sum_{j,j'} \int_{-\infty}^{\infty} \langle e^{-i\vec{q}\cdot\vec{R}_{j'}(0)} e^{i\vec{q}\cdot\vec{R}_j(t)} \rangle e^{-i\omega t} dt + \frac{k'}{k}\frac{1}{2\pi\hbar}\frac{\sigma_{inc}}{4\pi} \sum_{j} \int_{-\infty}^{\infty} \langle e^{-i\vec{q}\cdot\vec{R}_j(0)} e^{i\vec{q}\cdot\vec{R}_j(t)} \rangle e^{-i\omega t} dt \tag{4.2.1.37}$$

The first term of Eq.(4.2.1.37) is called coherent scattering:

$$\left.\frac{d^2\sigma}{d\Omega dE'}\right|_{coh} := \frac{k'}{k}\frac{1}{2\pi\hbar}\frac{\sigma_{coh}}{4\pi} \sum_{j,j'} \int_{-\infty}^{\infty} \langle e^{-i\vec{q}\cdot\vec{R}_{j'}(0)} e^{i\vec{q}\cdot\vec{R}_j(t)} \rangle e^{-i\omega t} dt \tag{4.2.1.38}$$

And second term is called incoherent scattering:

$$\left.\frac{d^2\sigma}{d\Omega dE'}\right|_{inc} := \frac{k'}{k}\frac{1}{2\pi\hbar}\frac{\sigma_{inc}}{4\pi} \sum_{j} \int_{-\infty}^{\infty} \langle e^{-i\vec{q}\cdot\vec{R}_j(0)} e^{i\vec{q}\cdot\vec{R}_j(t)} \rangle e^{-i\omega t} dt \tag{4.2.1.39}$$

[61] 4π is total solid angle for a sphere. This formulation is useful when we consider the total scattering cross section. For example, let us consider the total scattering cross section of Eq.(4.2.1.54):

$$\left.\frac{d\sigma}{d\Omega}\right|_{inc}^{sa} = \frac{\sigma_{inc}}{4\pi} N$$
$$\rightarrow \sigma_{tot} = \int \left.\frac{d\sigma}{d\Omega}\right|_{inc}^{sa} d\Omega = N\sigma_{inc}$$

This formulation gives us the clear physical meaning of σ_{inc}; Total scattering cross section is the sum of σ_{inc}.

Here, we define the following six functions:

$$I(\vec{q},t) := \frac{1}{N}\sum_{j,j'}\langle e^{-i\vec{q}\cdot\vec{R}_{j'}(0)}e^{i\vec{q}\cdot\vec{R}_j(t)}\rangle \tag{4.2.1.40}$$

$$I_s(\vec{q},t) := \frac{1}{N}\sum_{j}\langle e^{-i\vec{q}\cdot\vec{R}_{j}(0)}e^{i\vec{q}\cdot\vec{R}_j(t)}\rangle \tag{4.2.1.41}$$

$$G(\vec{r},t) := \frac{1}{(2\pi)^3}\int I(\vec{q},t)e^{-i\vec{q}\cdot\vec{r}}d\vec{q} = \frac{1}{(2\pi)^3}\frac{1}{N}\int\sum_{j,j'}\langle e^{-i\vec{q}\cdot\vec{R}_{j'}(0)}e^{i\vec{q}\cdot\vec{R}_j(t)}\rangle e^{-i\vec{q}\cdot\vec{r}}d\vec{q} \tag{4.2.1.42}$$

$$G_s(\vec{r},t) := \frac{1}{(2\pi)^3}\int I_s(\vec{q},t)e^{-i\vec{q}\cdot\vec{r}}d\vec{q} = \frac{1}{(2\pi)^3}\frac{1}{N}\int\sum_{j}\langle e^{-i\vec{q}\cdot\vec{R}_{j}(0)}e^{i\vec{q}\cdot\vec{R}_j(t)}\rangle e^{-i\vec{q}\cdot\vec{r}}d\vec{q} \tag{4.2.1.43}$$

$$S(\vec{q},\omega) := \frac{1}{2\pi\hbar}\int I(\vec{q},t)e^{-i\omega t}dt = \frac{1}{2\pi\hbar}\frac{1}{N}\int\sum_{j,j'}\langle e^{-i\vec{q}\cdot\vec{R}_{j'}(0)}e^{i\vec{q}\cdot\vec{R}_j(t)}\rangle e^{-i\omega t}dt \tag{4.2.1.44}$$

$$S_i(\vec{q},\omega) := \frac{1}{2\pi\hbar}\int I_s(\vec{q},t)e^{-i\omega t}dt = \frac{1}{2\pi\hbar}\frac{1}{N}\int\sum_{j}\langle e^{-i\vec{q}\cdot\vec{R}_{j}(0)}e^{i\vec{q}\cdot\vec{R}_j(t)}\rangle e^{-i\omega t}dt \tag{4.2.1.45}$$

where N is the number of molecules in the irradiated volume. Notice that $I_s(\vec{q},t)$ is similar to the self-intermediate scattering function defined by Eq.(4.1.2.14) [62]. $G_s(\vec{r},t)$ is similar to Eq.(4.1.2.15) (Fig.4.7). By using Eq.(4.2.1.44) and (4.2.1.45), we can represent Eq.(4.2.1.38) and (4.2.1.39) as follows:

$$\left.\frac{d^2\sigma}{d\Omega dE'}\right|_{coh} := \frac{\sigma_{coh}}{4\pi}\frac{k'}{k}NS(\vec{q},\omega) \tag{4.2.1.46}$$

$$\left.\frac{d^2\sigma}{d\Omega dE'}\right|_{inc} := \frac{\sigma_{inc}}{4\pi}\frac{k'}{k}NS_i(\vec{q},\omega) \tag{4.2.1.47}$$

Most of the quasi-elastic neutron scattering techniques measure $S(\vec{q},\omega)$ and $S_i(\vec{q},\omega)$ while neutron spin echo technique measures $I(\vec{q},t)$ and $I_s(\vec{q},t)$ as shown later.

Cross sections Eq.(4.2.1.38) and (4.2.1.39) are composed of time dependent quantities. However, some measurements such as small-angle neutron scattering do not care about the time dependence. From now, we derive more brief formulation of neutron scattering. Our starting point is the thermal average of Eq.(4.2.1.19):

$$\frac{d^2\sigma}{d\Omega dE'} = \sum_\lambda p_\lambda\sum_{\lambda'}\left.\frac{d^2\sigma}{d\Omega dE'}\right|_{\lambda\to\lambda'} = \frac{k'}{k}\sum_\lambda p_\lambda\sum_{\lambda'}\left|\sum_j b_j\langle\lambda'|e^{i\vec{q}\cdot\vec{R}_j}|\lambda\rangle\right|^2\delta(E_\lambda - E_{\lambda'} + E - E') \tag{4.2.1.48}$$

Now we decompose the matrix elements into the coherent and incoherent term:

$$\begin{aligned}\left|\sum_j b_j\langle\lambda'|e^{i\vec{q}\cdot\vec{R}_j}|\lambda\rangle\right|^2 &= \sum_{j\neq j'} b_j b_{j'}\langle\lambda|e^{-i\vec{q}\cdot\vec{R}_{j'}}|\lambda'\rangle\langle\lambda'|e^{i\vec{q}\cdot\vec{R}_j}|\lambda\rangle + \sum_j b_j^2|\langle\lambda'|e^{i\vec{q}\cdot\vec{R}_j}|\lambda\rangle|^2 \\ &\to (\bar{b})^2\sum_{j\neq j'}\langle\lambda|e^{-i\vec{q}\cdot\vec{R}_{j'}}|\lambda'\rangle\langle\lambda'|e^{i\vec{q}\cdot\vec{R}_j}|\lambda\rangle + \overline{b^2}\sum_j|\langle\lambda'|e^{i\vec{q}\cdot\vec{R}_j}|\lambda\rangle|^2 \\ &\quad + (\bar{b})^2\sum_j|\langle\lambda'|e^{i\vec{q}\cdot\vec{R}_j}|\lambda\rangle|^2 - (\bar{b})^2\sum_j|\langle\lambda'|e^{i\vec{q}\cdot\vec{R}_j}|\lambda\rangle|^2 \\ &= (\bar{b})^2\left|\sum_j\langle\lambda'|e^{i\vec{q}\cdot\vec{R}_j}|\lambda\rangle\right|^2 + (\overline{b^2} - (\bar{b})^2)\sum_j|\langle\lambda'|e^{i\vec{q}\cdot\vec{R}_j}|\lambda\rangle|^2\end{aligned} \tag{4.2.1.49}$$

[62] Notice that $\vec{r}_j$ in Eq.(4.1.2.14) implies the position of an atom and $\vec{R}_j$ in Eq.(4.2.1.41) implies the position of a nucleus.

Substitute Eq.(4.2.1.49) into Eq.(4.2.1.48):

$$\begin{aligned}\frac{d^2\sigma}{d\Omega dE'} &= \frac{\sigma_{coh}}{4\pi}\frac{k'}{k}\sum_{\lambda}p_\lambda\sum_{\lambda'}\left|\sum_j\langle\lambda'|e^{i\vec{q}\cdot\vec{R}_j}|\lambda\rangle\right|^2\delta(E_\lambda - E_{\lambda'} + E - E') \\ &+ \frac{\sigma_{inc}}{4\pi}\frac{k'}{k}\sum_{\lambda}p_\lambda\sum_{\lambda'}\sum_j|\langle\lambda'|e^{i\vec{q}\cdot\vec{R}_j}|\lambda\rangle|^2\delta(E_\lambda - E_{\lambda'} + E - E') \\ &=: \left.\frac{d^2\sigma}{d\Omega dE'}\right|_{coh} + \left.\frac{d^2\sigma}{d\Omega dE'}\right|_{inc} \end{aligned} \tag{4.2.1.50}$$

Now we apply the method called static approximation. In this approximation, we assume that the energy transfer is negligible [63]. Under this approximation, $k = k'$ and $E_\lambda = E_{\lambda'}$:

$$\begin{aligned}\left.\frac{d^2\sigma}{d\Omega dE'}\right|^{sa}_{coh} &\to \frac{\sigma_{coh}}{4\pi}\sum_{\lambda}p_\lambda\sum_{\lambda'}\left|\sum_j\langle\lambda'|e^{i\vec{q}\cdot\vec{R}_j}|\lambda\rangle\right|^2\delta(E - E') \\ &= \frac{\sigma_{coh}}{4\pi}\sum_{\lambda}p_\lambda\sum_{\lambda'}\sum_{j,j'}\langle\lambda|e^{-i\vec{q}\cdot\vec{R}_{j'}}|\lambda'\rangle\langle\lambda'|e^{i\vec{q}\cdot\vec{R}_j}|\lambda\rangle\delta(E - E') \\ &= \frac{\sigma_{coh}}{4\pi}\sum_{\lambda}p_\lambda\sum_{j,j'}\langle\lambda|e^{-i\vec{q}\cdot(\vec{R}_j - \vec{R}_{j'})}|\lambda\rangle\delta(E - E') \end{aligned} \tag{4.2.1.51}$$

Here, we used the closure relation, Eq.(4.2.1.24)[64]. Then integrate with respect to E' and substitute Eq.(4.2.1.40):

$$\left.\frac{d\sigma}{d\Omega}\right|^{sa}_{coh} := \int\left.\frac{d^2\sigma}{d\Omega dE'}\right|^{sa}_{coh}dE' = \frac{\sigma_{coh}}{4\pi}\sum_{j,j'}\langle e^{i\vec{q}\cdot(\vec{R}_j - \vec{R}_{j'})}\rangle = \frac{\sigma_{coh}}{4\pi}NI(\vec{q},0) \tag{4.2.1.52}$$

Similarly, apply the static approximation to incoherent part:

$$\begin{aligned}\left.\frac{d^2\sigma}{d\Omega dE'}\right|^{sa}_{inc} &\to \frac{\sigma_{inc}}{4\pi}\sum_{\lambda}p_\lambda\sum_{\lambda'}\sum_j|\langle\lambda'|e^{i\vec{q}\cdot\vec{R}_j}|\lambda\rangle|^2\delta(E - E') \\ &= \frac{\sigma_{inc}}{4\pi}\sum_{\lambda}p_\lambda\sum_{\lambda'}\sum_j\langle\lambda|e^{-i\vec{q}\cdot\vec{R}_j}|\lambda'\rangle\langle\lambda'|e^{i\vec{q}\cdot\vec{R}_j}|\lambda\rangle\delta(E - E') \\ &= \frac{\sigma_{inc}}{4\pi}\sum_{\lambda}p_\lambda N\delta(E - E') \end{aligned} \tag{4.2.1.53}$$

Then integrate with respect to E':

$$\left.\frac{d\sigma}{d\Omega}\right|^{sa}_{inc} := \int\left.\frac{d^2\sigma}{d\Omega dE'}\right|^{sa}_{inc}dE' = \frac{\sigma_{inc}}{4\pi}N \tag{4.2.1.54}$$

These simple formulations are valid when we do not care the energy transfer. These are also derived from classical calculation. The amplitude of the scattering wave from an atom whose position is $\vec{R}_j$ is represented as follows [14]:

$$A_j(\vec{q},t) = A_0 b_j e^{i(\omega t - \vec{q}\cdot\vec{R}_j)} \tag{4.2.1.55}$$

[63] In strict derivation, $\delta(\omega)$ is expanded like Eq.(4.2.1.20). Through this transformation, t is appeared in the formulation.
[64] Notice that E' does not depend on the state $|\lambda'\rangle$ in this approximation since $E_\lambda = E_{\lambda'}$.

b_j is determined by a type of nucleus and called scattering length, which is the same as that in Eq.(4.2.1.17). Notice that we ignore the time-dependence of $\vec{R}_j$. Then, total amplitude from an irradiated volume is the sum of Eq.(4.2.1.55) whose $\vec{R}$ is within the irradiated volume:

$$A(\vec{q},t) = A_0 \sum_j b_j e^{i(\omega t - \vec{q}\cdot\vec{R}_j)} \tag{4.2.1.56}$$

The flux of scattering wave, J, is a square of the total amplitude:

$$J(\vec{q}) = A^*(\vec{q},t)A(\vec{q},t) = A_0^2 \sum_{j,j'} b_j b_{j'} e^{-i\vec{q}\cdot(\vec{R}_j - \vec{R}_{j'})} \tag{4.2.1.57}$$

The differential scattering cross section is a normalized quantity of J:

$$\begin{aligned}
\frac{d\sigma}{d\Omega} = \frac{J(\vec{q})}{A_0^2} &= (\bar{b})^2 \sum_{j\neq j'} e^{-i\vec{q}\cdot(\vec{R}_j - \vec{R}_{j'})} + \overline{b^2} \sum_j 1 \\
&= (\bar{b})^2 \sum_{j\neq j'} e^{-i\vec{q}\cdot(\vec{R}_j - \vec{R}_{j'})} + \overline{b^2} \sum_j 1 + (\bar{b})^2 \sum_j 1 - (\bar{b})^2 \sum_j 1 \\
&= (\bar{b})^2 \sum_{j,j'} e^{-i\vec{q}\cdot(\vec{R}_j - \vec{R}_{j'})} + (\overline{b^2} - (\bar{b})^2)N \\
&= \frac{\sigma_{coh}}{4\pi} N I(\vec{q},0) + \frac{\sigma_{inc}}{4\pi} N
\end{aligned} \tag{4.2.1.58}$$

Here, we assume that b_j is independent from other atoms. This result is the same as the static approximation of strict derivation (Eq.(4.2.1.52) and (4.2.1.54)).

4.2.2 Small-angle neutron scattering

In the case of small-angle neutron scattering, phase difference of scattered wave originated from close atoms (around 1 Å) becomes very small (Figure 4.15). In this case, instead of one atom, we can regard one monomer as a scatterer. Here, scattering length, b (Table 4.1), is averaged over the volume of the monomer, $\Delta\rho v_n$. For example, the scattering length density of H_2O is calculated as follows.

$$\Delta\rho = \frac{\sum b}{\text{mol. density}} = \frac{(2\times(-3.7390)+5.803)\times10^{-15}\ \text{m}}{(18.0\ \text{g mol}^{-1}\ /\ 6.02214\times10^{23}\ \text{g mol}^{-1})/1.00\ \text{g cm}^{-3}} = -5.61\times10^{9}\ \text{cm}^{-2} \tag{4.2.2.1}$$

The scattering length density of several representative materials are shown in Table 4.2. By using the mixture of hydrated and deuterated solvent, we can tune the scattering length density of solvents as shown in Figure 4.16. This is one of the characteristic feature of neutron scattering.

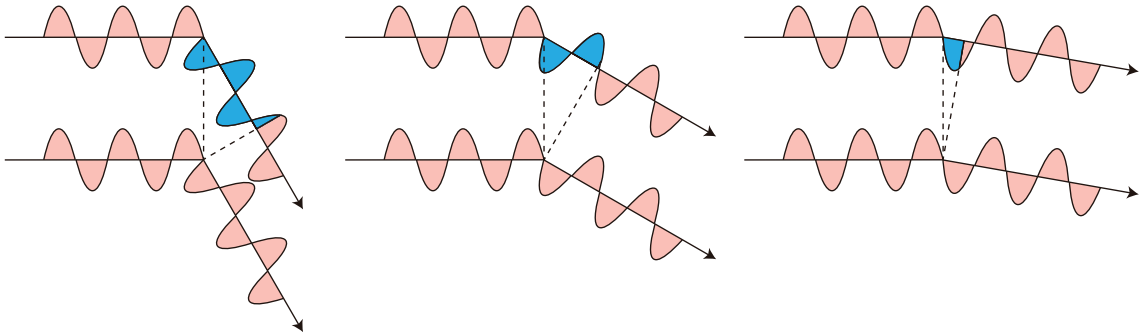

Figure 4.15: Relationship between phase difference and scattering angle.

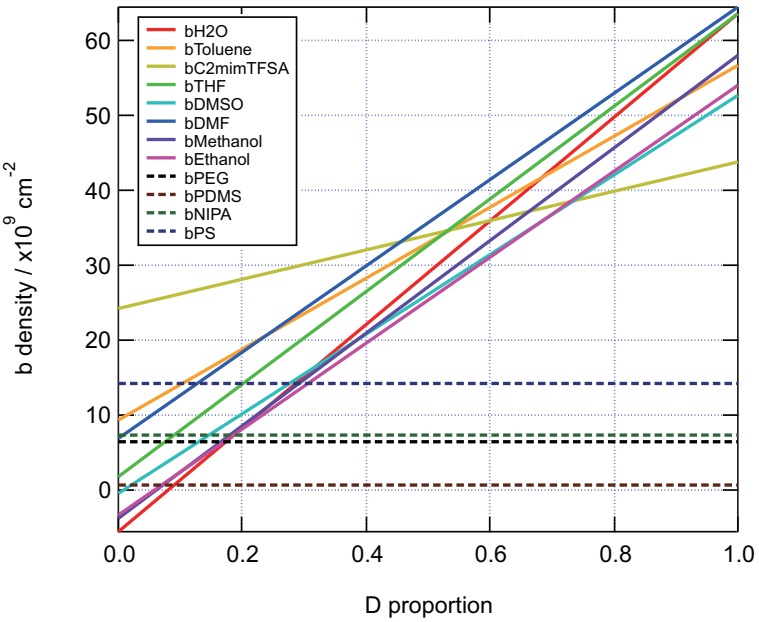

Figure 4.16: Effect of deuteration of solvent on their scattering length density. As a reference, scattering length densities of some polymers (not deuterated one) are also shown.

Table 4.1: List of scattering length [66]

Atom	b_{coh} / fm	b_{inc} / fm
H	-3.7390	—
^{1}H	-3.7406	25.274
^{2}H	6.671	4.04
C	6.6460	—
N	9.36	—
O	5.803	—
F	5.654	—
Si	4.1491	—
S	2.847	—

Table 4.2: List of scattering length density

Substance	Chemical formula	Density / g cm^{-3}	$\Delta\rho$ / $\times 10^9$ cm^{-2}
Water	H_2O	1.00	-5.60
Deuterated water	D_2O	1.1044	63.6
Methanol	CH_4O	0.7918	-3.73
Ethanol	C_2H_6O	0.789	-3.44
Toluene	C_7H_8	0.8669	9.41
THF	C_4H_8O	0.89	1.84
DMSO	C_2H_6OS	1.1004	-0.417
DMF	C_3H_7NO	0.944	6.94
[C_2mim][TFSA]	$C_8H_{11}N_3O_4F_6S_2$	1.53	24.2
PS	C_8H_8	1.05	14.1
PEG	C_2H_4O	1.13	6.40
PDMS	C_2H_6OSi	0.965	0.635
PNIPA	$C_6H_{11}NO$	—	7.4

4.2.3 Scattering by polarized neutrons

Until now, we do not care about spin. In general, neutrons and nuclei have their own spin. For example, a neutron has spin 1/2, a nucleus of hydrogen has spin 1/2, a nucleus of deuterium has spin 1 and so on. Although the manipulation of nuclei spin is difficult, we can choose the spin of neutrons by using appropriate apparatus such as a supermirror. Neutrons whose spin state is determined are called polarized. From now, we see the result of scattering from polarized neutrons.

Neutrons have spin $S = 1/2$. Let us assume that the nuclei have spin I. The quantum state of neutrons and nuclei are described as follows:

$$|S, s_z\rangle = |1/2, 1/2\rangle,\ |1/2, -1/2\rangle \tag{4.2.3.1}$$

$$|I, I_z\rangle = |I, I\rangle,\ |I, I-1\rangle,\ \ldots,\ |I, -I\rangle \tag{4.2.3.2}$$

Operators for these eigenstates are defined as follows:

$$\hat{S}^2|S, s_z\rangle = S(S+1)\hbar^2|S, s_z\rangle \tag{4.2.3.3}$$

$$\hat{S}_z|S, s_z\rangle = s_z\hbar|S, s_z\rangle \tag{4.2.3.4}$$

$$\hat{I}^2|I, I_z\rangle = I(I+1)\hbar^2|I, I_z\rangle \tag{4.2.3.5}$$

$$\hat{I}_z|I, I_z\rangle = I_z\hbar|I, I_z\rangle \tag{4.2.3.6}$$

To determine the wavefunction of the whole system, $\psi_{\vec{k}}\chi_\lambda$, now we have to designate the total spin of the

system, t. Since neutrons have spin 1/2, whole system is classified as up one and down one:

$$\hat{t}\,|+\rangle := \left(I + \frac{1}{2}\right)|+\rangle \tag{4.2.3.7}$$

$$\hat{t}\,|-\rangle := \left(I - \frac{1}{2}\right)|-\rangle \tag{4.2.3.8}$$

where $\hat{t}$ is the operator for the whole system:

$$\hat{t} := \hat{I} + \hat{S} \tag{4.2.3.9}$$

and $|+\rangle$ and $|-\rangle$ is the representation of whole system:

$$|S, s_z, I, I_z\rangle = \begin{cases} |1/2, 1/2, I, I_z\rangle =: |+\rangle \\ |1/2, -1/2, I, I_z\rangle =: |-\rangle \end{cases}$$

To consider the effect of polarization, we have to assume that the scattering length becomes an operator whose eigenvalue is the scattering length. This is because the scattering length depends on the spin state of neutrons and nuclei. From now, we derive the formulation of $\hat{b}$ such that:

$$\hat{b}\,|+\rangle = b^+\,|+\rangle \tag{4.2.3.10}$$

$$\hat{b}\,|-\rangle = b^-\,|-\rangle \tag{4.2.3.11}$$

Let us see the operator $\hat{t^2}$: [65]

$$\hat{t^2} = \hat{I^2} + \hat{S^2} + 2\hat{I}\cdot\hat{S} \tag{4.2.3.12}$$

Except for $\hat{I}\cdot\hat{S}$, we can calculate the eigenvalues of each term:

$$\hat{t^2}\,|+\rangle = \left(I + \frac{1}{2}\right)\left(I + \frac{3}{2}\right)\hbar^2\,|+\rangle \tag{4.2.3.13}$$

$$\hat{t^2}\,|-\rangle = \left(I - \frac{1}{2}\right)\left(I + \frac{1}{2}\right)\hbar^2\,|-\rangle \tag{4.2.3.14}$$

$$\hat{I^2}\,|+\rangle = I(I+1)\hbar^2\,|+\rangle \tag{4.2.3.15}$$

$$\hat{I^2}\,|-\rangle = I(I+1)\hbar^2\,|-\rangle \tag{4.2.3.16}$$

$$\hat{S^2}\,|+\rangle = \frac{3}{4}\hbar^2\,|+\rangle \tag{4.2.3.17}$$

$$\hat{S^2}\,|-\rangle = \frac{3}{4}\hbar^2\,|-\rangle \tag{4.2.3.18}$$

From Eq.(4.2.3.12) $\sim$ (4.2.3.18), we can derive the eigenvalue of $\hat{I}\cdot\hat{S}$:

$$2\hat{I}\cdot\hat{S}\,|+\rangle = (\hat{t^2} - \hat{I^2} - \hat{S^2})\,|+\rangle = I\hbar^2\,|+\rangle \tag{4.2.3.19}$$

$$2\hat{I}\cdot\hat{S}\,|-\rangle = (\hat{t^2} - \hat{I^2} - \hat{S^2})\,|-\rangle = -(I+1)\hbar^2\,|-\rangle \tag{4.2.3.20}$$

[65] Note that $\hat{I}$ and $\hat{S}$ commute.

By using the operator $\hat{I}\cdot\hat{S}$, let us define $\hat{b}$ as follows:

$$\hat{b} := A + B\hat{I}\cdot\hat{S} \tag{4.2.3.21}$$

where A and B are the constants which we determine. Both $|+\rangle$ and $|-\rangle$ are the eigenfunction of this operator:

$$\hat{b}\,|+\rangle = b^+\,|+\rangle = \left(A + B\frac{I\hbar^2}{2}\right)|+\rangle \tag{4.2.3.22}$$

$$\hat{b}\,|-\rangle = b^-\,|-\rangle = \left(A - B\frac{(I+1)\hbar^2}{2}\right)|-\rangle \tag{4.2.3.23}$$

Solve Eq.(4.2.3.22) and (4.2.3.23) for A and B:

$$A = \frac{1}{2I+1}((I+1)b^+ + Ib^-) \tag{4.2.3.24}$$

$$B = \frac{2}{(2I+1)\hbar^2}(b^+ - b^-) \tag{4.2.3.25}$$

Substitute Eq.(4.2.3.24) and (4.2.3.25) into Eq.(4.2.3.21):

$$\hat{b} = \frac{1}{2I+1}((I+1)b^+ + Ib^-) + \frac{2}{(2I+1)\hbar^2}(b^+ - b^-)\hat{I}\cdot\hat{S} \tag{4.2.3.26}$$

Let us consider the physical meaning of A. From Eq.(4.2.3.7) and (4.2.3.8), we can see that the number of states is $(I+1/2)\times 2+1 = 2I+2$ for $|+\rangle$ and $(I-1/2)\times 2+1 = 2I$ for $|-\rangle$. Take the number of state into account, we can write the average scattering length as A (Eq.(4.2.3.24)).

By using Eq.(4.2.3.26), we can calculate the spin-dependent scattering. Our starting point is Eq.(4.2.1.19). Here, $|\lambda\rangle$ is modified as $|\sigma,\lambda\rangle$ where σ implies the spin state of neutrons, $|\uparrow\rangle$ ($s_z = 1/2$) or $|\downarrow\rangle$ ($s_z = -1/2$). In addition to this, scattering length is modified as the operator ($b_j \to \hat{b_j}$)[66]:

$$\begin{aligned}\left.\frac{d^2\sigma}{d\Omega dE'}\right|_{\sigma,\lambda\to\sigma',\lambda'} &= \frac{k'}{k}\left|\sum_j \hat{b_j}\langle\sigma',\lambda'|e^{i\vec{q}\cdot\vec{R}_j}|\sigma,\lambda\rangle\right|^2 \delta(E_\lambda - E_{\lambda'} + E - E') \\ &= \frac{k'}{k}\left|\sum_j \langle\lambda'|e^{i\vec{q}\cdot\vec{R}_j}\langle\sigma'|\hat{b_j}|\sigma\rangle|\lambda\rangle\right|^2 \delta(E_\lambda - E_{\lambda'} + E - E')\end{aligned} \tag{4.2.3.27}$$

The effect of spin is appeared only in the term $\langle\sigma'|\hat{b_j}|\sigma\rangle$. From now, we evaluate this term. Let us calculate the eigenvalue of $|\uparrow\rangle$ for $\hat{b}$ by using Eq.(4.2.3.21):

$$\begin{aligned}\hat{b}\,|\uparrow\rangle &= (A + B(\hat{I}_x\hat{S}_x + \hat{I}_y\hat{S}_y + \hat{I}_z\hat{S}_z))\,|\uparrow\rangle \\ &= A\,|\uparrow\rangle + \frac{\hbar}{2}B\hat{I}_z\,|\uparrow\rangle + \frac{\hbar}{2}B(\hat{I}_x + i\hat{I}_y)\,|\downarrow\rangle\end{aligned} \tag{4.2.3.28}$$

$$\begin{aligned}\hat{b}\,|\downarrow\rangle &= (A + B(\hat{I}_x\hat{S}_x + \hat{I}_y\hat{S}_y + \hat{I}_z\hat{S}_z))\,|\downarrow\rangle \\ &= A\,|\downarrow\rangle - \frac{\hbar}{2}B\hat{I}_z\,|\downarrow\rangle + \frac{\hbar}{2}B(\hat{I}_x - i\hat{I}_y)\,|\downarrow\rangle\end{aligned} \tag{4.2.3.29}$$

[66] b_j does not relate to $|\lambda\rangle$ and $|\lambda'\rangle$ since we do not consider the magnetic scattering.

Here, we used the following relationship:

$$\hat{S}_x \,|\uparrow\rangle = \frac{\hbar}{2}\,|\downarrow\rangle \tag{4.2.3.30}$$

$$\hat{S}_x \,|\downarrow\rangle = \frac{\hbar}{2}\,|\uparrow\rangle \tag{4.2.3.31}$$

$$\hat{S}_y \,|\uparrow\rangle = i\frac{\hbar}{2}\,|\downarrow\rangle \tag{4.2.3.32}$$

$$\hat{S}_y \,|\downarrow\rangle = -i\frac{\hbar}{2}\,|\uparrow\rangle \tag{4.2.3.33}$$

$$\hat{S}_z \,|\uparrow\rangle = \frac{\hbar}{2}\,|\uparrow\rangle \tag{4.2.3.34}$$

$$\hat{S}_z \,|\downarrow\rangle = -\frac{\hbar}{2}\,|\downarrow\rangle \tag{4.2.3.35}$$

By using Eq.(4.2.3.28) and (4.2.3.29), four matrix elements are calculated as follows:

$$\langle\uparrow|\,\hat{b}\,|\uparrow\rangle = A + \frac{\hbar}{2}B\hat{I}_z \tag{4.2.3.36}$$

$$\langle\downarrow|\,\hat{b}\,|\uparrow\rangle = \frac{\hbar}{2}B(\hat{I}_x + i\hat{I}_y) \tag{4.2.3.37}$$

$$\langle\downarrow|\,\hat{b}\,|\downarrow\rangle = A - \frac{\hbar}{2}B\hat{I}_z \tag{4.2.3.38}$$

$$\langle\uparrow|\,\hat{b}\,|\downarrow\rangle = \frac{\hbar}{2}B(\hat{I}_x - i\hat{I}_y) \tag{4.2.3.39}$$

Notice that $|\uparrow\rangle$ and $|\downarrow\rangle$ are orthogonal.

From now, we average those matrix elements over the all nuclear spin states and isotopes. We write $\langle\cdots\rangle_{sp}$ for nuclear spin average and $\langle\cdots\rangle_{iso}$ for isotope average. We assume that the nuclear spin is randomly oriented:

$$\langle I_x\rangle_{sp} = \langle I_y\rangle_{sp} = \langle I_z\rangle_{sp} = 0 \tag{4.2.3.40}$$

For non spin-flip process:

$$\langle\langle\langle\uparrow|\,\hat{b}\,|\uparrow\rangle\rangle_{sp}\rangle_{iso} = \langle\langle\langle\downarrow|\,\hat{b}\,|\downarrow\rangle\rangle_{sp}\rangle_{iso} = \langle A\rangle_{iso} \tag{4.2.3.41}$$

For spin-flip process:

$$\langle\langle\langle\downarrow|\,\hat{b}\,|\uparrow\rangle\rangle_{sp}\rangle_{iso} = \langle\langle\langle\uparrow|\,\hat{b}\,|\downarrow\rangle\rangle_{sp}\rangle_{iso} = 0 \tag{4.2.3.42}$$

Substitute (4.2.3.41) and (4.2.3.42) into Eq.(4.2.1.35), we can apply the previous results to the case of polarized neutron scattering. For non spin-flip process:

$$\sigma_{coh}^{\uparrow\uparrow} = \sigma_{coh}^{\downarrow\downarrow} = 4\pi\langle A\rangle_{iso}^2 \tag{4.2.3.43}$$

For spin-flip process:

$$\sigma_{coh}^{\downarrow\uparrow} = \sigma_{coh}^{\uparrow\downarrow} = 0 \tag{4.2.3.44}$$

These results show that there is no spin-flip process for coherent scattering.

Then we calculate the cross section for incoherent scattering. What we have to calculate is $\overline{b^2}$. Since we assume that the nuclear spin is randomly oriented:

$$\langle I_x^2\rangle_{sp} = \langle I_y^2\rangle_{sp} = \langle I_z^2\rangle_{sp} = \frac{1}{3}I(I+1)\hbar^2 \tag{4.2.3.45}$$

Notice that the eigenvalue of $|+\rangle$ and $|-\rangle$ for $\hat{I}^2$ is $I(I+1)\hbar^2$ (Eq.(4.2.3.15) and (4.2.3.16)). By using Eq.(4.2.3.40) and (4.2.3.45), $\overline{b^2}$ for each process is calculated as follows:

$$\langle\langle|\langle\uparrow|\hat{b}|\uparrow\rangle|^2\rangle_{sp}\rangle_{iso} = \langle\langle A^2 + \frac{\hbar^2}{4}B^2I_z^2 + \hbar ABI_z\rangle_{sp}\rangle_{iso} = \langle A^2\rangle_{iso} + \frac{\hbar^4}{4}\frac{1}{3}\langle B^2I(I+1)\rangle_{iso} \tag{4.2.3.46}$$

$$\langle\langle|\langle\downarrow|\hat{b}|\uparrow\rangle|^2\rangle_{sp}\rangle_{iso} = \langle\langle\frac{\hbar^2}{4}B^2(I_x^2+I_y^2)\rangle_{sp}\rangle_{iso} = \frac{\hbar^4}{4}\frac{2}{3}\langle B^2I(I+1)\rangle_{iso} \tag{4.2.3.47}$$

$$\langle\langle|\langle\downarrow|\hat{b}|\downarrow\rangle|^2\rangle_{sp}\rangle_{iso} = \langle A^2\rangle_{iso} + \frac{\hbar^4}{4}\frac{1}{3}\langle B^2I(I+1)\rangle_{iso} \tag{4.2.3.48}$$

$$\langle\langle|\langle\uparrow|\hat{b}|\downarrow\rangle|^2\rangle_{sp}\rangle_{iso} = \frac{\hbar^4}{4}\frac{2}{3}\langle B^2I(I+1)\rangle_{iso} \tag{4.2.3.49}$$

Then let us substitute Eq.(4.2.3.41), (4.2.3.42), (4.2.3.46) $\sim$ (4.2.3.49) into Eq.(4.2.1.36). For non spin-flip process:

$$\sigma_{inc}^{\uparrow\uparrow} = \sigma_{inc}^{\downarrow\downarrow} = 4\pi\left(\langle A^2\rangle_{iso} - \langle A\rangle_{iso}^2 + \frac{\hbar^4}{4}\frac{1}{3}\langle B^2I(I+1)\rangle_{iso}\right) \tag{4.2.3.50}$$

For spin-flip process:

$$\sigma_{inc}^{\downarrow\uparrow} = \sigma_{inc}^{\uparrow\downarrow} = 4\pi\frac{\hbar^4}{4}\frac{2}{3}\langle B^2I(I+1)\rangle_{iso} \tag{4.2.3.51}$$

If the nuclei in the scattering system has $I = 0$, there is also no spin-flip process for incoherent scattering. A hydrogen atom is the most strong incoherent scatterer in the polymer system. If we do not use deuterium substitution, there is only one isotope in the polymer: ^{1}H ($I = 1/2$). In this case:

$$\langle A^2\rangle_{iso} = \langle A\rangle_{iso}^2 \quad \text{when there is only one isotope} \tag{4.2.3.52}$$

This means that:

$$\sigma_{inc}(\text{non spin-flip}) = \frac{1}{2}\sigma_{inc}(\text{spin-flip}) \tag{4.2.3.53}$$

This result implies that the incoherent scattering weaken the signal of neutron spin echo.

4.2.4 Neutron spin echo

Neutron spin echo technique is developed by F. Mezei in 1972 [67]. From now, we see the principle of neutron spin echo [68]. In the later section, I introduce the instrumentation of neutron spin echo.

Assume that the neutron spin is considered to be the classical vector quantity. When the spin $\vec{S}$ is in the magnetic field $\vec{B}$, this spin precesses around the field direction since this spin feels the torque $\vec{N}$ (Fig.4.17):

$$\vec{N} = \vec{S} \times \vec{B} \tag{4.2.4.1}$$

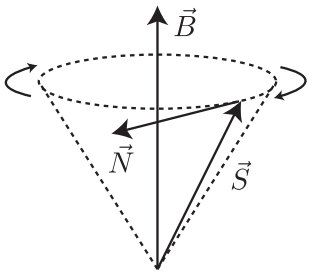

Figure 4.17: Precession of spin.

This precession is called Larmor precession. Larmor precession angle in a second is given by:

$$\gamma_L |\vec{B}| \tag{4.2.4.2}$$

where γ_L is called gyromagnetic ratio.

Let us consider the case where a neutron goes through in a homogeneous magnetic field $\vec{B}_1$ called precession field. By using the neutron's velocity, v, and the length of the precession field, l_1, we can calculate the total precession angle, φ:

$$\varphi = \gamma_L |\vec{B}_1| \frac{l_1}{v} \tag{4.2.4.3}$$

After this precession, we again make this neutron go thorough in the different precession field $\vec{B}_2$ whose direction[67] is oppose to $\vec{B}_1$. The length of the field is l_2. Then the total precession angle is:

$$\varphi = \gamma_L |\vec{B}_1| \frac{l_1}{v} - \gamma_L |\vec{B}_2| \frac{l_2}{v} \tag{4.2.4.4}$$

When the following relation is achieved, the total precession angle is zero:

$$|\vec{B}_1| l_1 = |\vec{B}_2| l_2 \tag{4.2.4.5}$$

This condition is called "spin echo condition" (Fig.4.18). Notice that the velocity of neutrons is not included in Eq.(4.2.4.5). This means that the total spin of polarized neutrons is precisely recovered after going through the two precession fields regardless of their velocity. Notice that the total spin becomes zero after passing the first precession field since the precession angle has broad distribution corresponding to their velocity. This recover is the phenomenon called neutron spin echo.

[67] In the case of the neutron spin echo experiment, the direction of the two precession fields are the same as mentioned later. Instead of this, the spin itself is rotated 180°.

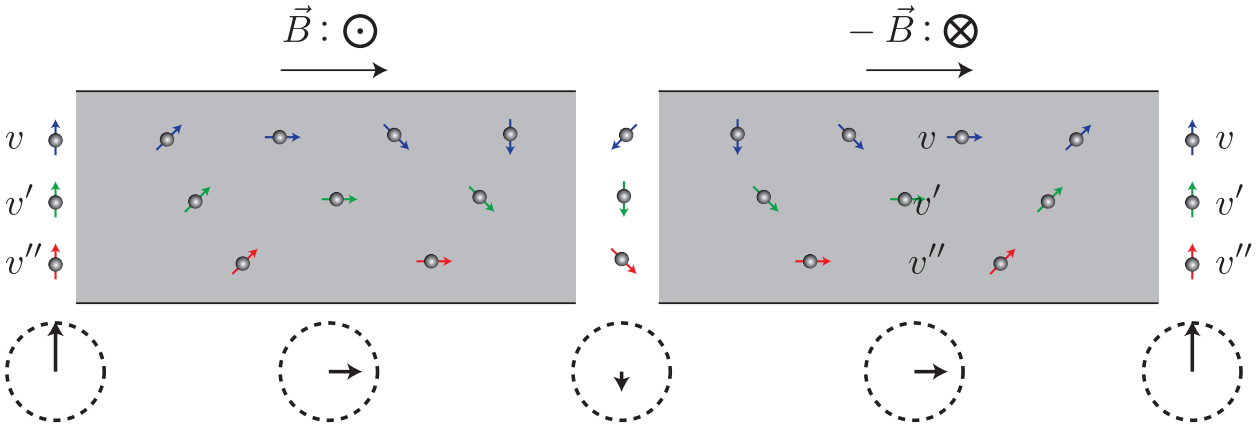

Figure 4.18: Concept of neutron spin echo. Here, we assume that $v < v' < v''$. Total spin of neutrons becomes small by the first precession field. However, second precession field reverse the spin of neutrons. As a result, total spin recovers completely after the second precession field.

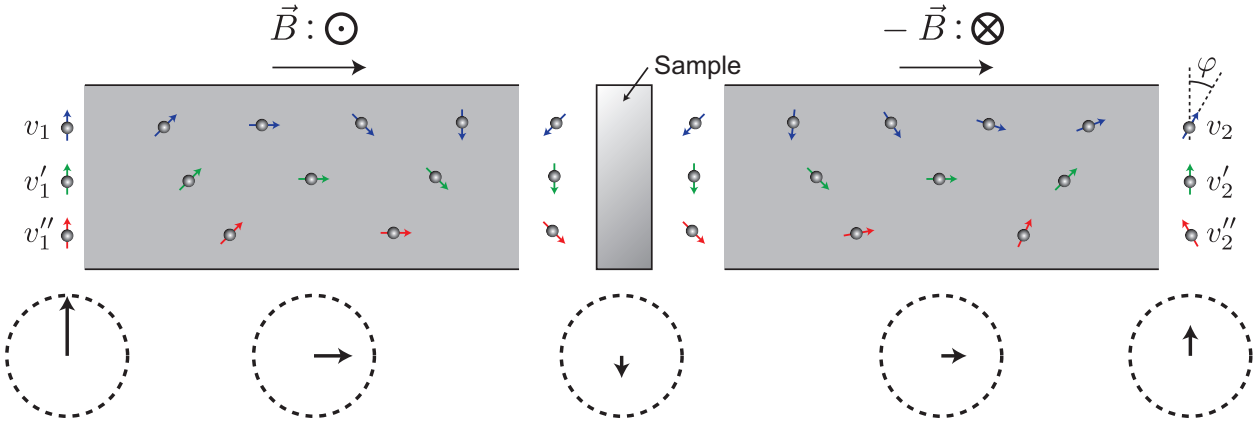

Figure 4.19: Disturbance of spin echo in the case of quasi-elastic scattering. Here, we assume that $v_1 < v_2 < v_1' = v_2' < v_2'' < v_1''$. Since a slow neutron ($v_1$) is accelerated, the time in the second precession field is shorter than that of the first precession field. As a result, the spin of the slow neutron does not go back to the original direction. Similar to this, the spin of a fast neutron (v_1'') overruns the original direction.

Neutron spin echo spectrometer utilizes this phenomenon to obtain high resolution quasi-elastic neutron scattering data. When the neutron after passing the first precession field is scattered quasi-elastically, the velocity is slightly changed. As a result, neutron spin echo becomes incomplete (Fig.4.19). Here, we assume that the spin does not change by scattering[68]. In this case, the total precession angle is written as:

$$\varphi = \gamma_L |\vec{B}_1| \frac{l_1}{v_1} - \gamma_L |\vec{B}_2| \frac{l_2}{v_2} \tag{4.2.4.6}$$

where v_1 is the velocity in the first precession field and v_2 is that in the second precession field.

We can relate this velocity change to the energy transfer, $\hbar\omega$, by the following equation:

$$\hbar\omega = \frac{m_n(v_2^2 - v_1^2)}{2} \tag{4.2.4.7}$$

[68] If we consider the change of the neutron spin, we should use the relation derived in the previous subsection. We treat this issue at the end of this subsection.

where m_n is the mass of a neutron.

Since what we obtain from the neutron spin echo experiment is φ, our aim is to relate φ to ω. From now, we demonstrate that the deviation of φ from its average value is proportional to the deviation of ω under a certain condition, not Eq.(4.2.4.5).

Although Eq.(4.2.4.7) is valid for each neutron, each neutron has different initial velocity, v_1. From now, we divide each φ and ω into the two components: the average value and the deviation:

$$\varphi = \overline{\varphi} + \delta\varphi \tag{4.2.4.8}$$

$$\omega = \overline{\omega} + \delta\omega \tag{4.2.4.9}$$

where

$$\overline{\varphi} := \gamma_L|\vec{B}_1|\frac{l_1}{\overline{v_1}} - \gamma_L|\vec{B}_2|\frac{l_2}{\overline{v_2}} \tag{4.2.4.10}$$

$$\overline{\omega} := \frac{m_n(\overline{v_2}^2 - \overline{v_1}^2)}{2\hbar} \tag{4.2.4.11}$$

$\delta\varphi$ and $\delta\omega$ differ from one neutron to another. First, we represent $\delta\varphi$ as a function of $\delta v_1 := v_1 - \overline{v_1}$ and $\delta v_2 := v_2 - \overline{v_2}$. We use the following Taylor expansion:

$$(1+\delta)^{-1} = 1 - \delta + \delta^2 - \delta^3 + \cdots \tag{4.2.4.12}$$

Then φ can be expanded as follows:

$$\begin{aligned}
\varphi &= \gamma_L|\vec{B}_1|\frac{l_1}{\overline{v_1} + \delta v_1} - \gamma_L|\vec{B}_2|\frac{l_2}{\overline{v_2} + \delta v_2} \\
&= \gamma_L|\vec{B}_1|l_1\left(\frac{1}{\overline{v_1}} - \frac{\delta v_1}{\overline{v_1}^2}\right) - \gamma_L|\vec{B}_2|l_2\left(\frac{1}{\overline{v_2}} - \frac{\delta v_2}{\overline{v_2}^2}\right) + O((\delta v)^2) \\
&= \overline{\varphi} - \frac{\gamma_L|\vec{B}_1|l_1}{\overline{v_1}^2}\delta v_1 + \frac{\gamma_L|\vec{B}_2|l_2}{\overline{v_2}^2}\delta v_2 + O((\delta v)^2)
\end{aligned} \tag{4.2.4.13}$$

Similarly, ω can be expanded as follows:

$$\begin{aligned}
\omega &= \frac{m_n}{2\hbar}((\overline{v_2} + \delta v_2)^2 - (\overline{v_1} + \delta v_1)^2) \\
&= \frac{m_n}{2\hbar}(\overline{v_2}^2 + 2\overline{v_2}\delta v_2 - \overline{v_1}^2 - 2\overline{v_1}\delta v_2) + O((\delta v)^2) \\
&= \overline{\omega} - \frac{m_n}{\hbar}\overline{v_1}\delta v_1 + \frac{m_n}{\hbar}\overline{v_2}\delta v_2 + O((\delta v)^2)
\end{aligned} \tag{4.2.4.14}$$

By substituting Eq.(4.2.4.13), (4.2.4.14) into Eq.(4.2.4.8), (4.2.4.9):

$$\delta\varphi \simeq -\frac{\gamma_L|\vec{B}_1|l_1}{\overline{v_1}^2}\delta v_1 + \frac{\gamma_L|\vec{B}_2|l_2}{\overline{v_2}^2}\delta v_2 \tag{4.2.4.15}$$

$$\delta\omega \simeq -\frac{m_n}{\hbar}\overline{v_1}\delta v_1 + \frac{m_n}{\hbar}\overline{v_2}\delta v_2 \tag{4.2.4.16}$$

As you can see, there is no special relationship between $\delta\varphi$ and $\delta\omega$. However, we can set $|\vec{B}_1|$ and $|\vec{B}_2|$ so as to realize the following linear relationship:

$$\boxed{\delta\varphi = t\delta\omega} \tag{4.2.4.17}$$

where t is the proportional constant. This constant is called Fourier time since it has the dimension of time.

Let us see when this proportionality is achieved. When Eq.(4.2.4.17) works out, the coefficient of δv_1 and δv_2 should be the same in both sides respectively since δv_1 and δv_2 are independent variables. Then,

$$-\frac{\gamma_L|\vec{B}_1|l_1}{\overline{v_1}^2} = -t\frac{m_n}{\hbar}\overline{v_1} \tag{4.2.4.18}$$

$$\frac{\gamma_L|\vec{B}_2|l_2}{\overline{v_2}^2} = t\frac{m_n}{\hbar}\overline{v_2} \tag{4.2.4.19}$$

By using these relations, we can see the representation of t:

$$t = \frac{\hbar\gamma_L|\vec{B}_1|l_1}{m_n\overline{v_1}^3} = \frac{\hbar\gamma_L|\vec{B}_2|l_2}{m_n\overline{v_2}^3} \tag{4.2.4.20}$$

From this formulation, neutron spin echo condition should be modified as follows:

$$\boxed{\frac{|\vec{B}_1|l_1}{\overline{v_1}^3} = \frac{|\vec{B}_2|l_2}{\overline{v_2}^3}} \tag{4.2.4.21}$$

Notice that this equation is reduced to Eq.(4.2.4.5) when $\overline{v_1} = \overline{v_2}$. In the case of quasi-elastic scattering, we can use Eq.(4.2.4.5). However, we have to use more general representation, Eq.(4.2.4.21), in the case of inelastic scattering such as the phonon scattering.

What we measure in the neutron spin echo experiment is not φ for each neutron but the ensemble-averaged φ. Usually we extract the z component of neutron spin at the end of the second precession field. The z component at this point is represented by $(1+\cos\varphi)/2$[69]. Since the scattering probability with the energy transfer ω is proportional to $S(\vec{q},\omega)$ for coherent scattering and $S_i(\vec{q},\omega)$ for incoherent scattering (Eq.(4.2.1.46) and (4.2.1.47)), ensemble-averaged z component for coherent scattering, J_{coh}, for a neutron whose initial energy is E is[70]:

$$\begin{aligned} J_{coh} &\propto \int_{-E/\hbar}^{\infty} S(\vec{q},\omega)\frac{1+\cos\varphi}{2}d\omega \\ &= \int_{-E/\hbar-\overline{\omega}}^{\infty} S(\vec{q},\overline{\omega}+\omega)\frac{1+\cos(\overline{\varphi}+\delta\varphi)}{2}d\omega \\ &= \int_{-E/\hbar-\overline{\omega}}^{\infty} S(\vec{q},\overline{\omega}+\omega)\frac{1+\cos(\overline{\varphi}+\omega t)}{2}d\omega \end{aligned} \tag{4.2.4.22}$$

Although E varies from each neutron, it does not matter since we can approximate that $-E \to -\infty$ in the case where only small energy transfer can occur. Then:

$$J_{coh} \propto \int_{-\infty}^{\infty} S(\vec{q},\overline{\omega}+\omega)\frac{1+\cos(\overline{\varphi}+\omega t)}{2}d\omega \tag{4.2.4.23}$$

Until now, we regard that the spin component is projected onto z direction which is defined as the direction of $\varphi = 0$. However, we can arbitrary decide the direction of projection. If we project the spin component

[69] Although z component itself should be represented as $z = \cos\varphi$, we modified this representation since what we obtain should be $0 < z < 1$. This contradiction arise from the oversimplification that we regard the spin as a classical vector quantity.

[70] The least value of ω is achieved when $v_2 = 0$. In this case, $\hbar\omega = -E$.

onto the direction of $\overline{\varphi}$, we can rewrite Eq.(4.2.4.23) to a more convenient form[71]:

$$J_{coh} \propto \int_{-\infty}^{\infty} S(\vec{q}, \overline{\omega} + \omega) \frac{1 + \cos \omega t}{2} d\omega \tag{4.2.4.24}$$

In the case of quasi-elastic scattering, $\overline{\omega} = 0$:

$$J_{coh} \propto \int_{-\infty}^{\infty} S(\vec{q}, \omega) \frac{1 + \cos \omega t}{2} d\omega \tag{4.2.4.25}$$

Since $S(\vec{q}, \omega)$ is an even function[72], we can rewrite Eq.(4.2.4.25):

$$\begin{aligned} J_{coh} &\propto \int_{-\infty}^{\infty} S(\vec{q}, \omega) d\omega + \int_{-\infty}^{\infty} S(\vec{q}, \omega) \cos(\omega t) d\omega \\ &= \int_{-\infty}^{\infty} S(\vec{q}, \omega) d\omega + \int_{-\infty}^{\infty} S(\vec{q}, \omega) \cos(\omega t) d\omega + \int_{-\infty}^{\infty} S(\vec{q}, \omega) i \sin(\omega t) d\omega \\ &= \int_{-\infty}^{\infty} S(\vec{q}, \omega) d\omega + \int_{-\infty}^{\infty} S(\vec{q}, \omega) e^{i\omega t} d\omega \\ &\propto I(\vec{q}, 0) + I(\vec{q}, t) \end{aligned} \tag{4.2.4.26}$$

We can calculate that for incoherent scattering. The proportion of coherent and incoherent component is determined by their scattering cross sections (Eq.(4.2.1.46) and (4.2.1.47)). Therefore, the signal of neutron spin echo, J, is represented as follows:

$$\begin{aligned} J \propto\ & \sigma_{coh}(I(\vec{q}, 0) + I(\vec{q}, t)) \\ & + (\sigma_{inc}(\text{non spin-flip}) - \sigma_{inc}(\text{spin-flip}))(I_s(\vec{q}, 0) + I_s(\vec{q}, t)) \end{aligned} \tag{4.2.4.27}$$

Here, we have to care the polarization-dependence of neutron scattering. As mentioned before (Eq.(4.2.3.50) and (4.2.3.51)), incoherent scattering partly shows spin-flip when the incident neutrons are polarized. In the case where the source of incoherent scattering is mainly ^{1}H, we can calculate how much the spins are flipped (Eq.(4.2.3.53)):

$$\sigma_{inc}(\text{non spin-flip}) = \frac{1}{3}\sigma_{inc} \tag{4.2.4.28}$$

$$\sigma_{inc}(\text{spin-flip}) = \frac{2}{3}\sigma_{inc} \tag{4.2.4.29}$$

Taking this fact into consideration, Eq.(4.2.4.27) is represented as follows:

$$J \propto \sigma_{coh}(I(\vec{q}, 0) + I(\vec{q}, t)) - \frac{1}{3}\sigma_{inc}(I_s(\vec{q}, 0) + I_s(\vec{q}, t)) \tag{4.2.4.30}$$

Therefore we can obtain $I(\vec{q}, t)$ and $I_s(\vec{q}, t)$ independently from the spin echo experiment by changing the ratio of σ_{coh} and σ_{inc}.

Here, I would like to show the principle of detailed balance. Let us start from the coherent part of

[71] In the case of symmetric quasi-elastic neutron scattering, $\overline{\varphi} = 0$.

[72] From the principle of detailed balance, $S(\vec{q}, -\omega) = \exp(-\hbar\omega\beta)S(\vec{q}, \omega)$ where $\beta = (k_B T)^{-1}$ is inverse temperature. In the case of quasi elastic scattering, $\exp(-\hbar\omega\beta) \sim 1$ and $S(\vec{q}, \omega)$ becomes an even function since $\hbar\omega \ll k_B T$. Notice that $\hbar\omega$ is neV order and $k_B T$ is meV order.

Eq.(4.2.1.50):

$$\left.\frac{d^2\sigma}{d\Omega dE'}\right|_{coh} = \frac{\sigma_{coh}}{4\pi}\frac{k'}{k}\sum_{\lambda}\frac{e^{-\beta E_\lambda}}{Z}\sum_{\lambda'}\left|\sum_j \langle\lambda'|e^{i\vec{q}\cdot\vec{R}_j}|\lambda\rangle\right|^2 \delta(E_\lambda - E_{\lambda'} + \hbar\omega) = \frac{\sigma_{coh}}{4\pi}\frac{k'}{k}NS(\vec{q},\omega) \tag{4.2.4.31}$$

Here, we used Eq.(4.2.1.29) and (4.2.1.46). Then we can write $S(\vec{q},\omega)$ as follows:

$$S(\vec{q},\omega) = \frac{1}{NZ}\sum_{\lambda,\lambda'} e^{-\beta E_\lambda}\left|\sum_j \langle\lambda'|e^{i\vec{q}\cdot\vec{R}_j}|\lambda\rangle\right|^2 \delta(E_\lambda - E_{\lambda'} + \hbar\omega) \tag{4.2.4.32}$$

Let us substitute $\vec{q} \to -\vec{q}$ and $\omega \to -\omega$. The physical meaning of this operation is the reverse process of the scattering; $|\lambda'\rangle$ is an initial state and $|\lambda\rangle$ is a final state. Taking these facts into consideration, $S(-\vec{q},-\omega)$ can be represented as follows:

$$\begin{aligned} S(-\vec{q},-\omega) &= \frac{1}{NZ}\sum_{\lambda,\lambda'} e^{-\beta E_{\lambda'}}\left|\sum_j \langle\lambda|e^{-i\vec{q}\cdot\vec{R}_j}|\lambda'\rangle\right|^2 \delta(E_{\lambda'} - E_\lambda - \hbar\omega) \\ &= e^{-\beta(E_{\lambda'}-E_\lambda)}\frac{1}{NZ}\sum_{\lambda,\lambda'} e^{-\beta E_\lambda}\left|\sum_j \langle\lambda'|e^{i\vec{q}\cdot\vec{R}_j}|\lambda\rangle\right|^2 \delta(E_\lambda - E_{\lambda'} + \hbar\omega) \\ &= e^{-\hbar\omega\beta}S(\vec{q},\omega) \end{aligned} \tag{4.2.4.33}$$

Notice that the value of $E_{\lambda'} - E_\lambda (\to \hbar\omega)$ does not depend on λ and λ'. Here we used the following facts:

$$\delta(x) = \delta(-x) \tag{4.2.4.34}$$

$$\langle\lambda|\hat{A}|\lambda'\rangle = \langle\lambda'|\hat{A}^\dagger|\lambda'\rangle^* \tag{4.2.4.35}$$

where $\hat{A}$ is an arbitrary operator.

The relationship represented by Eq.(4.2.4.33) is called the principle of detailed balance. This result is a consequence of the Boltzmann distribution of $|\lambda\rangle$ and $|\lambda'\rangle$.

To realize a neutron spin echo experiment, we manipulate the spin of neutrons by using appropriate devices [68]. The spin of neutrons is oriented randomly at the source. Therefore, we use the polarizer such as a supermirror to align the spin of neutrons to the direction of their motion. We define this direction as z. However, the direction of magnetic field is also z when the magnetic field is generated by a coil. Since the spin cannot precess in this condition, we flip the spin of neutrons from z direction to x direction. This manipulation is achieved by using the coil called $\pi/2$ flipper[73]. $\pi/2$ flipper is the device which impose the magnetic field in the direction of $x+z$. The neutron spin is rotated 180° around this axis and oriented to x direction (Fig.4.20).

After this alignment, the neutrons enter the first precession field and rotate in xy plane. Since we use the neutron beam without monochromating, neutrons have different velocities. Fast neutrons get out from the precession field earlier than slow neutrons. As a result, the spin of neutrons with different velocity points to different direction (Fig.4.21). Usually total spin of neutrons becomes zero at the end of precession field since neutrons rotates approximately 10000 times in the precession field and small difference of velocity becomes

[73]This name is derived from the fact that the eventual spin change is $\pi/2$ (from z to x) although the spin rotates π around $x+z$ direction.

large difference of precession angle.

After getting out from the precession field, the neutron spin is rotated 180° around x axis (Fig.4.22). This apparatus is called π flipper. We usually use π flipper instead of changing the direction of magnetic field in the second precession field.

After passing the π flipper, the neutrons are precessed by the second precession field. If there is no energy exchange (velocity change) between two precession fields, the direction of spins of all of the neutrons points to x direction by applying strictly the same quantity of $\vec{B}$. As a result, the neutron spin echo is achieved in x direction (Fig.4.23).

To detect this echo signal, we again move the spin to z direction by using $\pi/2$ flipper. This signal is finally detected as the projection on z component (Fig.4.24).

If we put a sample between the π flipper and the second precession field, neutrons exchange their energy with the sample. As a result of this quasi-elastic scattering, the velocity of neutrons can vary. Let us assume that fast neutrons are decelerated and slow neutrons are accelerated (Fig.4.25). In this case, fast neutrons precess more than the first precession field. In contrast to this, slow neutrons precess less than the first precession field. As a result, the neutron spin echo becomes incomplete. This signal is moved to z direction by using $\pi/2$ flipper (Fig.4.26). The projection on z component is smaller than that before the first precession field. From this decrease, we can calculate how the energy exchange is occurred.

Summary of neutron spin echo spectrometer is shown in Fig.4.27 and 4.28.

As you can see, the rotation angle in $\pi/2$ flipper and π flipper depends on the neutron velocity. This effect is discussed by Schärof by using Wolf net [68]. From now, we ignore this effect for simplicity.

In the actual measurements, we measure $I(\vec{q}, t)$ for several values of $\vec{q}$ and t by changing the scattering angle and the strength of magnetic fields with keeping the relationship Eq.(4.2.4.20). For each $\vec{q}$ and t, we measure the echo as a function of the magnetic field applied to the second precision field to obtain accurate data. Assume that we apply the additional magnetic field, δB, to the second precession coil. The effect of

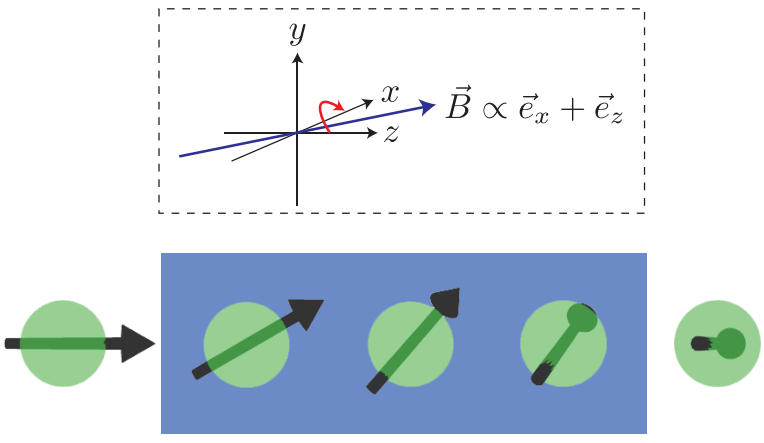

Figure 4.20: Motion of neutron spin by first $\pi/2$ flipper. Upper : Definition of the coordinate axis. A blue arrow implies the direction of magnetic field. A red arrow implies the motion of the total neutron spin. Lower : Variation of the total neutron spin by the first $\pi/2$ flipper.

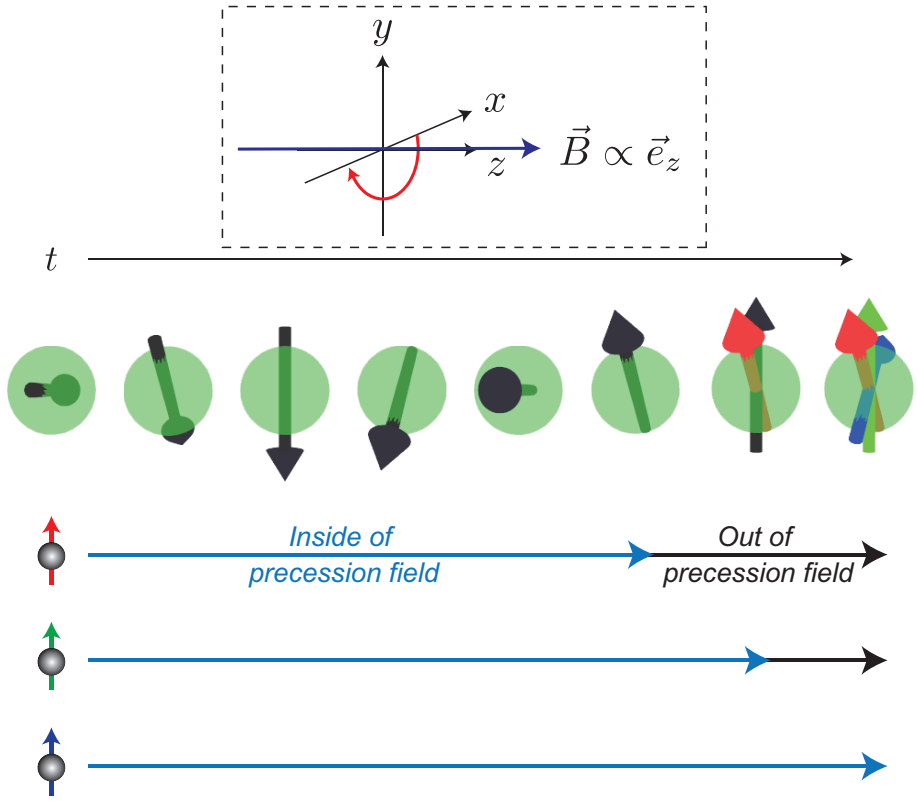

Figure 4.21: Motion of neutron spin in first precession field. Upper : Definition of the coordinate axis, magnetic field and the motion of the total neutron spin. Lower : Variation of the neutron spins by the first precession field. A red arrow implies a spin of a fast neutron. A green arrow implies a spin of a neutron with average velocity. A blue arrow implies a spin of a slow neutron.

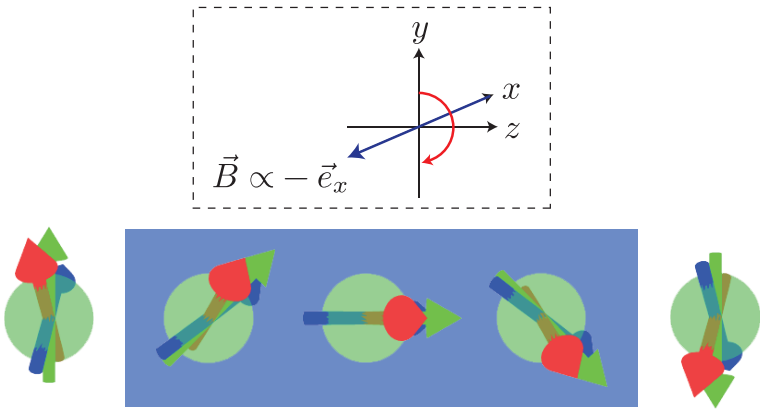

Figure 4.22: Motion of neutron spin by π flipper. Upper : Definition of the coordinate axis, magnetic field and the motion of the total neutron spin. Lower : Variation of the total neutron spin by the π flipper. Red, green and blue arrows implies a spin of a neutron with high, medium and low velocity, respectively.

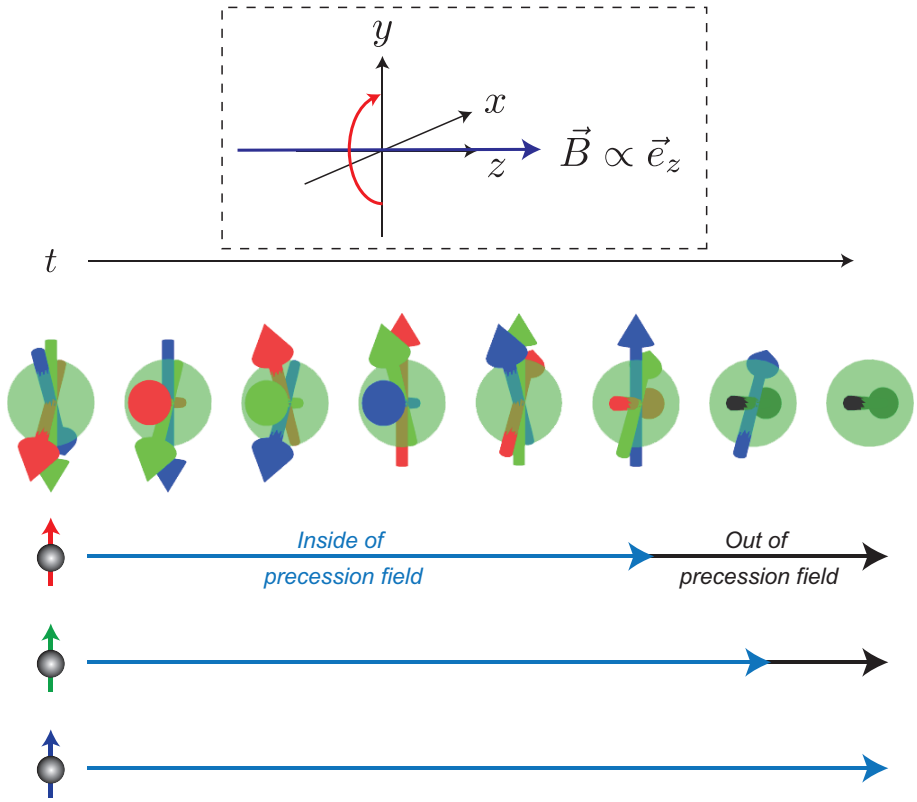

Figure 4.23: Motion of neutron spin in second precession field. Upper : Definition of the coordinate axis, magnetic field and the motion of the total neutron spin. Lower : Variation of the neutron spins by the second precession field. Red, green and blue arrows implies a spin of a neutron with high, medium and low velocity, respectively.

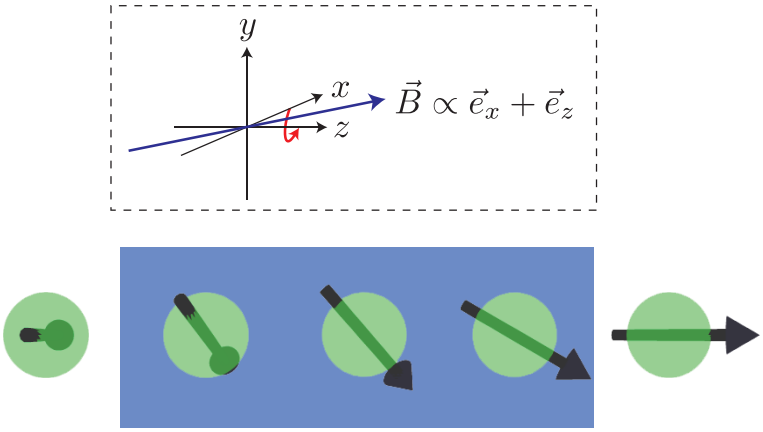

Figure 4.24: Motion of neutron spin by second $\pi/2$ flipper. Upper : Definition of the coordinate axis, magnetic field and the motion of the total neutron spin. Lower : Variation of the total neutron spin by the second $\pi/2$ flipper.

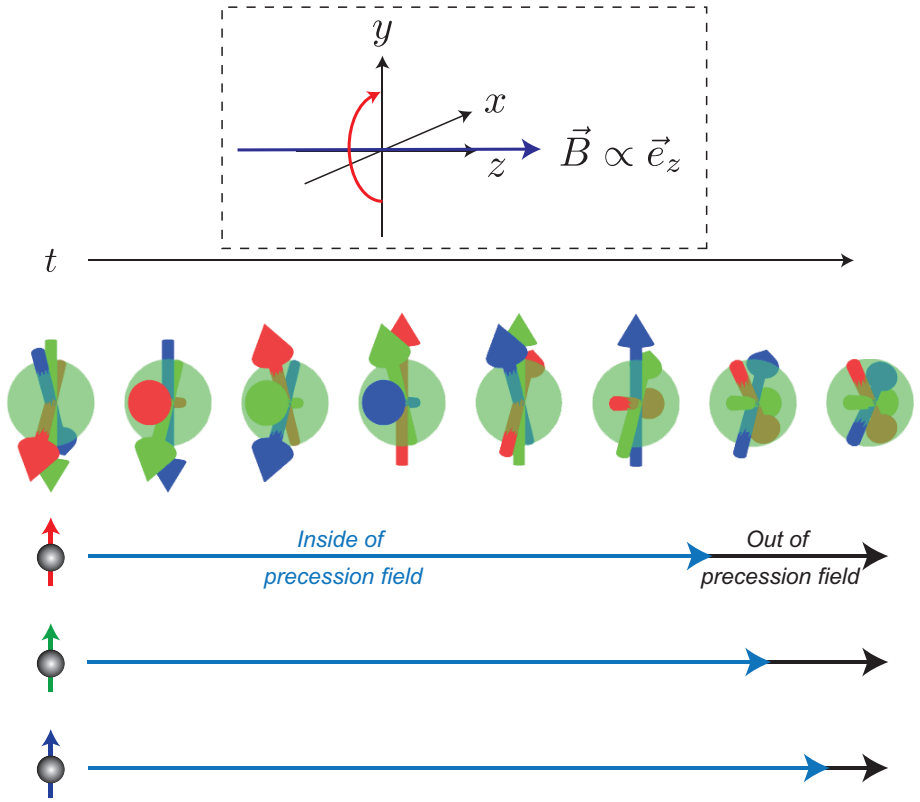

Figure 4.25: Motion of neutron spin in second precession field after quasi-elastic scattering. Here, we assume that fast neutrons (a red arrow) are decelerated, neutrons with average velocity (a green arrow) do not change their velocity and slow neutrons (a blue arrow) are accelerated. Upper : Definition of the coordinate axis, magnetic field and the motion of the total neutron spin. Lower : Variation of the neutron spins by the second precession field.

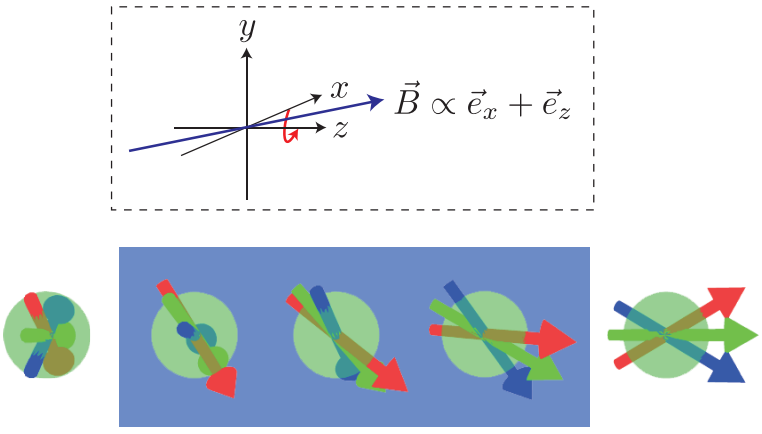

Figure 4.26: Motion of neutron spin by second $\pi/2$ flipper after quasi-elastic scattering. The assumption is the same as Fig.4.25. Upper : Definition of the coordinate axis, magnetic field and the motion of the total neutron spin. Lower : Variation of the total neutron spin by the second $\pi/2$ flipper.

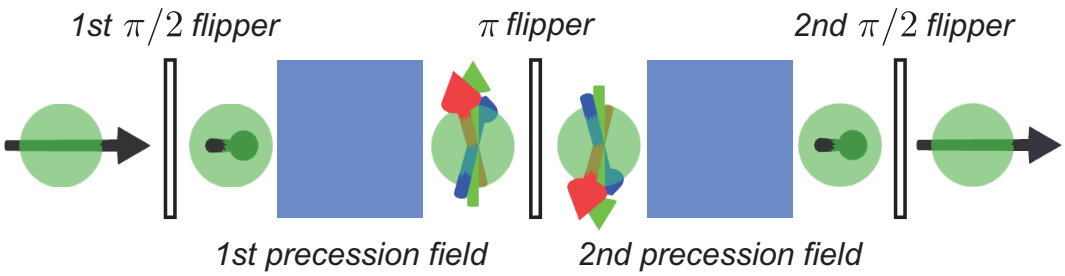

Figure 4.27: Summary of neutron spin echo spectrometer without quasi-elastic scattering.

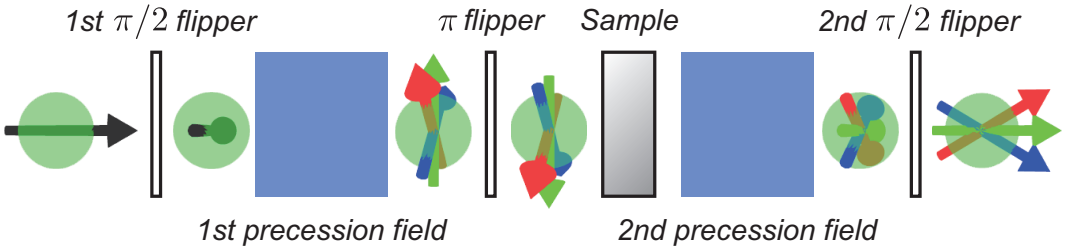

Figure 4.28: Summary of neutron spin echo spectrometer with quasi-elastic scattering.

the deviation of the precession angle, $\delta\varphi$, is expressed by (Eq.(4.2.4.3)):

$$\begin{aligned}\delta\varphi &= \frac{\gamma(\delta B)l_2}{v} \\ &= \frac{\gamma m\lambda l_2}{h}\delta B\end{aligned} \tag{4.2.4.36}$$

since v is represented by the following de Broglie wavelength, λ:

$$\lambda = \frac{h}{mv} \tag{4.2.4.37}$$

Then (4.2.4.25) is modified as follows:

$$J_{coh} \propto \int_{-\infty}^{\infty} S(\vec{q},\omega)[1+\cos(\omega t+\delta\varphi)]d\omega \tag{4.2.4.38}$$

Since $S(\vec{q},\omega)$ is an even function,

$$\begin{aligned}J_{coh} &\propto \int_{-\infty}^{\infty} S(\vec{q},\omega)d\omega + \int_{-\infty}^{\infty} S(\vec{q},\omega)\cos(\omega t+\delta\varphi)d\omega \\ &= I(\vec{q},0) + \int_{-\infty}^{\infty} S(\vec{q},\omega)[\cos(\omega t)\cos(\delta\varphi)+\sin(\omega t)\sin(\delta\varphi)]d\omega \\ &= I(\vec{q},0) + \int_{-\infty}^{\infty} S(\vec{q},\omega)\cos(\omega t)\cos(\delta\varphi)d\omega \\ &= I(\vec{q},0) + \cos(\delta\varphi)I(\vec{q},t) \\ &= I(\vec{q},0) + \cos\left(\frac{\gamma m\lambda l_n}{h}\delta B\right)I(\vec{q},t)\end{aligned} \tag{4.2.4.39}$$

By using Eq.(4.2.4.39), we can obtain $I(\vec{q},t)$ by changing the value of δB slightly and fit the echo data by a cosine function. The amplitude of the cosine function corresponds to $I(\vec{q},t)$ (Fig.4.29). For each q, we conduct this scan around several points of B (Fig.4.30). Each B corresponds to one t point and the data of

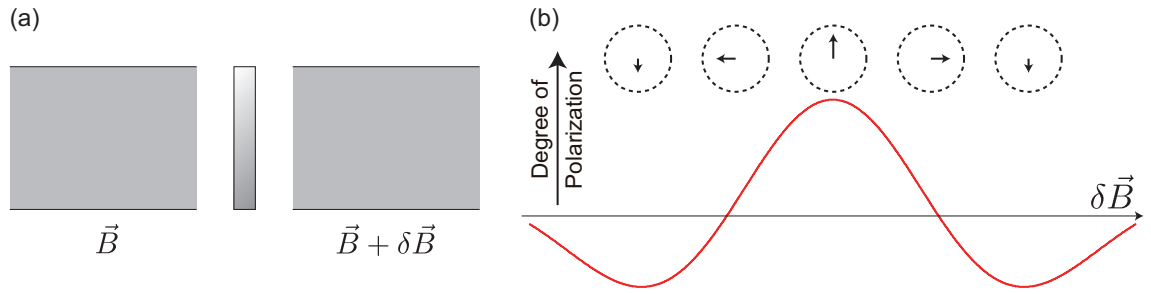

Figure 4.29: Measurement of one echo signal. (a) Experimental setup. (b) Measurement procedure. We measure a degree of polarization with changing the strength of magnetic field slightly. As a result, we can obtain the echo signal as a function of $\delta\vec{B}$. Usually, the amplitude attenuates because of the wide distribution of λ.

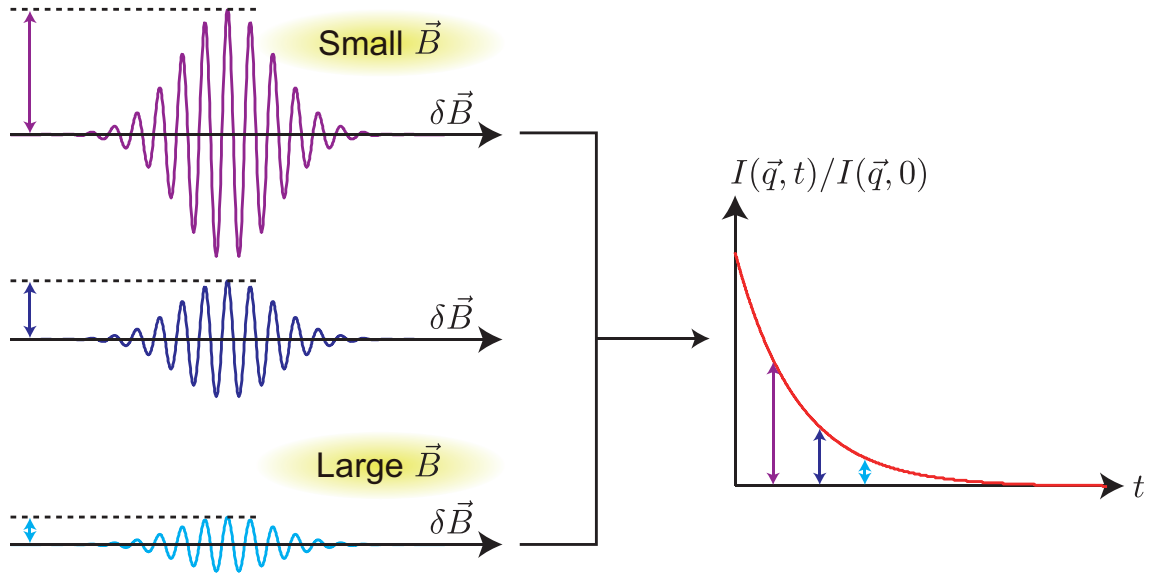

Figure 4.30: Construction of relaxation. We measure the amplitude of each spin echo signal. The amplitudes correspond to the values of normalized intermediate functions. This relaxation is usually represented by a function of Fourier time, shown in Eq.(4.2.4.20).

relaxation can be obtained (Eq.(4.2.4.20)).

In the case of our measurement, we measured the polarization data at 27 points for each q and t with changing δB[74]. We fit these data by using Eq.(4.2.4.39) and determine $I(\vec{q},t)$ as an amplitude of the echo. In the case of pulse source, we do not have to care the distribution of λ since we can apply a time-of-flight measurement. This means that the echo does not attenuate like Fig.4.30.

[74] In actual, we change the strength of the electric current applied to an electromagnetic coil.

5 Characterization of Tetra-PEG gels

5.1 Introduction

In the next section, I introduce amphiphilic gels produced by solvent-induced aggregation. Before the explanation about this amphiphilic gel, I would like to introduce the basic technique to produce it. In this section, I introduced the gel called "Tetra-PEG gel". Tetra-PEG gel is developed by Sakai *et al.* in 2008 [11] (Figure 5.1). This gel is created by mixing two prepolymers. Each prepolymer is tetra-arm PEG. Two prepolymer have different functional groups at the end of each arm. These functional groups react with each other and create a gel. Many experimental results strongly suggest that this preparation scheme introduce less inhomogeneities. In this section, I review the research related to Tetra-PEG gels from the viewpoint of physical properties. In addition, I would like to mention more about my research related to the dynamic behavior of Tetra-PEG gels in mesoscopic and microscopic scale.

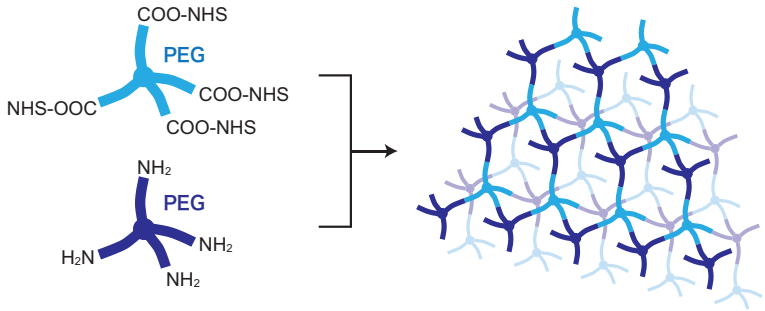

Figure 5.1: Preparation scheme of Tetra-PEG gels.

5.2 History of tough gels

As discussed in Section.3.2.1, the elasticity of polymer network is proportional to the number density of polymer chains, ν. In actual case, we have to consider the imperfection of networks such as entanglement, loop, loose ends and so on (Figure 5.2) [5]. Entanglement increases the number of crosslinks while loop and loose ends have no effect on elasticity. Since the maximum number density of polymer chains are determined by the preparation condition, the existence of loop and loose ends will weaken the network structure. By using this classical model, elasticity of elastomer is explained [69]. The same discussion holds true for gel materials. However, this kind of concept has been difficult to observe experimentally for gels. The reason is that it has been impossible to stretch or compress gels without breaking. The number density of polymer chain within gels is small because of the dilution by solvent. This means that the existence of inhomogeneities strongly affects the structure compared to elastomers. When the force is applied to homogeneous gel materials, the force is applied unevenly within the materials. As a result, weak parts become small cracks. These cracks will propagate in the gel and finally the gel is broken in macroscopic scale. Although elastomers also contain a lot of inhomogeneities, stress rupture less occurs compared to gel materials since the number density of polymer chains is so high that the variability of applied force are suppressed. On the other hand, there are strong demand of tough gels for biomedical and engineering applications (which I will introduce in the following subsection). To overcome this difficulty, a lot of effort has been paid. Here I'm going to review some representative tough gels developed recently. For recent reviews of tough gels, please refer to [70–74].

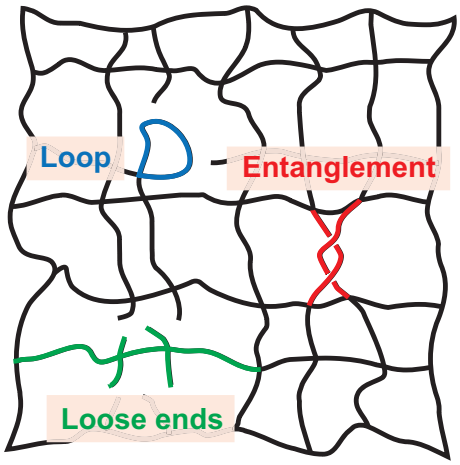

Figure 5.2: Inhomogeneities existing in conventional polymer network.

Slide-ring gel

Okumura and Ito first reported polyrotaxane gel, which is now usually called slide-ring gel [6]. The concept of slide-ring gel was proposed by de Gennes first [75]. This gel has unique crosslinking system, which moves along the main chain. The gel was prepared from polyrotaxane. Polyrotaxane is a polymer threading many cyclic molecules. These cyclic molecules are trapped by the bulky structure at the ends of polyrotaxane. In the first report of the slide-ring gel, PEG threading many α-cyclodextrin (CD) was used as a polyrotaxane. After synthesizing this polyrotaxane molecule, α-CD from different polyrotaxane molecules are covalently connected. As a result, two polyrotaxanes are interlocked by figure-of-eight crosslinks (Figure 5.3). Since the crosslinking points of slide-ring gels are movable, concentration of stress on one point induced by stretching will be relaxed. This effect is called pulley effect. Thanks to the pulley effect, the force applied to the gel is distributed evenly and the extensibility of this gel is enhanced. For recent reviews of slide-ring gels, please refer to [76].

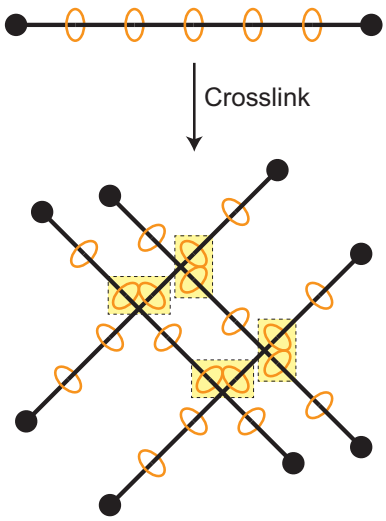

Figure 5.3: Schematics for the preparation of a slide-ring gel.

Nanocomposite gel

Haraguchi and Takehisa first reported network structure made from polymers and inorganic cray, named nanocomposite gel [7]. In this system, polymerization starts from the monomer on the inorganic clay (synthetic hectrite, ca. 30 nm ϕ (diameter) $\times$ 1 nm t (thickness)). Each clay is connected with the polymer originated from itself (Figure 5.4). As a monomer, NIPA is used. In this case, the amide group in NIPA will attach to the clay via hydrogen bonds. It is estimated that a few tens to more than 100 polymers grow from one clay. The clay can be regarded as a multifunctional crosslinker. Since the number of crosslinking point is much smaller compared to conventional polymer gels, the distance between crosslinking points are much longer. This is the origin of high extensibility, up to 1000 %. Multifunctionality is also good for the dissipation of local stress. Since there are a lot of polymer chains between each crosslinker, small cracks originated from one polymer chain do not propagate to the whole. For recent reviews of nanocomposite gels, please refer to [77].

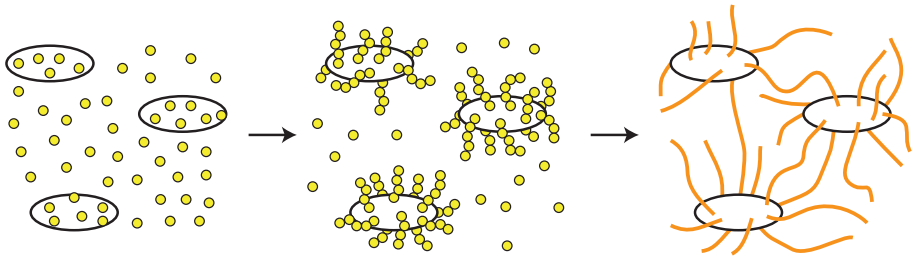

Figure 5.4: Schematics for the preparation of a nanocomposite gel.

Double-network gel

Gong *et al.* firstly reported tough gels by using two polymer networks (PAMPS and PAAm) [8]. Their synthetic scheme is a two-step network formation. First, PAMPS network is formed by conventional scheme by using crosslinkers. After this first network is created, this gel is immersed in the pre-gel solution for the second network. Since PAMPS is polyelectrolyte, the network is highly swollen. As a result, this first network becomes rigid and brittle. Under the existence of first network, the soft, ductile PAAm network is formed. Crosslinking for the second network is adjusted to low to make it soft. The gel created by this scheme is named "double network gel" and shows excellent mechanical characteristics. Their compression experiment showed that the double network can sustain a stress of 17.2 MPa and fracture strain was 92 %. The origin of this strength is explained by the concept of sacrifice bond (Figure 5.5). When the gels are compressed or stretched, PAMPS network breaks first since PAMPS are brittle compared to PAAm because of the swelling before the construction of the second network. Then the fragment of PAMPS works as new crosslinkers for PAAm networks. These new cross linkers will be produced much more at the position where the local force is stronger. As a result, the resultant gels become strong. The drawback of this gel is that the strength of double networks was lost by the first loading. However, the combination of two networks is versatile and this concept itself is very important. For recent reviews of double network gels, please refer to [78–80].

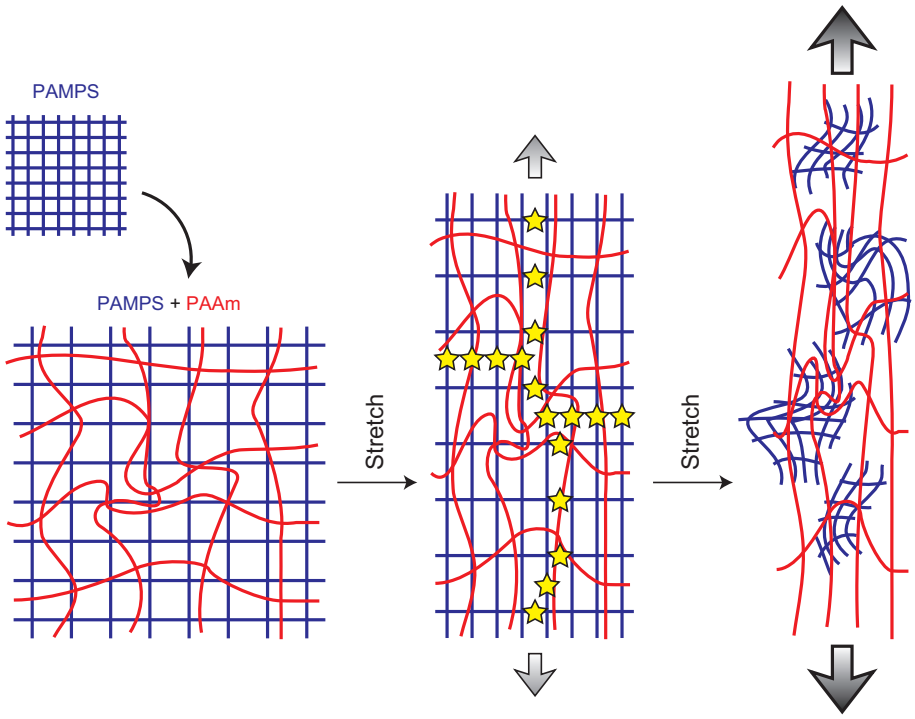

Figure 5.5: Schematics for stretching a double network gel. PAMPS networks break first. The broken fragment becomes additional crosslinking point.

Microsphere composite gel

Huang *et al.* reported strong hydrogel which does not break even at a compression stress of 10 MPa and a strain of 97 % [9]. The structure of this gel is similar to that of nanocomposite gel. Instead of inorganic clays, they used macromolecular microsphere as a multifunctional crosslinker. First, macromolecular microspheres were made from styrene, butyl acrylate, and acrylic acid. Then the microsphere emulsion was irradiated with γ-rays under oxygen. Through this process, peroxides are formed on the surface of the microspheres. After this treatment, monomers (acrylic acid) were added and heated. Though this process, radical on the surface of the microsphere initiates the polymerization. Through this polymerization, microspheres are connected with each other and gels are formed (Figure 5.6). Similar to the nanocomposite gels, multifunctionallity is the main origin of their strength. They proposed that we can add special electrical and magnetic properties by adding other inorganic nanoparticles.

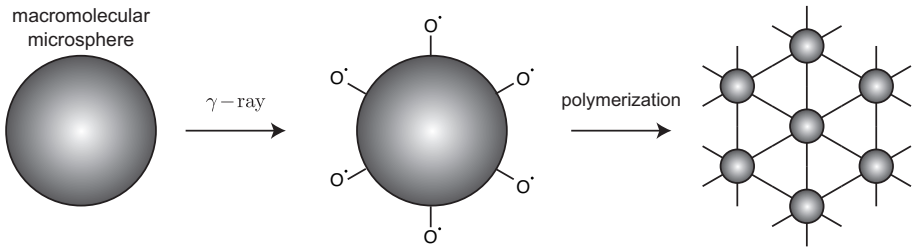

Figure 5.6: Schematics for the preparation of a microsphere composite gel.

Ionically crosslinked gel

Henderson *et al.* reported strong hydrogel by using ionic crosslinking [10]. The basic idea is similar to double-network gels. As mentioned before, one weak point of double-network gels is that the breaking process of the first network is irreversible. To solve this problem, ionic crosslinking is used to form the first network. They used amphiphilic triblock copolymer, PMMA–PMAA–PMMA (34k–114k–34k), as a sample. This copolymer was dissolved in DMSO and the solvent was exchanged to water by using vapor phase solvent exchange technique. During this process, hydrophobic PMMA made spherical aggregates which work as crosslinking points [81]. This relatively weak but homogeneous gel is regarded as a second network in the double-network gel. After the solvent substitution, the gel was immersed in buffered cation solution. Divalent cation can connect two strands via the coordination of carboxylate functionalities. These ionically crosslinked parts work as a first, strong network in the double-network gel (Figure 5.7). They showed that the gel was capable of attaining higher strains (around 5 times) by the introduction of ionic crosslinking.

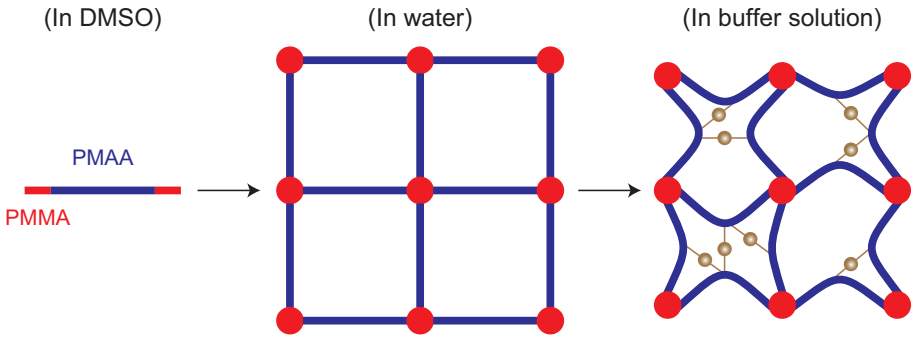

Figure 5.7: Schematics for the preparation of an ionically crosslinked gel.

Hydrogel with cooperative hydrogen bonding

Song *et al.* reported strong hydrogel without using any initiator and crosslinker [82]. Gel preparation scheme is very simple. Aqueous solution of Poly(*N*-vinylpyrrolidone) (PVP) and AAm monomers was degassed and heated at 56 °C for 36 hours. During the heating, AAm monomers were polymerized. Here, the hydrogen bonding between PVP and AAm plays an important roll. Before heating, some of AAm monomers were attached to PVP via hydrogen bonding. After heating, these AAm monomers become PAAm and connect PVPs via hydrogen bonding (Figure 5.8). Since the crosslinking is not permanent (physical crosslinking) and the hydrogen bonding was created like a zipper, the prepared gel becomes strong. Both tensile and compressive mechanical testing showed excellent mechanical properties. For examples, the tensile strength was approximately 1 MPa, which is 2 to 3 orders of magnitude higher than those of the conventional synthetic hydrogels.

Other representative examples

Gaharwar *et al.* reported strong hydrogel by the concept similar to those of nanocomposite gels and ionically crosslinked gels [83, 84]. They used the mixture of clays (hydroxyapatite nanoparticles, nHAp) and PEG to prepare hydrogels. Similar to the nanocomposite gels, nHAp works as a multifunctional cross linker and make the gel strong. In addition, they crosslinked PEG themselves by functionalizing the end of PEG to diacrylate. In other words, PEG is crosslinked twice; physical crosslinking to the nanoparticles and chemical

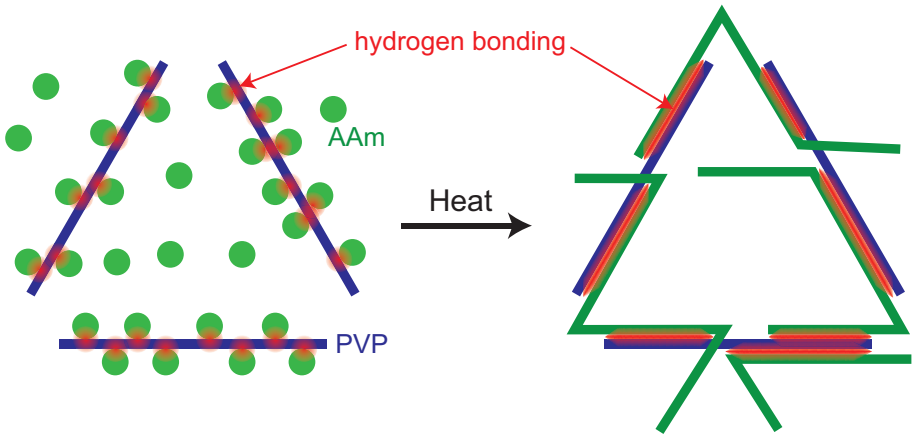

Figure 5.8: Schematics for the preparation of a hydrogel with cooperative hydrogen bonding.

crosslinking to themselves. The point that one polymer is crosslinked twice is the same as the ionically crosslinked gel. By using this technique, they successfully prepared gels whose ultimate strain reached 2000 %.

Sun *et al.* reported extremely stretchable and tough hydrogels by using the concept of double-network gels and ionically crosslinked gels [85]. As a first network, they used an alginate gel. An alginate chain is composed of two units; mannuronic acid and guluronic acid. Guluronic acid parts between different chains are connected via divalent cations similar to the ionically crosslinked gels. Since the alginate chain has blocks rich in Guluronic acids, this crosslinking becomes strong like a zipper. Second network is conventional PAAm gel. In addition, these two networks were also connected covalently. They showed that the prepared gels can be stretched beyond 20 times their initial length.

Bin Imran *et al.* reported slide-ring gel with improved functionality [86]. In the first report of slide-ring gels, pH of the gel should be high such as NaOH aqueous solution to prevent aggregation of α-CD. They showed that the aggregation of α-CD can be avoided by using ionic groups. Instead of figure-of-eight crosslinks, they connect α-CD of polyrotaxane directly to the polymer chains. When both polyrotaxane and polymer chains are non-ionic, prepared gels are not strong because of their low solubility. However, it was shown that the gels become strong when nonionic polyrotaxane are connected to ionic polymer chains such as NIPA-AAcNa. In this type of gels, NIPA-AAcNa copolymer will be stretched since the Na^+ counter ions cannot stay near the ionized polymers. Therefore, α-CDs attached to NIPA-AAcNa copolymer will also be prevented from aggregation. In addition, they also showed that the combination of ionic polyrotaxane with nonionic polymer chains also enhances the mechanical properties of gels. They used α-CD with carboxyl groups to make the polyrotaxane ionic. The gel prepared from this polyrotaxane and non-ionic PNIPA also showed high toughness.

Li *et al.* reported double-network gels by using other combination of chemical and physical crosslinking [87]. As a first network, they used PVA network whose crosslinking points are crystallites. As a second network, they used usual PAAm network prepared by crosslinkers. First, PAAm network is prepared from the mixture of AAm monomers and PVA chains. This gel is dried and annealed at 120 °C to promote crystallization. During this process, strong physical crosslinking is created. After the annealing, the gel is immersed in water to re-hydrate. The gel showed elastic modulus of 5 MPa.

5.3 Tetra-PEG gel and related materials

There are several techniques to prepare gel. When the gel is prepared by the copolymerization of monomers and crosslinkers, the crosslinking points are created randomly. Post-crosslinking by γ-ray irradiation also introduce crosslinking points randomly. Compared to this, preparation of gels by endlinking processes as been believed to give homogeneous networks of well-defined architectures. Therefore, the gels prepared by endlinking process is called model networks [88, 89]. However, it has also been clarified that even the gels are prepared by endlinking process, those gels contains significant amount of inhomogeneities as shown in Figure 5.2. In 2008, Sakai *et al.* reported hydrogels of ideally homogeneous network called Tetra-PEG gel (Figure 5.1) [11].[75] This gel is prepared by the crosslinking of two tetra-arm PEG units with different functionalities. One PEG has amine groups and the other has active ester groups. By mixing these two solutions with appropriate pH conditions, crosslinking occurs within several to several tens minutes to form a hydrogel (Figure 5.9). (For the synthesis of functional tetra-arm PEG, please refer to [91].) This preparation scheme has mainly there advantages to make the network homogeneous [92]. The first point is the control of reaction rate by adjusting pH. The second point is the presence of solvent, which allows homogeneous mixing and also prevents the overlapping of chains. The third point is the shape of prepolymers, which does not allow the formation of back-biting loop structures. Followed by this hypothesis, it was experimentally shown that the combination of active ester-terminated tetra-arm PEG and amine-terminated linear-PEG also form strong gels (Figure 5.10) [18].

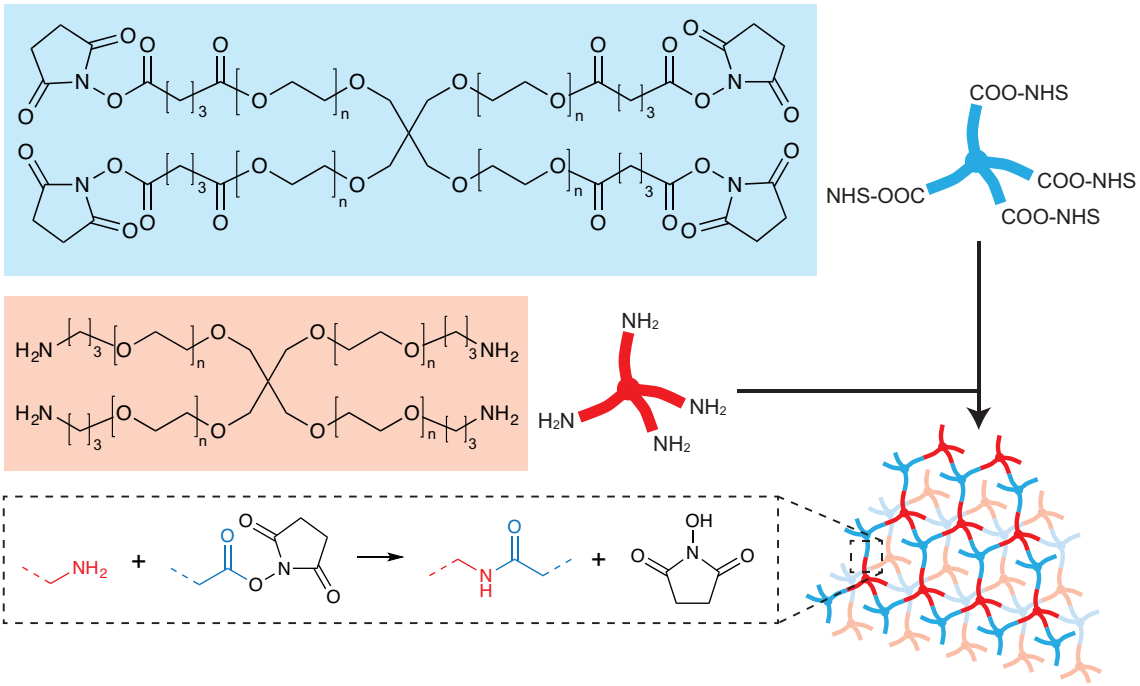

Figure 5.9: Synthesis of Tetra-PEG gel by endlinking of amine group and active-ester group.

[75] Conventionally, the polymer whose unit is CH_2CH_2O is called polyethylene glycol (PEG) when the molecular weight is small and called polyethylene oxide (PEO) when the molecular weight is large [90]. However, the threshold molecular weight is vague. In addition, there is no qualitative difference. In this thesis, I'm going to use the term PEG regardless of molecular weight.

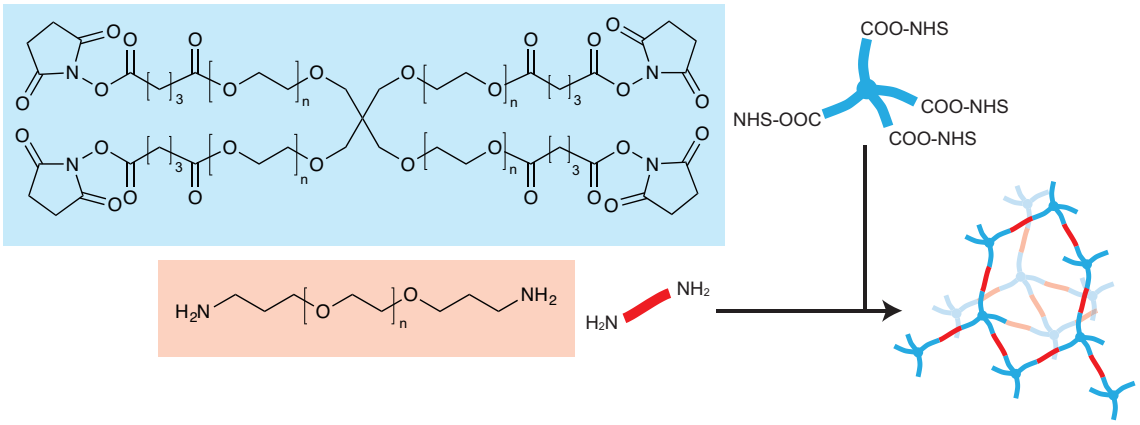

Figure 5.10: Synthesis of gel by endlinking of active ester-terminated tetra-arm PEG and amine-terminated linear PEG.

Inspired by this report, a variety of materials similar to Tetra-PEG gels have been prepared. Mortensen and Annaka reported preparation scheme of amphiphilic hydrogels from commercially available tetra-arm PEG-PPG (Figure 5.11) [93, 94]. Crosslinking procedure is the same as Figure 5.9. Meyerbrömer and Zharnikov reported similar scheme for the preparation of thin, freestanding nanomembrane (Figure 5.12) [95]. Instead of active ester, they used epoxy-terminated tetra-arm PEG. Jia *et al.* used the reaction between hydroxyl-terminated tetra-arm PEG and isocyanate-terminated short linker for the preparation of high strength gels (Figure 5.13). By introducing porphyrin unit, that gels gain sensitivity to heavy metal ions [96]. They also showed that we can tune redox-biodegradability of these gels by introducing disulfide bonds [97]. Yoshihara *et al.* developed rigid polyimide networks by using the same reaction scheme [98]. Oshima *et al.* developed homogeneous gels by end-linking of tetra-arm polymers with click chemistry (Figure 5.14) [99]. Here, Huisgen dipolar cycloaddition of azides and alkynes was used (Figure 5.15) [100–102]. This reaction has been used for the preparation of model networks due to its complete specificity and quantitative yields [103–106]. Qian *et al.* developed PEG-based high strength hydrogels by the crosslinking of $(\mathrm{PEG}_n(\mathrm{C{\equiv}CH}))_m$ and $\mathrm{PEG}_n(\mathrm{N_3})_2$ [107]. As the other click chemistry, reaction of thiol-ene reaction is also used for the preparation of gels [108, 109]. By using thiol-ene reaction, Saffer *et al.* developed highly resilient PEG hydrogels (Figure 5.16) [110]. They also succeeded in preparation of highly resilient amphiphilic PEG–PDMS hydrogels, which is the topic of next section [111]. Ikeda *et al.* developed gels by the crosslinking of 4-arm star-shaped ε-caprolactone oligomers [112]. In this report, they used Diels–Alder reaction between furan- and maleimide-terminated polymers (Figure 5.17). The mixture solution of these two polymers becomes gels through Diels–Alder reaction while the mixture becomes solution at 80 °C by retro-Diels–Alder reaction. The same group also reported other organogelation schemes; hydrogen bonding between carboxyl and pyridyl groups [113], and ionic and hydrogen-bonding interaction between sulfo and pyridyl groups [114]. Rossow and Seiffert developed gels by the crosslinking of tetra-arm PEG-terpyridine via the complex formation with transition metal ions (Figure 5.18) [115]. Physical properties of gels can be tuned by changing the type of transition metal ions. Schappache *et al.* attached tetraphenylporphyrin (TPP) with iron cations at the end of tetra-arm PEG (Figure 5.19) [116]. The aqueous solution of this polymer becomes chemical gel thanks to the formation of TPP–De–O–Fe–TPP bonds. This gel becomes physical gel by addition of HCl. Under the acidic condition, Fe–O–Fe bonds are broken. Instead of this chemical crosslinking, hydrophobic and $\pi - -\pi$

interactions between TPP become important to make them gel. Introduction of the concept of Tetra-PEG gel into other tough gels is also reported. For example, Fukasawa *et al.* prepared nanocomposite gel by using the mixture of clays and tetra-arm PEG and improvement of mechanical properties was shown [117]. Nakajima *et al.* prepared double-network gel by using Tetra-PEG gel as a first network and used for the analysis of fracture process [118].

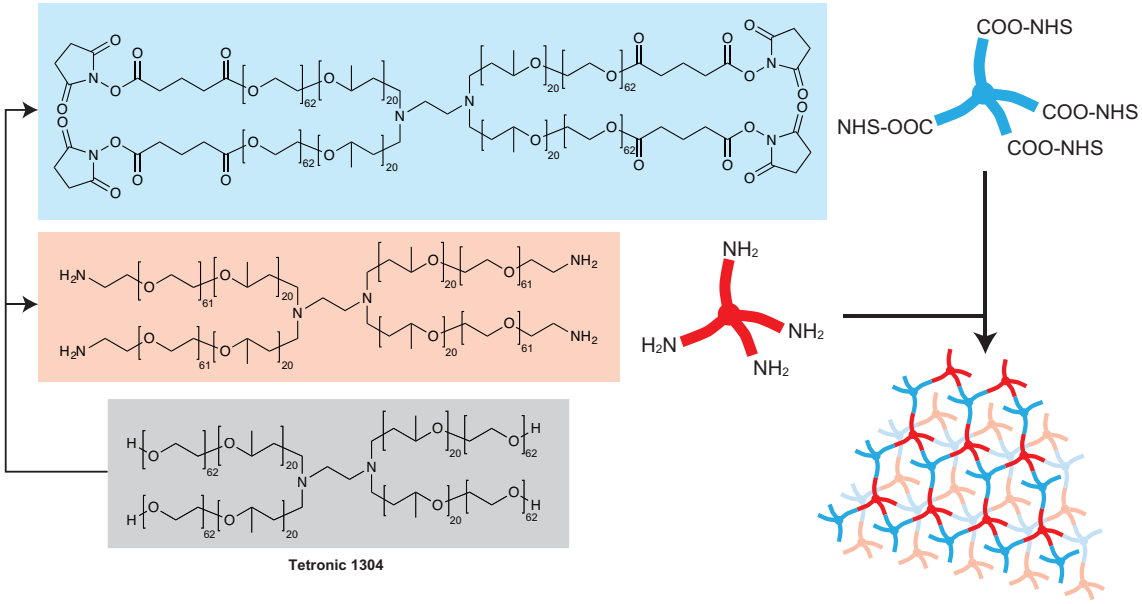

Figure 5.11: Synthesis of Tetra-(PEG-PPG) gel.

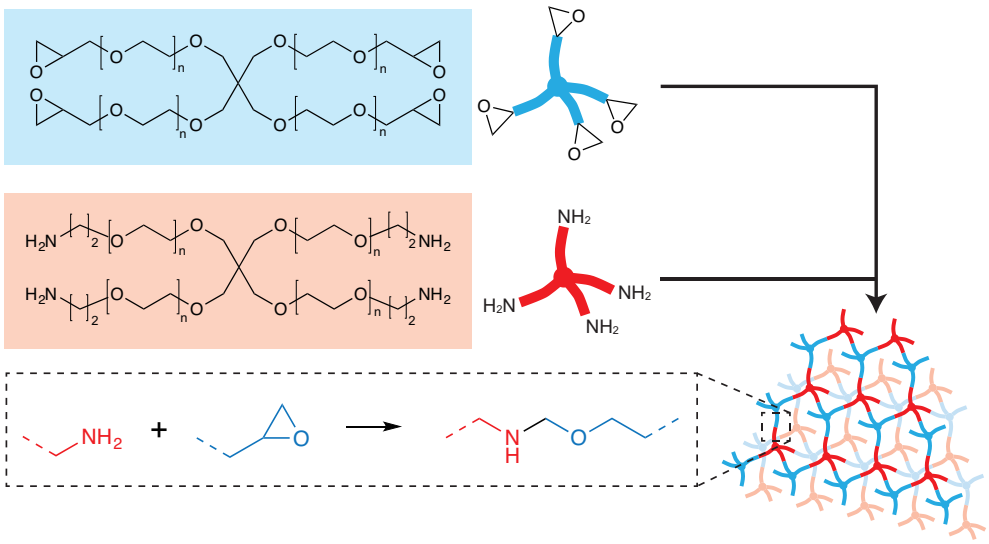

Figure 5.12: Synthesis of Tetra-PEG gel by the reaction of epoxy and amine.

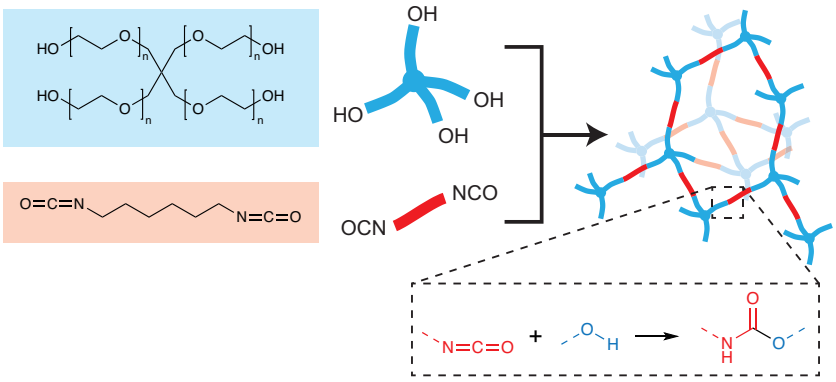

Figure 5.13: Synthesis of gel by endlinking of hydroxy-terminated tetra-arm PEG and hexamethylene diisocyanate.

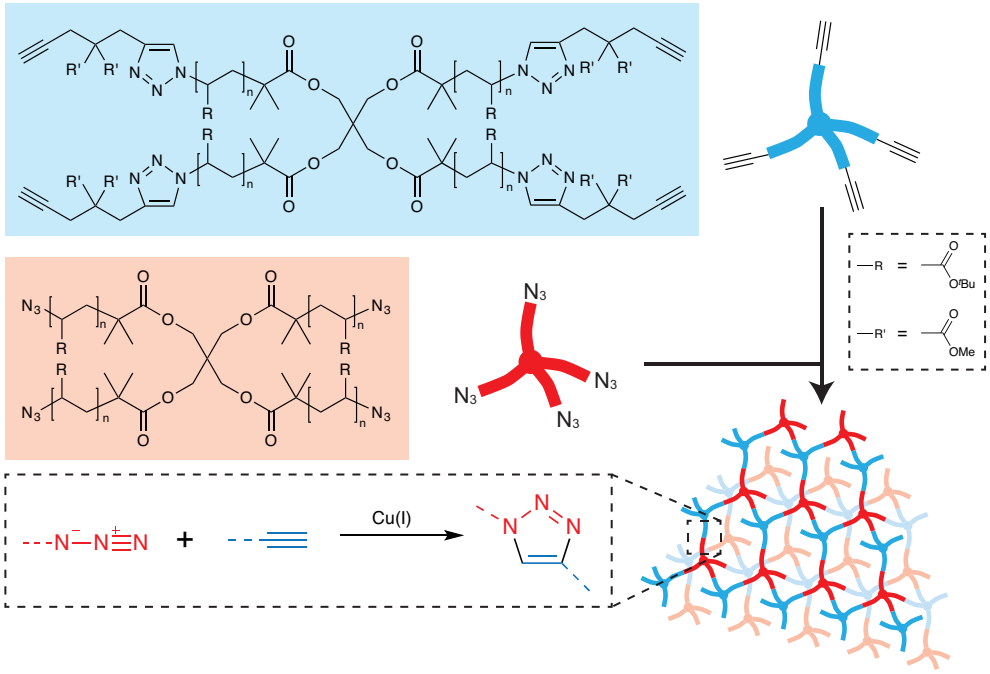

Figure 5.14: Synthesis of gel from tetra-arm polymers with click chemistry.

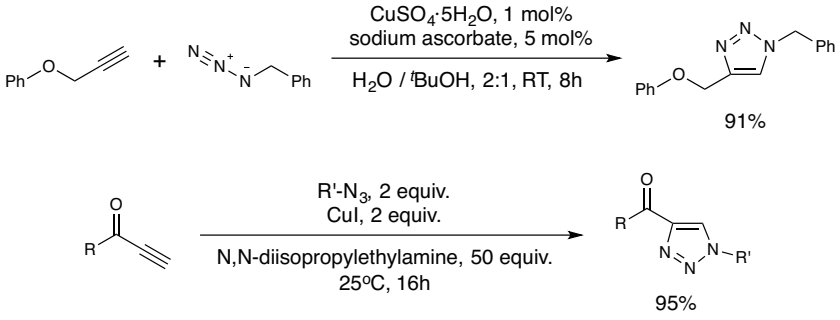

Figure 5.15: First reports of Huisgen dipolar cycloaddition of azides and alkynes.

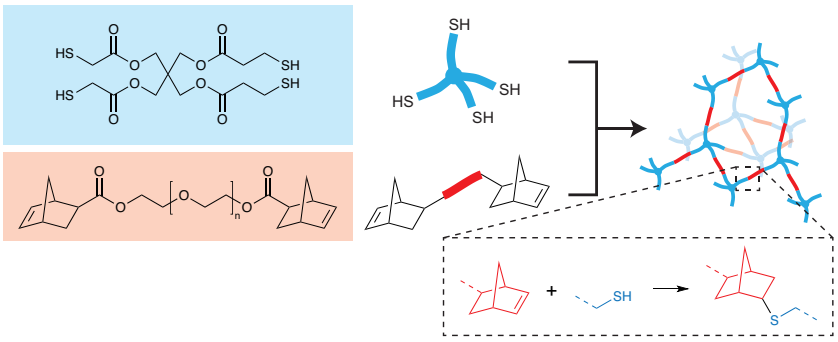

Figure 5.16: Synthesis of gel by endlinking of thiol-terminated tetra-arm PEG and ene-terminated linear PEG.

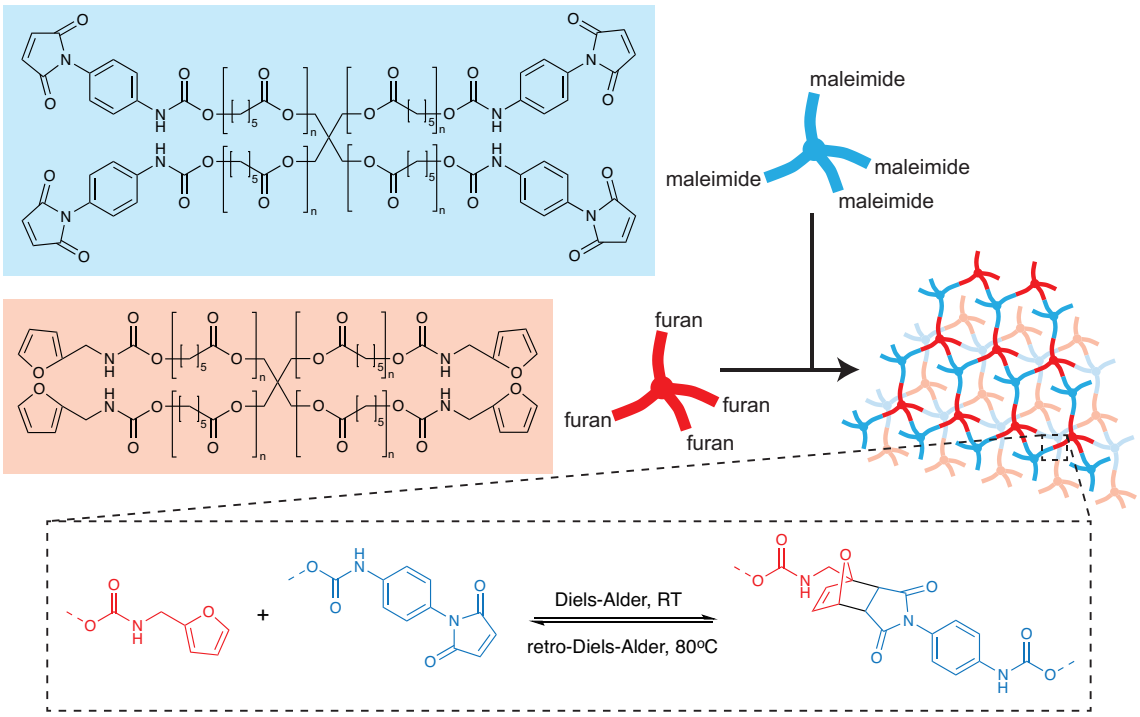

Figure 5.17: Synthesis of gel from tetra-arm oligomer using Diels–Alder reaction.

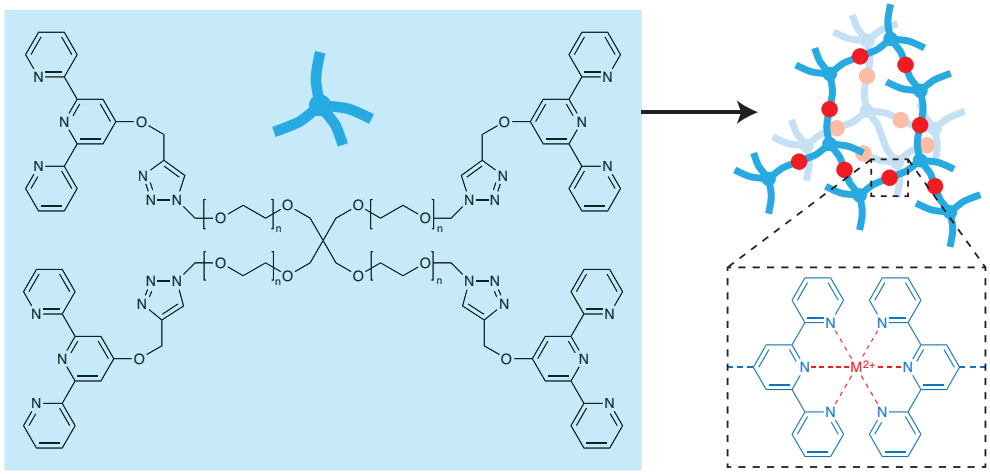

Figure 5.18: Synthesis of Tetra-PEG gel by using the complex formation with transition metal ions.

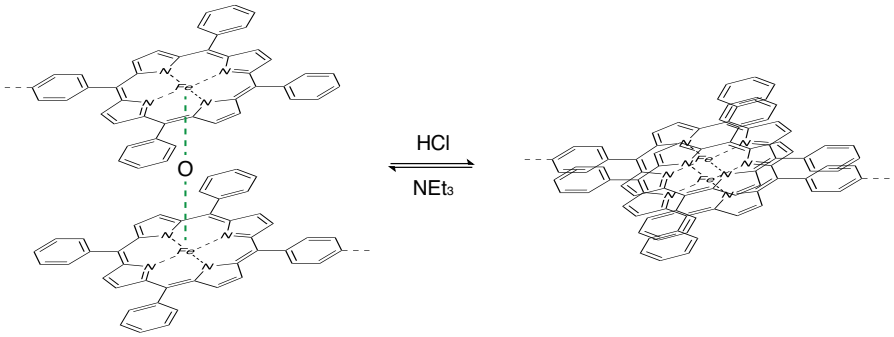

Figure 5.19: Synthesis of Tetra-PEG gel by using tetraphenylporphyrin.

5.4 Characterization of Tetra-PEG gel

After the invention of Tetra-PEG gel, characterization has been done thoroughly. Here I'm going to summarize previous research related to the characterization of Tetra-PEG gels. The basic knowledge for the quantitative description of soft matter is shown in Section 3.2.

5.4.1 Reaction

To elucidate the origins of the strength of Tetra-PEG gels, the efficiency and detailed mechanism of crosslinking reaction was investigated. Akagi *et al.* measured reaction efficiency from the amount of sol fraction [119]. By using Miller–Macosko theory [120], the proportion of sol fraction, ω_{sol} is written as a function of reaction efficiency, p, as follows:

$$\omega_{\mathrm{sol}} = \left[\left(\frac{1}{p} - \frac{3}{4} \right)^{1/2} - \frac{1}{2} \right]^4 \tag{5.4.1.1}$$

By using Eq.(5.4.1.1), reaction efficiency of Tetra-PEG whose molecular weight is 10 kg/mol was estimated to be $p \sim 0.75$ regardless of the polymer fraction, ϕ_0. Kurakazu *et al.* investigated the gelation kinetics [121]. By potentiometric titration, they showed that the pK_a of amine groups at the end of tetra-arm PEG is 9.27. Here, K_a is defined as follows.

$$K_a = \frac{[\mathrm{PEG\text{-}NH_2}][\mathrm{H^+}]}{[\mathrm{PEG\text{-}NH_3^+}]} \tag{5.4.1.2}$$

This result shows that most of the amine groups are protonated at neutral pH. Since the reaction between amine and active ester occurs only when amine is not protonated, gelation rate can be controlled by pH. They proved this fact quantitatively by using pH-dependence of gelation time. Here, gelation time was determined quantitatively by using the criteria of Chambon and Winter [122]; the time where $G' = G''$. In addition, they showed that the degradation of active ester-terminated tetra-arm PEG can be proved by the absorption at 290 nm. By using these partially degraded active ester-terminated tetra-arm PEG, we can tune the total connectivity at will. This is named p-tuned Tetra-PEG gel [123]. Later, direct determination of p by using IR spectra was developed [124]. In this technique, they focused on the absorption peaks originated from CO stretching vibration and amide II band. As the crosslinking proceeds, the intensity of amide II band

becomes strong. By using this technique, they showed that the terminal conversion efficiency is around 0.95. From the time-resolved IR spectroscopy measurement, it was clarified that this reaction can be described as a second-order reaction [125]. The reaction rate of crosslinking of Tetra-PEG gel was found to be much smaller than that of typical diffusion-controlled reaction [126]. This result suggests that the complete mixing of two types of prepolymer will be achieved before crosslinking and this may be the origin of homogeneous structure of Tetra-PEG gel. Simulation of this gelation is also reported [127].

5.4.2 Mechanical property

In the first report of Tetra-PEG gel [11], they performed compression test. The maximum value of breaking strength was obtained when the ratio of amine-terminated PEG and active ester-terminated PEG is 1:1 as expected from the preparation scheme. Later, gel preparation with an unbalanced stoichiometry was utilized for the research of sol-gel transition [128]. Typical Tetra-PEG gel can bear more than 90% strain and several MPa compression stress. Later, the maximum breaking stress and compression modulus were improved to be 25 MPa and 100 kPa, respectively [12]. Akagi *et al.* performed stretching measurement to investigate the elastic moduli of Tetra-PEG gel [119]. Elastic moduli is related to the density of elastically effective chain, ν, as shown in Eq.(3.2.1.19) under the approximation that all of the chains in the gel are deformed similar to the macroscopic deformation. This is called affine network model. If we consider the fluctuation of polymer chains, the elastic modulus of the gel will be decreased. One of the models which takes the fluctuation of polymer chains into consideration is phantom network model. Under this model, the elastic modulus is reduced to $(f-2)/f$ from affine network model where f is the functionality of crosslinking [23]. The model called junction affine network model predicts the intermediate value [124]. By using the density of crosslinking, μ, G of these models are written as follows.

$$G = \begin{cases} \nu RT & \text{for affine network model} \\ (\nu - \mu)RT & \text{for phantom network model} \\ (\nu - h\mu)RT & \text{for junction affine network model} \end{cases} \tag{5.4.2.1}$$

where h is a constant indicating the degree of thermal fluctuation of chemical crosslinks. From experimentally obtained G and p, they concluded that the elasticity of Tetra-PEG gel is well described by the affine theory. In addition, they found that the ϕ_0-dependence of ν is weak ($\nu \sim \phi_0^{1.28}$) compared to conventional gels ($\nu \sim \phi_0^{9/4}$). This result was interpreted as the absence of entanglements. Later, through more precise evaluation, the elasticity of Tetra-PEG gel described by the phantom theory was found [124]. At last, they conclude that there is a transition from the phantom network model to the affine network model at the overlapping polymer concentration [129]. Concentration dependence of the elastic modulus was investigated carefully by using Obukhov model and Panyukov model in the following paper [130, 131]. Kondo *et al.* showed that the heterogeneous distribution of strand length does not affect the mechanical properties of hydrogels by using Tetra-PEG bimodal gels, or size-mismatched Tetra-PEG gels [132, 133]. Simulation of the elasticity shown above was reported [134–137].

The stress-strain curve was also expressed analytically. In small strain, the relationship between stress

and strain is proportional like a spring. This is called Hooke's law.

$$\sigma = G\lambda \tag{5.4.2.2}$$

When the strain becomes large, ideal dependence between σ and λ is represented as follows (neo-Hookean material) [124].

$$\sigma = G(\lambda - \lambda^{-2}) \tag{5.4.2.3}$$

Here, σ is the experimentally observed stress called engineering stress.[76] However, this model did not reproduce the experimental results at large strain due to the finite extensibility. This problem was solved by using the extended Gent model [138].

$$\sigma = \frac{C_1(\lambda - \lambda^{-2})}{1 - \dfrac{\lambda^2 + 2\lambda^{-1} - 3}{\lambda_{\max}^2 + 2\lambda_{\max}^{-1} - 3}} + C_2(1 - \lambda^{-3}) \tag{5.4.2.4}$$

where C_1 and C_2 are the fitting parameter representing the number density of elastically effective strands and the strength of strain-coupling, respectively. Here, $C_1 + C_2 = G$ is satisfied. $\lambda_{\max}$ is the ultimate deformation ratio. Other function which reproduces the stress-strain curve is shown in [12].

$$\sigma = \frac{\nu RT}{3}\frac{N}{\lambda_{\max}}\left[\mathcal{L}^{-1}\left(\frac{\lambda}{\lambda_{\max}}\right) - \lambda^{-3/2}\mathcal{L}^{-1}\left(\frac{\lambda^{-1/2}}{\lambda_{\max}}\right)\right] \tag{5.4.2.5}$$

where $\mathcal{L}(x)$ represents Langevin function. Dynamic mechanical response of Tetra-PEG gels was also measured in the same paper. They showed that G'' was extremely small, which is lower than the measurable limit. This reflects the homogeneous nature of Tetra-PEG gels. Katashima *et al.* extended these stretching experiments in 2D by biaxial deformation [139, 140]. Akagi *et al.* also investigated fracture of Tetra-PEG gel [129]. Fracture energy, T, is defined as follows.

$$T := \frac{2F}{w} \tag{5.4.2.6}$$

where F is the tearing force and w is the thickness of the specimen. Fracture energy with infinitely slow stretching speed is called intrinsic fracture energy, T_0. In the Lake–Thomas model [141], T_0 is represented as follows.

$$T_0 = \frac{1}{2}L\nu NU \tag{5.4.2.7}$$

where L, N, U stand for the displacement strength, the degree of polymerization of the network, and the energy required to rupture a monomer unit. ϕ_0 and N dependence of T_0 showed good agreement with this model. Later, quantitative agreement was proved by multiplying an enhancement factor $k = 3$ to Eq.(5.4.2.7) [142, 143].

5.4.3 Static structure

Strength of Tetra-PEG gel is also explained from the viewpoint of static structure. Microscopic structure of Tetra-PEG gels was investigated by SANS experiment [15, 16]. In these experiments, hydrogels prepared by deuterated water were used as samples. Since the neutron scattering lengths of light hydrogen and heavy hydrogen are totally different, we can easily make contrast between solvent and polymer network (see Section 4.2.2 for further details). SANS profiles of Tetra-PEG solution were reproduced well by using form factor of star-polymer chains (Eq.(2.2.4.1)) with the single-contact theory of Zimm (Section 2.4.6). As for SANS

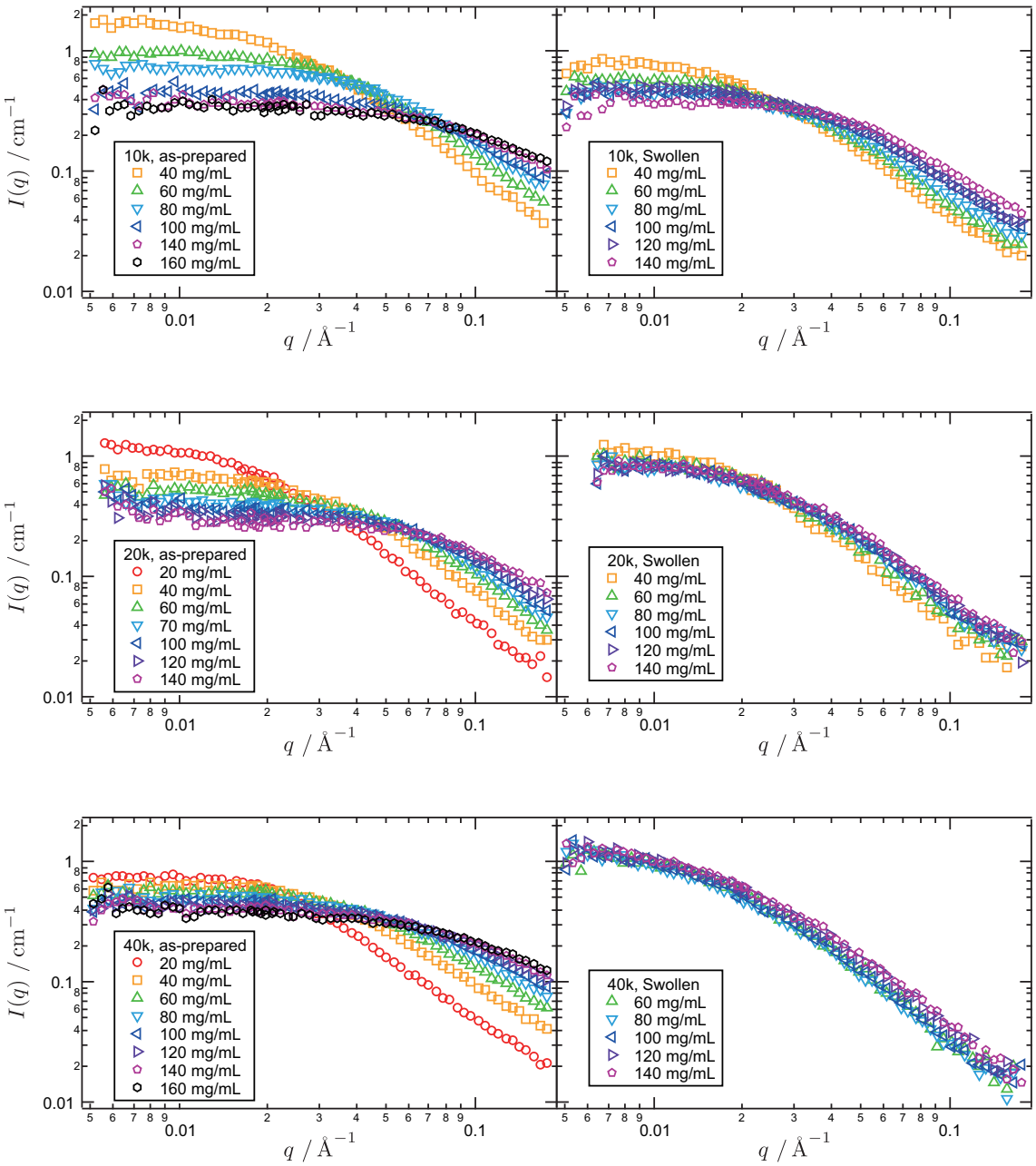

Figure 5.20: SANS profiles of Tetra-PEG gels [16].

[76] If we follow the definition of stress, we have to take the decrease of cross-section into consideration. This is called true stress.

profiles obtained from Tetra-PEG gels were shown in Figure 5.20. Figure 5.20 shows the SANS profiles obtained from Tetra-PEG gels with various concentration and molecular weight [15, 16]. In Figure 5.20, we can see concentration and molecular weight dependence and the effect of swelling on their SANS profiles. One of the most important features is that there is no upturn in low-q region for all of the samples shown in Figure 5.20. The upturn appearing in low-q region is a typical feature for conventional gels (Figure 5.21) and this upturn has been interpreted as inhomogeneities of gels. Therefore, the suppression of this upturn suggests that Tetra-PEG gels are homogeneous compared to the conventional gels. The effect of swelling on the microscopic structure is also clarified. SANS profiles of swollen gels whose molecular weight is 40 kg/mol are almost independent of their initial preparation concentration while that of 10 kg/mol show concentration dependence. The fact that the swollen gels did not show strong concentration dependence is that the network structure is unique regardless of preparation concentration. This is interpreted in such a manner that the resultant gels are inhomogeneity-free and microscopic structure is described as shown in Figure 5.9. In the case of short molecular weight, inhomogeneities (mainly loose ends) are introduced and small concentration dependence appears in their microscopic structure. This is consistent with the experimental result that the Tetra-PEG gels whose molecular weight is 5 kg/mol showed upturn in low-q region in as-prepared state. Note that the detailed analysis showed small concentration dependence of correlation length even for 40 kg/mol samples, which is also clarified in DLS measurements as shown later (Figure 5.25). For more detailed analysis, please refer to Ref [15, 16]. Structural analysis of Tetra-PEG gels under uniaxial deformation [144] and p-tune Tetra-PEG gels [123] was performed. Simulation of microscopic structure of Tetra-PEG gels was also reported [145–147].

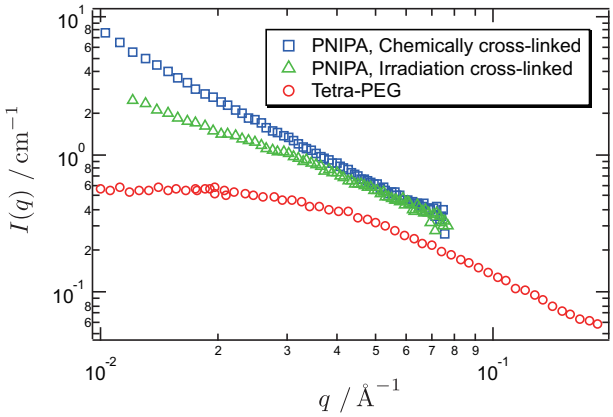

Figure 5.21: Comparison of SANS profiles obtained from three different gels [16, 148].

5.5 Multiscale dynamics of Tetra-PEG gel

Inhomogeneity-free nature of Tetra-PEG gels was also shown in dynamics of gels. Here I'm going to summarize the dynamics of Tetra-PEG gels elucidated by dynamic light scattering (DLS, Section 4.1.2) and neutron spin echo (NSE, Section 4.2.4) technique [29]. DLS was used to see the dynamics in the scale of 10∼100 nm, and NSE was used to see the dynamics in smaller scale (several nanometer).

5.5.1 Dynamic light scattering

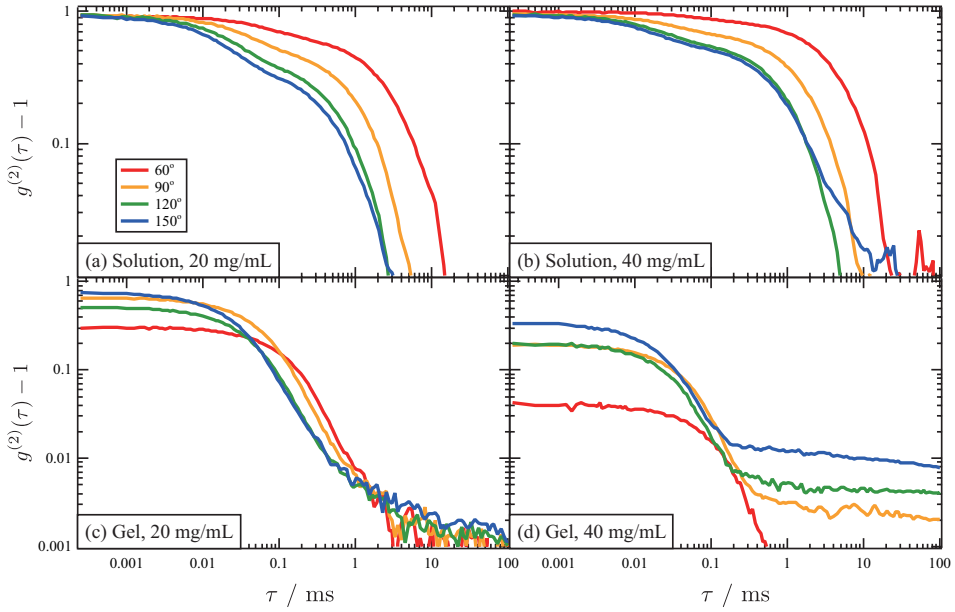

Figure 5.22: Normalized intensity time correlation functions of Tetra-PEG. (a) 20 mg/mL solution, (b) 40 mg/mL solution, (c) 20 mg/mL gel and (d) 40 mg/mL gel. In each graph, the data obtained at different scattering angles (60, 90, 120 and 150°) are shown.

In the first report of Tetra-PEG gels, time-resolved DLS was performed for the evaluation of gelation time [11]. Here I'm going to show the detailed analysis of Tetra-PEG gels by DLS. As a representative result, the normalized intensity time correlation functions of Tetra-PEG solutions and gels whose molecular weight is 20 kg/mol are shown in Figure 5.22. The concentration was set to 20 mg/mL ($c^*/2$) and 40 mg/mL (c^*). Overlap concentration, c^*, of Tetra-PEG in solution was determined by viscosity measurement [11,129]. The measurements were performed in four different scattering angles to obtain q-dependence of decays as shown later (Figure 5.24). Each time correlation function was converted into the characteristic decay time distribution functions by an inverse Laplace transform. These distribution functions are the function of decay rate, Γ. Then Γ is converted into the diffusion constant and the parameter called correlation length, ξ, as follows.

$$\Gamma = Dq^2 \tag{5.5.1.1}$$

$$\xi = \frac{k_B T}{6\pi\eta D} \tag{5.5.1.2}$$

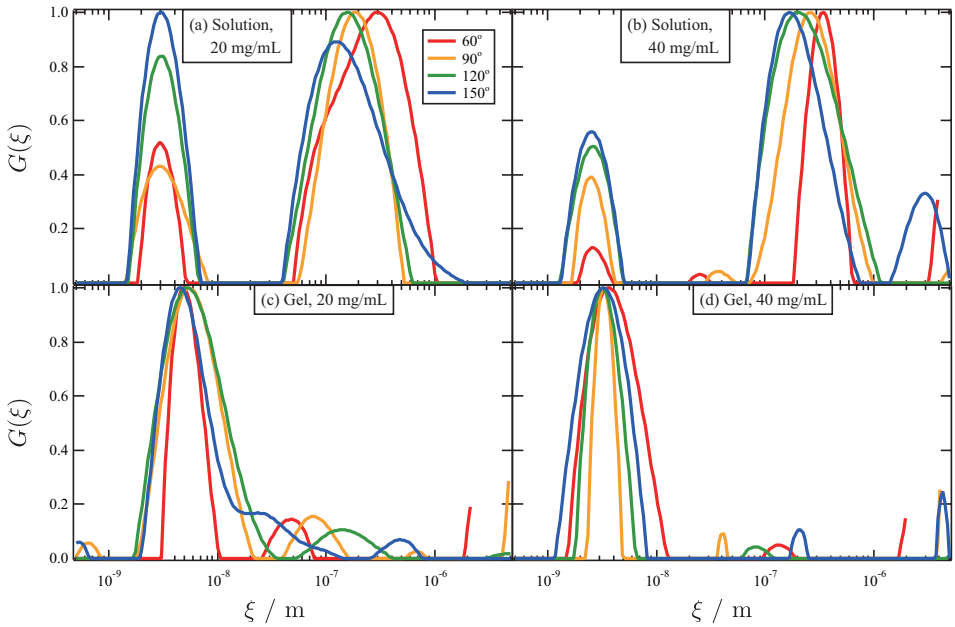

Figure 5.23: Probability distribution functions of ξ for Tetra-PEG solutions. (a) 20 mg/mL, (b) 40 mg/mL and for gels, (c) 20 mg/mL, (d) 40 mg/mL. In each graph, the data obtained at different scattering angles (60, 90, 120 and 150°) are shown.

where k_B, T and η are the Boltzmann constant, absolute temperature and the viscosity of the solvents (0.911 cP for sol buffer and 0.896 cP for gel buffer). q is a momentum transfer, $q := 4\pi n \sin\theta/\lambda$ and n is a refractive index of the solvent. As you can see in Eq.(5.5.1.2), ξ stands for the hydrodynamic radius for dilute solution. The results are shown in Figure 5.23. Figure 5.23 shows that there are two relaxation modes in solutions. Fast modes correspond to the relaxation originated from translational diffusion of single monomers [149,150]. In contrast to this, Wang reported that the slow modes can be attributed to the small bubbles [151]. For further analysis, the intensity time correlation functions are fitted as follows.

$$g^{(2)}(\tau) - 1 = [A_f \exp(-\Gamma_f \tau) + A_s \exp(-\Gamma_s \tau)]^2 \quad \text{for solutions} \tag{5.5.1.3}$$

$$g^{(2)}(\tau) - 1 = A \exp(-2\Gamma_A \tau) \quad \text{for gels} \tag{5.5.1.4}$$

A_f, A_s, and A represent the amplitude for the fast modes of solutions, slow modes of solutions, and decay of gels, respectively. In the case of solution, $A_f + A_s = 1$ since the smearing effect is negligibly small. In contrast to this, I applied partial heterodyne method for the analysis of gel samples (Section 4.1.3). Γ_A is converted into the genuine relaxation rate, Γ, by using the following relationship.

$$\Gamma_A = \frac{1 - \sqrt{1 - A}}{A}\Gamma \tag{5.5.1.5}$$

Figure 5.24 shows q-dependence of the relaxation rates, Γ_f, Γ_s, and Γ, calculated by the data with different scattering angles. They showed clear q^2-dependence. q^2-dependence implies that the observed relaxation originates from Brownian motion of objects. Γ_f, Γ_s, and Γ were then converted into the diffusion constants by using Eq.(5.5.1.1). In other words, the diffusion constants were estimated from the slopes in Figure 5.24. These diffusion constants were converted into the correlation length, ξ, through Eq.(5.5.1.2). The results are summarized in Table 5.1. Concentration and molecular weight dependence of ξ are shown in Figure 5.25.

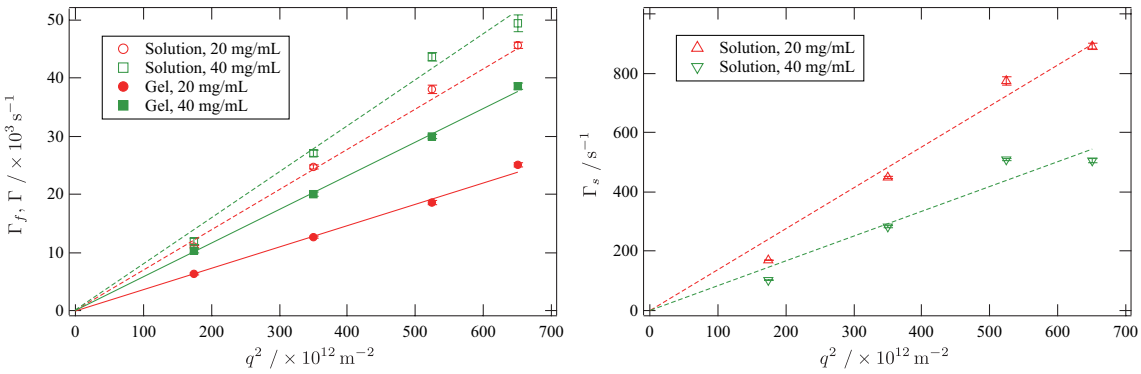

Figure 5.24: q^2-dependence of the decay rates of Tetra-PEG solutions (upper, Γ_f; lower, Γ_s) and gels (upper, Γ). The dashed lines show the best fit by Eq. 4.2.4.5 for solution samples, and the solid lines show that for gel samples.

Table 5.1: Diffusion constants and correlation lengths measured by DLS

State	Concentration / mg mL^{-1}	D / m^2 s^{-1}	ξ / nm
Solution, fast	20	$(6.9 \pm 0.1) \times 10^{-11}$	3.5 ± 0.1
Solution, fast	40	$(7.9 \pm 0.1) \times 10^{-11}$	3.1 ± 0.1
Solution, slow	20	$(1.4 \pm 0.1) \times 10^{-12}$	$(1.8 \pm 0.1) \times 10^2$
Solution, slow	40	$(8.4 \pm 0.6) \times 10^{-13}$	$(2.9 \pm 0.2) \times 10^2$
Gel	20	$(3.7 \pm 0.1) \times 10^{-11}$	6.7 ± 0.1
Gel	40	$(5.8 \pm 0.1) \times 10^{-11}$	4.2 ± 0.1

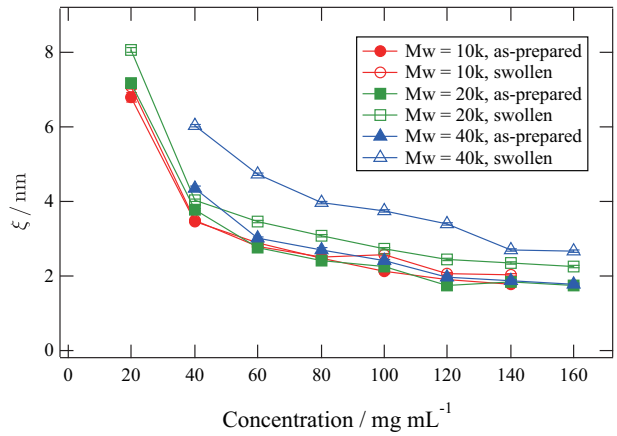

Figure 5.25: Concentration and molecular weight dependence of ξ for as-prepared and swollen Tetra-PEG gels.

In the case of solutions, ξ implies the size of solutes. Note that ξ is not exactly the same as the hydrodynamic radius in higher concentration region. Table 5.1 shows that ξ becomes small as the concentration increases. This result is consistent with the result obtained from SANS and interpreted that the monomers are compressed by the neighboring monomers as the concentration increases [16]. In the case of gels, ξ obtained from DLS is usually interpreted as an indicator of mesh size when the polymer network is far from its critical point [5]. Figure 5.25 is interpreted in line with this assumption. Molecular weight dependence

is not observed in as-prepared gels. This means that the mesh size is determined only by the concentration of polymers. In contrast to this, there are clear molecular weight dependence for swollen gels. This is because the mesh size is determined mainly by the molecular weight of polymers in the case of swollen gels. The decrease of ξ with the increase of polymer concentration is also reasonable since the distance between polymers becomes small as the concentration increases.

Comparison of the diffusion constant, D, of solution and gel samples shows interesting results. In the case of gels, D is related to the elastic modulus of longitudinal mode (Eqs.(3.2.3.26), (3.2.3.27)).

$$D = \frac{K_{os} + \frac{4}{3}G}{f} \tag{5.5.1.6}$$

where K_{os}, G, f are the osmotic modulus, the shear modulus, and the friction constant. From Eq.(5.5.1.6), it is clear that D for gels is decomposed into two. The first component is the osmotic modulus, K_{os}, which is the same as the solution sample. The second component is the shear modulus, $4G/3$, which is the characteristic point of gels. Since $G > 0$, D for gels is larger than that of solutions [152]. However, the result of Tetra-PEG gels showed opposite behavior. This discrepancy may arise from the assumption that the gel is regarded as a continuous elastic body. For conventional gels, this assumption is useful since the environment around each monomer is almost averaged because of the inhomogeneities. In contrast to this, in the case of Tetra-PEG gels, fluctuation of each monomer may be affected by the details of surrounding environment. For the elucidation of this point, further studies are required.

5.5.2 Neutron spin echo

Neutron spin echo measurement was performed at NSE-SNS neutron spin-echo spectrometers at the Spallation Neutron Source (SNS) at the Oak Ridge National Laboratory [153,154]. The sample solutions and gels were set in a sealed aluminum container of size $40 \times 30 \times 2$ mm under room temperature. Neutron wavelength was from 5 to 8 Å. Measurement angle covered $0.054 < q < 0.189$ Å^{-1}, which corresponds to $0.01 < t < 34$ ns for the measured intermediate dynamic structure factor. All of the samples were prepared by using D_2O as a solvent to reduce incoherent scattering from the solvent. Measurement time was approximately 50 hours for 40 mg/mL (c^*) samples and 60 hours for 20 mg/mL ($c^*/2$) samples.

As explained in Section 4.2.4, the measured quantity of NSE is the intermediate dynamic structure factor, $I(\vec{q}, t)$.

$$I(\vec{q}, t) = \frac{1}{N} \sum_{i}^{N} \sum_{j}^{N} \langle \exp[-i\vec{q} \cdot \vec{r}_i(0)] \exp[i\vec{q} \cdot \vec{r}_j(t)] \rangle \tag{5.5.2.1}$$

where N is the number of PEG monomers in the irradiated volume and $\vec{r}_i(t)$ is the position of PEG monomer i at time t. In this experiment, protonated PEG was used as a sample. In this case, main contribution in Eq.(5.5.2.1) is the part where $i \neq j$. This part is called coherent intermediate dynamic structure factor. In general, $I(\vec{q}, t)$ is a complicated function. However, the long-time behavior of the coherent factor can be expressed by a stretched-exponential form.

$$I(q, t) \propto \exp[-(\Gamma t)^{\beta}] \tag{5.5.2.2}$$

β and Γ are the characteristic parameters for the modes and summarized in Table 5.2. Derivation of $I(q, t)$ for Rouse mode and Zimm mode are shown in Section 3.1.2. Strictly speaking, Eq.(5.5.1.2) holds true only

for long-time region. However, in the following analysis, we assume that Eq.(5.5.2.2) is valid for all the time region. This approximation is common and good approximation [155,156]. In the following discussion, I use the normalized coherent intermediate dynamic structure factor and fit as follows.

$$\frac{I(q,t)}{I(q,0)} = A_0 + A_1 \exp[-(\Gamma t)^{\beta}] \tag{5.5.2.3}$$

A_0 represents the non-decay components. This component is typical for the gel system and regarded as a frozen component, which is explained later. We can see that $A_0 + A_1 = 1$ by substitute $t = 0$ into Eq.(5.5.2.3).

Table 5.2: Characterization of microscopic motion

Types of motion	β	Γ
collective diffusion	1	$\propto q^2$
Zimm mode	2/3	$\propto q^3$
Rouse mode	1/2	$\propto q^4$

Types of motion

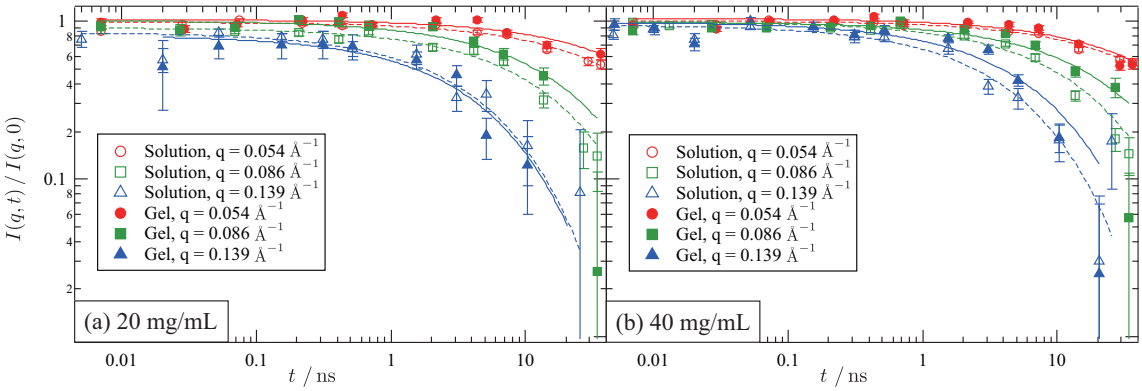

Figure 5.26: Normalized intermediate dynamic structure factors of Tetra-PEG solutions and gels. The dashed lines show the best fit by Eq. 4.2.4.12 for solution samples and the solid lines show that for gel samples with $\beta = 2/3$.

Figure 5.26 shows some of the obtained normalized intermediate dynamic structure factors, $I(q,t)/I(q,0)$, of Tetra-PEG solutions and gels. $I(q,t)/I(q,0)$ is fitted by Eq.(5.5.1.3). Fitting results showed that $\beta \simeq 2/3$ for all of the data. This result strongly suggests that the relaxation is represented as a Zimm mode in all q region. After the first fitting, fitting was performed again with fixing β as 2/3. The fitting results are also shown in Figure 5.26. From the fitting, Γ was obtained for each q region. q-dependence of Γ is shown in Figure 5.27. All of the data shows that $\Gamma \sim q^3$, which again suggests that the relaxation is represented as a Zimm mode. In addition to this, it is clarified that there are no difference between solutions and gels in Γ. Concentration dependence was also not observed. This result is also consistent with the Zimm mode since the decay rate of Zimm mode is described only by the temperature and the viscosity of the solvent (Eqs. (3.1.2.31) and (3.1.2.32)). This result that Zimm mode is observed in all q-region is different from the typical results for conventional gels. Reported NSE results for conventional gels showed the transition from Zimm mode (high-q region) to collective diffusion (low-q region) in the measured q-range [152,156,157]. Zimm mode is typical for polymer solutions and collective diffusion is typical for network systems. Therefore, the

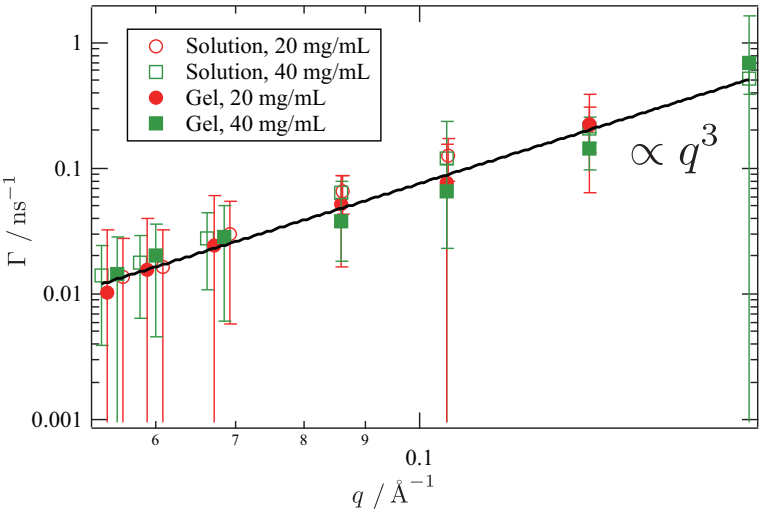

Figure 5.27: q-dependence of decay rate of NSE. The solid line implies q^3.

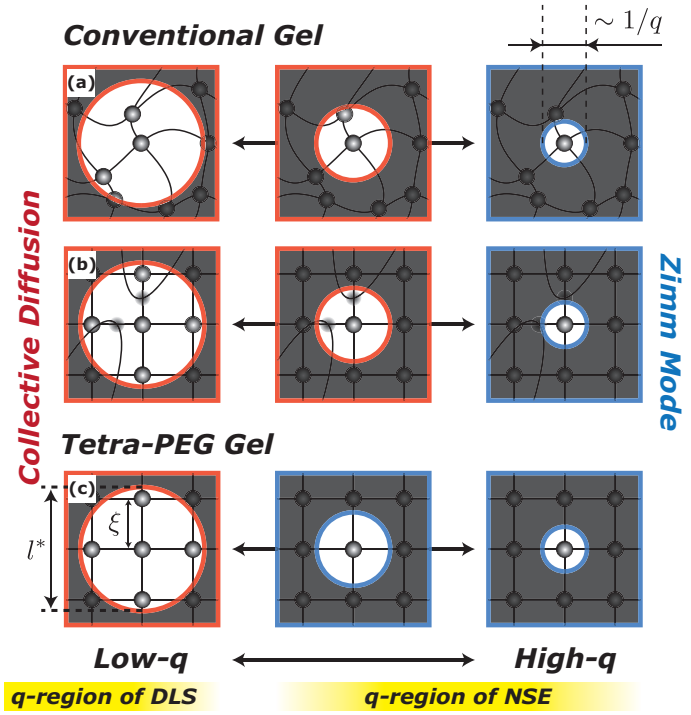

Figure 5.28: Comparison of conventional gels and Tetra-PEG gel from the viewpoint of neurons. In high-q region, monomers do not see other crosslinks. As q becomes lower, monomers begin to see the nearest crosslink and notice their connectivity (a). Entanglements are also regarded as crosslinks in the time region of NSE (b). In the case of Tetra-PEG gel, it requires lower q (i.e., large distance) to see other crosslinks since the length between crosslinks is strictly controlled and there are no entanglements (c).

transition point from Zimm mode to collective diffusion corresponds to the length where monomers "notice" that they are connected to the network systems. This situation is depicted in Figure 5.28(a) and (b). In the case of conventional gels, the fact that a monomer (the monomer at the center of each window in Figure 5.28) is connected to the crosslink point in small length scale compared to the average mesh size mainly by two reasons. First one is the connectivity inhomogeneities (Figure 5.28(a)). The distance between

crosslinks is uneven in the case of conventional gels, especially the gels prepared by the radical reaction. Since the monomer "notices" the existence of crosslinks by the nearest crosslink, transition from Zimm mode to collective diffusion occurs in relatively small length scale, which corresponds to high-q region. Second one is the entanglement (Figure 5.28(b)). Time scale of the phenomena which NSE observes is the order of nanosecond (Figure 5.26). In such a short time region, entanglements are regarded as crosslinking points. Therefore, the existence of entanglements makes the transition point in smaller length scale, or higher q region. In contrast to those conventional gels, Tetra-PEG gels have a few connectivity inhomogeneity and entanglement. Therefore, the fact that only Zimm mode was observed in the NSE measurement proved the inhomogeneity-free nature of Tetra-PEG gels from the viewpoint of dynamics (Figure 5.28(c)).

Disappearance of non-decay component

Fitting results in Figure 5.26 by Eq. 5.5.1.3 showed that the non-decay component, A_0, is almost zero for all of the measurement data. This is also different from the typical results for conventional gels; all of the NSE measurement for chemical crosslink gels showed significant amount of non-decay component. Disappearance of non-decay component was observed only for physical crosslink gels such as PVA with borax [156]. This non-decay component has been interpreted as the existence of frozen component, which is the origin of the upturn in low-q region of SANS profiles. In other words, this non-decay component originates from the inherent inhomogeneities of gels. This kind of inhomogeneity can be suppressed in the case of physical gels since the crosslinking occurs to decrease the inhomogeneity and increase the enthalpy gain by crosslinking. However, the inhomogeneities exist permanently in the case of chemical gels. Tetra-PEG gels solved this difficulty. Therefore, disappearance of non-decay component is also the sign of inhomogeneity-free nature of Tetra-PEG gels.

Quantitative analysis for this issue was performed by Richter *et al.* [158]. In their theory, the non-decay component is attributed to the restriction of the monomer movement as follows.

$$\frac{I(q,t)}{I(q,0)} = \exp\left[-\frac{q^2\langle l^2\rangle}{4}\right] + \left(1 - \exp\left[-\frac{q^2\langle l^2\rangle}{4}\right]\right)\exp[-(\Gamma t)^{\beta}] \tag{5.5.2.4}$$

where $\langle l^2\rangle$ is the square of the width of the Gaussian distribution of the monomer displacement from its equilibrium position. The meaning of Eq.(5.5.2.4) is that the non-decay component becomes large if the monomer movement is small ($\langle l^2\rangle$ is small). In the conventional gels, restriction of monomer movements is explained in two ways (Figure 5.29). The monomers in dense region cannot move significantly from their original position since there are a lot of monomers around them. This situation is similar to the packed commuter train. The monomers in sparse region also cannot move since the the monomers in such a region is in the stretched polymers. In contrast to this, Tetra-PEG gels have no such a density fluctuation. In addition, the number of monomers between crosslinking points is relatively large. For examples, the number of monomers between crosslinking points of typical PNIPA gels [159] is several dozen while that of Tetra-PEG gels used in this experiments is approximately 230. This indicates that the monomers can travel enough to make the first term of Eq.(5.5.2.4) negligibly small.

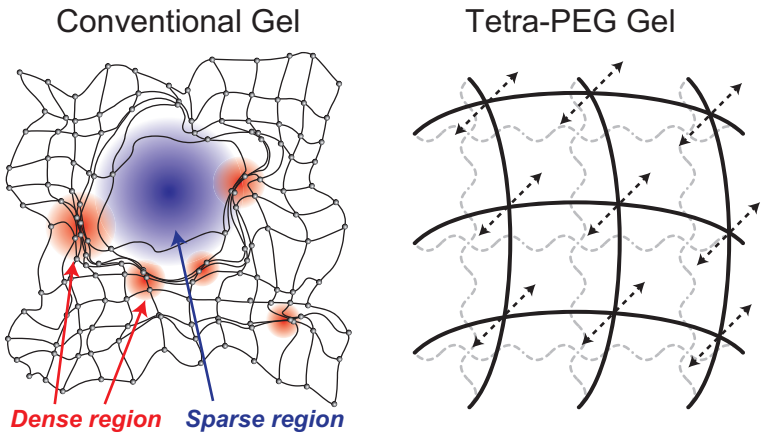

Figure 5.29: Origin and disappearance of non-decay component in $I(q,t)/I(q,0)$.

5.5.3 Integration of different scale motions

Both DLS and NSE measure the decay rate, Γ, in different length scale. Therefore, these results can be combined to see the dynamics in wide q-region. Figure 5.30 shows the q-dependence of Γ/q^2 measured by both DLS and NSE. Γ obtained from DLS (around 10^7 m^{-1}) shows q^{-2} dependence while that obtained from NSE (around 10^9 m^{-1}) shows q^{-3} dependence as mentioned in the previous subsections. In addition, these two results for gels are connected by two lines as shown in Figure 5.30. These two lines indicate the transition from Zimm mode (high-q region, q^{-3}) to collective diffusion (low-q region, q^{-2}), which is usually observed by using only NSE. In the case of solution samples, the connection cannot be achieved since Γ obtained from DLS is larger than that obtained from the low-q region of NSE. The origin of this discrepancy is the translational motion, which appears only in the DLS results. The transition point for the gels, q^*, can be converted into the characteristic length scale, l^*, as follows.

$$l^* := \frac{2\pi}{q^*} \tag{5.5.3.1}$$

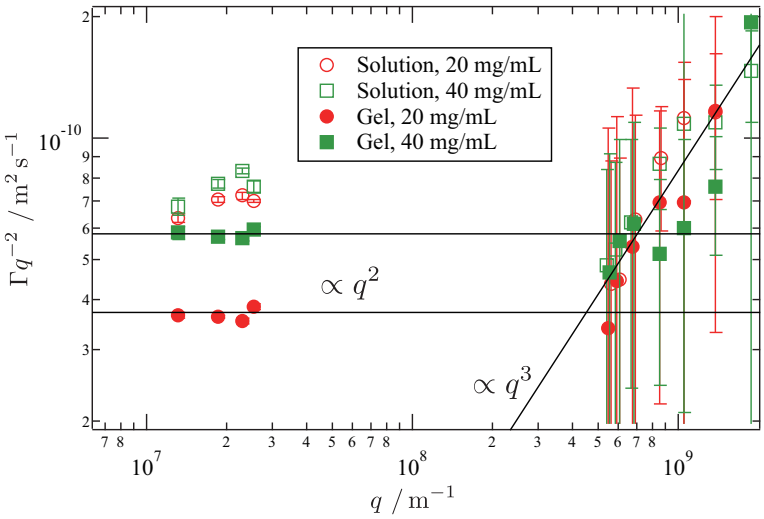

Figure 5.30: Decay rates of Tetra-PEG solutions and gels. The lines are the fitting results. The slopes of the lines are zero and unity.

l^* represents the size of window at the transition from Zimm mode to collective diffusion as shown in Figure 5.28(c). Calculated l^* is 14 nm for 20 mg/mL and 9.0 nm for 40 mg/mL. This value is approximately twice as large as the correlation length, ξ, of the corresponding gels obtained from DLS (Table 5.1); 6.7 nm for 20 mg/mL and 4.2 nm for 40 mg/mL. This result is consistent with the assumption that ξ is the mesh size (Figure 5.28(c)). Like this, through the combined analysis of DLS and NSE, quantitative analysis of the microscopic structure of Tetra-PEG gels is successfully performed.

5.5.4 Summary for the multiscale dynamics

Homogeneous nature of Tetra-PEG gels was examined from the viewpoint of dynamics for the first time. Through the DLS measurements, correlation lengths of solution and gel samples were obtained. Concentration dependence, molecular size dependence, and the effect of swelling for the correlation length of Tetra-PEG gels can be interpreted by considering that the correlation length stands for the mesh size of the gels. The validity of this assumption is quantitatively proved through the combined analysis of DLS and NSE. Furthermore, through the NSE measurements, inhomogeneity-free nature of Tetra-PEG gels was clarified in two aspects. From the q-dependence of the relaxation rates, it is clarified that Zimm mode appears in wide q-region. This result is interpreted that Tetra-PEG gels are free from connectivity inhomogeneity and entanglement. From the non-decay component of the intermediate dynamic structure factor, it is clarified that Tetra-PEG gels have no frozen component. In other words, the monomers in Tetra-PEG gels can move in wide space compared to conventional gels.

5.6 Application of Tetra-PEG gel

Thanks to their superior mechanical characteristics, simplicity of preparation, and biocompatibility, Tetra-PEG gels can be used for various applications. Fujii *et al.* developed Tetra-PEG ion gel to utilize the ion conductivities of ionic liquid in a solid-state material [160]. They prepared a free-standing gel with high strength by the crosslinking of Tetra-PEG macromers in room temperature ionic liquids, 1-ethyl-3-methylimidazolium-bis(trifluoromethanesulfonyl)amide, [C_2mIm$^+$][TFSA$^-$], and 1-ethyl-3-methylimidazolium bis(fluorosulfonyl)-amide, [C_2mIm$^+$][FSA$^-$]. A gel whose solvent is ionic liquid is called an ion gel. Since polymer fraction is small (around 5 wt%), the ionic conductivity of the prepared gel is almost equal to that of pure ionic liquid. Tetra-PEG ion gel can also be used for membrane-based CO_2 separation by utilizing CO_2 adsorption properties of ionic liquids. Structural analysis by using DLS and SANS [161, 162] and reaction control by using protic ionic liquid [163, 164] was performed for preparation of ideal network structure. The use of Tetra-PEG gels as gel electrolytes is also promising for Li ion batteries [165].

One of the other applications is electrophoresis. Li *et al.* investigated the migration behavior of double-stranded DNA in various kinds of Tetra-PEG gels by using capillary electrophoresis technique and revealed the different behavior compared to the existing models [166, 167] They proposed a new empirical model, which can also be applied to conventional inhomogeneous gels [168].

By modifying tetra-arm PEG units to other polymers, we can prepare functional materials without losing homogeneous nature of Tetra-PEG gels. Li *et al.* partially introduced degradation site in active-ester terminated PEG prepolymers to control degradation behavior of Tetra-PEG gels [169]. They also investigated the degradation behavior of Tetra-PEG gels by using H_2O_2 to accelerate the degradation [170]. Kamata *et al.*

partially introduced thermo-responsive polymer, poly(ethylglycidylether), to realize volume phase transition [17, 171, 172]. Thanks to their homogeneous nature, shrinking kinetics obeyed the theoretical prediction for homogeneous shrinking without creating skin layer. Kondo *et al.* partially introduced hydrophobic polymer, poly(dimethylsiloxane), to prepare homogeneous amphiphilic co-network [18]. The prepared gel showed high reliability, and the origin of the reliability is explained by the concept named "mechanical fuse link". Structural analysis of this gel is the topic of Section 9.

5.7 Summary

In this section, I reviewed the previous research related to tough gels. Among them, I focused on Tetra-PEG gels. Tera-PEG gel is prepared by the crosslinking of two tetra-arm PEG units. I reviewed Tetra-PEG gels and related materials that are prepared by similar scheme. Next, previous researches related to characterization of Tetra-PEG gels are reviewed from the viewpoint of reaction, mechanical property, and static structure. From these researches, inhomogeneity-free nature of Tetra-PEG gel is proved. Then, I investigated the inhomogeneity-free nature of Tetra-PEG gel from the viewpoint of dynamics. Through neutron spin echo measurements, it is proved that Tetra-PEG gels do not contain connectivity inhomogeneity, entanglement, and frozen component. The relaxation rates of Tetra-PEG gels obtained from neutron spin echo measurements and dynamic light scattering measurements were connected and the mesh size is evaluated quantitatively. Application of Tetra-PEG gels is also reviewed in the final subsection.

6 Construction of Dynamic Light Scattering Microscope

6.1 Introduction

Dynamic light scattering (DLS) is widely used for the assessment of polymer and colloid solutions. As explained in 4.1.2, the polydispersity of polymer solutions is measured by taking the time correlation function of the scattered light intensity. DLS has many advantages compared to other measurement techniques. Gel permeation chromatography (GPC) is a technique to measure the size distribution of polymer solution using a column filled with gels. The polymers are fractionated with their size. By combining other techniques such as static light scattering, UV-VIS spectrometry, and Raman spectroscopy, additional information such as absolute molecular weight and molecular species can also be extracted. However, a measurement by GPC takes long time (several tens of minutes) and the preparation is complicated. In the case of DLS, typical measurement time is several tens of seconds. In addition, what we have to do is only set the test tube filled with diluted sample solution. Other technique is an electron microscope. This technique realizes very high resolution (the order of angstrom), which cannot be accessed by using visible light. However, solution samples cannot be measured directly since the sample should be set under vacuum condition. Laser diffraction is the technique to measure the size distribution by using light diffraction. However, the measurable range of size is in principle on the order of the wavelength of light. The advantage of DLS compared to laser diffraction is its wide measurable range of size. By using the fluctuation of scattered light intensity, DLS can detect small polymer whose size is on the order of several nanometer, which cannot be measured by using laser diffraction.

Though DLS has many advantages mentioned above, there still exists room for improvements. Here I raise three drawbacks [173, 174]. The first one is that DLS cannot be used for turbid system. The origin of turbidity is the multiple scattering. As explained in 4.1.1, the intensity of scattered light is proportional to R^6 where R is the radius of scattered particles. Therefore, the particles whose radius is the order of 100 nm scatter light strongly. As a result, the light is scattered more than one before it escapes from the scatterer. Since this diffuse reflection has little relation to its wavelength, white turbidity is observed. The formula used for the analysis of DLS results are derived under the assumption of single scattering condition, multiple scattering should be suppressed for DLS measurement. The second drawback is that DLS cannot be used for light-absorbing system. This is obvious since the scattered light is not observed if it is absorbed by the sample itself. To overcome these two drawbacks, the sample is diluted before measurement. However, dilution may change the size distribution of the original sample significantly. In fact, this is true as we clarified by using carbon nanotube dispersion, which is explained later (Section 7). The third drawback is the poor spatial resolution. The spatial resolution of typical DLS system is on the order 100 μm. This poor resolution originates from practical difficulty and can be improved by applying another optical setup. By improving the spatial resolution of DLS, the applicability of DLS will be expanded significantly. For examples, the fluctuation of polymer brush at the interface of substrate will be measured directly. Another example is biological cells. The fluctuation of cell organelle can be measured, which cannot be accessed any existing apparatus. Interesting application is the measurement of number fluctuation. When the number of scatterers within the irradiated volume is so small, the intensity time correlation is strongly affected by the number fluctuation like FCS. If the high resolution DLS is applied for gel samples, spatial inhomogeneities and dynamic fluctuations can be measured simultaneously [5]. Many studies have been conducted on how

to overcome these disadvantages which I introduce in the next section [175–180]. However, no studies have been reported on the application of DLS to opaque media with high spatial resolution.

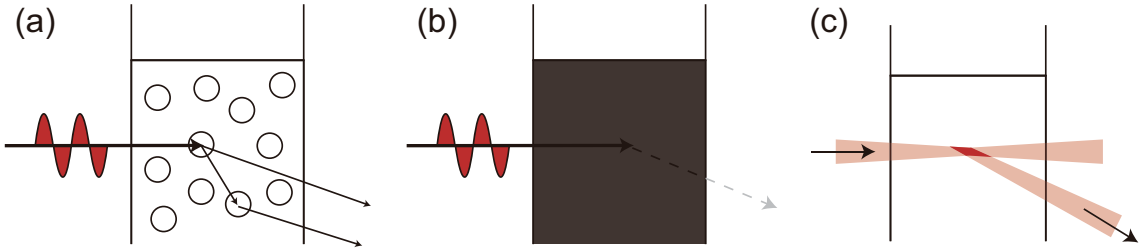

Figure 6.1: Drawbacks of DLS. (a) Multiple scattering. (b) Strong light absorption. (c) Poor spatial resolution.

In this section, I introduce a new technique named dynamic light scattering microscope [30]. This technique is the combination of DLS and an optical microscope. This combination itself has already reported in several papers [181–183] though all of them utilize forward scattering. In contrast to them, I applied backscattering geometry to reduce the optical path, similar to a Rayleigh light scattering microscope [184, 185]. This geometry enables us to measure opaque samples without dilution. In addition, spatial resolution close to diffraction limit is achieved by using an objective lens. First, I introduce existing DLS techniques to overcome its drawbacks. Next I introduce the optical setup of the DLS microscope. Then some representative results are shown to explain the applicability of the DLS microscope. The results obtained from carbon nanotube dispersions are especially interesting and explained in the next section.

6.2 Previous studies

A cross correlation spectroscopy is a technique to extract singly scattered light by using two-beam, two-detector light scattering spectrometer (Figure 6.2(a)) [175, 176]. In this experiment, a cross correlation was used to remove the effect from the multiply scattered light. To remove the multiply scattered light, two-color dynamic light scattering is also useful technique (Figure 6.2(b)) [13]. In this technique, they extract the same q component with different scattering angle by utilizing two different color of light. The different approach for the measurement of dense media is the evaluation of the intensity correlation function in consideration of multiple scattering explicitly, called diffusing wave spectroscopy [177, 178]. Another example is a low-coherence DLS (Figure 6.2(c)) [179]. The unique feature about this technique is the use of a superluminescent diode as the light source. Its short coherence length was efficiently utilized to remove multiple scattering. From a viewpoint of the application of DLS to biological cells, a novel technique was proposed by Dzakpasu and Axelrod [180]. They successfully created spatial maps of fluctuation decay rates with a high spatial resolution (μm order) by a combination of confocal microscopy and a streak camera. There is another technique to track the dynamics of solutes called total internal reflection microscopy [186, 187]. However, the applicability of this technique is limited to a thin layer.

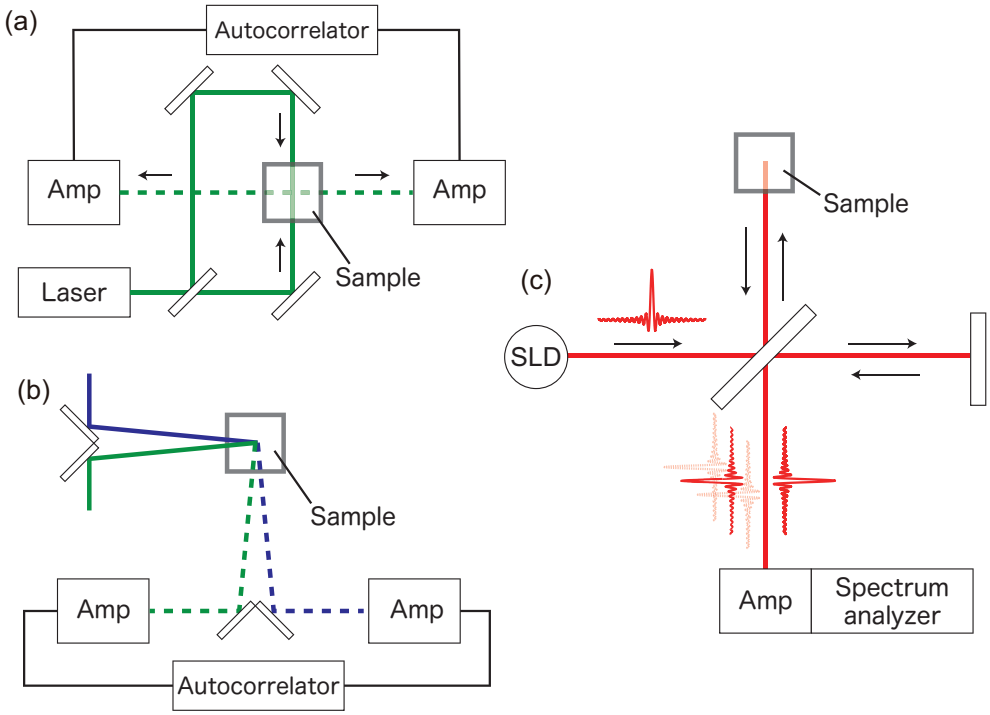

Figure 6.2: Representative techniques for the measurement of dense dispersion. (a) Cross correlation spectroscopy. (b) Two-color dynamic light scattering. (c) Low-coherence dynamic light scattering

6.3 Experimental

The schematic of the DLS microscope is shown in Figure 6.3. The laser light ($\lambda = 514.5$ nm, Stabilite 2018, Spectra-Physics) is reshaped by using the first pinhole and expanded by a factor of three. After that, the polarization is adjusted by using a $\lambda/2$ plate. This light is introduced into a microscope with a backscattering geometry (ECLIPSE Ti-U, Nikon Instech Co., Ltd.). The sample solution is shielded in a cavity slide. This sampling scheme reduces the required amount of samples to 50 μL. Note that a conventional DLS apparatus requires approximately 1 mL sample. In addition, the path length within the sample solution is reduced to the order 10 μm, which is approximately 10 mm for the conventional DLS system (Figure 6.4. Backscattered light is then guided to avalanche photodiode after passing through a second pinhole. To obtain an optical image, a long-pass filter is used as a launch mirror. The optical image is obtained with the same configuration since the light with long wavelength can be used as an illumination light.

The size of PH2 is determined as follows (Figure 6.5). In this experiment, I used an objective lens of Olympus. The focal length of secondary objective is set to 200 mm [77]. This means that the image of the objective lens is magnified nominal times by using the lens of $f = 200$. In our case, the size of focus at the stage of microscope is estimated to be 1 μm. Since this image is magnified 40 times by using the secondary objective, the size of focal point is 40 μm. Here, I used $f = 100$ lenses instead of precise secondary objective lens because of the space of our base. In this case, the magnification ratio is reduced to $40 \times (100/200) = 20$. Theoretically, the size of pinhole should be set to $\phi = 20$ μm. However, I set the size of pinhole to be $\phi = 50$ μm in consideration of the incompleteness of optical system.

[77] In the case of Nikon, that is set to 180 mm.

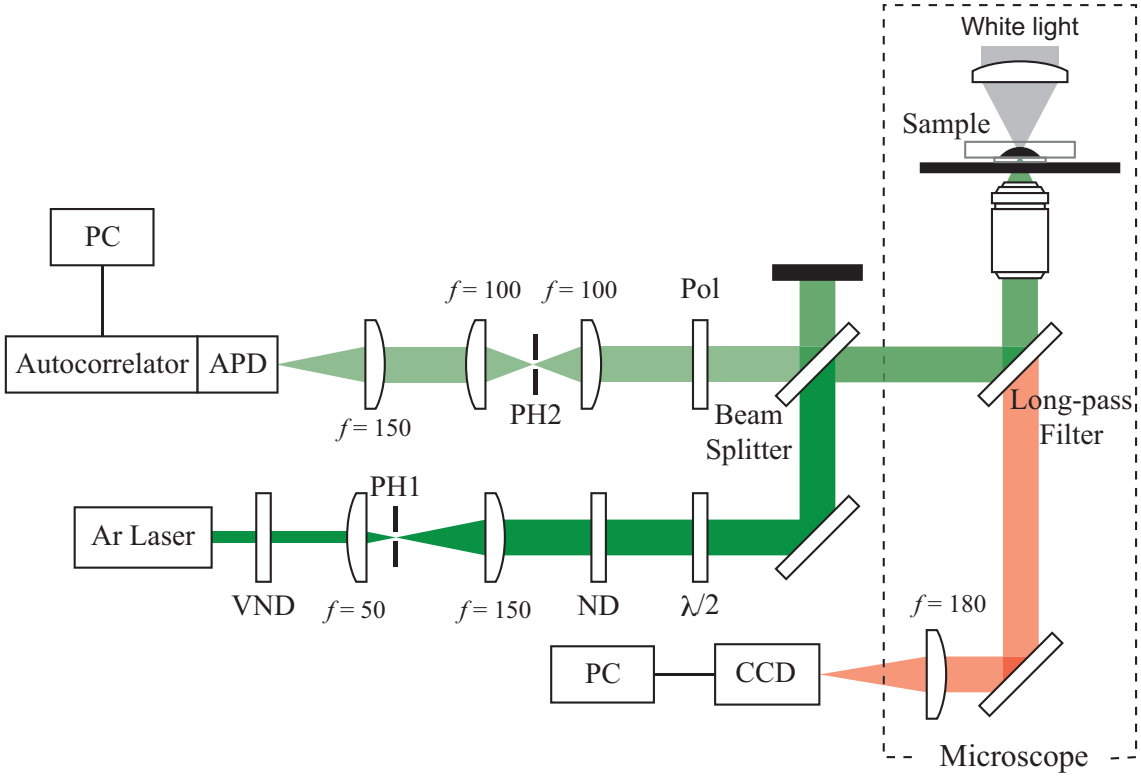

Figure 6.3: Schematic of the proposed DLS microscope: VND, variable neutral density filter; PH1, pinhole, $\phi = 25$ μm; HM, half mirror; BD, beam diffuser; PH2, pinhole, $\phi = 50$ μm; APD, avalanche photodiode.

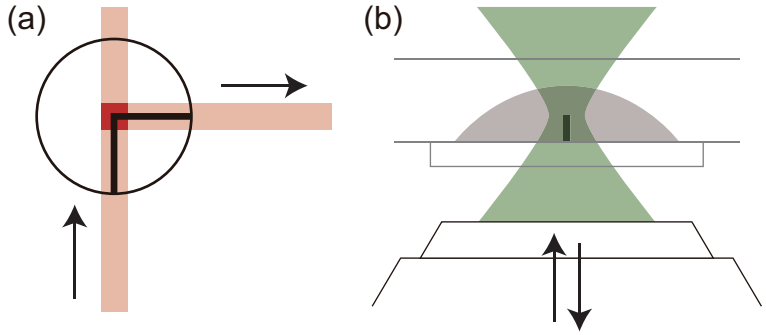

Figure 6.4: Comparison of the path length. (a) Conventional DLS system. (b) DLS microscope.

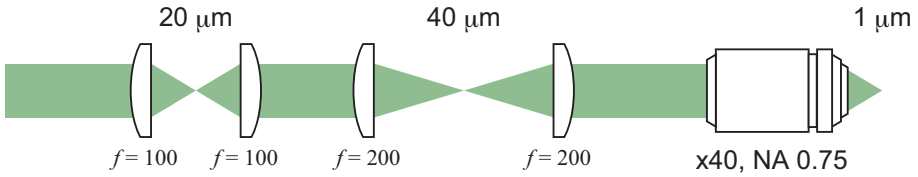

Figure 6.5: Calculation of the size of pinholes. We assume that the focal length of secondary objective is set to 200 mm. This means that the image of the objective lens is magnified 40 times by using the lens of $f = 200$.

By applying a confocal optical system, high spatial resolution is achieved (1 μm in a lateral direction and 10 μm in a vertical direction, Figure 6.6). Thanks to this small irradiated volume, the smearing effect [61,63] is negligible. In other words, the coherence factor is one and the initial amplitude $A := g^{(2)}(t=0)-1$ is equal to one. However, it is clarified that obtained A was significantly less than 1. The origin of this deviation is a reflection light from the boundary between glass and the sample solution. This reflection is so strong that considerable reflection light can pass PH2 (Figure 6.7). As a result, both the signal and reflected light are irradiated into the detector. This situation is the same as partial heterodyning, which is described in Section4.1.3. In this case, E_F in eq.(4.1.3.5) denotes the scattering from the sample solution and E_C denotes the reflected light. Therefore, eq.(4.1.3.42) is represented as follows:

$$1-\sqrt{1-A}=\frac{\langle I_s\rangle_T}{\langle I_{tot}\rangle_T} \tag{6.3.1}$$

where A is the initial amplitude of the time-correlation function of the scattered intensity, $g^{(2)}(0)-1$, $\langle I_s\rangle_T$ is the intensity from the sample, and $\langle I_{tot}\rangle_T$ is the total intensity. Similarly, eq.(4.1.3.45) is represented as follows:

$$D_A=\frac{1-\sqrt{1-A}}{A}D \tag{6.3.2}$$

where D_A is the apparent diffusion constant and D is the genuine diffusion constant which we want.

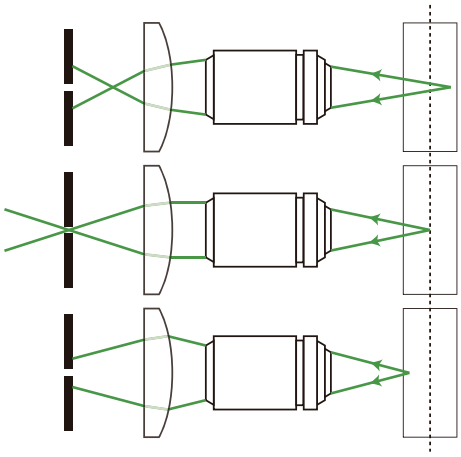

Figure 6.6: Principle of the confocal optical system. Only the light at focal point can go through a hole of the pinhole.

The samples were polystyrene latex suspensions (3000 Series Nanospheres, Duke Scientifc Cooperation), Chinese ink, and poly(N-isopropyl acrylamide) (PNIPA). As a comparison, measurement by using a conventional DLS system was also performed. The measurements were performed at 25 °C unless mentioned. To compare the results obtained from the DLS microscope, the measurements by using conventional DLS system were also performed (DLS/SLS-5000 compact goniometer (ALV, Langen), coupled with an ALV photon correlator). The incident light of the conventional DLS system is a 22 mW He–Ne laser whose wavelength is 632.8 nm. Scattered angle was set to be 90° and the measurement time was 30 seconds.

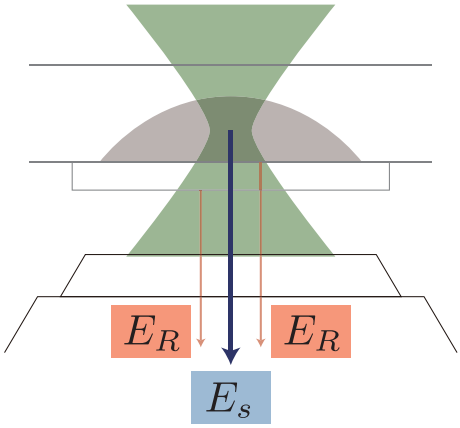

Figure 6.7: Explanation of partial heterodyning. E_s is the backscattered light from the sample solution and E_R is the reflection from the boundary.

6.4 Results and Discussion

6.4.1 Polystyrene beads: multiple scattering media

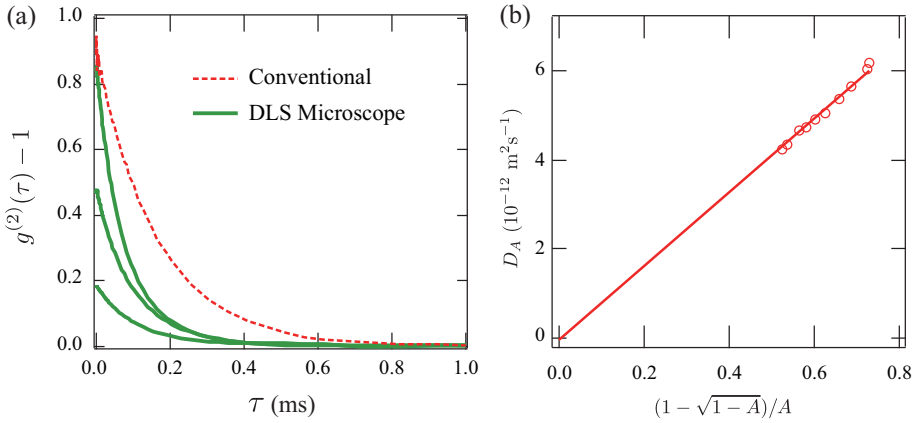

Figure 6.8: (a) Intensity correlation functions for a polystyrene latex suspension, 1 wt%. The nominal diameter of the polystyrene latex particles is 50 nm. Solid lines: Several data sets obtained from the DLS microscope ($\lambda = 514.5$ nm, $\theta = 180°$) at different points within the suspension. Dashed line: Data obtained from a typical DLS system (DLS/SLS 5000 compact goniometer, ALV, $\lambda = 632.8$ nm, $\theta = 90°$). (b) A plot of D_A vs. $(1 - \sqrt{1 - A})/A$. The solid line is the best fit result based on Eq. (6.3.2).

Figure 6.8(a) shows the time correlation functions of scattered light intensity from the polystyrene latex suspension whose diameter is 50 nm. The correlation function measured by the conventional DLS shows clear exponential curve whose initial amplitude, A, is almost 1. In contrast to this, the value of A obtained from the DLS microscope varies in the range between 0.2 and 0.9 when the focal point is varied. The relationship between the focal point and A is discussed later. Though the decay rate strongly depends on the focal position, the time correlation functions were measured from turbid suspension. In this experiment, the concentration was set to be 1% for the DLS microscope while 0.001 wt% for conventional DLS to suppress the effect of multiple scattering. To extract the diffusion constant from the data obtained from the DLS microscope, I utilized Eq. (6.3.2). Figure 6.8(b) shows a plot of D_A vs. $(1 - \sqrt{1 - A})/A$. The data shows

that D_A is proportional to $(1-\sqrt{1-A})/A$, which indicates the validity of Eq. (6.3.2). By fitting the data with Eq. (6.3.2), D is estimated to be 8.22×10^{-12} m^2 s^{-1}. By using Einstein–Stokes relationship, the hydrodynamic diameter is calculated to be 58 nm, which shows good agreement with the value obtained from the typical DLS system (57 nm).

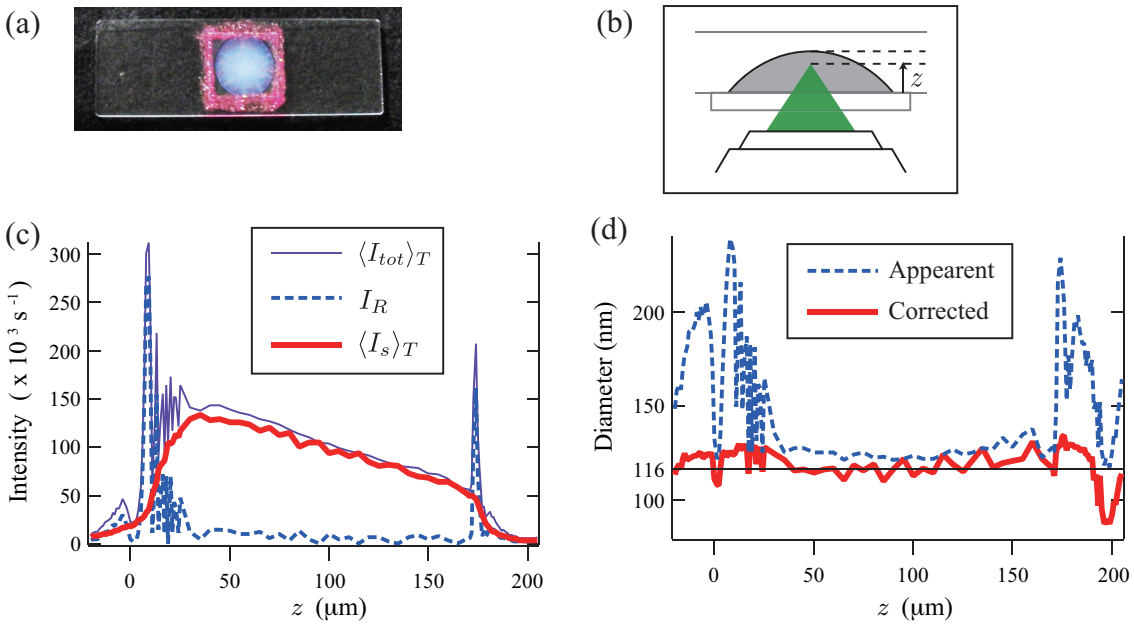

Figure 6.9: (a) The appearance of the sample. The cover glass is fixed with manicure. (b) The definition of z. (c) Position dependence of $\langle I_{tot} \rangle_T$ (thin solid line), I_R (dashed line), and $\langle I_s \rangle_T$ (thick solid line) for polystyrene latex suspension, 1 wt%. The nominal diameter of the polystyrene latex particles is 100 nm. The intensity is expressed in s^{-1}, the photon counts in a second. (d) Position dependence of the diameter of the polystyrene latex suspension. The diameter calculated from the typical DLS is 116 nm, which is indicated in the figure. Solid lines: The diameter corrected using Eq. (6.3.2). Dashed line: The apparent diameter calculated by using apparent diffusion constant, D_A.

To clarify the effect of reflected light quantitatively, DLS signals were measured with scanning the position of the focal point. The sample was 1 wt% polystyrene latex suspension whose nominal diameter is 100 nm. As shown in Figure 6.9(a), this suspension is so turbid that the conventional DLS system is not available. The time correlation functions were measured by scanning the focal point along the vertical direction (Figure 6.9(b)). Thanks to its high spatial resolution, the measurement can be achieved at 1 μm intervals. The thin solid line in Figure 6.9(c) shows the measured intensity, $\langle I_{tot} \rangle_T$. Around $z = 0 - 40$ μm and $170 - 180$ μm, the scattered light intensity shows sharp peaks. These strong light intensities originate from the reflection at the boundary between glass and the sample suspension. Around $z = 40 - 170$ μm, the measured scattered intensity shows monotonic decrease. This is due to the multiple scattering, which is eliminated by the pinhole. To clarify these points, the observed intensities were decomposed into I_R and $\langle I_s \rangle_T$ by using Eq. (6.3.1). The maximum value of the initial amplitude was 0.97, which indicates that the smearing effect is almost negligible. The broken line in Figure 6.9(c) shows the calculated I_R and the thick solid line shows the calculated $\langle I_s \rangle_T$. These data clearly shows that the observed sharp peaks around $z = 0 - 40$ μm and $170 - 180$ μm are due to the reflected light, I_R. In contrast to I_R, the scattered light intensity from the sample ($\langle I_s \rangle_T$) shows gradual change at the boundaries. The reason why the increase of

$\langle I_s \rangle_T$ is not sharp is that the irradiated volume along the vertical direction is larger than the mechanical spatial resolution of the microscope. From the decay of each time correlation function of the scattered light intensity, the diameter of the sample suspension was calculated as a function of z by using Eq. (6.3.2). The solid line in Figure 6.9(d) shows the result. As a comparison, the calculated result without taking the effect of partial heterodyning into consideration is also shown as the broken line. The diameter of diluted sample suspension measured by the conventional DLS system was 116 nm. The calculated result by using partial heterodyne method shows good agreement with this value in whole z. This result shows the importance of partial heterodyning. However, this result contradicts with the result of Xia *et al.* [188]. They observed the slowing down of the motion near the interface. This point should be further investigated by improving the signal to noise ratio of the DLS microscope.

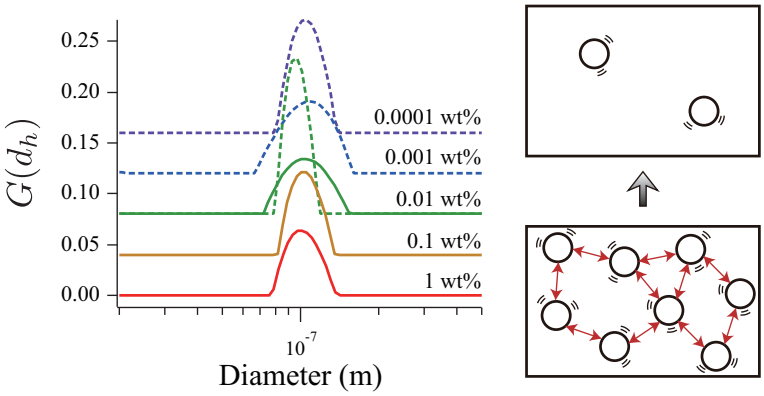

Figure 6.10: Concentration dependence of the size distribution of a polystyrene latex suspension. The nominal diameter of the polystyrene latex particles is 100 nm. The 1 - 0.01 wt%, as measured by the DLS microscope, is represented by the solid lines. The 0.01 - 0.0001 wt%, as measured by the typical DLS system, is represented by the dashed lines. The graphical image is shown on the right.

Figure 6.10 shows the concentration dependence of the size distribution function of polystyrene latex suspension. To check the consistency of a conventional DLS and the DLS microscope, the same sample (0.01 wt%) was measured by both instruments and show good agreement. In the case of polystyrene latex suspension, concentration dependence was not observed. This result is explained by the fact that the surface of the polystyrene latex particle is negatively charged. Because of this charge, the particles repel each other. As a result, the particle does not aggregate even at high concentration. This result agrees with the previous research investigated by using diffusing wave spectroscopy [189].

As a practical application, the size distribution functions of milk are shown in Figure 6.11. Original sample is so turbid that the conventional DLS system cannot be used (Figure 6.11(a)). The peaks are observed in the size distribution function of the diluted sample (Figure 6.11(c)). It is considered that the smaller particles are proteins and larger particles are fat globules. In contrast to this result, the size distribution function of the original sample is broader than that of the diluted sample. This indicates that the dilution process changes the dispersion states significantly. The surface charge of the particle is not so large to avoid aggregation. The aggregation process of proteins is investigated later (Section 8). From these results, the importance of measurement without dilution is clarified.

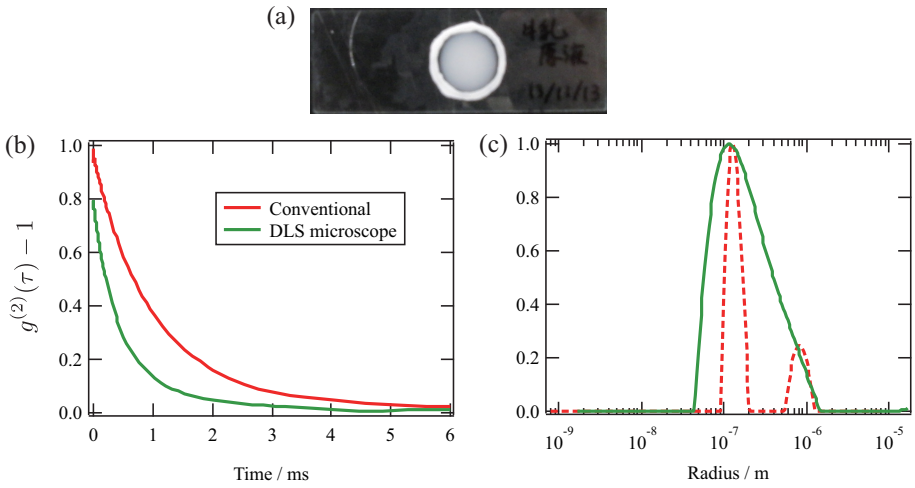

Figure 6.11: Measurement of the size distribution functions of milk. (a) Photograph of the sample. (b) Time correlation functions of scattered light intensity. (c) Size distribution functions calculated from the time correlation functions. Solid lines: Original sample measured by the DLS microscope. Broken lines: Diluted sample (1000 times) measured by the conventional DLS system.

6.4.2 Chinese ink: strong light-absorbing media

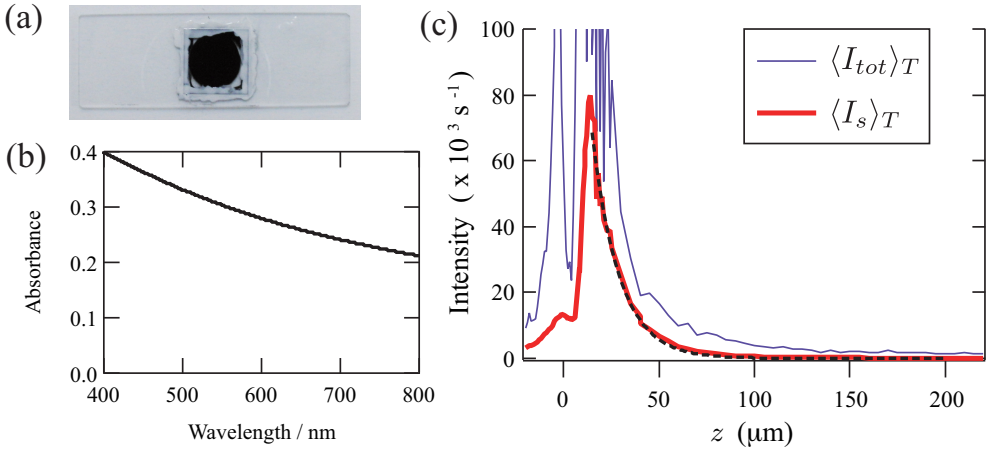

Figure 6.12: (a) The appearance of the sample. (b) Absorption spectrum of diluted Chinese ink (10000 times). (c) Position dependence of the scattered intensity from Chinese ink (10 wt%). Dashed line is the exponential fit.

As a representative of light-absorbing solution, I used Chinese ink. Chinese ink is a colloidal solution. Colloidal particles are carbons covered by animal glue. The Chinese ink is black and absorbs light strongly (Figure 6.12(a)). From the absorption spectrum (Figure 6.12(b)), absorption coefficient of the Chinese ink at 514.5 nm is calculated to be $\varepsilon = 3.23 \times 10^3$ cm^{-1}. This absorption of light was also measured by using the DLS microscope. As explained in the previous section, the scattered light intensity diminishes as z increases due to multiple scattering (Figure 6.9(c)). Similar intensity decrease was induced by light absorption. Figure 6.12(c) shows the observed light intensity as a function of z. Scattered light intensity, $\langle I_s \rangle_T$ is extracted by using Eq. (6.3.1). $\langle I_s \rangle_T$ shows exponential decay as a function of z. This decay can

be explained by Lambert-Beer's law. By fitting this decay curve, the absorption coefficient is estimated to be 3.10×10^3 cm^{-1}, which agrees well with the result measured by a conventional spectrometer. Note that the measurement was performed without dilution in the case of the DLS microscope. This is one of the promising way to use a DLS microscope as a tool of absorption measurement. The unique point is that we can extract the signal of sample solutions from the observed light intensity by using the initial amplitude of the time correlation function.

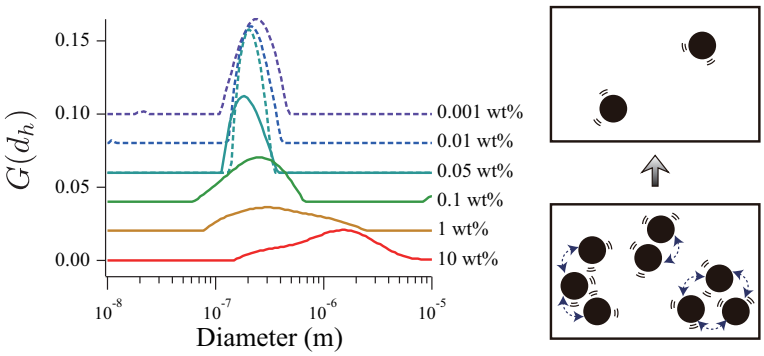

Figure 6.13: Concentration dependence of the size distribution of Chinese ink. The 10 - 0.05 wt%, as measured by the DLS microscope, is represented by the solid lines. The 0.05 - 0.001 wt%, as measured by the typical DLS system, is represented by the dashed lines. The graphical image is shown on the right.

Figure 6.13 shows the concentration dependence of the size distribution function of polystyrene latex suspension. As the concentration increases, the size distribution becomes broad and the average diameter becomes large. However, this is in contrast to the fact that the particles tend not to aggregate since the Chinese ink is a protective colloidal solution. This contradiction may be explained in such a manner that the Brownian motion is distorted at higher concentration region. As described on the right of Figure 6.13, the particles show collective motion at high concentration region driven by van der Waals interaction. This consideration agrees with the fact that the viscosity of Chinese ink is approximately five times larger than that of water.

6.4.3 Polymers with lower critical solution temperature

Poly(*N*-isopropyl acrylamide) (PNIPA) is known as a temperature-responsive polymer [56] whose lower critical solution temperature (LCST, see Section 3.2.4 for details) is 32 °C [190]. Temperature-responsive polymer can be utilized to many applications such as drug delivery system, and the investigation on PNIPA has been done by using calorimetry, DLS, and SANS [159]. However, there is no investigation on the aggregation process during heating. This is because there is no technique to measure the morphology change in high time resolution (several seconds) without dilution. DLS microscope can tackle with this difficulty. Here I report the size distribution change around LCST observed by the DLS microscope.

PNIPA is synthesized by following the procedure shown in [159]. 20 g *N*-isopropyl acrylamide was dissolve in 100 mL toluene with blocking out a light. This yellowish solution was filtrated under suction. The filtrate was mixed with 500 mL petroleum ether and cooled with ice-water until the monomers were precipitated (typically 30 minutes). Precipitated monomers were filtrated under suction and dried under reduced pressure over night (yield: 84 %). 6.9 mmol of recrystalized NIPA was dissolved in 9.5 mL degassed, deionized water.

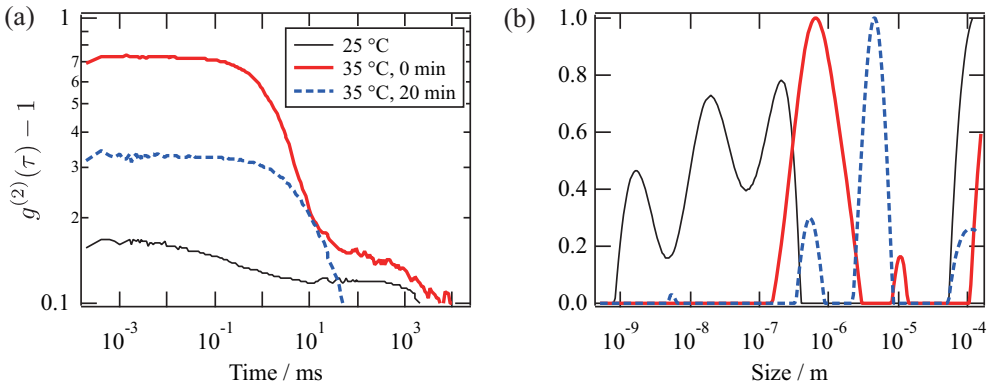

Figure 6.14: (a) Time correlation functions of scattered light intensity for the PNIPA solution. (b) Corresponding size distribution functions for the PNIPA solution obtained by the inverse Laplace transformation of Figure 2(a). Horizontal axis was calculated with considering the effect of partial heterodyning for each data. A thin solid line is the data obtained at 25 °C. A thick sold line is the data obtained just after the solution became turbid (35 °C). A broken line is the data obtained after 20 minutes of the measurement of the red line.

This solution was slowly stirred with introducing argon gas, cooled with ice-water, and blocking out a light for 10 minutes. Then 0.08 mmol of N,N,N',N'-tetramethylethylenediamine was added. After stirring for 1 minute, 0.5 mL of 0.035 M ammonium persulfate aqueous solution was added and stirred for 30 seconds. This solution was kept in a refrigerator (4 °C) over night and used as a sample solution.

The DLS measurement was done by using temperature-controlled stage (TP-108R-C, Tokai Hit CO.,Ltd). The PNIPA solution was shielded in a cavity slide. First, the time correlation function of scattered light intensity was measured at 25 °C. After that, the temperature of the stage was set to 35 °C. The measurement was done right after the solution becomes turbid. The solution was kept as it is and the measurement was done again after 20 minutes later. The size distribution functions were calculated by inverse Laplace transformation and rescaled by a partial heterodyne method.

Figure 6.14(a) and (b) show the results obtained by the DLS microscope. The thin solid lines show the results obtained from the PNIPA solution below LCST. The solution has broad size distribution and the average size is several tens nanometer, which is typical for polymer solutions. Since the irradiated volume is so small compared to the conventional DLS apparatus, the light intensity is also small. This means that the transparent solution is easily affected by a small amount of dusts. In Figure 6.14(a), the time correlation function is not decayed even at one second and this may be originated from the noise such as dusts. This kind of noise also affects at short time region and as a result the size distribution function becomes noisy as shown in Figure 6.14(b). However, it is usually not a problem since we can use the conventional DLS system for such transparent samples. The thick solid lines and the broken lines in Figure 6.14(a) and (b) show the results obtained just after and 20 minutes after the solution became turbid, respectively. The size of the aggregation just after the phase transition is around 1 μm while it becomes around 5 μm 20 minutes later. It clearly shows the aggregation growth during heating. Such a large size cannot be measured by SAXS, SANS and conventional light scattering techniques. This uniqueness of DLS will be utilized for further elucidation of aggregation growth processes. One of the examples is the aggregation state of carbon nanotube dispersions, which is introduced in the next section.

6.5 Summary

In this section, I introduced a new apparatus called a dynamic light scattering microscope. DLS microscope enables us to measure DLS from turbid system and light-absorbing system with high spatial resolution by applying backscattering geometry and confocal optical system. The contamination of reflected light originated from the boundary of the sample and glasses are analytically separated by using partial heterodyne method. This point is experimentally proved by using a polystyrene latex suspension as a sample. By using DLS microscope, concentration dependence of the size distribution is found in Chinese ink and milk. In the case of Chinese ink, this result is interpreted as a collective motion driven by van der Waals interaction. As another application, aggregation growth of PNIPA solution is measured around LCST for the first time. By using its high spatial resolution, I believe that this technique can also be applied to other systems such as polymer blush, biological cells and so on.

7 Concentration-induced Aggregation: Carbon Nanotube Suspension

7.1 Introduction

As shown in the previous section, the size distribution of dispersions can vary by dilution. However, the mechanism of size distribution variation as a function of concentration is not clarified yet in the previous section. To clarify the mechanism of size distribution variation in details, I focus on carbon nanotube (CNT) dispersions. This research is directly connected to the theme of this thesis, "Aggregation structure of polymers induced by hydrophilic and hydrophobic interaction". The reason why I chose a carbon nanotube as a sample is that CNT is a typical hydrophobic material. To investigate the aggregation structure induced by hydrophobic interaction, CNT is one of the best materials since CNT is composed of only carbons, which has hydrophobic character. From the viewpoint of application, CNT is taking center stage thanks to its distinguished physical properties such as chemical sensing [191], electrical and thermal management [192], photoemission [193], stretchable electro-device [194,195], electromagnetic shielding [196,197], energy storage performance [198] and so on. To use CNT for the products, CNT is usually dispersed to the solvent since the solution is easy to handle compared to powder samples. As a solvent of CNT, non-polar organic solvent is preferable thanks to its high solubility for CNT. However, such organic solvents are harmful to our body and environment in many cases. Therefore, for mass consumption of CNT for the products, water is the best solvent if only CNT is dissolved. Although CNT is extremely hydrophobic, it is possible to dissolve CNT to water with the aid of surfactant. Currently, CNT dispersed in water is widely used for the production of materials, which utilize the prominent feature of CNT. However, the dispersion state of CNT is complicated because of their strong tendency to aggregate via van der Waals interactions [199]. I believe that the deep understanding of the dispersion state of CNT in water will improve the efficiency and quality of those products.

There are many techniques to investigate the dispersion state of CNTs (Figure 7.1). Here I introduce their advantages and disadvantages. Direct observation of aggregates is realized by using microscope techniques such as atomic force microscope (AFM), transmission electron microscope (TEM), and scanning electron microscope (SEM) [200, 201]. Since these microscopes can see each aggregate as it is, not only the size distribution but also their shape is clarified. As for TEM and SEM, solution samples cannot be measured directly since the sample should be dried up. There is a technique to measure the solution sample by using freeze-dried sample. However, this technique is not common and difficult to implement. These microscopic techniques are the observation in real space. Similar information can be obtained even in reciprocal space. Observation in reciprocal space is performed by scattering technique. Among the scattering techniques, SANS and SAXS are the best for the measurement of several to several tens nanometer size [202–204]. Since the obtained scattering image is the space-average within the irradiated volume, it is impossible to determine the shape of each aggregate. In addition, large nuclear plant or proton accelerator is required for SANS measurement. However, we can still extract abundant information as a form factor and a structure factor. In addition, both diluted and concentrated samples (even dried solid samples) can be measured by these scattering techniques. More classical technique is rheological measurements [205, 206]. From the rheological properties of the dispersions such as sheer thinning, the degree of orientation and aggregation can be obtained. Rheological measurement is easy to implement compared to the microscope techniques and small-angle scattering technique. In addition, both diluted and concentrated dispersions can be mea-

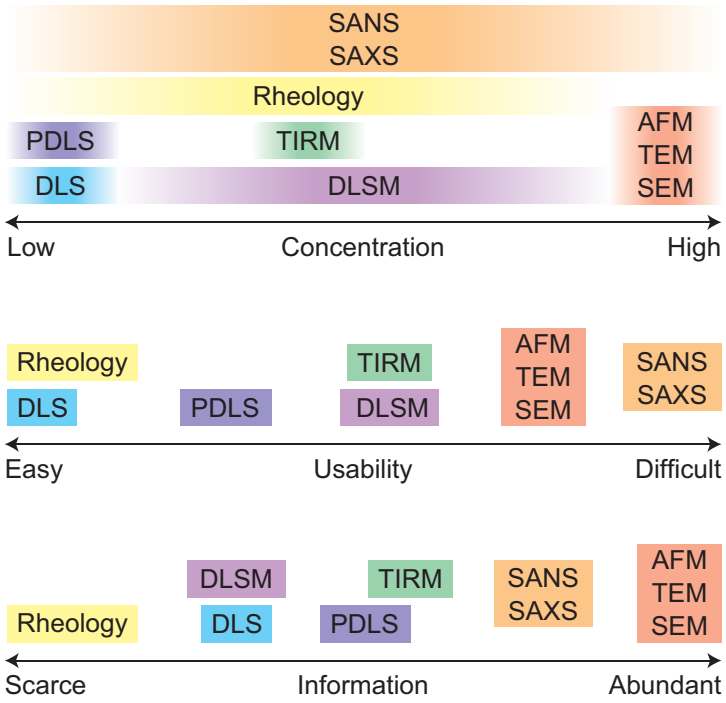

Figure 7.1: Comparison of techniques to measure dispersion states.

sured. The main drawback is that the extracted information is not directly related to the shape and size of aggregates. There are also many measurement techniques by using light as a probe. DLS is the one of the representative technique for the measurement of CNT dispersions. The advantage and disadvantage of DLS compared to other measurement techniques are discussed in Section 6. To dissolve the drawbacks of DLS, I developed DLS microscope, which is also discussed in Section 6. As a characteristic technique for the measurement of rod-like solutes like CNT, polarized DLS is important [65,207,208]. Polarized DLS is almost the same as DLS. However, the polarizations of incident and scattered light are set in appropriate geometry. Different polarization geometry gives different time correlation functions of scattered light intensity. From this information, not only the size but also aspect ratio is obtained from rod-like solutes. Total internal reflection microscopy (TIRM) is another technique to measure diffusion of solute by using light [186,187]. The image of one particle confined in thin layer is measured in real space, and information such as diffusion constant and interaction between solutes and surfaces can be extracted. Although this technique is used only for a thin layer, high spatial resolution greater than the optical diffraction limit is achieved by using an evanescent wave as an illumination.

In this section, I introduce a research to clarify the concentration dependence of CNT dispersion states by the combination of DLS microscope and polarized DLS. First, I introduce the characteristic feature of CNT by referring to previous researches. Next I introduce the experiment details. To find appropriate sample preparation scheme, I tried three scheme, which are introduced in the following subsection. Then the concentration dependence of the size distribution is discussed. First I compare the size distributions at low and middle concentration by using conventional DLS system and DLS microscope. Then the concentration dependence of the size distribution of several CNT dispersions are shown in wide concentration range. In addition, anisotropy is also discussed by using polarized DLS, which is explained in Section 4.1.4. These results are summarized as a form of dispersion state transition.

7.2 Experimental

7.2.1 Materials and sample preparation

Preparation scheme for CNT sample dispersion is shown in Figure 7.2. To disperse CNT in water, CNT and surfactant (sodium deoxycholate (SDOC), Tokyo Chemical Industry Co., LTD.) were mixed and dispersed by cyclic probe sonicator (UX-050, Mitsui Electric CO., LTD.) at 50 W power and 20 kHz for 12 hours. Concentration of CNT and SDOC were 0.1 wt%. This suspension was concentrated by evaporating the solvent. This scheme is called scheme I. Scheme II is followed by the additional SDOC (triple volume of the Scheme I's sample) and vortex in five hours. Scheme III is followed by centrifugation (6000 rpm, five hours) of Scheme II's sample and supernatants were used as samples. Five kinds of CNTs were used as samples (Table 7.1); Nanocyl (NC7000, Nanocyl S.A.), VGCF-X (Showa Denko K.K.), HiPCO (purified, Unidyme Inc.), CoMoCAT (CG200, Southwest Nano Technologies), SG (AIST) [209].

Table 7.1: List of CNTs

Product	ID	Single / Multi	Diameter / nm	Length / μm	Specific area / $m^2\ g^{-1}$	G/D ratio
NC7000	Nanocyl	Multi	9.5	1.5	280	0.8
VGCF-X	VGCF-X	Multi	10-15	3.0	250	0.9
CoMoCAT	CoMoCAT	Single	0.8	5.0	450	15
HiPCO	HiPCO	Single	0.8	1.0	300 [210]	50
Super growth	SG	Single	3.7	1200	1150	5

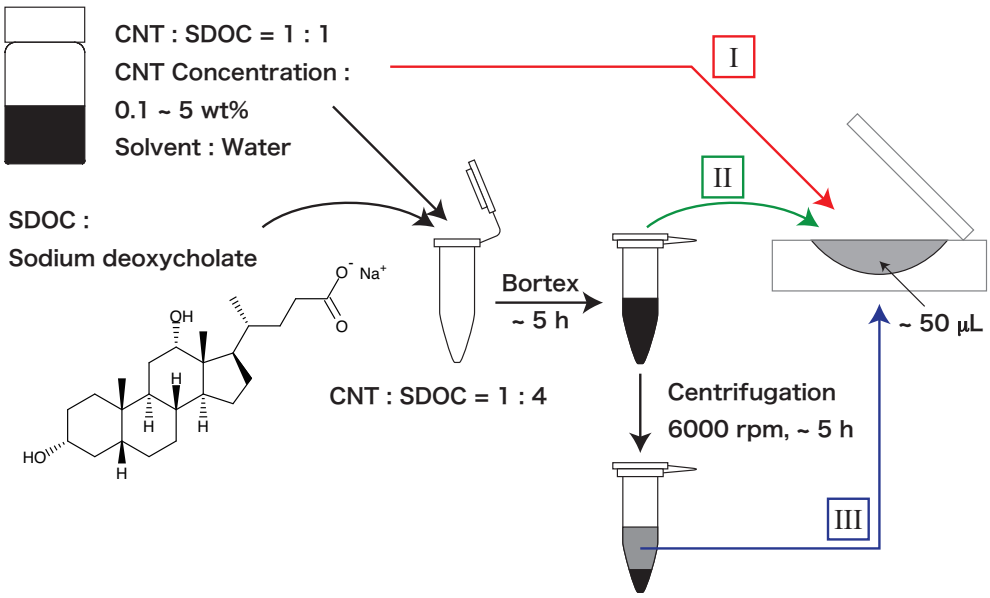

Figure 7.2: Preparation scheme of the sample dispersion.

7.2.2 UV-VIS measurement

The concentration of Scheme III's sample was measured by UV-VIS spectrometer (V-630, JASCO, Japan). Since the absorbance of light is very strong, the measurement was done by using diluted samples with 0.2 cm optical path. Then absorbance of original samples was calculated by using Lambert–Beer law.

7.2.3 Dynamic light scattering

Measurement was performed by using both conventional DLS system (DLS/SLS 5000 compact goniometer, ALV, $\lambda = 632.8$ nm, $\theta = 90°$) and DLS microscope ($\lambda = 514.5$ nm, $\theta = 180°$). See Chapter 6 for details. As for the data analysis of DLS microscope, the effect of partial heterodyning is taken into account. The initial amplitudes of time correlation functions of scattered light intensity in most of the measurements were around 0.1. In this case, the coefficient of eq.(6.3.1) is approximately 0.5. Therefore, the apparent diffusion constant, D_A, is a half of actual diffusion constant, D.

In addition, polarized DLS was measured by using both conventional DLS system and DLS microscope. To perform polarized DLS for conventional DLS system, two polarizers are used as shown in Figure 4.12. Here I call polarized scattering as VV configuration and depolarized scattering as VH configuration. In the case of DLS microscope, $\lambda/2$ plate is used to set the polarization of incident light (see Figure 6.3). Details of data analysis for polarized DLS is described in Section 4.1.4.

7.3 Results and Discussion

7.3.1 Appropriate preparation scheme

Figure 7.3(a) shows concentration dependence of $g^{(2)}(t) - 1$ for Nanocyl. Strong AC noise may come from incompleteness of optical alignment. It is clear that there is no systematic change of $g^{(2)}(t) - 1$ as a function of concentration. The reason for this is the existence of large aggregates as shown in Figure 7.3(b). The existence of aggregates whose size is several μm will disturb the scattered light from dispersion whose size is sub μm since the scattered intensity from large particles is much larger than that from small particles. This is similar to the conventional DLS system; large dust should be eliminated for the measurement of conventional DLS. Then I tried to remove large aggregates by vortex (Scheme II). Figure 7.4(a) shows concentration dependence of $g^{(2)}(t) - 1$ for HiPCO, 3 wt%. It is clarified that the $g^{(2)}(t) - 1$ varies as time advances. The reason is clarified by checking the optical images (Figure 7.4(b)). Since the sample mount is set with the cover glass facing downward, relatively large aggregates do not appear at the focal point. However, these large aggregates go to the bottom as time goes on. Therefore, it is difficult to obtain reproducible data from the sample of Scheme II. To solve this problem, the large aggregates were removed

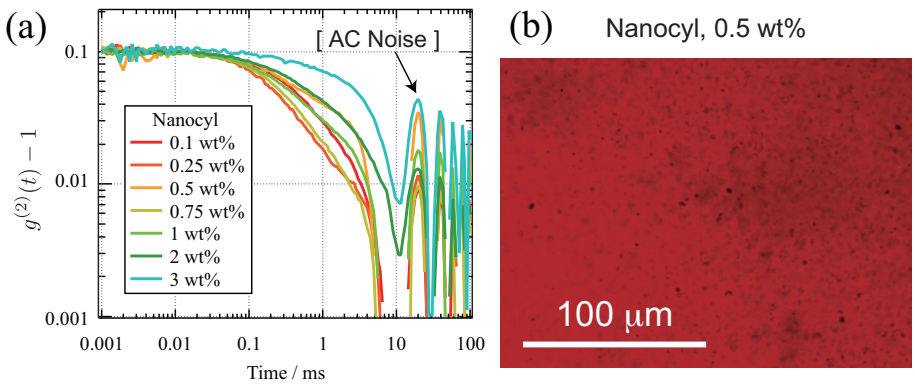

Figure 7.3: Experimental results obtained from the sample prepared by Scheme I. (a) Concentration dependence of $g^{(2)}(t) - 1$ for Nanocyl. (b) Optical image for Nanocyl, 0.5 wt%.

by centrifugation and the supernatants were used as samples (Scheme III). Figure 7.5 is the optical images of Scheme III's samples whose initial concentration were 3 wt%. Except for CoMoCAT, no aggregates were observed. In the case of CoMoCAT, the aggregates might be created within supernatant though the amount of aggregates was decreased significantly compared to other two schemes. This point becomes more clear in the case of super growth CNT (Figure 7.6). Although the aggregates cannot be removed completely, still I can apply DLS measurements since the DLS microscope has high spatial resolution. For CNT suspension, the measurement points were marked as an x mark. In the following sections, only the data obtained from Scheme III's samples were shown.

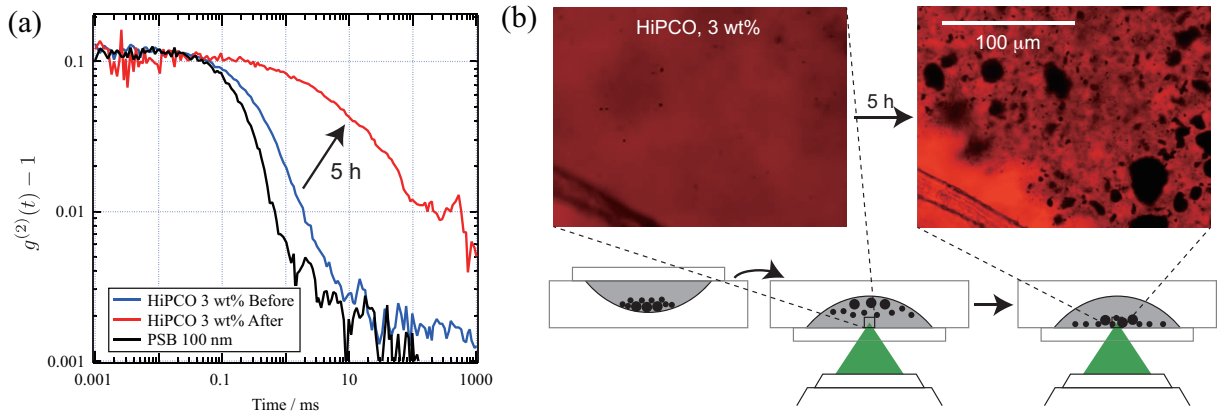

Figure 7.4: Experimental results obtained from the sample prepared by Scheme II. (a) Time dependence of $g^{(2)}(t) - 1$ for polystyrene latex and HiPCO. (b) Time dependence of optical image for HiPCO, 3 wt%.

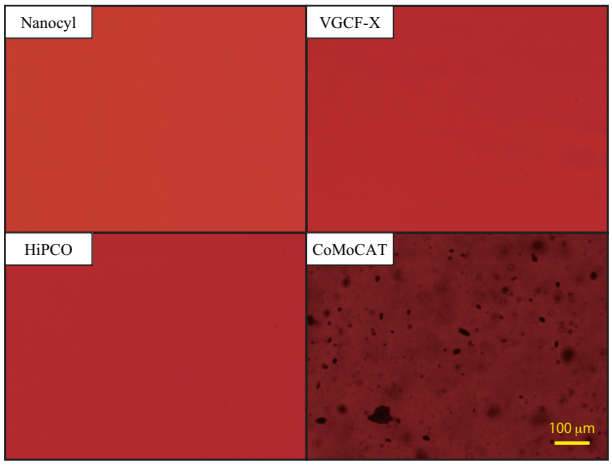

Figure 7.5: Optical image of CNT dispersions prepared by Scheme III. Initial concentration is 3 wt%. Scale bar is common and shown in the photo of CoMoCAT.

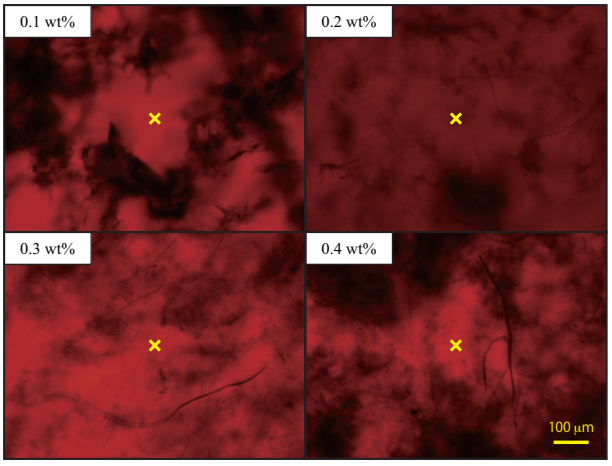

Figure 7.6: Optical image of super growth CNT dispersions prepared by Scheme III. Initial concentration is shown in each image. Yellow x indicates the position of laser spot. Scale bar is common and shown in the photo of 0.4 wt% sample.

7.3.2 Characterization of dispersions

As explained in previous section, the centrifugation is applied to remove large aggregates whose size is approximately 1 μm. This means that the concentration of CNT dispersions before and after centrifugation is different. To determine the amount of removed aggregates, absorption spectra were measured in visible region as shown in Figure 7.7. Single-walled (SW) CNTs (HiPCO and CoMoCAT, upper figures) and multi-walled (MW) CNTs (Nanocyl and VGCF-X, lower figures) show different feature. First, the absorbance of MW-CNTs is approximately five times larger than that of SW-CNTs. In addition, SW-CNTs show many peaks. These peaks originates from discontinuous density of states, known as van Hove singularity transitions [211]. However, SG shows MW-CNT-like features; strong light absorbance and no peak structure. This may be originated from their extremely large aspect ratio.

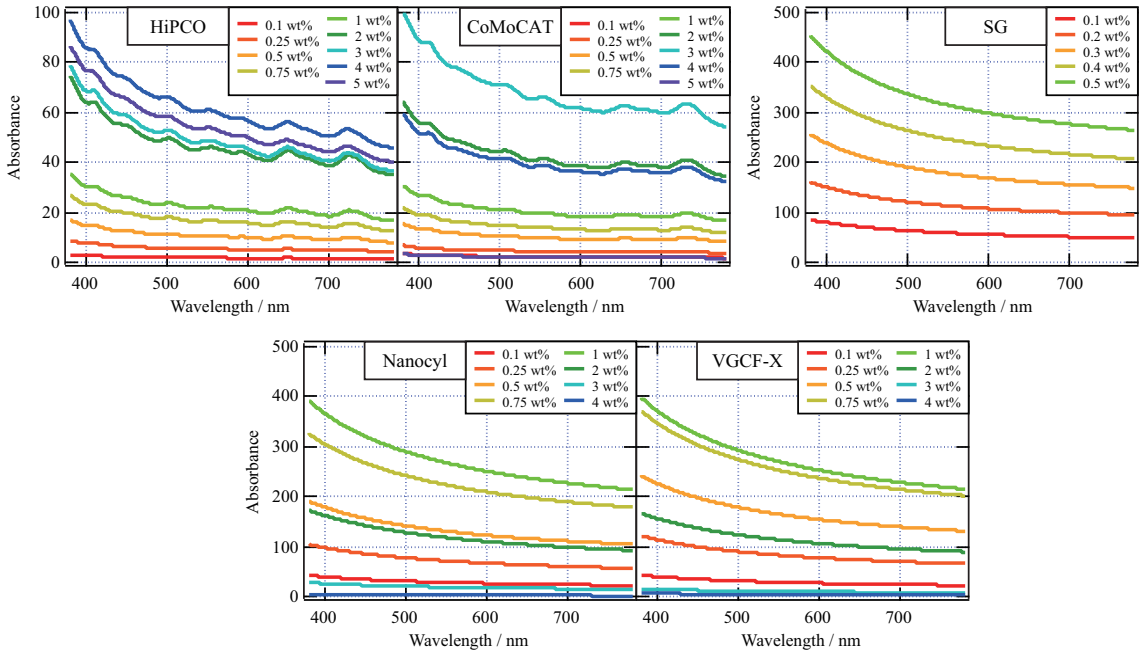

Figure 7.7: Photo absorption spectra for CNT dispersions. Concentration shown in each graph indicates their preparation concentration before vortex and centrifugation.

Figure 7.7 shows that the absorbance of CNT dispersions after centrifugation are not proportional to their concentration before centrifugation. This means that the large aggregates were removed as sedimentation. By using Lambert-Beer's law, the proportion of removed aggregates, P, can be calculated as follows:

$$P = 1 - \frac{A_{obs}(c)}{cA_{obs}(1 \text{ mg mL}^{-1})} \tag{7.3.2.1}$$

where c is the concentration before centrifugation (mg mL^{-1}) and $A_{obs}(c)$ is the observed absorbance whose initial concentration is c. When there is no sedimentation, $A_{obs}(c) = cA_{obs}(1 \text{ mg mL}^{-1})$ and $P = 0$. Some samples showed small negative value of P, which originate from experimental error. In these samples, I set $P = 0$. Concentration dependence of P was shown in Figure 7.8. It seems that there are threshold concentrations to start making sedimentation and that concentrations are different for each CNT species. The threshold concentration of MW-CNTs seems smaller than that of SW-CNTs. At these threshold concentrations, the aggregation energy (van der Waals interaction) may become larger than the thermal energy.

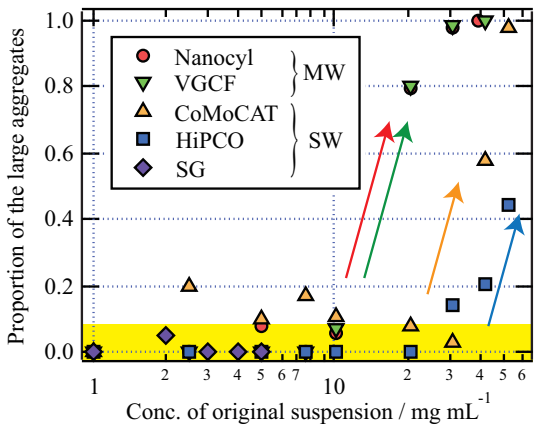

Figure 7.8: Concentration dependence of proportion of large aggregates for five kinds of CNT dispersions evaluated by the UV-VIS spectrometer. At low concentration, several points are overlapped at the bottom region (shown in a yellow band). Deviation points from this region are shown for each CNT as arrows.

7.3.3 Determination of size distribution

To measure size distributions of the CNT dispersions, DLS microscope was applied for concentrated CNT dispersions. The result at 0.5 wt% is shown in Figure 7.9. In the case of SG, the result at 0.1 wt% is shown since 0.5 wt% dispersion shows totally different behavior as shown later (Figure 7.14), reflecting their high aspect ratio. Note that the absorbance of some samples reached larger than 100 (when optical length is set to 1 cm) at this concentration (Figure 7.7). It was completely impossible to measure such strong light absorbing dispersion by using conventional DLS system. To clarify the effect of dilution, CNT suspensions diluted before vortex treatment (Scheme I) were also measured by using conventional DLS system. These results are also shown in Figure 7.9. Note that the initial amplitude of time correlation functions obtained by DLS microscope is small (typically < 0.2). This is because of an effect of reflected light from prepared slide. Concerning the data of DLS microscope, their initial amplitudes were set to 0.1 by multiplying appropriate constant for clarity.

These time correlation functions do not show single exponential decay. This reflects the polydisperse nature of CNT dispersions. By applying inverse Laplace transformation using the algorithm called CONTIN (see Section 6), the time correlation functions were converted into the distribution functions of decay time. Then, the decay time is converted into the hydrodynamic radius by using Einstein–Stokes equation. Results are shown in the lower part of Figure 7.9. One of the drawbacks of CONTIN is its weakness against the noise. In addition to this, use of Einstein–Stokes equation is also a coarse approximation in this concentration region. Therefore, quantitative discussion by using size distribution functions shown in Figure 7.9 should be avoided.

These results show that the aggregation state in diluted sample is similar to that of moderate concentration dispersion. This information is important in many practical situations. Usually a high concentration sample used for DLS measurement is diluted before measurement to suppress the effect of multiple scattering and light absorption. Although this is a de-facto standard, there is no guarantee that the aggregation state in high concentration is similar to that of diluted one. This experimental result shows one of the rationalizations for that. However, it is also clarified that this de-facto standard does not actually hold true for higher concentration region as shown in the following results.

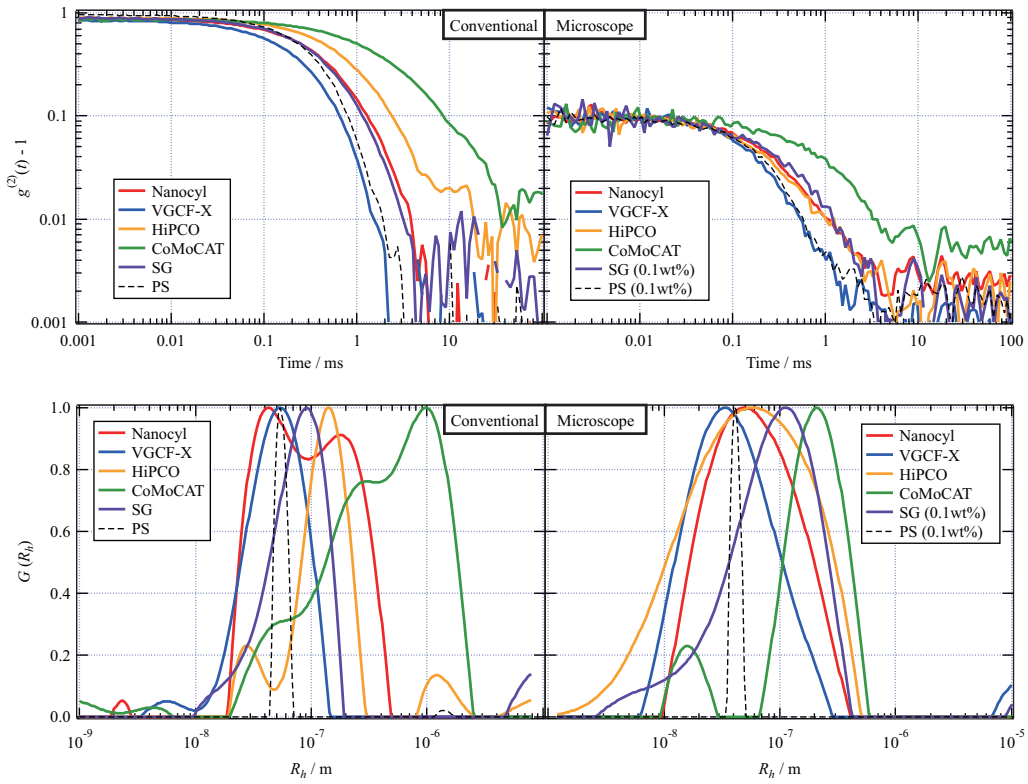

Figure 7.9: (Upper) Time correlation functions of (left) 0.001 wt % CNT dispersions measured by conventional DLS system and (right) 0.5 wt% CNT dispersions measured by DLS microscope. Concerning the data of DLS microscope, their initial amplitudes are set to 0.1 by multiplying appropriate constant for clarity. (Lower) Size distribution functions of (left) 0.001 wt% CNT dispersions and (right) 0.5 wt% CNT dispersions calculated from the time correlation functions. Only SG the result of 0.1 wt% is shown for DLS microscope. In each figure, results of polystyrene latex suspension (PS) are shown as a standard sample. The diameter of polystyrene latex is 100 nm. The concentration of polystyrene latex suspension is 0.001 wt% for conventional results (left) and 0.1 wt% for DLS microscope results (right).

Only the data of HiPCO shows significant difference between diluted one and concentrated one; the decay time of HiPCO becomes short as concentration becomes high. The most likely reason for this is that aggregates of HiPCO are efficiently broken via the process of vortex. It is known that HiPCO prefers to form sphere shape than rod shape because of their relatively thin form. This characteristic shape is easy to break by vortex compared to other CNTs. This is the reason why the size of HiPCO measured by DLS microscope is smaller than that measured by conventional DLS.

Next the concentration dependences of the size distribution for each CNT are measured in details by using DLS microscope. Figure 7.10(a) shows the concentration dependence of the time correlation functions for Nanocyl dispersions measured by DLS microscope. As shown in Figure 7.7, the absorption coefficient of these dispersions is so large (several hundreds) that it is impossible to measure by a conventional DLS system. Figure 7.10(b) shows the size distribution function converted from Figure 7.10(a) by using CONTIN program. Here the size distribution function for the diluted sample (0.01 wt%) measured by the conventional DLS system is also shown. Taking the uncertainty of inverse Laplace transformation into consideration, the size distribution functions obtained from the conventional DLS system and DLS microscope shows good

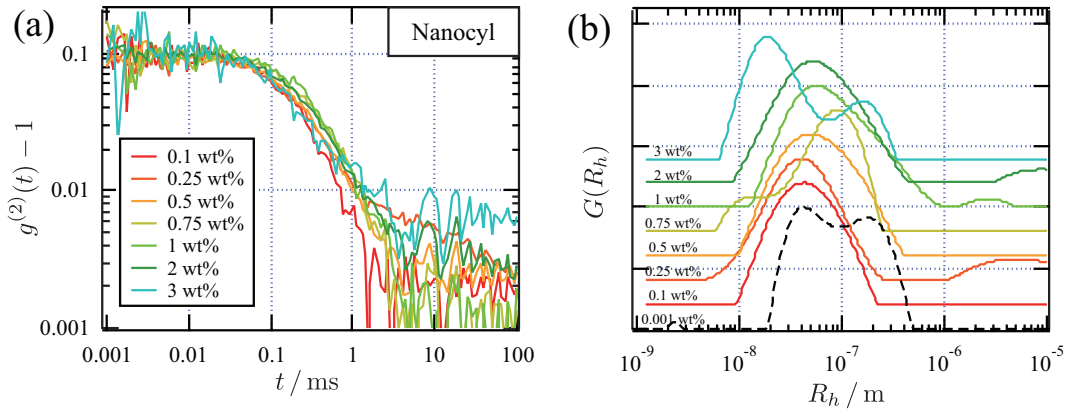

Figure 7.10: Concentration dependence of (a) time correlation functions and (b) size distribution functions for Nanocyl dispersions measured by DLS microscope. Labels in the figure stands for the concentration of original suspension. Initial amplitudes are set to be 0.1 by multiplying appropriate factor to each time correlation function for (a).

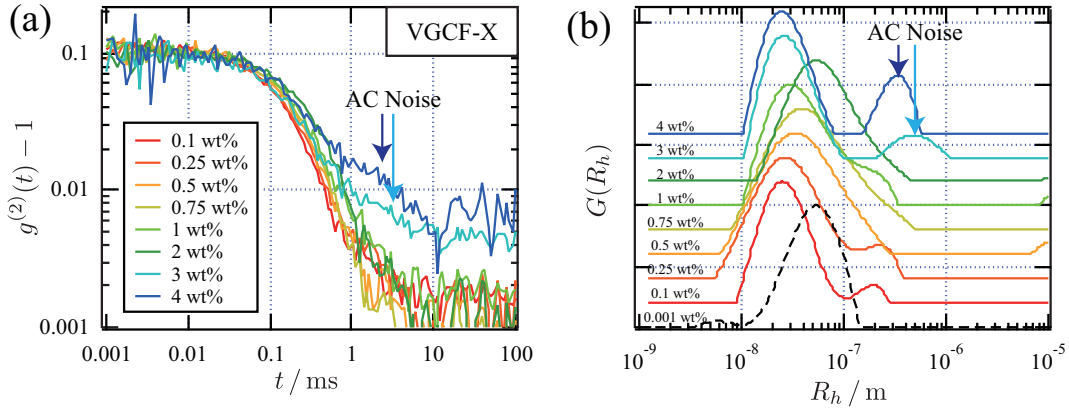

Figure 7.11: Concentration dependence of (a) time correlation functions and (b) size distribution functions for VGCF-X dispersions measured by DLS microscope. Labels in the figure stands for the concentration of original suspension. Initial amplitudes are set to be 0.1 by multiplying appropriate factor to each time correlation function for (a).

agreement. In the case of Nanocyl dispersions, the size distributions of aggregates are almost the same for all concentration regions. Similar results were obtained for VGCF-X (Figure 7.11) and HiPCO (Figure 7.12). The length of these CNTs is short compared to other CNTs (CoMoCAT and SG). Therefore, the chance for collision between CNTs is small even at high concentration region. As a result, each tube can be separated regardless of their concentration. As for VGCF-X, the signal originated from AC noise was appeared for 3 wt% and 4 wt% samples. Note that these high concentration samples become low concentration after centrifugation because of the sedimentation of large aggregates (Figure 7.8). Therefore, the origin of AC noise may be due to scarce signal intensity.

In contrast to this, CoMoCAT and SG show clear concentration dependence in their size distribution as shown in Figure 7.13 and 7.14. In the case of CoMoCAT, the decay of the time correlation functions becomes slow at the concentration higher than 2 wt% (Figure 7.13(a)). This slowing down reflects the existence of large aggregates. This fact is also clearly shown in their size distribution function (Figure 7.13(b), shown by a

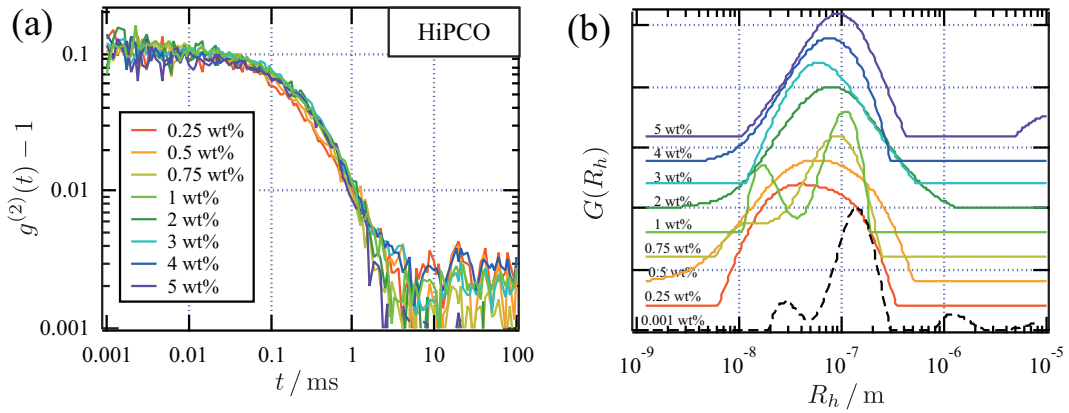

Figure 7.12: Concentration dependence of (a) time correlation functions and (b) size distribution functions for HiPCO dispersions measured by DLS microscope. Labels in the figure stands for the concentration of original suspension. Initial amplitudes are set to be 0.1 by multiplying appropriate factor to each time correlation function for (a).

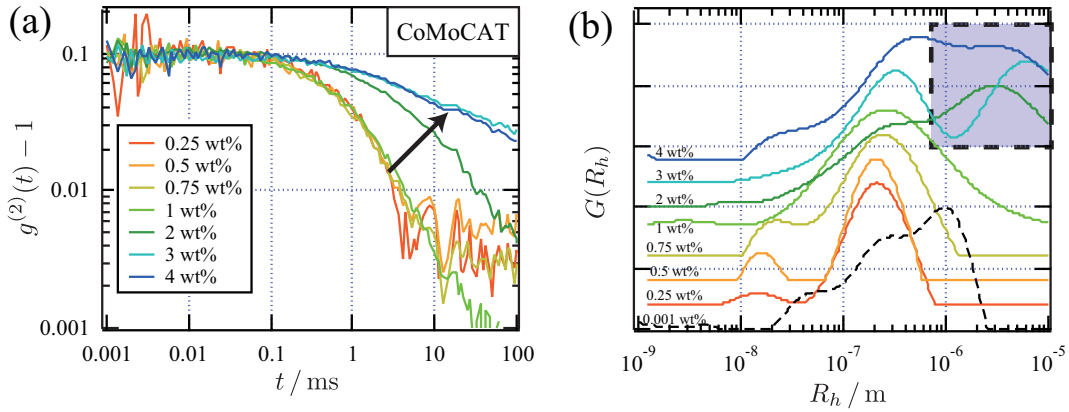

Figure 7.13: Concentration dependence of (a) time correlation functions and (b) size distribution functions for CoMoCAT dispersions measured by DLS microscope. Labels in the figure stands for the concentration of original suspension. Initial amplitudes are set to be 0.1 by multiplying appropriate factor to each time correlation function for (a).

hatched rectangular). Similar aggregation growth was also appeared for SG at the concentration higher than 0.3 wt% (Figure 7.14). This is consistent with the fact that these two CNTs are relatively long. Because of their length, each solute collides to other solutes frequently. As a result, the solutes are combined and large aggregates are created. The difference of the threshold concentration for this aggregation process can also be explained by this line. SG is exceptionally long tube and each solute collides at relatively low concentration compared to CoMoCAT. Therefore, the threshold concentration for aggregation process of SG is low (0.3 wt%) compared to CoMoCAT (2 wt%).

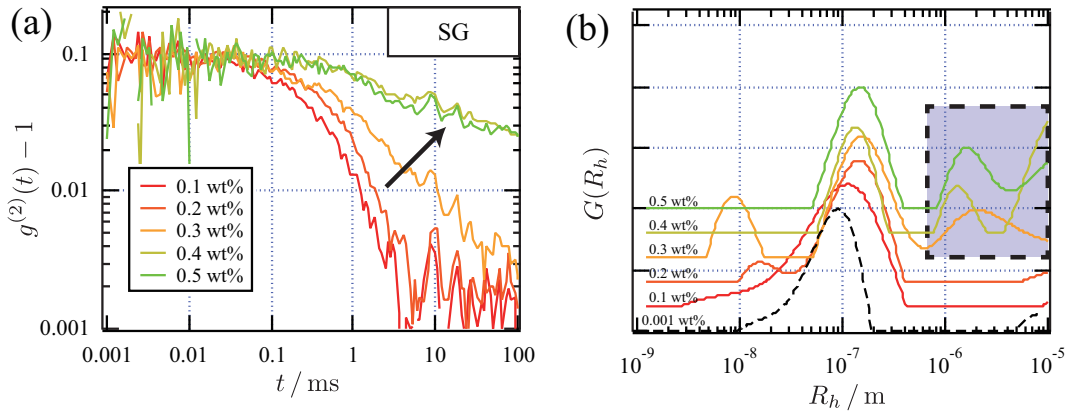

Figure 7.14: Concentration dependence of (a) time correlation functions and (b) size distribution functions for SG dispersions measured by DLS microscope. Labels in the figure stands for the concentration of original suspension. Initial amplitudes are set to be 0.1 by multiplying appropriate factor to each time correlation function for (a).

7.3.4 Estimation of anisotropy

As explained in the Introduction, the aspect ratio of solutes can be measured by polarization-resolved DLS [207]. The basic theory is written in Section 4.1.4. Before implementation of polarized DLS to DLS microscope, polarized DLS measurement was performed by using conventional DLS system. Diluted polystyrene latex suspension and SG suspension were used as a representative sample. The measurement was performed in VV and VH configuration and the results are shown in Figure 7.15(a). In the case of polystyrene latex, both VV and VH show almost the same time correlation functions. Since the difference of decay rates between VV and VH configuration originates from the rotational diffusion coefficient, D_r, this result means that $D_r = 0$ for polystyrene latex suspension (eq.(4.1.4.1) and (4.1.4.2)). This is consistent with the fact that the polystyrene latex is a sphere. In contrast to this, the decay of time correlation functions for VV configuration is slower than that for VH configuration in the cace of SG. This is because $D_r \neq 0$ for rod-like solute such as CNT. From this result, both D_t and D_r can be obtained.

Here, to obtain the numerical value of these diffusion coefficients more precisely, the measurement results obtained from different scattering angles are used. The time correlation functions for different scattering angles are shown in Figure 7.16. These time correlation functions are fitted by an exponential curve and decay rates, Γ, are obtained. Figure 7.17 shows the q^2-dependence of Γ. As shown in eq.(4.1.4.1), Γ_{VV} is proportional to q^2 and the proportional coefficient is D_t. In the case of Γ_{VH}, the slope is the same as that of Γ_{VV} and D_r is a y-intercept (eq.(4.1.4.2)). Therefore, the linear fitting of Figure 7.17 give us the numerical values of D_t and D_r. First, D_t is obtained from the linear fitting of Γ_{VV} whose y-intercept is fixed to 0. Then, D_r is obtained from the linear fitting of Γ_{VH} whose slope is fixed to D_t. Fitting results are also shown in Figure 7.17. Again, it is shown that $D_r = 0$ for polystyrene latex suspension since the shape of solutes are sphere. In the case of SG, the calculated results are $D_t = 3.6 \times 10^{-12}$ m^2 s^{-1} and $D_r = 1.1 \times 10^2$ s^{-1}. From these values, eq.(4.1.4.3) and (4.1.4.4), the average size of SG solute is estimated to be $a = 300$ nm and $b = 7$ nm. Although the length of SG CNT becomes short though the preparation of the sample, it is clarified that the solute shows still high aspect ratio.

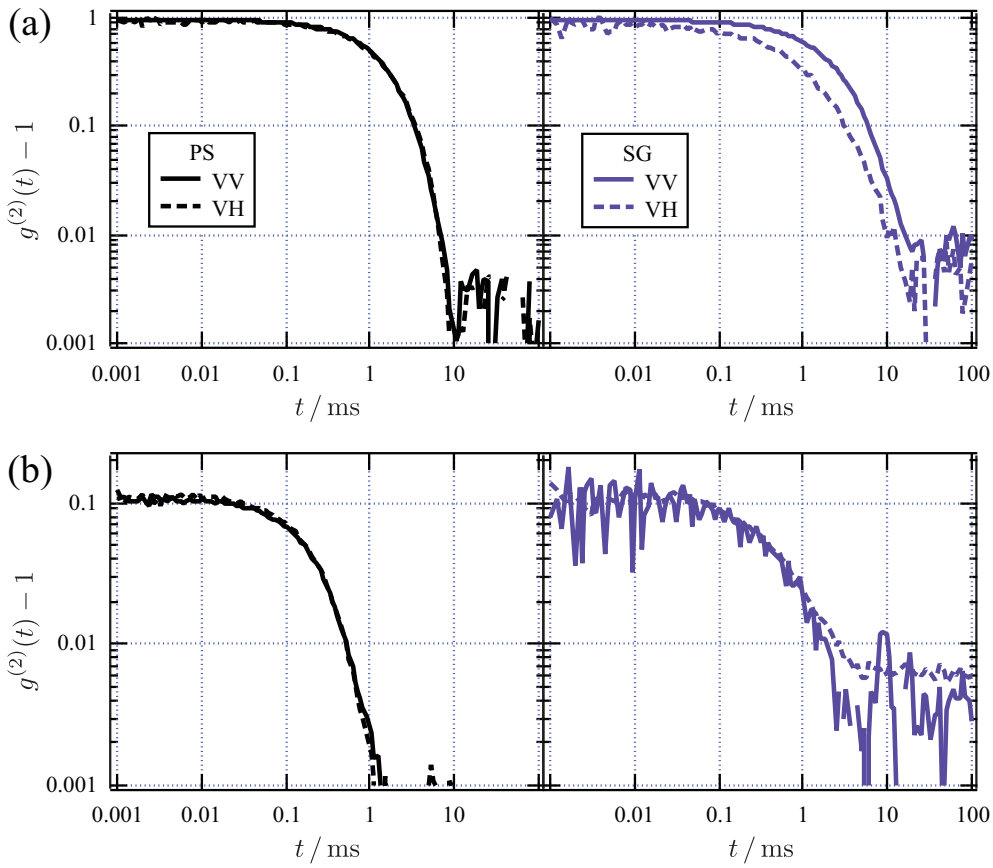

Figure 7.15: Polarization dependence of representative time correlation functions for polystyrene latex suspension (PS, diameter: 100 nm) and SG dispersion. (a) Time correlation functions of (left) 0.001 wt% PS and (right) 0.001 wt% SG measured by conventional DLS system ($\theta = 50°$). (b) Time correlation functions for (left) 0.1 wt% PS and (right) 0.1 wt% SG measured by DLS microscope. Solid line: VV configuration. Broken line: VH configuration.

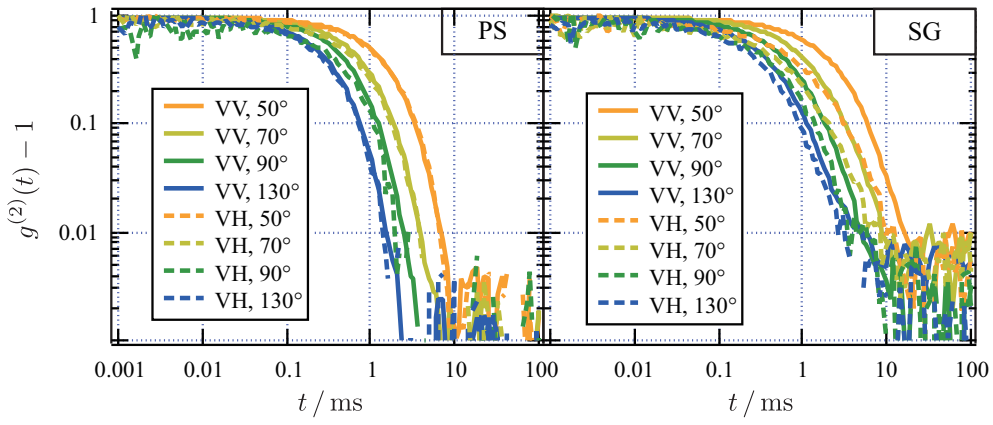

Figure 7.16: Scattering angle and polarization dependence of time correlation functions measured by conventional DLS system. Solid line: VV configuration. Broken line: VH configuration. (Top) Polystyrene latex suspension (PS), diameter: 100 nm, concentration: 0.001 wt%. (Bottom) SG suspension, concentration: 0.001 wt%.

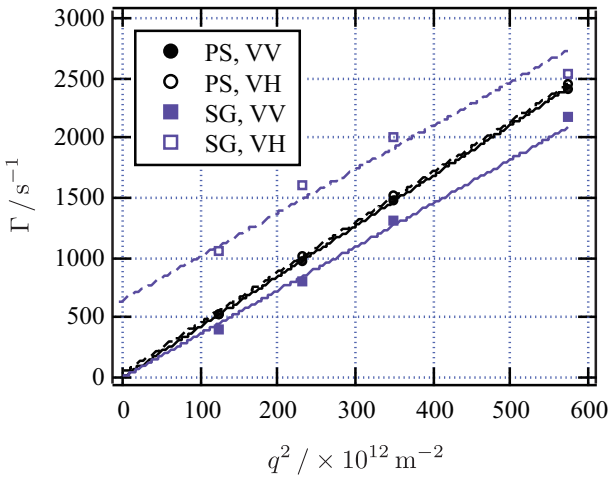

Figure 7.17: Polarization dependence of relaxation rates measured by a conventional DLS system. Solid line: Fitting results for VV configuration. Broken line: Fitting results for VH configuration.

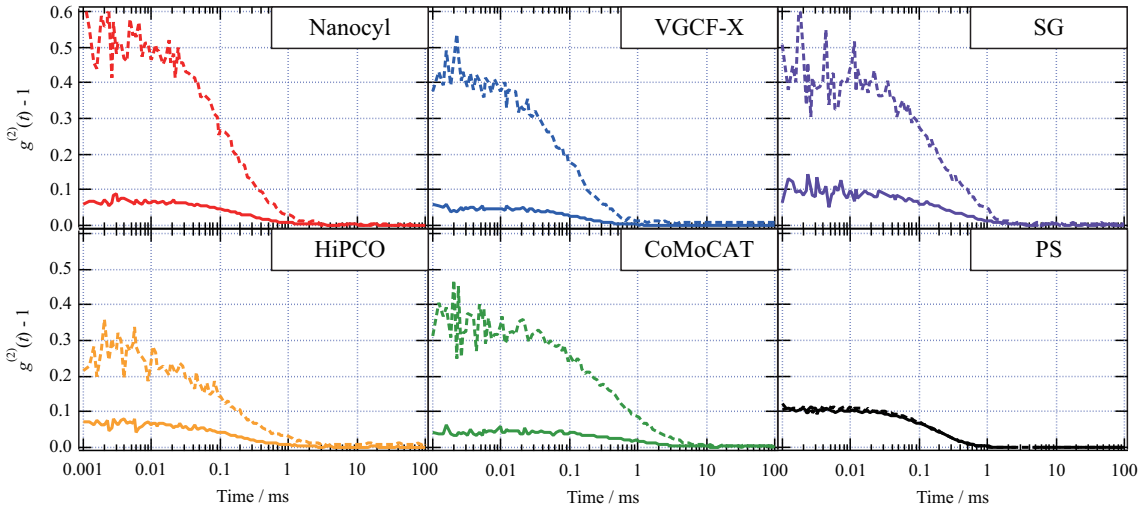

Figure 7.18: Polarization dependence of time correlation functions observed by DLS microscope. Solid line: VV configuration. Broken line: VH configuration. Concentration of CNT dispersions is 0.5 wt%. Only SG shows the result of 0.1 wt%. PS : Polystyrene latex suspension, diameter: 100 nm, concentration : 0.1 wt%.

Then polarized DLS was applied for concentrated samples by using DLS microscope. Figure 7.18 shows representative time correlation functions measured with VV and VH configurations at the same position. The solid lines are the results obtained with usual VV configurations. In this case, the detected signal is the mixture of backscattered light from the sample and reflected light from boundary between sample and cover glass. Usually the amount of reflected light is large compared to the scattered light from the sample. Because of this, initial amplitudes of the time correlation function are very small (typically 0.1). Then the time correlation functions from the same position with VH configuration were measured. The results are shown as broken lines in Figure 7.18. These figures show that the initial amplitudes become large compared to VV configuration except for the case of polystyrene latex. This can be explained as follows. In the case of polystyrene latex, there is no VH scattering in principle because polystyrene latex is isotropic. The detected signal in this case is the polarization-distorted VV scattering originated from the focusing of an objective

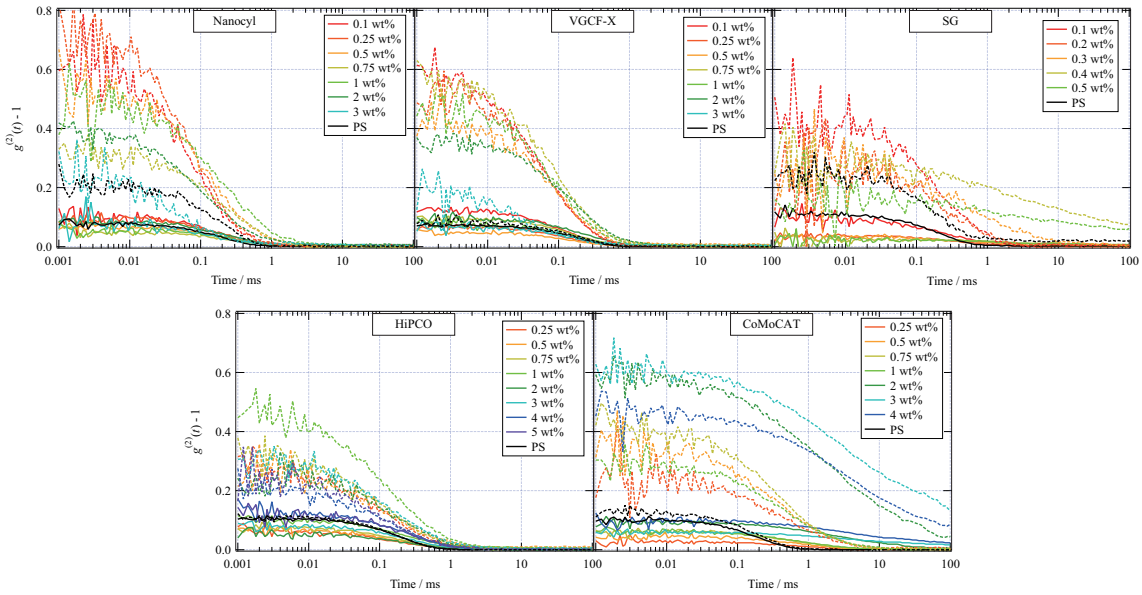

Figure 7.19: Polarization dependence of time correlation functions. Solid line: VV configuration. Broken line: VH configuration. PS : Polystyrene latex suspension, diameter: 100 nm, concentration : 0.1 wt%.

lens. In this case, the initial amplitude for each configuration is the same. However, if the sample solute is anisotropic, there is depolarized (VH) scattering. In the case of CNT dispersions, this depolarized scattering overwhelms the effect of polarization distortion originated from the objective lens. In this case, the initial amplitude becomes large because unfavorable reflection from the boundary is effectively reduced. Note that the reflection from the boundary is VV (polarized) scattering. From these considerations, it is proved that anisotropy of CNT dispersion was clearly observed by polarized DLS microscopy. This anisotropy was observed for all of CNT dispersions whose concentrations are larger than 0.1 wt% (Figure 7.19).

Then the time correlation functions of relatively high concentration dispersion were measured for VV and VH configurations by using polarized DLS microscope. Figure 7.15(b) shows the results for the suspension of polystyrene latex and SG. The concentration of each suspension is 100 times higher than that measured by the conventional DLS system (Figure 7.15(a)). The result for polystyrene latex is almost the same as the diluted sample; the decay rates of VV and VH configuration are almost the same. Note that the decay rate itself is different between the conventional DLS system and DLS microscope because of the different scattering angle and wavelength. The interesting feature is shown in the results of SG; the decay rates of VV and VH configuration are almost the same even for SG suspension in the case of high concentration. This result is completely different from the result for the diluted sample (Figure 7.15(a)). The overlap of the time correlation functions for VV and VH configurations indicates $D_r = 0$. It seems that the solute becomes isotropic due to the aggregation. However, since it is proved that the size distribution function of SG is almost the same in this concentration region (Figure 7.14(b)), the shape of solute itself may be still rod-like. Here, I propose the concept, "rotational restriction" to explain the reason for $D_r = 0$. The physical meaning of $D_r = 0$ is that the object does not rotate. In the case of concentrated CNT dispersion, the rotational motion of a rod-like CNT may be restricted due to other CNTs around it. This restriction will occur when the concentration is so high that the distance between each CNT becomes close and can interact with each other. This kind of effect may appear only when the solute has high aspect ratio like SG CNT.

7.3.5 Dispersion-state transition

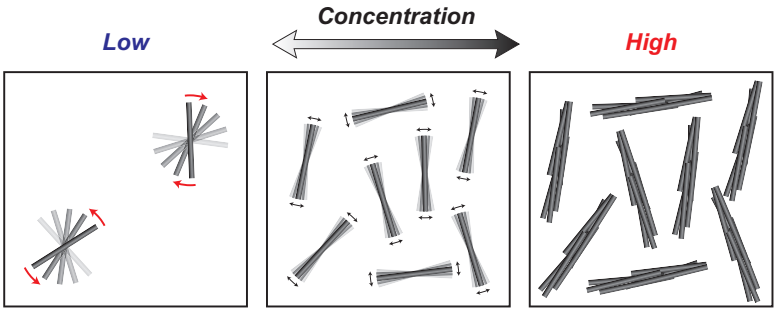

Nanocyl	0.001 wt%	0.1 ~ 3 wt%	
HiPCO	0.001 wt%	0.25 ~ 5 wt%	
VGCF-X	0.001 wt%	0.1 ~ 4 wt%	
CoMoCAT	0.001 wt%	0.25 ~ 1 wt%	2 wt% ~
SG	0.001 wt%	0.1 ~ 0.2 wt%	0.3 wt% ~

Figure 7.20: Proposed concentration dependence for aggregation state of CNT dispersions.

The previous results are summarized in Figure 7.20. I propose that there are three dispersion states in the dispersion of rod-like solutes. When the concentration of dispersion is low, each solute is described as a translational and rotational Brownian motion. Translational Brownian motion is observed by any kind of DLS system (for examples, Figure 7.9) and rotational Brownian motion is observed by polarized DLS (Figure 7.15(a)). When the concentration becomes high, rotational Brownian motion is restricted due to the intermolecular interaction. This phenomenon is observed by the overlap of the time correlation functions of scattered light intensity with VV and VH configuration measured by the polarized DLS (Figure 7.15(b)). Note that the size of solute itself does not change as shown in Figure 7.9. For long CNT such as CoMoCAT and SG, another dispersion state transition is observed as a form of aggregation growth. These aggregation growth is clearly observed as a form of the slowing down of the decay of the time correlation functions measured by the DLS microscope (Figure 7.13 and 7.14).

7.4 Summary

In this section, I showed the application of DLS microscope to the investigation of dispersion state of CNT as a function of concentration. Several kinds of CNT dispersions were prepared and measured by using polarized DLS microscope after removing large aggregates (> 1 μm), which disturb the measurement. As for translational Brownian motion, long CNTs such as CoMoCAT and SG showed slowing down at relatively high concentration (several wt%). This indicates the aggregation growth induced by the increase of concentration. As for rotational Brownian motion, the restriction of rotation was observed at relatively low concentration (0.1 wt%). This is the first report of rotational restriction. I believe that this kind of dispersion state transition is universal for rod-like shape solutes. This concept will improve the production scheme of CNT-containing materials.

8 Heat-induced Aggregation: Ovalbumin

8.1 Introduction

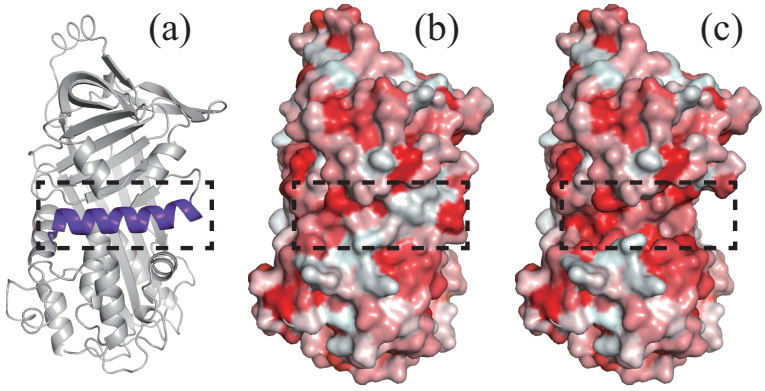

Figure 8.1: (a) Schematic illustration of a 3D ribbon model OVA (PDB code, 1OVA) drawn with Pymol. After pepsin treatment, the residues from 1 to 22 (the helix part colored purple in the figure) are removed. (b) Hydrophobicity map of OVA evaluated from the hydrophobicity of each amino acid [18]. White parts correspond to hydrophilic parts and red parts correspond to hydrophobic parts. Dashed rectangle shows the position of the residues from 1 to 22. (c) Estimated hydrophobicity map of pOVA. (d), (e) Hydrophobicity map of the residues from 1 to 22 from the viewpoint of (d) outside and (e) inside of OVA molecule.

As an example of aggregation of hydrophilic substance, I focus on ovalbumin (OVA) in this section. OVA is a major protein in egg white. Egg white contains approximately 10 % of proteins and half of those proteins is OVA [212]. OVA is composed of 385 amino acids and the complete sequence of OVA was revealed in 1978 [213]. Later, crystal structure of OVA was determined by X-ray diffraction as shown in Figure 8.1(a) and (b) [214, 215]. Gelation mechanism of OVA has been investigated for a long time. One of the most well-known mechanism proposed by Koseki *et al.* is shown in Figure 8.2 [20]. At room temperature (or, to say precisely, below denaturation temperature), the surface of OVA in solution is covered by hydrophilic amino acids. As the temperature increases, OVA is denatured. Denature induces the exposure of inner hydrophobic part. Hydrophobic parts of OVAs will get together to hide hydrophobic parts from water. This tendency is called hydrophobic interaction. When the solution is salt-free condition, we have to consider Coulomb repulsion since each OVA is negatively charged. Note that the isoelectric point of OVA is 4.5 [22]. As a result, heat-induced OVA aggregates are fibrillar structure. As the ionic strength of solution increases, resultant aggregates become dense since Coulombic interaction is weakened. This is experimentally proved by using cryo-TEM [216]. Weijers *et al.* showed the size change during heat-induced aggregation by using DLS [217]. DLS is suitable for the measurement of size distribution of solutes. They clearly showed the decrease of monomers and growth of aggregates.

To elucidate the gelation mechanism, structural analysis of heat-induced aggregates and gels has been performed by rheology [218–220], light scattering [217, 221, 222], SAXS and SANS [223–225], transmission electron microscope (TEM) [20, 216] and so on. Main topic of these researches are the relationship between the ionic strength and structure of heat-induced aggregates, which support the gelation mechanism shown in Figure 8.2. Here, I focus on the relationship between hydrophilicity and structure of heat-induced aggregates. Recently, modification of the primary structure of OVA was reported [21, 22]. It was found that the pepsin

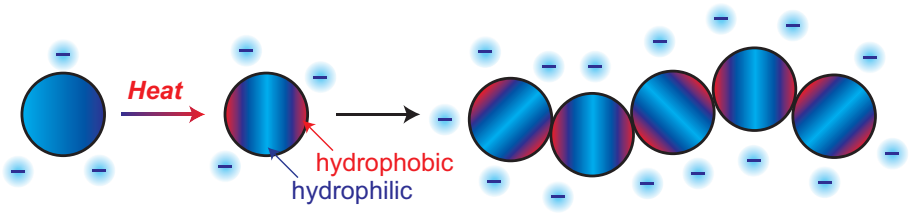

Figure 8.2: Mechanism of heat-induced gelation of OVA under salt-free condition, proposed by Koseki *et al* [20].

hydrolysis of OVA at pH 4 cleaves the peptide bond between His22 and Ala23. Cleaved peptide region is colored purple in Figure 8.1(a). The resultant large OVA fragment is called pOVA (Figure 8.1(c)). Physical properties of pOVA such as intrinsic viscosity, the secondary structure, and the denaturation temperature are almost the same as that of OVA [226]. However, it is known that the heat-induced aggregates and gels of pOVA are different from that of OVA. Figure 8.3 shows the photographs of heat-induced OVA and pOVA solution under salt-free, neutral condition. As clearly seen, the OVA gel is transparent while the pOVA gel is turbid [78]. Although the reason for this is not clear yet, one of the key factors of this difference is hydrophicility. Figure 8.1(b) and (c) show the hydrophobicity map of OVA and pOVA, respectively. Cleaved region is shown by a dashed rectangular. Red parts are hydrophobic amino acids and white parts are hydrophilic amino acids. It is shown that the removal of N-terminal peptide region expose hydrophobic (red) region to the solvent. This will induce difference in their dispersion state even before heating.

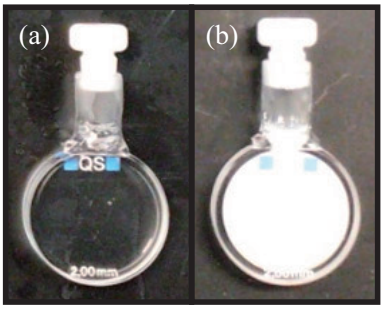

Figure 8.3: Photographs of (a) OVA and (b) pOVA gels. Protein solutions (6 wt%) were heated at 85 °C for an hour. No salts were added and pH was 7.

In this section, I introduce a research to clarify the difference of heat-induced aggregates and gels between OVA and pOVA from the viewpoint of hydrophilicity. First, I clarify the difference of heat-induced aggregates and gels between OVA and pOVA quantitatively by using rheological measurement and DLS. Then structural analysis was performed by SANS. From the concentration dependence of microscopic structures, detailed gelation mechanism of OVA and pOVA under salt-free, neutral condition is proposed. Structural analysis of OVA and pOVA gels under acidic condition was also performed. In addition, structural analysis during heating was performed by using time-resolved SANS measurement. Time-resolved measurement is one of the unique point of SANS. In the case of SAXS, time-resolved measurement is difficult since irradiation of intense X-ray will damage the samples. In contrast to SAXS, SANS gives less damage.

[78] Since OVA is the main component of egg "white", it seems strange that the OVA gel is transparent. The point is that Figure 8.3 is salt-free condition. Salt concentration of typical egg white is 0.5 wt%. The existence of salt makes the heat-induced aggregates more dense as explained in the main text. As a result, egg white becomes white (turbid) by heating.

8.2 Experimental

8.2.1 Materials

OVA (purity: $\geq$ 98 %) was purchased from Sigma-Aldrich (A5503). Pepsin was purchased from Worthington Biochemicals. Other chemicals were purchased from Wako Pure Chemical Industries. All of these materials were used without further purification. pOVA was synthesized from OVA as follows [22]. First, 100 mM buffer solution whose pH is 4 was prepared by dissolving 488 μL acetic acid and 121.3 mg sodium acetate with 100 mL deionized water. Then, 1.00 g OVA was dissolved with 80 mL buffer solution. Next, 20 mg pepsin was dissolved with 20 mL buffer solution. These two solutions were mixed and stirred for 15 hours at room temperature. During this process, *N*-terminal residues were cleaved. After the reaction, pH of the solution was adjusted to 7 by adding 1 M sodium hydroxide to terminate the reaction. This solution was dialyzed overnight against 0.5 mM ammonium acetate by using cellulose tube whose cutoff molecular weight is between 12000 and 14000. After the dialysis, the white powder was obtained by freeze dehydration of the solution. The yield was 89.6 %.

8.2.2 Dynamic light scattering

The DLS measurements were performed by the conventional DLS system, which is the same as the previous sections. The temperature was set to be 25 °C and the scattering angle was set to be 90°. Detail of the data analysis is given in Section 4.1.2. Samples were filtered by 0.2 μm filter before the measurements to remove the dust and large aggregates.

8.2.3 Rheology

The rheological measurements were performed by a stress-control rheometer (MCR-501, Anton Paar, Austria). Sample solution was set on a temperature-controlled stage and the solution is sheared by a cone plate whose radius is 25.0 mm and the cone angle is 1°. Oscillatory shear with 0.5 % distortion was applied and the stress was measured as a function of shear rate (0.01 $\sim$ 100 rad s^{-1}).

8.2.4 Small-angle neutron scattering

SANS experiments were performed at the GP-SANS and Bio-SANS beamline at the High Flux Isotope Reactor at the Oak Ridge National Laboratory. The experimental conditions are summarized in Table 8.1. Sample solutions were filled in banjo cells or demountable cells whose thickness were 2 mm. Most of the measurement, the temperature of the holders were set to be 25 °C. In the case of time-resolved SANS measurements, the temperature was increased in stepwise manner to induce gelation (See the following section).

Table 8.1: Experimental conditions of SANS

	GP-SANS	Bio-SANS
Average wavelength	4.72 Å	4.72 Å
Sample-to-detector distance (SDD)	2.0 m / 18.5 m	1.7 m / 14.5 m
q-range	$0.02\ \text{Å}^{-1} < q < 0.5\ \text{Å}^{-1}$ (SDD: 2.0 m) $0.003\ \text{Å}^{-1} < q < 0.07\ \text{Å}^{-1}$ (SDD: 18.5 m)	$0.02\ \text{Å}^{-1} < q < 0.4\ \text{Å}^{-1}$ (SDD: 1.7 m) $0.003\ \text{Å}^{-1} < q < 0.04\ \text{Å}^{-1}$ (SDD: 14.5 m)

$q = 4\pi \sin\theta/\lambda$ where λ and 2θ represent the wavelength and the scattering angle, respectively.

8.3 Results and Discussion

8.3.1 Rheological behavior

Figure 8.4 shows angular frequency dependence of G' and G'' of heat-induced gels (85 °C, 1 hour) under neutral, salt-free condition. Threshold concentration of gelation under this condition is 6 wt% for OVA and 5 wt% for pOVA. Therefore, the data under these threshold concentrations is difficult to obtain because of the lack of torque (shown by open symbols in the figure). By comparing the data of OVA and pOVA whose concentration is 6 wt%, it is clarified that the pOVA gel is stronger (large G') than the OVA gels. Interestingly, opposite results were obtained under acidic condition with 100 mM salt concentration (Figure 8.5). These results indicate that the gelation mechanism for these two conditions is different.

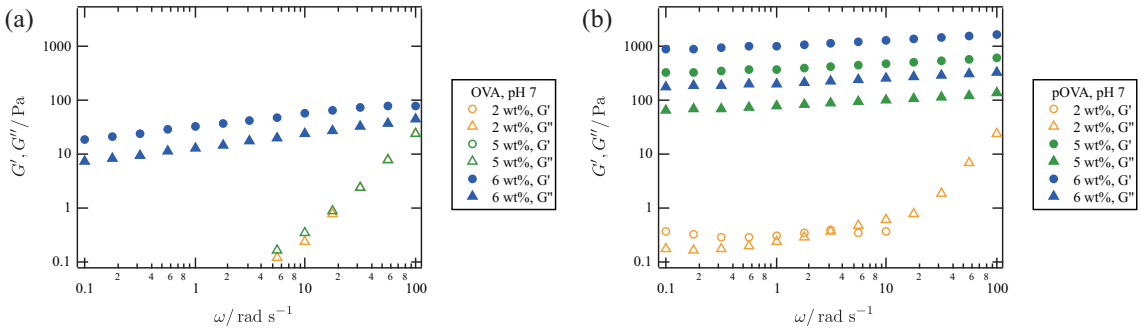

Figure 8.4: Angular frequency dependence of the storage (G') and the loss (G'') moduli of heat-induced gels under neutral, salt-free condition. Heating condition is 85 °C, 1 hour. (a) OVA. (b) pOVA.

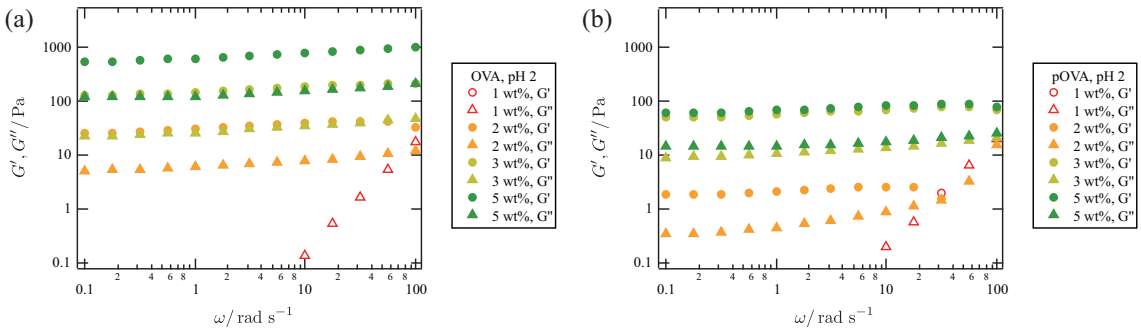

Figure 8.5: Angular frequency dependence of the storage (G') and the loss (G'') moduli under acidic condition (100 mM buffer solution). Heating condition is 65 °C, 1 hour. (a) OVA. (b) pOVA.

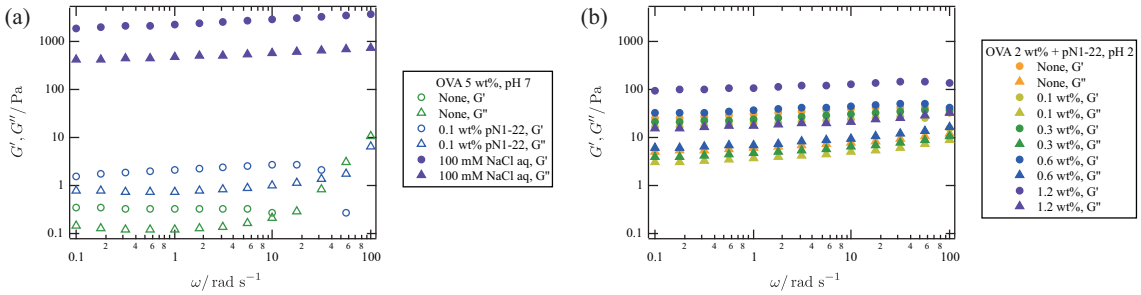

Figure 8.6: Angular frequency dependence of the storage (G') and the loss (G'') moduli for the mixture of OVA and addtives. (a) OVA under neutral, salt-free condition. Heating condition is 85 °C, 1 hour. (b) pOVA under acidic condition (100 mM buffer solution). Heating condition is 65 °C, 1 hour.

Rheological behavior can also be controlled by adding salt. Figure 8.6(a) shows the rheological behavior of heated 5 wt% OVA solution with and without NaCl (100 mM) under neutral condition. As shown in Figure 8.4, the solution does not become gel. However, addition of NaCl induced gelation. In addition, the resultant gel is stronger than any other gels shown in this subsection. This enhancement of OVA gel strength is induced not only by salt but also the peptide, pN1-22. Figure 8.6(b) shows the rheological behavior of heated 2 wt% OVA solution with pN1-22 under acidic condition with 100 mM salt concentration. It is clear that the strength of the resultant gels increases as the amount of pN1-22 increases. This phenomenon is characteristic for acidic condition since the peptide does not dissolve in neutral, salt free condition so much to induce significant change in its rheological behavior (Figure 8.6(a)). To clarify the gelation mechanism under these conditions, microscopic measurements were performed by DLS and SANS. In this section, I focus mainly on neutral, salt-free condition. Preliminary investigation under acidic condition is also shown.

8.3.2 Size distributions of OVA and pOVA molecules in solution

To see the dispersion state of OVA and pOVA in neutral water, DLS measurements were performed. Figure 8.7 shows (a) the time correlation functions of scattered light intensity and (b) corresponding size distribution of OVA (solid lines) and pOVA (broken lines) solutions whose concentration are 2 wt%. The size distributions of both solutions show two peaks. One peak corresponds to several nanometers. This size corresponds to the order of one OVA (3 nm [214]). However, it is difficult to know whether they are monomers or dimers because the scattering light from small particle is weaker than larger particles. In the next subsection, it is clarified that this peak corresponds to the dimers. Another peak corresponds to several tens nanometer. This may corresponds to the cluster consisting of several tens OVA or pOVA monomers. Note that the peak height of each peak in Figure 8.7(b) does not corresponds to the proportion of dimers and clusters. The measurements by other concentrations also show the similar tendency (Figure 8.8). This clustering indicates that both OVA and pOVA are not hydrated completely.

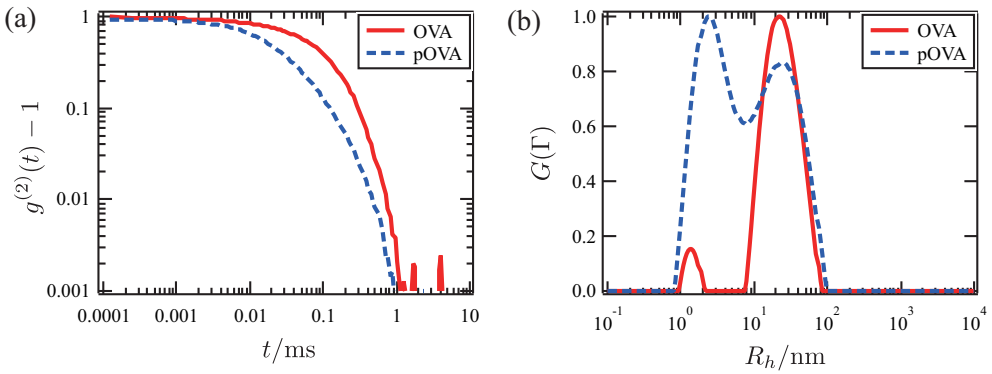

Figure 8.7: (a) Time correlation functions and (b) size distribution functions of OVA and pOVA solutions (2 wt%) measured by DLS. pH was set to be 7.

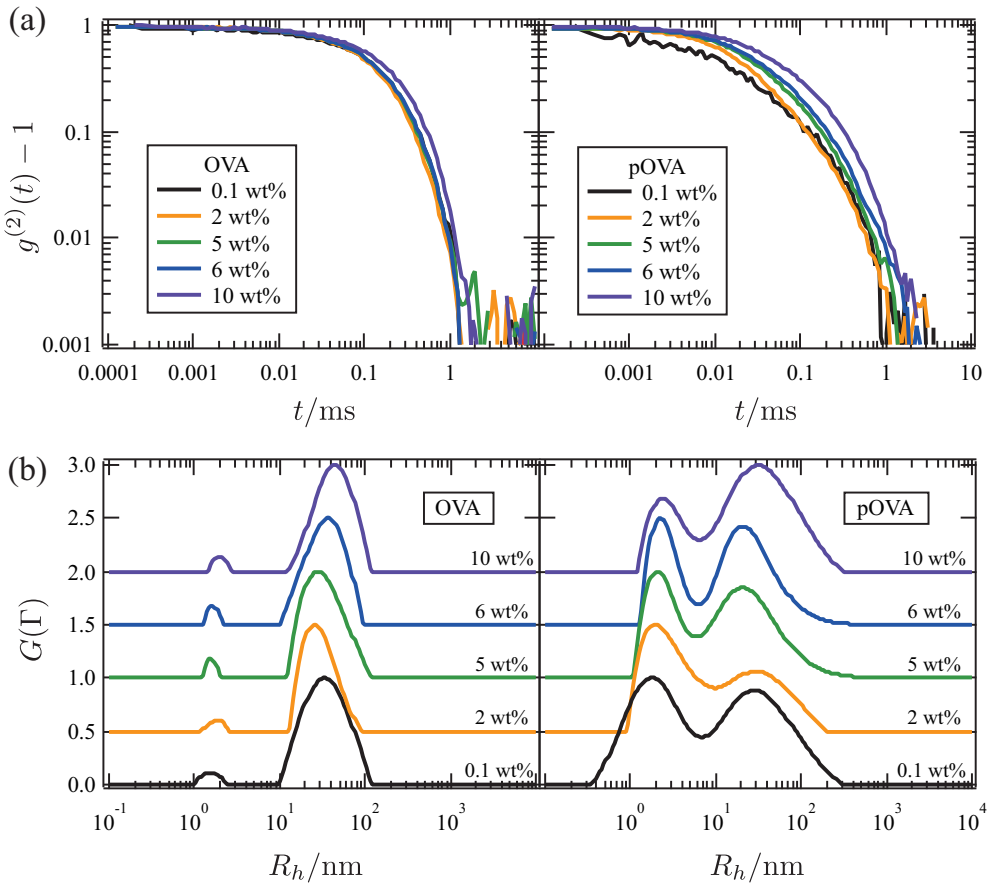

Figure 8.8: Concentration dependence of (a) time correlation functions and (b) size distribution function of OVA (left) and pOVA (right) solutions measured by DLS. In Figure (b), each profile is equally shifted vertically for clarity. pH was set to be 7.

8.3.3 Gelation mechanism of OVA

From this subsection, I focused on neutral, salt-free condition. Figure 8.9(a) shows the SANS profiles of OVA solution before heating. Clear peak structure was observed in all of the concentration. These peaks indicate the existence of characteristic length between the solutes. Since these solutions are salt-free condition, the charges on each solute are not shielded. Therefore, origin of these peaks is the electric repulsion between the solutes. To clarify this point, the characteristic correlation length (d^*) is calculated from the peak position (q^*) as follows:

$$d^* := \frac{2\pi}{q^*} \tag{8.3.3.1}$$

The relationship between d^* and protein concentration is shown in Figure 8.10. Power law is observed as $d^* \sim C^{-0.29}$ where C is the protein concentration (g/L). This power law is consistent with the previous research of SAXS, which shows $d^* \sim C^{-0.28}$ [224]. It is also theoretically proved that the power law should become $d^* \sim C^{-0.28}$ for the dispersion of monodisperse charged particles [227].

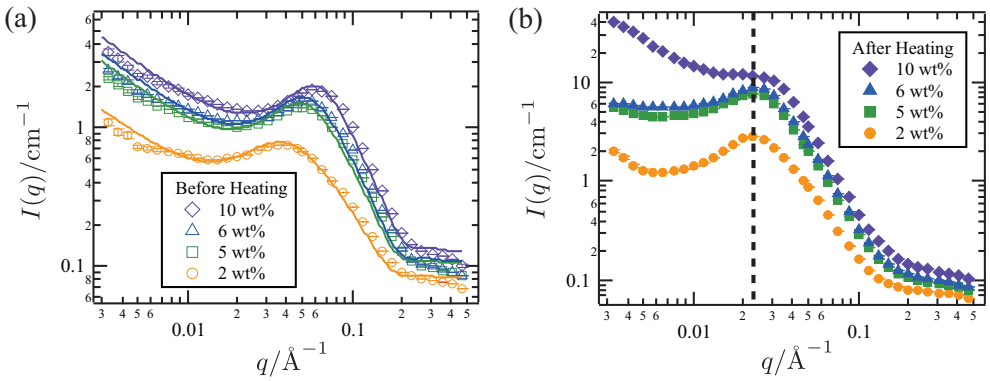

Figure 8.9: SANS profiles of OVA solutions (a) before and (b) after heat treatment with different concentrations. Solid lines in (a) show the fitting results. A dashed line shown in (b) represents the position of the peaks.

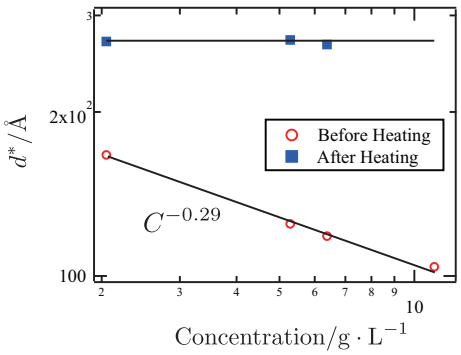

Figure 8.10: Relationship between the concentration and the characteristic length of the OVA solutions before and after heating. Solid lines show the power law of d^* against C.

This situation is quantitatively analyzed by using Hayter-Penfold structure factor (Sec. 2.4.5). As a form factor, ellipsoid shape is chosen as reported [225]. Hayter-Penfold structure factor is not directly applied to the dispersion of ellipsoids. Therefore, the radius of equivalent sphere, called the effective radius, is used for the fitting [228]. To obtain the absolute intensity, the number of solutes was calculated from the concentration

and molecular weight of the solutes. Here, each solute is regarded as a dimer [229]. Scattering length density is calculated by taking D/H exchange effect into consideration [230–232], which is summarized in Table 8.2. However, Hayter-Penfold structure factor cannot reproduce the upturn in low-q region which is clearly seen in Figure 8.9(a). There are various explanations for this upturn such as inhomogeneous hydrophobic hydration [233], equilibrium cluster formation [234], long-range attraction [235,236], aging [237], permanent aggregates [238] and so on. Although the detail of their explanation is different, most of the research indicates the existence of large aggregates. The existence of large aggregates is also suggested from the DLS results (Figure 8.7(b)) though no structural information is obtained from the DLS results. The power law of the upturn in Figure 8.9(a) is found to be $I(q) \sim q^{-1}$. This power law is characteristic for rod-shape solute. Therefore, additional form factor is added to the fitting function by assuming the large rod-shape aggregates [204]. The fitting function is summarized as follows:

$$I(q) = N_P(\Delta\rho)^2 V_P^2 S(q;\phi,R,z_m,c_{\mathrm{salt}},\varepsilon,T)P_{ellip}(q;R_a,R_b) + A_{rod}P_{rod}(q) + I_{bkg} \tag{8.3.3.2}$$

$$R = R_a^{1/3}R_b^{2/3}f^{1/3} \tag{8.3.3.3}$$

$$f := \frac{1}{4} + \frac{3}{16}\left(1 + \frac{1}{(1+\varepsilon^2)^{1/2}}\frac{\arcsin\varepsilon}{\varepsilon}\right)\left(1 + \frac{1-\varepsilon^2}{2\varepsilon}\ln\frac{1+\varepsilon}{1-\varepsilon}\right) \tag{8.3.3.4}$$

$$\varepsilon := \frac{R_a^2 - R_b^2}{R_a^2} \tag{8.3.3.5}$$

The definitions of characters are summarized in Table 8.3.

Table 8.2: Scattering length densities of amino acids

Amino acids	Chemical formula	b in H_2O / fm	b in D_2O / fm	V / Å^3	ρ in H_2O / 10^9 cm^{-2}	ρ in D_2O / 10^9 cm^{-2}
GLY	C_2H_3NO	18.91	29.32	66.4	28.5	44.2
SER	$C_3H_5NO_2$	23.88	44.70	99.1	24.1	45.1
ILE	$C_6H_{11}NO$	15.57	25.98	168.8	9.2	15.4
ALA	C_3H_5NO	18.08	28.49	91.5	19.8	31.1
MET	C_5H_9NOS	19.25	29.66	170.8	11.3	17.4
GLU	$C_5H_6NO_3$	39.23	49.65	140.6	27.9	35.3
PHE	C_9H_9NO	42.99	53.40	203.4	21.1	26.3
CYS	C_3H_5NOS	20.92	41.75	105.6	19.8	39.5
ASP	$C_4H_4NO_3$	40.07	50.48	113.6	35.3	44.4
VAL	C_5H_9NO	16.41	26.82	141.7	11.6	18.9
LYS	$C_6H_{13}N_2O$	17.45	59.10	176.2	9.9	33.5
LEU	$C_6H_{11}NO$	15.57	25.98	167.9	9.3	15.5
HIS	$C_6H_{6.5}N_3O$	51.12	66.74	167.3	30.6	39.9
ASN	$C_4H_6N_2O_2$	36.14	67.38	135.2	26.7	49.8
TYR	$C_9H_9NO_2$	48.79	69.62	203.6	24.0	34.2
PRO	C_5H_7NO	23.89	23.89	129.3	18.5	18.5
THR	$C_4H_7NO_2$	23.04	43.87	122.1	18.9	35.9
ARG	$C_6H_{13}N_4O$	36.17	98.64	180.8	20.0	54.6
GLN	$C_5H_8N_2O_2$	35.31	66.54	161.1	21.9	41.3
TRP	$C_{11}H_{10}N_2O$	61.90	82.72	237.6	26.1	34.8

The parameters z_m and c_{salt} are independent parameters. However, these parameters can be unified. In the analysis of Figure 8.9, the fitting can be done by setting $c_{\mathrm{salt}} = 0$. Strictly speaking, this analysis is rough approximation since the existence of ions originated from the dissociation from OVA is ignored [225]. However, this error is compensated by the decrease of z_m. In this case, the parameter z_m is re-interpreted as the effective charge of the solute, z (Figure 8.11).

Table 8.3: Definitions of characters

N_P	Number of solutes per unit volume
$\Delta\rho$	Scattering length density difference
V_P	Volume of the solute
$S(q)$	Hayter-Penfold structure factor
$P_{ellip}(q)$	Form factor of ellipsoids
A_{rod}	Scaling factor of the intensity of scattering from rods
P_{rod}	Form factor of rods
I_{bkg}	Background intensity including incoherent scattering
R	Effective radius
R_a	Length of long axis for the ellipsoids
R_b	Length of short axis for the ellipsoids
L	Length of the rods
d	Diameter of the rods
f	Correction parameter
ε	Eccentricity of the ellipsoids

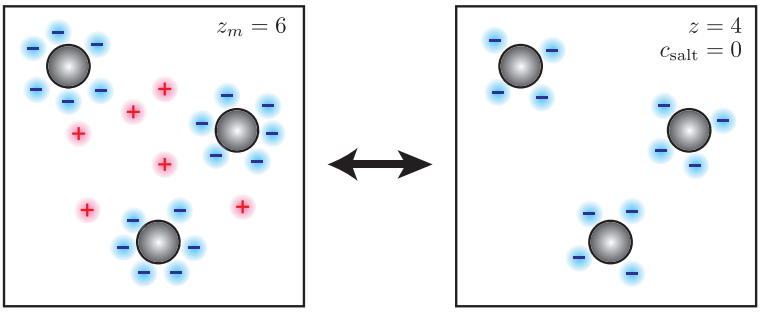

Figure 8.11: The meaning of z_m and z.

The diameter of the rods, d is also fixed (40 Å). The reason for this is that the convergence of d was poor since the profile change induced by the difference of d is overwhelmed by the peak structure in the SANS profile. The assumed value of 40 Å is taken from the characteristic size of one OVA solute. In other words, rod-like aggregates made from OVA are assumed to be a chain of OVA solutes, which was proposed by Koseki *et al.* [20]. Through these assumptions, the number of fitting parameters were reduced to 6; $R_a, R_b, z, A_{rod}, L, I_{bkg}$.

Table 8.4: Fitting parameters of SANS profiles for OVA before heating

Sample	R_a / Å	R_b / Å	z
2 wt%	50	19	8.6
5 wt%	50	19	9.4
6 wt%	52	18	9.7
10 wt%	55	17	9.7

The fitting results for OVA solution before heating are shown in Figure 8.9(a) and Table 8.4. At first, N_P is calculated by assuming that the solute is one monomer. However, the size of solutes indicates that the solute is not a monomer but a dimer as explained below. Therefore, N_P is assumed to be a half of its

original value. Through this modification, the SANS profiles are reproduced well in absolute scale. Fitting results for R_a and R_b are a little bit larger than the size of one monomer ($R_a = 35\,\text{Å}$, $R_b = 25\,\text{Å}$) [214]. This indicates that the OVA exists in dimeric form in the aqueous solution, as mentioned before. This result is supported by the DLS results (Figure 8.7(b)) and previous reports [225, 229]. The value of z is smaller than that of reported z_m (11e [225]), which is also consistent with the difference of the physical meaning of z and z_m. q^{-1} power law in low-q region is also reproduced by using a form factor of rods. To discuss the length of rods quantitatively, the information of lower-q region is necessary since the length is very long. Therefore, what we can see in the present data is that the length of the rods may be the order of several hundreds nanometer. The hydrodynamic radius for such a rod-like structure is calculated to be the order of several hundreds nanometer [239]. This estimation is consistent with the DLS results (Figure 8.7(b)). Such a long rod-like shape is formed when there are both hydrophobic (attractive) interaction and electrostatic (repulsive interaction) [20]. Note that the amount of these rod-like aggregates is small since the OVA before heating is mostly covered by hydrophilic part. Therefore, the analysis by the linear combination of the contribution of the rod term and the contribution of the Hayter-Penfold term is rationalized. Note that this addition is useless if there are so many rod-like aggregates that disturb the correlations between OVA dimers.

Interestingly, the SANS profiles of OVA solutions after the heating (85 °C, 1 hour) show totally different behavior (Figure 8.9(b)). As shown in Figure 8.4(a) and previous research [224], the samples whose concentrations are smaller than 5 wt% are sol while larger than 6 wt% are gels. Since each solute is connected with each other, Eq. 8.3.3.2 is no longer available. In contrast to the clear difference in rheological measurements, the SANS profile change is continuous as a function of concentration. As for 10 wt%, strong upturn originated from inhomogenieties [5] make the peak structure dull. Other three SANS profiles show clear peak structure whose peak position is 0.023 Å^{-1} for all of the samples (indicated as the dashed line). This result indicates that the distance between solutes is independent of the concentration ($d^* \sim 270\,\text{Å}$). This is surprising since the distance between solutes decrease in general. Similar phenomenon was reported for the solution of lysozyme [234]. This unusual behavior can be explained by using aggregation growth. The fact that the distance between solutes is constant suggests that the number of solutes does not change even we change the solution. This means that the number of monomers in each solute is proportional to their concentration.

The discussion above is summarized in Figure 8.12. The solute before heating is explained well by using Hayter-Penfold type structure factor with ellipsoidal form factor. The distance between each solute (dimeric form) decreases as the concentration becomes high. The heating induces the exposure of hydrophobic parts that were inside of the original conformation. This exposure of hydrophobic parts induces the aggregation of solutes. It is clarified that the size of the resultant aggregates is proportional to the concentration. Note that the resultant aggregates are in fibrillar form under salt-free condition [20]. When the size of these aggregates becomes larger than the distance between each solute (percolation), the solution becomes a gel. Since each aggregate repels with each other due to electrostatic force, the resultant gel is relatively homogeneous. This is one of the reasons why the resultant gels are transparent.

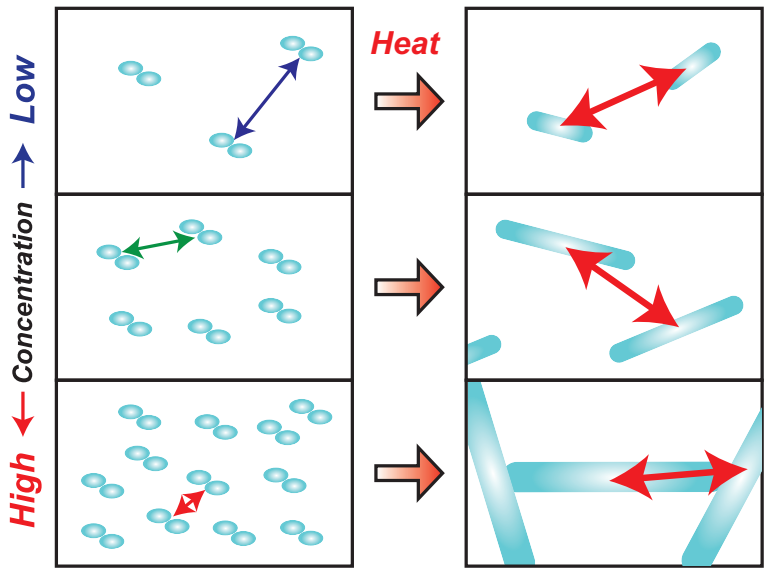

Figure 8.12: Proposed aggregation / gelation mechanism of OVA solutions.

8.3.4 Gelation mechanism of pOVA

Next, the measurement by using pOVA instead of PVA was performed with the same setup. The SANS profiles of the pOVA solutions under salt-free condition are shown in Figure 8.13(a). Although there is no peak structure, Eq. 8.3.3.2 is also used for the fitting and the observed profiles are reproduced well. The fitting results are shown in Figure 8.13(a) and Table 8.5. By comparing the value of A_{rod}, it is clarified that the amount of rod-like aggregates in pOVA solution is larger than that in OVA solution. This is rationalized by the fact the pOVA is more hydrophobic than OVA (Figure 8.1). Under salt-free condition, electrostatic and hydrophobic interactions induce the formation of rod-like aggregates like heated OVA solutes [226]. The existence of large amount of aggregates will disturb the repulsive interaction between small pOVA solutes. This is the reason for the disappearance of the peak structure. Because of the existence of these large aggregates, Hayter–Penfold type description may not be accurate. Therefore, it is difficult to conclude whether pOVA exists in monomeric form or larger form in the aqueous solution. Here, I assume that pOVA also exists in dimeric form (similar to OVA). I believe that this assumption is somehow rationalized by taking the exposure of hydrophobic part in pOVA into consideration (Figure 8.1(c)).

Table 8.5: Fitting parameters of SANS profiles for pOVA

Before heating			
Sample	R_a / Å	R_b / Å	z
2 wt%	51	18	5.1
6 wt%	63	16	5.6
After heating			
Sample	R / Å	Ξ_L / Å	Ξ_S / Å
2 wt%	$(5.9 \pm 1.9) \times 10^2$		47
6 wt%		9.3×10^2	38

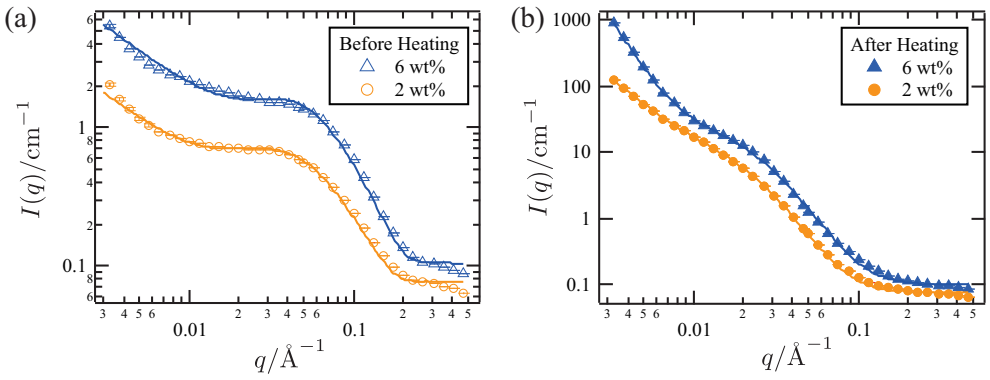

Figure 8.13: SANS profiles of pOVA solutions (a) before and (b) after heat treatment with different concentrations. Solid lines in (a) and (b) show the fitting results.

The SANS profiles after the heating (85 °C, 1 hour) of pOVA solutions also show qualitative difference with that of OVA solutions (Figure 8.13(b)). As shown in Figure 8.4(b), the sample whose concentration is 2 wt% is a sol while 6 wt% is a gel. In contrast to the case of OVA, the SANS profiles for sol and gel are qualitatively different in low-q region. The sol sample (2 wt%) shows shoulder at around 0.03 $\mathrm{Å}^{-1}$ Interestingly, q^{-2} power law is observed at $0.04 < q < 0.07$ $\mathrm{Å}^{-1}$. This indicates that Hayter–Penfold structure factor may be no longer available. Instead of Hayter–Penfold structure, I tried other structure factors which are introduced in Section 2.4. In addition, low-q region is no longer represented by q^{-1} power law but more steep. To express this obtained SANS profile, a form factor of a sphere is introduced. This assumption is based on the fact that the heat-induced aggregates of pOVA in acidic condition is spherical form [22] though there is no report in neutral, salt-free condition. Finally, it was clarified that the following fitting function reproduce the obtained SANS profile well.

$$I(q) = A_L P_{sph}(q) + \frac{A_S}{(1+q^2\Xi_S^2)^2} + I_{bkg} \tag{8.3.4.1}$$

The fitting result is shown in Figure 8.13(b). The first term in Eq. (8.3.4.1) is the form factor of spherical aggregates, which express the low-q region. The second term is known as Debye–Bueche function (Section 2.5.2). The fact that Debye–Bueche function reproduced the observed profile indicates the existence of glass-like inhomogeneities. To summarize, the heat-induced pOVA aggregates is spherical and has glass-like inhomogeneities. Note that this glass-like inhomogeneities is different from inhomogeneities originated from concentration fluctuations, which is described by Ornstein–Zernike function (Section 2.5.3).

The gel sample (6 wt%) shows q^{-2} power law in two region; $0.003 < q < 0.01$ $\mathrm{Å}^{-1}$ and $0.04 < q < 0.07$ $\mathrm{Å}^{-1}$. From this experimental finding, double Debye–Bueche function was used for fitting.

$$I(q) = \frac{A_L}{(1+q^2\Xi_L^2)^2} + \frac{A_S}{(1+q^2\Xi_S^2)^2} + I_{bkg} \tag{8.3.4.2}$$

The fitting result is shown in Figure 8.13(b). First term represents large inhomogeneities, Ξ_L, and second term represents small inhomogeneities, Ξ_S. However, these two inhomogeneities have qualitative difference. The meaning of Ξ_S is similar to that for low-concentration case (Eq. (8.3.4.1)); glass-like inhomogeneities. Fitting results show that Ξ_S decreases as the concentration increases (Table 8.5). This indicates that the aggregation structure becomes dense as the concentration increases. In contrast to this, the meaning of Ξ_L is

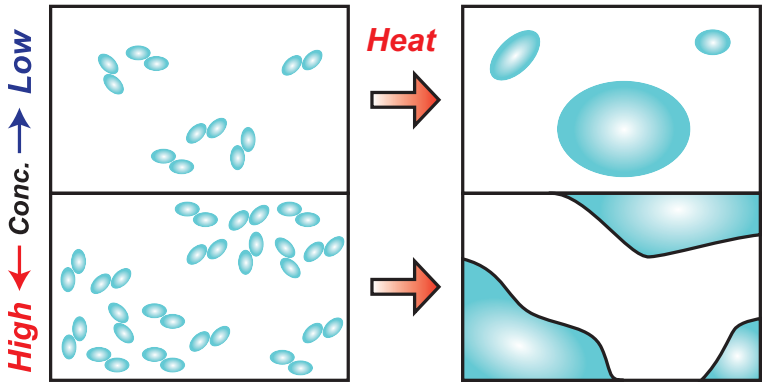

Figure 8.14: Proposed aggregation / gelation mechanism of pOVA solutions.

considered to be a correlation length for two-phase separated structure [240]. Two-phase separated structure in 100 nm scale will induce turbidity, which is shown in Figure 8.3(b).

The gelation mechanism for pOVA is summarized in Figure 8.14. Dispersion state of pOVA before heating is similar to that of OVA; each solute is in dimeric form and described by using Hayter-Penfold structure factor. However, the amount of aggregates is larger in the case of pOVA compared to OVA. This difference may be originated from the hydrophobic nature of pOVA. As a result, the distance between each solute will have wide distribution. This feature is clearly shown experimentally as a form of the disappearance of correlation peak (Figure 8.13(a)). After heating, the dispersion state showed striking difference below and above gelation concentration. Below the gelation concentration, large aggregates are produced whose inside has glass-like inhomogeneities. The origin of this glass-like inhomogeneities may be the wide distribution of inter-solute distance before heating. In contrast to this, two-phase separated structure whose inside also have glass-like inhomogeneities is produced above the gelation concentration.

8.3.5 Effect of peptide in acidic condition

In the previous report [22], it is proved that the heat-induced gels of OVA become strong with the existence of N-terminal residues from 1 to 22 (pN1-22) under acidic condition. To investigate the conformation of the solutions and the resultant gels, SANS measurements were performed.

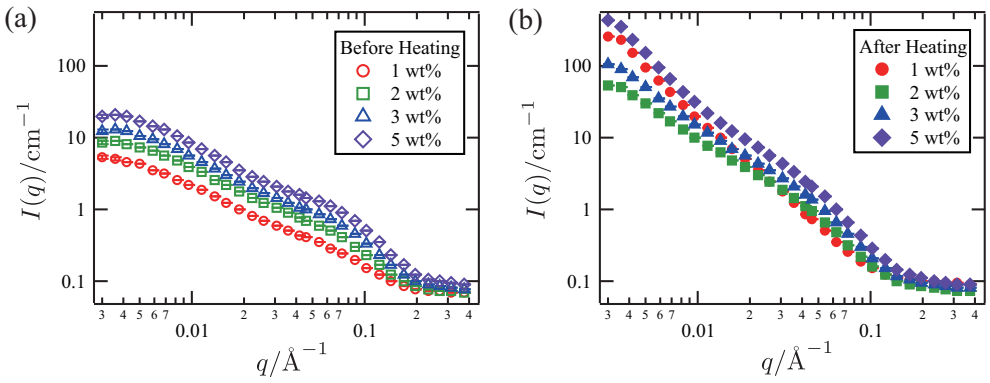

Figure 8.15: SANS profiles of OVA solutions (a) before and (b) after heat treatment with different concentrations under acidic condition. Salt concentration was 100 mM.

Figure 8.15 shows the SANS profile of OVA in 100 mM potassium phosphate buffer solution before (a) and after (b) heating. These profiles are totally different from that for salt-free, neutral solution (Figure 8.9). The most striking difference is the disappearance of the correlation peaks. This can be explained that charges on the solutes are screened by the buffer solution. The profiles after heating show different behavior below and above gelation concentration. Below the gelation concentration (1 wt%), the SANS profile shows q^{-2} dependence in wide q-region. This SANS profile does not show shoulder even in low-q region. In contrast to this, the SANS profile above the gelation concentration (2, 3, and 5 wt%) shows one shoulder around $q \sim 0.05$ Å^{-1}, which is similar to the case of pOVA in neutral condition. This indicates that the resultant gels may have glass-like inhomogeneities and two-phase separated structure. Note that the resultant gels were moderately turbid under this condition.

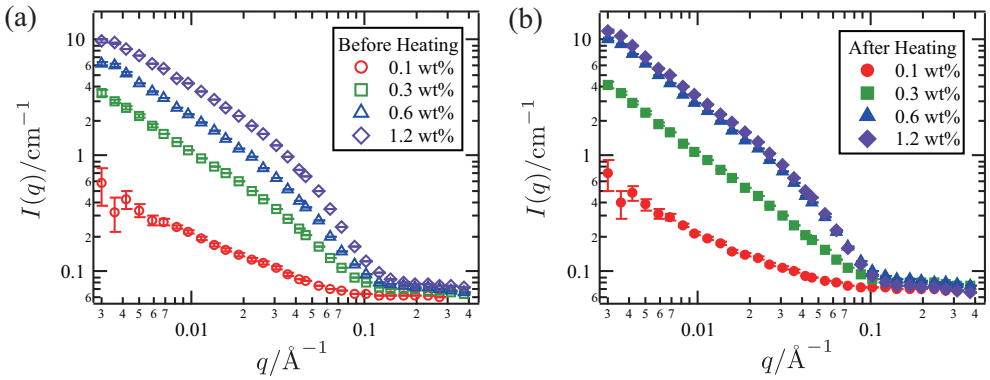

Figure 8.16: SANS profiles of pN1-22 solutions (a) before and (b) after heat treatment with different concentrations under acidic condition. Salt concentration was 100 mM.

Figure 8.16 shows the SANS profile of pN1-22 in 100 mM potassium phosphate buffer solution before (a) and after (b) heating. These graphs show that the heat-induced conformational change of pN1-22 is not so large. This is reasonable since denaturation is not so drastic for this small peptide region.

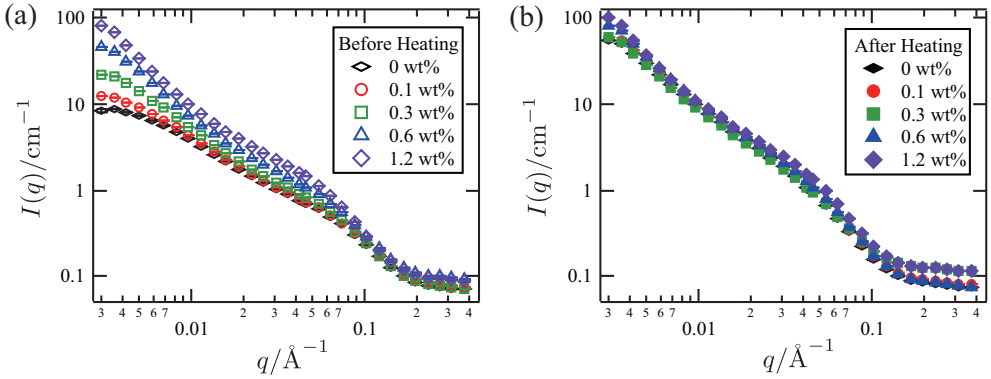

Figure 8.17: SANS profiles of the mixture of 2 wt% OVA and pN1-22 solutions (a) before and (b) after heat treatment with different concentrations under acidic condition. Salt concentration was 100 mM.

Figure 8.17 shows the SANS profile of the mixture of OVA and pN1-22 in 100 mM potassium phosphate buffer solution before (a) and after (b) heating. The concentration of OVA was fixed to 2 wt%. Interestingly, the obtained SANS profiles cannot be expressed as the summation of two SANS profiles obtained independently (Figure 8.15(a) and 8.16(a)). This result strongly suggests that pN1-22 can create aggregates

with OVA even before heat treatment. Note that the previous research clarified the pN1-22 binds to OVA only after denaturation. However, the heat-induced gels did not show significant difference in their SANS profiles. The shapes of SANS profiles obtained from the heat-induced gels are almost the same, regardless of the concentration of pN1-22. This result suggests that the pN1-22 does not induce microscopic change to the resultant gels. Slight increase of overall $I(q)$ with the increase of pN1-22 concentration shows that pN1-22 strengthen the heat-induced gels by just thicken the network strand.

8.3.6 Time-resolved measurement

To investigate the dynamical conformational change during heating, time-resolved measurements will be effective. There were many researches which focus on the dynamic aspect of heat-induced gelation of OVA [241]. Here, I introduced preliminary three time-resolved measurements; rheology, light scattering, and SANS.

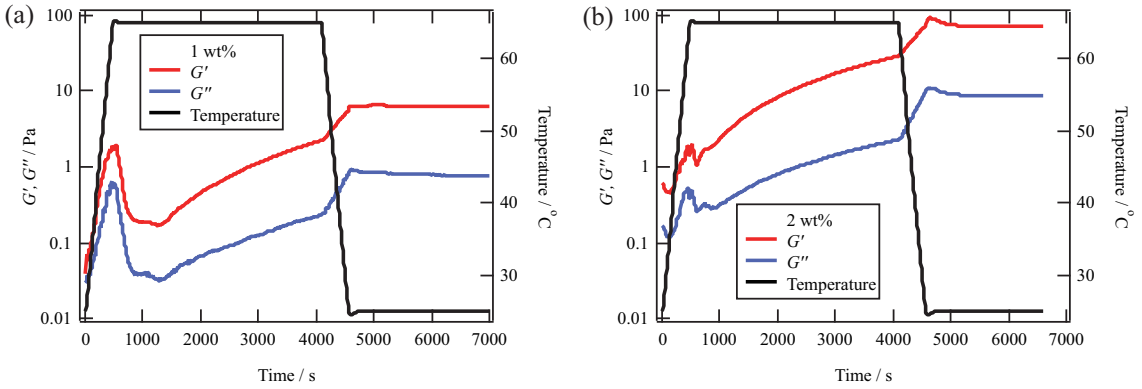

Figure 8.18: Time-resolved measurement of rheological behavior for (a) 1 wt% and (b) 2 wt% OVA solutions under acidic condition. Salt concentration was 100 mM. Temporal profiles for G', G'', and temperature are shown.

Figure 8.18 shows the dynamical change of G' and G'' of OVA solutions during heating. pH was set to be 2.2 and the salt concentration of buffer solution was 100 mM. In contrast to Figure 8.5, G' and G'' were obtained as a function of heated time. Temperature of the stage was first increased from 25 °C to 65 °C with the speed of 5 °C / min. Then the temperature was kept to 65 °C for one hour. After that, the temperature was decreased to 25 °C with the speed of 5 °C / min. First, G' and G'' were increased by the increase of temperature. After the temperature was set to 65 °C, both G' and G'' were decreased for a while. Although the degree of this decrease is different, the same feature appears in both 1 wt% and 2 wt% samples. This result indicates that the character of the heat-induced gels will be affected not only by the final temperature but heating process. After the decrease, G' and G'' increased again under 65 °C condition. Then the degree of the increase of G' and G'' becomes large by the decrease of temperature. From these measurements, the importance of temperature change is highlighted.

It is well known that DLS is one of the useful tools for the measurement of gelation [242]. Here, I applied time-resoled DLS technique to OVA solutions. Figure 8.19 shows the dynamical change of scattered light intensity, $\langle I \rangle_T$, the apparent diffusion constant, D_A and the time correlation functions of $\langle I \rangle_T$, $g^{(2)}(t) - 1$, of OVA solutions during heating. These measurements were performed by setting the OVA solution to the

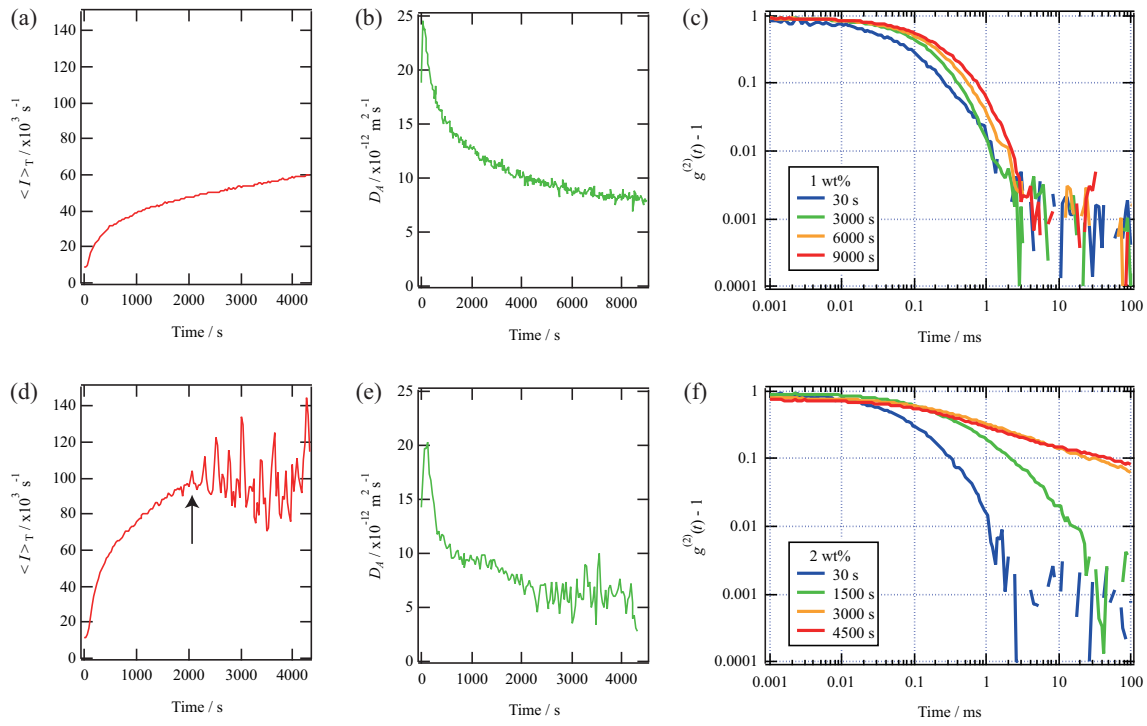

Figure 8.19: Time-resolved DLS measurements under acidic condition. Salt concentration was 100 mM. (a),(d): Time variation of scattered light intensity for 1 wt% (a) and 2 wt% (d) solution. (b),(e): Time variation of apparent diffusion constant for 1 wt% (b) and 2 wt% (e) solution. (c),(f): Some representative time correlation functions of scattered light intensity for 1 wt% (c) and 2 wt% (f) solution.

sample holder of DLS units which was set to 65 °C. pH was set to be 2.2 and the salt concentration of buffer solution was 100 mM. Striktly speaking, the apparent diffusion constant should be converted into the genuine diffusion constant by using heterodyne method since the initial amplitude ($g^{(2)}(t=0)-1$) is not exactly 1. However, it is good approximation to regard D_A as the genuine diffusion constant since the initial amplitude is almost 1.

For 1 wt% solution, the aggregation of solutes was clearly observed. As the time goes on, the scattered light intensity increased (Figure 8.19(a)). This indicates that the solute becomes large. In addition, the diffusion constant decreased as the time goes on (Figure 8.19(b)). This also indicates the aggregation of the solutes. Note that the diffusion constant is inversely proportional to the hydrodynamic radius (Einstein–Stokes equation). In contrast to this, not only aggregation but also gelation was observed for 2 wt% solution. At the gelation point, the scattered light intensity started fluctuation (around 2000 s, shown by an arrow in Figure 8.19(d)). The gelation is also clearly observed in $g^{(2)}(t)-1$ (Figure 8.19(f)). $g^{(2)}(t)-1$ for 30 s and 1500 s can be expressed approximately by one single exponential function. This is the characteristic feature for solution. In contrast to this, $g^{(2)}(t)-1$ for 3000 s and 4500 s can be expressed by using power law function. This is the characteristic feature for gel.

Figure 8.20 shows the time-resolved SANS measurements for 6 wt% OVA solution under neutral, salt-free condition. Temperature of the sample holder was first increased from 25 °C to 85 °C by 5 °C every 5 minutes (discontinuously, see Figure 8.20(a)). Then the temperature was kept to 85 °C for one hour. Figure 8.20(b) shows the SANS profiles at several points. The SANS profile did not change at the temperature below 60

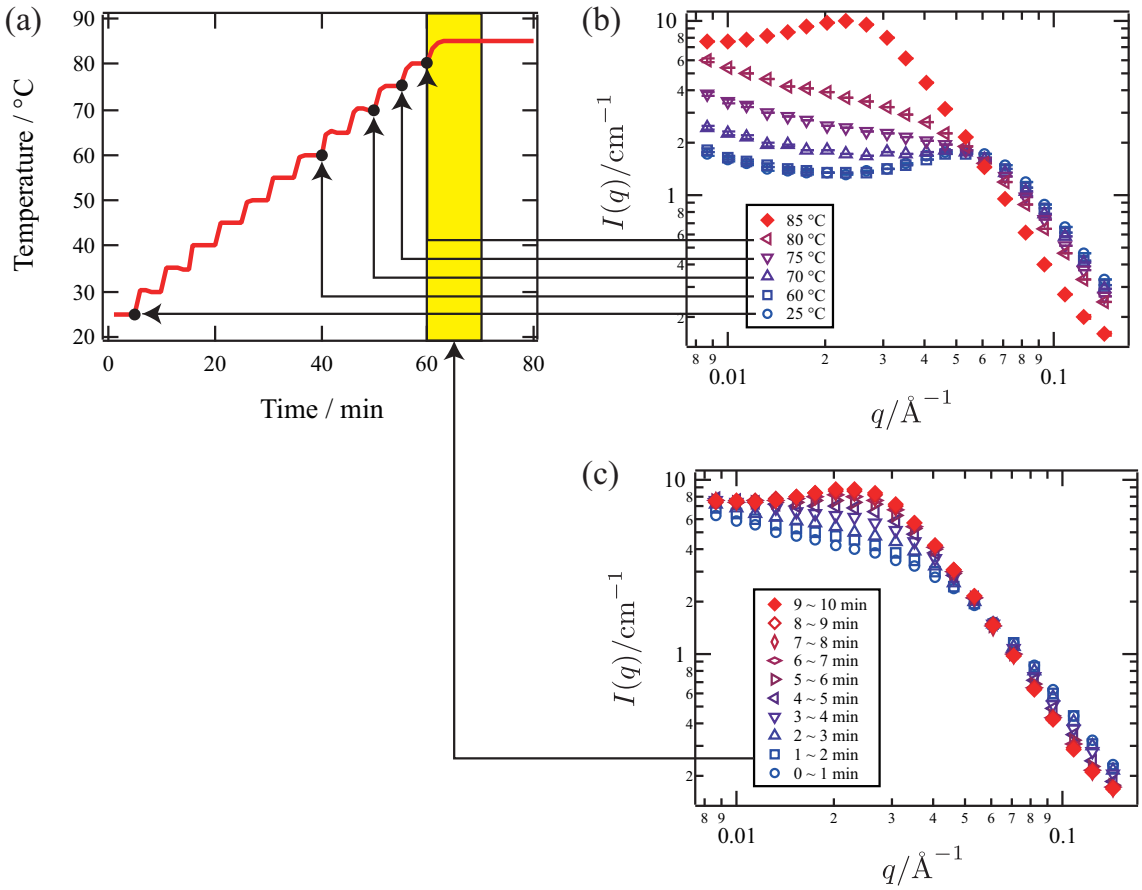

Figure 8.20: (a) Measured temperature variation of the sample cell. (b) Temperature dependence of SANS profiles during heating. Each profile except for 85 °C corresponds to the profile 5 minute after the cell temperature reaches that temperature. The profile labeled "85 °C" is the profile 1 hour after the cell temperature becomes 85 °C. (c) Time resolved SANS profiles at 85 °C. Each profile is obtained every 1 minute after setting the cell temperature at 85 °C. The sample was OVA solution, 6 wt%.

°C. Then the profile started changing at around 70 °C. This is consistent with the fact that the denaturation occurs at around 75 °C, measured by DSC [22]. As the temperature increased, the intensity at high-q region decreased while that at low-q region increased. In addition, the intensity at $q = 0.055$ Å^{-1} does not change at any temperature. The existence of this iso-scattering point has already been reported by Nicolai *et al.* [241]. In usual case, iso-scattering point is explained by two-component system. Here, two components stand for the dispersion states before heating and after heating. However, the SANS profile cannot be reproduced by the simple linear combination of the SANS profiles at 25 °C (before heating) and 85 °C (after heating). This is because the structure factor is not expressed by each component. However, it is clear that the gelation process started at the denaturation temperature. Figure 8.20(c) shows the SANS profiles after setting the sample holder at 85 °C. The SANS profile stopped changing within 10 minutes. This result tells us the time scale of gelation. Like this, time-resolved measurements give us useful information about gelation.

8.4 Summary

Gelation mechanism of OVA and its derivatives were investigated under neutral, salt-free condition and acidic, 100 mM buffer solution. Under neutral, salt-free condition, both OVA and pOVA are regarded as a charged dimeric form. However, reflecting the hydrophobic nature of pOVA, the amount of large aggregates is larger in pOVA solution than OVA solution. This difference drastically changes the character of their heat-induced gels. For OVA, the aggregation growth induced by heating proceeds homogeneously. The size of the resultant aggregates is proportional to the initial concentration. When the concentration is larger than 5 wt%, each aggregate percolates and becomes a gel. Since each aggregate repels with each other, this percolation occurs homogeneously and the resultant gel is transparent. In contrast to this, the correlation between each aggregate is disturbed by the large aggregates in the case of pOVA. As a result, the resultant gel is turbid. The inhomogeneities of this gel are clarified as glass-like inhomogeneities described by the Debye–Bueche function. The analysis for acidic condition and time-resolved measurements are incomplete at this stage. I would like to investigate more in the future.

9 Solvent-induced Aggregation: PEG–PDMS Gels

9.1 Introduction

Amphiphilic network is the system composed of hydrophilic and hydrophobic polymers [25,26]. This unique architecture is utilized for many applications such as drug release systems [243], antifouling coatings [244], gas and biosensors [245], chiral separation membranes [246], activating carriers for biocatalysts [247] and so on. Amphiphilic network is also promising for drug delivery system [27,248,249] (Figure 9.1(a)). If the carrier of drugs is made from amphiphilic network, both hydrophilic and hydrophobic medicines are available. Another representative application is soft contact lenses [28] (Figure 9.1(b)). Contact lenses should be hydrophilic since our eyes are hydrophilic. However, hydrophilic materials tend to decrease oxygen permeability. This drawback will be solved by using amphiphilic network as a material since hydrophobic part can pass oxygen.

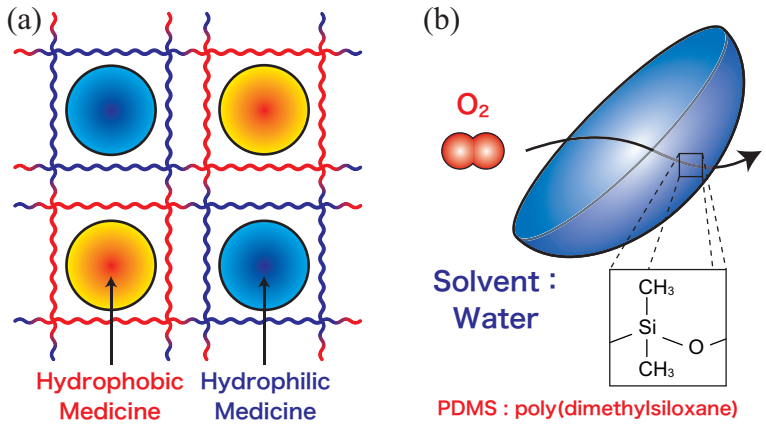

Figure 9.1: Examples for the application of amphiphilic co-networks. (a) Drug delivery system. (b) Contact lenses.

Structure of such amphiphilic conetwork system is also interesting from the viewpoint of basic science. Starting from de Gennes' theoretical investigation [50, 250], there are many reports on structural analysis for conetwork systems [111, 251–265]. Small-angle X-ray / neutron scattering techniques (SAXS / SANS) revealed microscopic structures in amphiphilic conetwork system such as a bicontinuous structure [49, 251], a weakly ordered local structure [252], a hydrophobic domain structure [266] and so on. One of the major problems for these analysis is that the prepared networks have inhomogeneities, which makes the quantitative analysis difficult. Such inhomogeneities are inevitable as far as the networks are prepared by radical or γ-ray radiation reactions since the crosslink point is introduced randomly. Here I focus on inhomogeneity-free amphiphilic gels prepared by hydrophilic tetra-arm poly(ethylene glycol) (Tetra-PEG) and hydrophobic linear poly(dimethylsiloxane) (linear-PDMS) as building blocks which was reported recently [18]. This preparation scheme is similar to Tetra-PEG gel (Section 5) and therefore resultant gels contain less inhomogeneities. In general, structural analysis of gels in real space such as TEM and SEM is difficult since the sample should be set under vacuum condition. Here I report the structural analysis of the inhomogeneity-free amphiphilic gels, PEG–PDMS gels, performed by SANS and SAXS. Complimentary use of SANS and SAXS is useful for this system since they give us different profiles in a qualitative manner. The effect of the solvent, the volume fraction of PDMS, and the molecular weight of the polymers on their structure are investigated.

9.2 Experimental

9.2.1 Sample preparation

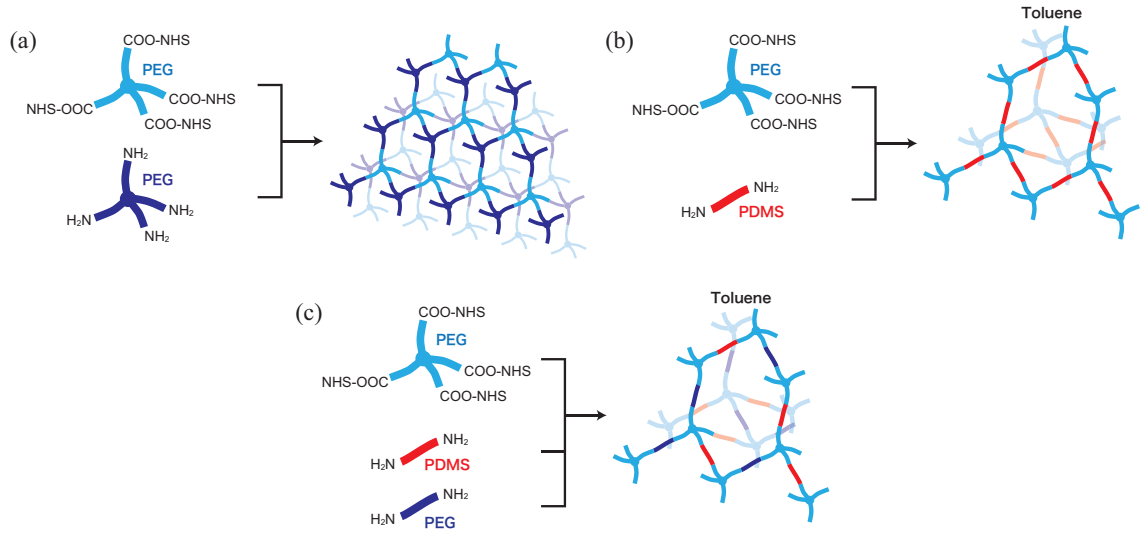

Figure 9.2: Schematics of sample preparation. (a) Conventional Tetra-PEG gels. (b) PEG–PDMS gels, $r = 1$. (c) PEG–PDMS gels, $r = 0.5$.

Figure 9.2(a) shows the preparation scheme of conventional Tetra-PEG gels. Two prepolymer solutions are prepared with appropriate pH (For details, please see Appendix) to control reaction rate. By exchanging amine-terminated tetra-arm PEG to amine-terminated linear PDMS[79], PEG–PDMS gels are prepared (Figure 9.2(b)). Because PDMS is not dissolved in water, toluene is used as a solvent. When part of amine-terminated linear PDMS is substituted to amine-terminated linear PEG, we can tune the PDMS content rate at will (Figure 9.2(c)). Here, I call the molar ratio of linear-PDMS to the total linear polymers r. In other words, $r \equiv$ (linear-PDMS)/(linear-PDMS + linear-PEG). Functionalized Tetra-PEG and linear-PEG are purchased from NOF Cooperation and the -NH_2 terminated linear PDMS was purchased from Sigma-Aldrich. Total polymer concentration in as-prepared state is set to 75 mg/mL except for Figure 9.6(a) and 9.12(a).

To prepare amphiphilic hydrogels, I utilized solvent substitution technique (Figure 9.3). After gelation proceeds completely (typically 12 hours), each gel was immersed into toluene to allow complete swelling. After swelling was over, each gel was immersed into the mixture of toluene and methanol. This procedure was repeated 3 times with changing the proportion of methanol to 25 %, 50 %, and 75%. Then these gels were immersed into pure methanol. Next, these methanol-substituted gels were immersed into the mixture of methanol and water 3 times. The proportion of water was changed to 25 %, 50 %, and 75%. At last, these gels were immersed into pure water. This procedure was repeated again to prepare the amphiphilic hydrogels. Figure 9.4 shows photographs of these gels. When PDMS is short, all of the hydrogels are transparent. In contrast to this, the gel becomes translucent for PEG 10k-PDMS 27k hydrogels. When $r = 0.5$, resultant gel becomes brittle. In the case of PEG 10k-PDMS 27k hydrogels, the gels of $r = 0.5$ and $r = 0.75$ are brittle. The origin of this may be incompatibility of amine-terminated linear PEG and PDMS in toluene solution.

[79]The reason why I use a linear polymer is simply because there is no commercially-available amine-terminated tetra-arm PDMS.

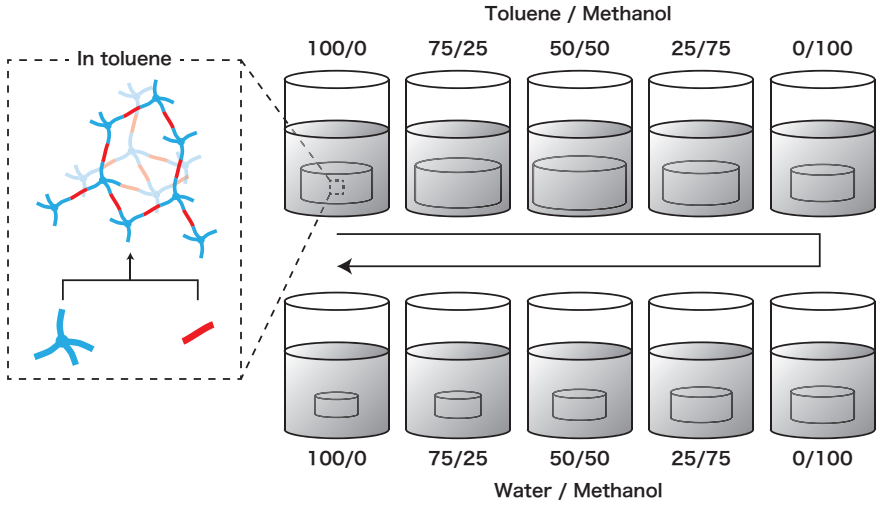

Figure 9.3: Schematics of solvent substitution.

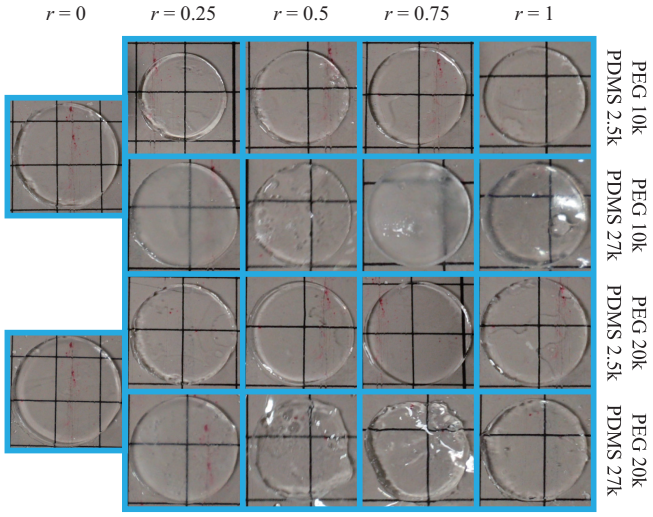

Figure 9.4: Photographs of the gels. All of them are cut to the same size by cork borer.

9.2.2 Small-angle neutron and X-ray scattering

The SANS experiments were performed on the 40m SANS at High-flux Advanced Neutron Application Reactor (HANARO) [267] at Korea Atomic Energy Research Institute (KAERI), Korea, and QUOKKA [268] at the OPAL Reactor at the Australian Nuclear Science and Technology Organization (ANSTO), Australia. The SAXS experiment was performed on BL03XU at SPring-8, Japan. The experimental conditions are summarized in Table 9.1. The sample gels were cut by using cork borer. The radius was approximately 10 mm. Thickness was controlled (around 2 mm) by changing the thickness of molds. Actual thickness was measured by a CCD laser displacement sensor (LK-G30A, KEYENCE). For SANS measurement, cut gels were immersed in the deuterated solvents to decrease incoherent scattering from hydrogen. These gels were set in demountable cells and immersed in the deuterated solvents. The scattered intensities were converted to an absolute intensity scale by using direct beam attenuation method. For SAXS measurement, cut gels were attached directly to the sample holder. The measurement was performed before drying. The scattered intensity was converted to the absolute intensity scale by using glassy carbon as a secondary standard.

Table 9.1: Experimental conditions of SANS and SAXS

	40m SANS	QUOKKA	SPring-8
Source	Neutron	Neutron	X-ray
Average wavelength	6.0 Å	5.0 Å	1.0 Å
Sample-to-detector distance (SDD)	2.0 m / 17.5 m	3.1 m / 16.1 m	1.2 m / 4.4 m
q-range	$0.02\ \text{Å}^{-1} < q < 0.3\ \text{Å}^{-1}$ (SDD: 2.0 m) $0.003\ \text{Å}^{-1} < q < 0.04\ \text{Å}^{-1}$ (SDD: 17.5 m)	$0.02\ \text{Å}^{-1} < q < 0.3\ \text{Å}^{-1}$ (SDD: 3.1 m) $0.004\ \text{Å}^{-1} < q < 0.05\ \text{Å}^{-1}$ (SDD: 16.1 m)	$0.02\ \text{Å}^{-1} < q < 1.0\ \text{Å}^{-1}$ (SDD: 1.2 m) $0.003\ \text{Å}^{-1} < q < 0.2\ \text{Å}^{-1}$ (SDD: 4.2 m)
Temperature	room temperature	25 °C	room temperature

$q = 4\pi \sin\theta/\lambda$ where λ and 2θ represent the wavelength and the scattering angle, respectively.

9.2.3 Rheological measurement

Rheological measurements were performed by using a rheometer (MCR 501, Anton Paar) with a cone plate geometry whose radius is 25.0 mm and a cone angle is 1°. Mixture of active ester-terminated prepolymer solution and amine-terminated prepolymer solution (100 mg/mL) was poured directly on a stage, and the storage modulus G' and the loss modulus G'' were measured as a function of time. The strain, angular frequency and temperature were set to 2 %, 1 rad s^{-1} and 25 °C, respectively.

9.3 Results and Discussion

9.3.1 Determination of gelation time

In the case of conventional Tetra-PEG gels, gelation time (reaction rate) can be controlled by pH. In contrast to this, gelation time of PEG–PDMS gels is out of control since we have to use toluene as a solvent. Gelation time was measured by rheological measurement. Figure 9.5 shows the variation of the storage modulus G' and the loss modulus G'' as a function of time. When the sample is liquid like, G'' is larger than G'. As the reaction proceeds, elasticity of the sample increases, which is shown as the form of G' increase. Therefore, a point where $G' = G''$ is regarded as a good indicator of gelation time, known as Winter's criteria [122]. Gelation time determined by this criteria is summarized in Table 9.2. As shown in Figure 9.5 and Table 9.2, gelation time becomes longer as r increases. This means that the reaction between Tetra-PEG and linear-PDMS is slower than that for Tetra-PEG and linear-PEG. However, quantitative discussion is difficult since the number density of crosslinking also depends on r since the molecular weights of linear-PEG and linear-PDMS are different.

Table 9.2: r-dependence of the gelation time of PEG–PDMS gels.

r	0	0.25	0.5	0.75	1
Time / s	270	210	410	720	920

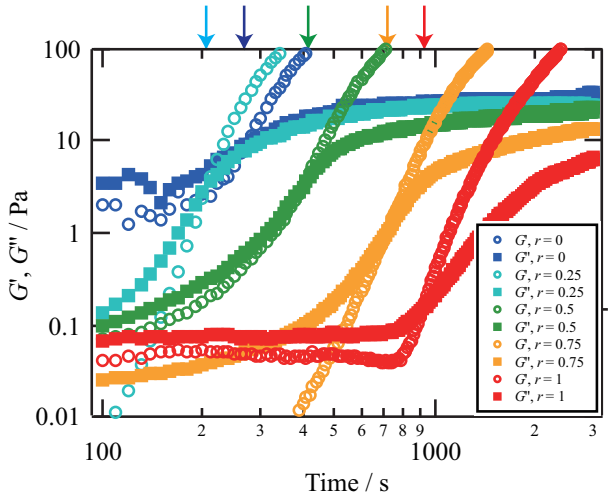

Figure 9.5: r-dependence of the time variation of G' and G'' during the gelation process of PEG–PDMS gels (75 mg/mL, Tetra-PEG: 10 kg/mol, linear-PEG: 10 kg/mol, linear-PDMS: 2.5 kg/mol). The arrows in the figure indicate the gelation point.

9.3.2 Microphase separation induced by solvent substitution

To see the structure before solvent substitution, SANS profiles of as-prepared gels were measured. Figure 9.6(a) shows the r-dependence of SANS profiles obtained from the as-prepared gels. Except for $r = 0$ (no PDMS component), upturn in low-q region is suppressed. As explained in Figure 5.21, strong upturn is the sign of inhomogeneities and typical feature of conventional gels. Therefore, Figure 9.6(a) indicates that the introduction of PDMS component decrease the inhomogeneities. The reason of the decrease of inhomogeneieties may be the difference of reaction rate. As explained in the previous subsection, the reaction first proceeds between Tetra-PEG and linear-PEG when $r > 0$. After this reaction, the reaction between remaining active-ester terminated part of Tetra-PEG and linear-PDMS proceeds. This two-step reaction may make the gel homogeneous. When $r = 0$, reaction proceeds relatively fast and inhomogeneities remain. In contrast to this, reaction proceeds slowly in the case of $r = 1$. Therefore, $r = 1$ gel is also homogeneous though the reaction is one-step. SANS profiles shown in Figure 9.6(a) are fitted by Ornstein–Zernike function (Section 2.5.3):

$$I(q) = \frac{I(0)}{1 + (q\xi)^2} + I_{BKG} \tag{9.3.2.1}$$

where ξ and I_{BKG} stands for the correlation length and the background scattering including incoherent scattering, respectively. Fitting results are also shown as solid lines in Figure 9.6(a), which show good agreement. For $r = 0$, the fitting resin is restricted to $q > 0.01$ Å^{-1} to neglect the effect of strong upturn in low-q region. The fact that the SANS profiles are reproduced well by Ornstein–Zernike function means that the structure of gels are the same as semidilute solutions [50]. Therefore, it is clarified that the crosslinking of PEG–PDMS gels are introduced without creating static inhomogeneities. Figure 9.6(b) shows the relationship between the obtained correlation length, ξ, and the average molecular weight between cross-link points (see Figure 9.7). They show positive correlation. This is consistent with the assumption that the correlation length is a measure of the mesh size of the gels as explained in Sec. 5.5.

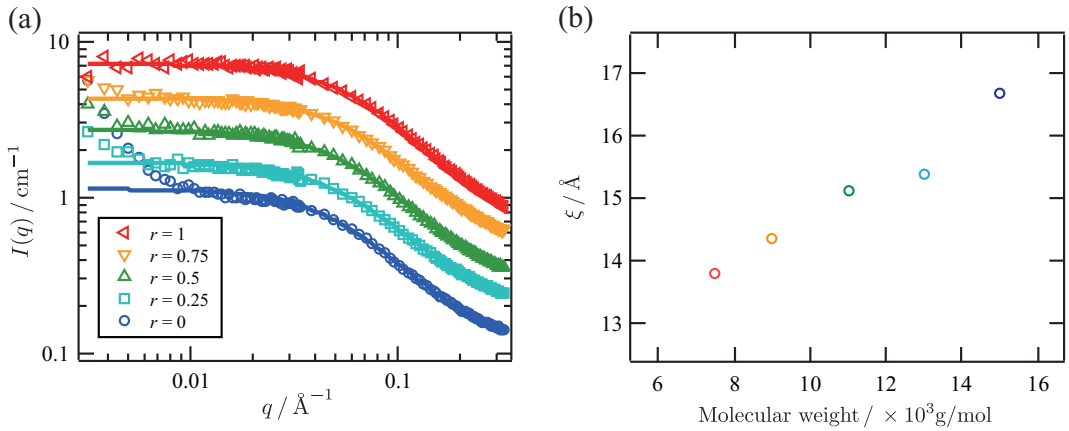

Figure 9.6: (a) r-dependence of SANS profiles of as-prepared PEG–PDMS gels (100 mg/mL, Tetra-PEG: 10 kg/mol, linear-PEG: 10 kg/mol, linear-PDMS: 2.5 kg/mol). Solid lines are the fitting results by using Eq. 9.3.2.1. Each profile except for $r = 0$ is vertically shifted for clarity. (b) The relationship between correlation length and average molecular weight between cross-link points. The correlation length was evaluated from fitting.

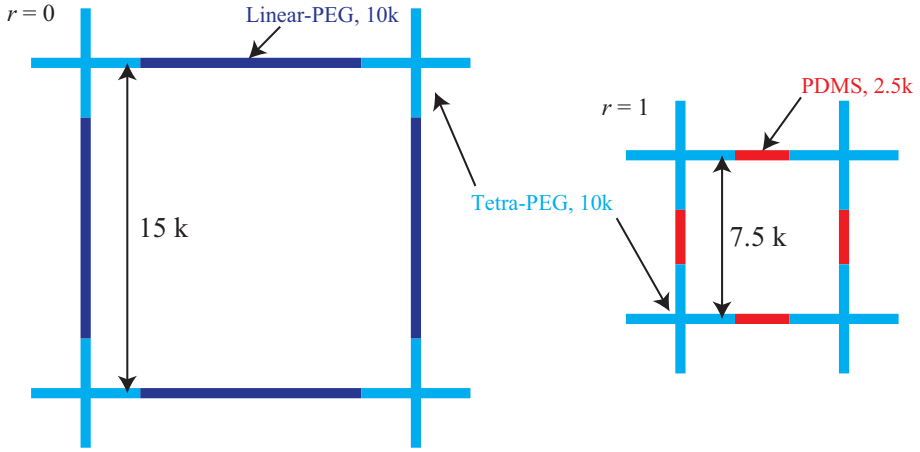

Figure 9.7: Schematics for the calculation of the average molecular weight between cross-link points.

Next, let us see the structural change induced by solvent substitution. Figure 9.8(a) shows the SANS profiles of swollen PEG–PDMS gels of $r = 1$ (Figure 9.2(b)) with various solvents. In contrast to the result that there was no upturn in low-q region for as-prepared gel (Figure 9.6(a)), the gel swollen by toluene shows upturn in low-q region. This is because swelling enhance the inhomogeneities [5]. As explained in Figure 5.29, conventional gel has dense region and sparse region. By swelling, sparse region becomes more sparse. This is the origin of the enhancement of the inhomogeneities. Although the inhomogeneities of PEG–PDMS gel is small as shown in Figure 9.2, small inhomogeneities may cause small upturn in low-q region induced by swelling. By substituting solvent from toluene to the mixture of methanol and toluene, the upturn in low-q region is suppressed. This indicates that the affinity of polymers and solvent is improved. This is also clarified by the swelling ration as shown in Figure 9.8(b). Figure 9.8(b) shows the variation of swelling ratio by the solvent substitution. Swelling ratio is defined as the gel size (measured by their length) compared to the as-prepared gel. By the substitution of solvent to the mixture of methanol and toluene,

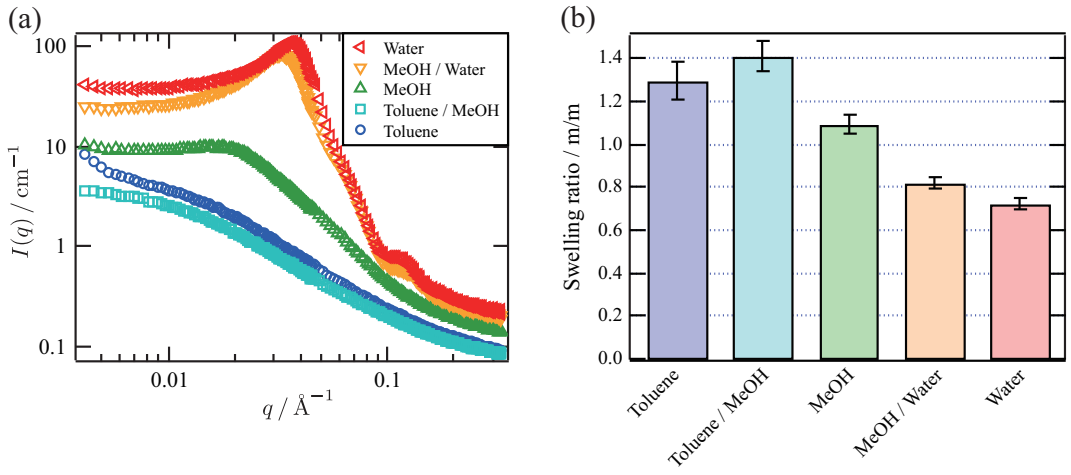

Figure 9.8: (a) SANS profiles and (b) swelling ratios of PEG–PDMS gels ($r = 1$) with different solvents (75 mg/mL). The ratios of toluene/MeOH and MeOH/water are both 1/1 (volume fraction).

swelling ratio is increased. This also supports the idea that the affinity of polymers and solvent becomes better. The decrease of $I(q)$ is simply due to the decrease of polymer fraction due to the dilution by solvent. Note that the scattering length density of *d*-toluene and *d*-methanol is almost the same (Figure 4.16).

By substituting the solvent to pure methanol, broad peak is appeared at around $q = 0.02$ Å^{-1}. This peak becomes sharp as the solvent becomes more hydrophilic. In addition, the position of peak center moves to higher q. This indicates that the characteristic length becomes short as the solvent becomes hydrophilic. Appearance of the scattering peak in amphiphilic block copolymers or amphiphilic conetworks was reported in several papers [251, 252, 266]. Qualitatively speaking, the origin of this peak is explained by using the concept of microphase separation as explained in Section 3.3. When the solvent becomes hydrophilic, PDMS components will shrink due to their incompatibility to the hydrophilic component. Sharpness of the peak correspond to the sharp boundary between hydrophilic solvent and hydrophobic PDMS components. Shrinkage of the PDMS components induces the shrinkage of the gel itself as shown in Figure 9.8(b) (Schematically shown in Figure 9.3). This shrinkage may be the origin of peak shifts to higher-q region. However, the second peak at around $q = 0.11$ Å^{-1} cannot be explained by the theory discussed in Section 3.3. In addition, the length scale of microphase separation is too large compared to the estimation by the theory of microphase separation used for diblock copolymer melt. The inter-domain size, d^*, is estimated from the peak position, q^*, by $d^* := 2\pi/q^*$. The estimated value of d^* is approximately 200 Å for the gel in pure water. This value is significantly larger than the size of one Tetra-PEG; the radius of gyration of Tetra-PEG whose molecular weight is 10 kg/mol is around 15 Å (measured from Figure 5.20 [16]). This result suggests that the microphase separation does not occur in the scale of one PDMS unit but accompanies many PDMS units and Tetra-PEG units around one PDMS unit. Therefore, the morphology of the resultant gels may be manipulated by varying the compositions of PEG and PDMS. To investigate this hypothesis, preparation and characterization of PEG–PDMS gels with various compositions of PEG and PDMS was performed.

9.3.3 r-dependence of microphase separation

First, PDMS composition is decreased by exchanging linear-PDMS component to linear-PEG component as shown in Figure 9.2(c). Table 9.3 shows the estimated volume fraction of polymers for each gel. These values were calculated from the preparation conditions and the observed swelling ratios. Figure 9.9(a) shows the SANS profiles of water-swollen PEG–PDMS gels for various r values. Except for $r = 0$ (no PDMS component), clear peak structures were observed. Note that the peak appear even when the volume fraction of PDMS is 0.2 % ($r = 0.25$, Table 9.3). This indicates a uniform distribution and strong aggregation of PDMS components in water solvent. Figure 9.8(b) shows the variation of swelling ratio by the change of PDMS composition, r. This result also supports the idea that PDMS units shrinks and aggregates in water. Figure 9.8(c) shows the relationship between the swelling ratio (Figure 9.8(b)) and the inter-domain size of corresponding gels, d^*, estimated from the peak position of Figure 9.8(a). Although d^* shows positive correlation to the swelling ratio, the relation is not proportional. This indicates that the morphology is not the same for all r. This is consistent with the fact that the SANS profiles higher than their first peak strongly depends on r. For examples, shoulder structure is seen at around $q = 0.06$ Å^{-1} for $r = 0.5$ while it is blurred for $r = 0.75$. In the case of $r = 1$, secondary peak appears at around $q = 0.1$ Å^{-1}. These qualitative differences indicate the different morphology. However, it is difficult to determine the morphology only from the SANS profiles, Figure 9.9(a). For more precise analysis, I performed SAXS measurements. In next section, I explain the advantage of the complimentary use of SANS and SAXS for this system.

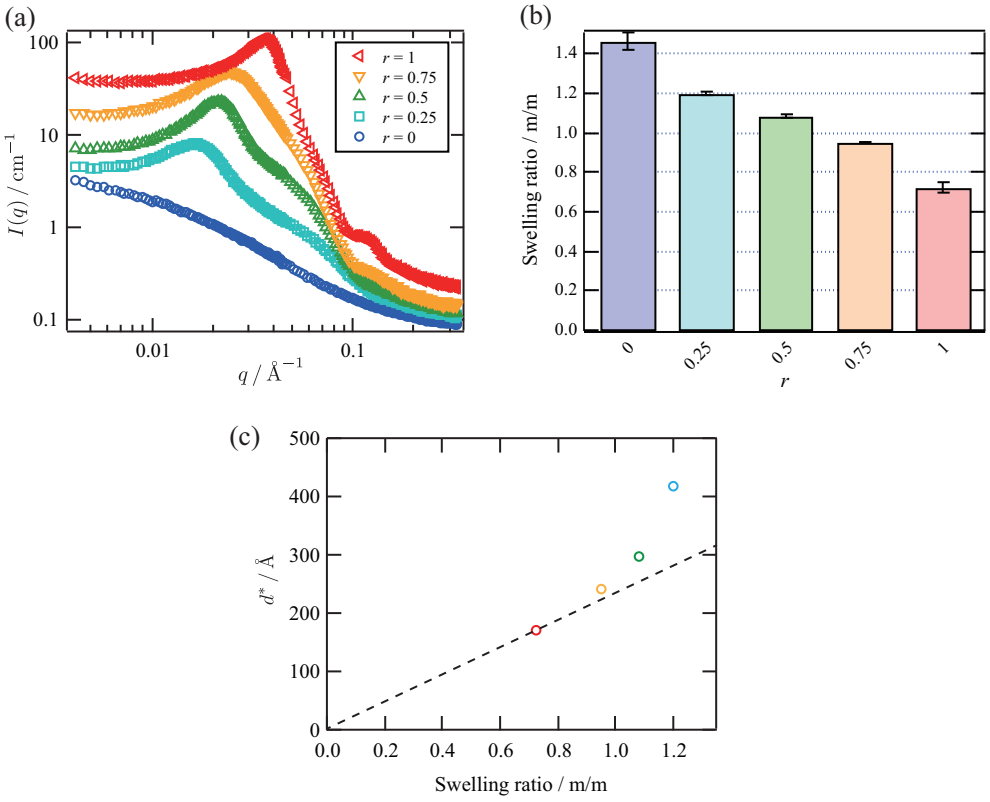

Figure 9.9: r-dependence of (a) SANS profiles and (b) swelling ratios in water (deuterated) (75 mg/mL). (c) Relationship between the inter-domain distance and the swelling ratio. The inter-domain distance was evaluated from the peak positions of Figure 9.9(a). Dashed line is guide for eyes.

Table 9.3: r-dependence of the estimated volume fractions of swollen PEG-rich PEG–PDMS gels in water

r	PEG	PDMS	Water
0	0.021(3)	0	0.979(3)
0.25	0.035(3)	0.0021(2)	0.963(3)
0.5	0.044(4)	0.006(1)	0.950(4)
0.75	0.058(4)	0.017(1)	0.925(5)
1	0.098(12)	0.058(7)	0.844(18)

9.3.4 Analysis of microphase-separated structure

Figure 9.10 shows the comparison of scattering length densities (SLD) of water, PEG and PDMS for SANS and SAXS. Please refer to Section 4.2.2 for the calculation of SLD. Important difference is that the scattering length has positive correlation to an atomic number in the case of SAXS while there is no correlation in the case of SANS. As a result, the contrast for SANS and SAXS experiment is totally different. In the case of SANS, the contrast between D_2O and PEG is similar to that between D_2O and PDMS. In contrast to this, the difference of SLD between water and PEG has different sign of that between water and PDMS in the case of SAXS. Therefore, the complimentary use of SANS and SAXS will give us rich information.

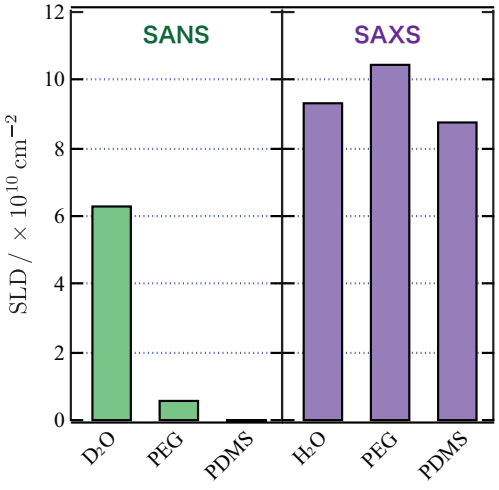

Figure 9.10: Scattering length densities of water, PEG, and PDMS for (left) SANS and (right) SAXS.

Figure 9.11 shows the SANS and SAXS profiles of PEG–PDMS gels of $r = 1$. Note that the intensity is given in absolute scale. The profiles show clear difference; the SAXS profile shows dip structure while the SANS profile shows peak structure at around $q = 0.04$ Å^{-1}. To reproduce this difference, fitting analysis is performed. When the solvent of the gel is water, PDMS components will aggregates and PDMS-rich region will be created. This means that there should be PEG-rich region to compensate the aggregation of PDMS. In addition, the simplest model to reproduce dip structure is form factors of three-component system such as core-shell-solvent structure [269, 270]. Therefore, in the analysis, the gel is regarded as three-component system; PEG-rich region, PDMS-rich region, and solvent. However, only the form factor of three-component system cannot explain the peak structure shown in SANS profile. To solve this point, I introduced a modified Percus–Yevick structure factor (Section 2.4.3). Modified Percus–Yevick structure factor has been used for

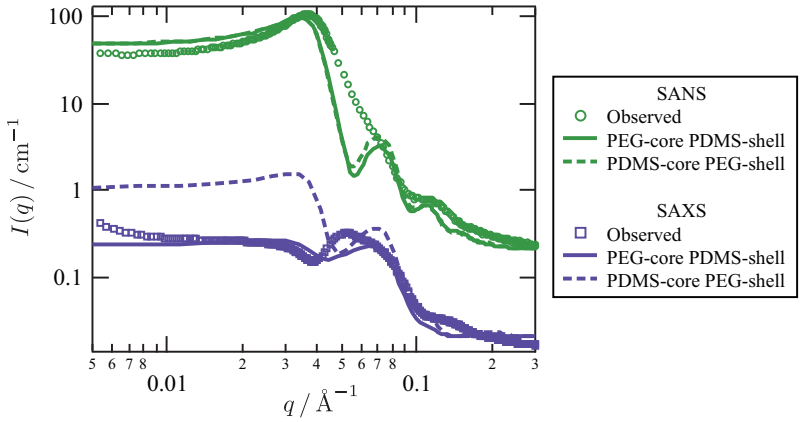

Figure 9.11: SANS and SAXS profiles of PEG–PDMS gels with $r = 1$ (75 mg/mL). The molecular weights of Tetra-PEG and PDMS are 10 kg/mol and 2.5 kg/mol, respectively. The solid lines are the simulated profiles obtained from the model described (see main text).

the analysis of other amphiphilic gels [266]. To summarize, the model curve is described as follows.

$$I(q) = nS_{mPY}(q;\phi', R+L)P_{cs}(q;R,dR,L) + I_{BKG} \tag{9.3.4.1}$$

where $n, S_{mPY}(q;\phi', R+L)$, and $P_{cs}(q;R,dR,L)$ correspond to the number density of core-shell particles, the modified Percus–Yevick structure factor, and the core-shell form factor (Section 2.2.3), respectively. Here, ϕ', R, L, and dR corresponds to the effective volume fraction, the mean radius of core, the thickness of the shell, and the polydispersity of the core, respectively. A Schulz distribution for the radius is assumed for the analysis [271]:

$$G(r) = \frac{r^Z}{\Gamma(Z+1)}\left(\frac{Z+1}{R}\right)^{Z+1}\exp\left[-\frac{r}{R}(Z+1)\right] \tag{9.3.4.2}$$

where

$$\left(\frac{dR}{R}\right)^2 = \frac{\langle\,(R-r)^2\,\rangle}{\langle\,R-r\,\rangle^2} - 1 =: \frac{1}{Z+1} \tag{9.3.4.3}$$

At this stage, there is no information whether the form factor is PEG-core PDMS-shell or PDMS-core PEG-shell. Therefore, I tested both two form factors for the modeling of SANS and SAXS profiles. The parameters were determined by trial-and-error. The results are shown in Figure 9.11. The parameters used is $n = 2.8 \times 10^{16}$ cm$^{-3}, \phi' = 0.32, R = 36$ Å$, L = 45$ Å, and $dR = 7.5$ Å for PEG-core PDMS-shell, and $n = 3.2 \times 10^{16}$ cm^{-3} for PDMS-core PEG-shell. Here, SLDs for core and shell were assumed to be pure PEG or PDMS for simplicity. The size of core-shell structure is significantly larger than the radius of gyration of Tetra-PEG (15 Å) [16], which indicates the aggregation of many polymer units as suggested from Figure 9.9. Although the model is simple, both models qualitatively reproduce the SANS profiles. As for the SAXS profile, both models reproduce the dip though the position is slightly higher than the actual profile in the case of PDMS-core PEG-shell model. In addition, PEG-core PDMS-shell model reproduced absolute intensity of both SANS and SAXS profiles very well. From these results, it seems that PEG-core PDMS-shell model is better than PDMS-core PEG-shell model.

To support this, let us estimate the number density of core-shell particles, n, for both models. First, let us calculate the weight of PDMS in a unit volume. 1 cm^3 of the water-swollen $r = 1$ gel corresponds to 2.63 cm^3 of the as-prepared gel since the swelling ratio is $(0.724)^3 = 0.38$ (Figure 9.9(b)). For $r = 1$ gel,

the concentration of as-prepared gel of PDMS is 25 mg/mL. From this value, the weight of PDMS in the water-swollen gel is estimated to be 66 mg/cm^3. Next, let us calculate the weight of PDMS for each core-shell particle. The volume of core and shell of each core-shell structure ($R = 36$ Å, $L = 45$ Å) is estimated to be 1.95×10^5 Å^3 and 2.03×10^6 Å^3, respectively. By using the density of PDMS, 0.965 g/cm^3, the weight of PDMS for each core-shell particle is 2.0×10^{-15} mg for PEG-core PDMS-shell model and 1.9×10^{-16} mg for PDMS-core PEG-shell model. From these values, n is estimated to be 3.3×10^{16} cm^{-3} for PEG-core PDMS-shell model and 3.5×10^{17} cm^{-3} for PDMS-core PEG-shell model. The parameters used for the model in Figure 9.11 is 2.8×10^{16} cm^{-3} for PEG-core PDMS-shell model, which agrees well, and 3.2×10^{16} cm^{-3} for PDMS-core PEG-shell model, which does not agree. This estimation strongly supports the validity of the use of PEG-core PDMS-shell model.

9.3.5 PDMS size-dependence of microphase separation

As explained in Section 3.3, the morphology of microphase-separated structure of diblock copolymer melt is determined by the affinity of two components, χN, and the proportion of two components, f (Figure 3.18). Similar to this, the morphology of PEG–PDMS hydrogel may be manipulated by varying the volume fraction of PEG, PDMS, and water. To investigate this point, I prepared PEG–PDMS with different molecular weight. Figure 9.12(a) shows the SANS profiles of $r = 1$ as-prepared PEG–PDMS gels with different molecular weight. Similar to Figure 9.6(a) [80] , upturn in low-q region is small. This indicates that all of the gels are relatively homogeneous. These data are fitted by using Eq.(9.3.2.1), and the obtained ξ is plotted as a function of molecular weight between crosslinking points in Figure 9.12(b). It shows positive correlation, which is consistent with the concept that ξ is regarded as the size of mesh. Figure 9.13 shows the SANS profiles of $r = 1$ PEG–PDMS gels with different molecular weight after solvent substitution to water. It is clearly shown that the morphology of PEG–PDMS hydrogels strongly depends on the molecular weight. As a representative sample, I focus on PEG 10k / PDMS 27k samples from now. I call this gel PDMS-rich gel while PEG 10k / PDMS 2.5k samples is called PEG-rich gel.

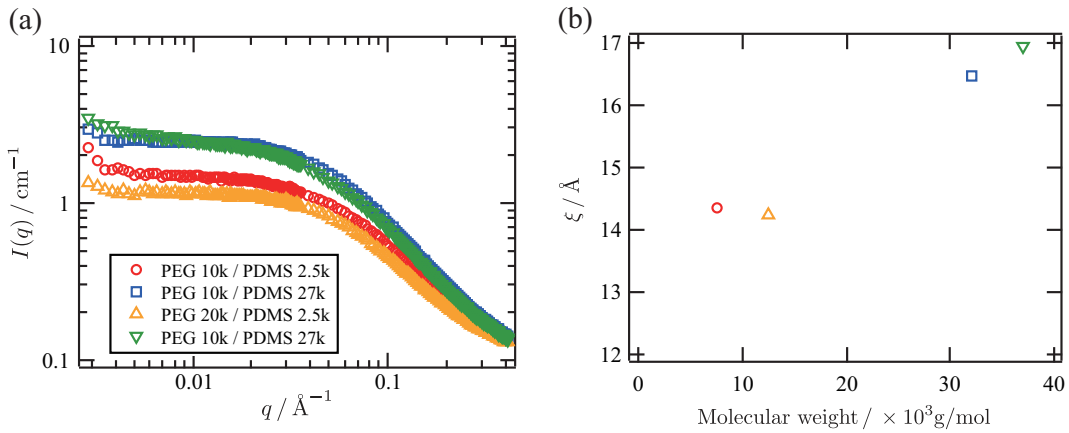

Figure 9.12: (a) SANS profiles of as-prepared PEG–PDMS gels with different molecular weight (100 mg/mL, $r = 1$). (b) The relationship between correlation length and average molecular weight between cross-link points. The correlation length was evaluated from fitting.

[80] The data in Figure 9.6 was measured on the beam time July 1st to 5th, 2013. The data in Figure 9.12 was measured on the beam time January 6th to 10th, 2014. Therefore, the data of PEG 10k / PDMS 2.5k shown in each graph is slightly different.

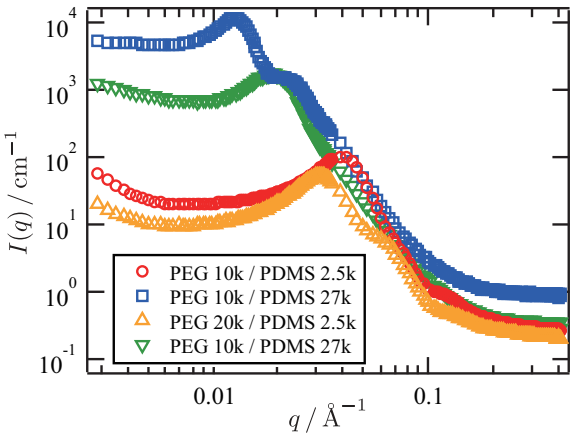

Figure 9.13: SANS profiles of water-swollen PEG–PDMS gels with different molecular weight (75 mg/mL, $r = 1$).

To investigate the morphology of PDMS-rich gel, complimentary use of SANS and SAXS were performed. Figure 9.14 shows the SANS and SAXS profiles of PDMS-rich gel. Both SANS and SAXS profiles show peak structure. The peaks of the SAXS profile are more sharp compared to the SANS profile. The main origin of this is the difference in the instrumental broadening. In the SAXS profile, up to 4th order peak is seen. The relative peak position is approximately 1:2:3:4 with respect to the first order peak. This strongly suggest lamellar structure. Peak assignment using other typical structure factors are shown in Figure 9.15. The reciprocal space position ratios for these structures (up to $\sqrt{20}$) are summarized in Table 9.4. Compared to the assignment of lamellar structure (1:2:3:4), these structure factors are not reasonable. Figure 9.16 shows the r-dependence of SANS and SAXS profiles of PDMS-rich PEG–PDMS gels. Lamellar-like peak structure is observed only for $r = 1$ sample. This result is reasonable since lamellar structure is observed only when enough amount of PDMS exists. Table 9.5 is the volume fractions of PEG, PDMS, and water estimated from the preparation conditions and the observed swelling ratios. The volume fraction of PDMS in $r = 1$ hydrogel is more than 0.3 and it may form lamellar structure. The peak structure at $q \sim 0.8$ Å^{-1} is an amorphous halo of PDMS [272]. This peak indicates the strong aggregation of PDMS chains.

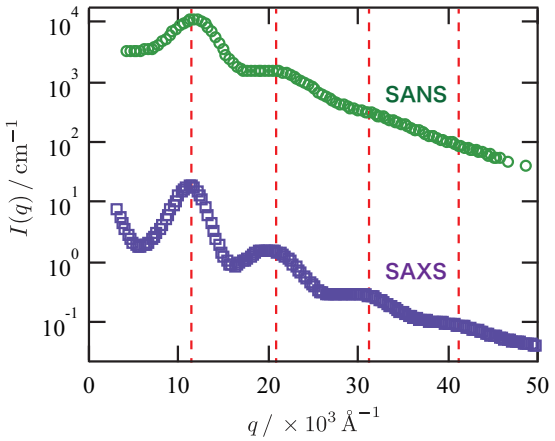

Figure 9.14: SANS and SAXS profiles of $r = 1$ PEG–PDMS gels (75 mg/mL). The molecular weights of PEG and PDMS are 10 kg/mol and 27 kg/mol, respectively. The dashed lines indicate the peak positions.

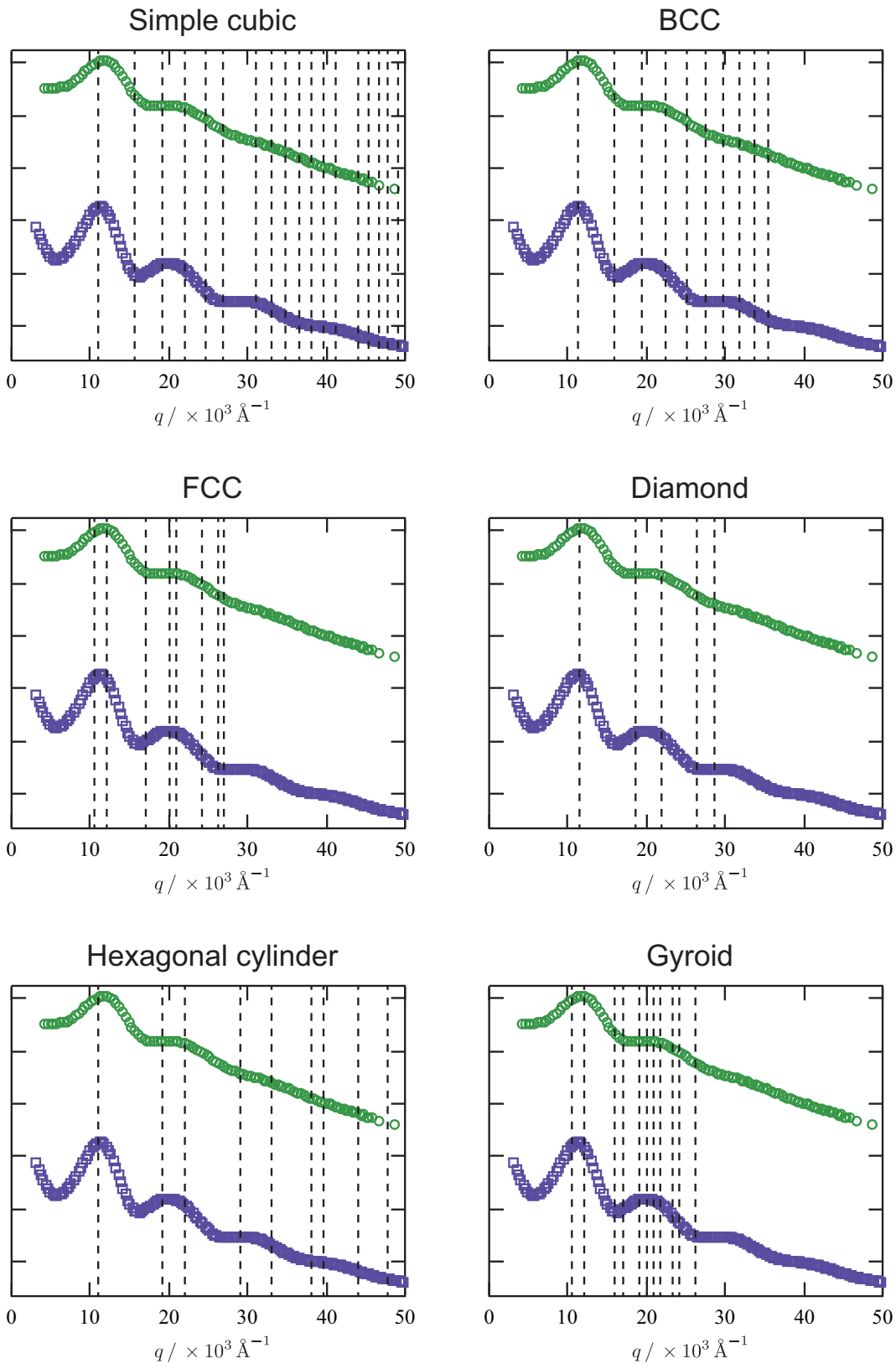

Figure 9.15: Representative results of indexing for $r = 1$ gels with water solvent. Green line is the SANS profile and purple line is the SAXS profile.

Table 9.4: List of index for representative structures.

Simple cubic	$\sqrt{1}, \sqrt{2}, \sqrt{3}, \sqrt{4}, \sqrt{5}, \sqrt{6}, \sqrt{8}, \sqrt{9}, \sqrt{10}, \sqrt{11}, \sqrt{12}, \sqrt{13}, \sqrt{14}, \sqrt{16}, \sqrt{17}, \sqrt{18}, \sqrt{19}, \sqrt{20}$
BCC	$\sqrt{2}, \sqrt{4}, \sqrt{6}, \sqrt{8}, \sqrt{10}, \sqrt{12}, \sqrt{14}, \sqrt{16}, \sqrt{18}, \sqrt{20}$
FCC	$\sqrt{3}, \sqrt{4}, \sqrt{8}, \sqrt{11}, \sqrt{12}, \sqrt{16}, \sqrt{19}, \sqrt{20}$
Diamond	$\sqrt{3}, \sqrt{8}, \sqrt{11}, \sqrt{16}, \sqrt{19}$
Hexagonal cylinder	$\sqrt{1}, \sqrt{3}, \sqrt{4}, \sqrt{7}, \sqrt{9}, \sqrt{12}, \sqrt{13}, \sqrt{16}, \sqrt{19}$
Gyroid [273]	$\sqrt{3}, \sqrt{4}, \sqrt{7}, \sqrt{8}, \sqrt{10}, \sqrt{11}, \sqrt{12}, \sqrt{13}, \sqrt{15}, \sqrt{16}, \sqrt{19}$

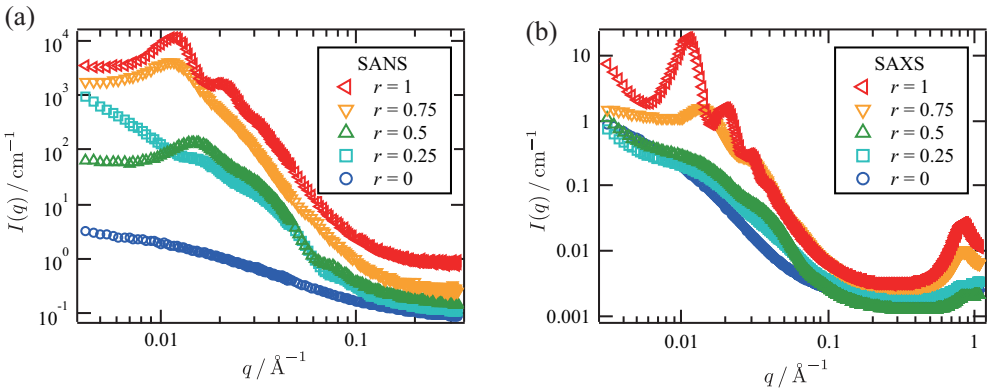

Figure 9.16: SANS and SAXS profiles of PEG–PDMS gels with $r = 1$ (75 mg/mL). The molecular weights of Tetra-PEG and PDMS are 10 kg/mol and 27 kg/mol, respectively. The dashed lines indicate the peak positions.

Table 9.5: r-dependence of the estimated volume fractions of swollen PDMS-rich PEG–PDMS gels in water

r	PEG	PDMS	Water
0	0.021	0	0.979
0.25	0.026	0.017	0.957
0.5	0.022	0.035	0.943
0.75	0.035	0.109	0.856
1	0.050	0.313	0.637

Let us consider more about the formation of lamellar structure for $r = 1$ PDMS-rich gel. In the case of block copolymers, lamellar structure is observed when the volume fraction of two components is almost the same (Figure 3.18). The volume fraction of PEG, PDMS, and water of PEG-rich and PDMS-rich hydrogels are summarized in Table 9.6. The volume fraction of PDMS in $r = 1$ PDMS-rich hydrogel, $\phi = 0.313$, may not be enough to form lamellar structure although this gel is not the same as block copolymer system. To consider more about this issue, let us assume that the gel is decomposed into two components; PEG domain and PDMS domain (Figure 9.17). In as-prepared gel in toluene solution, both PEG and PDMS dissolved in toluene. Therefore, we can attribute the solvent part to PEG domain and PDMS domain evenly. In this case, the volume fraction of PEG domain (PEG + toluene phase, $\phi = 0.14$) of PDMS-rich gel is much smaller than that of PDMS domain (PDMS + toluene phase, $\phi = 0.86$). However, all of the solvent should be attributed to PEG domain when the solvent is substituted to water since PDMS is insoluble to water. In this case, the volume fraction of PEG domain (PEG + water phase, $\phi = 0.69$) of PDMS-rich gel is much larger than that of PDMS domain (PDMS phase, $\phi = 0.31$) although the volume fraction of

Table 9.6: Comparison of the estimated volume fractions of each component of PEG–PDMS gels composed of short and long PDMS

PDMS: 2.5 kg/mol	PEG	PDMS	Water
As-prepared (toluene)	0.041(1)	0.024(1)	0.935(1)
Swollen (water)	0.098(12)	0.058(7)	0.844(18)

PDMS: 27 kg/mol	PEG	PDMS	Water
As-prepared (toluene)	0.010(1)	0.061(1)	0.929(1)
Swollen (water)	0.050(3)	0.313(19)	0.637(22)

PEG itself ($\phi = 0.05$) is much smaller than that of PDMS. This means that the volume fraction of PEG domain and PDMS domain is inverted before and after the solvent substitution. As a result, there is a point where the volume fraction of PEG domain and PDMS domain becomes almost the same during the solvent substitution. At this point, the morphology will become lamellar structure. However, this lamellar structure may be broken by the further solvent substitution since the volume fraction of PDMS domain will decrease up to 0.31. To consider this point, let us consider a non-equilibrium aspect of microphase separation. When the rearrangement of the chemical junctions of diblock copolymers at the interface of microphase-separated structure is slow, resultant morphology may be different from a thermodynamically favorable morphology. In this case, morphology will be determined kinetically. This phenomena has already been observed in AB-type diblock polymers in neutral solvents and called non-equilibrium effect [274]. In the case of solution, the origin of the slowing down of the rearrangement is the high concentration of the polymers. This concept may also be applied to the PDMS-rich gels. In the case of the PDMS-rich gel, the origin of the slowing down will be the existence of crosslinking. Once lamellar structure is constructed, it is kinetically unfavorable to create cylindrical or spherical domains because the potential barrier for the transport of the chains is higher. As a result, lamellar structure will remain even the PDMS domain fraction becomes less than 0.5. In contrast to this case, lamellar structure will not be observed for PEG-rich gel or PDMS-rich gel with $r < 1$ since the fraction of PEG domain for these gels is always larger than that of PDMS domain during solvent substitution. The molecular weight dependence of microphase-separated structure of the PEG–PDMS gels is summarized in Figure 9.18.

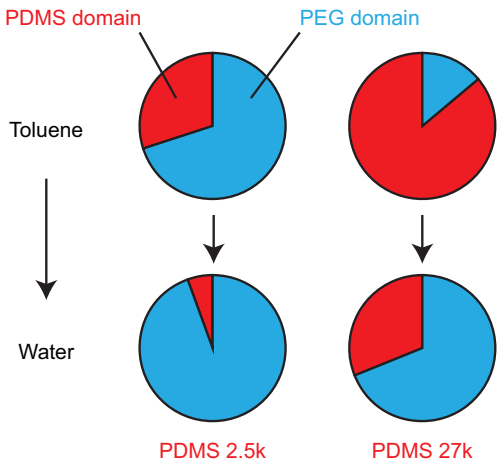

Figure 9.17: Schematics of the composition variation of the PEG–PDMS gels.

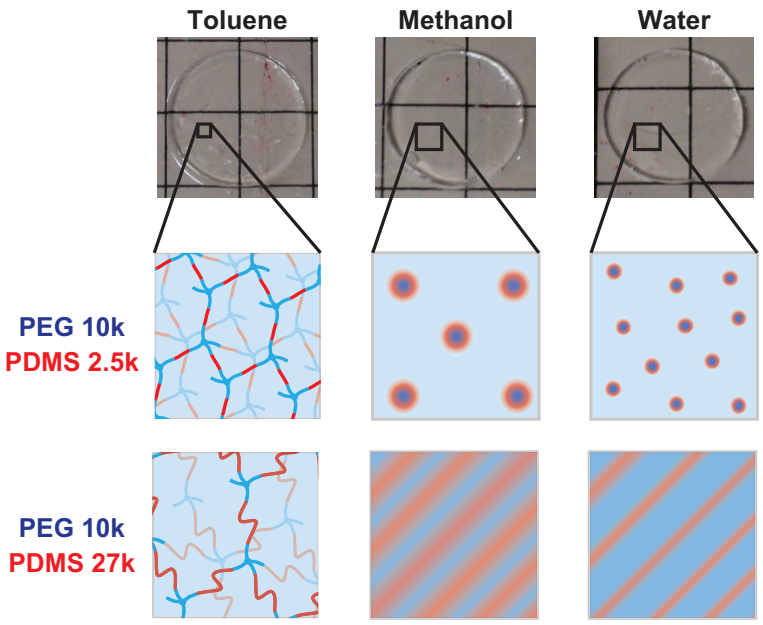

Figure 9.18: Proposed phase separation mechanism during solvent substitution.

9.3.6 Summary

Structural analysis of inhomogeneity-free PEG–PDMS gels was performed by the complementary use of SANS and SAXS. From the small upturn in low-q region of SANS profiles of as-prepared toluene gels, homogeneities of PEG–PDMS gels were proved. The SANS profiles showed drastically change by the solvent substitution from toluene to water. The origin of this change was attributed to the aggregation of hydrophobic PDMS units under the hydrophilic condition. This point is also clarified by the macroscopic change of the gel size. Microphase separation was clearly observed even when the volume fraction of PDM is 0.2 %. The morphology of microphase-separated structure was examined by finding the model that reproduce both SANS and SAXS with absolute scale. The result suggested PEG-core PDMS-shell structure for PEG-rich gels and lamellar structure for PDMS-rich gels. Lamellar structure of PDMS-rich gels were rationalized by taking non-equilibrium effect during the solvent substitution into consideration. From this study, it is clarified that the microphase-separated structure can be manipulated by varying the molecular weight of PEG and PDMS. This may open the door for the precise design of the mesoscopic structure of amphiphilic gels.

10 Conclusion

10.1 Summary of this thesis

In this thesis, I treat mainly two topics. The first topic is the investigation of homogeneous gels called Tetra-PEG gel. The second topic is the investigation of aggregation phenomena caused by hydrophilic and hydrophobic interactions. These two topics are summarized by the work of amphiphilic Tetra-PEG gel.

In Section 5, the history of tough gels is reviewed at first. Among those tough gels, I focused on the gel called Tetra-PEG gel. Tetra-PEG gel is prepared by crosslinking of tetra-arm PEG units. It was known that this preparation scheme suppresses inherent inhomogeneities in static structure. In addition to this, I investigated whether homogeneities appear in the dynamics of Tetra-PEG gel or not. By using dynamic light scattering (DLS) and neutron spin echo (NSE), fluctuations of polymer network of Tetra-PEG gel were investigated in a wide q-region ($10^7 \sim 10^9$ m^{-1}). From these two techniques, it was clarified that the transition from collective diffusion to Zimm mode occurred in lower q compared to the conventional gels. The collective diffusion is typical dynamics observed in network systems while the Zimm mode is typical dynamics observed in solution systems. Therefore, the observation result is interpreted that solution-like dynamics was observed in large length scale in real space. There are two reasons why the solution-like dynamics was observed in a large scale. The first one is that the distance between crosslinking points is the same. The second one is that there are no entanglements, which are regarded as a nominal crosslinking point. In other words, it was revealed that the homogeneous nature of Tetra-PEG gels is reflected not only in static but also dynamic structure.

In addition, it was clarified that we can measure the mesh size of Tetra-PEG gel from the correlation length obtained from DLS. This means that we can map mesh size of Tetra-PEG gels by performing DLS with the combination of microscope. This measurement may clarify the small inhomogeneity in Tetra-PEG in a large length scale which was indicated in a very low-q region of the SANS profile. To achieve this goal, I constructed a DLS microscope, which is described in Section 6. Through operating the DLS microscope, a very interesting feature of this apparatus was clarified; DLS measurement from opaque samples. This is unique since it has been common knowledge that DLS can be measured only from transparent, dilute samples. DLS microscope has overcome this difficulty by utilizing confocal optical system. As a proof-of-principle experiment, I showed that DLS microscope enables us to obtain the size distribution of opaque systems such as Chinese ink, milk, and phase transition of PNIPA solution.

The finding that DLS microscope can measure opaque systems significantly expands my research target. I started the research of aggregation induced by hydrophilic and hydrophobic interactions, which has been beyond the scope of DLS technique. As a first example, I investigated the concentration-induced aggregation of carbon nanotube dispersion (Section 7). Here, the carbon nanotube is a model compound of hydrophobic substance. By using DLS microscope, it was clarified that the solute of CNT dispersion aggregates in higher concentration. The threshold concentration for the production of these aggregates becomes lower when the CNT becomes longer. In addition, the restriction of rotational motion was also observed for the first time. This is a characteristic feature for rod-like shape solutes such as CNT. This dynamical information is obtained relatively easily by using polarized DLS. The finding of the restriction of rotational motion showed the power of the combination of polarized DLS technique and DLS microscope.

As a second example of the system governed by hydrophilic/hydrophobic interaction, I investigated the

temperature-induced aggregation of ovalbumin, the main protein in egg white (Section 8). Here, ovalbumin is the model compound of hydrophilic substance. In this research, I used *N*-terminus cleaved OVA (pOVA) as a comparison material. The major difference between OVA and pOVA is their hydrophilicity. By cutting the *N*-terminal peptide region, a hydrophobic part in the OVA is exposed. This small difference induced large difference in the heat-induced gelation. Under neutral, salt-free condition, OVA gels were transparent while pOVA gels were turbid. The reason for this result was investigated by using DLS and SANS. It is clarified that the dispersion state of OVA and pOVA was different before heating. In pOVA, large aggregates induced by their relatively high hydrophobicity exist even before heating. These large aggregates disturb the correlation between dimers. As a result, the heat-induced gel of pOVA becomes inhomogeneous. In contrast to this, OVA in a salt-free solution is dispersed well thanks to the charges on the surface of each solute. As a result, though heating induce the exposure of hydrophobic region in OVA, the aggregation growth of OVA proceeds homogeneously.

The experimental result of OVA showed that homogeneous gels could be prepared even when the solutes have hydrophobic region. By combining this concept and Tetra-PEG gels, I prepared homogeneous (transparent) amphiphilic Tetra-PEG gels (Section 9). The preparation scheme is similar to that of original Tetra-PEG gels. Instead of amine-terminated tetra-arm PEG, amine-terminated linear PDMS was used as a unit. SANS experiments showed that the crosslinking of active ester-terminated tetra-arm PEG and amine-terminated linear PDMS makes a homogeneous gel in toluene solvent. When the solvent of these gels was substituted from toluene to water, a microphase separation occurred. The morphology of this microphase separation was investigated by the combined use of SANS and SAXS. It was clarified that the morphology can be manipulated by changing the proportion of PEG and PDMS. In other words, by manipulating hydrophilicity and hydrophobicity, we can prepare amphiphilic gels with desired morphology.

10.2 Future perspective

There are mainly two directions for the next step of these researches. The first direction is the application of the developed techniques and materials to industrial products. Since the working principle of DLS microscope is simple, this technique can be combined in the product line. Therefore, DLS microscope can be utilized for the quality control of turbid material such as food, painting, cosmetics and so on as shown in the case of CNT suspension. As for OVA, next step is the control of texture. This will be done by the combination of OVA, pOVA, and cleaved peptide. Now the structure of heat-induced gel prepared from the mixture of OVA and the cleaved peptide is under investigation. This peptide may be utilized for the effective additive to the food. As the application of PEG–PDMS gels, contact lenses are promising. This is because the prepared PEG–PDMS gels are transparent in spite of their relatively high PDMS content rate. In addition, its high mechanical stability has already been proved. Furthermore, it is relatively easy to incorporate a new function to the PEG–PDMS gels since this can be done by using new unit in the preparation. This characteristic feature is good for the product development.

The second direction is the basic research towards the elucidation of gel inhomogeneities. Originally, DLS microscope was developed for the mapping of mesh size in real space. This aim has not been accomplished yet due to the weak scattered light intensity. However, we can perform this mapping by using turbid gels such as PNIPA gels, amphiphilic PEG–PDMS with high PDMS ratio and so on. In addition, the problem of weak signal will be solved by reducing background signal. Now DLS microscope with an oil immersion

lens is examined. By using oil immersion lens, the refractive index mismatch between glass and air is removed. Therefore, reflection from the boundary of glass and air will be decreased significantly. Through this improvement, the mapping of mesh size can be achieved. This experiment will give us a new evaluation perspective to the network system.

As for dynamic light scattering microscope, I hope that this technique will extend the scope of DLS significantly. Several ideas are shown in Figure 10.1. As explained in Section 6.4.3, DLS microscope can be used for the observation of the aggregation of polymer solutions during LCST transition. As a future work, I would like to observe polymer gels during LCST transition. It is well known that LCST changes when the polymer forms gels. For examples, LCST of PNIPA solution is 32 °C while that of gel is 34 °C [159]. This means that LCST transition is affected by the crosslinking point. This phenomena may be clarified by DLS microscope. Of course, other measurements such as time-resolved SANS will give us additional information. By utilizing very small irradiated volume, DLS microscope may be used for the measurement of number fluctuation. This idea is similar to fluorescence correlation spectroscopy. However, we do not have to label the target particles if DLS microscope could detect number fluctuation. By utilizing high spatial resolution, fluctuation from surface may be extracted. For examples, fluctuation of polymer brush may be detected by DLS. Characterization of polymer brash in static form can be performed by neutron reflectometry. DLS microscope may give us additional information about dynamics. By using DLS microscope, we may be able to measure samples that are difficult to measure by conventional DLS. One of the examples is rubber. Measurement of fluctuation of rubber was achieved by using X-ray photon correlation spectroscopy (XPCS) [275]. XPCS is dynamic light scattering by using X-ray as a light source [276, 277]. One of the drawbacks of XPCS is that strong light source such as synchrotron radiation is required for measurements. If similar measurements can be conducted by DLS, the research of network system will advance. Another example of new sample is biological system. For example, dynamics of molecular motors can be detected by using heterodyne-detected DLS, which is used for the detection of linear motion. Previously, research of molecular motors have been performed mainly by single molecule detection such as optical tweezer [278, 279]. Combination of optical tweezer and DLS is fine since DLS microscope can be performed with the same setup of optical tweezer. In the future, I would like to conduct these experiments.

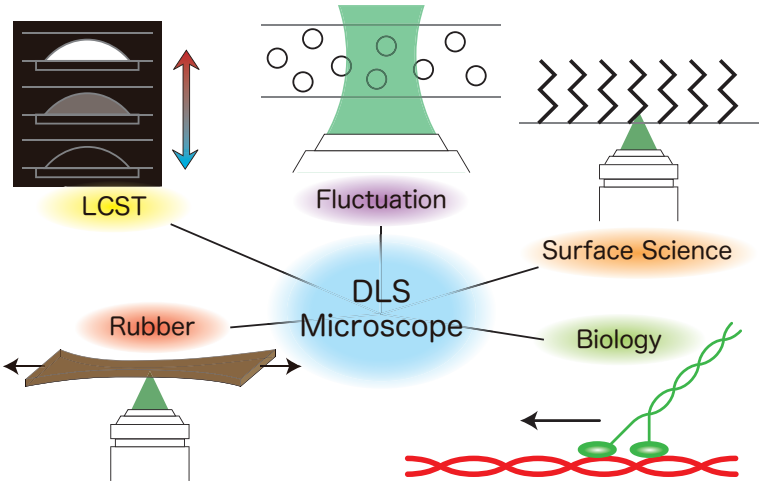

Figure 10.1: Proposed applications of DLS microscope.

11 Appendix

11.1 List of symbols and abbreviations

Table 11.1: List of symbols and abbreviations

Abbreviation	Formal nomenclature
PAMPS	poly(2-acrylamido-2-methylpropanesulfonic acid)
PAAm	poly(acrylamide)
PMMA	poly(methyl methacrylate)
PMAA	poly(methacrylic acid)
PNIPA	poly(*N*-isopropylacrylamide)
PDMAA	poly(*N*,*N*-dimethylacrylamide)
PEG	poly(ethylene glycol)
PEGDA	poly(ethylene glycol) diacrylate
PVP	poly(vinylpyrrolidone)
PDMS	poly(dimethylpolysiloxane)
BIS	*N*,*N*′-methylenebis(acrylamide)
TEMED	*N*,*N*,*N*′,*N*′-Tetramethyl ethylenediamine
APS	ammonium persulfate
[C_2mim][TFSA]	1-ethyl-3-methylimidazolium bis(trifluoromethanesulfonyl)amide
[C_2mim][FSA]	1-ethyl-3-methylimidazolium bis(fluorosulfonyl)amide

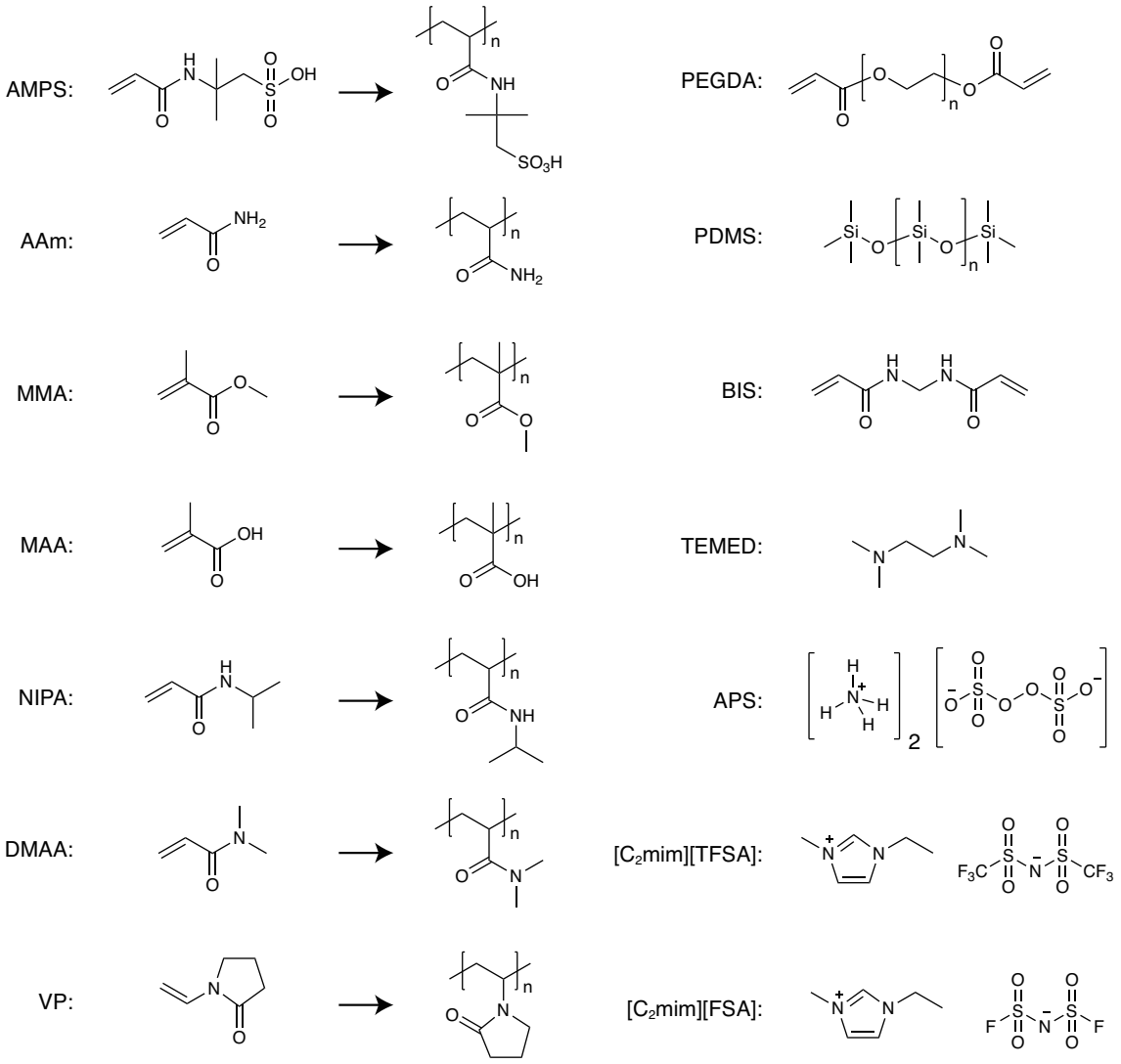

Figure 11.1: Chemical structures of Table 11.1.

11.2 Parameters of Hayter-Penfold function

$$\delta := 1 - \phi \tag{11.2.1}$$

$$a_1 := \frac{24\phi\gamma\exp(-k)(\alpha_1 + \alpha_2 + (1+k)\alpha_3) - (2\phi+1)^2}{\delta^4} \tag{11.2.2}$$

$$a_2 := \frac{24\phi(\alpha_3(\sinh k - k\cosh k) + \alpha_2\sinh k - \alpha_1\cosh k)}{\delta^4} \tag{11.2.3}$$

$$a_3 := \frac{24\phi((2\phi+1)^2/k^2 - \delta^2/2 + \alpha_3(\cosh k - 1 - k\sinh k) - \alpha_1\sinh k + \alpha_2\cosh k)}{\delta^4} \tag{11.2.4}$$

$$\alpha_1 := -\frac{(2\phi+1)\delta}{k} \tag{11.2.5}$$

$$\alpha_2 := -\frac{14\phi^2 - 4\phi - 1}{k^2} \tag{11.2.6}$$

$$\alpha_3 := -\frac{36\phi^2}{k^4} \tag{11.2.7}$$

$$b_1 := \frac{3\phi(\phi+2)^2/2 - 12\phi\gamma\exp(-k)(\beta_1 + \beta_2 + (1+k)\beta_3)}{\delta^4} \tag{11.2.8}$$

$$b_2 := \frac{12\phi(\beta_3(k\cosh k - \sinh k) - \beta_2\sinh k + \beta_1\cosh k)}{\delta^4} \tag{11.2.9}$$

$$b_3 := \frac{12\phi(\delta^2(\phi+2)/2 - 3\phi(\phi+2)^2/k^2 - \beta_3(\cosh k - 1 - k\sinh k) + \beta_1\sinh k - \beta_2\cosh k)}{\delta^4} \tag{11.2.10}$$

$$\beta_1 := -\frac{(\phi^2 + 7\phi + 1)\delta}{k} \tag{11.2.11}$$

$$\beta_2 := -\frac{9\phi(\phi^2 + 4\phi - 2)\delta}{k^2} \tag{11.2.12}$$

$$\beta_3 := -\frac{12\phi(2\phi^2 + 8\phi - 1)\delta}{k^4} \tag{11.2.13}$$

$$\omega_0 := \omega_{14}^2 - \omega_{12}\omega_{24} \tag{11.2.14}$$

$$\omega_1 := 2\omega_{15}\omega_{14} - \omega_{13}\omega_{24} - \omega_{12}(\omega_{34} + \omega_{25}) \tag{11.2.15}$$

$$\omega_2 := \omega_{15}^2 + 2\omega_{16}\omega 14 - \omega_{13}(\omega_{34} + \omega_{25}) - \omega_{12}(\omega_{35} + \omega_{26}) \tag{11.2.16}$$

$$\omega_3 := 2\omega_{16}\omega 15 - \omega_{13}(\omega_{35} + \omega_{26}) - \omega_{12}\omega_{36} \tag{11.2.17}$$

$$\omega_4 := \omega_{16}^2 - \omega_{13}\omega_{36} \tag{11.2.18}$$

$$\omega_{ij} := \mu_i\lambda_j - \mu_j\lambda_i \tag{11.2.19}$$

$$\mu_1 := t_2 a_2 - 12\phi v_2^2 \tag{11.2.20}$$

$$\mu_2 := t_1 a_2 + t_2 a_1 - 24\phi v_1 v_2 \tag{11.2.21}$$

$$\mu_3 := t_2 a_3 + t_3 a_2 - 24\phi v_2 v_3 \tag{11.2.22}$$

$$\mu_4 := t_1 a_1 - 12\phi v_1^2 \tag{11.2.23}$$

$$\mu_5 := t_1 a_3 + t_3 a_1 - 24\phi v_1 v_3 \tag{11.2.24}$$

$$\mu_6 := t_3 a_3 - 12\phi v_3^2 \tag{11.2.25}$$

$$\lambda_1 := 12\phi p_2^2 \tag{11.2.26}$$

$$\lambda_2 := 24\phi p_1 p_2 - 2b_2 \tag{11.2.27}$$

$$\lambda_3 := 24\phi p_2 p_3 \tag{11.2.28}$$

$$\lambda_4 := 12\phi p_1^2 - 2b_1 \tag{11.2.29}$$

$$\lambda_5 := 24\phi p_1 p_3 - 2b_3 - k^2 \tag{11.2.30}$$

$$\lambda_6 := 12\phi p_3^2 \tag{11.2.31}$$

$$p_1 := \frac{\gamma \exp(-k)(\varphi_1 - \varphi_2)^2 - (\phi + 2)/2}{\delta^2} \tag{11.2.32}$$

$$p_2 := \frac{(\varphi_1^2 - \varphi_2^2)\sinh k + 2\varphi_1\varphi_2 \cosh k}{\delta^2} \tag{11.2.33}$$

$$p_3 := \frac{(\varphi_1^2 - \varphi_2^2)\cosh k + 2\varphi_1\varphi_2 \sinh k + \varphi_1^2 - \varphi_2^2}{\delta^2} \tag{11.2.34}$$

$$t_1 := \tau_3 + \tau_4 a_1 + \tau_5 b_1 \tag{11.2.35}$$

$$t_2 := \tau_4 a_2 + \tau_5 b_2 + 12\phi(\tau_1 \cosh k - \tau_2 \sinh k) \tag{11.2.36}$$

$$t_3 := \tau_4 a_3 + \tau_5 b_3 + 12\phi(\tau_1 \sinh k - \tau_2(\cosh k - 1)) - \frac{2\phi(\phi + 10)}{5} - 1 \tag{11.2.37}$$

$$v_1 := \frac{(2\phi+1)(\phi^2-2\phi+10)/4 - \gamma\exp(-k)(\nu_4+\nu_5)}{5\delta^4} \tag{11.2.38}$$

$$v_2 := \frac{\nu_4\cosh k - \nu_5\sinh k}{5\delta^4} \tag{11.2.39}$$

$$v_3 := \frac{(\phi^3-6\phi^2+5)\delta - 6\phi(2\phi^3-3\phi^2+18\phi+10)/k^2 + 24\phi\nu_3 + \nu_4\sinh k - \nu_5\cosh k}{5\delta^4} \tag{11.2.40}$$

$$\nu_1 := -\frac{(\phi^3+3\phi^2+45\phi+5)\delta}{k} \tag{11.2.41}$$

$$\nu_2 := \frac{2\phi^3+3\phi^2+42\phi-20}{k^2} \tag{11.2.42}$$

$$\nu_3 := \frac{2\phi^3+30\phi-5}{k^4} \tag{11.2.43}$$

$$\nu_4 := \nu_1 + 24\phi k\nu_3 \tag{11.2.44}$$

$$\nu_5 := 6\phi(\nu_2+4\nu_3) \tag{11.2.45}$$

$$\varphi_1 := \frac{6\phi}{k} \tag{11.2.46}$$

$$\varphi_2 := \delta - \frac{12\phi}{k^2} \tag{11.2.47}$$

$$\tau_1 := \frac{\phi+5}{5k} \tag{11.2.48}$$

$$\tau_2 := \frac{\phi+2}{k^2} \tag{11.2.49}$$

$$\tau_3 := -12\phi\gamma\exp(-k)(\tau_1+\tau_2) \tag{11.2.50}$$

$$\tau_4 := 3\phi k^2(\tau_1^2-\tau_2^2) \tag{11.2.51}$$

$$\tau_5 := \frac{3\phi(\phi+8)}{10} - \frac{2(2\phi+1)^2}{k^2} \tag{11.2.52}$$

11.3 Isserlis's theorem

Here I'm going to show the proof of Isserlis's theorem, or Wick's theorem [280]. This theorem is extended to mixed-Gaussian random variables [281, 282]. Isserlis's theorem is summarized as follows.

If $x_1x_2\dots x_{2N}$ are normalized, jointly Gaussian random variables,

$$\mathbb{E}[X_1X_2\dots X_{2N}] = \sum\prod \mathbb{E}[X_iX_j] \tag{11.3.1}$$

where $\mathbb{E}[\cdots]$ stands for the mean value of $\cdots$, and $\sum\prod$ stands for summing over all distinct ways of partitioning $X_1X_2\dots X_{2N}$ into pairs. For example, when $2N=4$,

$$\mathbb{E}[X_1X_2X_3X_4] = \mathbb{E}[X_1X_2]\mathbb{E}[X_3X_4] + \mathbb{E}[X_1X_3]\mathbb{E}[X_2X_4] + \mathbb{E}[X_1X_4]\mathbb{E}[X_2X_3] \tag{11.3.2}$$

Here, I prove Eq.(11.3.2), which corresponds to Eq.(4.1.2.10). Let us set that the probability density

function of random variables x_i $(i = 2, 3, 4)$ are written as follows.

$$f_i(X_i = x_i) = \frac{1}{\sqrt{2\pi}\sigma_i} \exp\left[-\frac{x_i^2}{2\sigma_i^2}\right] \tag{11.3.3}$$

Expectation value of a power of x_i is called moment and calculated as follows.

$$\mathbb{E}[X_i] = \frac{1}{\sqrt{2\pi}\sigma_i} \int_{-\infty}^{\infty} x_i \exp\left[-\frac{x_i^2}{2\sigma_i^2}\right] = 0 \tag{11.3.4}$$

$$\mathbb{E}[X_i^2] = \frac{1}{\sqrt{2\pi}\sigma_i} \int_{-\infty}^{\infty} x_i^2 \exp\left[-\frac{x_i^2}{2\sigma_i^2}\right] = \sigma_i \tag{11.3.5}$$

$$\mathbb{E}[X_i^3] = \frac{1}{\sqrt{2\pi}\sigma_i} \int_{-\infty}^{\infty} x_i^3 \exp\left[-\frac{x_i^2}{2\sigma_i^2}\right] = 0 \tag{11.3.6}$$

$$\mathbb{E}[X_i^4] = \frac{1}{\sqrt{2\pi}\sigma_i} \int_{-\infty}^{\infty} x_i^4 \exp\left[-\frac{x_i^2}{2\sigma_i^2}\right] = 3\sigma_i^4 \tag{11.3.7}$$

Let us calculate the expectation value of X_i when $X_1 = x_1$. Here, we define X_i as follows.

$$X_i =: \rho_{1i}\frac{\sigma_i}{\sigma_1}X_1 + \Delta_i \tag{11.3.8}$$

where ρ_{ij} is the correlation coefficient defined as follows.

$$\rho_{ij} := \frac{\mathbb{E}[X_i X_j]}{\sigma_i \sigma_j} \tag{11.3.9}$$

The first term and second term of Eq.(11.3.8) is independent since the expectation value of the product of these two terms is zero.

$$\mathbb{E}\left[X_1\Delta_i\right] = \mathbb{E}\left[X_1 X_2\right] - \mathbb{E}\left[\rho_{1i}\frac{\sigma_i}{\sigma_1}X_1^2\right] = \rho_{1i}\sigma_1\sigma_i - \rho_{1i}\frac{\sigma_i}{\sigma_1}\sigma_i^2 = 0 \tag{11.3.10}$$

Moment of Δ_i is calculated as follows.

$$\mathbb{E}\left[\Delta_i\right] = 0 \tag{11.3.11}$$

$$\begin{aligned}\mathbb{E}\left[\Delta_i^2\right] &= \mathbb{E}\left[\left(X_i - \rho_{1i}\frac{\sigma_i}{\sigma_1}X_1\right)^2\right] \\ &= \mathbb{E}[X_i^2] - 2\rho_{1i}\frac{\sigma_i}{\sigma_1}\mathbb{E}[X_1 X_i] + \rho_{1i}^2\frac{\sigma_i^2}{\sigma_1^2}\mathbb{E}[X_1] \\ &= \sigma_i^2 - 2\rho_{1i}\frac{\sigma_i}{\sigma_1}\rho_{1i}\sigma_1\sigma_i + \rho_{1i}^2\frac{\sigma_i^2}{\sigma_1^2}\sigma_1^2 = (1-\rho_{1i}^2)\sigma_i^2\end{aligned} \tag{11.3.12}$$

Therefore, the expectation value of X_i when $X_1 = x_1$ is:

$$\mathbb{E}[X_i | X_1 = x_1] = \mathbb{E}\left[\rho_{1i}\frac{\sigma_i}{\sigma_1}x_1\right] + \mathbb{E}[\Delta_i] = \rho_{1i}\frac{\sigma_i}{\sigma_1}x_1 \tag{11.3.13}$$

By using Eq.(11.3.8), $\mathbb{E}[X_1X_2X_3X_4]$ is written as follows.

$$
\begin{aligned}
&\mathbb{E}[X_1X_2X_3X_4] \\
&= \mathbb{E}[X_1\mathbb{E}[X_2X_3X_4|X_1 = X_1]] \\
&= \mathbb{E}\left[X_1\mathbb{E}\left[\left(\rho_{12}\frac{\sigma_2}{\sigma_1}X_1 + \Delta_2\right)\left(\rho_{13}\frac{\sigma_3}{\sigma_1}X_1 + \Delta_3\right)\left(\rho_{14}\frac{\sigma_4}{\sigma_1}X_1 + \Delta_4\right)\middle| X_1 = X_1\right]\right] \\
&= \mathbb{E}\left[X_1\rho_{12}\frac{\sigma_2}{\sigma_1}\rho_{13}\frac{\sigma_3}{\sigma_1}\rho_{14}\frac{\sigma_4}{\sigma_1}X_1^3\right] \\
&+ \mathbb{E}\left[X_1\rho_{12}\frac{\sigma_2}{\sigma_1}\rho_{13}\frac{\sigma_3}{\sigma_1}\mathbb{E}\left[\Delta_4\right]X_1^2\right] + \mathbb{E}\left[X_1\rho_{12}\frac{\sigma_2}{\sigma_1}\rho_{14}\frac{\sigma_4}{\sigma_1}\mathbb{E}\left[\Delta_3\right]X_1^2\right] + \mathbb{E}\left[X_1\rho_{13}\frac{\sigma_3}{\sigma_1}\rho_{14}\frac{\sigma_4}{\sigma_1}\mathbb{E}\left[\Delta_2\right]X_1^2\right] \\
&+ \mathbb{E}\left[X_1\rho_{12}\frac{\sigma_2}{\sigma_1}\mathbb{E}\left[\Delta_3\Delta_4\right]X_1\right] + \mathbb{E}\left[X_1\rho_{13}\frac{\sigma_3}{\sigma_1}\mathbb{E}\left[\Delta_2\Delta_4\right]X_1\right] + \mathbb{E}\left[X_1\rho_{14}\frac{\sigma_4}{\sigma_1}\mathbb{E}\left[\Delta_2\Delta_3\right]X_1\right] \\
&+ \mathbb{E}\left[X_1\mathbb{E}\left[\Delta_2\Delta_3\Delta_4\right]\right]
\end{aligned}
\tag{11.3.14}
$$

2nd to 4th terms of Eq.(11.3.14) are zero (Eq.(11.3.11)). 8th term of Eq.(11.3.14) is also zero since Δ_i is symmetric with respect to zero.

$$
\mathbb{E}[\Delta_2\Delta_3\Delta_4] = \mathbb{E}[(-\Delta_2)(-\Delta_3)(-\Delta_4)] = -\mathbb{E}[\Delta_2\Delta_3\Delta_4] = 0 \tag{11.3.15}
$$

$\mathbb{E}[\Delta_i\Delta_j]$ in 5th to 7th terms of Eq.(11.3.14) is calculated as follows.

$$
\begin{aligned}
\mathbb{E}[\Delta_i\Delta_j] &= \mathbb{E}\left[\left(X_i - \rho_{1i}\frac{\sigma_i}{\sigma_1}X_1\right)\left(X_j - \rho_{1j}\frac{\sigma_j}{\sigma_1}X_1\right)\right] \\
&= \mathbb{E}\left[\left(X_iX_j - \rho_{1i}\frac{\sigma_i}{\sigma_1}X_1X_j - \rho_{1j}\frac{\sigma_j}{\sigma_1}X_1X_i + \rho_{1i}\frac{\sigma_i}{\sigma_1}\rho_{1j}\frac{\sigma_j}{\sigma_1}X_1^2\right)\right] \\
&= \sigma_i\sigma_j\rho_{ij} - \rho_{1i}\frac{\sigma_i}{\sigma_1}\sigma_1\sigma_j\rho_{1j} - \rho_{1j}\frac{\sigma_j}{\sigma_1}\sigma_1\sigma_i\rho_{1i} + \rho_{1i}\rho_{1j}\frac{\sigma_i\sigma_j}{\sigma_1^2}\sigma_1^2 \\
&= [\rho_{ij} - \rho_{1i}\rho_{1j}]\sigma_i\sigma_j
\end{aligned}
\tag{11.3.16}
$$

By substituting Eqs.(11.3.5), (11.3.7), (11.3.9), (11.3.11), (11.3.15), and (11.3.16) into Eq.(11.3.14), Eq.(11.3.2) is proved.

$$
\begin{aligned}
&\mathbb{E}[X_1X_2X_3X_4] \\
&= \rho_{12}\rho_{13}\rho_{14}\frac{\sigma_2\sigma_3\sigma_4}{\sigma_1^3}\mathbb{E}[X_1^4] \\
&+ \rho_{12}\frac{\sigma_2}{\sigma_1}(\rho_{34} - \rho_{13}\rho_{14})\sigma_3\sigma_4\mathbb{E}[X_1^2] + \rho_{13}\frac{\sigma_3}{\sigma_1}(\rho_{24} - \rho_{12}\rho_{14})\sigma_2\sigma_4\mathbb{E}[X_1^2] + \rho_{14}\frac{\sigma_4}{\sigma_1}(\rho_{23} - \rho_{12}\rho_{13})\sigma_2\sigma_3\mathbb{E}[X_1^2] \\
&= 3\rho_{12}\rho_{13}\rho_{14}\sigma_1\sigma_2\sigma_3\sigma_4 \\
&+ (\rho_{12}\rho_{34}\sigma_1\sigma_2\sigma_3\sigma_4 - \rho_{12}\rho_{13}\rho_{14}\sigma_1\sigma_2\sigma_3\sigma_4) \\
&+ (\rho_{13}\rho_{24}\sigma_1\sigma_2\sigma_3\sigma_4 - \rho_{12}\rho_{13}\rho_{14}\sigma_1\sigma_2\sigma_3\sigma_4) \\
&+ (\rho_{14}\rho_{23}\sigma_1\sigma_2\sigma_3\sigma_4 - \rho_{12}\rho_{13}\rho_{14}\sigma_1\sigma_2\sigma_3\sigma_4) \\
&= \sigma_1\sigma_2\sigma_3\sigma_4(\rho_{12}\rho_{34} + \rho_{13}\rho_{24} + \rho_{14}\rho_{23}) \\
&= \mathbb{E}[X_1X_2]\mathbb{E}[X_3X_4] + \mathbb{E}[X_1X_3]\mathbb{E}[X_2X_4] + \mathbb{E}[X_1X_4]\mathbb{E}[X_2X_3]
\end{aligned}
\tag{11.3.17}
$$

11.4 Preparation scheme

11.4.1 PNIPA solutions and gels

H_2O, 9 mL
→ Add NIPA, 780.8 mg [6.9 mmol]
→ Stir, Ar bubbling[81], 5 min [Dark]
→ Add BIS, 34.5 mg [0.224 mmol] to make the solution gel, otherwise skip this part
→ Stir, 5 min [Slow, Dark]
→ in ice bath, 10 min [Slow, Dark]
→ Add TEMED, 11.92 μL [0.08 mmol]
→ Stir, 1 min [Fast, Dark]
→ Add APS solution, 1 mL ← 7.98 mg [0.0350 mmol] / mL
→ Stir, 30 sec [Fast, Dark]
→ Mold

11.4.2 Tetra-PEG gels

Citric acid-phosphate buffer (CP-Buffer, pH $\sim$ 5.8)
Citric acid monohydrate: 0.1 M, 78.8 mL: 7.88 mmol, Mw: 210.14 → 1.6559 g
$Na_2HPO_4 \cdot 12\,H_2O$: 0.2 M, 121.2 mL: 24.24 mmol, Mw: 358.14 → 8.6813 g
→ Add 200 mL deionized water[82]: "200 mM CPB"

Phosphate buffer (P-Buffer, pH $\sim$ 7.4)
$NaH_2PO_4 \cdot 2\,H_2O$: 0.2 M, 38.0 mL: 7.60 mmol, Mw: 156.01 → 1.1857 g
$Na_2HPO_4 \cdot 12\,H_2O$: 0.2 M, 162.0 mL: 32.40 mmol, Mw: 358.14 → 11.6037 g
→ Add 200 mL deionized water: "200 mM PB"

Tetra-PEG gel (100 mg/mL, 4 mL)
Amine-terminated PEG (PA) 200 mg + PB 0.5 mL + Water 1.5 mL
Active ester-terminated PEG (HS) 200 mg + CPB 0.5 mL + Water 1.5 mL[83]
→ Mix, filterate the pregel solution with 5 μm filter to remove air bubbles and dusts
Under this condition, the solution becomes a gel within one hour.

11.4.3 Acidic buffer solution for OVA gels

KH_2PO_4 (Mw: 136.09) → 400 mL, 0.1 M: 40 mmol = 5.4436 g
K_2HPO_4 (Mw: 174.18) → 50 mL, 0.1 M: 5 mmol = 0.8709 g
→ KH_2PO_4 aq 400 mL + K_2HPO_4 aq 50 mL → Phosphate buffer 450 mL

[81] N_2 is also available.
[82] For precise preparation, we have to decrease the amount of deionized water since the solutes contains water molecule. However, in most cases, this slight difference affects anything.
[83] Active ester is susceptible to hydrolysis. Use fresh solution for preparation of conventional Tetra-PEG gels. In other words, we can tune the crosslinking density by using hydrolysis. The gel prepared by using this technique is named *p*-tuned gel.

→ Add 1.2 M HCl aq, ∼ 20 mL, dropwise up to pH = 2.2

Let us calculate pH of these solutions analytically.

$$\mathrm{H_3PO_4} \rightleftharpoons \mathrm{H^+ + H_2PO_4^-}, \qquad K_{a1} = 10^{-1.96} = \frac{[\mathrm{H^+}][\mathrm{H_2PO_4^-}]}{[\mathrm{H_3PO_4}]} \tag{11.4.1}$$

$$\mathrm{H_2PO_4^-} \rightleftharpoons \mathrm{H^+ + HPO_4^{2-}}, \qquad K_{a2} = 10^{-7.12} = \frac{[\mathrm{H^+}][\mathrm{HPO_4^{2-}}]}{[\mathrm{H_2PO_4^-}]} \tag{11.4.2}$$

$$\mathrm{HPO_4^{2-}} \rightleftharpoons \mathrm{H^+ + PO_4^{3-}}, \qquad K_{a3} = 10^{-12.32} = \frac{[\mathrm{H^+}][\mathrm{PO_4^{3-}}]}{[\mathrm{HPO_4^{2-}}]} \tag{11.4.3}$$

To calculate pH of 0.1 mol/L $\mathrm{KH_2PO_4}$ aq, set $[\mathrm{H^+}] = [\mathrm{HPO_4^{2-}}] = x$ mol/L. Eq.(11.4.2) is expressed as follows.

$$K_{a2} = \frac{x^2}{0.1 - x} \rightarrow x = 8.66 \times 10^{-5} \text{ mol/L, pH} = 4.1 \tag{11.4.4}$$

To calculate pH of 0.1 mol/L $\mathrm{K_2HPO_4}$ aq, set $[\mathrm{OH^-}] = [\mathrm{H_2PO_4^-}] = x$ mol/L. Eq.(11.4.2) is expressed s follows in basic condition.

$$\mathrm{HPO_4^{2-} + H_2O} \rightleftharpoons \mathrm{H_2PO_4^- + OH^-}, \qquad K_{b2} = \frac{[\mathrm{H_2PO_4^-}][\mathrm{OH^-}]}{[\mathrm{HPO_4^{2-}}]} = \frac{K_w}{K_{a2}} = 10^{-6.88} \tag{11.4.5}$$

Then pH of 0.1 mol/L $\mathrm{K_2HPO_4}$ aq is calculated as follows.

$$K_{b2} = \frac{x^2}{0.1 - x} \rightarrow x = 1.15 \times 10^{-4} \text{ mol/L, pOH} = 3.9, \text{ pH} = 10.1 \tag{11.4.6}$$

pH of mixture of these two solutions before adding HCl is calculated by using Henderson-Hasselbalch equation [283].

$$\mathrm{pH} = \mathrm{p}K_{a2} + \log \frac{[\mathrm{HPO_4^{2-}}]}{[\mathrm{H_2PO_4^-}]} = 7.12 + \log \frac{50}{400} = 6.2 \tag{11.4.7}$$

Addition of 21.44 mmol of HCl (17.87 mL) makes the amount of $\mathrm{H_2PO_4^-}$ from 40 mmol to 28.56 mmol while that of $\mathrm{H_3PO_4}$ from 5 mmol to 16.44 mmol. Then pH becomes 2.2 as follows.

$$\mathrm{pH} = \mathrm{p}K_{a1} + \log \frac{[\mathrm{H_2PO_4^-}]}{[\mathrm{H_3PO_4}]} = 1.96 + \log \frac{28.56}{16.44} = 2.2 \tag{11.4.8}$$

11.5 Function and Functional

Here, I list the formula for the calculation of functionals. Instead of precise proof, I showed the similarity between calculation of functions and functionals.

$$e^{ax} = \int dx' \delta(x' - x) e^{ax'} \tag{11.5.1}$$

$$e^{af(x)} = \int D[g(x)] \delta[g(x) - f(x)] e^{ag(x)} \tag{11.5.2}$$

$$\delta(x) = \frac{1}{2\pi}\int dk \exp[ikx] \tag{11.5.3}$$

$$\delta[f(x)] = \int D\{g(x)\} \exp\left[i\int dx f(x)g(x)\right] \tag{11.5.4}$$

Taylor expansion:

$$f(x) = \sum_n \frac{1}{n!}\left.\frac{d^n f(x)}{dx^n}\right|_{x=0} x^n \tag{11.5.5}$$

$$f(x_1,\cdots,x_m) = \sum_n \frac{1}{n!}\sum_{i_1}^{m}\cdots\sum_{i_n}^{m}\left.\frac{\partial^n f(x_1,\cdots,x_m)}{\partial x_{i_1}\cdots\partial x_{i_n}}\right|_{x_1,\cdots,x_m=0} x_{i_1}\cdots x_{i_n} \tag{11.5.6}$$

$$F[f(\vec{r})] = \sum_n \frac{1}{n!}\int d\vec{r}_1\cdots\int d\vec{r}_n \left.\frac{\delta^n F[f(\vec{r})]}{\delta f(\vec{r}_1)\cdots\delta f(\vec{r}_n)}\right|_{f(\vec{r})=0} f(\vec{r}_1)\cdots f(\vec{r}_n) \tag{11.5.7}$$

$$F[f_1(\vec{r}),\cdots,f_M(\vec{r})] = \sum_n \frac{1}{n!}\sum_{i_1}^{M}\cdots\sum_{i_n}^{M}\int d\vec{r}_1\cdots\int d\vec{r}_n \left.\frac{\delta^n F[f_1(\vec{r}),\cdots,f_M(\vec{r})]}{\delta f_{i_1}(\vec{r}_1)\cdots\delta f_{i_n}(\vec{r}_n)}\right|_{f_1(\vec{r}),\cdots,f_M(\vec{r})=0} f_{i_1}(\vec{r}_1)\cdots f_{i_n}(\vec{r}_n) \tag{11.5.8}$$

Saddle point method:

$$\begin{aligned} I &:= \int dx e^{f(x)} \simeq \int dx e^{f(x_0)+\frac{1}{2}f''(x_0)(x-x_0)^2} = Ce^{f(x_0)} \ s.t. \ \left.\frac{df(x)}{dx}\right|_{x=x_0} = 0 \\ &\to \ln I \simeq e^{f(x_0)} \ s.t. \ \left.\frac{df(x)}{dx}\right|_{x=x_0} = 0 \\ I(x) &:= \int D\{\varphi(x)\} e^{f[\varphi(x)]} \simeq Ce^{f[\phi(x)]} \ s.t. \ \left.\frac{\delta f[\varphi(x)]}{\delta\varphi(x)}\right|_{\varphi(x)=\phi(x)} = 0 \\ &\to \ln I(x) \simeq e^{f[\phi(x)]} \ s.t. \ \left.\frac{\delta f[\varphi(x)]}{\delta\varphi(x)}\right|_{\varphi(x)=\phi(x)} = 0 \end{aligned} \tag{11.5.9, 11.5.10}$$

Moment and cumulant:

For random variable X whose probability that $X = x$ is represented by $p(x)$, nth order moment, m_n, is defined as follows.

$$m_n := \int_{-\infty}^{\infty} x^n p(x) dx \tag{11.5.11}$$

Here, we define the function called generating function as follows.

$$M(\xi) := \langle\, e^{\xi X} \,\rangle = \int_{-\infty}^{\infty} e^{\xi x} p(x) dx \tag{11.5.12}$$

Taylor expansion of Eq.(11.5.12) is:

$$\begin{aligned} M(\xi) &= \int_{-\infty}^{\infty}\sum_{n=0}^{\infty}\frac{1}{n!}(\xi x)^n p(x)dx \\ &= \sum_{n=0}^{\infty}\frac{m_n}{n!}\xi^n \end{aligned} \tag{11.5.13}$$

By using Eq.(11.5.13), moment is "generated" from the generating function as follows.

$$m_n = \left.\frac{d^n}{d\xi^n} M(\xi)\right|_{\xi=0} \tag{11.5.14}$$

Similar to this, cumulant is defined as follows.

$$\ln M(\xi) =: \sum_{n=1}^{\infty} \frac{c_n}{n!}\xi^n \tag{11.5.15}$$

$$c_n = \left.\frac{d^n}{d\xi^n} \ln M(\xi)\right|_{\xi=0} \tag{11.5.16}$$

c_n is called nth order cumulant.

Let us see the relationship between m_n and c_n. Differentiation of $M(\xi)$ and $\ln M(\xi)$ is calculated as follows.

$$\frac{dM(\xi)}{d\xi} = \sum_{n=1}^{\infty} \frac{m_n}{(n-1)!}\xi^{n-1} \tag{11.5.17}$$

$$\frac{d(\ln M(\xi))}{d\xi} = \sum_{n=1}^{\infty} \frac{c_n}{(n-1)!}\xi^{n-1} \tag{11.5.18}$$

Eq.(11.5.18) is also calculated as follows.

$$\frac{d(\ln M(\xi))}{d\xi} = \frac{1}{M(\xi)}\frac{dM(\xi)}{d\xi} \tag{11.5.19}$$

By using Eqs.(11.5.13) and (11.5.17) $\sim$ (11.5.19), moment and cumulant is related as follows.

$$\begin{aligned} &\frac{dM(\xi)}{d\xi} = M(\xi)\frac{d(\ln M(\xi))}{d\xi} \\ &\to \sum_{n=1}^{\infty} \frac{m_n}{(n-1)!}\xi^{n-1} = \left(\sum_{n=0}^{\infty} \frac{m_n}{n!}\xi^n\right)\left(\sum_{n=1}^{\infty} \frac{c_n}{(n-1)!}\xi^{n-1}\right) \end{aligned} \tag{11.5.20}$$

By comparing the same order term of ξ, the relationship between m_n and c_n is derived as follows. [84]

$$m_1 = c_1 \tag{11.5.21}$$

$$m_2 = c_2 + m_1 c_1 = c_2 + c_1^2 \tag{11.5.22}$$

$$m_3 = 2!\left(\frac{1}{2!}c_3 + m_1 c_2 + \frac{1}{2!}m_2 c_1\right) = c_3 + 3c_2 c_1 + c_1^3 \tag{11.5.23}$$

$$m_4 = 3!\left(\frac{1}{3!}c_4 + \frac{1}{2!}m_1 c_3 + \frac{1}{2!}m_2 c_2 + \frac{1}{3!}m_3 c_1\right) = c_4 + 4c_3 c_1 + 3c_2^2 + 6c_2 c_1^2 + c_1^4 \tag{11.5.24}$$

Eqs.(11.5.21) $\sim$ (11.5.24) can also be solved for c_n.

$$c_1 = m_1 \tag{11.5.25}$$

$$c_2 = m_2 - c_1^2 = m_2 - m_1^2 \tag{11.5.26}$$

$$c_3 = m_3 - 3c_2 c_1 - c_1^3 = m_3 - 3m_2 m_1 + 2m_1^3 \tag{11.5.27}$$

$$c_4 = m_4 - 4c_3 c_1 - 3c_2^2 - 6c_2 c_1^2 - c_1^4 = m_4 - 4m_3 m_1 - 3m_2^2 + 12m_2 m_1^2 - 6m_1^4 \tag{11.5.28}$$

[84] Note that $m_0 = 1$ since m_0 represents the normalization of $p(x)$.

Similar to Eqs.(11.5.14) and (11.5.16), we define moment and cumulant for certain functional $Z[\{V_K(\vec{r})\}]$.

$$M_n^{K_1,\cdots,K_n}(\vec{r}_1,\cdots,\vec{r}_n) := \left.\frac{\delta^n Z[\{V_K(\vec{r})\}]}{\delta V_{K_1}(\vec{r}_1)\cdots\delta V_{K_n}(\vec{r}_n)}\right|_{\{V_K\}=\{0\}} \tag{11.5.29}$$

$$C_n^{K_1,\cdots,K_n}(\vec{r}_1,\cdots,\vec{r}_n) := \left.\frac{\delta^n (\ln Z[\{V_K(\vec{r})\}])}{\delta V_{K_1}(\vec{r}_1)\cdots\delta V_{K_n}(\vec{r}_n)}\right|_{\{V_K\}=\{0\}} \tag{11.5.30}$$

Similar to Eqs.(11.5.13), Taylor expansion of $Z[\{V_K(\vec{r})\}]$ is expressed as follows.

$$\begin{aligned} Z[\{V_K(\vec{r})\}] &= 1 + \sum_{K_1}\int d\vec{r}_1 M_1^{K_1}(\vec{r}_1)V_{K_1}(\vec{r}_1) + \frac{1}{2!}\sum_{K_1}\sum_{K_2}\int d\vec{r}_1\int d\vec{r}_2 M_2^{K_1,K_2}(\vec{r}_1,\vec{r}_2)V_{K_1}(\vec{r}_1)V_{K_2}(\vec{r}_2)+\cdots \\ &= \sum_{n=0}^{\infty}\frac{1}{n!}\sum_{K_1,\cdots,K_n}\int d\vec{r}_1\cdots\int d\vec{r}_n M_n^{K_1,\cdots,K_n}(\vec{r}_1,\cdots,\vec{r}_n)V_{K_1}(\vec{r}_1)\cdots V_{K_n}(\vec{r}_n) \end{aligned} \tag{11.5.31}$$

Let us see the relationship between $M_n^{K_1,\cdots,K_n}(\vec{r}_1,\cdots,\vec{r}_n)$ and $C_n^{K_1,\cdots,K_n}(\vec{r}_1,\cdots,\vec{r}_n)$. Differentiation of $Z[\{V_K(\vec{r})\}]$ and $\ln Z[\{V_K(\vec{r})\}]$ is calculated as follows.

$$\begin{aligned} \frac{\delta Z[\{V_K(\vec{r})\}]}{\delta V_{K'}(\vec{r})} &= M_1^{K'}(\vec{r}) + \sum_{K_2}\int d\vec{r}_2 M_2^{K',K_2}(\vec{r},\vec{r}_2)V_{K_2}(\vec{r}_2) \\ &\qquad + \frac{1}{2!}\sum_{K_2}\sum_{K_3}\int d\vec{r}_2\int d\vec{r}_3 M_3^{K',K_2,K_3}(\vec{r},\vec{r}_2,\vec{r}_3)V_{K_2}(\vec{r}_2)V_{K_3}(\vec{r}_3)+\cdots \\ &= \sum_{n=0}^{\infty}\frac{1}{(n-1)!}\sum_{K_2,\cdots,K_n}\int d\vec{r}_2\cdots\int d\vec{r}_n M_n^{K',K_2,\cdots,K_n}(\vec{r},\vec{r}_2,\cdots,\vec{r}_n)V_{K_2}(\vec{r}_2)\cdots V_{K_n}(\vec{r}_n) \end{aligned} \tag{11.5.32}$$

$$\frac{\delta(\ln Z[\{V_K(\vec{r})\}])}{\delta V_{K'}(\vec{r})} = \sum_{n=0}^{\infty}\frac{1}{(n-1)!}\sum_{K_2,\cdots,K_n}\int d\vec{r}_2\cdots\int d\vec{r}_n C_n^{K',K_2,\cdots,K_n}(\vec{r},\vec{r}_2,\cdots,\vec{r}_n)V_{K_2}(\vec{r}_2)\cdots V_{K_n}(\vec{r}_n) \tag{11.5.33}$$

Eq.(11.5.33) is also calculated as follows.

$$\frac{\delta(\ln Z[\{V_K(\vec{r})\}])}{\delta V_{K'}(\vec{r})} = \frac{1}{Z[\{V_K(\vec{r})\}]}\frac{\delta Z[\{V_K(\vec{r})\}]}{\delta V_{K'}(\vec{r})} \tag{11.5.34}$$

By using Eqs.(11.5.31) $\sim$ (11.5.34), moment and cumulant is related as follows.

$$\begin{aligned} &\frac{\delta Z[\{V_K(\vec{r})\}]}{\delta V_{K'}(\vec{r})} = Z[\{V_K(\vec{r})\}]\frac{\delta(\ln Z[\{V_K(\vec{r})\}])}{\delta V_{K'}(\vec{r})} \\ &\to \sum_{n=0}^{\infty}\frac{1}{(n-1)!}\sum_{K_2,\cdots,K_n}\int d\vec{r}_2\cdots\int d\vec{r}_n M_n^{K',K_2,\cdots,K_n}(\vec{r},\vec{r}_2,\cdots,\vec{r}_n)V_{K_2}(\vec{r}_2)\cdots V_{K_n}(\vec{r}_n) \\ &= \left(\sum_{n=0}^{\infty}\frac{1}{n!}\sum_{K_1,\cdots,K_n}\int d\vec{r}_1\cdots\int d\vec{r}_n M_n^{K_1,\cdots,K_n}(\vec{r}_1,\cdots,\vec{r}_n)V_{K_1}(\vec{r}_1)\cdots V_{K_n}(\vec{r}_n)\right) \\ &\quad \left(\sum_{n=0}^{\infty}\frac{1}{(n-1)!}\sum_{K_2,\cdots,K_n}\int d\vec{r}_2\cdots\int d\vec{r}_n C_n^{K',K_2,\cdots,K_n}(\vec{r},\vec{r}_2,\cdots,\vec{r}_n)V_{K_2}(\vec{r}_2)\cdots V_{K_n}(\vec{r}_n)\right) \end{aligned} \tag{11.5.35}$$

By comparing the same order term of V, the relationship between $M_n^{K_1,\cdots,K_n}(\vec{r}_1,\cdots,\vec{r}_n)$ and $C_n^{K_1,\cdots,K_n}(\vec{r}_1,\cdots,\vec{r}_n)$

is derived as follows.

$$M_1^{K_1}(\vec{r}_1) = C_1^{K_1}(\vec{r}_1) \tag{11.5.36}$$

$$\begin{aligned}
&\sum_{K_2} \int d\vec{r}_2 M_2^{K',K_2}(\vec{r},\vec{r}_2) V_{K_2}(\vec{r}_2) \\
&= \sum_{K_2} \int d\vec{r}_2 C_2^{K',K_2}(\vec{r},\vec{r}_2) V_{K_2}(\vec{r}_2) + \left(\sum_{K_1} \int d\vec{r}_1 M_1^{K_1}(\vec{r}_1) V_{K_1}(\vec{r}_1) \right) \left(C_1^{K'}(\vec{r}) \right)
\end{aligned}$$

$$\begin{aligned}
\rightarrow M_2^{K_1,K_2}(\vec{r}_1,\vec{r}_2) &= C_2^{K_1,K_2}(\vec{r}_1,\vec{r}_2) + M_1^{K_2}(\vec{r}_2) C_1^{K_1}(\vec{r}_1) \\
&= C_2^{K_1,K_2}(\vec{r}_1,\vec{r}_2) + C_1^{K_1}(\vec{r}_1) C_1^{K_2}(\vec{r}_2)
\end{aligned} \tag{11.5.37}$$

$$\begin{aligned}
&\frac{1}{2!} \sum_{K_2} \sum_{K_3} \int d\vec{r}_2 \int d\vec{r}_3 M_3^{K',K_2,K_3}(\vec{r},\vec{r}_2,\vec{r}_3) V_{K_2}(\vec{r}_2) V_{K_3}(\vec{r}_3) \\
&= \frac{1}{2!} \sum_{K_2} \sum_{K_3} \int d\vec{r}_2 \int d\vec{r}_3 C_3^{K',K_2,K_3}(\vec{r},\vec{r}_2,\vec{r}_3) V_{K_2}(\vec{r}_2) V_{K_3}(\vec{r}_3) \\
&+ \left(\sum_{K_1} \int d\vec{r}_1 M_1^{K_1}(\vec{r}_1) V_{K_1}(\vec{r}_1) \right) \left(\sum_{K_2} \int d\vec{r}_2 C_2^{K',K_2}(\vec{r},\vec{r}_2) V_{K_2}(\vec{r}_2) \right) \\
&+ \left(\frac{1}{2!} \sum_{K_1} \sum_{K_2} \int d\vec{r}_1 \int d\vec{r}_2 M_2^{K_1,K_2}(\vec{r}_1,\vec{r}_2) V_{K_1}(\vec{r}_1) V_{K_2}(\vec{r}_2) \right) \left(C_1^{K'}(\vec{r}) \right)
\end{aligned}$$

$$\begin{aligned}
\rightarrow &M_3^{K_1,K_2,K_3}(\vec{r}_1,\vec{r}_2,\vec{r}_3) + M_3^{K_1,K_3,K_2}(\vec{r}_1,\vec{r}_3,\vec{r}_2) \\
&= C_3^{K_1,K_2,K_3}(\vec{r}_1,\vec{r}_2,\vec{r}_3) + C_3^{K_1,K_3,K_2}(\vec{r}_1,\vec{r}_3,\vec{r}_2) \\
&\quad + 2(M_1^{K_2}(\vec{r}_2) C_2^{K_1,K_3}(\vec{r}_1,\vec{r}_3) + M_1^{K_3}(\vec{r}_3) C_2^{K_1,K_2}(\vec{r}_1,\vec{r}_2)) \\
&\quad + M_2^{K_2,K_3}(\vec{r}_2,\vec{r}_3) C_1^{K_1}(\vec{r}_1) + M_2^{K_3,K_2}(\vec{r}_2,\vec{r}_3) C_1^{K_1}(\vec{r}_1)
\end{aligned}$$

Since the indices of moments and cumulants can be exchanged:

$$\begin{aligned}
\rightarrow &M_3^{K_1,K_2,K_3}(\vec{r}_1,\vec{r}_2,\vec{r}_3) \\
&= C_3^{K_1,K_2,K_3}(\vec{r}_1,\vec{r}_2,\vec{r}_3) \\
&+ C_2^{K_1,K_2}(\vec{r}_1,\vec{r}_2) C_1^{K_3}(\vec{r}_3) + C_2^{K_2,K_3}(\vec{r}_2,\vec{r}_3) C_1^{K_1}(\vec{r}_1) + C_2^{K_3,K_1}(\vec{r}_3,\vec{r}_1) C_1^{K_2}(\vec{r}_2) \\
&+ C_1^{K_1}(\vec{r}_1) C_2^{K_2}(\vec{r}_2) C_3^{K_3}(\vec{r}_3)
\end{aligned} \tag{11.5.38}$$

List of Publication

Publications related to this thesis

1. Hiroi, T; Shibayama, M. Dynamic light scattering microscope- Accessing opaque samples with high spatial resolution, Opt. Express, 21, 20260-20267 (2013)

2. Asai, H; Nishi, K; Hiroi, T; Fujii, K; Sakai, T; Shibayama, M. Gelation Process of Tetra-PEG Ion-gel Investigated by Time-Resolved Dynamic Light Scattering, Polymer, 54, 1160-1166 (2013)

3. Nishi, K; Hiroi, T; Hashimoto, K.; Fujii, K.; Hang, Y.-S; Kim, T.-H; Katsumoto, Y.; Shibayama, M. SANS and DLS Studies of the tacticity effects on the hydrophobicity and the phase separation of poly(*N*-isopropylacrylamide), Macromolecules, 46, 6225-6232 (2013)

4. Hiroi, T; Ohl, M; Sakai, T; Shibayama, M. Multiscale Dynamics of Inhomogeneity-Free Polymer Gels, Macromolecules, 47, 763-770 (2014)

5. Shibayama, M; Nishi, K; Hiroi, T. Gelation Kinetics and Polymer Network Dynamics of Homogeneous Tetra-PEG Gels, Macromol. Symp., 348, 9-13 (2015)

6. Kondo, S; Hiroi, T; Han,Y.S; Kim, T.H; Shibayama, M; Chung, U; Sakai, T. Reliable hydrogel with mechanical 'fuse link' in an aqueous environment, Adv. Mater., 27, 7407-7411 (2015)

7. Hiroi, T; Ata, S.; Shibayama, M. Transitions of Aggregation States for Concentrated Carbon Nanotube Dispersion, J. Phys. Chem. C, 120, 5776-5782 (2016)

8. Hiroi, T; Okazumi,Y: Littrell, K. C; Narita, Y; Tanaka, N; Shibayama, M. Mechanism of Heat-induced Gelation for Ovalbumin and Its *N*-terminus Cleaved Form, Polymer, 93, 152-158 (2016)

9. Hiroi, T; Kondo, S; Sakai, T; Gilbert, E. P; Han, Y.-S; Kim, T.-H; Shibayama, M. Fabrication and Structural Characterization of Module-Assembled Amphiphilic Conetwork Gels, Macromolecules, 49, 4940-4947 (2016)

10. Hiroi, T; Shibayama, M. Dynamic Light Scattering Microscope: Measurement of Particle Size Distribution for Turbid Solutions, J. Vis. Exp. (119), e54885 (2017)

Publications not related to this thesis

1. Kusano, T; Hiroi, T; Amemiya, K; Ando, M; Takahashi, T; Shibayama, M. Structure evolution of catalyst ink for fuel cell in drying process investigated by CV-SANS, Polym. J., 47, 546-555 (2015)

2. Nishi, K; Tochioka, S; Hiroi, T; Yamada, T; Kokado, K; Tae-Hwan Kim, T-H; Gilbert, E. P; Sada, K; Shibayama, M. Structural Analysis of Lipophilic Polyelectrolyte Solutions and Gels in Low-Polar Solvents Macromolecules, 48, 3613-3621 (2015)

3. Saha, S; Hiroi, T, Iwata, K; Hamaguchi, H. Raman Spectroscopy and the Heterogeneous Liquid Structure in Ionic Liquids, in Ionic Liquids Completely UnCOILed: Critical Expert Overviews (eds N. V. Plechkova and K. R. Seddon), John Wiley & Sons, Inc, Hoboken, NJ. (2015)

References

[1] P.-G. de Gennes. "Soft Matter (Nobel Lecture)". *Angew. Chem. Int. Ed. Engl.*, **31**, 1992.

[2] S. Kumar, A. K. Panda, R. K. Singh. "A review on tertiary recycling of high-density polyethylene to fuel". *Resour. Conserv. Recycl.*, **55**, 2011.

[3] A. Manuel Stephan. "Review on gel polymer electrolytes for lithium batteries". *Eur. Polym. J.*, **42**, 2006.

[4] M. J. Zohuriaan-Mehr, K. Kabiri. "Superabsorbent Polymer Materials: A Review". *Iran. Polym. J.*, **17**, 2008.

[5] M. Shibayama. "Spatial inhomogeneity and dynamic fluctuations of polymer gels". *Macromol. Chem. Phys.*, **199**, 1998.

[6] Y. Okumura, K. Ito. "The Polyrotaxane Gel: A Topological Gel by Figure-of-Eight Cross-links". *Adv. Mater.*, **13**, 2001.

[7] K. Haraguchi, T. Takehisa. "Nanocomposite Hydrogels: A Unique Organic-Inorganic Network Structure with Extraordinary Mechanical, Optical, and Swelling/De-swelling Properties". *Adv. Mater.*, **14**, 2002.

[8] J. P. Gong *et al.* "Double-Network Hydrogels with Extremely High Mechanical Strength". *Adv. Mater.*, **15**, 2003.

[9] T. Huang *et al.* "A Novel Hydrogel with High Mechanical Strength: A Macromolecular Microsphere Composite Hydrogel". *Adv. Mater.*, **19**, 2007.

[10] K. J. Henderson *et al.* "Ionically Cross-Linked Triblock Copolymer Hydrogels with High Strength". *Macromolecules*, **43**, 2010.

[11] T. Sakai *et al.* "Design and Fabrication of a High-Strength Hydrogel with Ideally Homogeneous Network Structure from Tetrahedron-like Macromonomers". *Macromolecules*, **41**, 2008.

[12] T. Sakai *et al.* "Highly Elastic and Deformable Hydrogel Formed from Tetra-arm Polymers". *Macromol. Rapid Commun.*, **31**, 2010.

[13] A. Moussaïd, P. N. Pusey. "Multiple scattering suppression in static light scattering by cross-correlation spectroscopy". *Phys. Rev. E*, **60**, 1999.

[14] R. Roe. *Methods of X-ray and Neutron Scattering in Polymer Science.* Oxford University Press, 2000.

[15] T. Matsunaga *et al.* "Structure Characterization of Tetra-PEG Gel by Small-Angle Neutron Scattering". *Macromolecules*, **42**, 2009.

[16] T. Matsunaga *et al.* "SANS and SLS Studies on Tetra-Arm PEG Gels in As-Prepared and Swollen States". *Macromolecules*, **42**, 2009.

[17] H. Kamata *et al.* "Anomalous volume phase transition in a polymer gel with alternative hydrophilic-amphiphilic sequence". *Soft Matter*, **8**, 2012.

[18] S. Kondo *et al.* "Reliable Hydrogel with Mechanical " Fuse Link " in an Aqueous Environment". *Adv. Mater.*, **27**, 2015.

[19] J. N. Israelachvili. *Intermolecular and surface forces.* Academic Press, Burlington, MA, 2011.

[20] T. Koseki, N. Kitabatake, E. Doi. "Irreversible thermal denaturation and formation of linear aggregates of ovalbumin". *Food Hydrocoll.*, **3**, 1989.

[21] N. Tanaka *et al.* "The Mechanism of Fibril Formation of a Non-inhibitory Serpin Ovalbumin Revealed by the Identification of Amyloidogenic Core Regions". *J. Biol. Chem.*, **286**, 2011.

[22] Y. Kawachi *et al.* "Role of the N-Terminal Amphiphilic Region of Ovalbumin during Heat-Induced Aggregation and Gelation". *J. Agric. Food Chem.*, **61**, 2013.

[23] M. Rubinstein, R. Colby. *Polymer Physics*. OUP Oxford, 2003.

[24] I. Hamley. *The Physics of Block Copolymers*. Oxford University Press, 1998.

[25] C. S. Patrickios, T. K. Georgiou. "Covalent amphiphilic polymer networks". *Curr. Opin. Colloid & Interface Sci.*, **8**, 2003.

[26] G. Erdodi, J. P. Kennedy. "Amphiphilic conetworks: Definition, synthesis, applications". *Prog. Polym. Sci.*, **31**, 2006.

[27] I. Barakat *et al.* "Macromolecular engineering of polylactones and polylactides. XXV. Synthesis and characterization of bioerodible amphiphilic networks and their use as controlled drug delivery systems". *J. Polym. Sci. Part A: Polym. Chem.*, **37**, 1999.

[28] P. C. Nicolson, J. Vogt. "Soft contact lens polymers: an evolution". *Biomater.*, **22**, 2001.

[29] T. Hiroi *et al.* "Multiscale Dynamics of Inhomogeneity-Free Polymer Gels". *Macromolecules*, **47**, 2014.

[30] T. Hiroi, M. Shibayama. "Dynamic light scattering microscope: Accessing opaque samples with high spatial resolution". *Opt. Express*, **21**, 2013.

[31] T. Hiroi, M. Shibayama. "Measurement of Particle Size Distribution in Turbid Solutions by Dynamic Light Scattering Microscopy". *J. Vis. Exp.*, **119**, 2017.

[32] T. Hiroi, S. Ata, M. Shibayama. "Transitions of Aggregation States for Concentrated Carbon Nanotube Dispersion". *J. Phys. Chem. C*, **120**, 2016.

[33] T. Hiroi *et al.* "Mechanism of heat-induced gelation for ovalbumin and its N-terminus cleaved form". *Polymer*, **93**, 2016.

[34] T. Hiroi *et al.* "Fabrication and Structural Characterization of Module-Assembled Amphiphilic Conetwork Gels". *Macromolecules*, **49**, 2016.

[35] G. Squires. *Introduction to the Theory of Thermal Neutron Scattering*. Cambridge University Press, 2012.

[36] J. S. Higgins, H. Benoit, H. Benoît. *Polymers and Neutron Scattering*. Clarendon Press, 1994.

[37] A. Furrer, T. Strässle, J. Mesot. *Neutron Scattering in Condensed Matter Physics*. World Scientific, 2009.

[38] B. Hammouda. *Probing nanoscale structures - The SANS Toolbox*. National Institute of Standards and Technology, 2017.

[39] J. Hansen, I. McDonald. *Theory of Simple Liquids: with Applications to Soft Matter*. Elsevier Science, 2013.

[40] J. K. Percus, G. J. Yevick. "Analysis of Classical Statistical Mechanics by Means of Collective Coordinates". *Phys. Rev.*, **110**, 1958.

[41] M. S. Wertheim. "Exact Solution of the Percus-Yevick Integral Equation for Hard Spheres". *Phys. Rev. Lett.*, **10**, 1963.

[42] E. Thiele. "Equation of State for Hard Spheres". *The J. Chem. Phys.*, **39**, 1963.

[43] M. S. Wertheim. "Analytic Solution of the Percus- Yevick Equation". *J. Math. Phys.*, **5**, 1964.

[44] H. Krienke. "The Kelbg solution of the Percus-Yevick equation for hard spheres by direct differentiation of the Oz equation". *J. Mol. Liq.*, **78**, 1998.

[45] H. Kawada *et al.* "Structure and Rheology of a Self-Standing Nanoemulsion". *Langmuir*, **26**, 2010.

[46] R. V. Sharma, K. C. Sharma. "The structure factor and the transport properties of dense fluids having molecules with square well potential, a possible generalization". *Phys. A: Stat. Mech. its Appl.*, **89**, 1977.

[47] J. B. Hayter, J. Penfold. "An analytic structure factor for macroion solutions". *Mol. Phys.*, **42**, 1981.

[48] M. E. Fisher. "Correlation Functions and the Critical Region of Simple Fluids". *J. Math. Phys.*, **5**, 1964.

[49] M. Teubner, R. Strey. "Origin of the scattering peak in microemulsions". *J. Chem. Phys.*, **87**, 1987.

[50] P. G. de Gennes. *Scaling concepts in polymer physics.* Cornell University Press, Ithaca, N.Y, 1979.

[51] V. SAKAI, C. Alba-Simionesco, S. Chen. *Dynamics of Soft Matter: Neutron Applications.* Springer US, 2011.

[52] B. Ewen, D. Richter. *Neutron Spin Echo Investigations on the Segmental Dynamics of Polymers in Melts, Networks and Solutions*, pages 1–129. Springer Berlin Heidelberg, Berlin, Heidelberg, 1997.

[53] T. Tanaka, L. O. Hocker, G. B. Benedek. "Spectrum of light scattered from a viscoelastic gel". *J. Chem. Phys.*, **59**, 1973.

[54] P. Flory. *Principles of Polymer Chemistry.* Cornell University Press, 1953.

[55] S. Fujishige, K. Kubota, I. Ando. "Phase transition of aqueous solutions of poly(N-isopropylacrylamide) and poly(N-isopropylmethacrylamide)". *J. Phys. Chem.*, **93**, 1989.

[56] M. Shibayama, T. Tanaka. *Volume phase transition and related phenomena of polymer gels*, pages 1–62. Springer Berlin Heidelberg, Berlin, Heidelberg, 1993.

[57] A. Matsuyama, F. Tanaka. "Theory of solvation-induced reentrant phase separation in polymer solutions". *Phys. Rev. Lett.*, **65**, 1990.

[58] Y. Okada, F. Tanaka. "Cooperative Hydration, Chain Collapse, and Flat LCST Behavior in Aqueous Poly(N-isopropylacrylamide) Solutions". *Macromolecules*, **38**, 2005.

[59] Y. Ono, T. Shikata. "Hydration and Dynamic Behavior of Poly(N-isopropylacrylamide)s in Aqueous Solution: A Sharp Phase Transition at the Lower Critical Solution Temperature". *J. Am. Chem. Soc.*, **128**, 2006.

[60] L. D. Barron. *Molecular Light Scattering and Optical Activity.* Cambridge University Press, 2009.

[61] B. Berne, R. Pecora. *Dynamic Light Scattering: With Applications to Chemistry, Biology, and Physics.* Dover Publications, 2000.

[62] C. Johnson, D. Gabriel. *Laser Light Scattering.* Dover Publications, 2015.

[63] B. Chu. *Laser Light Scattering: Basic Principles and Practice.* Dover Publications, 2007.

[64] M. Shibayama, T. Norisuye, S. Nomura. "Cross-link Density Dependence of Spatial Inhomogeneities and Dynamic Fluctuations of Poly(N-isopropylacrylamide) Gels". *Macromolecules*, **29**, 1996.

[65] A. M. Shetty *et al.* "Multiangle Depolarized Dynamic Light Scattering of Short Functionalized Single-Walled Carbon Nanotubes". *J. Phys. Chem. C*, **113**, 2009.

[66] V. F. Sears. "Neutron scattering lengths and cross sections". *Neutron News*, **3**, 1992.

[67] F. Mezei. "Neutron spin echo: A new concept in polarized thermal neutron techniques". *Z. Phys. A*, **255**, 1972.

[68] F. Mezei. *Neutron spin echo : proceedings of a Laue-Langevin Institut workshop, Grenoble, October 15-16, 1979.* Lecture notes in physics; 128. Springer-Verlag, Berlin; New York, 1980.

[69] L. Treloar. *The Physics of Rubber Elasticity.* OUP Oxford, 2005.

[70] M. Shibayama. "Structural Investigation of Supertough Polymer Gels by Small-Angle Neutron Scattering Measurement". *J. Phys. Soc. Jpn.*, **78**, 2009.

[71] A. B. Imran, T. Seki, Y. Takeoka. "Recent advances in hydrogels in terms of fast stimuli responsiveness and superior mechanical performance". *Polym. J*, **42**, 2010.

[72] M. Shibayama. "Structure-mechanical property relationship of tough hydrogels". *Soft Matter*, **8**, 2012.

[73] C. W. Peak, J. J. Wilker, G. Schmidt. "A review on tough and sticky hydrogels". *Colloid Polym. Sci.*, **291**, 2013.

[74] W. Richtering, B. R. Saunders. "Gel architectures and their complexity". *Soft Matter*, **10**, 2014.

[75] P.-G. de Gennes. "Sliding gels". *Phys. A: Stat. Mech. its Appl.*, **271**, 1999.

[76] K. Ito. "Novel entropic elasticity of polymeric materials: why is slide-ring gel so soft[quest]". *Polym. J.*, **44**, 2012.

[77] K. Haraguchi. "Synthesis and properties of soft nanocomposite materials with novel organic/inorganic network structures". *Polym. J.*, **43**, 2011.

[78] J. P. Gong. "Why are double network hydrogels so tough?". *Soft Matter*, **6**, 2010.

[79] Q. Chen *et al.* "Fundamentals of double network hydrogels". *J. Mater. Chem. B*, **3**, 2015.

[80] T. Nonoyama, J. P. Gong. "Double-network hydrogel and its potential biomedical application: A review". *Proc. Inst. Mech. Eng. Part H: J. Eng. Medicine*, **229**, 2015.

[81] M. E. Seitz *et al.* "Self-Assembly and Stress Relaxation in Acrylic Triblock Copolymer Gels". *Macromolecules*, **40**, 2007.

[82] G. Song *et al.* "Facile Fabrication of Tough Hydrogels Physically Cross-Linked by Strong Cooperative Hydrogen Bonding". *Macromolecules*, **46**, 2013.

[83] A. K. Gaharwar *et al.* "Highly Extensible, Tough, and Elastomeric Nanocomposite Hydrogels from Poly(ethylene glycol) and Hydroxyapatite Nanoparticles". *Biomacromolecules*, **12**, 2011.

[84] A. K. Gaharwar *et al.* "Transparent, elastomeric and tough hydrogels from poly(ethylene glycol) and silicate nanoparticles". *Acta Biomater.*, **7**, 2011.

[85] J.-Y. Sun *et al.* "Highly stretchable and tough hydrogels". *Nature*, **489**, 2012.

[86] A. Bin Imran *et al.* "Extremely stretchable thermosensitive hydrogels by introducing slide-ring polyrotaxane cross-linkers and ionic groups into the polymer network". *Nat. Commun.*, **5**, 2014.

[87] J. Li, Z. Suo, J. J. Vlassak. "Stiff, strong, and tough hydrogels with good chemical stability". *J. Mater. Chem. B*, **2**, 2014.

[88] G. Hild. "Model networks based on 'endlinking' processes: synthesis, structure and properties". *Prog. Polym. Sci.*, **23**, 1998.

[89] D. J. Waters *et al.* "Morphology of Photopolymerized End-Linked Poly(ethylene glycol) Hydrogels by Small-Angle X-ray Scattering". *Macromolecules*, **43**, 2010.

[90] Y. Yamaguchi *et al.* "Polyethylene Oxide (PEO) and Polyethylene Glycol (PEG) Polymer Sieving Matrix for RNA Capillary Electrophoresis". *PLoS ONE*, **10**, 2015.

[91] G. Lapienis. "Star-shaped polymers having PEO arms". *Prog. Polym. Sci.*, **34**, 2009.

[92] T. Sakai. "Experimental verification of homogeneity in polymer gels". *Polym. J.*, **46**, 2014.

[93] M. Fujiki *et al.* "Friction Coefficient of Well-Defined Hydrogel Networks". *Macromolecules*, **49**, 2016.

[94] K. Mortensen, M. Annaka. "Structural Study of Four-Armed Amphiphilic Star-Block Copolymers: Pristine and End-Linked Tetronic T1307". *ACS Macro Lett.*, **5**, 2016.

[95] N. Meyerbröker, M. Zharnikov. "Ultraflexible, Freestanding Nanomembranes Based on Poly(ethylene glycol)". *Adv. Mater.*, **26**, 2014.

[96] H. Jia *et al.* "Facile functionalization of a tetrahedron-like PEG macromonomer-based fluorescent hydrogel with high strength and its heavy metal ion detection". *J. Mater. Chem. A*, **3**, 2015.

[97] H. Jia *et al.* "One-pot synthesis of highly mechanical and redox-degradable polyurethane hydrogels based on tetra-PEG and disulfide/thiol chemistry". *RSC Adv.*, **6**, 2016.

[98] N. Yoshihara *et al.* "Rigid Polyimide Networks End-Linked with Tri- and Tetra-armed Crosslinkers". *Macromol. Chem. Phys.*, **215**, 2014.

[99] K. Oshima *et al.* "Model Polyelectrolyte Gels Synthesized by End-Linking of Tetra-Arm Polymers with Click Chemistry: Synthesis and Mechanical Properties". *Macromolecules*, **47**, 2014.

[100] H. C. Kolb, M. G. Finn, K. B. Sharpless. "Click Chemistry: Diverse Chemical Function from a Few Good Reactions". *Angew. Chem. Int. Ed.*, **40**, 2001.

[101] V. V. Rostovtsev *et al.* "A Stepwise Huisgen Cycloaddition Process: Copper(I)-Catalyzed Regioselective " Ligation " of Azides and Terminal Alkynes". *Angew. Chem. Int. Ed.*, **41**, 2002.

[102] C. W. Tornøe, C. Christensen, M. Meldal. "Peptidotriazoles on Solid Phase: [1,2,3]-Triazoles by Regiospecific Copper(I)-Catalyzed 1,3-Dipolar Cycloadditions of Terminal Alkynes to Azides". *J. Org. Chem.*, **67**, 2002.

[103] M. Malkoch *et al.* "Synthesis of well-defined hydrogel networks using Click chemistry". *Chem. Commun.*, **26**, 2006.

[104] B. D. Polizzotti, B. D. Fairbanks, K. S. Anseth. "Three-Dimensional Biochemical Patterning of Click-Based Composite Hydrogels via Thiolene Photopolymerization". *Biomacromolecules*, **9**, 2008.

[105] V. Truong, I. Blakey, A. K. Whittaker. "Hydrophilic and Amphiphilic Polyethylene Glycol-Based Hydrogels with Tunable Degradability Prepared by " Click " Chemistry". *Biomacromolecules*, **13**, 2012.

[106] K. W. Li *et al.* "Well-Defined Poly(ethylene glycol) Hydrogels with Enhanced Mechanical Performance Prepared by Thermally Induced Copper-Catalyzed Azide-Alkyne Cycloaddition". *Macromol. Mater. Eng.*, **301**, 2016.

[107] S. Qian *et al.* "High strength biocompatible PEG single-network hydrogels". *RSC Adv.*, **4**, 2014.

[108] C. J. Kloxin, T. F. Scott, C. N. Bowman. "Stress Relaxation via Addition − Fragmentation Chain Transfer in a Thiol-ene Photopolymerization". *Macromolecules*, **42**, 2009.

[109] M. A. Cole, C. N. Bowman. "Evaluation of thiol-ene click chemistry in functionalized polysiloxanes". *J. Polym. Sci. Part A: Polym. Chem.*, **51**, 2013.

[110] E. M. Saffer *et al.* "SANS study of highly resilient poly(ethylene glycol) hydrogels". *Soft Matter*, **10**, 2014.

[111] J. Cui *et al.* "Mechanical Properties of End-Linked PEG/PDMS Hydrogels". *Macromolecules*, **45**, 2012.

[112] T. Ikeda *et al.* "Organogelation behavior, thermal and mechanical properties of polymer network formed by the Diels-Alder reaction of furan- and maleimide-terminated four-arm star-shaped ε-caprolactone oligomers". *Polymer*, **54**, 2013.

[113] T. Nakamura *et al.* "Organogelation behavior and thermal properties of supramolecular polymer network composed of carboxy- and pyridyl-terminated 4-arm star-shaped ε -caprolactone oligomers". *J. Colloid Interface Sci.*, **404**, 2013.

[114] T. Nakamura, T. Fuke, M. Shibata. "Organogelation behavior and thermal properties of supramolecular polymer networks using pyridyl-terminated 4-arm star-shaped ε -caprolactone oligomers and disulfonic acids". *Colloid Polym. Sci.*, **292**, 2014.

[115] T. Rossow, S. Seiffert. "Supramolecular polymer gels with potential model-network structure". *Polym. Chem.*, **5**, 2014.

[116] M. Schappacher, A. Deffieux, J.-F. Le Meins. "Soft dynamic covalent hydrogels based on iron(iii)tetraphenylporphyrinato-functionalized 4-arm poly(ethylene oxide)". *Polym. Chem.*, **4**, 2013.

[117] M. Fukasawa *et al.* "Synthesis and Mechanical Properties of a Nanocomposite Gel Consisting of a Tetra-PEG/Clay Network". *Macromolecules*, **43**, 2010.

[118] T. Nakajima *et al.* "Synthesis and Fracture Process Analysis of Double Network Hydrogels with a Well-Defined First Network". *ACS Macro Lett.*, **2**, 2013.

[119] Y. Akagi *et al.* "Evaluation of Topological Defects in Tetra-PEG Gels". *Macromolecules*, **43**, 2010.

[120] D. R. Miller, C. W. Macosko. "A New Derivation of Post Gel Properties of Network Polymers". *Macromolecules*, **9**, 1976.

[121] M. Kurakazu *et al.* "Evaluation of Gelation Kinetics of Tetra-PEG Gel". *Macromolecules*, **43**, 2010.

[122] H. H. Winter, M. Mours. *Rheology of Polymers Near Liquid-Solid Transitions*, pages 165–234. Springer Berlin Heidelberg, Berlin, Heidelberg, 1997.

[123] K. Nishi *et al.* "Small-Angle Neutron Scattering Study on Defect-Controlled Polymer Networks". *Macromolecules*, **47**, 2014.

[124] Y. Akagi *et al.* "Examination of the Theories of Rubber Elasticity Using an Ideal Polymer Network". *Macromolecules*, **44**, 2011.

[125] K. Nishi *et al.* "Kinetic Study for AB-Type Coupling Reaction of Tetra-Arm Polymers". *Macromolecules*, **45**, 2012.

[126] K. Nishi *et al.* "Kinetic Aspect on Gelation Mechanism of Tetra-PEG Hydrogel". *Macromolecules*, **47**, 2014.

[127] Y. Hashimoto *et al.* "Structure and dynamics of tetra-PEG gel by Brownian dynamics". *Trans. Mater. Res. Soc. Jpn.*, **35**, 2010.

[128] T. Sakai *et al.* "Sol-gel transition behavior near critical concentration and connectivity". *Polym. J.*, **48**, 2016.

[129] Y. Akagi *et al.* "Transition between Phantom and Affine Network Model Observed in Polymer Gels with Controlled Network Structure". *Macromolecules*, **46**, 2013.

[130] T. Sakai *et al.* "Effect of swelling and deswelling on the elasticity of polymer networks in the dilute to semi-dilute region". *Soft Matter*, **8**, 2012.

[131] T. Katashima *et al.* "Mechanical properties of tetra-PEG gels with supercoiled network structure". *J. Chem. Phys.*, **140**, 2014.

[132] S. Kondo *et al.* "Mechanical Properties of Polymer Gels with Bimodal Distribution in Strand Length". *Macromolecules*, **46**, 2013.

[133] S. Kondo, U.-i. Chung, T. Sakai. "Effect of prepolymer architecture on the network structure formed by AB-type crosslink-coupling". *Polym. J.*, **46**, 2014.

[134] K. Nishi *et al.* "Rubber elasticity for incomplete polymer networks". *J. Chem. Phys.*, **137**, 2012.

[135] A. Sugimura *et al.* "Mechanical properties of a polymer network of Tetra-PEG gel". *Polym. J.*, **45**, 2013.

[136] K. Nishi *et al.* "Rubber elasticity for percolation network consisting of Gaussian chains". *J. Chem. Phys.*, **143**, 2015.

[137] E. Wang, F. A. Escobedo. "Mechanical Properties of Tetrapolyethylene and Tetrapoly(ethylene oxide) Diamond Networks via Molecular Dynamics Simulations". *Macromolecules*, **49**, 2016.

[138] Y. Akagi *et al.* "Ultimate elongation of polymer gels with controlled network structure". *RSC Adv.*, **3**, 2013.

[139] T. Katashima *et al.* "Strain energy density function of a near-ideal polymer network estimated by biaxial deformation of Tetra-PEG gel". *Soft Matter*, **8**, 2012.

[140] T. Katashima *et al.* "Probing the cross-effect of strains in non-linear elasticity of nearly regular polymer networks by pure shear deformation". *J. Chem. Phys.*, **142**, 2015.

[141] G. J. Lake, A. G. Thomas. "The Strength of Highly Elastic Materials". *Proc. Royal Soc. Lond. Ser. A. Math. Phys. Sci.*, **300**, 1967.

[142] Y. Akagi *et al.* "Fracture energy of polymer gels with controlled network structures". *J. Chem. Phys.*, **139**, 2013.

[143] T. Sakai *et al.* "Experimental verification of fracture mechanism for polymer gels with controlled network structure". *Soft Matter*, **10**, 2014.

[144] T. Matsunaga *et al.* "SANS Studies on Tetra-PEG Gel under Uniaxial Deformation". *Macromolecules*, **44**, 2011.

[145] M. Asai *et al.* "Correlation between Local and Global Inhomogeneities of Chemical Gels". *Macromolecules*, **46**, 2013.

[146] K. Takagi *et al.* "A computer simulation of the networked structure of a hydrogel prepared from a tetra-armed star pre-polymer". *Soft Matter*, **10**, 2014.

[147] M. Asai *et al.* "Supercoiling transformation of chemical gels". *Soft Matter*, **11**, 2015.

[148] T. Norisuye *et al.* "Small angle neutron scattering studies on structural inhomogeneities in polymer gels: irradiation cross-linked gels vs chemically cross-linked gels". *Polymer*, **43**, 2002.

[149] L. Fang, W. Brown. "Decay time distributions from dynamic light scattering for aqueous poly(vinyl alcohol) gels and semidilute solutions". *Macromolecules*, **23**, 1990.

[150] Y. Matsuda *et al.* "Structural analysis of aggregates formed by a thermoresponsive homopolymer in dilute aqueous solutions". *J. Polym. Sci. Part B: Polym. Phys.*, **44**, 2006.

[151] J. Wang. "The Origin of the Slow Mode in Dilute Aqueous Solutions of PEO". *Macromolecules*, **48**, 2015.

[152] A. M. Hecht *et al.* "Structure and dynamics of a poly(dimethylsiloxane) network: a comparative investigation of gel and solution". *Macromolecules*, **25**, 1992.

[153] M. Ohl *et al.* "The high-resolution neutron spin-echo spectrometer for the SNS with $\tau \geq 1$ μs". *Phys. B: Condens. Matter*, **350**, 2004.

[154] M. Ohl *et al.* "The spin-echo spectrometer at the Spallation Neutron Source (SNS)". *Nucl. Instrum. Methods Phys. Res. Sect. A*, **696**, 2012.

[155] A.-M. Hecht *et al.* "Thermal Fluctuations in Polymer Gels Investigated by Neutron Spin Echo and Dynamic Light Scattering". *Macromolecules*, **35**, 2002.

[156] T. Kanaya *et al.* "Neutron spin-echo studies on dynamic and static fluctuations in two types of poly(vinyl alcohol) gels". *Phys. Rev. E*, **71**, 2005.

[157] S. Koizumi *et al.* "Frozen concentration fluctuations in a poly(N-isopropyl acrylamide) gel studied by neutron spin echo and small-angle neutron scattering". *Appl. Phys. A*, **74**, 2002.

[158] R. Oeser *et al.* "Dynamic fluctuations of crosslinks in a rubber: A neutron-spin-echo study". *Phys. Rev. Lett.*, **60**, 1988.

[159] M. Shibayama, T. Tanaka, C. C. Han. "Small angle neutron scattering study on poly(N- isopropyl acrylamide) gels near their volume- phase transition temperature". *J. Chem. Phys.*, **97**, 1992.

[160] K. Fujii *et al.* "High-performance ion gel with tetra-PEG network". *Soft Matter*, **8**, 2012.

[161] H. Asai *et al.* "Structural Analysis of High Performance Ion-Gel Comprising Tetra-PEG Network". *Macromolecules*, **45**, 2012.

[162] H. Asai *et al.* "Gelation process of Tetra-PEG ion-gel investigated by time-resolved dynamic light scattering". *Polymer*, **54**, 2013.

[163] K. Hashimoto *et al.* "Gelation Mechanism of Tetra-armed Poly(ethylene glycol) in Aprotic Ionic Liquid Containing Nonvolatile Proton Source, Protic Ionic Liquid". *J. Phys. Chem. B*, **119**, 2015.

[164] K. Hashimoto *et al.* "Nearly Ideal Polymer Network Ion Gel Prepared in pH-Buffering Ionic Liquid". *Macromolecules*, **49**, 2016.

[165] T. Hazama *et al.* "High-performance gel electrolytes with tetra-armed polymer network for Li ion batteries". *J. Power Sources*, **286**, 2015.

[166] X. Li *et al.* "Migration Behavior of Rodlike dsDNA under Electric Field in Homogeneous Polymer Networks". *Macromolecules*, **46**, 2013.

[167] X. Li *et al.* "Electrophoretic Mobility of Double-Stranded DNA in Polymer Solutions and Gels with Tuned Structures". *Macromolecules*, **47**, 2014.

[168] K. Khairulina *et al.* "Electrophoretic mobility of semi-flexible double-stranded DNA in defect-controlled polymer networks: Mechanism investigation and role of structural parameters". *J. Chem. Phys.*, **142**, 2015.

[169] X. Li *et al.* "Precise Control and Prediction of Hydrogel Degradation Behavior". *Macromolecules*, **44**, 2011.

[170] X. Li *et al.* "Degradation Behavior of Polymer Gels Caused by Nonspecific Cleavages of Network Strands". *Chem. Mater.*, **26**, 2014.

[171] H. Kamata, U.-i. Chung, T. Sakai. "Shrinking Kinetics of Polymer Gels with Alternating Hydrophilic/Thermoresponsive Prepolymer Units". *Macromolecules*, **46**, 2013.

[172] H. Kamata *et al.* "“Nonswellable” Hydrogel Without Mechanical Hysteresis". *Science*, **343**, 2014.

[173] H. van de Hulst. *Light Scattering by Small Particles*. Dover Publications, 2012.

[174] C. Bohren. *Clouds in a Glass of Beer: Simple Experiments in Atmospheric Physics*. Dover Publications, 2013.

[175] G. D. J. Phillies. "Suppression of multiple scattering effects in quasielastic light scattering by homodyne cross- correlation techniques". *J. Chem. Phys.*, **74**, 1981.

[176] G. D. J. Phillies. "Experimental demonstration of multiple-scattering suppression in quasielastic-light-scattering spectroscopy by homodyne coincidence techniques". *Phys. Rev. A*, **24**, 1981.

[177] G. Maret, P. E. Wolf. "Multiple light scattering from disordered media. The effect of brownian motion of scatterers". *Z. Phys. B*, **65**, 1987.

[178] D. J. Pine *et al.* "Diffusing wave spectroscopy". *Phys. Rev. Lett.*, **60**, 1988.

[179] K. Ishii, R. Yoshida, T. Iwai. "Single-scattering spectroscopy for extremely dense colloidal suspensions by use of a low-coherence interferometer". *Opt. Lett.*, **30**, 2005.

[180] R. Dzakpasu, D. Axelrod. *Dynamic Light Scattering Microscopy*, book section 10, pages 319–353. Wiley-VCH Verlag GmbH & Co. KGaA, 2007.

[181] Y. Takagi, K. Kurihara. "Application of a microscope to Brillouin scattering spectroscopy". *Rev. Sci. Instrum.*, **63**, 1992.

[182] P. D. Kaplan, V. Trappe, D. A. Weitz. "Light-scattering microscope". *Appl. Opt.*, **38**, 1999.

[183] D. C. Liptak *et al.* "On the development of a confocal Rayleigh-Brillouin microscope". *Rev. Sci. Instrum.*, **78**, 2007.

[184] C. Casiraghi *et al.* "Rayleigh Imaging of Graphene and Graphene Layers". *Nano Lett.*, **7**, 2007.

[185] G. Louit *et al.* "Spectral and 3-Dimensional Tracking of Single Gold Nanoparticles in Living Cells Studied by Rayleigh Light Scattering Microscopy". *J. Phys. Chem. C*, **113**, 2009.

[186] D. C. Prieve. "Measurement of colloidal forces with TIRM". *Adv. Colloid Interface Sci.*, **82**, 1999.

[187] S. L. Eichmann *et al.* "Imaging Carbon Nanotube Interactions, Diffusion, and Stability in Nanopores". *ACS Nano*, **5**, 2011.

[188] X. Hui, I. Katsuhiro, I. Toshiaki. "Hydrodynamic Radius Sizing of Nanoparticles in Dense Polydisperse Media by Low-Coherence Dynamic Light Scattering". *Jpn. J. Appl. Phys.*, **44**, 2005.

[189] P. Navabpour *et al.* "Influence of concentration on the particle size analysis of polymer latexes using diffusing-wave spectroscopy". *Colloid Polym. Sci.*, **283**, 2005.

[190] S.-i. Takata, T. Norisuye, M. Shibayama. "Small-Angle Neutron-Scattering Study on Preparation Temperature Dependence of Thermosensitive Gels". *Macromolecules*, **35**, 2002.

[191] C. Staii *et al.* "DNA-Decorated Carbon Nanotubes for Chemical Sensing". *Nano Lett.*, **5**, 2005.

[192] H. Huang *et al.* "Aligned Carbon Nanotube Composite Films for Thermal Management". *Adv. Mater.*, **17**, 2005.

[193] J. Choi *et al.* "Band filling and correlation effects in alkali metal doped carbon nanotubes". *Phys. Lett. A*, **299**, 2002.

[194] T. Yamada *et al.* "A stretchable carbon nanotube strain sensor for human-motion detection". *Nat Nano*, **6**, 2011.

[195] K.-Y. Chun *et al.* "Highly conductive, printable and stretchable composite films of carbon nanotubes and silver". *Nat. Nanotechnol.*, **5**, 2010.

[196] N. Li *et al.* "Electromagnetic Interference (EMI) Shielding of Single-Walled Carbon Nanotube Epoxy Composites". *Nano Lett.*, **6**, 2006.

[197] W.-S. Jou, H.-Z. Cheng, C.-F. Hsu. "The electromagnetic shielding effectiveness of carbon nanotubes polymer composites". *J. Alloy. Compd.*, **434-435**, 2007.

[198] J.-H. Kim *et al.* "Synthesis and Electrochemical Properties of Spin-Capable Carbon Nanotube Sheet/MnOx Composites for High-Performance Energy Storage Devices". *Nano Lett.*, **11**, 2011.

[199] X. Q. He, S. Kitipornchai, K. M. Liew. "Buckling analysis of multi-walled carbon nanotubes: a continuum model accounting for van der Waals interaction". *J. Mech. Phys. Solids*, **53**, 2005.

[200] Y. Wang, J. Wu, F. Wei. "A treatment method to give separated multi-walled carbon nanotubes with high purity, high crystallization and a large aspect ratio". *Carbon*, **41**, 2003.

[201] L. Zhu *et al.* "Growth and electrical characterization of high-aspect-ratio carbon nanotube arrays". *Carbon*, **44**, 2006.

[202] W. Zhou *et al.* "Small angle neutron scattering from single-wall carbon nanotube suspensions: evidence for isolated rigid rods and rod networks". *Chem. Phys. Lett.*, **384**, 2004.

[203] H. Wang *et al.* "Dispersing Single-Walled Carbon Nanotubes with Surfactants: A Small Angle Neutron Scattering Study". *Nano Lett.*, **4**, 2004.

[204] B. J. Bauer, E. K. Hobbie, M. L. Becker. "Small-Angle Neutron Scattering from Labeled Single-Wall Carbon Nanotubes". *Macromolecules*, **39**, 2006.

[205] Z. Fan, S. G. Advani. "Rheology of multiwall carbon nanotube suspensions". *J. Rheol.*, **51**, 2007.

[206] W. K. A. Ma *et al.* "Rheological modeling of carbon nanotube aggregate suspensions". *J. Rheol.*, **52**, 2008.

[207] D. Lehner, H. Lindner, O. Glatter. "Determination of the Translational and Rotational Diffusion Coefficients of Rodlike Particles Using Depolarized Dynamic Light Scattering". *Langmuir*, **16**, 2000.

[208] S. Badaire *et al.* "In Situ Measurements of Nanotube Dimensions in Suspensions by Depolarized Dynamic Light Scattering". *Langmuir*, **20**, 2004.

[209] K. Hata *et al.* "Water-Assisted Highly Efficient Synthesis of Impurity-Free Single-Walled Carbon Nanotubes". *Science*, **306**, 2004.

[210] V. Krungleviciute *et al.* "Gas Adsorption on HiPco Nanotubes: Surface Area Determinations, and Neon Second Layer Data". *Nano Lett.*, **4**, 2004.

[211] R. Saito, G. Dresselhaus, M. S. Dresselhaus. "Trigonal warping effect of carbon nanotubes". *Phys. Rev. B*, **61**, 2000.

[212] H. McGee. *On Food and Cooking: The Science and Lore of the Kitchen.* Scribner, 2007.

[213] L. McReynolds *et al.* "Sequence of chicken ovalbumin mRNA". *Nature*, **273**, 1978.

[214] P. E. Stein *et al.* "Crystal structure of ovalbumin as a model for the reactive centre of serpins". *Nature*, **347**, 1990.

[215] P. E. Stein *et al.* "Crystal structure of uncleaved ovalbumin at 1.95 Åresolution". *J. Mol. Biol.*, **221**, 1991.

[216] M. Pouzot *et al.* "X-ray and light scattering study of the structure of large protein aggregates at neutral pH". *Food Hydrocoll.*, **19**, 2005.

[217] M. Weijers, R. W. Visschers, T. Nicolai. "Light Scattering Study of Heat-Induced Aggregation and Gelation of Ovalbumin". *Macromolecules*, **35**, 2002.

[218] B. Egelandsdal. "HEAT-INDUCED GELLING IN SOLUTIONS OF OVALBUMIN". *J. Food Sci.*, **45**, 1980.

[219] A. Koike, N. Nemoto, E. Doi. "Structure and dynamics of ovalbumin gels: 1. Gel induced by high-temperature heat treatment". *Polymer*, **37**, 1996.

[220] A. Koike, A. Takada, N. Nemoto. "Structure and dynamics of ovalbumin gels: II. Gels induced by heat treatment at 80 ° C". *Polym. Gels Networks*, **6**, 1998.

[221] M. Pouzot, D. Durand, T. Nicolai. "Influence of the Ionic Strength on the Structure of Heat-Set Globular Protein Gels at pH 7. β-Lactoglobulin". *Macromolecules*, **37**, 2004.

[222] M. Weijers, R. W. Visschers, T. Nicolai. "Influence of the Ionic Strength on the Structure of Heat-Set Globular Protein Gels at pH 7. Ovalbumin". *Macromolecules*, **37**, 2004.

[223] M. Sugiyama *et al.* "Effect of Salt and Heating on a Mesoscopic Structure Composed of Ovalbumin Globules in Aqueous Solution". *Biomacromolecules*, **2**, 2001.

[224] M. Weijers *et al.* "Heat-induced formation of ordered structures of ovalbumin at low ionic strength studied by small angle X-ray scattering". *Colloids Surfaces A: Physicochem. Eng. Aspects*, **270-271**, 2005.

[225] L. Ianeselli *et al.* "Protein − Protein Interactions in Ovalbumin Solutions Studied by Small-Angle Scattering: Effect of Ionic Strength and the Chemical Nature of Cations". *J. Phys. Chem. B*, **114**, 2010.

[226] E. Doi, T. Koseki, N. Kitabatake. "Effects of limited proteolysis on functional properties of ovalbumin". *J. Am. Oil Chem. Soc.*, **64**, 1987.

[227] D. Renard *et al.* " " Ordered " structure in solutions and gels of a globular protein as studied by small angle neutron scattering". *Biopolym.*, **39**, 1996.

[228] A. Isihara. "Determination of Molecular Shape by Osmotic Measurement". *J. Chem. Phys.*, **18**, 1950.

[229] T. Matsumoto, J. Chiba. "Rheological and small-angle X-ray scattering investigations on the shape and ordered arrangement of native ovalbumin molecules in aqueous colloids". *J. Chem. Soc. Faraday Trans.*, **86**, 1990.

[230] B. Jacrot. "The study of biological structures by neutron scattering from solution". *Reports on Prog. Phys.*, **39**, 1976.

[231] T. Suzuki *et al.* "Nonuniformity in Cross-Linked Natural Rubber as Revealed by Contrast-Variation Small-Angle Neutron Scattering". *Macromolecules*, **43**, 2010.

[232] V. Pipich *et al.* "Nucleation and Growth of CaCO3 Mediated by the Egg-White Protein Ovalbumin: A Time-Resolved in situ Study Using Small-Angle Neutron Scattering". *J. Am. Chem. Soc.*, **130**, 2008.

[233] M. Shibayama, T. Tanaka. "Small- angle neutron scattering study on weakly charged poly(N- isopropyl acrylamide- co- acrylic acid) copolymer solutions". *J. Chem. Phys.*, **102**, 1995.

[234] A. Stradner *et al.* "Equilibrium cluster formation in concentrated protein solutions and colloids". *Nature*, **432**, 2004.

[235] F. Sciortino *et al.* "Equilibrium Cluster Phases and Low-Density Arrested Disordered States: The Role of Short-Range Attraction and Long-Range Repulsion". *Phys. Rev. Lett.*, **93**, 2004.

[236] Y. Liu *et al.* "Effective Long-Range Attraction between Protein Molecules in Solutions Studied by Small Angle Neutron Scattering". *Phys. Rev. Lett.*, **95**, 2005.

[237] A. Stradner, F. Cardinaux, P. Schurtenberger. "Comment on "Effective Long-Range Attraction between Protein Molecules in Solution Studied by Small Angle Neutron Scattering"". *Phys. Rev. Lett.*, **96**, 2006.

[238] A. Shukla *et al.* "Absence of equilibrium cluster phase in concentrated lysozyme solutions". *Proc. Natl. Acad. Sci.*, **105**, 2008.

[239] W. Van de Sande, A. Persoons. "The size and shape of macromolecular structures: determination of the radius, the length and the persistance length of rod-like micelles of dodecyldimethylammonium chloride and bromide". *J. Phys. Chem.*, **89**, 1985.

[240] A. Onuki. "Scattering from deformed swollen gels with heterogeneities". *J. Phys. II France*, **2**, 1992.

[241] T. Nicolai *et al.* "Iso-scattering points during heat-induced aggregation and gelation of globular proteins indicating micro-phase separation". *Europhys. Lett.*, **73**, 2006.

[242] M. Shibayama, T. Norisuye. "Gel Formation Analyses by Dynamic Light Scattering". *Bull. Chem. Soc. Jpn.*, **75**, 2002.

[243] C. Lin, I. Gitsov. "Preparation and Characterization of Novel Amphiphilic Hydrogels with Covalently Attached Drugs and Fluorescent Markers". *Macromolecules*, **43**, 2010.

[244] C. S. Gudipati *et al.* "Hyperbranched fluoropolymer and linear poly(ethylene glycol) based amphiphilic crosslinked networks as efficient antifouling coatings: An insight into the surface compositions, topographies, and morphologies". *J. Polym. Sci. Part A: Polym. Chem.*, **42**, 2004.

[245] M. Hanko *et al.* "Nanophase-Separated Amphiphilic Conetworks as Versatile Matrixes for Optical Chemical and Biochemical Sensors". *Anal. Chem.*, **78**, 2006.

[246] J. Tobis *et al.* "Amphiphilic polymer conetworks as chiral separation membranes". *J. Membr. Sci.*, **372**, 2011.

[247] G. Savin *et al.* "Nanophase Separated Amphiphilic Microbeads". *Macromolecules*, **38**, 2005.

[248] B. Iván, J. P. Kennedy, P. W. Mackey. *Amphiphilic Networks*, volume 469 of *ACS Symposium Series*, book section 18, pages 194–202. American Chemical Society, 1991.

[249] B. Iván, J. P. Kennedy, P. W. Mackey. *Amphiphilic Networks*, volume 469 of *ACS Symposium Series*, book section 19, pages 203–212. American Chemical Society, 1991.

[250] R. M. Briber, B. J. Bauer. "Effect of crosslinks on the phase separation behavior of a miscible polymer blend". *Macromolecules*, **21**, 1988.

[251] K. Yamamoto *et al.* "Phase-Separated Conetwork Structure Induced by Radical Copolymerization of Poly(dimethylsiloxane)-α,ω-diacrylate and N,N-Dimethylacrylamide". *Macromolecules*, **42**, 2009.

[252] A. Domján *et al.* "Structural Studies of Nanophase-Separated Poly(2-hydroxyethyl methacrylate)-l-polyisobutylene Amphiphilic Conetworks by Solid-State NMR and Small-Angle X-ray Scattering". *Macromolecules*, **36**, 2003.

[253] B. Iván *et al.* "Synthesis, Characterization, and Structural Investigations of Poly(ethyl acrylate)-l-polyisobutylene Bicomponent Conetwork". *Macromolecules*, **34**, 2001.

[254] G. Erdödi, B. Iván. "Novel Amphiphilic Conetworks Composed of Telechelic Poly(ethylene oxide) and Three-Arm Star Polyisobutylene". *Chem. Mater.*, **16**, 2004.

[255] G. Erdodi, J. P. Kennedy. "Ideal tetrafunctional amphiphilic PEG/PDMS conetworks by a dual-purpose extender/crosslinker. II. Characterization and properties of water-swollen membranes". *J. Polym. Sci. Part A: Polym. Chem.*, **43**, 2005.

[256] S. R. Gomes *et al.* "SANS investigation of PDMS hybrid materials prepared by gamma-irradiation". *Nucl. Instrum. Methods Phys. Res. Sect. B*, **266**, 2008.

[257] C. Fodor, G. Kali, B. Iván. "Poly(N-vinylimidazole)-l-Poly(tetrahydrofuran) Amphiphilic Conetworks and Gels: Synthesis, Characterization, Thermal and Swelling Behavior". *Macromolecules*, **44**, 2011.

[258] G. Kali *et al.* "Thermally Responsive Amphiphilic Conetworks and Gels Based on Poly(N-isopropylacrylamide) and Polyisobutylene". *Macromolecules*, **46**, 2013.

[259] N. Bruns *et al.* "Nanophase Separated Amphiphilic Conetwork Coatings and Membranes". *Macromolecules*, **38**, 2005.

[260] M. Haraszti, E. Tóth, B. Iván. "Poly(methacrylic acid)-l-Polyisobutylene: A Novel Polyelectrolyte Amphiphilic Conetwork". *Chem. Mater.*, **18**, 2006.

[261] G. Kali *et al.* "Synthesis and Characterization of Anionic Amphiphilic Model Conetworks Based on Methacrylic Acid and Methyl Methacrylate: Effects of Composition and Architecture". *Macromolecules*, **40**, 2007.

[262] T. K. Georgiou *et al.* "Amphiphilic Model Conetworks of Polyisobutylene Methacrylate and 2-(Dimethylamino)ethyl Methacrylate Prepared by the Combination of Quasiliving Carbocationic and Group Transfer Polymerizations". *Macromolecules*, **40**, 2007.

[263] G. Kali *et al.* "Synthesis and Characterization of Anionic Amphiphilic Model Conetworks of 2-Butyl-1-Octyl-Methacrylate and Methacrylic Acid: Effects of Polymer Composition and Architecture". *Langmuir*, **23**, 2007.

[264] J. Scherble *et al.* "Formation of CdS nanoclusters in phase-separated poly(2-hydroxyethyl methacrylate)-l-polyisobutylene amphiphilic conetworks". *J. Polym. Sci. Part B: Polym. Phys.*, **39**, 2001.

[265] W. H. Binder *et al.* "Magnetic and Temperature-Sensitive Release Gels from Supramolecular Polymers". *Adv. Funct. Mater.*, **17**, 2007.

[266] M. Vamvakaki *et al.* "Amphiphilic Networks Based on Cross-Linked Star Polymers: A Small-Angle Neutron Scattering Study". *Langmuir*, **23**, 2007.

[267] Y.-S. Han *et al.* "Design of 40M SANS instrument at HANARO, Korea". *Phys. B: Condens. Matter*, **385-386, Part 2**, 2006.

[268] E. P. Gilbert, J. C. Schulz, T. J. Noakes. " ' Quokka ' —the small-angle neutron scattering instrument at OPAL". *Phys. B: Condens. Matter*, **385-386, Part 2**, 2006.

[269] S. Manet *et al.* "Structure of Micelles of a Nonionic Block Copolymer Determined by SANS and SAXS". *J. Phys. Chem. B*, **115**, 2011.

[270] M. Groenewolt *et al.* "Polyisobutylene-block-Poly(ethylene oxide) for Robust Templating of Highly Ordered Mesoporous Materials". *Adv. Mater.*, **17**, 2005.

[271] P. Bartlett, R. H. Ottewill. "A neutron scattering study of the structure of a bimodal colloidal crystal". *J. Chem. Phys.*, **96**, 1992.

[272] K. A. Andrianov *et al.* "Some physical properties of polyorganosiloxanes. I. Linear polyorganosiloxanes". *J. Polym. Sci. Part A: Polym. Chem.*, **10**, 1972.

[273] D. A. Hajduk *et al.* "The Gyroid: A New Equilibrium Morphology in Weakly Segregated Diblock Copolymers". *Macromolecules*, **27**, 1994.

[274] M. Shibayama, T. Hashimoto, H. Kawai. "Ordered structure in block polymer solutions. 5. Equilibrium and nonequilibrium aspects of microdomain formation". *Macromolecules*, **16**, 1983.

[275] Y. Shinohara *et al.* "X-ray Photon Correlation Spectroscopy of Filler in Rubber". *Jpn. J. Appl. Phys.*, **46**, 2007.

[276] B. Chu *et al.* "An X-ray Photon Correlation Experiment". *Langmuir*, **11**, 1995.

[277] S. B. Dierker *et al.* "X-Ray Photon Correlation Spectroscopy Study of Brownian Motion of Gold Colloids in Glycerol". *Phys. Rev. Lett.*, **75**, 1995.

[278] A. Ashkin. "Acceleration and Trapping of Particles by Radiation Pressure". *Phys. Rev. Lett.*, **24**, 1970.

[279] K. C. Neuman, A. Nagy. "Single-molecule force spectroscopy: optical tweezers, magnetic tweezers and atomic force microscopy". *Nature Methods*, **5**, 2008.

[280] L. Isserlis. "On a Formula for the Product-Moment Coefficient of any Order of a Normal Frequency Distribution in any Number of Variables". *Biom.*, **12**, 1918.

[281] J. V. Michalowicz *et al.* "A general Isserlis theorem for mixed-Gaussian random variables". *Stat. & Probab. Lett.*, **81**, 2011.

[282] C. Vignat. "A generalized Isserlis theorem for location mixtures of Gaussian random vectors". *Stat. & Probab. Lett.*, **82**, 2012.

[283] G. Christian, P. Dasgupta, K. Schug. *Analytical Chemistry, 7th Edition: Seventh Edition.* Wiley Global Education, 2013.

Acknowledgement

First of all, I would like to express the deepest appreciation to my supervisor, Prof. Mitsuhiro Shibayama. His attitude towards research strongly affects my research style and way of thinking. I would like to thank my secondary supervisor, Prof. Kaoru Yamanouchi for his support and helpful discussion.

I could not conduct the experiments in this thesis without the help and discussion with collaborators. I would like to thank Dr. Takamasa Sakai and Prof. Ungil Chung for their support related to the work on Tetra-PEG gels (Section 5.5, 9). My research starts from the study of Tetra-PEG gels, which are developed by them. It results in the work of PEG–PDMS gels, which is the core of this thesis. Their advices from the viewpoint of mechanical characteristic were always helpful for the analysis from the viewpoint of structural analysis. I am also grateful to the members of their laboratory. Especially, I would like to thank Dr. Shinji Kondo for his assistance of the preparation of PEG–PDMS gels (Section 9). My structural analysis of PEG–PDMS gels is based on his research for the preparation and mechanical characteristic investigation of PEG–PDMS gels. I would like to thank Dr. Seisuke Ata for inviting me the research of carbon nanotube dispersion (Section 7). From the collaboration work with him, I learned the importance of application of basic research to engineering product. I would like to thank Prof. Naoki Tanaka for his advices related to the chemistry of OVA and pOVA (Section 8). The research related to egg protein is different from more simple chemicals such as Tetra-PEG and CNT. It was very tough to analyze but interesting. I would also like to thank Ms. Yuri Narita for her assistance of the preparation of OVA and pOVA gels and buffer solutions.

To conduct the research of small-angle neutron and X-ray scattering, I would like to thank the technical support from the researchers in the institutes and the financial support. I would like to thank Dr. Young-Soo Han and Dr. Tae-Hwan Kim for their support at 40m SANS at HANARO, Korea (Section 9). It was my first SANS experiment, and I never forget the moment when I saw the SANS pattern of my sample. I would like to thank Dr. Michael Ohl and Dr. Malcolm Cochran for their support at Neutron Spin Echo Spectrometer in Spallation Neutron Source, USA (Section 5.5). It was my first time to conduct the experiment by myself in the institute abroad. I could not accomplish the experiment without their strong support. I would like to thank Dr. Ken Littrell for his support at GP-SANS at High Flux Isotope Reactor, USA (Section 8). Thanks to well-organized experimental setup, I could conduct my experiment without any difficulty. I would like to thank Dr. Sai Venkatesh Pingali for his support at Bio-SANS at High Flux Isotope Reactor, USA (Section 8). Even though Bio-SANS is a kind of twin of GP-SANS, I could learn a lot from this instrument. I would like to thank Dr. Elliot Paul Gilbert for his support at QUOKKA at Australia's Open Pool Australian Lightwater, Australia (Section 9). It was my first time to visit without senior researchers. His kind support and instruction was very helpful for me.

Neutron spin echo experiment (Section 5.5) was performed by SNS-NSE (BL15) at SNS, Oak Ridge, TN. I acknowledge the financial support provided by JCNS and the use of the JCNS-NSE instrument at the Spallation Neutron Source (SNS), Oak Ridge, USA. Part of this research conducted at SNS was sponsored by the Scientific User Facilities Division, Office of Basic Energy Sciences, US Department of Energy. This work was carried out under the Joint-Use Research Program for Neutron Scattering, Institute for Solid State Physics (ISSP), the University of Tokyo, at the Research Reactor JRR-3, JAEA (Proposal No. 13612). The

experiments of OVA (Section 8) was supported by the US-Japan Cooperative Program on Neutron Scattering (IPTS-10925 for GP-SANS, 12590 for Bio-SANS). As for the experiments of PEG–PDMS gels (Section 9), the SANS experiment at 40 m SANS at HANARO was transferred from SANS-U at the Research Reactor JRR-3 with the approval of Institute for Solid State Physics (ISSP), The University of Tokyo (Proposal No. 13592). The SANS experiment at QUOKKA at OPAL was also transferred from SANS-U with the approval of ISSP (Proposal No. 14587). The SAXS experiment was performed at the second hutch of the Frontier Soft Matter Beamline (FSBL; BL03XU), SPring-8, Hyogo, Japan, with the assistance of Atsushi Izumi, Sumitomo Bakelite, Co., Ltd. (Proposal No. 2014B7260).

I would also like to thank all of the members in Neutron Science Laboratory, both staffs and students. Especially, I appreciate the members of Shibayama Laboratory. I would like to thank Dr. Kenta Fujii and Dr. Xiang Li, assistant professors of Shibayama Laboratory, for their support in conducting experiments. I learned almost all of my experimental skills from Dr. Takumi Kusano and Dr. Kei Hashimoto, my senior students. My junior students also helped me a lot. Especially, Mr. Kazu Hirosawa conducted the SANS experiments of OVA with me. Ms. Saki Tochioka conducted the SANS experiments of PEG–PDMS with me. Thanks to them, I could conduct SANS experiments without any difficulty.

I acknowledge the financial support, Advanced Leading Graduate Course for Photon Science, Program for Leading Graduate Schools (ALPS) and Research Fellowships for Young Scientists (DC1), from Japan Society for the Promotion of Science.

Last but most importantly, I would like to thank my parents.